# DEFORMATION AND METAMORPHISM OF THE SUKHOTHAI FOLD BELT, NORTHERN THAILAND

by

Sampan Singharajwarapan

B.S. (Chiang Mai University), M.Sc. (Asian Institute of Technology)


Submitted in fulfilment of the requirements for the degree of
**Doctor of Philosophy**

University of Tasmania
Hobart

December, 1994

*This thesis contains no material which has been accepted for the award of any other degree or diploma in any tertiary institution and, to the best of my knowledge and belief, contains no copy or paraphase of material previously published or written by another person, except when due reference is made in the text of the thesis.*

Sampan Singharajwarapan

# ABSTRACT

A structural and metamorphic study across the Sukhothai fold belt in Northern Thailand provides new evidence for testing many of the tectonic models currently proposed to explain the geological evolution of this part of Southeast Asia. A brief study was also made of the structure and metamorphism of the Doi Inthanon metamorphic complex located about 80 km to the west of the fold belt.

The oldest rocks recognised in the Sukhothai fold belt, particularly the eastern part, are arc volcanics and a subduction-accretion complex sequence represented by the Permo-Carboniferous Pha Som Metamorphic Complex. This complex consists of a metasedimentary unit and a serpentinite melange unit (ophiolite association). The metasedimentary unit is characterised by a multiply-deformed, coherent sequence of metagreywackes and minor phyllites. The metagreywackes are interpreted to have been derived from two different sources, i.e. an accretionary complex/continental magmatic arc source and a volcanic arc source. The serpentinite melange unit consists dominantly of blocks of igneous and meta-igneous rocks that originated in an oceanic arc setting together with less abundant backarc and oceanic within-plate counterparts. Greywacke, argillite, chert and limestone blocks are minor components. Four structural phases were recognised in the coherent metasedimentary unit. The earliest recognisable structure is compositional layering ($S_1$). $D_2$ structures include tight $F_2$ folds, differentiated layering/phyllitic cleavage ($S_2$) and a stretching lineation ($L_2$). The $D_1$ and $D_2$ structures are interpreted to be the results of deformation in a thrust environment during which diffusional mass transfer was the dominant deformation mechanism. The $D_1$-$D_2$ events are consistent with subduction-accretion models. $D_3$ produced open folds with associated crenulations and crenulation cleavage. $D_4$ kinks and angular folds are probably related to thrusting. A single metamorphic episode was recognised in the metasedimentary rocks. The *P-T* estimates are constrained via thermodynamic calculations and $b_0$ and illite crystallinity studies. A newly calibrated phengite-chlorite geothermometer, applied to this suite of rocks, yields temperatures in the range 300-400 °C. The $b_0$ values of the pelitic rocks are indicative of a low to medium pressure facies series whereas petrogenetic grids constrain the pressures to between 3 and 6 kbar. The peak metamorphic condition was attained during $D_2$. Blocks of igneous rocks within the serpentinite melange

have been variably metamorphosed to sub-greenschist through to middle amphibolite facies.

A Permian sequence (the Ngao or Phrae Group), distributed mainly in the eastern and central part of the fold belt, is characterised by turbidites and limestones probably deposited in a forearc setting. The deposition of the forearc sediments may have persisted into the Triassic, during which period the upper forearc volcaniclastic sediments and ramp carbonates (the Lampang Group) dominated. Petrographic and geochemical data support the previous interpretations that the Triassic turbiditic sandstones were derived from a volcanic arc source. Only one phase of folding with associated thrusting was recognised in the Permian and Triassic sequences. This deformation event resulted in the upright to inclined folds with axial-plane cleavage, and thrusts. The timing of folding and thrusting is constrained by the age of the youngest rock unit affected by this deformation event (i.e. the middle Carnian-lower Norian Wang Chin Formation) and the age of post-kinematic granites (Late Triassic-Early Jurassic). Metamorphic grades of the Permian and Triassic rocks, based on the illite crystallinity values of pelitic rocks, increase from west to east (i.e. from diagenetic-lower anchizone grade to upper anchizone-epizone grade).

The Jurassic strata, east of the Sukhothai fold belt, contain post-orogenic continental sediments. Petrographic criteria and observed sedimentary features suggest that the Jurassic sandstones (the Phra Wihan Formation) were derived from a quartzose recycled orogenic source or craton interior and deposited in fluvial plains. Late Triassic-Early Jurassic S-type granites are widespread in northern Thailand and post-date the regional cleavage in the Permian and Triassic sequences.

The Doi Inthanon metamorphic complex is a mantled gneiss dome which is characterised by core orthogneisses and mantling paragneisses detached from the Lower Palaeozoic cover rocks by a low-angle fault surface. The gneisses have been intruded by S-type granites of Late Triassic-Early Jurassic and younger ages. Compositional layering and folds in the gneisses are widely overprinted by mylonitic fabrics subparallel to the layering. The compositional layering and folds are likely to be the result of a compressional event as suggested by inclined isoclinal folds in similar gneissic rocks further south, e.g. the Bhumipol Dam area. At this stage, it is uncertain whether this compressional event is related to the Late Triassic folding and thrusting event in the Sukhothai fold belt or some other older events. On the other hand, mylonitisation of the gneisses is probably due to Cretaceous-Middle Tertiary tectonic unroofing and uplift. The peak metamorphism of the

gneissic rocks occurred under low $P$ - high $T$ conditions (i.e. around 4 kbar and 700 °C) which may be related to the extensive Late Triassic-Early Jurassic S-type granitic intrusions. The peak metamorphism was overprinted by a later retrograde event that is contemporaneous with mylonitisation.

During Late Carboniferous to Permian times, the tectonism of northern Thailand was dominated by subduction and arc volcanism. The accretion of trench and ocean basin sediments and igneous rocks occurred during this time interval and eventually culminated in the collision between the Shan-Thai and the Indochina terranes in Late Triassic. The collision phase is best exemplified by folding and thrusting of the Triassic turbiditic sequences followed by extensive intrusions of Late Triassic-Early Jurassic S-type granites and post-orogenic Jurassic-Cretaceous continental redbeds. There has been extensive mid-Tertiary faulting which resulted in the formation of widespread extensional basins in northern Thailand.

# ACKNOWLEDGEMENTS

I would like to express my sincere gratitude to my supervisor, Dr. Ron Berry, for his invaluable advice, support, interest, and encouragement throughout the course of this study. I also thank him and his wife, Kate, for their friendship and hospitality over the past few years.

I am also very much indebted to Drs. Clive Burrett, Tony Crawford and Yuenyong Panjasawatwong for their stimulating discussion, support and more importantly initiation of the project.

I am grateful for the support of Charn Tantisukrit, my former teacher and present colleague.

Financial support for this study was kindly provided by the Australian Government through the Australian International Development Assistance Bureau (AIDAB) Postgraduate Training Award. Special thanks are extended to the AIDAB staff, particularly Kevin MacCormack, Robin Bowden, Peter Robin and Diane Smith who helped me go through various stages of my study from the beginning until the completion of this thesis.

Drs. Tony Crawford and Joe Stolz are thanked for their helpful discussion, critical reading and comments on Chapter 6 and Drs. Garry Davidson and Prasada Rao are thanked for their critical reading and comments on Chapter 7.

The determination of illite crystallinity and $b_0$ values was carried out by Ralph Bottrill and Ritchie Wooley of the Tasmania Department of State Development and Resources (formerly the Tasmania Department of Mines) and their tremendous effort is genuinely appreciated.

Thanks are extended to Dr. Robin Offler and Professor Hanan Kisch for providing the illite crystallinity standards and for their comments on the technique of illite crystallinity measurement used in Hobart. Dr. Robin Offler and his staff at the University of Newcastle generously re-measured illite crystallinity of five samples to verify the results obtained in Hobart.

Kathy Stait and Dr. Maxwell Banks kindly identified fossils and gave a great deal of useful advice.

Wieslaw Jablonski of the Central Science Laboratory is thanked for his instruction and technical assistance in the operation of electron microprobe and scanning electron microscope.

Thanks are extended to the staff of Geology Department who assisted me during this study particularly: Simon Stevens for his skillful work in preparing

hundreds of thin sections and polished thin sections; Philip Robinson for his technical assistance in XRF analytical work; Keith Harris for an introductory session on the operation of electron microprobe; Nilar Hlaing for her advice in preparing pressed-powder pellets and fusion discs for XRF analysis; Jeanette Hankin and Peter Cornish for their efficient handling of all bureaucratic work and June Pongratz for her advice on Macintosh software.

Pornchai Konglim is thanked for his assistance in the field, especially during two adventurous trips across the Sirikit Reservoir in a small boat.

Laurie Zambon and Louise Oxley are thanked for their assistance in editing the manuscript of this thesis.

Thanks are extended to post-doctoral fellows and PhD students of this department for their friendship and support : Drs. Ai Yang, Andrew McNiel, Andrew Tunks, Anthea Hill, Aung Pwa, David Cooke, David Huston, Djojomihardjo Soetijos, Fernando Della Pasqua, Geoff Nichols, Greg Yaxley, Ian Harte, Ingvar Sigurdsson, Jamie Rogers, Khin Zaw, Kim Hein, Marcel Kamperman, Mark Doyle, Massimo Gasparon, Matthew White, Memet Rahmat Hermanto, Michael Roach, Paul Kitto, Peter McGoldrich, Pol Chaodumrong, Rob Lewis, Ruth Lanyon, Sjafra Dwipa, Thanis Wongwanich and Udi Hartono.

I am deeply grateful for the support from my parent and sisters. And finally, I would like to thank for the continual support and encouragement given to me by my wife, Fongsaward, and my sons, Silpa and Sarana, who have been patiently waiting for me to return from Down Under.

Part of Chapter 4 has been published in the Journal of Southeast Asian Earth Sciences:

Singharajwarapan, S. and Berry, R.F., 1993, Structural analysis of the accretionary complex in Sirikit Dam area, Uttaradit, Northern Thailand, Journal of Southeast Asian Earth Sciences, v. 8, p. 233-245.

# TABLE OF CONTENTS

# LIST OF FIGURES

# LIST OF TABLES

# ABBREVIATIONS, SYMBOLS AND THAI GEOGRAPHICAL NAMES

## Mineral abbreviations and formulae

*Note* : Mineral abbreviations are from Kretz (1983) where practicable. Mineral formulae are from Deer *et al.* (1966) except * from Holland and Powell (1990). All Fe is $Fe^{2+}$ unless otherwise indicated.

| | | |
|---|---|---|
| Act | actinolite | $Ca_2(Fe,Mg)_5Si_8O_{22}(OH,F)_2$ |
| Ab | albite | $NaAlSi_3O_8$ |
| Alm | almandine | $Fe_3Al_2Si_3O_{12}$ |
| Ames* | amesite | $Mg_4Al_2(Si_2Al_2)O_{10}(OH)_8$ |
| Amph | amphibole | |
| And | andalusite | $Al_2SiO_5$ |
| Adr | andradite | $Ca_3Fe^{3+}{}_2Si_3O_{12}$ |
| Ank | ankerite | $Ca(Mg,Fe)(CO_3)_2$ |
| An | anorthite | $CaAl_2Si_2O_8$ |
| Atg | antigorite | $Mg_3Si_2O_5(OH)_4$ |
| Ap | apatite | $Ca_5(PO_4)_3(OH,F,Cl)$ |
| Aug | augite | $(Ca,Na,Mg,Fe,Mn,Fe^{3+},Al,Ti)_2(Al,Si)_2O_6$ |
| Bt | biotite | $K(Mg,Fe)_{3-2}(Fe^{3+},Al,Ti)_{0-1}Si_{3-2.5}Al_{1-1.5}O_{10}(OH,F)_2$ |
| Cal | calcite | $CaCO_3$ |
| Cats* | Ca-Tschermak pyroxene | $CaAl(SiAl)O_6$ |
| Cel* | celadonite | $KMgAlSi_4O_{10}(OH)_2$ |
| Clin* | clinochlore | $Mg_4(MgAl)Si_2(SiAl)O_{10}(OH)_8$ |
| Chl | chlorite | $(Mg,Fe,Al)_6(Si,Al)_4O_{10}(OH)_8$ |
| Chr | chromite | $FeCr_2O_4$ |
| Ctl | chrysotile | $Mg_3Si_2O_5(OH)_4$ |
| Cpx | clinopyroxene | |
| Czo | clinozoisite | $Ca_2AlAl_2Si_3O_{12}(OH)$ |
| Di | dioside | $CaMgSi_2O_6$ |
| Dol | dolomite | $CaMg(CO_3)_2$ |
| East* | eastonite | $KMg(MgAl)Si_2Al_2O_{10}(OH)_2$ |
| Ed | edenite | $NaCa_2Mg_5Si_7AlO_{22}(OH,F)_2$ |
| En | enstatite (ortho) | $Mg_2Si_2O_6$ |
| Ep | epidote | $Ca_2(Fe^{3+}Al_2)Si_3O_{12}(OH)$ |
| Fs | ferrosilite (ortho) | $Fe_2Si_2O_6$ |
| Ftr* | Fe-tremolite | $Ca_2Fe_5Si_8O_{22}(OH)_2$ |
| Grt | garnet | |
| Grs | grossular | $Fe_3Al_2Si_3O_{12}$ |
| Hem | haematite | $Fe_2O_3$ |
| Hs | hastingsite | $NaCa_2Fe_4Fe^{3+}Si_6Al_2O_{22}(OH,F)_2$ |
| Hd | hedenbergite | $CaFeSi_2O_6$ |
| Hbl | hornblende | $(Na,K)_{0-1}Ca_2(Mg,Fe,Fe^{3+},Al)_5Si_{6-7}Al_{2-1}O_{22}(OH,F)_2$ |
| Ill | illite | $K_{0.5-0.75}Al_2(Al_{0.5-0.75}Si_{3.5-3})O_{10}(OH)_2$ |
| Ilm | ilmenite | $FeTiO_3$ |
| Jd | jadeite | $NaAlSi_2O_6$ |
| Kfs | K-feldspar | $KAlSi_3O_8$ |
| Ky | kyanite | $Al_2SiO_5$ |
| Mgs | magnesite | $MgCO_3$ |

| | | |
|---|---|---|
| Mag | magnetite | $FeFe^{3+}{}_2O_4$ |
| Mc | microcline | $KAlSi_3O_8$ |
| Ms | muscovite | $KAl_2(AlSi_3)O_{10}(OH,F)_2$ |
| Or | orthoclase | $KAlSi_3O_8$ |
| Pg | paragonite | $NaAl_2(AlSi_3)O_{10}(OH,F)_2$ |
| Prg | pargasite | $NaCa_2Mg_4AlSi_6Al_2O_{22}(OH,F)_2$ |
| Phl | phlogopite | $KMg_3(AlSi_3)O_{10}(OH,F)_2$ |
| Pm | piemontite | $Ca_2(Mn^{3+},Fe^{3+}Al)_3Si_3O_{12}(OH)$ |
| Ps | pistacite | $Ca_2(Fe^{3+}Al_2)Si_3O_{12}(OH)$ |
| Pl | plagioclase | $(Na,Ca)Al_{1-2}Si_{3-2}O_8$ |
| Prh | prehnite | $Ca_2Al(AlSi_3O_{10})(OH)_2$ |
| Pmp | pumpellyite | $Ca_4(Mg,Fe)(Al,Fe^{3+})_5Si_6O_{21}(OH)_7$ |
| Prp | pyrope | $Fe_3Al_2Si_3O_{12}$ |
| Qtz | quartz | $SiO_2$ |
| Rt | rutile | $TiO_2$ |
| Srp | serpentine | $Mg_3Si_2O_5(OH)_4$ |
| Sd | siderite | $CaFe(CO_3)_2$ |
| Sil | sillimanite | $Al_2SiO_5$ |
| Sps | spessartine | $Fe_3Al_2Si_3O_{12}$ |
| Spn | sphene | $CaTi(SiO_4)(O,OH,F)$ |
| Tlc | talc | $Mg_3Si_4O_{10}(OH)_2$ |
| Tur | tourmaline | $Na(Mg,Fe,Mn,Li,Al)_3Al_6(Si_6O_{18})(BO_3)_3(OH,F)_4$ |
| Tr | tremolite | $Ca_2Mg_5Si_8O_{22}(OH,F)_2$ |
| Ts | tschermakite | $Ca_2Mg_3Al_2Si_6Al_2O_{22}(OH,F)_2$ |
| Wo | wollastonite | $CaSiO_3$ |
| Zrn | zircon | $ZrSiO_4$ |
| Zo | zoisite | $Ca_2AlAl_2Si_3O_{12}(OH)$ |

## Thermodynamic and unit symbols

| | |
|---|---|
| $a_i^A$ | activity of component *i* in phase A |
| $\Delta G$ | Gibbs free energy change of a reaction (J) |
| $\gamma_i$ | activity coefficient of component *i* |
| $\Delta H$ | enthalpy change of a reaction (J) |
| $K$ | equilibrium constant |
| $K_D$ | distribution coefficient |
| $K\gamma$ | product of activity coefficients of end-members for a given reaction |
| $K_X$ | product of mole fractions of end-members for a given reaction |
| R | gas constant = 8.3143 J $mol^{-1}$ $K^{-1}$ |
| $\Delta S$ | entropy change of a reaction (J $K^{-1}$) |
| $\Delta V$ | volume change of a reaction (J $bar^{-1}$) |
| $W_{ij}^A$ | Margules interaction parameter for mixing between component *i* and *j* in phase A (J) |
| $X_i^A$ | mole fraction of component *i* in phase A |
| J | joule |
| K | Kelvin |
| $P$ | pressure (bar or kbar as specified) |
| $T$ | temperatute in Kelvin (K) unless indicated as degree Celcius (°C) |

## Structural symbols

| | |
|---|---|
| C | Cisaillement (*French*) or shear |
| $D_i$ | denotes the $i^{th}$ deformation |
| $L_i$ | denotes the $i^{th}$ lineation |
| $F_i$ | denotes the $i^{th}$ folding phase |
| S | denotes foliation |
| $S_i$ | denotes the $i^{th}$ foliation |
| $M_i$ | denotes the $i^{th}$ metamorphism |

## Miscellaneous symbols

| | |
|---|---|
| k (prefix) | kilo ($10^3$) |
| m (prefix) | milli ($10^{-3}$) |
| μ (prefix) | micro ($10^{-6}$) |
| n (prefix) | nano ($10^{-9}$) |
| m | metre |
| km | kilometre |
| mm | millimetre |
| μm | micron |
| nm | nanometre |
| Å | angstrom ($10^{-10}$ m) |
| A | ampere |
| V | volt |
| nA | nanoampere |
| kV | kilovolt |

## Thai geographical names

| | |
|---|---|
| Ban | : village |
| Amphoe | : district |
| Changwat | : province |
| Doi | : mountain |
| Khao | : mountain |
| Phu | : mountain |
| Khuen | : dam |
| Huai | : rivulet, creek |
| Mae Nam | : river |
| Nam | : river |

# Chapter 1

# INTRODUCTION

## 1.1 Purpose and Scope of Study

The objective of the present study is to document the structure and metamorphism across the Sukhothai fold belt in northern Thailand and to test the tectonic models that have been used to explain the geological evolution of this part of Southeast Asia. In order to carry out this aim, a regional transect was studied across the fold belt concentrating on the structure. Detailed mapping was carried out in some selected areas to delineate the style and history of deformation and metamorphism of some key rock units where this was appropriate to the aim of the study.

The Sirikit Dam area was chosen for detailed mapping because of its position on the boundary between the Sukhothai and Loei fold belts of mainland Southeast Asia (Fig. 1.1). There are sufficient accessible outcrops to suggest many of the tectonic models could be tested against the structural and metamorphic history of this area.

The transect across the Sukhothai fold belts includes two geological traverses (Figs. 1.1 and 1.2). One traverse is along Highway 11 between Lampang and Denchai covering a distance of about 70 km. Another 50 km traverse is along the road from Phrae to the Sirikit Reservoir. These two traverses were chosen for the following reasons: (i) the traverses cross almost normal to the trend of regional structure, and (ii) sufficient outcrops of the Upper Palaeozoic and Triassic sequences in this fold belt are available so that the structural and metamorphic history of these sequences can be documented.

In addition, a brief study was made of petrology and structure of the Doi Inthanon metamorphic complex, located to the west of the Sukhothai fold belt (Fig. 1.1). The purpose is to obtain supplementary data for testing the relevant tectonic models. The significance of the Doi Inthanon metamorphic complex in the tectonic evolution of the northern Thailand region is still a subject of debate. Thus,

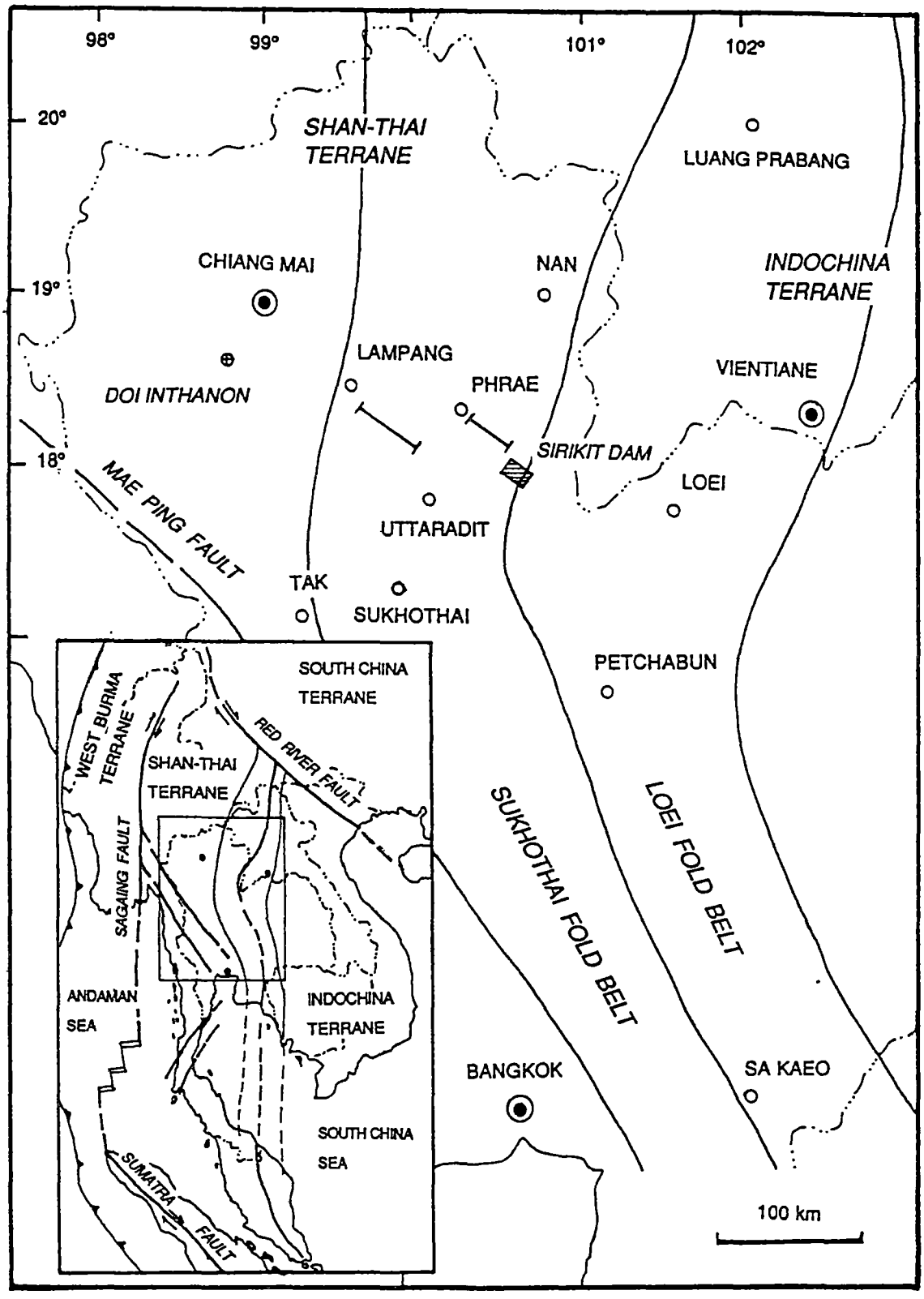


Figure 1.1 Map showing the Sukhothai and Loei fold belts and major towns referred to in the text. Bars indicate two transects across the Sukhothai fold belt. A shaded rectangle indicates the Sirikit Dam area. Inset is a tectonic map of Southeast Asia showing terrane boundaries (modified after Bunopas, 1981; Metcalfe, 1986; Mitchell, 1992).

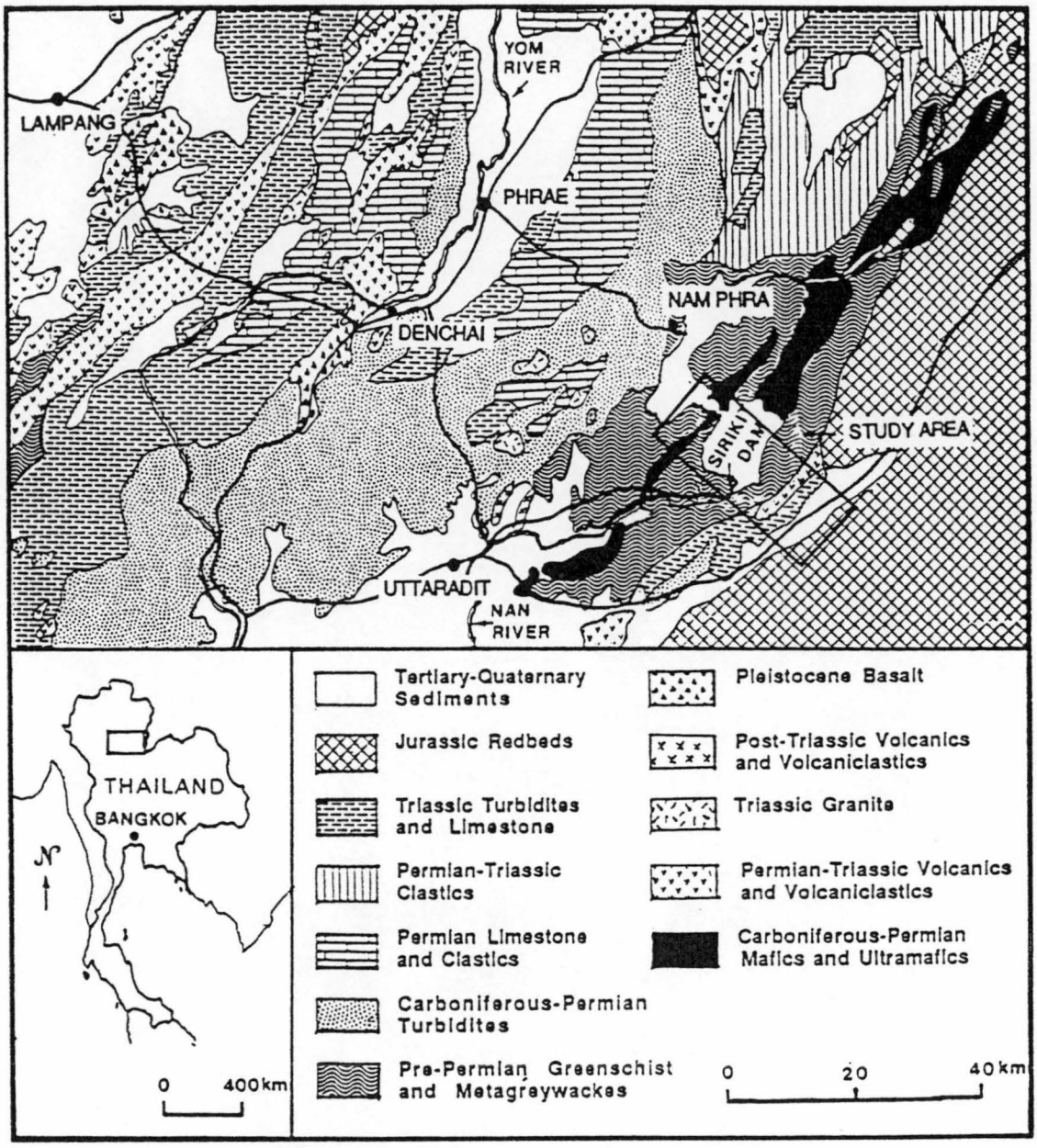


Figure 1.2 Generalised geological map of the Lampang-Phrae-Uttaradit area showing the distribution of major stratigraphic units and the location of the Sirikit Dam area and two transects along the Lampang-Denchai highway and the Phrae-Sirikit Reservoir (Nam Phra) road (modified from Suensilpong *et al.*, 1984; Hess and Koch, 1975; Lumjuan and Sinpoon-anant, 1987)

understanding the evolution of this metamorphic complex is very crucial to any tectonic modelling.

## 1.2 Geographical Setting

### 1.2.1 Physiography and access

Northern Thailand is situated between latitude 16.5-20.5 °N and longitude 97.5-101.5 °E (Fig. 1.1). The physiography of this region is characterised by a series of N-S trending basins and ranges, largely the result of faulting that took place in Middle Tertiary time.

The study area around the Sirikit Dam is approximately 12 x 30 $km^2$ in areal extent. The Sirikit Dam, built across the Nan River nearly 25 year ago, is located 50 km northeast of Uttaradit and can be accessed via Highway 1045 (Fig. 1.2). The area has rugged topography consisting of small stream valleys and hills with moderate relief. The lowest elevation in the area is 100 m above sea level at the Nan River and the highest elevation is 505 m above sea level at the ridge near Phu Khon Kaen. Road-cuttings and streams as well as the wave-cut banks of the reservoir provide reasonably good outcrops for detailed mapping.

The 60 km long unpaved road from Ban Pa Daeng, 8 km east of Phrae, to Ban Nam Phra on the bank of the Sirikit Reservoir (about 25 km northwest of the Sirikit Dam) provides good access for geological traverse from Phrae towards the Sirikit Dam area (Fig. 1.2). This road passes through a rugged terrain with mountain ranges reaching more than 1000 m above sea level.

The traverse from Lampang to Denchai, a small town about 25 km southwest of Phrae, was carried out from km 7.00 to km 75.00 on Highway 11 (Fig. 1.2). The road-cuttings provide excellent outcrops for a detailed structural study.

The gneissic rocks selected for this study are from the Doi Inthanon area, approximately 70 km south of Chiang Mai (Fig. 1.1). The area can be reached via Highway 108 from Chiang Mai to Chom Thong. This area has a very high relief and the Doi Inthanon itself is the highest mountain in Thailand with its peak reaching 2528 m above sea level. Excellent outcrops along the streams and road-cuttings provide a good opportunity for detailed structural and metamorphic studies.

### 1.2.2 Climate

The climate of northern Thailand is tropical savannah and is characterised by distinct wet and dry seasons. This region is under the influence of regional southwest and northeast monsoons. The wet season, influenced by the southwest monsoon from the Indian Ocean, begins around middle of May and continues until the end of September. The intermonsoon period in October is reflected by a retreat of the southwest monsoon and an advance of the northeast monsoon that brings the cold airmass from Central Asia into the region. The cool and dry period, under the influence of the northeast monsoon, lasts from November to early March. Another intermonsoon period, from late March to early May, is marked by a retreat of the northeast monsoon and a slow advance of the southwest monsoon.

The weather pattern of northern Thailand region may be represented by the weather records at Chiang Mai, given a minor variation due to local topographic effects. The mean annual rainfall is 1260 mm. Rains during a period from May to October contribute more than 90% to this annual rainfall (Fig. 1.3a). January is the coolest month with the average temperature range of 13-28 °C and April is the warmest month with the average temperature range of 22-36 °C (Fig. 1.3b). Humidity is relatively low during November to April compared to the remaining period (Fig. 1.3c). Apparently, the humidity is closely related to the amount of rainfall. The weather in Lampang, Phrae and Nan is very similar to that in Chiang Mai, but Uttaradit and Tak are warmer than the rest of northern Thailand.

### 1.2.3 Vegetation and cultivation

The mountain ranges in the study area are generally covered by tropical forests consisting of bamboo, teak and other deciduous trees. However, during the last few decades, extensive deforestation due to illegal logging and encroachment by local people has caused a severe reduction in the forest area. The result is the widespread patches of thorny bush and grassland on the hill sides which can easily be detected from aerial or landsat photographs. The forest conditions have been improved since the Thai government introduced a nationwide logging ban in 1990.

The lowlands in the river basins, e.g. Chiang Mai, Lampang, Phrae, Nan and Nam Pat basins, are mainly occupied by rice paddies with scattered patches of fruit orchards. The major fruit trees include mango, longan, durian, lychee, tangerine and rambutan. The drier and higher grounds (e.g. river terraces) are

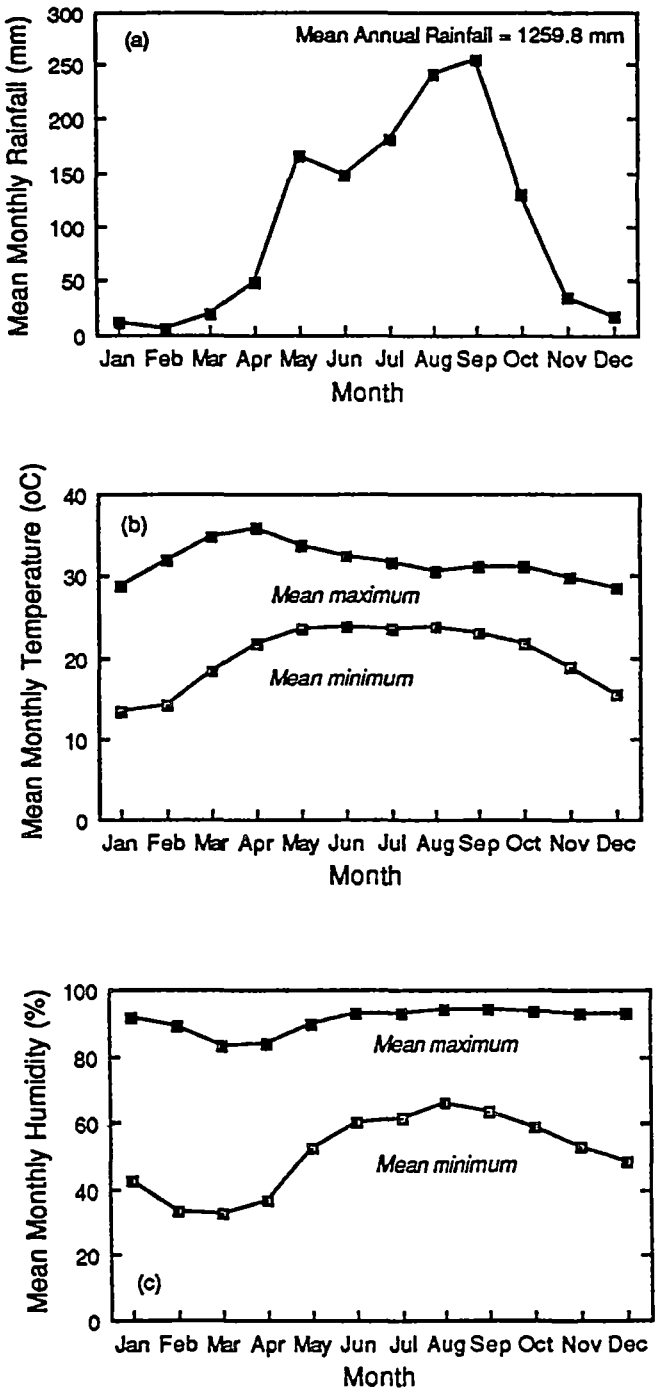


Figure 1.3 Plots of (a) mean monthly rainfall, (b) mean monthly temperature, and (c)mean monthly humidity for Chiang Mai (Royal Thai Department of Meteorology, 1982, unpublished data).

normally used to grow crops such as corn, cassava, sugar cane, cotton, banana and pineapple. Common domestic animals are poultry, pigs and cattle.

## 1.3 Geological Setting

The Sirikit Dam area and two traverses extend across the Sukhothai fold belt and a discontinuous belt of mafic-ultramafic rocks (Fig. 1.2). The mafic-ultramafic belt has been inferred to mark the suture (known as the Nan River Suture zone or the Nan Suture in short) between the Shan-Thai terrane on the west and the Indochina terrane on the east (Bunopas and Vella, 1978; Bunopas, 1981). The Sukhothai and Loei fold belts on either side of the terrane boundary define a large-scale deformation zone in the northern Thailand region (Fig. 1.1). These two terranes are separated from the South China terrane to the north by a large-scale dextral strike-slip fault known as the Red River fault. This fault extends from North Vietnam to the Yunnan province in southern China. The Shan-Thai terrane is separated from the West Burma terrane by another large-scale dextral strike-slip fault known as the Sagaing fault in central Burma. This fault is probably linked with the Sumatra (Semangko) fault in Indonesia through a backarc rifting system in the Andaman Sea (Fig. 1.1).

Northern Thailand is characterised by approximately N-S trending outcrop pattern and major fold structures possibly due to an E-W compression during the amalgamation of the Shan-Thai and Indochina terranes. These features were later modified by faulting in Tertiary time and their present sigmoidal pattern is related to the NW-SE-trending sinistral wrench faults, e.g. the Mae Ping fault (Fig. 1.1).

The geological map in Figure 1.2 shows distribution of major stratigraphic units in this part of northern Thailand. A mafic-ultramafic complex is tectonically enclosed within low-grade metasedimentary rocks. These two rock units are probably the oldest rocks in the Sukhothai fold belt, but their ages are not very well constrained. Hess and Koch (1975) and Charoenpravat *et al.* (1976) assigned a Permo-Carboniferous age for the mafic-ultramafic complex and this age has later been supported by some radiometric dates (Drs. Y. Panjasawatwong and A.J. Crawford, pers. comm., 1993). The age of the low-grade metasedimentary unit has been widely inferred to be Silurian-Devonian by geologists from the Royal Thai Department of Mineral Resources (Piyasin, 1975; Bunopas,1981; Charoenpravat *et al.*, 1976). However, it has been thought to be Permo-Carboniferous on a stratigraphic basis (Hess and Koch, 1975). Barr and Macdonald (1987) reported the metamorphic age as Middle Permian for this metasedimentary unit.

The Jurassic continental redbeds spread across the boundary between the Sukhothai and the Loei fold belts. They are relatively less deformed compared to the older rock units in this region.

In the west, the elongate outcrops of Permo-Triassic volcanic and volcaniclastic rocks extend from north of Tak to Lampang. The area between these Permo-Triassic volcanics and the Permo-Carboniferous mafic-ultramafic belt is occupied by two major turbidite sequences of different ages. The turbidite sequence in the west belongs to the Triassic Lampang Group (Piyasin, 1972). The other sequence in the east is the Permian turbidites of the Phrae Group (Bunopas, 1981).

To the west of the Sukhothai fold belt, a continuous belt of middle to upper amphibolite facies gneissic rocks extends over 400 km along the western mountain range of Thailand (Fig. 10.1). This gneiss belt has been inferred to represent a Precambrian basement. Overlying this high-grade basement are Palaeozoic sedimentary sequences probably deposited in a shelf environments (Bunopas and Vella, 1983). The basement and the cover sequence have been extensively invaded by granitic plutons of mainly Triassic age.

## 1.4 Previous Work

### 1.4.1 The Sirikit Dam area

The area around the Sirikit Dam (originally the Pha Som Dam) and its surrounding was first mapped by Bunopas (1969). The geology of this area, as summarised later by Bunopas (1981), is largely characterised by lower-greenschist facies metasedimentary rocks which have been subjected to more than one period of deformation. Within the metasedimentary rocks, tectonic slices of mafic-ultramafic rocks including gabbro, peridotite, serpentinite and pillow lavas were reported. The stratigraphic schemes for the Sirikit Dam area proposed by Bunopas (1981) and the one adopted in this study are shown in Table 1.1.

The geology of the Sirikit Dam area was also summarised on the geological maps of Uttaradit (Piyasin, 1975) and Loei (Charoenpravat *et al.*, 1976). Mapping of the area around the Sirikit Dam was repeated by Lamjuan and Sinpoonanant (1987) and Chairangsee *et al.* (1989). However, their information remain largely the same as those published previously.

Macdonald and Barr (1984) gave a first detailed account on petrochemistry and tectonic setting of the mafic and ultramafic rocks of the Nan River area near the Sirikit Dam. Later, they reported the occurrence of epidote-crossite blueschists in the metasedimentary unit and a metamorphic age (269±12 Ma) of associated

Table 1.1 Stratigraphic schemes of rock units in the Sukhothai Fold Belt

| Age | SIRIKIT DAM AREA | | PHRAE-SIRIKIT RESERVOIR AREA | | | LAMPANG - DENCHAI AREA | | | |
|---|---|---|---|---|---|---|---|---|---|
| | Bunopas (1981) | This study | Piyasin (1972) | Bunopas (1981) | This study | Piyasin (1972) | Bunopas (1981) | Chaodumrong (1992) | This study |
| Jurassic | Lower Khorat Group | Phra Wihan Fm | | | | | | | |
| Triassic | NAM PAT GROUP<br>Huai Bo Khong Fm<br>Huai Lat Fm | NAM PAT GROUP<br>Huai Bo Khong Fm<br>Huai Lat Fm | LAMPANG GROUP<br>Pha Daeng Fm<br>Doi Chang Fm<br>Hong Hoi Fm<br>Pha Kan Fm<br>Phra That Fm | | Wang Chin Fm | LAMPANG GROUP<br>Pha Daeng Fm<br>Doi Chang Fm<br>Hong Hoi Fm<br>Pha Kan Fm<br>Phra That Fm | | LAMPANG GROUP<br>Wang Chin Fm<br>Kang Pla Fm<br>Pha Daeng Fm<br>Doi Long Fm<br>Hong Hoi Fm<br>Pha Kan Fm<br>Phra That Fm | LAMPANG GROUP<br>Wang Chin Fm (Tr7)<br>Kang Pla Fm (Tr6)<br>Pha Daeng Fm (Tr5)<br>Doi Long Fm (Tr4)<br>Hong Hoi Fm (Tr3)<br>Pha Kan Fm (Tr2)<br>Phra That Fm (Tr1) |
| Permo-Triassic | Pak Pat Volcanics | Pak Pat Volcanics | Volcanic Group | | | Volcanic Group | P-Tr Volcanics | | Doi Luang volcanics |
| Permian | | | RATBURI GROUP<br>Huai Thak Fm<br>Pha Huat Fm<br>Kiu Lom Fm | PHRAE GROUP<br>Rong Kwang Fm | Rong Kwang Fm | RATBURI GROUP<br>Huai Thak Fm<br>Pha Huat Fm<br>Kiu Lom Fm | NGAO GROUP<br>Huai Thak Fm<br>Pha Huat Fm<br>Kiu Lom Fm | | Huai Thak Fm |
| Permo-Carboniferous | Pha Som Group<br>Pha Som Ultramafics | PHA SOM META-MORPHIC COMPLEX<br>metasediments<br>ophiolite association | Mae Tha Fm<br>Don Chai Group | Mae Sai Fm<br>Pha Som Group | Pha Som Group | Mae Tha Fm<br>Don Chai Group | | | |

actinolite-quartz schists (Barr and Macdonald, 1987). The geochemistry and petrology of the mafic-ultramafic complex in the Nan River area was later studied in much more detail by Panjasawatwong (1991). In this latest study, the petrogenetic diversity of the mafic-ultramafic complex was revealed.

In April 1991, a number of undergraduate students from Chiang Mai University led by Dr. Y. Panjasawatwong mapped the areas adjacent to the present study area. Their work yields additional data that are useful for the present study (i.e. Charungrum *et al.*, 1991; Nutperean *et al.*, 1991; Promma *et al.*, 1991).

### 1.4.2 The Phrae-Sirikit Reservoir transect

The pre-existing geological data along the traverse from Phrae to the Sirikit Reservoir are rather limited compared to the other areas covered in the present study. Some useful data available from published and unpublished reports and maps include a broad account on the stratigraphy of the area (Piyasin, 1972; Bunopas, 1981) as summarised in Table 1.1. This area was mapped again by geologists from the Royal Thai Department of Mineral Resources (i.e. Charoenpravat *et al.*, 1987; Maranate *et al.*, 1987) and additional Permian and Triassic fossils were reported.

### 1.4.3 The Lampang-Denchai transect

The geology of the area between Lampang and Phrae is well documented (e.g. Piyasin, 1972; Bunopas, 1981; Chaodumrong, 1992). However, most workers have paid little attention to the structure and deformation in this area. The rock units in the area include Permian sedimentary strata, Permo-Triassic volcanics, Triassic sedimentary sequences, small intrusive bodies of Late Triassic granite and Pleistocene basalts (Piyasin, 1972). The stratigraphic schemes for the Lampang-Denchai area proposed by these authors are summarised in Table 1.1

The stratigraphy of the Triassic sequence have been subject of several studies since the pioneering work of Piyasin (1972). These include the work of Chonglakmani (1981, 1983), Wolfart (1987) and Chaodumrong (1992).

### 1.4.4 The Doi Inthanon area

The metamorphic complex in the Doi Inthanon area is part of a continuous belt of amphibolite facies gneissic rocks which extends over 400 km along the western mountain range of Thailand (Fig. 10.1). The deformation and

metamorphism of the complex have been studied by a few workers (e.g. Mongkolthip, 1986; Macdonald *et al.*, 1993). A common agreement among these workers is that the gneissic rocks have been metamorphosed under low pressure - high temperature conditions. Radiometric dating has been carried out on some of the granitic plutons within this metamorphic complex (e.g. Teggin, 1975; von Braun *et al.*, 1976; Macdonald *et al.*, 1993).

# 1.5 Methods of Study

## 1.5.1 Field methods

The fieldwork was designed to cover the areas expected to yield useful data on the structure and metamorphism across the Sukhothai fold belt. Two field seasons were arranged for this purpose. The first field season (3 months) was done during December, 1990 to February, 1991 and the second one (4 months) was carried out between November, 1991 and February, 1992.

The fieldwork along Highway 11 (the Lampang-Denchai Highway) and the Phrae-Sirikit Reservoir road focused on mesoscopic structures observed in the road-cuttings and nearby streams. More than 300 samples were collected at appropriate interval (i.e. every 200-250 m on the highway) for general petrographic, metamorphic and microstructural studies. The traverse was done on 1:25,000 scale map base. More detailed mapping (1:1000 scale) was carried out in a few localities to obtain details of mesoscopic structures.

The Sirikit Dam area was mapped on a scale 1: 25,000 with the aid of air-photo interpretation from 1: 15,000 aerial photographs. The area was traversed along the streams, the Sirikit reservoir bank and Highway 1045. Detailed 1:1,000 mapping was carried out on particular outcrops or road-sections where structures are well-exposed. The aim was to obtain sufficient data for detailed structural analysis. About 50 oriented samples for microstructural study were collected from the high-strain or thrust zones in particular. All together, more than 250 samples were collected from this area for general petrographic, metamorphic and microstructural studies..

Fieldwork carried out in the Doi Inthanon area is reconnaissance in nature with emphasis on metamorphic petrology. The structural information was based on previous studies (e.g. Macdonald *et al.*, 1993). Additional data were acquired by field observation of critical outcrops.

## 1.5.2 Analytical methods

Analytical work was carried out to determine mineral compositions, whole-rock chemical compositions, illite crystallinity and $b_O$ values. These data are needed to constrain the petrogenesis and tectonic settings of the key lithologies. The analytical techniques involved are discussed below.

### Mineral analysis

Constituent minerals of rocks were analysed using a CAMECA CAMEBAX SX50 electron microprobe at the Central Science Laboratory, University of Tasmania at Hobart. The electron beam current was set at 10, 15 or 20 nA at a fixed voltage of 15 kV depending on the alkali and water components in each mineral. Counting time for each element was set differently depending on the amount present in the mineral, i.e. 10 s for Si and Al, 10-20 s for Ti, Cr, Fe, Mn, Mg, Ca and Na, 20-60 s for K, 20 s for Ba, Sr, Zn, Cl and F. Data were stored and processed by on-line DEC minicomputer using a specific software routine for each type of mineral (e.g. MISCELLAN, FELDSPAR, MICA, AMPHIBOLE, CHLORITE, SPINEL and CARBONATE). Standard checks, using Delegate clinopyroxene as a mineral standard, were carried out before and after the analysis batch to ensure the consistency of the results. The precision of the analysis is estimated to be within 3% relative to the amount of the element present.

### Whole-rock analysis

Whole-rock analyses were carried out on volcanic and hypabyssal rocks, greywackes and metagreywackes to obtain their chemical compositions which could provide valuable information on their tectonic settings. The samples were carefully selected to avoid rocks containing (i) abundant amygdale minerals, (ii) extensive mesoscopic domains of secondary minerals such as albite, epidote or chlorite, and (iii) quartz, epidote or calcite veins or patches totalling >5 modal%; as these may lead to misleading interpretation of the tectonic setting. Fifty samples were analysed for major elements (Si, Ti, Al, Fe, Mn, Mg,Ca, Na, K, P and ignition loss) and trace elements (Nb, Zr, Y, Ba, Sr, Rb, Pb, Th, Ni, Cr, V, Sc, La, Ce and Nd). From these samples, four basalts were selected and analysed for rare-earth elements (La, Ce, Nd, Sm, Eu, Tb, Ho, Yb and Lu) by instrumental neutron activation analysis (INAA).

The selected samples were prepared for the analysis by splitting hand specimens into fragments of about 10-20 mm in the longest dimension. Chips with weathered surfaces were discarded. The fragments were then crushed with a steel jaw crusher and cleaned with an airhose. Approximately 30-50 g aliquots of the crushed fragments showing no sign of weathered surfaces, veins and amygdales minerals were ground for 2-3 minutes using a tungsten-carbide Tema disc mill.

The analyses were carried out by an automated Philips PW 1480 X-ray fluorescence (XRF) spectrometer at the Department of Geology, University of Tasmania at Hobart, using the technique of Norrish and Chappell (1967) and Norrish and Hutton (1969). Major elements were determined from fusion discs prepared with 3.75 g Norrish flux (lithium borate and lanthanum oxide mix), 0.05 g lithium nitrate and 0.7 g sample powder. Trace elements were determined on pressed powder pellets backed by boric acid. Mass absorption coefficients calculated from major element concentration were used for the determinations of trace elements. Ignition loss was determined gravimetrically by heating about 1 g of sample at 1000 °C for 12 hours.

REE analyses for four basaltic samples were done by instrumental neutron activation analysis at Becquerel Laboratories, Lucas Heights, New South Wales. The detection limits for the analysed elements are: 2 ppm for Nd; 1 ppm for Ce; 0.5 ppm for Tb and Ho; 0.1 ppm for La, Eu and Yb; and 0.05 ppm for Sm and Lu.

## Determination of illite crystallinity and $b_0$ values

The illite crystallinity measurements of white micas in shale, slate and phyllite were made on the < 2 μm fraction using the technique of Offler *et al.* (1987). The < 2 μm fraction was obtain from approximately 20 g of sample crushed in a Tema disc mill for 20 seconds and dispersed in the sedimentation cylinders. After appropriate settling period, the < 2 μm fraction was drained off and sedimented with the controlled thickness of 1-2 mg/cm$^2$ onto a glass slide. Scans were carried out over the range 7.5 - 10° 2θ at 0.5° 2θ/min with a chart speed of 40 mm/min and a time constant of 2. Divergence and scatter slits of 1° and receiving slit of 0.2 mm were used. Peak width at half-height was calculated in terms of Δ° 2θ (Kisch, 1980a) and samples with illite crystallinity values greater than 0.21 Δ° 2θ were glycolated and heated at 550 °C to determine the presence of other components interlayered with illites.

The $b_0$ measurements were made on polished slabs of slate and phyllite cut normal to the cleavage. The range 58-63° 2θ was scanned at 0.25° 2θ and $b_0$ determined from (060) peak using the (211) quartz reflection as an internal

standard. Mean $b_0$ was calculated from six determinations for each specimen. The following settings were used: divergence and scatter slits of 2° and receiving slit of 0.1 mm, a goniometer speed of 20 mm/min and a time constant of 2.

All illite crystallinity and $b_0$ analyses were carried out on an automated Philips PW-1729 X-ray diffractometer at the Tasmania Department of Mines. The machine was set up with 40 kV and 30 mA using Cu-$K_\alpha$ radiation and graphite monochromator.

# 1.6 Classification and Terminology

## 1.6.1 Classification of rocks

For sedimentary rocks, sandstones are classified according to McBride (1963) and Pettijohn *et al.* (1972). The classification of limestones based on depositional texture of Dunham (1962) is adopted in this study. In the petrographic description of limestones; the following terms taken from Tucker (1981) for fine aggregates of equant-polyhedral calcite grains are used: micrite (less than 4 μm), microspar (4-10 μm) and pseudospar (10-50 μm).

Naming the metamorphic rocks follows Winkler (1976). In this scheme, the exact designation of the rock is done by placing the name of subordinate constituents in front of the rock name, starting with the least abundant. Textural and microstructural descriptions follow Spry (1969).

The plutonic rocks are classified following the modal classification scheme recommended by the IUGS Subcommission, i.e. Streckeisen (1976).

## 1.6.2 Classifications and terminology of structures

Fold classification and terminology outlined by Turner and Wise (1963), Fleuty (1964), Whitten (1966), Ramsay (1967) and Suppe (1985) are adopted in this study. The morphological classification of rock cleavage follows Powell (1979) and Borradaile *et al.* (1982).

Fault terminology used herein is discussed in Hobbs *et al.* (1976). For fault-related rocks, the terminology suggested by Wise *et al.* (1982) is used.

# Chapter 2

# AN EMPIRICALLY CALIBRATED PHENGITE-CHLORITE GEOTHERMOMETER

## 2.1 Introduction

The geothermometry for pelitic rocks in the low temperature range encompassing sub-greenschist, lower greenschist and blueschist facies (i.e. 180 - 450 °C) relies heavily on illite crystallinity which is essentially a semi-quantitative approach (e.g. Weaver, 1960; Kubler, 1967; Kisch, 1980a, 1980b, 1987,1990; Blenkinsop, 1988; Robinson *et al.*, 1990). The high-variance nature of the mineral assemblages limits the use of phase equilibrium calculations for pelitic rocks at these conditions. No substantial changes in equilibrium assemblages occur over the wide range of *P-T* conditions in contrast to high-temperature pelitic assemblages.

Thermodynamic calculations (e.g. Powell and Holland, 1988) have been applied with very limited success to pelitic rocks in this low temperature range. Problems include the lack of well-constrained phase equilibria and appropriate activity-composition relations.

Simple calibrations from equilibrium mineral pairs are probably the better options in quantitative thermometry of the low temperature pelitic rocks. For pelitic metasedimentary rocks which contain plagioclase and white mica, Green and Usdansky (1986) have developed a geothermometer based on a K-Na exchange reaction between plagioclase and muscovite. This geothermometer was tested against garnet-biotite thermometry (e.g. Ferry and Spear, 1978; Hodges and Spear, 1982) and was found to give comparable results to the latter. However, the plagioclase-muscovite thermometer has only been tested in rocks which have equilibration temperatures greater than 420 °C. Therefore, it is useful to investigate the possibility of applying this geothermometer to low-temperature pelitic rocks (see detailed discussion in Chapter 5).

Likewise, the exchange reactions, e.g. Fe-Mg or Mg-Tschermak exchange between phengite and chlorite which are abundant phases in very-low and low grade pelitic rocks, could also be calibrated for geothermometric purposes. Essene

(1989) recommended that chlorite-phengite $K_D$ thermometry could ultimately prove useful in blueschists which, at present, are constrained by petrogenetic grids to 250 - 450 °C range. Unfortunately, a large number of studies have shown that an Fe-Mg exchange between phengite and chlorite, though having a reasonable partitioning trend (e.g. Ernst *et al.*, 1970; Black, 1975; Coombs *et al.*, 1976; Rao, 1977), is not appropriate to be calibrated as a geothermometer due to high variation in $K_D$ values. This high variation is probably due to complicated coupled substitutions between phengite and chlorite (e.g. Miyashiro and Shido, 1985; Wang and Banno, 1987) as well as problems in estimating $Fe^{3+}$ in phengite.

However, it has been noted that white micas become enriched in muscovite component and depleted in celadonite component with increasing temperature in the chlorite, biotite and lower garnet zone (Miyashiro and Shido, 1985). This has been attributed mainly to Tschermak substitution, particularly a Mg-Tschermak exchange, which may have strong potential in geothermometry. A Mg-Tschermak exchange reaction is much less sensitive to errors in $Fe^{3+}$ estimation than the Fe-Mg exchange thermometer. However, this type of substitution involves complex multi-site mixing of atoms of different sizes and charges where ordering and dis-ordering are not well understood. At the present state of our knowledge, it is not possible to evaluate the effect of ignoring ordering in the calibration.

Kotov (1975) has formulated muscovite-chlorite as a geothermometer based on Mg-Fe Tschermak substitution. Application of Kotov's geothermometer to the data set used in this study yields unsatisfactory results. This is probably due to (i) insufficient and/or poor quality data used in his calibration, and (ii) failure to include $Al^{iv}$ and Si (in tetrahedral sites of muscovite and chlorite) in the formulation. However, his attempt has greatly contributed to the fundamental concept of the present study.

Jahren and Aagaard (1992) and Aagaard and Jahren (1992) have studied compositional variations of diagenetic illites and chlorites from the oil fields in the North Sea area, offshore Norway. They use the ideal-mixing-on-sites model to calculate the end-member activities and predict that the stability of muscovite and clinochlore components increases with increasing temperature while increasing pressure stabilises celadonite and amesite. The present study adopts their approach but also takes into account non-ideal behaviour of the illite and chlorite solid-solutions.

A thermodynamic formulation and empirical calibration are used in this study to investigate the possibility of using a Mg-Tschermak exchange reaction between phengite and chlorite as a practical geothermometer for sub-greenschist, greenschist and blueschist facies pelitic or semi-pelitic rocks.

The approach adopted herein is similar to, but somewhat different in detail from that of Hoisch (1989) who developed the muscovite-biotite geothermometer based also on the Mg-Tschermak exchange reaction.

## 2.2 Thermodynamic Formulation

The Mg-Tschermak exchange between phengite and chlorite may be represented by the end-member reaction:

$$\underset{\text{celadonite}}{KMgAlSi_4O_{10}(OH)_2} + \underset{\text{amesite}}{Mg_4Al_2Al_2Si_2O_{10}(OH)_8}$$
$$= \underset{\text{muscovite}}{KAl_2AlSi_3O_{10}(OH)_2} + \underset{\text{clinochlore}}{Mg_5AlAlSi_3O_{10}(OH)_8} \qquad (2.1)$$

The equilibrium constant can be written:

$$K = a_{ms}^{Ms}.a_{clin}^{Chl} / a_{cel}^{Ms}.a_{ames}^{Chl} \qquad (2.2)$$

where $a_i^A = \gamma_i^A .X_i^A$ and $K = K\gamma.K_X$

and K = equilibrium constant, $a_i^A$ = activity of component $i$ in phase A, $\gamma_i^A$ = activity coefficient of component $i$ in phase A, $X_i^A$ = mole fraction of component $i$ in phase A, $K\gamma$ = equilibrium constant for activity coefficient terms, and $K_X$ = equilibrium constant for mole fraction terms.

$$K\gamma = \gamma_{ms}^{Ms}.\gamma_{clin}^{Chl} / \gamma_{cel}^{Ms}.\gamma_{ames}^{Chl} \qquad (2.3)$$

$$K_X = X_{ms}^{Ms}.X_{clin}^{Chl} / X_{cel}^{Ms}.X_{ames}^{Chl} \qquad (2.4)$$

In complex solid solutions such as muscovite and chlorite, there are a number of possible formulations for the mole fractions. Unfortunately, the constraints on ordering are poorly known at this stage and I therefore have taken a very simple model as most appropriate for this empirical approach. This has the advantage of being very little affected by errors in $Fe^{3+}$, here treated as $Fe^{3+} = 0$ for this process. The simplified ideal-mixing-on-sites models (e.g. Powell, 1978; Aagaard and Jahren, 1992), assuming two identical octahedral sites and four identical tetrahedral sites in phengite and six identical octahedral sites and four identical tetrahedral sites in chlorite, were chosen to calculate the mole fraction of

the end-members in the solid-solutions of phengite (Ms) and chlorite (Chl) as follows:

$$X^{Ms}_{ms} = 9.4815(X_{K,A})(X_{Al,O})^2[X_{Al,T}][X_{Si,T}]^3 \quad (2.5.1)$$

$$X^{Ms}_{cel} = 4(X_{K,A})(X_{Mg,O})(X_{Al,O})[X_{Si,T}]^4 \quad (2.5.2)$$

$$X^{Chl}_{clin} = 141.5578(X_{Mg,O})^5(X_{Al,O})[X_{Al,T}][X_{Si,T}]^3 \quad (2.5.3)$$

$$X^{Chl}_{ames} = 729(X_{Mg,O})^4(X_{Al,O})^2[X_{Al,T}]^2[X_{Si,T}]^2 \quad (2.5.4)$$

where subscripts A, O and T denote A-, octahedral-, and tetrahedral-sites respectively, and therefore,

$$K_X = \frac{0.4604[(X_{Al,O}).(X_{Al,T})/(X_{Mg,O}).(X_{Si,T})]^{Ms}}{[(X_{Al,O}).(X_{Al,T})/(X_{Mg,O}).(X_{Si,T})]^{Chl}} \quad (2.6)$$

for phengite:

$X_{Al,O} = X^{Ms}_{Al} = Al^{vi}/2$; $X_{Mg,O} = X^{Ms}_{Mg} = Mg/2$; $X_{Fe,O} = X^{Ms}_{Fe} = Fe/2$;

and $X_{Al,T} = Al^{iv}/4$; $X_{Si,T} = Si/4$

and for chlorite:

$X_{Al,O} = X^{Chl}_{Al} = Al^{vi}/6$; $X_{Mg,O} = X^{Chl}_{Mg} = Mg/6$; $X_{Fe,O} = X^{Chl}_{Fe} = Fe/6$;

and $X_{Al,T} = Al^{iv}/4$; $X_{Si,T} = Si/4$

it follows:

$$K_X = 0.4604\ [Al^{vi}.Al^{iv}/Mg.Si]^{Ms}/[Al^{vi}.Al^{iv}/Mg.Si]^{Chl} \quad (2.7)$$

For reaction (2.1), the equilibrium thermodynamic expression was approximated using a simple form of the Gibbs free energy equation (i.e. the heat capacity difference ($\Delta Cp$) was assumed to be zero for an exchange reaction) :

$$\Delta\mu = 0 = \Delta G + RT\ \ln K = \Delta H - T\Delta S + P\Delta V + RT\ \ln K_X + RT\ \ln K\gamma \quad (2.8)$$

where $\Delta\mu$ = change in chemical potential of a reaction, $\Delta G$ = Gibbs free energy change of a reaction (joule), $\Delta H$ = enthalpy change of a reaction (joule), $\Delta S$ = entropy change change of a reaction (joule/°K), $\Delta V$ = volume change of a reaction (joule/bar), $R$ = universal gas constant (8.3143 joule/mole/°K), $T$ = temperature (°K), $P$ = pressure (bar).

A solid-solution between muscovite and celadonite end-members in phengite is non-ideal (Miyashiro and Shido, 1985). For simplicity, the solid-solution was expressed in terms of octahedral mixing assuming ideal mixing on A- and T-sites. Additionally, other substitutions such as $Fe^{3+}$, pyrophyllite and trioctahedral mica were ignored. The non-ideality was modelled using a symmetric regular solution model (Wohl, 1946) for mixing of Mg, Fe and Al in octahedral sites, to express activity-composition relations of phengite,

$$RT \ln \gamma_{Al}^{Ms} = W_{MgAl}^{Ms}[(X_{Mg}^{Ms})^2 + X_{Mg}^{Ms}X_{Fe}^{Ms}] + W_{FeAl}^{Ms}[(X_{Fe}^{Ms})^2 + X_{Mg}^{Ms}X_{Fe}^{Ms}] - W_{MgFe}^{Ms}(X_{Mg}^{Ms}X_{Fe}^{Ms}) + C(2X_{Al}^{Ms}-1)(X_{Mg}^{Ms}X_{Fe}^{Ms}) \quad (2.9.1)$$

$$RT \ln \gamma_{Mg}^{Ms} = W_{MgAl}^{Ms}[(X_{Al}^{Ms})^2 + X_{Al}^{Ms}X_{Fe}^{Ms}] + W_{MgFe}^{Ms}[(X_{Fe}^{Ms})^2 + X_{Al}^{Ms}X_{Fe}^{Ms}] - W_{FeAl}^{Ms}(X_{Al}^{Ms}X_{Fe}^{Ms}) + C(2X_{Mg}^{Ms}-1)(X_{Al}^{Ms}X_{Fe}^{Ms}) \quad (2.9.2)$$

where $W_{MgAl}^{Ms}$, $W_{FeAl}^{Ms}$, $W_{MgFe}^{Ms}$ are the binary Margules parameters of mixing between Mg-Al, Fe-Al, Mg-Fe in octahedral sites of phengite and C is a ternary term. For mixing on two sites:

$$RT \ln \gamma_{ms}^{Ms} = 2RT \ln \gamma_{Al}^{Ms} \quad (2.10.1)$$

$$RT \ln \gamma_{cel}^{Ms} = RT \ln \gamma_{Mg}^{Ms} + RT \ln \gamma_{Al}^{Ms} - 1/2\, W_{MgAl}^{Ms} \quad (2.10.2)$$

and hence,

$$RT \ln [\gamma_{ms}^{Ms} / \gamma_{cel}^{Ms}] = RT \ln \gamma_{Al}^{Ms} + RT \ln \gamma_{Mg}^{Ms} - 1/2\, W_{MgAl}^{Ms} \quad (2.11)$$

Substituting equation (2.11) by equations (2.9.1) and (2.9.2) yields:

$$RT \ln [\gamma_{ms}^{Ms} / \gamma_{cel}^{Ms}] = W_{MgAl}^{Ms}[(X_{Mg}^{Ms})^2 - (X_{Al}^{Ms})^2 + X_{Mg}^{Ms}X_{Fe}^{Ms} - X_{Al}^{Ms}X_{Fe}^{Ms}] + W_{FeAl}^{Ms}[(X_{Fe}^{Ms})^2 + X_{Mg}^{Ms}X_{Fe}^{Ms} + X_{Al}^{Ms}X_{Fe}^{Ms}] - W_{MgFe}^{Ms}[X_{Mg}^{Ms}X_{Fe}^{Ms} + (X_{Fe}^{Ms})^2 + X_{Al}^{Ms}X_{Fe}^{Ms}] + C[X_{Al}^{Ms}X_{Fe}^{Ms} - X_{Mg}^{Ms}X_{Fe}^{Ms}] + 1/2\ W_{MgAl}^{Ms} \quad (2.12)$$

Assuming that Mg-Fe binary solution is near ideal behaviour and ignoring the ternary term, that is $W_{MgFe}^{Ms} = C = 0$, equation (2.12) simplifies to

$$RT \ln [\gamma^{Ms}_{ms} / \gamma^{Ms}_{cel}] = W^{Ms}_{MgAl}[(X^{Ms}_{Mg})^2 - (X^{Ms}_{Al})^2 + X^{Ms}_{Mg}X^{Ms}_{Fe} - X^{Ms}_{Al}X^{Ms}_{Fe}] + W^{Ms}_{FeAl}[(X^{Ms}_{Fe})^2 + X^{Ms}_{Mg}X^{Ms}_{Fe} + X^{Ms}_{Al}X^{Ms}_{Fe}] + 1/2\ W^{Ms}_{MgAl} \quad (2.13)$$

This is still too complex for the level of data available so I have simplified by assuming $W^{Ms}_{MgAl} \sim W^{Ms}_{FeAl}$ which gives a formulation

$$RT \ln [\gamma^{Ms}_{ms} / \gamma^{Ms}_{cel}] = W^{Ms}_{MgAl}[(X^{Ms}_{Mg})^2 + (X^{Ms}_{Fe})^2 - (X^{Ms}_{Al})^2 + 2X^{Ms}_{Mg}X^{Ms}_{Fe} + 1/2] \quad (2.14)$$

Since $X^{Ms}_{Fe}$ is always less than 0.1, its square, $(X^{Ms}_{Fe})^2$ , and the product, $X^{Ms}_{Mg}.X^{Ms}_{Fe}$, can be neglected; and equation (2.14) is approximated by :

$$RT \ln [\gamma^{Ms}_{ms} / \gamma^{Ms}_{cel}] = W^{Ms}_{MgAl}[(X^{Ms}_{Mg})^2 - (X^{Ms}_{Al})^2 + 1/2] \quad (2.15)$$

The solid-solution between clinochlore and amesite in chlorite can be treated in the same manner and thus,

$$RT \ln [\gamma^{Chl}_{clin} / \gamma^{Chl}_{ames}] = W^{Chl}_{MgAl}[(X^{Chl}_{Al})^2 - (X^{Chl}_{Mg})^2 - (X^{Chl}_{Fe})^2 - 2(X^{Chl}_{Mg}X^{Chl}_{Fe}) - 1/2] \quad (2.16)$$

where $W^{Chl}_{MgAl}$ is the Margules parameter of mixing between Mg and Al in octahedral sites of chlorite (assumed to be equal to $W^{Chl}_{FeAl}$).

By substituting equations (2.15) and (2.16) in equation (2.8), then the thermodynamic expression is :

$$\Delta\mu = 0 = \Delta H - T\Delta S + P\Delta V + RT \ln K_X + W^{Ms}_{Mg\text{-}Al}[(X^{Ms}_{Mg})^2 - (X^{Ms}_{Al})^2 + 1/2] + W^{Chl}_{MgAl}[(X^{Chl}_{Al})^2 - (X^{Chl}_{Mg})^2 - (X^{Chl}_{Fe})^2 - 2(X^{Chl}_{Mg}X^{Chl}_{Fe}) - 1/2] \quad (2.17)$$

To perform the regression, equation (2.17) may be recast in the form:

$$T = \Delta H^*/\Delta S + P\Delta V/\Delta S + RT \ln K_X/\Delta S + W^{Ms}_{MgAl}/\Delta S[(X^{Ms}_{Mg})^2 - (X^{Ms}_{Al})^2] + W^{Chl}_{MgAl}/\Delta S[(X^{Chl}_{Al})^2 - (X^{Chl}_{Mg})^2(X^{Chl}_{Fe})^2 - 2(X^{Chl}_{Mg}X^{Chl}_{Fe})] \quad (2.18)$$

where $\Delta H^* = \Delta H + 1/2\ W^{Ms}_{Mg\text{-}Al} - 1/2\ W^{Chl}_{MgAl}$

## 2.3 Calibration Data Set

Temperature, pressure and mineral compositional data used in the calibration were taken from rocks apparently containing equilibrium assemblages including phengite and chlorite pairs. The data were selected in such a manner as to encompass the possible pressure and temperature ranges of sub-greenschist, lower greenschist and blueschist facies metamorphism. The pressure range of 182 - 15,000 bars and the temperature range of 162 - 450 °C of the data set (Table 2.1) adequately fulfil this purpose.

After an extensive search through literatures, more than one-hundred mineral pairs were compiled from published and unpublished data. From this original data set, twenty-one samples were selected as representing the best analyses. After regression, the number of selected samples was reduced to fourteen. The criteria that were applied for the acceptance or rejection of data for calibration of the phengite-chlorite geothermometer are :

(i) The samples whose temperature and pressure estimates are doubtful were rejected. This was done to ensure accuracy of the final result. Those with well-established independent *P-T* estimates have to fulfil other criteria as well.

(ii) The samples with low Mg and Si contents of phengites (Mg <0.09 and Si <3.15 per 11 oxygens in formula unit) were not considered. The reason for excluding low Mg and Si phengites is because analytical errors become paramount especially when considering alternative site occupancy.

(iii) The samples, which were diagnosed as prominent outliers during regression, were also eliminated. For this purpose prominent was taken as more than $2\sigma$ from the regression line.

Low temperature data of diagenetic chlorites and illites in clastic reservoir sandstones from the North Sea, offshore Norway, were taken from Jahren and Aagaard (1992). The three samples (samples XIV, XV and XVI) included in the data set represent the lower-end of the temperature spectrum of very low-grade metamorphism. Also included are three samples (samples 439, 622 and 675) of McDowell and Elders (1980) from the Salton Sea geothermal field, California. The temperature and depth of these samples were measured in drill holes. To convert depth to pressure the density of rocks was taken as 2.7 g/cc.

Samples 29173, 29199 and 38443 are quartzofeldspathic schists from western Otago, New Zealand (Kawachi *et al.*, 1983). The metamorphic temperatures of these schists were estimated at 390±30 °C. The sphalerite

Table 2.1 Data for phengite-chlorite assemblages used for calibration of phengite-chlorite geothermometer.

| Sample no. | References | Phengite | | | | Chlorite | | | | X MgAl | Kx | P | T est | T MsChl | T diff | σT |
|---|---|---|---|---|---|---|---|---|---|---|---|---|---|---|---|---|
| | | Mg | Fe | Alvi | Si | Mg | Fe | Alvi | Si | | | (bar) | (°C) | (°C) | (°C) | (°C) |
| XIV | J&A92 | 0.150 | 0.220 | 1.650 | 3.370 | 0.800 | 3.160 | 1.780 | 2.720 | -0.6750 | 0.9042 | 1194 | 162 | 185 | 23 | 14 |
| XV | " | 0.110 | 0.280 | 1.650 | 3.340 | 0.460 | 3.540 | 1.760 | 2.720 | -0.6776 | 0.7579 | 1299 | 175 | 176 | 1 | 14 |
| XVI | " | 0.090 | 0.080 | 1.860 | 3.240 | 0.390 | 4.130 | 1.460 | 2.680 | -0.8629 | 1.2105 | 1316 | 180 | 178 | -2 | 15 |
| 432m | M&E80 | 0.306 | 0.275 | 1.507 | 3.600 | 1.669 | 2.831 | 1.304 | 2.990 | -0.5444 | 0.9546 | 118 | 190 | 192 | 2 | 14 |
| 622m | " | 0.339 | 0.185 | 1.613 | 3.335 | 2.616 | 2.097 | 1.203 | 2.886 | -0.6217 | 2.4608 | 168 | 251 | 243 | -8 | 18 |
| 675m | " | 0.203 | 0.132 | 1.733 | 3.359 | 2.143 | 2.026 | 1.569 | 2.936 | -0.7405 | 2.8268 | 182 | 264 | 235 | -29 | 18 |
| 29173 | K&Co83 | 0.290 | 0.190 | 1.520 | 3.310 | 4.320 | 0.350 | 1.220 | 2.710 | -0.5566 | 3.7420 | 6400 | 390 | 385 | -5 | 23 |
| 29199 | " | 0.300 | 0.200 | 1.520 | 3.270 | 4.630 | 0.060 | 1.200 | 2.750 | -0.5551 | 4.4203 | 6400 | 390 | 402 | 12 | 24 |
| 38443 | " | 0.300 | 0.200 | 1.510 | 3.210 | 4.370 | 0.060 | 1.340 | 2.720 | -0.5475 | 3.9523 | 6400 | 390 | 392 | 2 | 23 |
| GP-18 | Chopin81 | 0.430 | 0.050 | 1.550 | 3.420 | 3.740 | 0.870 | 1.310 | 2.820 | -0.5544 | 1.9203 | 15000 | 450 | 451 | 1 | 23 |
| 7-172 | " | 0.390 | 0.080 | 1.530 | 3.450 | 3.300 | 1.460 | 1.220 | 2.810 | -0.5472 | 1.8392 | 15000 | 450 | 447 | -3 | 22 |
| 7-230 | " | 0.430 | 0.260 | 1.340 | 3.510 | 3.320 | 1.440 | 1.200 | 2.830 | -0.4027 | 1.3403 | 15000 | 450 | 438 | -12 | 21 |
| 6-255 | " | 0.580 | 0.160 | 1.250 | 3.570 | 4.550 | 0.000 | 1.170 | 2.980 | -0.3065 | 1.3579 | 15000 | 450 | 453 | 3 | 21 |
| 3119 | S&M85 | 0.137 | 0.143 | 1.721 | 3.223 | 2.425 | 2.203 | 1.258 | 2.848 | -0.7353 | 6.6481 | 8000 | 431 | 444 | 13 | 27 |

Notes: X MgAl = (X Mg,Ms)^2 - (X Al,Ms)^2

P = estimated pressure, T est = estimated temperature, T MsChl = phengite-chlorite temperature, T diff = temperature difference between T MsChl and T est, σ T = uncertainty in T MsChl.

J&A92 = Jahren and Aagaard (1992), M&E80 = McDowell and Elders (1980), K&Co83 = Kawachi et al. (1983), Chopin81 = Chopin (1981) and S&M85 = Storey and Menecilly (1985)

geobarometry for sulphide mineralisation in similar schists in the nearby area suggested a pressure of 6.4±0.4 kbar for these schists.

The sample 3118.6 from the Scotia metamorphic complex, South America (Storey and Meneilly, 1985) provides the data point for medium pressure and moderate temperature range, i.e. a pressure of 8±1 kbar and a temperature of 431± 37 °C.

High-temperature and high-pressure data were taken from four high-grade pelitic blueschists (samples GP-18, 7-172, 7-230 and 6-255) from western Alps, Italy (Chopin, 1981) that contain talc-phengite plus chlorite. These rocks were quoted as being metamorphosed at a temperature of 450±50 °C and a pressure of greater than 7 kbar. Later Massonne and Chopin (1989) based on the experimental study of Massonne and Schreyer (1987) estimated the pressure at 15±1 kbar.

These data, though carefully selected, still have considerable uncertainties. However, they are the best available from the literature for calibrating the Mg-Tschermak exchange reaction between coexisting phengite and chlorite. Direct experimental calibration of reactions involving these complex phases at low temperature is extremely difficult to achieve and may never be possible.

## 2.4 Empirical Calibration

The calibration of the phengite-chlorite geothermometer involves fitting equation (2.18) to the data tabulated in Table 2.1.

A FORTRAN program modified from the multiple correlation program RMULT of Davis (1973) was used to find the unknowns in equation (2.18). This program provides the coefficient of multiple correlation and goodness of fit and also performs the F-test. The same results (to the fourth decimal points) were also obtained using the FORTRAN subroutines of Press *et al.* (1986) based on least square minimisation methods with singular value decomposition (SVD). The subroutines perform the $\chi^2$ test and provide uncertainties for the regressed variables.

To select the best regression equation, the regressed variables were re-examined to see which one of them can be discarded without significantly affecting the multiple regression. The standardised partial regression coefficients indicated that the $W^{Chl}_{MgAl}$ variable did not make a significant contribution to the regression; thus it was eliminated. Elimination of this variable caused a considerable improvement of the quality of fit. The results of the best possible regression are:

$\Delta H^*/\Delta S = 539.5242 \pm 3.8142$ °K
$\Delta V/\Delta S = 0.01334 \pm 0.00013$ °K/bar
$1/\Delta S = 0.01507 \pm 0.00016$ °K/joule
$W^{Ms}_{MgAl}/\Delta S = 135.4304 \pm 5.4863$ °K

with $2\sigma$ uncertainties indicated and a correlation matrix,

| | $\Delta H^*/\Delta S$ | $\Delta V/\Delta S$ | $1/\Delta S$ | $W^{Ms}_{MgAl}/\Delta S$ |
|---|---|---|---|---|
| $\Delta H^*/\Delta S$ | 1 | 0.8925 | 0.5946 | 0.6092 |
| $\Delta V/\Delta S$ | | 1 | 0.1986 | 0.6744 |
| $1/\Delta S$ | | | 1 | -0.0394 |
| $W^{Ms}_{MgAl}/\Delta S$ | | | | 1 |

The quality of fit is indicated by a multiple correlation coefficient of 0.991. A geothermometric expression in which temperatures are solved with respect to the given pressure and compositional data can be formulated from the regressed variables by rearranging equation (2.18):

$$T = \frac{539.5242 + 0.01334P + 135.4304\,[(X^{Ms}_{Mg})^2 - (X^{Ms}_{Al})^2]}{1 - 0.01507\,R\,\ln K_X} \qquad (2.19)$$

Equation (2.19) will be useful as a geothermometer if temperatures calculated are not too sensitive to uncertainties in the assumed pressures. The sensitivity of the calculated temperature to the pressure may be assessed by differentiating equation (2.19) with respect to pressure, $P$ :

$$dT/dP \approx 0.01334 / (1-0.01507\,R\,\ln K_X) \qquad (2.20)$$

For the end-member reaction ($\ln K_X = 0$), $dT/dP = 0.01334$ °K/bar, indicating that 1 kbar uncertainty in assumed pressure causes a 13 °K uncertainty in temperature.

Temperatures calculated using the regressed variables are compared to the temperature data used in the calibration. For all fourteen rocks, the difference is less than 30 °K. For nine rocks, the difference is less than 8 °K. The multiple correlation coefficient of 0.991 is reflected in the small scatter data about a line of hypothetical perfect correlation (Fig. 2.1).

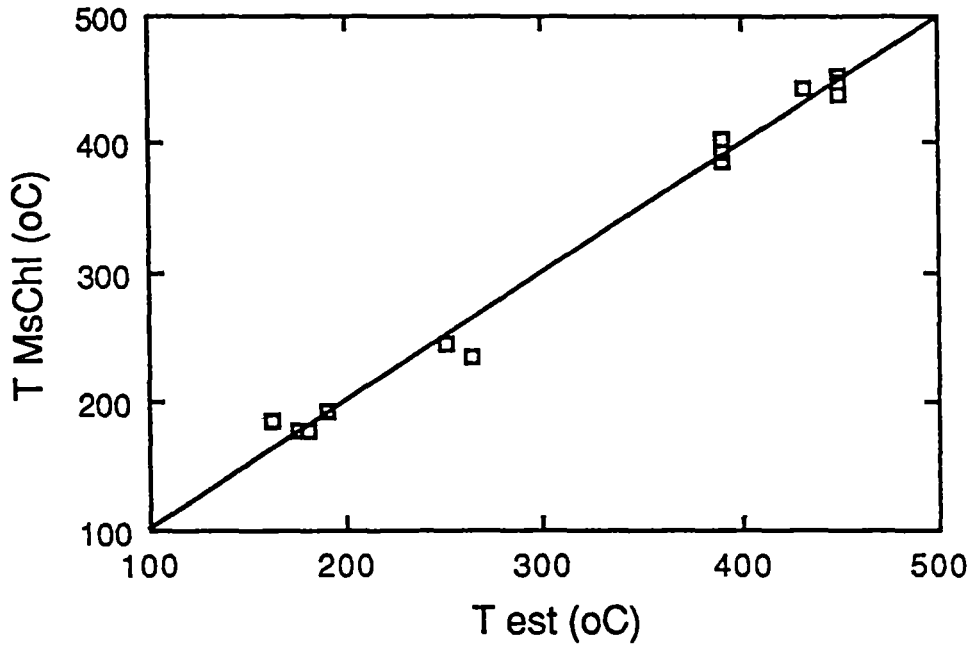


Figure 2.1 Plot of phengite-chlorite temperatures versus estimated temperatures used in the calibration. A straight line represents hypothetical perfect correlation.

## 2.5 Uncertainties

There are various possibilities which may cause the phengite-chlorite geothermometer to give unrealistic results regardless of the goodness of fit of the calibration data by equation (2.19). The errors may be systematic or non-systematic. The systematic errors may be inherited from the the assumptions made in the calibration which include the simplified ideal-mixing-on-sites models, the omission of ternary terms in the regular solution model and also the selection of the calibration data. The errors of this nature may lead to substantial uncertainties for the calculated values of temperature. The accuracy of the calculation can only be evaluated by comparing the results with the known values obtained from independent geothermometry or from phase equilibrium consideration by reference to a petrogenetic grid. Non-systematic errors involve uncertainties introduced by disequilibrium among the phases and/or uncertainties associated with analytical data. Equilibrium may be recognisable by petrographic study and intra- or inter-

sample consistency of phase compositions. Uncertainties associated with analytical data, especially electron microprobe data may be quantified together with uncertainties inherited from the regression. Crude error propagation calculation (Powell, 1978) was considered to be sufficient in dealing with the problem of this type where elaborate techniques may not be justified. The error propagation equation is:

$$\sigma_y = \{\sum (\partial y/\partial x_i)^2 x_{j(j\neq i)} \sigma^2_{xi}\}^{1/2} \qquad (2.21)$$

where $y = f(x_1,x_2,...)$ and $\sigma_y$ is the uncertainty on y caused by the uncertainties on $x_i$. Assuming that the uncertainties on the $x_i$ are not correlated, then equation (2.8) which may be recast in the form:

$$T = \frac{\Delta H + P\,\Delta V + RT\,\ln K\gamma}{\Delta S - R\,\ln K_X} \qquad (2.22)$$

in which $RT\,\ln K\gamma = W^{Ms}_{MgAl}[(X^{Ms}_{Mg})^2 - (X^{Ms}_{Al})^2]$ and by substituting $\Delta H$ by $\Delta H^*$ then,

$$T = \frac{\Delta H^* + P\,\Delta V + W^{Ms}_{MgAl}[(X^{Ms}_{Mg})^2 - (X^{Ms}_{Al})^2]}{\Delta S - R\,\ln K_X} \qquad (2.23)$$

For convenience, $W = W^{Ms}_{MgAl}$ and $X = (X^{Ms}_{Mg})^2 - (X^{Ms}_{Al})^2$ then consider:

$T = f(\Delta H^*, \Delta V, \Delta S, K_X, W, X)$

and

$\partial T/\partial \Delta H^* = 1/(\Delta S - R\,\ln K_X)$

$\partial T/\partial \Delta V = P/(\Delta S - R\,\ln K_X)$

$\partial T/\partial \Delta S = -(\Delta H^* + P\,\Delta V + WX)/(\Delta S - R\,\ln K_X)^2$

$\partial T/\partial K_X = R\,(\Delta H^* + P\,\Delta V + WX)/K_X(\Delta S - R\,\ln K_X)^2$

$\partial T/\partial W = X/(\Delta S - R\,\ln K_X)$

$\partial T/\partial X = W/(\Delta S - R\,\ln K_X)$

Therefore:

$$\sigma_T = \{(\partial T/\partial \Delta H^*)^2 \sigma^2_{\Delta H} + (\partial T/\partial \Delta V)^2 \sigma^2_{\Delta V} + (\partial T/\partial \Delta S)^2 \sigma^2_{\Delta S} + (\partial T/\partial \Delta Kx)^2 \sigma^2_{\Delta Kx} + (\partial T/\partial \Delta W)^2 \sigma^2_{\Delta W} + (\partial T/\partial \Delta X)^2 \sigma^2_{\Delta X}\}^{1/2} \qquad (2.24)$$

where the thermodynamic parameters (with $2\sigma$ uncertainties) derived from the regressed variables in equation (2.19) are:

$\Delta H^* = 35{,}798.8322 \pm 253.0823$ joules
$\Delta V = 0.88508 \pm 0.00849$ joules/bar
$\Delta S = 66.3526 \pm 0.7082$ joules/ °K
$W = 8986.1588 \pm 364.0329$ joules

Uncertainties in $K_X$ and X were estimated from the counting statistics of the electron microprobe data. Counting statistics for Mg and Si in phengite and chlorite were conservatively computed at 3% and 2% respectively. The counting statistics of Si were used to calculate uncertainties in $Al^{vi}$ in phengite and chlorite from which a value of about 5% was obtained. Random checks indicate that these lead to the uncertainty in $K_X$ up to 15% and the uncertainty in X up to 3%. Taking into account uncertainties in $Fe^{2+}$ and $Fe^{3+}$ which are partly constrained, then the uncertainty in $K_X$ of 20% and the uncertainty in X of 5% were adopted in the error propagation calculation. The uncertainties in estimated temperature from equation (2.19) can then be calculated from equation (2.24) using the parameters with $2\sigma$ uncertainties given above. Within the range of the data set, the uncertainties are in the order of 14-27 °C (Table 2.1).

## 2.6 Testing of Geothermometer

The phengite-chlorite geothermometer was tested for its reliability when applied to rocks that also contain probable equilibrium pairs of phengite and chlorite. The test data were selected from the published mineral compositional data where the temperatures and/or pressures are known or estimated. It is found that for those rocks with the compositions of phengite and chlorite falling within the range of the calibration data set, the calculated temperatures using equation (2.19) are reasonably close to the reported values or lie within the possible range deduced from relevant petrogenetic grids (Table 2.2).

The lower greenschist facies phyllites and greywackes from the Tennant Creek area, Australia were implied by Rao (1977) to have a possible temperature range of 200-400 °C and a pressure range of 2-4 kbar. The calculated temperatures using data on phengite-chlorite pairs are in the range 282-355 °C at an assumed pressure of 3 kbar which is considered to be the reasonable estimates with good

Table 2.2 Data for phengite-chlorite assemblages used to test the phengite-chlorite geothermometer.

| Sample no. | References | Phengite Mg | Phengite Fe | Phengite Alvi | Phengite Si | Chlorite Mg | Chlorite Fe | Chlorite Alvi | Chlorite Si | X MgAl | Kx | P (kbar) | T est (°C) | T MsChl (°C) | σT (°C) |
|---|---|---|---|---|---|---|---|---|---|---|---|---|---|---|---|
| 54 | Rao77 | 0.170 | 0.180 | 1.630 | 3.490 | 3.330 | 1.270 | 1.240 | 3.070 | -0.6570 | 5.7187 | 3 | 200-400 | 355 | 24 |
| 73 | " | 0.160 | 0.160 | 1.760 | 3.180 | 3.080 | 2.060 | 1.050 | 2.560 | -0.7680 | 6.8101 | 3 | 200-400 | 353 | 25 |
| 71 | " | 0.180 | 0.220 | 1.490 | 3.720 | 2.780 | 1.850 | 1.210 | 3.120 | -0.5469 | 2.3367 | 3 | 200-400 | 292 | 19 |
| D174 | " | 0.240 | 0.200 | 1.640 | 3.240 | 2.600 | 1.590 | 1.550 | 2.930 | -0.6580 | 3.3897 | 3 | 200-400 | 306 | 20 |
| 70D | " | 0.150 | 0.240 | 1.670 | 3.240 | 1.190 | 2.680 | 1.310 | 2.850 | -0.6916 | 2.7068 | 3 | 200-400 | 282 | 19 |
| 2/6291 | This study | 0.262 | 0.175 | 1.550 | 3.241 | 4.510 | 0.060 | 1.269 | 2.894 | -0.5835 | 5.9318 | 7 | 400-450 | 440 | 26 |
| 82-RRJ-39a | S&Co91 | 0.370 | 0.170 | 1.370 | 3.380 | 1.780 | 2.910 | 1.260 | 2.850 | -0.4350 | 1.0948 | 6 to 9 | 270-350 | 321 | 17 |
| T61 | C&Co76 | 0.305 | 0.220 | 1.505 | 3.335 | 2.250 | 2.390 | 1.290 | 2.720 | -0.5430 | 1.6790 | 4 | 250-370 | 282 | 17 |
| T62 | " | 0.155 | 0.245 | 1.630 | 3.340 | 2.050 | 2.610 | 1.280 | 2.730 | -0.6582 | 3.2938 | 4 | 250-370 | 319 | 21 |
| T63 | " | 0.115 | 0.145 | 1.815 | 3.115 | 2.110 | 2.470 | 1.330 | 2.750 | -0.8203 | 7.2053 | 4 | 250-370 | 367 | 26 |
| 11 | Mather70 | 0.240 | 0.180 | 1.370 | 3.300 | 1.800 | 2.550 | 1.270 | 2.770 | -0.4548 | 1.7794 | - | chlorite zone | 314 | 18 |
| 14 | " | 0.480 | 0.280 | 1.140 | 3.270 | 2.350 | 2.100 | 1.360 | 2.800 | -0.2673 | 0.9842 | - | " | 296 | 16 |
| 16 | " | 0.220 | 0.150 | 1.520 | 3.210 | 1.700 | 2.510 | 1.510 | 2.810 | -0.5655 | 2.0812 | - | biotite zone | 310 | 19 |
| 17 | " | 0.230 | 0.120 | 1.450 | 3.280 | 1.660 | 2.530 | 1.450 | 2.790 | -0.5124 | 1.6819 | - | " | 301 | 18 |
| 18 | " | 0.200 | 0.110 | 1.560 | 3.190 | 1.850 | 2.390 | 1.540 | 2.820 | -0.5984 | 2.6178 | - | " | 324 | 20 |

Notes: X MgAl = (X Mg,Ms)^2 - (X Al,Ms)^2
P = estimated pressure, T est = estimated temperature, T MsChl = phengite-chlorite temperature, σ T = uncertainty in T MsChl.
Rao77 = Rao (1977), S&Co91 = Shau et al. (1991), C&Co76 = Coombs et al. (1976b), Mather70 = Mather (1970)

precision. The point to note is that the metamorphic temperatures for these rocks become better constrained as a result of this geothermometer.

A piemontite-bearing quartz schist from the Sirikit Dam area, northern Thailand, with the assemblage quartz + phengite + Mg-chlorite + piemontite + magnetite + haematite, has a possible equilibration temperature between 400-450 °C deduced from the similar rock types in western Otago, New Zealand (Yardley, 1982; Kawachi *et al.*, 1983). The phengite-chlorite geothermometry yields the temperature of 440 °C at a minimum pressure of 7 kbar derived from phengite geobarometry of Massonne and Schreyer (1987).

The data on the intergrown phengite-chlorite pairs in a blueschist sample 82-RRJ-39a from the South Folk Mountain Schist of the eastern Franciscan belt, northern California (Shau *et al.*, 1991) give the temperature range of 294-334 °C for the pressure range of 6-9 kbar respectively. This temperature range is considered to be more realistic than $T < 200$ °C at $P < 7.4$ kbar calculated by Shau *et al.* (1991) from the thermodynamic data of Holland and Powell (1990). Brown and Ghent (1983) estimated the peak metamorphic temperatures and pressures to be in the vicinity of 270-310 °C and 6-8 kbar for rocks from the same belt. Jayko *et al.* (1986), based on oxygen isotope and mineral phase equilibria, estimated a maximum temperature of 330-350 °C and pressures of 7-9 kbar for rocks of the South Folk Mountain Schist. The temperatures obtained from this calibration of the phengite-chlorite geothermometry are in excellent agreement with the estimates given by Brown and Ghent (1983) and are slightly lower than those of Jayko *et al.* (1986). The calibration produced here gives a realistic result for blueschist facies pelites.

Coombs *et al.* (1976b) studied the semi-schistose Taveyanne Formation of the pumpellyite-actinolite facies in Switzerland and suggested a temperature of about 250-370 °C and pressure of greater than 2.5 kbar. At an assumed pressure of 4 kbar, the phengite-chlorite geothermometry yields, with one exception, the temperature of 282-319 °C which is a reasonable estimate for pumpellyite-actinolite facies metamorphism compared to the values of about 230-310 °C at 4 kbar constrained from a recently published petrogenetic grid for metabasites (Frey *et al.*, 1991).

A phengite-chlorite geothermometer yields reasonably good estimates for the rocks from the chlorite zone of the Dalradian (Mather, 1970) but yields very low temperatures, about 100 °C less than the appropriate values for the biotite zone. This large discrepancy may be explained by the fact that the mineral analyses were done on the separates which may contain substantial contamination due to poor separation at the fine grained sizes. They may also suffer from containing a mixed

set of mineral compositions if the original materials included some retrograde compositions.

## 2.7 Summary

The Mg-Tschermak substitution between phengite and chlorite was found through empirical calibration to be a useful geothermometer for high-temperature diagenesis to lower greenschist and blueschist facies metamorphic regimes. Testing of the phengite-chlorite geothermometer to rocks from low-grade terranes showed that reliable results can be obtained. However, the application of this geothermometer should be restricted to white micas and chlorites which have the composition ranges similar to those used in the calibration.

# Chapter 3

# LITHOSTRATIGRAPHY OF THE SIRIKIT DAM AREA

## 3.1 Introduction

The aim of this thesis is not to revise the lithostratigraphy of northern Thailand. Lithostratigraphic revisions ,and the erection of new units and names, is the responsibility of the officers of the Royal Thai Department of Mineral Resources in Bangkok. In this chapter and in Chapters 8 and 9, the author has attempted to apply the established terminology, with the minimum possible modification (Table 1.1), to support the regional structural study which forms the basis of this thesis. The major aspects of the lithostratigraphy relevant to this work are the correlations of units between basins, their thickness and the nature of the boundaries between the units.

Rocks in the Sirikit Dam area are genetically diverse and complex. On one hand, they range from unmetamorphosed non-marine siliciclastics and marine turbiditic sandstones and conglomerates to lower-greenschist facies metasedimentary rocks; on the other, they include metavolcanic rocks, mafic-ultramafic intrusive rocks and amphibolite facies metabasites. These rocks have been grouped into several lithostratigraphic units by geologists from the Royal Thai Department of Mineral Resources where general accounts of the geology of the area have been given through a series of published and unpublished reports and geological maps (e.g. Bunopas, 1969; 1981; Piyasin, 1974, Charoenpravat *et al.*, 1976; Lumjuan and Sinpoon-anant, 1987). Detailed petrochemistry of mafic and ultramafic igneous rocks in this area and the neighbouring region has been reported by Macdonald and Barr (1984), Barr and Macdonald (1987) and Panjasawatwong (1991). These papers provided the basis for understanding the complex geologic history of the area. In the present study, the original stratigraphic nomenclature of the Sirikit Dam area proposed by Bunopas (1969; 1981) is retained with only minor modification. Four major lithostratigraphic units which were recognised include the Pha Som Metamorphic Complex of a probable Permo-Carboniferous age, the Permo-Triassic

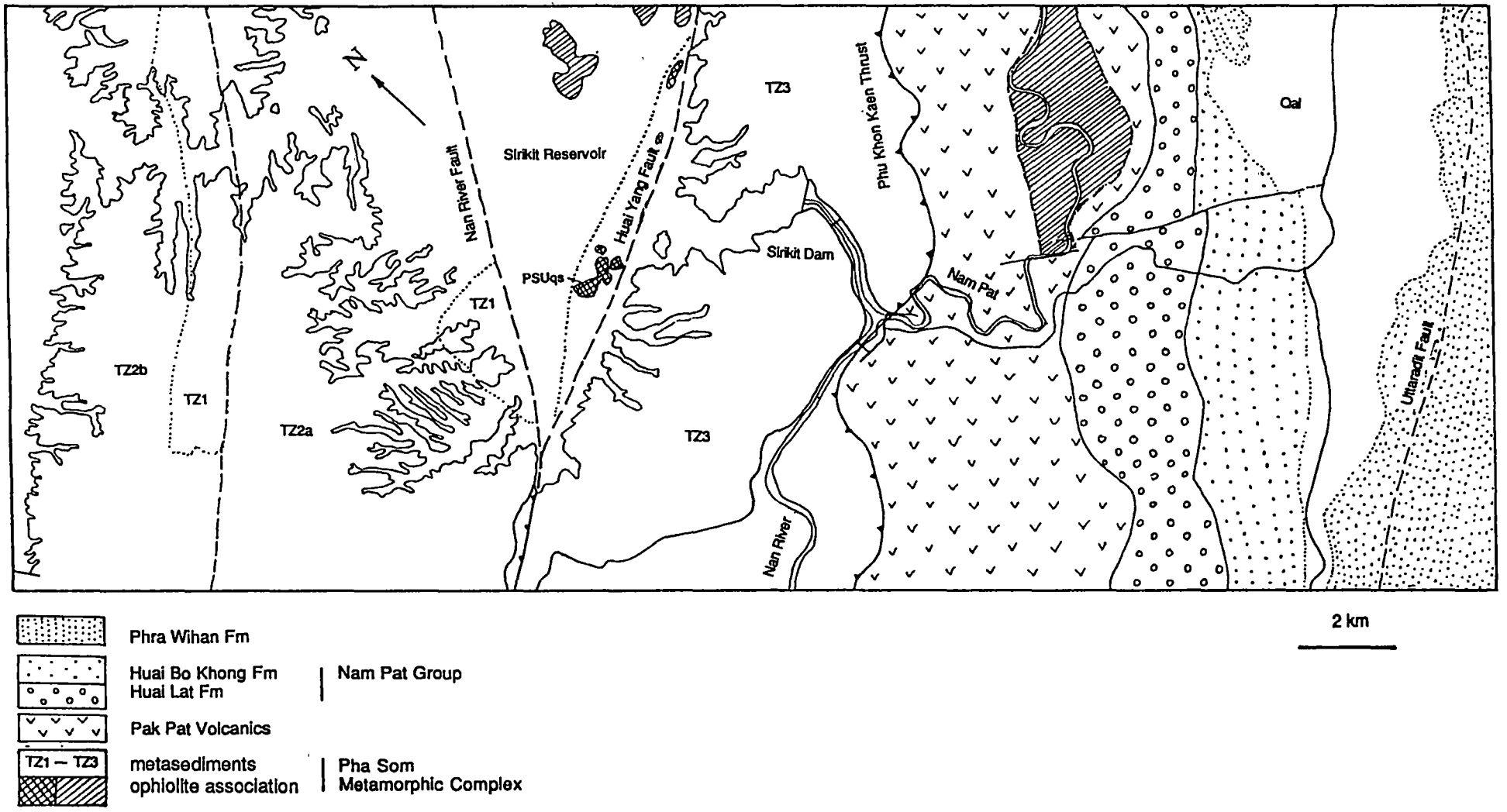


Figure 3.1 Simplified geological map of the Sirikit Dam area showing distribution of lithostratigraphic units. Detailed structural data are presented in Figure 4.1.

Pak Pat Volcanics, the Triassic Nam Pat Group and the Middle Jurassic Phra Wihan Formation. These rock units have either unconformable or fault contacts with one another as shown in Figure 3.1.

## 3.2 The Pha Som Metamorphic Complex

The Pha Som Metamorphic Complex is used here as a collective name for the "Pha Som Ultramafics" and the "Pha Som Group" of Bunopas (1981). These two units, though markedly differ from each other in terms of lithology, have a similar structural history.

### 3.2.1 The ophiolite association of the Pha Som Metamorphic Complex

The ophiolite association ("Pha Som Ultramafics" of Bunopas, 1981) was originally defined as a suite of mafic and ultramafic igneous rocks. However, it was shown later that this rock unit contains a sedimentary component as well (Macdonald and Barr, 1984; Panjasawatwong, 1991; and this study). It comprises a mixed variety of rocks, ranging from metavolcanic rocks, mafic-ultramafic plutonic rocks and amphibolites to metamorphosed pelagic-hemipelagic sediments. The mafic-ultramafic igneous rocks which are the dominant rock types are basalt, dolerite, microgabbro, gabbro, hornblendite, pyroxenite and peridotite. Basalts and related shallow intrusives have been subjected to low-grade metamorphism of sub-greenschist to lower-greenschist facies. Peridotites including rare dunite are almost completely altered to serpentinite whereas pyroxenites are largely amphibolitised. Amphibolites were believed to be derived from gabbros (Macdonald and Barr, 1984; Panjasawatwong, 1991) but it is also possible that some of them may simply be amphibolitised pyroxenite or metahornblendite. Previous workers described metahornblendites as hornblendites of a cumulate origin (Thanasuthipitak, 1978; Macdonald and Barr, 1984) though some of these hornblendites were better classified as amphibolites of a metamorphic origin. Minor metachert, greywacke, argillite and marble are the relic sedimentary rocks associated with the mafic and ultramafic rocks. The internal structure of this stratigraphic unit is rather complicated, due to extensive shearing and faulting. The structural complexity coupled with the discontinuity and scarcity of the outcrops preclude the possibility of mapping individual lithological units independently. Panjasawatwong (1991) described the dismembered mafic-ultramafic-dominated bodies in this area and elsewhere along the Nan River region as a serpentinite melange.

The ophiolite association can be traced for a distance of approximately 100 km from Uttaradit along the Nan River, via the Sirikit Dam area, to Nan and probably across the border into Laos (see Figs. 1.1 and 1.2). In the map area, the main part of this mafic-ultramafic complex has been submerged in the Sirikit Reservoir and outcrops and float rocks can only be seen on some small islands (formerly ridges). Further northeast from the map area, the mafic-ultramafic rocks crop out intermittently within the residual soils and occupy a low landscape compared to neighbouring ridges formed by a volcanic sequence of the Pak Pat Volcanics and metasediments of the Pha Som Metamorphic Complex. Apart from the main body, a small fault sliver of rocks including metabasaltic lavas, dolerite, gabbro, peridotites and serpentinite in close association with bedded chert, marble, greywacke and argillite is found along the Nam Pat River, a tributary of the Nan River, as an inlier within the Pak Pat Volcanics. This suite of mafic-ultramafic rocks and associated sediments is considered to be part of the ophiolite association of the Pha Som Metamorphic Complex on the basis of close lithological similarity. Elsewhere, several small bodies of similar lithological assemblages have been found scattered within the metasediments and the Pak Pat Volcanics (Bunopas, 1981; and this study). These small bodies of mainly mafic-ultramafic rocks are probably thrust slices as suggested by observable thrust contacts with the enclosing phyllites and metagreywackes and also by their complex internal geometry contrasting with the surrounding Pak Pat Volcanics.

**Lithology:** In the study area, the ophiolite association consists chiefly of mafic-ultramafic plutonic rocks including gabbro, dolerite, serpentinised peridotite and serpentinite in close association with amphibolites which show either foliated or granoblastic texture. Other minor rock types also included in this unit are metabasaltic volcanics, chromitite, muscovite-quartz schist, piemontite-bearing quartz schist, chert, greywacke, argillite and marble.

Serpentinised peridotites, including dunite and pyroxenite, were found as float rocks on small islands in the Sirikit Reservoir a few kilometres north of the Sirikit Dam and also occur as lenses wrapped around by foliated serpentinite along the Nam Pat River about 6 km east of the Sirikit Dam. They were almost completely serpentinised with only a very small amount of relic orthopyroxene and olivine grains.

Amphibolites were found on the small islands in the Sirikit Reservoir and a small outcrop was seen along the reservoir bank to the north of the Sirikit Dam. They are intimately associated with serpentinite, amphibolitised pyroxenite and gabbro. Their mineralogy varies markedly. They may be metahornblendite, zoisite amphibolite or garnet amphibolite.

Garnet amphibolites are medium-grained granoblastic rocks consisting of clinopyroxene and amphibole with patches of pink garnet. They occur as blocks within abundant serpentinite matrix that are exposed in an exploratory trench on the reservoir bank (grid reference 668757 of map sheet 5144 IV).

Zoisite amphibolite is dark grey, medium-grained gneissic rock with well-developed foliation. The foliation trends northeasterly and dips steeply towards the northwest. This rare outcrop is probably a large block because no serpentinite was seen within its immediate vicinity.

Metahornblendite is either coarse-grained granoblastic rock or medium-grained schistose rock. This rock type was found only as float on a small island in the Sirikit Reservoir (grid reference 648697 of map sheet 5144 IV).

Serpentinites are always found together with peridotites and occasionally amphibolites and gabbros. They are strongly foliated and lineated rocks, light green to dark green in colour, and usually wrap around lensoid blocks of serpentinised peridotites.

Chromitites are closely associated with peridotite and garnet amphibolite. They were found as float within a serpentinite body together with peridotite and garnet amphibolite. The rocks are black with irregular white patches and have medium- to coarse-grained glomero-porphyritic texture. They consist almost entirely of chromite with serpentine along the grain boundaries.

Dolerites occur as dykes cutting across the body of mafic-ultramafic rocks. They are green, fine- to medium-grained non-porphyritic rocks.

Metabasalts are green, fine-grained porphyritic rocks found as float together with amphibolites and serpentinised peridotites.

Quartz schist and piemontite-bearing quartz schist are found on the small islands in the Sirikit Reservoir. Because the majority of these rock types are submerged under water, it is not possible to map their exact boundary. However, from the outcrop trend, it is likely to be part of the ophiolite association which is enclosed within the metasediments (Fig. 3.1). They are light grey to brown with reddish tint and show either medium-grained granoblastic texture or indistinct compositional layering.

Cherts were found as float within the ultramafic body on the small island in the Sirikit Reservoir and also as outcrops along the Pat River, 6 km east of the Sirikit Dam. They are well-bedded and tightly folded. At one locality, they are interbedded with dark grey argillite and greywackes. They are very fine-grained, brown to green rocks made up chiefly of cryptocrystalline to microcrystalline quartz.

Marble was found to have a shear contact with serpentinised peridotites and serpentinites. The thickness of the marble layer is about 0.3 m. It is characterised by alternating white and dark bands which are tightly folded.

Greywackes are grey to dark grey, thin- to thick-bedded with parallel bedform and are intercalated with laminated argillites and bedded chert. In some places, they appear as blocks in an argillaceous matrix probably formed by transposition of bedding.

Argillites are dark grey and occasionally laminated rocks interbedded with greywackes and chert beds. They have a parallel bedform and range from thinly laminated to medium bedded (5-200 mm).

**Contacts:** The contact between the ophiolite association and the surrounding low-grade metasediments of the Pha Som Metamorphic Complex has a tectonic rather than intrusive characteristic. This evidence rules out the possibility that the meta-igneous rocks were emplaced by intruding into the Pha Som Metamorphic Complex as envisaged by a few workers, e.g. Thanasuthipitak (1978) and Lumjuan and Sinpoon-anant (1987). The contact between the ultramafic unit and the surrounding Pak Pat Volcanics is obscured due to poor exposure and weathering. Phromma *et al.* (1991) reported a thrust contact between the ophiolite association and the Pak Pat Volcanics exposed at Huai Sai Laeng, a small creek that flows into the Sirikit Reservoir about 2 km north of the map area (approximately 6 km north of the Sirikit Dam).

**Age:** The age of the ophiolite association varies markedly, e.g., Hada (1990) reported that most of the radiolaria in red chert blocks indicate upper Middle Permian to lower Upper Permian. The age range from Upper Devonian to Lower Carboniferous (361±22 to 327±20 Ma) was reported by Helmcke (1985) based on K-Ar dating of amphiboles. Hahn (1985) reported the Permo-Carboniferous age (more probably Carboniferous) based on foraminifera and bryozoan in a calcareous cement of the volcanic breccia. The Ar-Ar dating of the basic lavas and associated plutonic rocks indicates an age range of 356-256 Ma (Lower Carboniferous - Upper Permian) with the exception that one rock sample yields the age of 97±7 Ma (Lower Cretaceous) (Drs. Y. Panjasawatwong and A.J. Crawford, pers. comm., 1993). This is not surprising when taking into account the chaotic nature of these rocks which are basically blocks in a serpentinite matrix. In spite of a wide range in age, the majority of these blocks probably formed in Carboniferous time with only minor portion formed in the Early and Middle Permian.

### 3.2.2 The metasediments of the Pha Som Metamorphic Complex

The name "Pha Som Group" was first introduced by Bunopas (1969) for a sequence of sedimentary rocks which has been metamorphosed under greenschist facies conditions. The type section was then designated as the excavations prepared for the abutments of the Pha Som Dam (an original name of the Sirikit Dam) which are now concealed beneath the dam structure. The recrystallisation and complex deformation of these metasedimentary rocks has destroyed most of primary features and hence restrict the sedimentological interpretations for the these rocks. Likewise, detailed stratigraphic subdivision of the metasediments is impracticable due to the monotony of the succession, the structural complexity, and the scarcity of marker horizons.

**Lithology:** The dominant rock types of the metasediments are metagreywackes with associated minor phyllites. The term metagreywackes used in the present study includes various rocks described by previous workers in the Nan River area as banded quartzite, muscovite-quartz schist, epidote-quartz schist and actinolite-quartz schist (Thanasuthipitak, 1978; Bunopas, 1981). Epidote-crossite schist interlayered with quartzite was found in the Doi Phuk Sung area about 70 km northeast of the Sirikit Dam by Barr *et al.* (1985) and was correlated with this unit.

Metagreywackes are the dominant rock types in the Sirikit Dam area. They make up more than 90% of the unit. The vast majority of metagreywackes have a quartzofeldspathic composition. A few rocks, particularly in the northwestern corner of the map area, contain abundant volcanic lithic fragments suggesting a volcanogenic source. Regardless of the texture, metagreywackes contain typical lower greenschist facies mineral assemblage: quartz, albite, muscovite and chlorite with or without calcite, epidote and/or actinolite. A micaceous sheen on the foliation surface is common. No biotite was found in the metasediments. The metagreywackes and associated phyllites in the Sirikit Dam area therefore fall within the chlorite zone of the greenschist facies. Texturally, the metagreywackes can be classified as slightly sheared greywacke (TZ1), semischist (TZ2a and TZ2b) and fine-grained schists (TZ3) following the scheme devised by Turner (1938) in which four textural zones (Chl 1 through Chl 4), reflecting increasing intensity of deformation, were used as subdivisions of the chlorite zone of the greenschist facies Otago Schist in southern New Zealand. These textural zones have been used extensively in New Zealand (e.g. Bishop, 1972; Kawachi, 1974) and a similar procedure has been followed in California where textural zones have been successfully mapped in rocks of metagreywacke lithology of the Franciscan Terrane (Ghent, 1965; Blake *et al.*, 1967). Detailed discussion concerning the textural zonation is presented in Chapter 5. The TZ3 textural zone is widespread throughout

the Sirikit Dam area to the east of the Nan River fault. In the area west of the Nan River fault, the TZ1 textural zone is bounded within the TZ2a and TZ2b textural zone (Fig. 3.1). The boundary between successive textural zones is only approximate due to the scarcity of outcrops.

Phyllites are the minor lithology in the metasedimentary unit of the Pha Som Metamorphic Complex. They occur as partings or very thin layers within a package of more abundant metagreywackes. A few varieties of phyllites were recognised depending on the varying proportion of constituent minerals, these include muscovite phyllite, chlorite-muscovite phyllite, muscovite-chlorite phyllite and quartz-muscovite phyllite. They are dark grey to greyish green rocks with shiny surfaces.

**Thickness:** The stratigraphic thickness of the metasediments could not be determine in this study. Bunopas (1981) estimated the thickness was at least 2 km, but his estimate did not allow for the structural complexity recognised in the present study and is not reliable.

**Contact:** The base of the metasediments has not been seen. It is thrust over the Pak Pat Volcanics along the Phu Khon Kaen Thrust (Fig. 3.1) and encloses the ophiolite association. The boundary between the two rock units is marked by the Nan River fault on the west side. The contact with a mudrock-dominated sequence of the Permian Phrae Group further to the west (on the Phrae-Sirikit Reservoir transect) has not been directly observed but it is likely to be a thrust fault (detailed discussion in Chapter 8). Bunopas (1981), however, reported that the metasediments were unconformably overlain by the Permian Phrae Group in the area northeast of Phrae.

**Age and correlation:** The age of the metasediments unit of the Pha Som Metamorphic Complex remains controversial. No fossils have been found in the rocks of this group. On the basis of regional stratigraphy, Bunopas (1981) thought that this rock unit was pre-Permo-Carboniferous and suggested a Silurian-Devonian age whereas Hess and Koch (1975) assigned a Permo-Carboniferous age. Barr and Macdonald (1987), on the other hand, suggested Middle Permian (269± 12 Ma) as a minimum metamorphic age according to a K-Ar date of actinolite-quartz schist in the metasediments. On the basis of this metamorphic age and the presumed subduction zone setting of the area, it is quite reasonable to suggest that the sedimentation of the metasediments took place within a short time-span during Carboniferous to the beginning of Permian. However, a Middle Cretaceous metamorphic age of phyllites based on a K-Ar date of muscovite has recently been reported (Ahrendt *et al.*, 1993). This latest date is not compatible with metamorphic, structural and sedimentological evidence presented in the rock units of known ages

especially the Triassic Nam Pat Group and the Middle Jurassic Phra Wihan Formation. It is best considered as a reset age.

## 3.3 The Pak Pat Volcanics

The Pak Pat Volcanics was named after Ban Pak Pat, a small community located about 3 km downstream from the Sirikit Dam, by Bunopas (1981).

**Lithology:** The Pak Pat Volcanics consists of basalts, basaltic andesites and minor dacites and tuffs. The rocks have undergone sub-greenschist or lower-greenschist facies metamorphism.

Basaltic andesite is the most abundant volcanic rocks of the Pak Pat Volcanics. They are characterised by aphanitic-porphyritic texture. Abundant white plagioclase feldspar phenocrysts and a few dark green chlorite spots are disseminated throughout the lighter green groundmass. The best outcrop of this rock type can be seen at a quarry near Ban Pak Pat (grid reference 650610 of map sheet 5144 III). The rocks have a massive appearance and are locally cut by numerous calcite veins.

Basalts, andesites and dacites are minor components of the Pak Pat Volcanics. They are closely associated with the basaltic andesites and are difficult to distinguish from the latter without chemical analysis.

Tuffs including lapilli varieties also constitute an important proportion of the Pak Pat Volcanics apart from the lavas. They vary in colour from green to reddish purple probably due to the effects of low-grade metamorphism rather than the original mineralogy. They typically have a fragmental texture. Primary stratification was rare owing to their massive character. However, at km 5.5 on Highway 1146 from Ban Pak Pat to Nam Pat town, laminated tuffs are interbedded with sheared tuffaceous conglomerate.

**Thickness:** The exact thickness of the Pak Pat Volcanics is not possible to measure due to the massive character of the rocks. However, it is estimated to be more than 1500 m judging from the outcrop width and the attitudes of the adjacent units.

**Contact:** The Pak Pat Volcanics was considered to rest on top of the metasediments of the Pha Som Metamorphic Complex by Bunopas (1981) but field evidence in the present study argues for juxtaposition by overthrusting of the latter along the Phu Khon Kaen Thrust. On the eastern side, it is unconformably overlain by a sequence of conglomerates of the Huai Lat Formation. A small body of mafic-ultramafic intrusives and related rocks (part of the ophiolite association) is enclosed within the Pak Pat Volcanics probably as a thrust slice.

**Age and correlation:** There is no radiometric-age dating to constrain the actual age of the Pak Pat Volcanics. On the stratigraphic ground, Bunopas (1981) proposed the Permo-Triassic age for this rock unit. Judging from the fact that it is unconformably overlain by the conglomerate units of the Huai Lat Formation which, in turn, underlies the Huai Bo Khong Formation that contains Middle Triassic *Halobia*, it is suggested the age range must be Middle Permian to Lower Triassic. The Pak Pat Volcanics is different from the Permo-Triassic volcanics in Lampang-Phrae area. The volcanic rocks of the latter unit are more felsic, i.e. they are dominated by dacites, rhyolites and associated tuffs rather than the basaltic andesites and related rocks of the Pak Pat Volcanics.

## 3.4 The Nam Pat Group

The Nam Pat Group was introduced by Bunopas (1981) to include two formations, the lower Huai Lat Formation of volcaniclastic conglomerates and the upper Huai Bo Khong Formation of marine turbidites which were originally named by Bunopas (1969). The Nam Pat Group can be traced further southwest from the map area before it is covered by Quaternary alluvium near Uttaradit. Further northeast this rock unit is known to extend for a considerable distance but has not been mapped (Bunopas, 1981). A stratigraphic column of the Nam Pat Group based on the traverse along Huai Bo Khong is shown in Figure 3.2.

### 3.4.1 The Huai Lat Formation

The name of this formation was given by Bunopas (1969) after a small creek, Huai Lat, running from north to south to join the Nam Pat River at a bend 6 km northwest of the Nam Pat town. This formation is characterised by a thick sequence of volcaniclastic conglomerates and minor sandstones (Fig. 3.2).

**Lithology:** The dominant rocks in the Huai Lat Formation are volcaniclastic conglomerates. Minor interbedded sandstones are found locally and increase towards the upper part particularly near the base of the Huai Bo Khong Formation.

Conglomerates are polymict having clasts made up of andesite, basalt, granodiorite, epidosite, chert, limestone and vein-quartz set in a tuffaceous sandy matrix (Fig. 3.3a, b, c &d). They are greyish green to purplish red and are generally matrix-supported with subangular to rounded clasts. Sorting is very-poor and the clasts range in size from gravel to large boulders (up to 4 m across). Bed thickness varies from about 1 metres to more than 10 metres.

Sandstones are greenish-grey tuffaceous and slightly calcareous, very coarse-grained to conglomeratic and poorly sorted. Bed thickness ranges from medium to very thick and bedding varies from moderately- to well-bedded. Pebbles in conglomeratic sandstone beds are generally rounded and include vein-quartz, limestone, chert, epidosite and volcanic rocks.

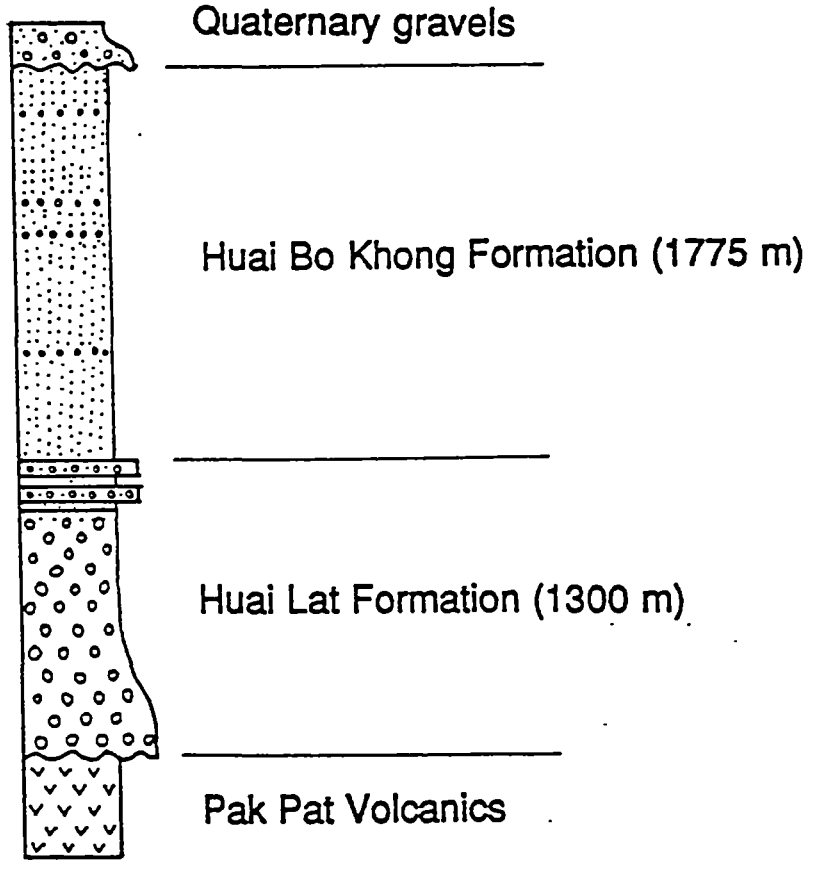


Figure 3.2 Stratigraphic column of the Nam Pat Group based on the traverse along Huai Bo Khong.

**Thickness:** The thickness of the Huai Lat Formation at its type section was estimated at 500 m (Bunopas, 1981). Along the Huai Bo Khong traverse, it is approximately 1300 m thick.

**Contact:** The Huai Lat Formation unconformably overlies the Pak Pat Volcanics on the west as seen on the road between the Ban Pak Pat to Nam Pat town. It grades upwards into the Huai Bo Khong Formation on the east. The

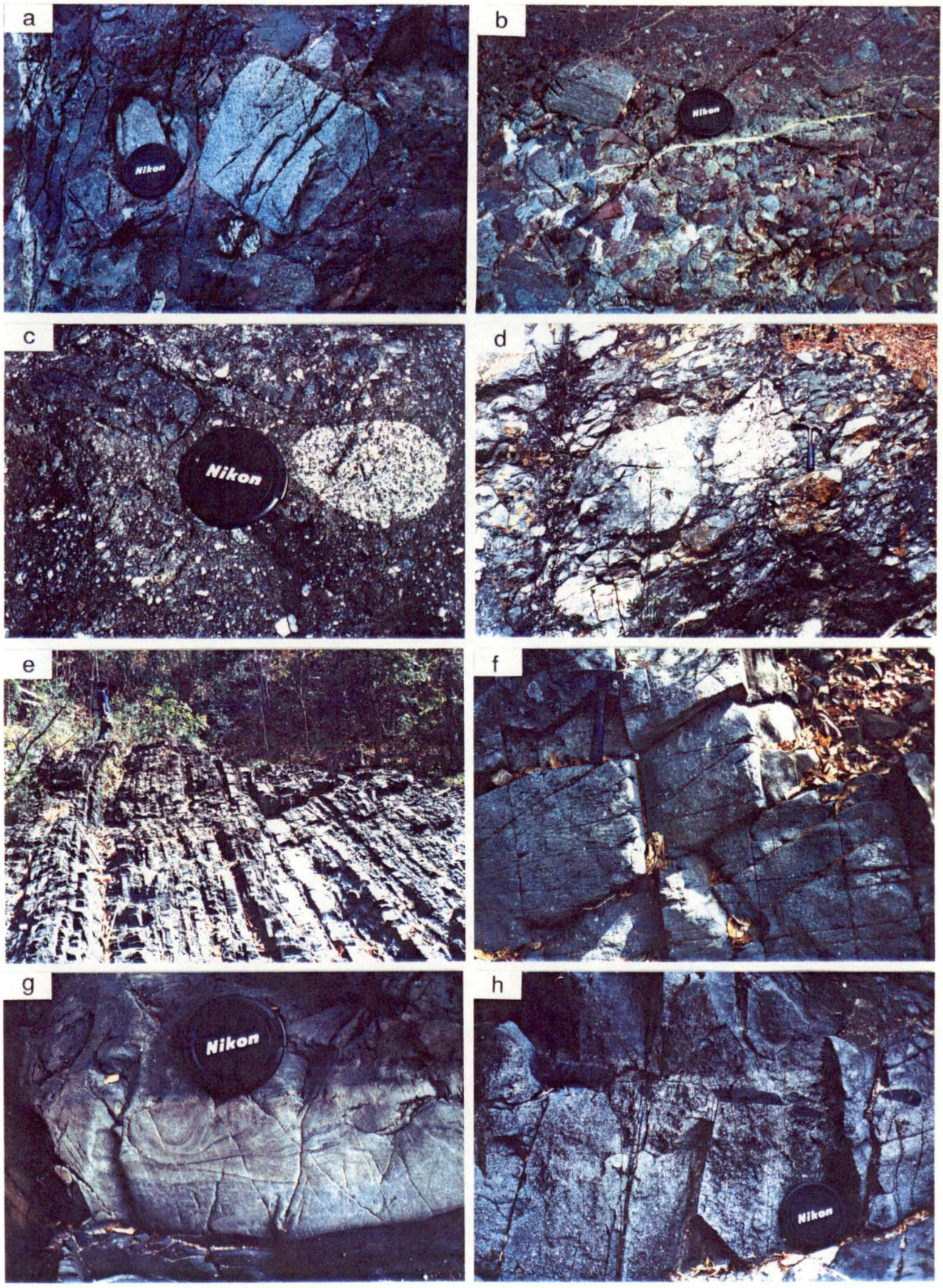
a
b
c
d
e
f
g
h
Nikon

boundary between these two formations is taken where massive conglomerates give way to alternating beds of sandstone and mudrocks.

**Age and correlation:** The age of the Huai Lat Formation was inferred from the age of fusulinids found in the limestone clasts in conglomerates at a few places east of Sirikit Dam by Bunopas (1981). The fusulinids *Neofusilinella saraburiensis*, *Neofusulinella sp.*, *Pseudofusulina sp.*, and *Schwagerinella solida* indicate a lower Upper Permian age for the limestone from which the clasts were derived and hence provided the lower limit for the age of the Huai Lat Formation. In addition, foraminifera *Globivalvulina sp.*, *Schubertella sp.* and *Verbeekina sp.* of lower Middle Permian (identified by J. Jamnongthai of the Royal Thai Department of Mineral Resources) were also found in the boulders of grey limestones embedded in the conglomerates (Dr Y. Panjasawatwong, pers. comm., 1992). These fossil-bearing limestones were located on top of a small hill near Ban Wang Bang on the Highway 1146 from Ban Pak Pat to Nam Pat town (Grid Reference 678591 of map sheet 5144 III). Fossils in limestones from the same location were identified as *Pseudostaffella sp.* (Upper Carboniferous), *Klamathina elongata* (Lower Permian), and *Pseudoschwagerina sp.* (Lower-Middle Permian) (K. Stait, pers. comm., 1993). An upper age limit is provided by the Middle Triassic *Halobia* in the overlying Huai Bo Khong Formation. The age of the Huai Lat Formation was considered to be Lower Triassic by Bunopas (1981). However, limestone pebbles containing Middle Triassic fossils (identified by R. Ingavat-Helmcke) has recently been reported (Lüddecke *et al.*, 1991).

### 3.4.2 The Huai Bo Khong Formation

The name of this formation was derived from Huai Bo Khong, a small tributary of the Nam Pat River east of the Sirikit Dam (Bunopas, 1969). Huai Bo Khong, running from east to west across the general strike of the Nam Pat Group and subparallel to Highway 1146, provides a good access for measuring a stratigraphic section. The Huai Bo Khong Formation encompasses a monotonous sequence of turbiditic sandstone and interbedded shale and siltstone.

**Lithology:** The thick sequence of this turbidite unit consists of long laterally continuous, even sandstone beds interbedded with shale and siltstone (Fig. 3.3e).

Sandstones are grey to greenish grey and consist of framework grains of quartz, volcanic fragments and plagioclase feldspar in a matrix of chlorite and clay minerals. They are thin- to very thick-bedded but mainly medium-bedded, medium- to very coarse-grained to conglomeratic (Fig. 3.3f) and moderately- to poorly-

sorted. Laminations occasionally occur within a single bed. Sedimentary features typical of turbidites such as Bouma sequence (Fig. 3.3g), graded bedding, convoluted lamination, flame structure, rip-up clasts (Fig. 3.3h) are common. These features are very useful indicators for younging direction of the sequence as does the cleavage-bedding relationship. They all indicate the southeastward overturning of the sequence in the same sense as the younging direction. In contrast, sole structures which are the most reliable palaeocurrent indicators, are rare.

Shale and siltstone are dark grey, thin to medium bedded. Laminations are also quite common.

**Thickness:** The thickness of the incomplete sequence of turbiditic sandstones and mudrocks of the Huai Bo Khong Formation is estimated at 1775 m in this study contrasting to a previous estimate of 900 m by Bunopas (1981) based on the same section along Huai Bo Khong. Elsewhere, it has been estimated to be up to 1450 m (Bunopas, 1981).

**Contact:** The Huai Bo Khong Formation conformably overlies the Huai Lat Formation on the west. It appears to have either a fault contact or an unconformity with the sequence of non-marine siliciclastics of the Phra Wihan Formation on the eastern part of the map area. Bunopas (1981) who mapped a larger area reported that the Huai Bo Khong Formation was faulted against the Lower Khorat Group in all known sections. However, he also pointed out the existence of an angular unconformity between both units further south.

**Age and correlation:** The Middle Triassic age of the Huai Bo Khong Formation was given by Bunopas (1981) on the basis of the bivalve *Halobia* or *Daonella* found in a mudstone bed south of the present map area. He noted that there was no lithological equivalent in the marine Triassic Lampang Group 80 km to the west (the more detailed discussion of the Lampang Group is presented in Chapter 9).

## 3.5 The Phra Wihan Formation

The name Phra Wihan Formation is adopted in this study for non-marine strata consisting chiefly of quartzose sandstones after Charoenpravat *et al.* (1976). This formation is probably a lithostratigraphic correlative of the Ms4 Formation of Hahn (1976). The outcrops of this unit are distributed in the eastern part of the Sirikit Dam area, notably in the northeast-trending mountain range east of the Nam Pat river valley that extends from Tron, a small town near Uttaradit, to Fak Tha through to the Laos border.

**Lithology:** Quartzose sandstone is the dominant rock type of the Phra Wihan Formation together with minor siltstone and mudstone.

The sandstones can be classified as quartz arenites based on modal composition. Muscovite is occasionally present whereas feldspar is virtually absent. They are whitish-grey to yellowish-grey, well to very well-sorted, medium- to thick bedded and are interbedded with thin-bedded mudstone and siltstone. Sedimentary structures particularly current ripple-marks are common on the bedding planes.

Siltstone and mudstone are reddish-brown or occasionally light-grey, mainly thin-bedded intercalated with sandstone beds.

**Thickness:** The thickness of this unit was not measured due to the lack of appropriate section in the map area. However, it has been known to be much thicker than the Phra Wihan Formation in northeastern Thailand which is 56 to 136 m as measured by Ward and Bunnag (1964). Further north in the Nan and Phayao areas, Hahn (1976) reported the Ms4 Formation, the probable equivalent of the Phra Wihan Formation in the map area, as having the thickness in the range 400-500 m.

**Contact:** The contact between the Pha Wihan Formation and the underlying Huai Bo Khong Formation is either a fault or an angular unconformity. In the map area, it appears to be an unconformity. Bunopas (1981) also mentioned the unconformity between the two formations further to the south. The top of the Phra Wihan Formation is not exposed in the map area. Further east, the quartzose sandstone beds of this formation grades into red, fine-grained clastic, non-marine strata of the Sao Khua Formation.

**Age and correlation:** A Middle Jurassic age has been assigned to the Phra Wihan Formation in the map area based on the correlation with the Phra Wihan Formation in the Khorat Plateau region where fossil plants were found by Iwai *et al.* (1966) and identified as *Sphenopteris sp.* and *Brachyphyllum sp.* of Middle Jurassic time. Drumm *et al.* (1993) reported the finding of *Corollina sp.* (*Classiopollis sp.* Upper Triassic to Middle Jurassic) in the palynological samples from the Ms4 Formation in the Phrae-Nan area which was also found in the Phra Wihan Formation in northeastern Thailand as well.

## 3.6 Summary

Four major lithostratigraphic units which were recognised include the Pha Som Metamorphic Complex of a probable Permo-Carboniferous age, the Pak Pat Volcanics of a Permo-Triassic age, the Triassic Nam Pat Group and the Middle

Jurassic Phra Wihan Formation. These rock units have either unconformable or fault contacts with one another.

The ophiolite association of the Pha Som Metamorphic Complex is characterised by blocks of various rock types in serpentinite matrix for which the term serpentinite melange was introduced (Panjasawatwong, 1991). Blocks include mainly mafic-ultramafic plutonic rocks (i.e. gabbro, dolerite, serpentinised peridotite and amphibolites). Other minor rock types which also occur as blocks are metabasaltic rocks, chromitite, muscovite-quartz schist, piemontite-bearing quartz schist, chert, greywacke, argillite and marble. The contact between the ophiolite association and the surrounding metasediments is tectonic rather than intrusive. The age of blocks in the ophiolite association vary markedly. The probable age range is from Carboniferous to Middle Permian.

The dominant rock types of the metasedimentary unit of the Pha Som Metamorphic Complex are metagreywackes with minor phyllites. Texturally, the metagreywackes can be classified as slightly sheared greywackes (TZ1), semischists (TZ2a and TZ2b), fine-grained schist following the scheme devised by Turner (1938) and Bishop (1972). Phyllites, the minor lithology in the metasediments, occur as partings or very thin layers within a package of more abundant metagreywackes. The thickness of the metasediments is still unknown due to a complex deformational style of the rocks. The age of the metasediments remains controversial but the a Permo-Carboniferous age is the most likely.

The Pak Pat Volcanics (Middle Permian to Lower Triassic) consists of basaltic andesites and minor basalts, dacites and tuffs. The thickness of the Pak Pat Volcanics is estimated to be more than 1500 m. The Pak Pat Volcanics are different in composition to the time-equivalent volcanics in Lampang-Phrae area.

The Nam Pat Group consists of two formations, the Huai Lat Formation (lower unit, Middle Permian to Middle Triassic) and the Huai Bo Khong Formation (upper unit, Middle Triassic). The dominant lithology of the Huai Lat Formation is volcaniclastic conglomerates. Minor interbedded sandstones are found locally and tend to increase towards the upper part. The thickness of the Huai Lat Formation is approximately 1300 m. The Huai Bo Khong Formation is a sequence of turbiditic sandstone and interbedded shale and siltstone. The thickness of the incomplete sequence of turbiditic sandstones and mudrocks of the Huai Bo Khong Formation is estimated at 1775 m.

The Phra Wihan Formation (Middle Jurassic) consists dominantly of quartzose sandstone with minor siltstone and mudstone. The thickness of this formation is estimated between 400 and 500 m.

# Chapter 4

# STRUCTURE OF ROCKS IN THE SIRIKIT DAM AREA

## 4.1 Introduction

The aim of this chapter is to document the structure of rock units in the Sirikit Dam area. The mesoscopic structures were studied in detail and were used to place constraints on the interpretation of the major structure and structural history of the area. The structural study in combination with stratigraphic and metamorphic investigation places additional constraints on tectonic models for northern Thailand.

Each rock unit in the Sirikit Dam area (Figs. 4.1 and 4.2) has a different structural style and history. The rocks of the Pha Som Metamorphic Complex have been multiply deformed, whereas the Pak Pat Volcanics, the Nam Pat Group and the Phra Wihan Formation have suffered only a single phase of deformation. These rock units may be grouped into three distinct structural-stratigraphic units: (i) the Pha Som Metamorphic Complex, (ii) the cover sequence (the Pak Pat Volcanics and the Nam Pat Group) and (iii) the continental redbeds (the Phra Wihan Formation). The description and the analysis of these three structural units are given below.

## 4.2 Structure of the Pha Som Metamorphic Complex

Between the two rock units of the Pha Som Metamorphic Complex, the deformation style in the metasediments is relatively coherent in contrast to the disrupted rocks of the ophiolite association. The metasediments are better exposed and more suitable for a classical approach to structural history. The major emphasis in the structural study has been to define the deformation history of these rocks. The ophiolite association was given less attention, largely because the outcrop was too poor to support a detailed structural analysis.

### 4.2.1 Structure of the metasediments

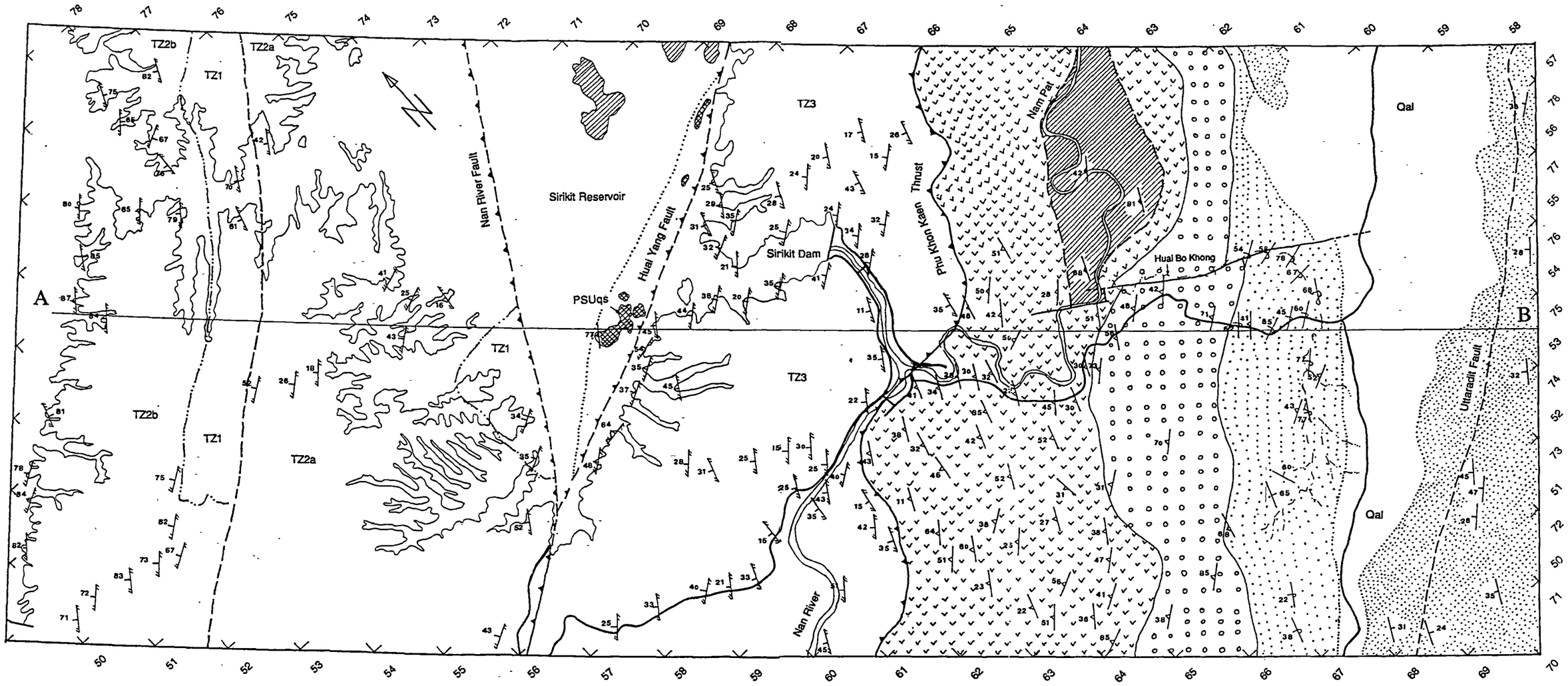


Figure 4.1 Structural map of the Sirikit Dam area

## LEGEND

| | | | |
|---|---|---|---|
| Qal | Alluvium | | *Quaternary* |
| | Phra Wihan Fm | | *Middle Jurassic* |
| | Huai Bo Khong Fm<br>Huai Lat Fm | Nam Pat Group | *Tnassic* |
| | Pak Pat Volcanics | | *Permo-Triassic* |
| TZ1-TZ3 | metasediments<br>ophiolite association | Pha Som<br>Metamorphic Complex | *Permo-Carboniferous* |

PSUqs : *Quartz schist*

## SYMBOLS

- Textural zone boundary
- Lithological boundary
- Lithological boundary (approximate)
- Fault
- Fault (inferred)
- Thrust fault
- Thrust fault (inferred)
- 35 / 66 — Bedding and overturned bedding
- 72 — Cleavage in volcanics and sedimentary rocks
- 81 — Foliation in the Pha Som Ultramafics
- 21 — $S_2$ in the Pha Som Group
- 2 km

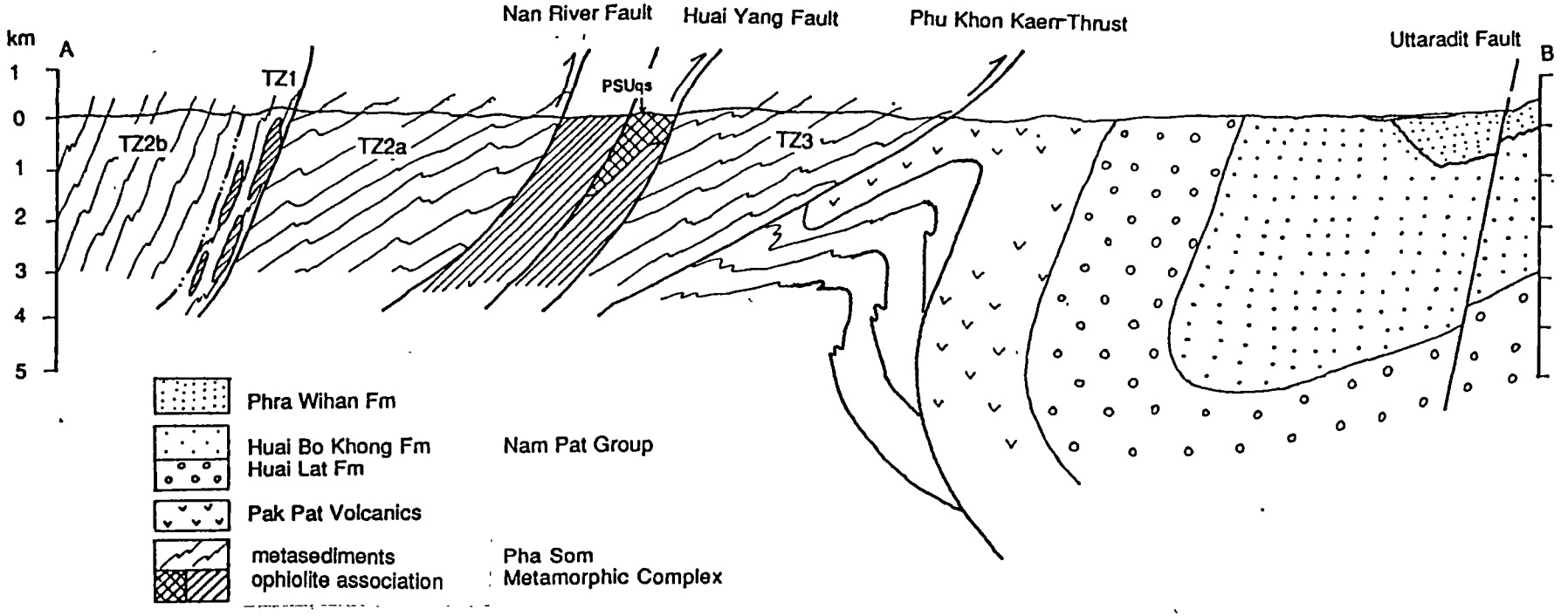


Figure 4.2 Interpretive cross-section across the Sirikit Dam area along line AB in Figure 4.1.

The metasedimentary rocks of the Pha Som Metamorphic Complex are multiply deformed. However, parts of the deformation history in the Sirikit Dam area is probably progressive rather than episodic in nature. The structures, especially folds and foliations, produced by these multiple deformation episodes are classified into generations on the basis of style and overprinting relationships recognisable on mesoscopic or microscopic scale (following Hobbs *et al.*, 1976; Williams, 1985). Orientation criterion was used only locally. In this study, overprinting relationships are the most reliable criteria in assigning a group of structures into a particular generation. At a few locations, overprinting relationships had to be established on microscopic scale due to the lack of recognisable mesoscopic features. In the Sirikit Dam area, the style has also proven to be a useful criterion. The style of folds of the same generation is relatively uniform but the style of the foliations varies significantly with lithology.

Four deformation phases were recognised in the metasediments. The mesoscopic and microscopic structural characteristics of each phase are described below.

## $D_1$ structures

The rocks are intensely deformed and recrystallised, so that the sedimentary structures are obscured. Recognisable $S_1$ is rare in the field area. This is due to the effect of later deformation, especially the development of strong $S_2$ cleavage/layering which extensively transposes and obliterates the pre-existing structures. Where $S_1$ was seen, all layering was transposed parallel to it and primary bedding features could not be distinguished from the compositional or differentiated layering which defines $S_1$. In outcrop, this planar structure is defined by fine colour bands of light-coloured quartz-rich and dark-coloured phyllosilicate-rich domains. (Fig. 4.3a). $S_1/S_2$ intersection lineations occurring as colour bands were observed on $S_2$ cleavage surfaces in a few outcrops (Fig. 4.3b). The $S_1/S_2$ intersection lineation is invariably sub-horizontal and trends northeasterly. The orientation data are insufficient to allow for further detailed geometrical analysis.

No proven examples of $D_1$ folds were observed on any scale. In metagreywackes and phyllites, the relics of $S_1$ are cut by a discrete crenulation cleavage or phyllitic cleavage, $S_2$ (Figs. 4.3c &d). Thin seams of opaque phases accentuate the $S_1$ cleavage and are folded by $F_2$ folds. The presumed original lamination ($S_0$) is sub-parallel to $S_1$ (Fig. 4.3c).

Common quartz veins, probably formed during $D_1$, are sub-parallel to $S_1$ and folded into tight to isoclinal folds with axial planes parallel or sub-parallel to $S_2$

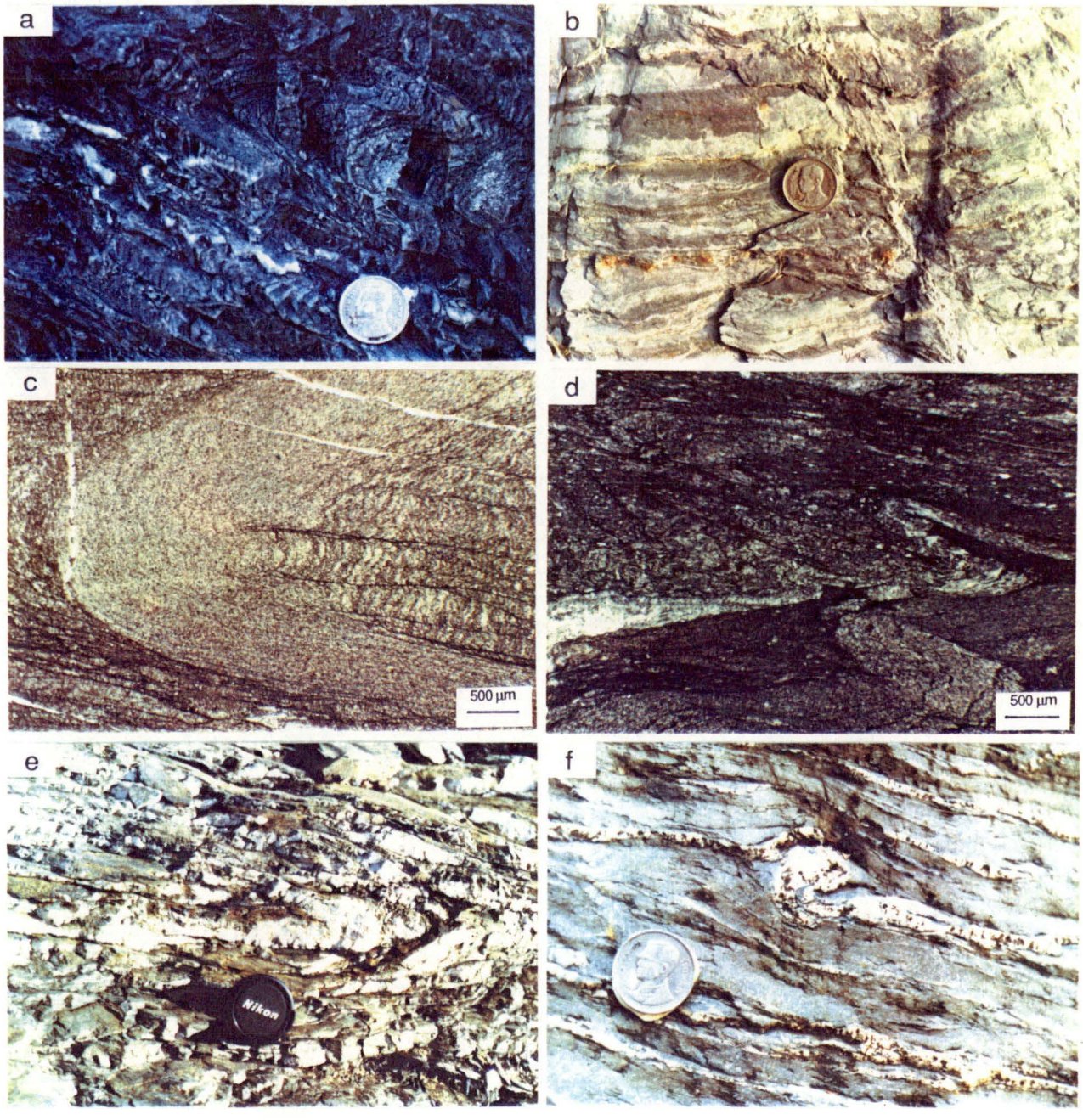


Figure 4.3 Photographs (a,b,e&f) and photomicrographs (c,d) of structures in the Pha Som M.C.. (a) $S_1$ folded by $F_2$ folds in TZ3 fine-grained quartzofeldspathic schist at grid reference 586618/5044II. Note the spaced cleavage ($S_2$) coincides with shear out fold limb. (b) Traces of $S_1$ on $S_2$ surface ($S_1/S_2$ intersection lineation) at grid reference 663636/5144IV. (c) $F_2$ fold with axial-plane crenulation cleavage (sample 7/9291). Note continuous phyllitic cleavage outside the fold. (d) Asymmetrical $F_2$ fold in phyllite (sample 6/9291). (e) Quartz veins tightly folded by $F_2$ fold at grid reference 645655/5144IV. (f) Sigmoidal quartz veins indicating clockwise rotation at grid reference 661659/5144IV. Scale: coin is 32 mm in diameter and lens cap is 52 mm in diameter.

phyllitic cleavage (Fig. 4.3e). At one stream outcrop probably located on a limb of a larger fold, quartz veins are folded into small-scale southeast-verging Z-shaped folds (Fig. 4.3f).

The mineral assemblages formed during $D_1$ phase are described in more detail in Chapter 5 (section 5.3). The dominant minerals defining $S_1$ layering are quartz, albite, muscovite and chlorite.

## $D_2$ structures

$D_2$ deformation produced close to isoclinal folds ($F_2$) with strongly-developed axial-plane foliation ($S_2$). The $S_2$ foliation is the dominant fabric element in rocks of all textural zones in the Sirikit Dam area. It is characterised by phyllitic cleavage in phyllites and discrete spaced cleavage/differentiated layering in metagreywackes. The variation in microscopic character of $S_2$ foliation in metagreywackes is used as a basis for establishing textural zonation (see details in Chapter 5). Transposition of $S_1$ layering by $S_2$ axial-plane foliation is so strong that distinction between these two generations of foliations is almost impossible, except where $F_2$ fold closures are observed. In most outcrops, the dominant foliation along which the rocks tend to split is $S_2$ foliation (Fig 4.4a).

**$F_2$ folds:** Folding associated with $D_2$ deformation folded original lamination or bedding ($S_0$) and cleavage/layering ($S_1$) into close to isoclinal folds with wavelength less than 100 mm (Figs. 4.3a, c, d &e and Figs. 4.4 b & c). The limbs in some of these folds are strongly sheared and thinned while the hinge zones are thickened. These folds have developed axial-plane foliation ($S_2$) which generally transposes $S_1$ layering. Based on dip-isogon pattern (Ramsay, 1967; Huddleston, 1973), the folds in quartz-rich layers can be classified as class 1C (flattened parallel folds) and those in phyllosilicate-rich layers belong to class 3 (folds with divergent dip isogon) as illustrated in Figure 4.4d. These two classes of folds appear to approach class 2 (similar fold). Huddleston(1973) and Gray (1979) have shown that this style of folding develops while the layers are still mechanically active and hence buckling is the principal mechanism rather than slip folding (passive folding) as in case of an ideal similar fold. Asymmetrical nature of many of these folds is reasonably clear, so that it can be used as kinematic indicator. The sense of shear is deduced on the basis of fold vergence. These small-scale folds are generally east verging. This phase of folding affected the semischists (TZ2a and TZ2b metagreywackes) sequence as well. The layering ($S_2$) dips uniformly to the northwest (Fig. 4.5a) in these zones. The scatter of poles to $S_2$ in a NW-SE-

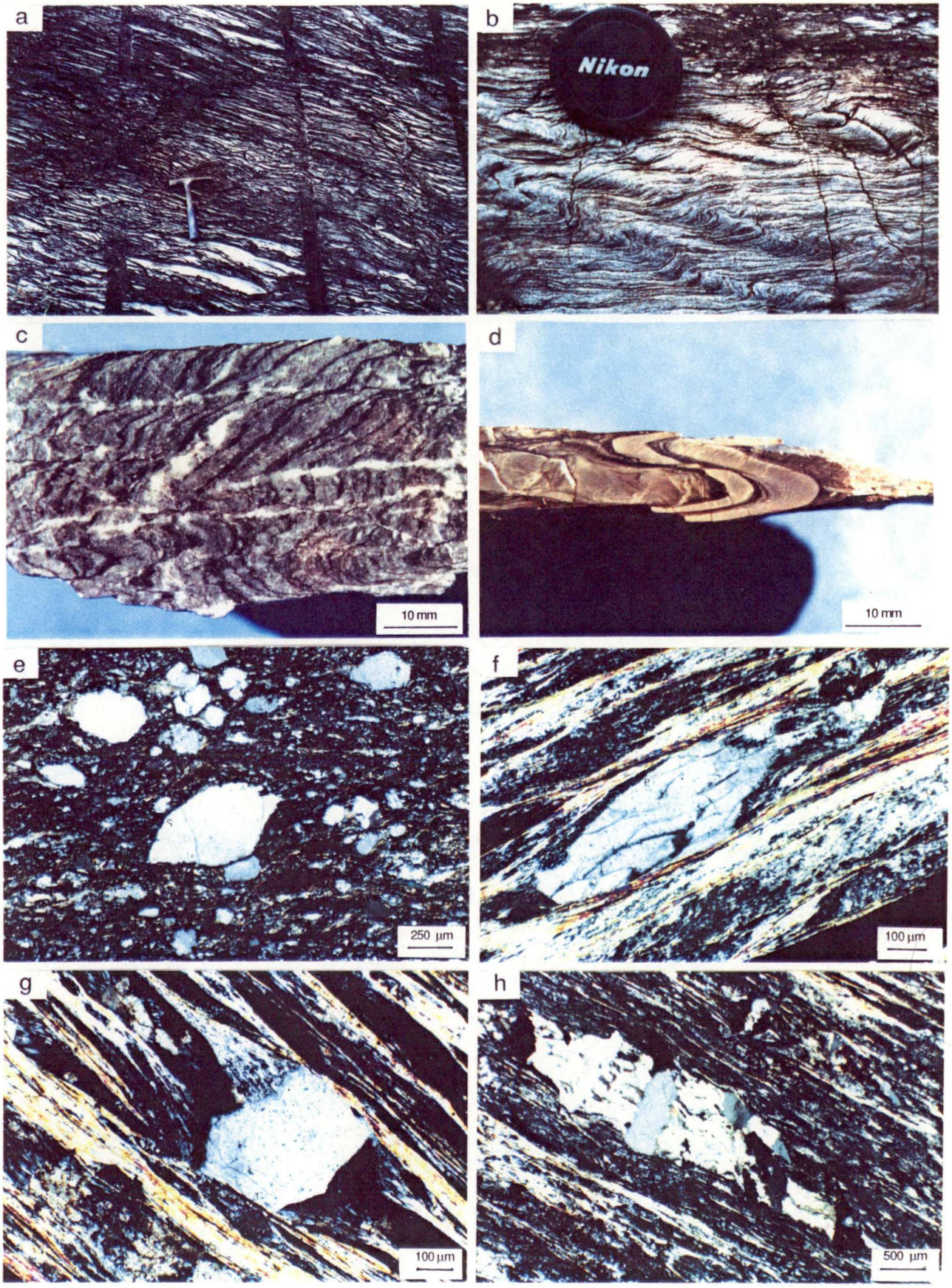
a
b
Nikon
c
10 mm
d
10 mm
e
250 µm
f
100 µm
g
100 µm
h
500 µm

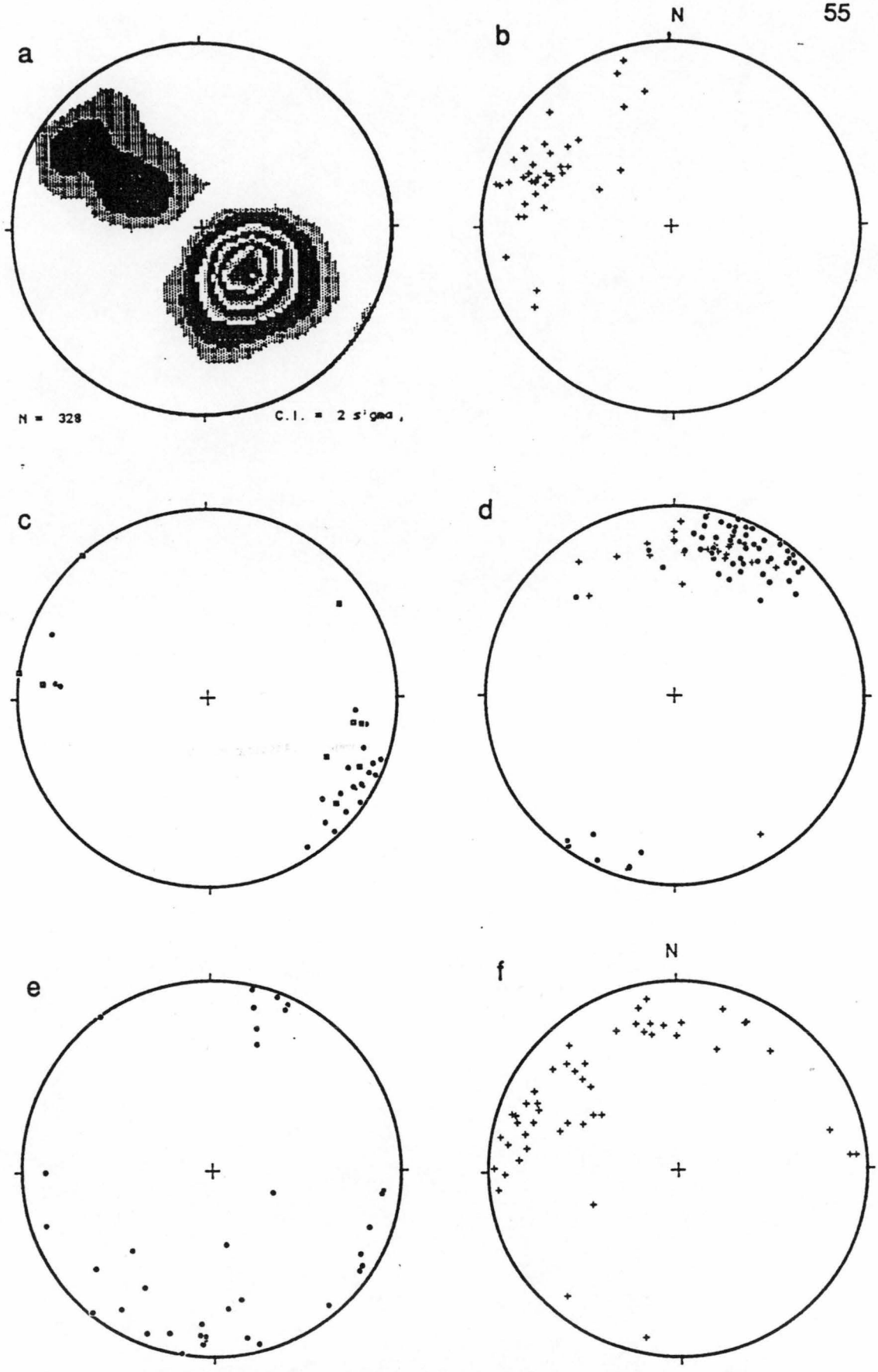


Figure 4.5 Lower-hemisphere equal-area stereographic projections of structures in the Pha Som M.C. (a) Contoured poles to $S_2$ (n=328). (b) Stretching lineation ($L_2$) in phyllites (n=40). (c) Poles to axial planes of open $F_3$ folds (dots) and crenulation cleavage (squares). (d) F3 fold axes (+) and crenulation axes (dots). (e) Poles to kink bands (n=39). (f) Kink axes (n=51).

trending great circle is due to the effect of later small-scale folds (especially $F_4$ kink folds).

Limited orientation data indicates that $F_2$ folds plunge shallowly to the northeast or southwest and the axial plane strikes northeast and dips northwest.

**$S_2$ foliation:** $S_2$ is characterised by phyllitic cleavage in phyllites and discrete spaced cleavage or differentiated layering in TZ3 metagreywackes. In outcrop or hand specimen, the phyllitic cleavage is apparently continuous (using the terminology of Hobbs *et al.*, 1976; Powell, 1979; Borradaile *et al.*, 1982) but appears to be domainal in thin section. It commonly transposes an $S_1$ compositional layering. The $S_2$ phyllitic cleavage is defined by strong parallelism of muscovite and chlorite in combination with the alignment of inequant grains of quartz and albite. In TZ3 metagreywacke, discrete spaced cleavage is defined by a very thin cleavage domain separating the microlithon domains (less than 10 mm in width). In some metagreywacke samples, differentiated layering which is calcite-rich and quartz-phyllosilicate-rich is also present.

Diffusional mass transfer (i.e. pressure solution) plays an important role as the dominant deformation mechanism in $D_2$ deformation. This is clearly evident in TZ2 and TZ3 metagreywackes where large quartz grains were dissolved along the high-pressure sides and the dissolved materials precipitated in the pressure shadows forming beards of fibrous quartz, calcite and minor chlorite (Fig. 4.4e). In higher strain zones, differentiation between phyllosilicate-rich and quartz-rich domains is more extensive giving rise to the strong schistose appearance of the rocks (Figs. 4.4 f & g). Quartz porphyroclasts are relatively flattened parallel to the cleavage plane. Some of them, especially in phyllites, are highly elongate and slightly rotated resulting in the formation of asymmetrical boudins (Fig. 4.4h).

Near the Phu Khon Kaen thrust the metasediments show higher strain. The style of deformation is brittle-ductile (Ramsay 1980), with the fault walls having higher strain but lacking a mylonitic fabric. There is only weak evidence for a non-coaxial deformation in these rocks, e.g. weak asymmetry of quartz porphyroclasts and pressure shadows.

$S_2$ cleavage uniformly strikes northeasterly and dips to the northwest and southeast (Fig. 4.5a). However, the overall dip direction (in terms of enveloping surface) is northwesterly. The variation in dip directions of $S_2$ surfaces is mainly due to the effect of folding during $D_4$ deformation event which is characterised by asymmetrical kink folds or angular folds ($F_4$). The long limbs of these $F_4$ folds dip to the northwest whereas the short limbs dip to the southeast.

The mineral assemblages formed during $D_2$ deformation are very similar to the $D_1$ assemblages. They are characterised by typical lower greenschist facies assemblage quartz-albite-muscovite-chlorite-calcite-epidote-actinolite.

**Stretching lineation ($L_2$):** A mineral stretching lineation ($L_2$) is another prominent structural feature produced during $D_2$ deformation. $L_2$ is well-developed within phyllite layers where it is easily recognised on $S_2$ cleavage surface (Fig. 4.6a). It has previously been recognised in phyllite in the area west of Tha Pla by Lumjuan and Sinpoon-anant (1987). In general, $L_2$ plunges shallowly to the northwest (Figs. 4.5b and 4.7).

## $D_3$ structures

The $D_3$ deformation episode produced mesoscopic $F_3$ open folds (Fig. 4.6b) and associated crenulations (microfolds) which crenulate $S_2$ phyllitic cleavage and is recognised almost everywhere on the $S_2$ surface in pelitic layers. However, the associated crenulation cleavage ($S_3$) is only incipiently to moderately developed and very finely-spaced (Figs. 4.6 c, d, e, f & g). This makes it very difficult to recognise in the outcrop. A crenulation cleavage, as seen in thin section is either of discrete or zonal type according to the classification of Gray (1977). In some cases, a discrete crenulation cleavage can be traced into a zonal type and dies out over short distances (Fig. 4.6b). Crenulation folding is characterised by rounded-hinge microfolds in contrast to later angular folds ($F_4$).

$F_3$ open folds and crenulations are not significantly affected by $F_4$ folding. The fold axes generally plunge to the north-northeast (Fig. 4.5c) whereas the crenulation cleavage strikes northeasterly and dips steeply to the northwest (Fig. 4.5d).

## $D_4$ structures

The structural features produced during $D_4$ deformation event are kink folds and angular folds ($F_4$) and thrust faults.

**$F_4$ kink and angular folds:** The geometry of most kink folds is characterised by asymmetrical monoclinal kink folds (Fig. 4.8a) but symmetrical conjugate kink folds are formed locally (Fig 4.8b). Kink bands ($S_4$) are rather narrow ranging from a few centimetres to a few tens of centimetres in width. In the outcrop of TZ3 metagreywackes, asymmetrical close angular folds have amplitudes of 40-400 mm and wavelengths of 20-300 mm (Figs. 4.8 c & d).

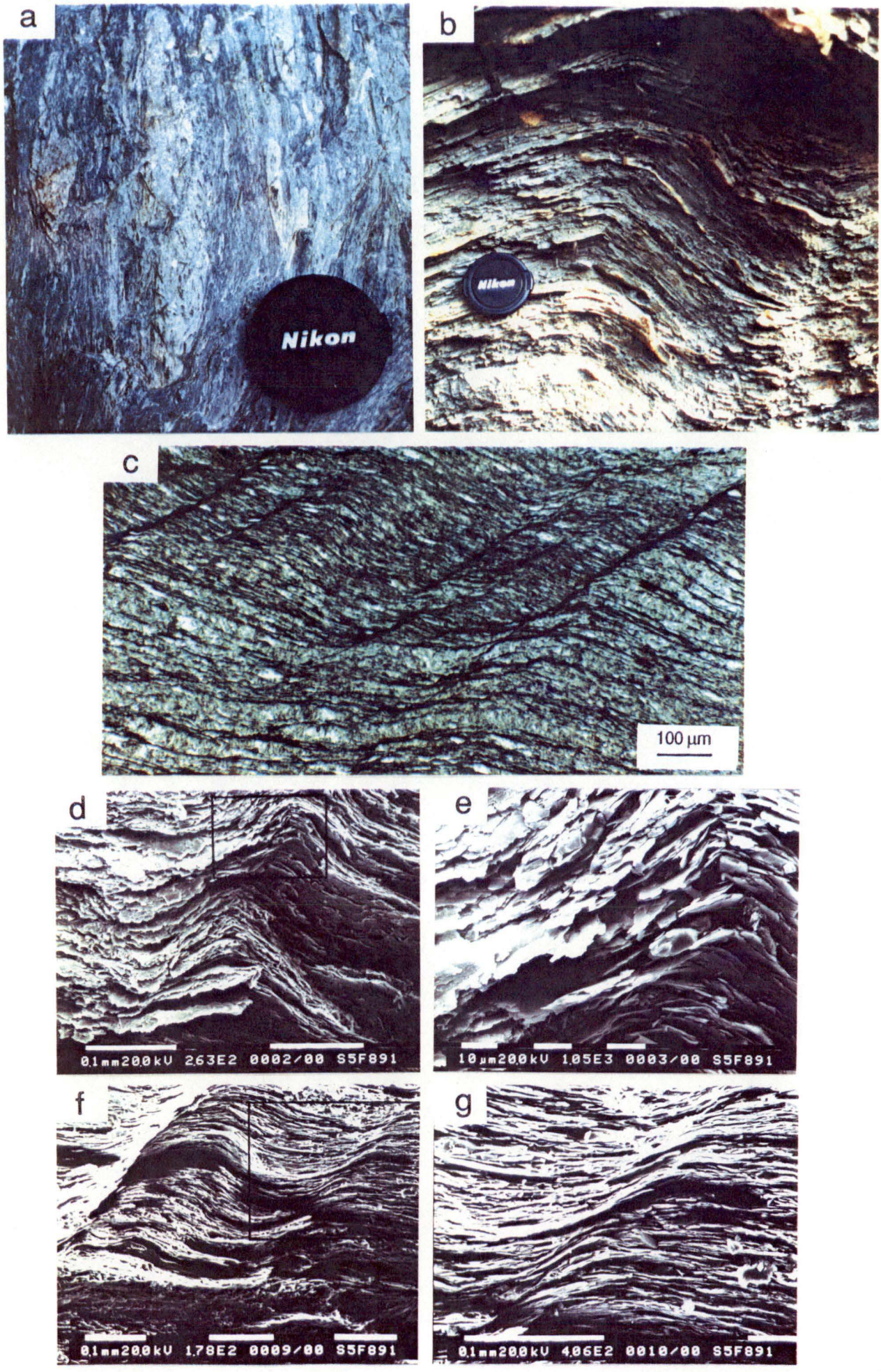
a
Nikon
b
Nikon
c
100 µm
d
0.1mm20.0kV 263E2 0002/00 S5F891
e
10µm20.0kV 1.05E3 0003/00 S5F891
f
0.1mm20.0kV 1.78E2 0009/00 S5F891
g
0.1mm20.0kV 4.06E2 0010/00 S5F891

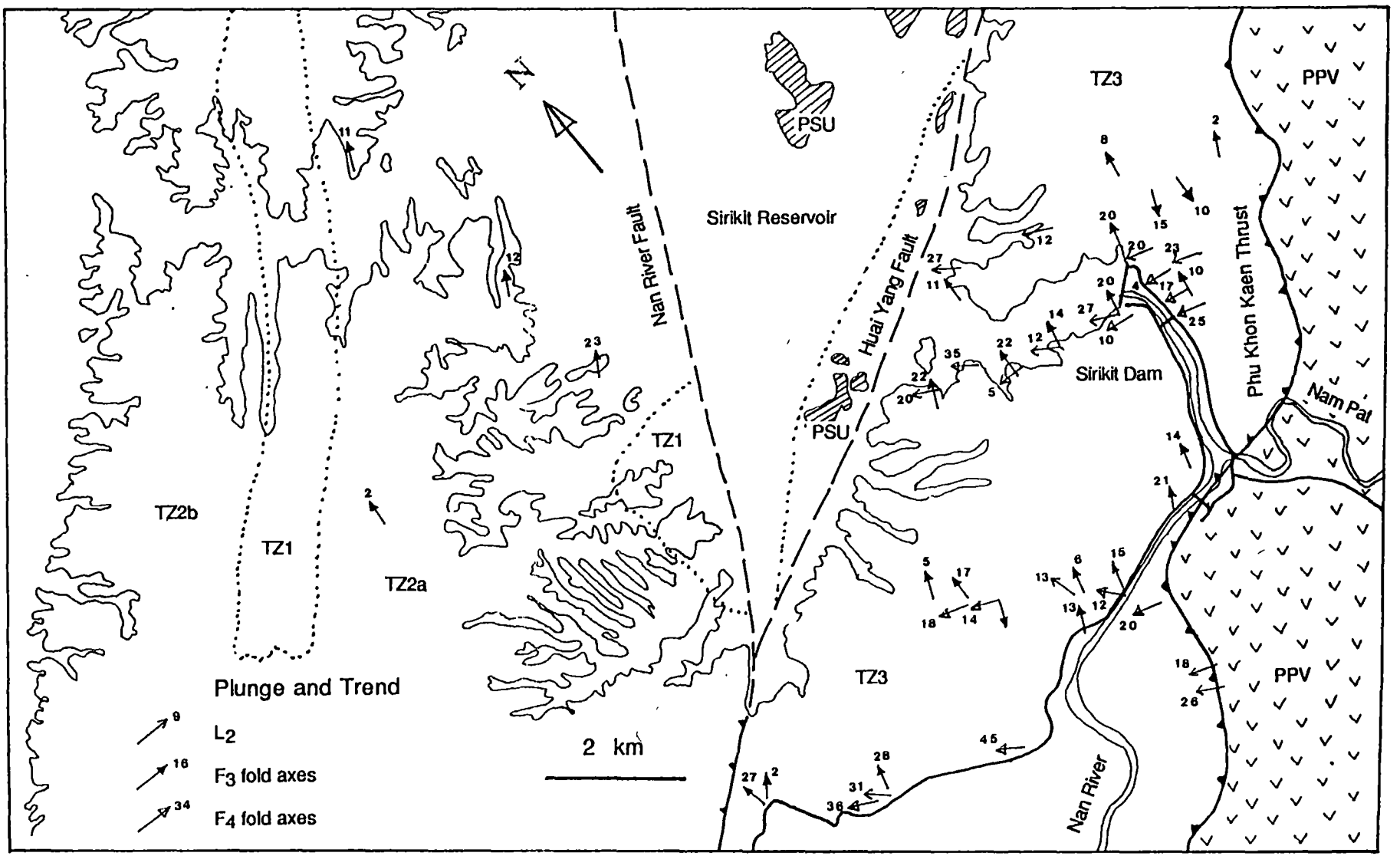


Figure 4.7 Structural map showing orientation of the linear fabric elements of the Pha Som M.C.

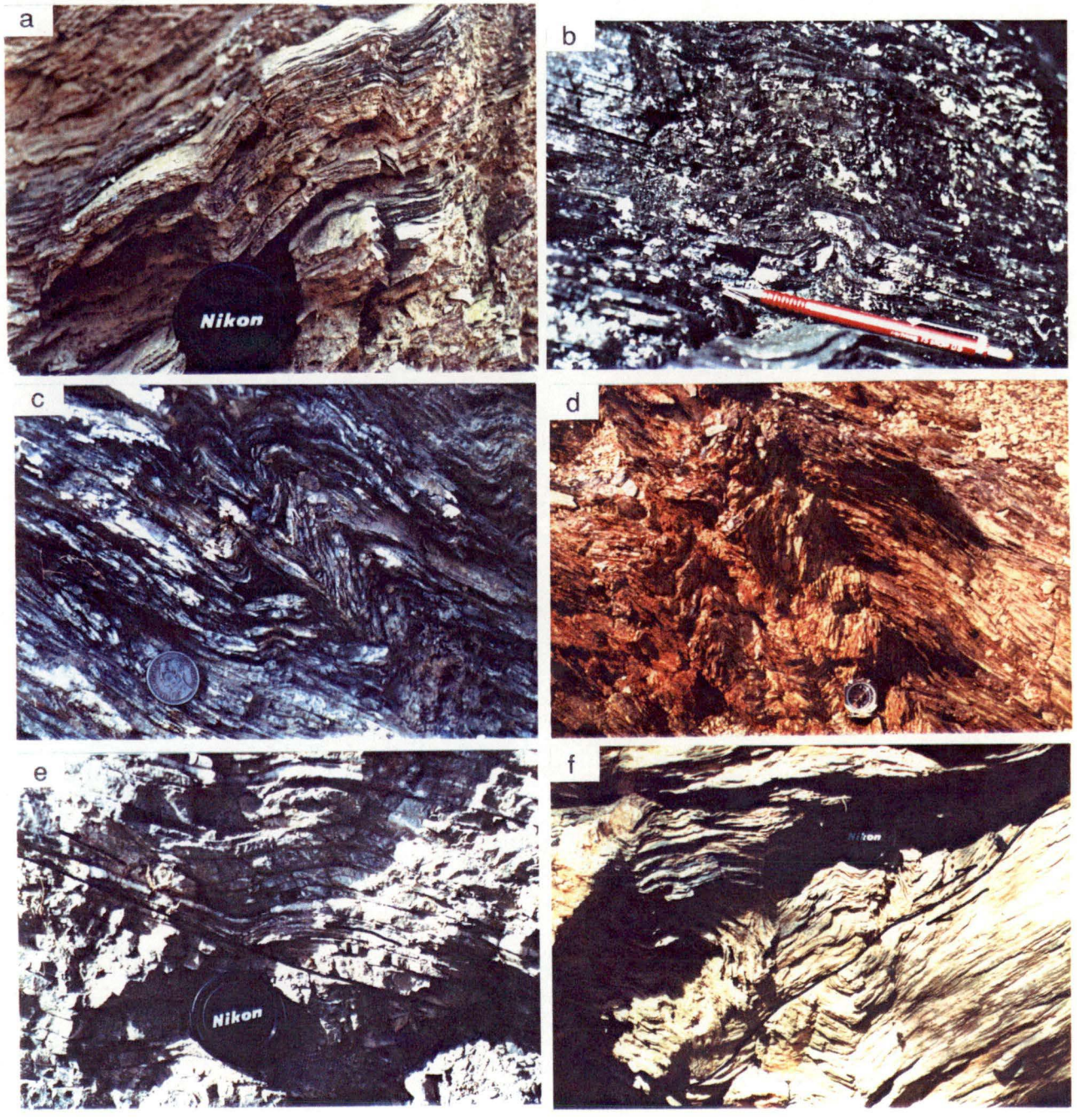


Figure 4.8 Photographs of D4 structures. (a) Asymmetrical kink folds in phyllite (looking north) at grid reference 629612/5144III. (b) Conjugate kink fold in TZ3 fine-grained quartzofeldspathic schist at grid reference 657644/5144IV. (c) Asymmetrical angular folds in phyllite at grid reference 582619/5044II (looking southwest). (d) Asymmetrical angular folds in phyllite at grid reference 604648/5144IV (looking south). (e) Small-scale thrust duplex in phyllite at grid reference 582619/5044II (looking southwest). (f) Small-scale thrust duplex in phyllite at grid reference 628617/5144III (looking northeast). Note deformed hanging wall and footwall. Scale: lens cap is 52 mm in diameter, pen is 140 mm long, coin is 32 mm in diameter and compass is 65 mm in diameter.

The orientations of kink bands and angular fold axial plane ($S_4$) are relatively variable (Fig. 4.5d). Angular fold axes and kink axes ($L_4$) plunge rather shallowly but trend variably (Fig. 4.5e). The variable trends of the $F_4$ kink folds could be partly explained by the conjugate form typical of this fold type but the range in axial plane orientation suggests this style group may include both N-S and E-W compression events.

**$D_4$ thrusts:** Thrusts associated with $F_4$ folding are exposed at a few localities. In an outcrop of TZ3 metagreywackes near the Sirikit damsite, thrust surfaces apparently truncate layering ($S_2$) and curve into parallelism with the layering at the upper part with a flat-ramp-flat geometry of thrusting. Similar thrust geometry was observed at km 47.00 on Highway 1045 (Fig. 4.8e). At this locality, the orientation data of fault striations on the thrust surfaces (Fig. 4.9) indicate northeast-directed thrusting. However, this movement direction may not simply represent the major transport direction during $D_4$ deformation as the variable trends of kink axes suggest a complex pattern. An example of $D_4$ thrust (Fig. 4.8f) where folding of $S_2$ cleavage occurs on both hanging wall and footwall blocks is present at some localities.

The form of these small scale thrusts indicates the $S_2$ cleavage was reactivated as a thrust surface during $D_4$, The early faults have a similar orientation and are probably also reactivated during $D_4$.

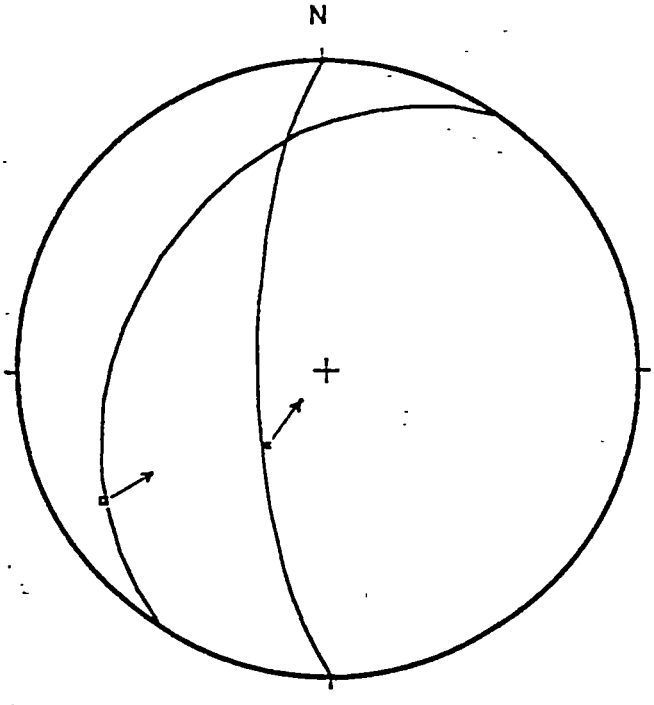


Figure 4.9 Lower-hemisphere equal-area stereographic projection of fault planes with striations at km 47.00 on Highway 1045 (grid reference 582619/5044II).

## 4.2.2 Structure of the ophiolite association

The main part of ophiolite association is enclosed within the metasedimentary package bounded by the Nan River and Huai Yang faults (Fig. 4.1). In addition, several small bodies of serpentinite are embedded within the metasedimentary rocks as well as within the Permo-Triassic Pak Pat volcanics. The gross structure of the ophiolite association is characterised by blocks of mafic-ultramafic rocks (pyroxenite, gabbro, dolerite and basalt) and equivalent metamorphic rocks (amphibolites). The blocks are commonly bounded by faults or shear boundaries and surrounded by a sheared serpentinite matrix (e.g. Fig. 4.10a). Other rock types found as blocks include sedimentary and metasedimentary rocks which are dominantly quartz schists and bedded chert with minor argillite, greywacke and marble. Each of these blocks have complex internal structures, e.g. tight to isoclinal folds in quartz schists and foliation in amphibolite blocks. The exposed boundaries of blocks are all faults or shears. The blocks have been affected by a wide range of metamorphic conditions indicating that at least some of them record a deformation history which predates the assembly of the blocks into their present structural environment. This complexity combined with the difficulty in finding exposed boundaries to blocks, and good quality exposures of the matrix have prevented detailed structural analysis of the ophiolite association. The data on mesoscopic structures of these blocks and the nature of contact with adjacent blocks that is available are described below to illustrate their deformation styles.

**Amphibolite blocks:** The dominant structural element of amphibolite blocks (i.e. garnet amphibolite, epidote/zoisite amphibolite and metahornblendite) is schistosity or gneissosity. Folds have not been observed in any of these amphibolites. Schistosity is defined by parallel to sub-parallel alignment of amphibole crystals whereas gneissosity is defined by compositional layering of amphibole and epidote/zoisite and/or plagioclase. The paucity of outcrops of amphibolites make it difficult to obtain adequate orientation data for meaningful geometrical analysis. The available data suggest that schistosity and/or gneissosity strikes northeasterly and dips steeply to the northwest (e.g. 035° 85°NW at grid reference 668757 of map sheet 5144 IV). The amphibolite blocks are always enclosed within the sheared serpentinite bodies. The relationships with blocks of other rock types are unknown.

**Serpentinites:** Serpentinites occur mainly as a sheared matrix surrounding blocks of mafic-ultramafic rocks of varying dimensions. They contain numerous shear or fault surfaces with pronounced striations. The orientation of


a

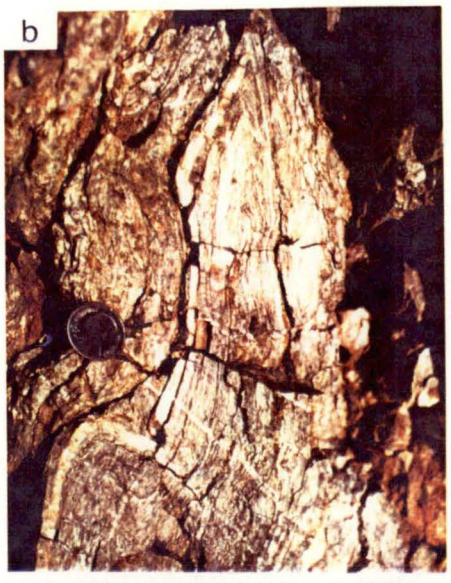
b

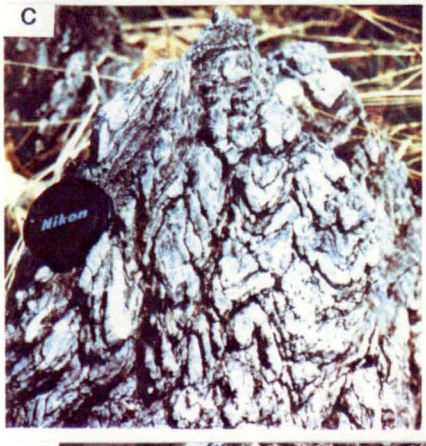
c
Nikon


d
2 1 0 1 2
CM


e


f
Nikon

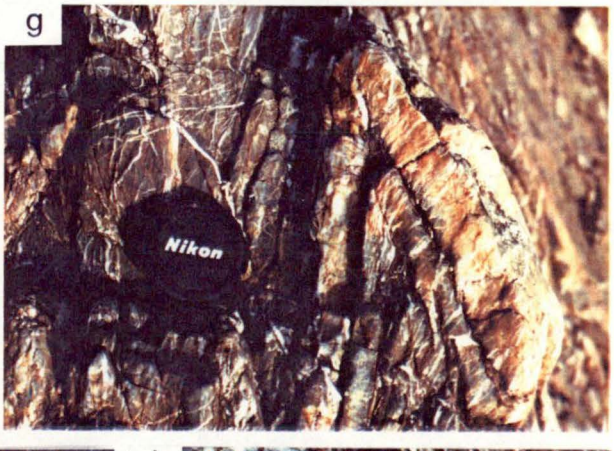
g
Nikon


h


i
Nikon


j

fault surfaces and striations varies greatly. At grid reference 668757 (map sheet 5144 IV), fault surfaces strike WNW and dip moderately or steeply to the SW and striations indicate oblique-reverse slip.

At a the small tributary creek of the Nam Pat (grid reference 709608 of map sheet 5144 III), anastomosing cleavage of serpentinites (Fig. 4.10a) strikes 010-030° and dips 64-80°NW.

Apart from the map area in Figure 4.1, slivers of serpentinite and talc schist were found within metagreywackes and phyllites in several places. For instance, at a small talc and asbestos mine near Ban Khlong Na Pong (grid reference 332515 of map sheet 5044 II), talc schist and serpentinite are enclosed in phyllites with phyllitic cleavage dipping 65°-80° NW. A fault surface between serpentinite and phyllite strikes 80° and dips 70°SW.

**Quartz schist blocks:** Quartz schists including the piemontite-bearing quartz schists occur as a large isolated block in the serpentinite melange unit (Fig. 4.1). The quartz schist block is bounded on the eastern side by the Huai Yang fault but the contact with the mafic-ultramafic blocks on the western side is not exposed. Quartz schists are characterised by a compositional layering folded into tight to isoclinal angular folds (Figs. 4.10 b, c & d). Axial planes of mesoscopic folds trend NNE and dip steeply to the WNW (Fig. 4.11).

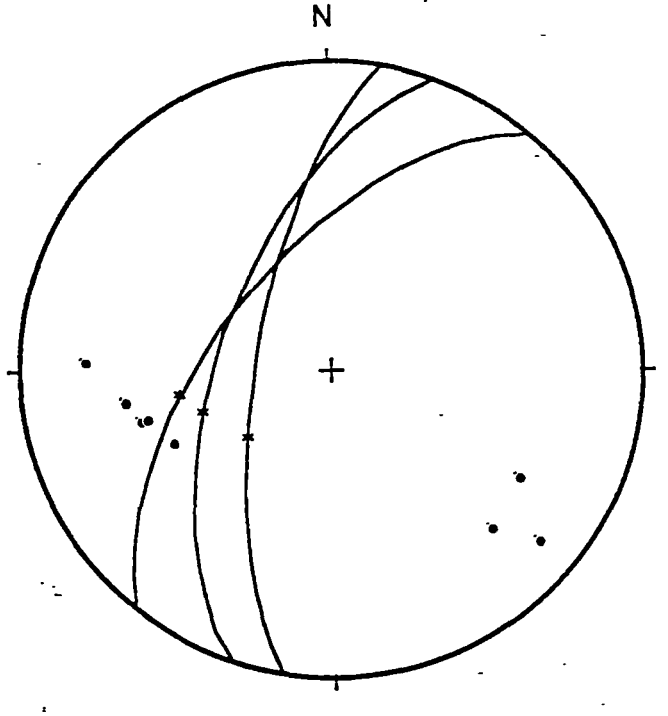


Figure 4.11 Lower-hemisphere equal-area stereographic projection of structural data of the piemontite-bearing quartz schist. Poles to differentiated layering (dots), axial-planes of tight to isoclinal ?$F_2$ folds (great circle) and fold axes (*). Poles to layering folded around a ?$F_3$ fold.

Transposition of layering is common (Fig. 4.10e). The isoclinal fold axial plane and compositional layering are apparently refolded by later kink folds (e.g. Fig. 4.10b). In thin section (e.g. sample 2/6291) schistosity is defined by parallel to sub-parallel alignment of phengitic muscovite and piemontite together with elongate quartz grains.

**Chert blocks:** Blocks of bedded chert are common in the serpentinite melange unit. At one outcrop along the Nam Pat (grid reference 713634 of map sheet 5144 III), bedded chert is interbedded with argillite and greywacke. The bedded chert blocks are characterised by close folds with narrow hinge zones (Fig. 4.10 f & g). The amplitude to wavelength ratio of these folds is relatively high. Numerous quartz veins cross-cut the bedding. At grid reference 713634 of map sheet 5144 III, the fold axial plane strikes 335°, dips 55°SW and the fold axis plunges 8° to 160°.

**Marble blocks:** Marble was observed to have a shear contact with serpentinite at grid reference 709608 (map sheet 5144 III). The recognised structure is close to isoclinal folds with high amplitude to wavelength ratio (Fig. 4.10h). The fold axial plane strikes 015° and dips 75°NW, sub-parallel to the shear boundary.

**Greywacke and argillite:** Greywacke and argillite are interbedded and locally they are also interbedded with chert. In some localities, e.g. at a small talc and asbestos mine near Ban Khlong Na Pong (grid reference 332515 of map sheet 5044 II), greywacke and argillite are in fault contact with serpentinite body. In laminated argillite, the lamination was folded into rounded close fold (Fig. 4.10i). The axial plane of this fold strikes 040° and dips 70°NW (grid reference 700623). A small-scale duplex structure of sandstone beds is observed at grid reference 708627 of map sheet 5144 III (Fig. 4.10j).

## 4.3 Structure of the Cover Sequences

The cover sequences in the Sirikit Dam area includes the Pak Pat Volcanics and the Nam Pat Group (the Huai Lat and Huai Bo Khong Formations). The cover rocks are separated from the underlying Pha Som Metamorphic Complex either by faults or unconformity. All of these cover rocks have experienced only a single phase of folding.

### 4.3.1 Structure of the Pak Pat Volcanics

The Pak Pat Volcanics are overthrust by the Pha Som Metamorphic Complex on the western side along the Phu Khon Kaen thrust (Figs. 4.1 and 4.2). On the east, they are unconformably overlain by the conglomerate beds of the Triassic Nam Pat Group. Locally, a thrust fault is also suggested by an increase in cleavage intensity towards the contact. The Pak Pat Volcanics are dominated by massive lavas. Rare folds are developed in the volcaniclastic facies. A variably-developed cleavage strikes northeasterly and dips to the northwest (Fig. 4.12). Cleavage steepens from west to east away from the Phu Khon Kaen thrust (Figs. 4.1 and 4.2).

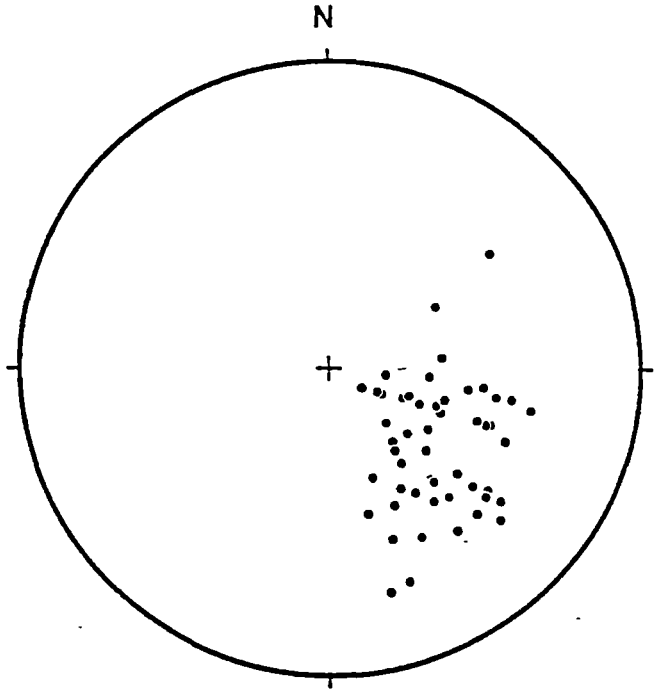


Figure 4.12 Lower-hemisphere equal-area stereographic projection of poles to cleavage in the Pak Pat volcanics (n=52).

## 4.3.2 Structure of the Nam Pat Group

### Structure of the Huai Lat Formation

The Huai Lat Formation, the lower unit of the Triassic Nam Pat Group, is characterised by very thick bedded to massive volcaniclastic conglomerate. In contrast to the well-bedded sequence of the Huai Bo Khong Formation, the conglomerate unit does not show short-wavelength folding. The cleavage developed

in this unit is variable. The cleavage intensity is strongest near the contact with the Pak Pat Volcanics in the west and decreases towards the east. Locally, the contact between the Pak Pat Volcanics and the Huai Lat conglomerates is a high strain zone possibly as a result of the rheological contrast between the units.

The other common structural features in this conglomerate unit are the high-angle faults. Fault surfaces are steeply dipping or sub-vertical and strike northeasterly. Fault striations defined by slickensides or fibrous minerals (e.g. quartz and calcite fibres) are very common. In most cases, field observation of fault striations using the techniques of Petit (1987) indicates normal dip slip that are apparently overprinted by dextral strike-slip movement. However, much of the normal slip evidence has been obliterated by late strike-slip, therefore the striation data are dominated by the strike-slip (Fig. 4.13).

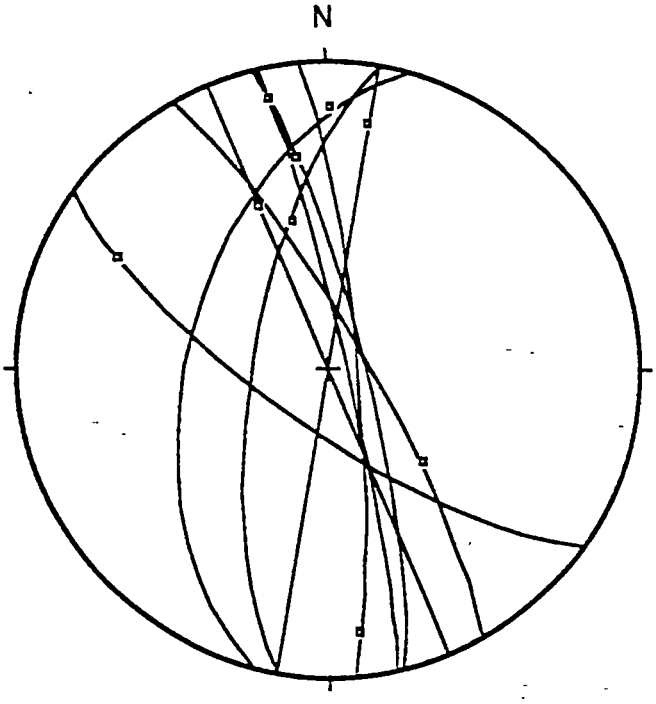


Figure 4.13 Lower-hemisphere equal-area stereographic projection of fault planes with striations in the Huai Lat Formation.

### Structure of the Huai Bo Khong Formation

The Huai Bo Khong Formation is characterised by alternating beds of sandstone and mudstone. Only one phase of folding is recognised in this turbidite. The strata have been folded into upright fold with associated axial plane cleavage and joints and small-scale limb thrusts.

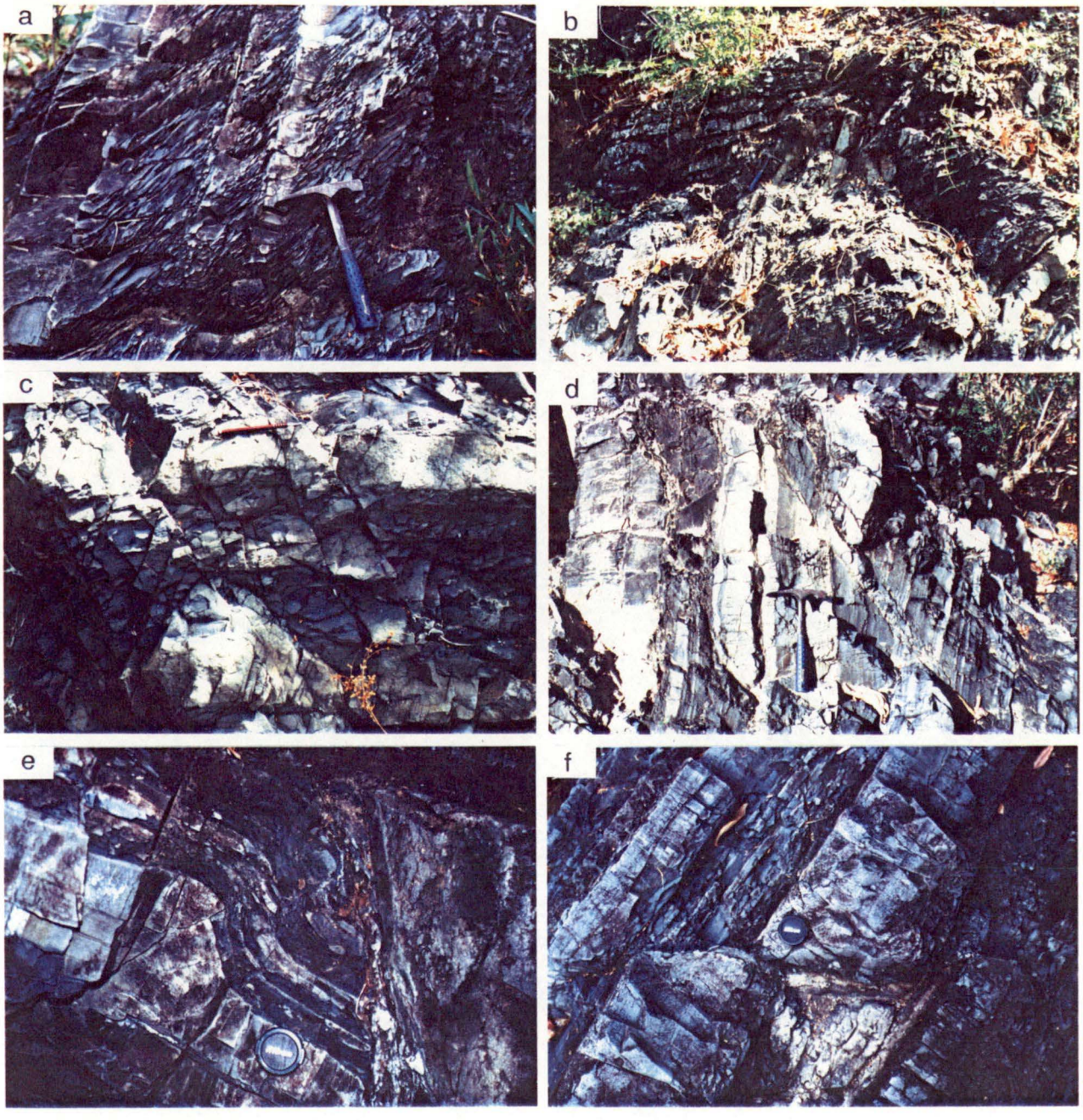


Figure 4.14 Photographs of structures in the Huai Bo Khong Formation. (a) Pencil cleavage intersects bedding in mudstone interbedded with sandstone at grid reference 717567/5144III. (b) Inclined close fold in interbedded sandstone and mudstone at grid reference 718569/5144III (looking north). (c) Small-scale conjugate faults at grid reference 716566/5144III. (d) Small-scale sinistral strike-slip fault at grid reference 717567/5144 III. (e) Small-scale fault cross cut fold hinge at grid reference 717567/5144 III. (f) Small-scale dextral strike-slip fault at grid reference 718570/5144III. Scale: hammer is 280 mm long, pen is 140 mm long and lens cap is 52 mm in diameter.

The structure commonly seen are steeply to moderately dipping strata cross-cut by a spaced cleavage (Fig. 4.14a). The cleavage is disjunctive spaced cleavage which is responsible for a crude pencil structure in mudstone beds. Locally, small-scale overturned angular folds were formed (Fig. 4.14b). Bedding ($S_0$) is largely overturned to the southeast as indicated by the cleavage-bedding relationships and sedimentary structures such as graded bedding. However, northwest-younging beds due to small-scale folds are also present. Poles to bedding surfaces are distributed in a NNW-SSE-trending great circle (Fig. 4.15a). Mesoscopic fold axes plunge to the northeast or southwest sub-parallel to cleavage/bedding intersection lineation (Fig. 4.15b). Cleavage strikes northeasterly and dips moderately to steeply to the northwest (Fig. 4.15c). Conjugate set of joints cross-cut sub-perpendicular to the axial plane cleavage (Fig. 4.15d). The geometrical relationships with major fold suggests that these joints were probably formed during folding as diagonal joints.

At grid reference 717567 (map sheet 5144 III), a detailed map (Fig. 4.16) of the stream outcrop reveals the relationships between folding and related deformational features. Bedding at this location has been overturned to the southeast. Along the bedding plane, calcite fibres indicate reverse movement. These calcite fibres plunge moderately to the NW (Fig. 4.16). It should be noted that the bedding at this location mainly strikes ENE-WSW or E-W which is different from the NE-SW strikes in most locations. At the upper left-hand corner of the map, a fold closure plunging to the north was cut off by a northeast-trending fault. On the eastern side of this fault the bedding swings from NE-SW to ENE-WSW or E-W strike. This suggests that this fault has significant strike-slip component. A series of NW-trending faults have a similar effect, e.g. on the easternmost portion of the map where an abrupt change in the orientation of bedding occurs across the fault. These brittle faults cross-cut and offset bedding (Figs. 4.14 c, d, e & f). These two sets of faults lack clear cross-cutting relationships suggesting that they are conjugate faults. Based on the geometrical relationships with the bedding, these faults are interpreted as having formed late in the folding of these Triassic turbidites.

## 4.4 Structure of the Continental Redbeds

In northern Thailand, the continental redbeds unconformably overlies the marine Triassic and Permian sequences (e.g. the 1:1,000,000 geological map of Thailand published by the Department of Mineral Resources, 1982). Locally, fault contacts between the redbeds and older rocks have been recognised. These faults are either normal or strike-slip. In the Sirikit Dam area, the continental redbeds are represented by the Middle Jurassic Phra Wihan Formation which is characterised by

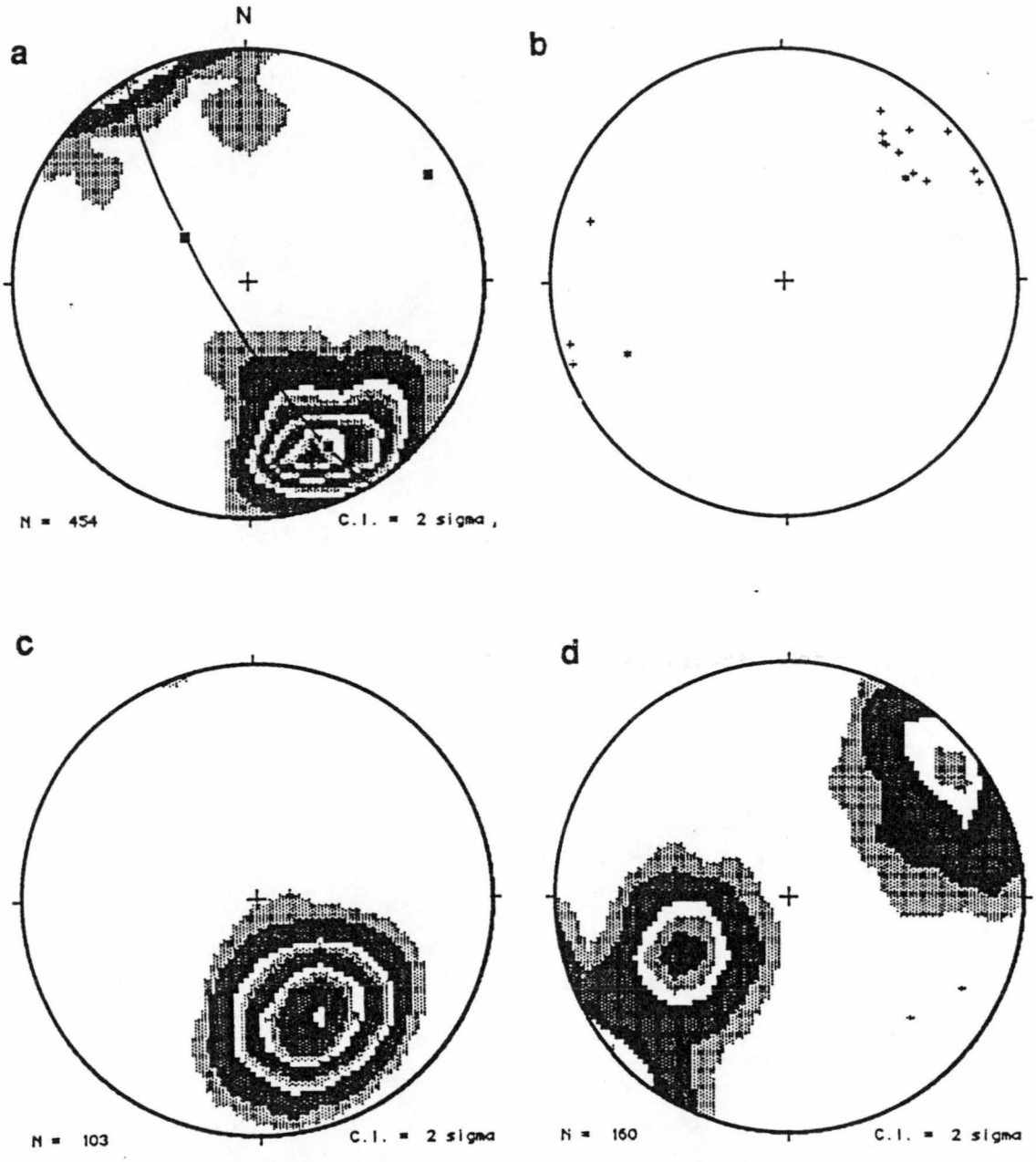


Figure 4.15 Lower-hemisphere equal-area stereographic projection of structural data of the Huai Bo Khong Formation. (a) Poles to bedding (n=454). (b) Bedding-cleavage intersection lineation (+) and mesoscopic fold axes (*). (c) Poles to spaced (pencil) cleavage (n=103). (d) Poles to joints in sandstone beds (n=160).

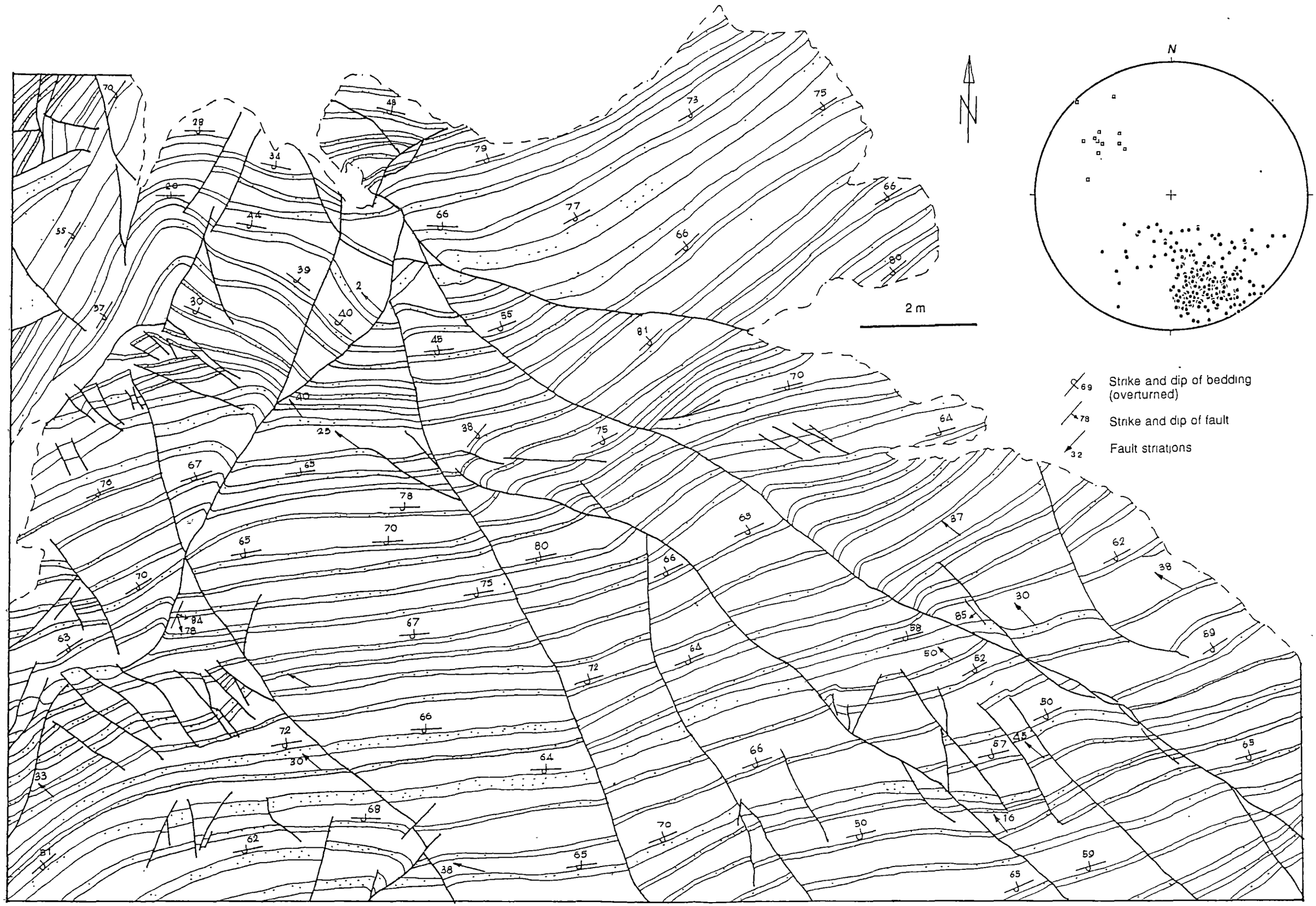


Figure 4.16 Form-line map of the Triassic Huai Bo Khong turbidites at grid reference 717567/ 5144III. Stippled layers represent sandstone beds and heavy lines indicate high-angle faults. Also shown is the lower-hemisphere equal-area projection of poles to bedding (dots) and fault striations (open squares).

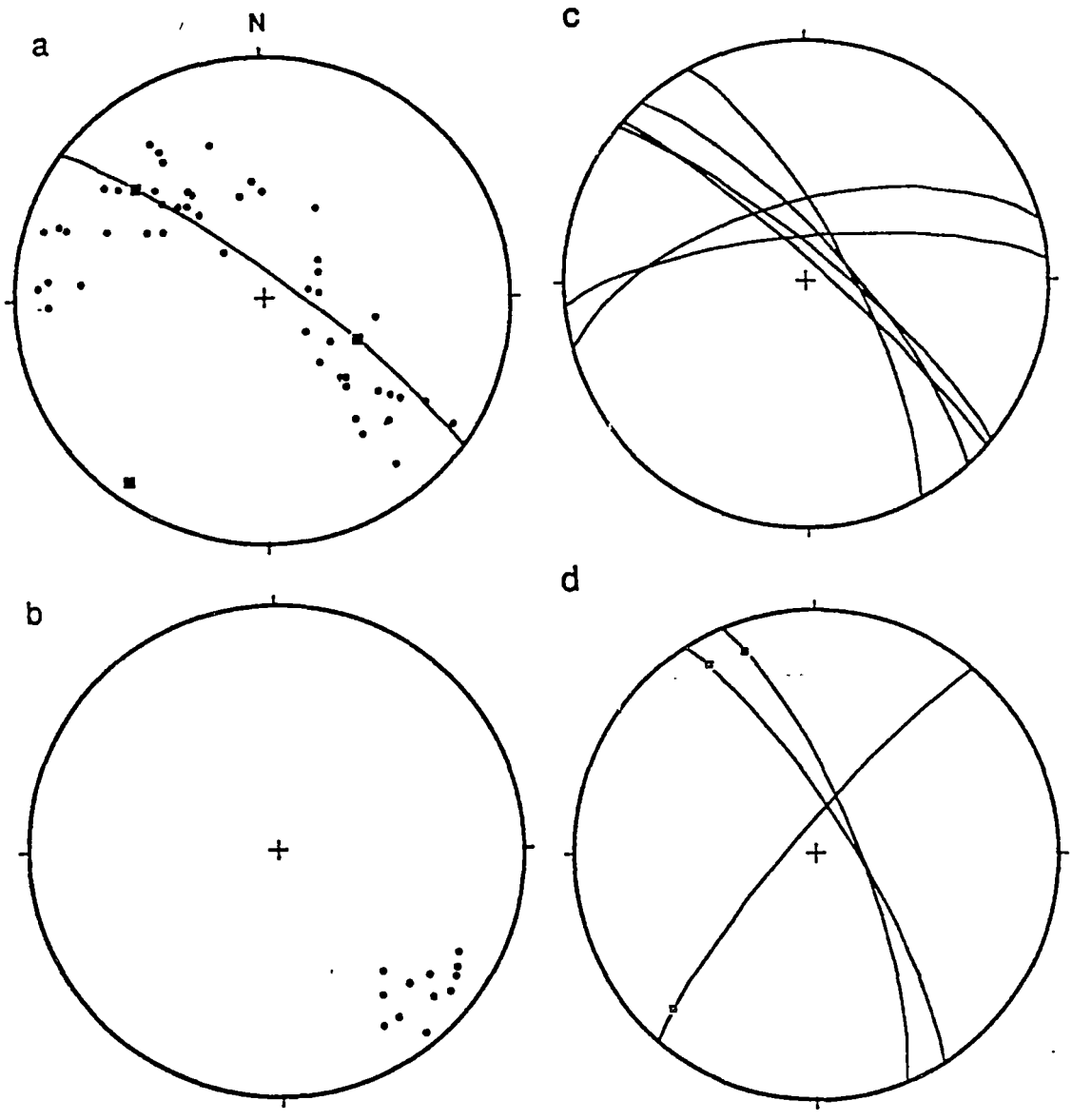


Figure 4.17 Lower-hemisphere equal-area stereographic projection of structural data of the Phra Wihan Formation. (a) Poles to bedding (n=49). (b) Poles to spaced cleavage. (c) Joints. (d) Faults with striations.

shallow to moderately dipping strata buckled into upright folds with rounded hinges in discrete zones. Poles to bedding are distributed in a NW-SE-trending great circle and the corresponding β-axis indicates a shallow-plunging open macroscopic fold (Fig. 4.17a). In the outcrop, these open folds lack axial-plane cleavage. However, a poorly-developed disjunctive spaced cleavage is locally present in siltstone and mudstone. The cleavage strikes northeasterly and dips steeply to the northwest (Fig. 4.17b). The style of folds in this formation differs markedly from that observed in the Triassic Huai Bo Khong Formation in that they lack axial-plane cleavage and are more open (i.e. with greater interlimb angles). For example the large-scale east-facing limb, east of Huai Bo Khong (Fig 4.1), is overturned and dips moderately W in the Huai Bo Khong Formation, but dips moderately E in the Phra Wihan Formation. This is interpreted as a late Triassic fold which has been tightened after the deposition of the Phra Wihan Formation. The form of the fold is typical of fault propagation folds (Fig. 4.2) suggesting that reactivation of older faults controlled the tightening of this structure.

Two sets of joints are recognised in the Phra Wihan Formation, the NW-SE-striking and ENE-WSW-striking joints (Fig. 4.17c). Two sets of small-scale high-angle faults were recognised locally, NNW-SSE-trending and NE-SW-trending faults (Fig. 4.17d). Both fault systems have strike-slip movement as indicated by fault striations.

## 4.5 Major faults

**Nan River fault and Huai Yang fault:** The ophiolite association is faulted against the metasediments of Pha Som Metamorphic Complex (Fig. 4.1). The western boundary fault is referred to as the Nan River fault after the Nan River. The eastern boundary fault is referred to as the Huai Yang fault after the small creek where outcrop of this fault was reported (Promma *et al.*, 1991). These two faults were shown on the geological map of the Sirikit Dam area prior to the impounding of the Sirikit Reservoir (Bunopas, 1981). In the present map, the Nan River fault coincides with the boundary between the TZ2a and TZ3 textural zones within the metasediments and appears to truncate the Huai Yang fault. No outcrops of these two faults have been observed in the present study. However, the traces of these faults suggest that they have steep orientation. The sense of movement along these two faults are unconstrained. The steep orientation of the faults in contrast with the shallow orientation of $S_2$ adjacent to the faults, indicates that $S_2$ has been truncated. This geometry could be explained either by rotational normal faults or out-of-sequence thrusts. The latter interpretation is favoured here for a number of reasons.

Other faults of this orientation, within the study area, have been shown to be reverse faults. Faults in the area with proven normal displacements have fault scarps or control Tertiary basins, e.g. the Tertiary Nam Pat basin in the east. The style of faulting and the juxtaposition of very different elements within the metamorphic complex suggest these faults have an early history which is interpreted here as occurring in an accretionary complex. In this environment contractional faults are more common (e.g. Hada and Suzuki, 1983; Sample and Moore, 1987). Reactivation of these structures on the Mesozoic or Tertiary may have a different sense of movement but no evidence has been found for this.

**Phu Khon Kaen thrust:** The thrust fault that juxtaposes TZ3 metagreywacke against the Pak Pat Volcanics is referred to as the Phu Khon Kaen thrust after a prominent peak about 8 km northeast of the Sirikit Dam (see Fig 6.1). This thrust fault is marked by a narrow shear zone between these two rock units. The outcrops of this shear zone were observed in several places, e.g. the Nam Pat, road-cuttings and small creeks running across the boundary between the volcanic rocks and TZ3 metagreywacke. Outcrop-scale shear bands are common within this shear zone (Fig. 4.18a). L-S tectonites and extensive quartz veins are also common within this shear zone. Shear band and quartz vein geometry together with asymmetrical kink folds consistently indicate southeast-directed thrusting. In thin section, an asymmetrical quartz porphyroclast with pressure-solution tails (Fig. 4.18b) supports southeast-directed transport based on the shear sense criteria of Simpson and Schmid (1983) and Simpson (1986). Asymmetrical pressure shadows around pyrite crystals (Figs. 4.18 c& d) also indicate non-coaxial flow path but the component of rotational strain is relatively small. The thrusting is partly contemporaneous with the $F_4$ kink style folds. The presence of a strong zone of cleavage along this fault suggests a substantial ductile component to the strain more compatible with a $D_3$ age for the thrusting. The cleavage in the footwall Pak Pat Volcanics is also correlated with this thrusting event. Correlation of structures between units is considered further in section 4.6.2.

**Uttaradit fault:** The fault which bounds the eastern side of the Nam Pat river valley is referred to as the Uttaradit fault by Piyasin (1991). The Uttaradit fault has been shown in previous geological maps (Bunopas, 1981; Charoenpravat *et al.*, 1976) but was not named. The trace of the Uttaradit fault is clearly expressed by a topographic break within the Phra Wihan Formation. It is readily recognised both from the topographic map and aerial photographs. The outcrop trace and the associated small-scale faults indicate that the Uttaradit fault is high-angle normal

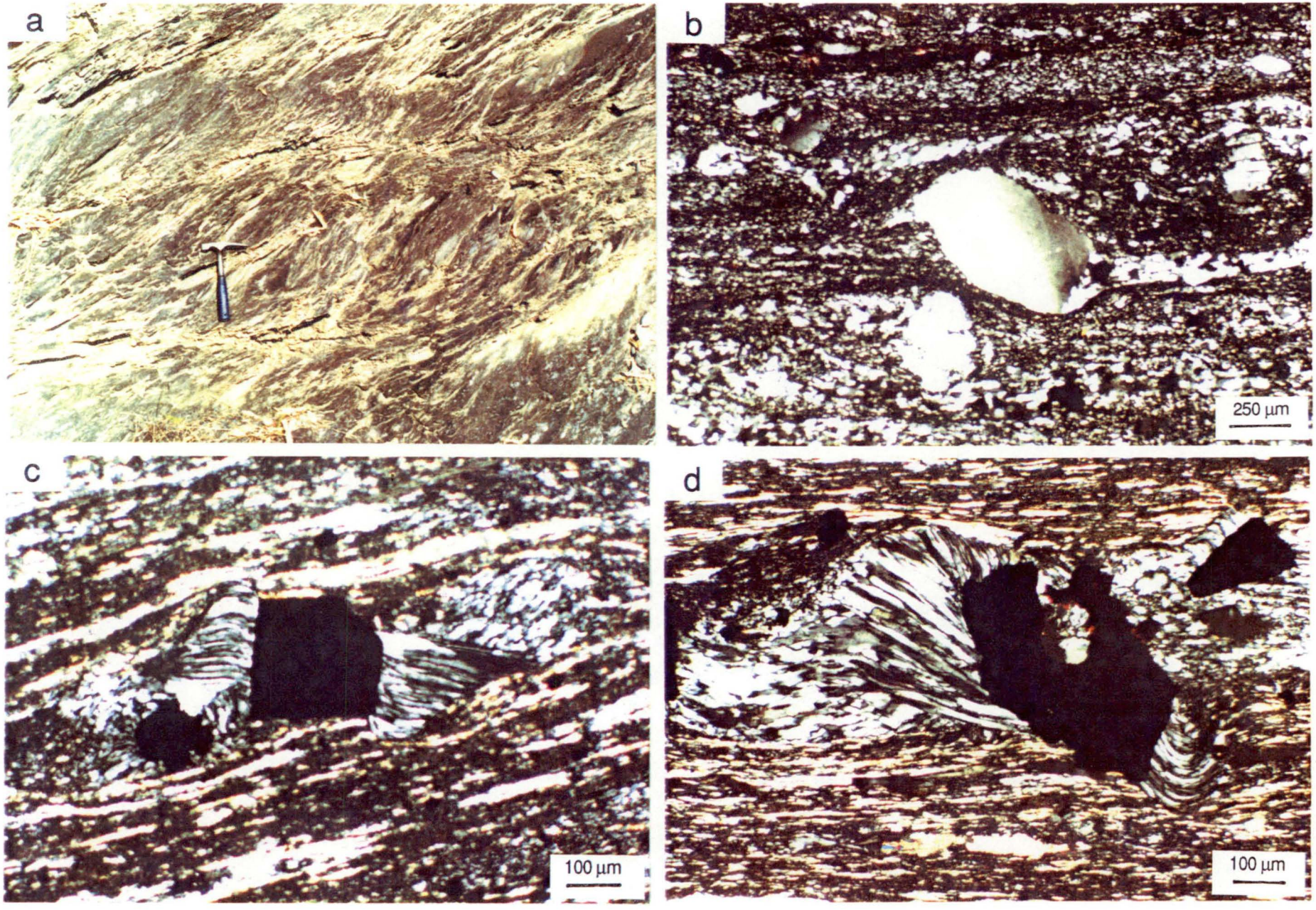
a
b
250 µm
c
100 µm
d
100 µm

fault. The fault throw is less than the thickness of the Phra Wihan Formation (i.e. less than 500 m) as the strata are repeated only within this formation (Fig. 4.2).

In addition to these major faults, there are some other faults which are recognised in the Sirikit Dam area. For example, a high-angle fault cut across the Nam Pat Group sub-parallel to Huai Bo Khong (Fig. 4.1). This fault offsets the boundary of this rock unit probably as a tear fault associated with thrusting between the volcanics and the conglomerates of the Huai Lat Formation. There are probably a great number of small-scale faults in the ophiolite association but they are not discernible due to poor exposure. These faults are at least partly responsible for juxtaposition of rocks of diverse origins within this melange unit.

## 4.6 Structural interpretation

### 4.6.1 Macroscopic structure

The interpretive structural cross-section across the Sirikit Dam area is presented in Figure 4.2. The structures shown in this cross-section are discussed from west to east as follows:

The TZ1 zone occupies a central part of the TZ2 zone. It is interpreted to be bounded on the eastern side by a fault. The boundary between the TZ1 zone and TZ2b zone on the west appears to be gradational. Serpentinised ultramafic bodies shown to be enclosed in the TZ1 zone are projected from the outcrops further south.

The structural domains within the metasediments can be established on the basis of $S_2$ orientation (see Fig. 4.1). Three domains were recognised and the domain boundaries coincide with the boundaries of textural zones. The TZ3 textural zone occupying the eastern domain have variably dipping $S_2$ due to later folding (Fig. 4.19a). The TZ2a zone is similar to a TZ3 zone in that $S_2$ also dips shallowly to the northwest (Fig. 4.19b). The TZ2b textural zone has steeply NW-dipping $S_2$ (Fig. 4.19c). Minor $F_2$ folds consistently verge to the east. This could indicate that they are on a single limb of a F2 fold but more likely this consistent vergence is a result of fault related cleavage development in a zone of imbricate thrusting and there are no large scale F2 folds.

The ophiolite association which is characterised by a serpentinite melange are shown to be bounded by the Nan River and the Huai Yang faults on either side (see discussion in section 4.5). These faults are shown here as high-angle reverse faults (i.e. out-of-sequence thrusts).

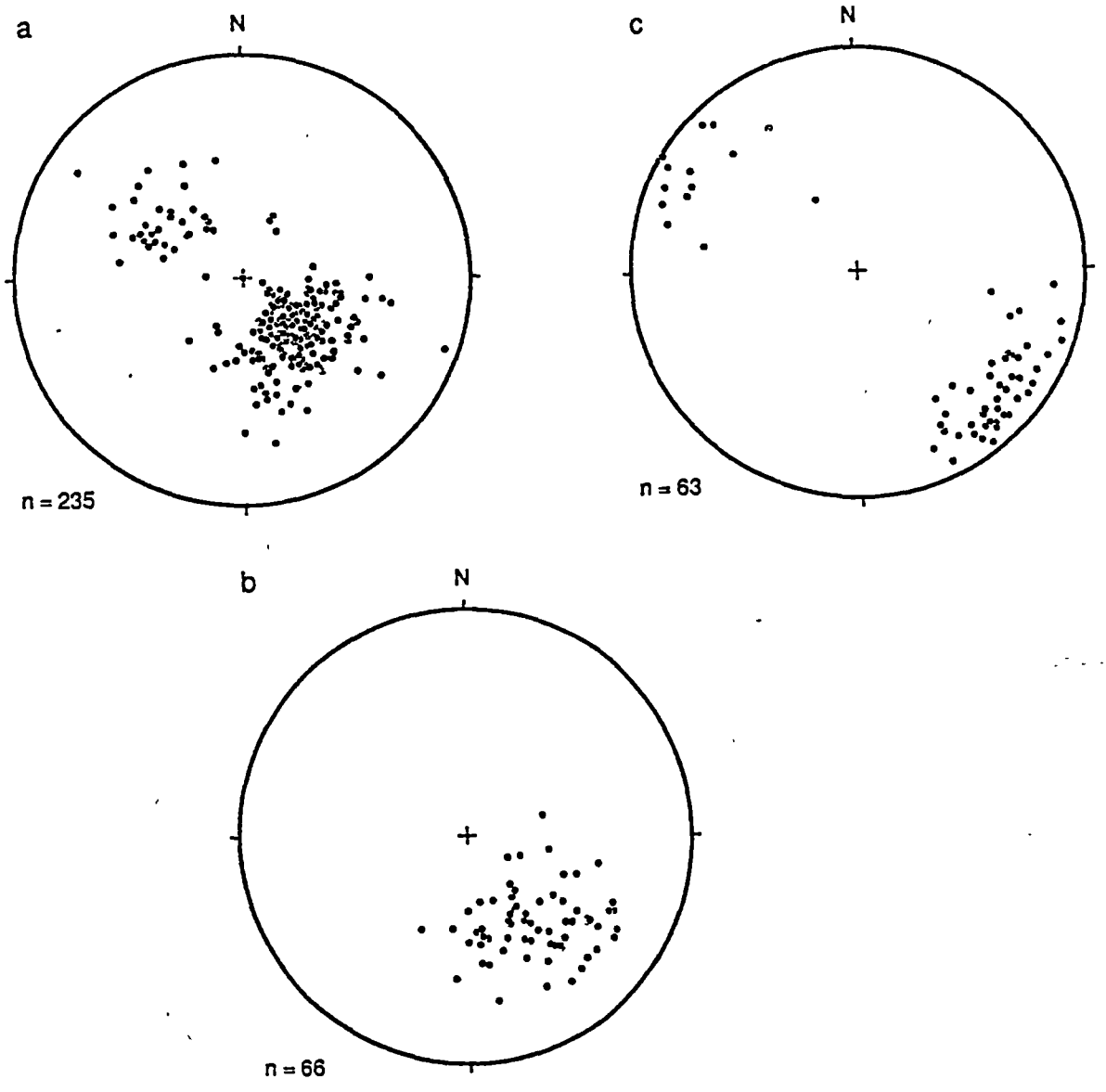


Figure 4.19 Lower-hemisphere equal-area stereographic projection of poles to S2 in each textural zone of the Pha Som M.C. (a) TZ3 textural zone. (b) TZ2a textural zone. (c) TZ2b textural zone.

The Phu Khon Kaen thrust is marked by a narrow shear zone (about 200 m wide) between the Pha Som Metamorphic Complex and the Pak Pat Volcanics. The field evidence (discussed in section 4.5) indicates southeast-directed movement for this fault.

The Pak Pat Volcanics are shown to be unconformably underlain the lower part of the Triassic Nam Pat Group (the Huai Lat Formation). The cleavage-bedding relationships and graded bedding demonstrate that the Huai Bo Khong Formation is overturned to the south east on the western limb of a gently-plunging syncline (Fig. 4.2). The Middle Jurassic Phra Wihan formation is unconformably on the Huai Bo Khong Formation and is offset by the Uttaradit fault.

## 4.6.2 Structural development

The structural history of the Sirikit Dam area can be divided into three stages. First is the development of the Permo-Carboniferous Pha Som Metamorphic Complex, second is the deformation of the Permian and Triassic cover sequences and third is the deformation of the Jurassic continental redbeds. The correlation of structural elements in these rock units are summarised in Table 4.1.

Table 4.1 Structural correlation in the Sirikit Dam area

| Structural Elements | | | | |
|---|---|---|---|---|
| Rock Unit | Pha Som Metamorphic Complex | Cover Sequence | | Phra Wihan Formation |
| | | Pak Pat Volcanics | Nam Pat Group | |
| Structural Events | | | | |
| D1 | Compositional layering (S1) | - | - | - |
| D2 | F2 folds, Stretching lineation (L2), spaced/ phyllitic cleavage (S2) | - | - | - |
| D3 | Crenulations, crenulation cleavage (S3) | Spaced cleavage | Overturned folds, axial plane spaced/ pencil cleavage | - |
| D4 | Kink and angular folds (F4), kink bands (S4), thrust faults | | | - |
| Later folding and faulting | Not recognised | High-angle faults | High-angle faults | Folds, high-angle faults |

The earliest stage in the structural evolution of the Pha Som Metamorphic Complex is represented by the compositional layering ($S_1$) which is probably associated with the first generation folds. $D_1$ structures are almost completely obliterated by $D_2$ deformational features.

$D_2$ structures are interpreted to be the results of ductile thrusting where $F_2$ folds, stretching lineation ($L_2$) and cleavages ($S_2$) developed. The *P-T* condition during $D_2$ was sub-greenschist to lower greenschist facies.

$F_3$ open folds with associated crenulations and crenulation cleavages produced by $D_3$ deformation are asymmetrical features. These can be interpreted either as the extensional structures developed under rotational deformation regime (Platt and Vissers, 1980) or the result of layer shortening with non-parallel minimum principal strain axis. At present, the latter model is more likely because some crenulations are symmetrical in profile and it can be postulated that crenulations and crenulation cleavage are the result of shortening of the $S_2$ foliation. This deformation event probably corresponds to the shortening of the accretionary wedge.

$D_4$ kink and angular folds are interpreted as the result of late thrusting which is strongly variable in movement direction.

The upright open folds and thrusts in the Triassic Huai Bo Khong turbidite sequence are similar in style and orientation to the upright open to close folds in marine Triassic sedimentary rocks exposed along the Lampang-Denchai and Phrae-Sirikit Reservoir transects (detailed discussions are given in Chapters 8 and 9). The Triassic rocks have been subjected to only a single phase of folding with which the associated regional cleavage strikes northeasterly. The folding event together with the cleavage formation are constrained to be Late Triassic. However, the radiometric age of white mica in the Sirikit Dam area of around 90 Ma (Upper Cretaceous) has been reported (Ahrendt *et al.*, 1993). This age is interpreted here to be the result of resetting during later movement along the Uttaradit fault rather than to the folding.

The correlation of this single phase of folding and related thrusting with the structures in the Pha Som Metamorphic Complex is ambiguous. The direct correlation based on orientation would suggest that $D_3$ in the Pha Som Group correlates with the folding in the cover sequence. In contrast there is a spatial correlation of some $D_4$ kinks with late thrusting in the Pha Som Group. The most likely correlation is that $D_3$ correlates with folding in the cover sequence and some of the D4 kinks are equivalent structures forming along fault surfaces. The orientation of these structures is similar to but steeper than the $S_2$ surface in the Pha Som Metamorphic Complex. Many of the high strain zones involved rotated and enhanced $S_2$ even where the faults have demonstrable post-Permian movement. The

dominance of southeast directed thrusting in this Sirikit Dam area may be a result of extensive reactivation of older structures.

The Phra Wihan Formation, and correlates, have an unusual structural history. Over most of the area they are very gently folded but along discrete linear zones there are steep limbs within these late Mesozoic redbeds. One of these zones of steep bedding forms the eastern margin of the Sirikit Dam area (Fig 4.1). This zone is interpreted as the result of reactivation of a Late Triassic fault propagation fold.

High angle faults common in the Huai Lat conglomerates and Phra Wihan sandstones are interpreted here as the Tertiary structures based on the cross-cutting relationship with the Jurassic-Cretaceous redbeds. These faults have normal displacements that are partly overprinted and obliterated by strike slip movements. An alternative interpretation is that the normal faults were formed as the result of extension following the main collision in Late Triassic and were reactivated by later Tertiary strike-slip faults.

## 4.7 Summary

Four structural phases ($D_1$-$D_4$) and upright folding and high-angle faulting are recognised in the metasediments of the Sirikit Dam area. The earliest recognisable structure is compositional or differentiated layering. $D_2$ structures are characterised by $F_2$ folds, differentiated layering/phyllitic cleavage ($S_2$) and a stretching lineation ($L_2$). These structures are interpreted to correlate with early thrusting. $D_3$ produced open folds with an associated crenulation cleavage. $D_4$ deformation produced kink folds and angular folds related to late thrusting.

The upright close to open folds in the Triassic Huai Bo Khong turbidite sequence is similar in style and orientation to the upright close to open folds in Triassic sequence along the Lampang-Denchai and Phrae-Sirikit Reservoir transects (Chapters 8 and 9). Only a single phase of folding was recognised in the Triassic sedimentary rocks. It produced northeast-trending folds and thrusts.

High-angle faults with normal displacement partly overprinted by strike-slip movements are interpreted as Tertiary structures.

$D_1$ and $D_2$ in the metasediments pre-date deformation of the cover sequence. $D_3$ structures in the metasediments are probable correlates of the cleavage in the Pak Pat Volcanics and upright folds in the Triassic Nam Pat Group turbidites. $D_4$ structures are probably correlates of thrusting in the cover sequence.

# Chapter 5

# METAMORPHISM OF ROCKS IN THE SIRIKIT DAM AREA

## 5.1 Introduction

In the present study, a suite of complexly deformed metamorphic rocks in the Sirikit Dam area are collectively referred to, for convenience, as the Pha Som Metamorphic Complex. This new name encompasses the previous two separate rock units, i.e. the "Pha Som Group" and the "Pha Som Ultramafics" of Bunopas (1969, 1981). The dominant metamorphic rocks in the Sirikit Dam area are low-grade psammites (metagreywackes) and associated pelites (phyllites) which form the metasedimentary unit of the Pha Som Metamorphic Complex. Tectonically emplaced into these low-grade metasedimentary rocks is the ophiolite association containing blocks of amphibolites and serpentinised mafic-ultramafic rocks including piemontite-bearing quartz schists. In addition to these important metamorphic units, the Pak Pat Volcanics has also been subjected to sub-greenschist facies regional metamorphism. The rocks which have largely undergone diagenesis include greywackes and shale of the Nam Pat Group and quartzose sandstones of the Phra Wihan Formation.

The metamorphic grade of the metasediments was inferred to be greenschist facies on the basis of mineral assemblages by Thanasuthipitak (1978) and Bunopas (1981). Mafic rocks containing hornblende were simply referred to as hornblendite or hornblende peridotite implying an igneous origin.

Macdonald and Barr (1984) was the first to report the occurrence of amphibolite and garnet amphibolite in association with the mafic and ultramafic plutonic rocks of the ophiolite association in the Nan River area. Later, Barr *et al.* (1985) reported the occurrence of crossite blueschist associated with quartzite of the metasediments in Doi Phuk Sung area about 70 km NNE of the Sirikit Dam. Their studies concentrated on petrochemistry and tectonic setting of the ophiolite association and no precise *P-T* estimates were given for the metamorphic rocks.

For garnet amphibolites from the same area, Panjasawatwong (1991) reported the chemistry of coexisting metamorphic minerals and calculated the equilibration temperature to be 600-780 °C at 5 kbar. The crossite-epidote blueschists, on the other hand, were inferred from a petrogenetic grid to have formed at a pressure of about 7 kbar and a temperature in the range 390-450 °C.

In many regions around the world, metamorphic study has been proven to be very useful to complement structural work and aid interpretation of relevant tectonic processes (e.g. Turner, 1981; Berry and Grady, 1981; Kemp *et al.*, 1985; Jaygo and Blake, 1989; Gottschalk, 1990). Understanding the metamorphic history of the Sirikit Dam area is an important additional constraint in the reconstruction of tectonic scenario of the northern Thailand region. The aims of this chapter are to document the *P-T* conditions and timing of metamorphism of the important metamorphic units and to outline the metamorphic history of the Sirikit Dam area.

## 5.2 Geothermobarometric Techniques and Age Constraints

The *P-T* conditions of metamorphism of rocks in the Sirikit Dam area can be approximated using petrogenetic grids of the relevant mineral assemblages. For more precise estimations, various techniques in quantitative geothermobarometry were applied. These techniques include:

(i) experimentally-calibrated geothermobarometry or "directly-calibrated method" such as garnet-clinopyroxene geothermometers of Ellis and Green (1979), Pattison and Newton (1987) and Yang (1992), and phengite geobarometry of Massonne and Schreyer (1987).

(ii) empirically-calibrated geothermometers such as garnet-hornblende geothermometer (Graham and Powell, 1984), phengite-chlorite geothermometer (Chapter 2), plagioclase-muscovite geothermometer (Green and Usdansky, 1986) and chlorite geothermometer (Cathelineau and Nieva, 1985; Cathelineau, 1988).

(iii) thermodynamic calculations or "internally-consistent methods" (e.g. Powell and Holland, 1988; Brown *et al.*, 1988).

The precision of each geothermobarometric technique depends on various factors which will be discussed together with the estimates derived from each of them. Most techniques yield reasonably good *P-T* estimates for these rocks. However, the estimates from thermodynamic calculations have high uncertainties due to lacks of well-constrained phase equilibria and appropriate activity-composition relations among relevant end-member components as well as problems in estimating $Fe^{2+}$ / $Fe^{3+}$ for the phases involved .

The relative ages of the metamorphic units were inferred from structural and stratigraphic relationships with sedimentary units that have well-established stratigraphic ages. Timing of metamorphism was further constrained using available radiometric-age data (e.g. Barr and Macdonald, 1987; Drs. Y. Panjasawatwong and A.J. Crawford, pers. comm., 1993).

# 5.3 Metamorphism of the metasediments of the Pha Som Metamorphic Complex

## 5.3.1 Psammites

Psammites are the principal component of the metasediments. The vast majority of psammites have quartzofeldspathic lithology except in a few localities where psammitic rocks contain abundant volcanic lithic fragments. Systematic textural change from clastic sandstone to fine-grained schist with increasing deformation and metamorphism has been observed. Regardless of textures, psammites contain typical lower-greenschist facies mineral assemblage, quartz + albite + phengitic muscovite + chlorite ± calcite ± epidote ± actinolite ± pumpellyite. In terms of texture, they can be classified as greywacke, semischist, and fine-grained schist (Spry ,1969) corresponding to psammitic rocks of Chl1, Chl2 and Chl3 textural zones of Turner (1938) respectively. To avoid metamorphic connotation of the abbreviation "Chl" (derived from chlorite zone), a textural zones, TZ1, TZ2 and TZ3 are used herein instead of Chl1, Chl2 and Chl3 textural zones of Turner (1938). TZ2 zone is subdivided into TZ2a and TZ2b subzones based on variation in textural development (see petrographic description below). The distribution of the textural zones in the Sirikit Dam area is shown in Figure 5.1.

### Petrography

#### Greywackes (TZ1 textural zone)

On the basis of mineralogical composition, greywackes can be divided into two distinct types, i.e. quartzose lithic or feldspathic greywacke and quartz-poor lithic greywacke.

(i) Quartzose lithic or feldspathic greywacke (Fig.5.2a) consists chiefly of monocrystalline and polycrystalline quartz (greater than 50%) with subordinate schist and phyllite fragments, small amounts of albitised plagioclase and chert. Quartz is of volcanic origin and shows either straight or slightly undulatory

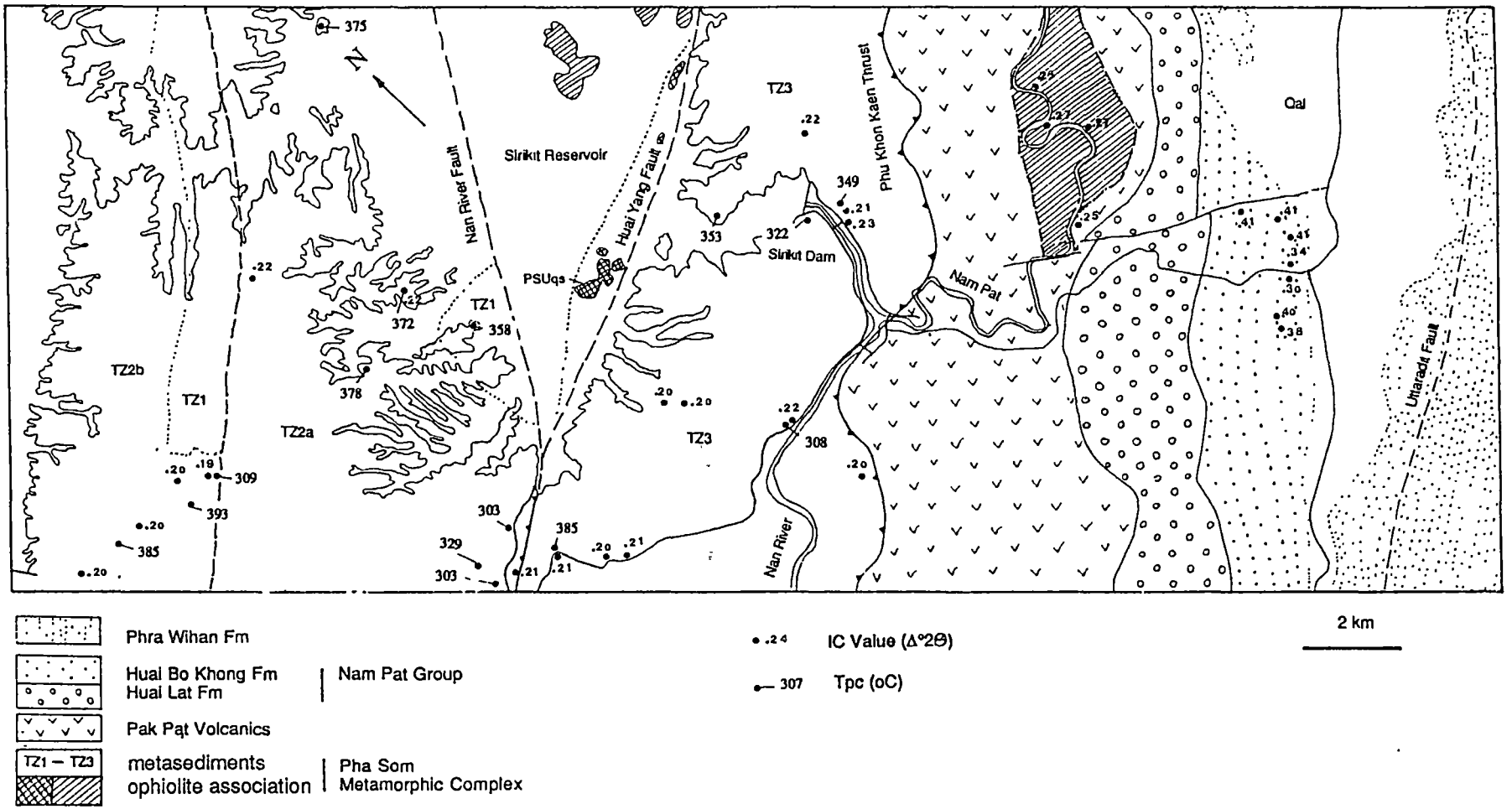


Figure 5.1 Geological map of the Sirikit Dam area showing distribution of the Pha Som M.C. and textural zones TZ1, TZ2a, TZ2b and TZ3 (PSUqs = quartz schist and Qal = Quaternary alluvium). Also shown are the illite crystallinity (IC) values of pelites and the calculated temperatures based on phengite-chlorite geothermometer for psammites and pelites.

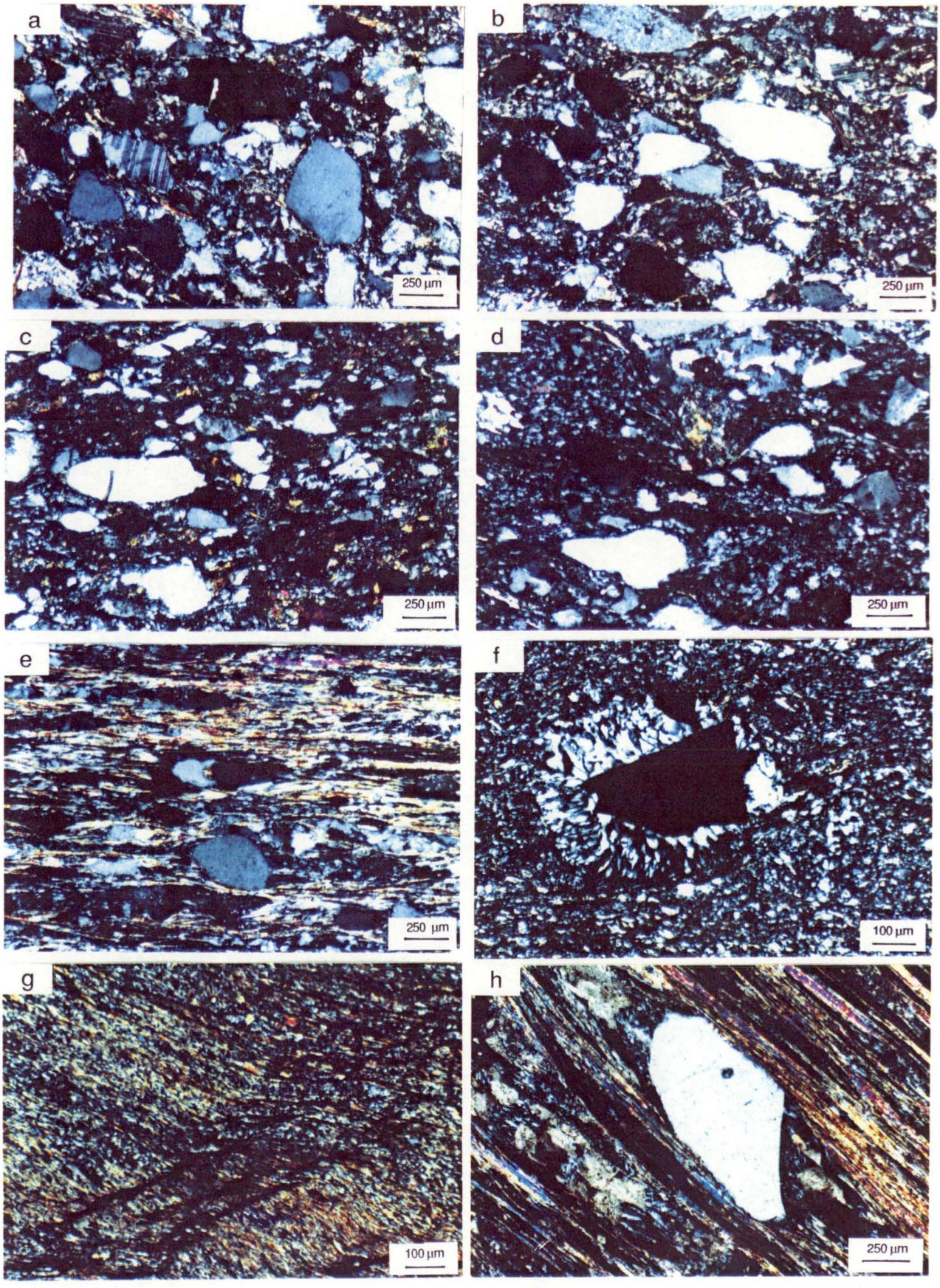
a
250 µm
b
250 µm
c
250 µm
d
250 µm
e
250 µm
f
100 µm
g
100 µm
h
250 µm

extinction. Polysynthetic twinning in albite is common. Tourmaline and pyrite are present as accessories. Grains are poorly- to moderately-sorted and angular to subangular with mean grain size of 250 μm to 500 μm and are largely intact with weakly developed mortar texture. Partially recrystallised matrix (5-10%) is made up of microcrystalline quartz, fine-grained muscovite, albite, chlorite and epidote. Grains are partly cemented by calcite. The arrangement of platy muscovite flakes is either random or defines cleavage. Schistosity has not developed.

(ii) Quartz-poor lithic greywacke has a volcanic source. The framework grains consist chiefly of volcanic lithic fragments and subordinate albitised plagioclase and monocrystalline and polycrystalline quartz. Haematite is present as an accessory mineral. Grains are moderately-sorted and subangular with mean grain size of 400-600 μm. Grains commonly show lobate grain boundaries. Partially recrystallised matrix (less than 15 %) is made up of microcrystalline quartz, fine-grained muscovite, albite and chlorite. Plagioclase is largely replaced by epidote, calcite and to a lesser extent fine-grained muscovite. Chloritisation of mafic minerals is common.

### Semischists (TZ2 textural zone)

The semischists (Figs 5.2b&c) are metagreywackes that show slight to moderate recrystallisation of the original clastic grains and correspond to the metagreywackes of Chl2 textural zone of Turner (1938). TZ2a semischists (Fig. 5.2b) are distinguished from TZ2b semischists (TZ2c) on the basis of degree of recrystallisation of clastic grains. The framework grains of both TZ2a and TZ2b semischists consist chiefly of monocrystalline and polycrystalline quartz with small amounts of chert, albitised plagioclase, muscovite and chlorite. Tourmaline and zircon are present as accessories. Grains are poorly-sorted and angular to subangular with mean grain size of 400 μm. The sheared and partially recrystallised matrix is over 15 % (this probably includes deformed unstable grains) and grains are partly cemented by calcite. A weakly-developed schistosity is defined by parallel to subparallel alignment of fine-grained platy muscovite in combination with dimensional-preferred orientation of quartz and albite. Clastic biotite is completely replaced by chlorite. Pyrite is also present presumably as a diagenetic mineral.

### Fine-grained schist (TZ3 textural zone)

The rocks of the fine-grained schist texture (Figs. 5.2d&e) are those that develop more pronounced schistosity and have been subjected to more intense

recrystallisation than semischists. In thin section, they are characterised by a strongly sheared rock consisting of porphyroclasts of quartz and plagioclase set in a recrystallised and schistose matrix of microcrystalline quartz, phengitic muscovite, chlorite, epidote, actinolite, calcite and rare pumpellyite. Accessory zircon is also present. Porphyroclasts have a mean grain size of 300 μm and are flattened. Asymmetrical quartz grains commonly show undulatory extinction and possess serrated grain boundaries. Muscovite porphyroclasts display mica-fish structure. In the matrix, fine-grained platy muscovite invariably shows strong parallelism and wrap around porphyroclasts of quartz and plagioclase. Pressure shadows are also common around some pyrite crystals (Fig. 5.2f).

### 5.3.2 Pelites

#### Petrography

A few varieties of pelites (Figs. 5.2g&h) were recognised. They differs from each other in the proportions of constituent minerals. These include muscovite phyllite, chlorite-muscovite phyllite, muscovite-chlorite phyllite and quartz-muscovite phyllite.

The assemblage phengitic muscovite + chlorite + quartz + albite ± epidote ± K-feldspar ± calcite is the most common among the studied pelitic samples. Rare ankerite occurs as rhomb-shaped grains in some samples (e.g. 2/5291 in Fig. 5.2h).

### 5.3.3 Mineralogy of psammites and pelites

The mineral assemblages in psammites and associated pelites are given in Table 5.1. The most common assemblage is quartz + albite + muscovite + chlorite + epidote, with or without actinolite, pumpellyite, calcite and sphene.

**Quartz :** Quartz is a ubiquitous phase in all psammitic rocks of all textural zones. It occurs in two modes, i.e. larger clastic grains and microcrystalline matrix. With increasing intensity of textural adjustment (i.e. from TZ1 to TZ3 textural zone), wavy extinction and deformation lamellae become more common in clastic grains. In pelites, quartz is a minor phase. It occurs as tiny grains interspersed with more abundant muscovite and chlorite.

**Albite :** All plagioclase feldspars in psammitic and pelitic rocks are albite ($An_{0-6}$). Albite is present in 95% of psammitic samples. In thin section, albite is generally clear and albite twinning is fairly common. XRD analyses indicate the

Table 5.1 Mineral assemblages of the studied psammites and pelites of the Pha Som M.C.

| Sample no. | Rock Type | Qtz | Kfs | Ab | Ms | Chl | Cal | Ep | Act | Pump | Spn | Pyrt | Hem | Rt | Cpx |
|---|---|---|---|---|---|---|---|---|---|---|---|---|---|---|---|
| 5/8291 | Phyllite | X | | X | X | X | | X | | | | X | | | |
| 3/9291 | " | X | | | X | X | X | | | | | | | X | |
| 6/9291 | " | X | | X | X | X | | | | | | | | | |
| 3/8291 | Greywacke | X | | X | X | X | | X | | | | | | | |
| SD-97 | " | X | | X | X | X | | | | | | | | | |
| SD-225 | " | X | | X | | X | X | X | | | | | | | |
| SD-227 | " | X | | X | | X | X | X | | | | | | | X |
| 1/7291 | Semischist | X | | X | X | X | X | | | | | | | | |
| SD-60 | " | X | | X | X | X | X | X | | | | | | | |
| SD-61 | " | X | | X | X | X | X | X | | | | | | | |
| SD-97 | " | X | | X | X | X | X | X | | | | | | | |
| SD-99 | " | X | | X | X | X | X | | | | | | | | |
| SD-193 | " | X | | X | X | X | | | | | | | | | |
| P-102 | " | X | | X | | X | | X | X | | X | | | | |
| P-104 | " | X | | X | | X | | X | X | | X | | | | |
| P-106 | " | X | | X | X | | | X | X | | | | | | |
| P-107 | " | X | | X | X | | | X | X | | X | | | | |
| 1/6291 | Fine-grained schist | X | | X | X | | | X | | | X | | | | |
| 15/6291 | " | X | | | X | X | X | X | | | | | | | |
| SD-42 | " | X | | X | X | X | X | | | | | | | | |
| SD-64 | " | X | | X | X | X | X | | | | | | | | |
| SD-104 | " | X | | X | X | | X | X | | X | X | | | | |
| SD-148 | " | X | | | | X | X | | | | | | | | |
| SD-148.1 | " | X | | X | | X | X | X | | | | | | | |
| SD-150 | " | X | | X | | X | | X | | | | | | | |
| SD-165 | " | X | | X | X | X | X | | | | X | | | | |
| SD-198 | " | X | | X | X | X | | X | X | X | | | | | |
| SD-209 | " | X | X | X | | X | | X | | | | | | | |
| SD-211 | " | X | | X | X | X | X | | | | | | | | |
| SD-213 | " | X | | X | X | X | X | | | | | | | | |
| SD-217 | " | X | | X | X | X | X | X | | | | | | | |
| SD-221 | " | X | | X | X | X | X | X | | X | | | | | |

Table 5.2 Representative electron microprobe analyses of albites in psammites and pelites of the Pha Som Metamorphic Complex.

| Sample no. | 2/5291 | 6/9291 | 3/8291 | SD-97 | 1/7291 | SD-60 | SD-99 | SD-193 | 1//6291 | SD-42 | SD-64 | SD-104 | SD-165 | SD-198 | SD-211 | SD-213 | SD-217 | SD-221 | P-106 | P-107 |
|---|---|---|---|---|---|---|---|---|---|---|---|---|---|---|---|---|---|---|---|---|
| Point no. | Ab1 | Ab5 | Ab2 | Ab6 | Ab1 | Ab4 | Abm | Ab3 | Ab1 | Ab4 | Ab3 | Ab1 | Abm | Abm | Abm | Ab5 | Ab4 | Abm | Abm | Abm |
| SiO2 | 68.52 | 69.20 | 68.35 | 67.85 | 68.47 | 67.11 | 68.34 | 68.32 | 68.96 | 68.29 | 68.53 | 68.02 | 68.23 | 68.21 | 68.25 | 66.12 | 68.20 | 68.11 | 68.09 | 68.01 |
| Al2O3 | 19.33 | 19.53 | 19.32 | 19.68 | 19.38 | 20.09 | 19.87 | 19.54 | 19.36 | 19.89 | 19.43 | 19.27 | 19.58 | 19.61 | 19.60 | 20.36 | 19.86 | 19.65 | 19.66 | 19.69 |
| FeO* | 0.07 | 0.15 | 0.04 | 0.10 | 0.04 | 0.03 | 0.07 | 0.00 | 0.00 | 0.09 | 0.00 | 0.00 | 0.04 | 0.04 | 0.03 | 0.05 | 0.01 | 0.03 | 0.03 | 0.03 |
| MgO | 0.00 | 0.00 | 0.00 | 0.00 | 0.00 | 0.01 | 0.01 | 0.02 | 0.00 | 0.00 | 0.00 | 0.02 | 0.01 | 0.01 | 0.01 | 0.02 | 0.00 | 0.01 | 0.01 | 0.01 |
| CaO | 0.07 | 0.05 | 0.44 | 0.16 | 0.08 | 0.59 | 0.15 | 0.22 | 0.13 | 0.10 | 0.09 | 0.19 | 0.22 | 0.19 | 0.20 | 1.13 | 0.26 | 0.27 | 0.28 | 0.29 |
| Na2O | 11.31 | 11.37 | 11.05 | 10.81 | 11.15 | 10.75 | 11.06 | 11.23 | 11.09 | 10.65 | 11.18 | 11.55 | 11.05 | 11.05 | 11.08 | 10.44 | 10.60 | 10.99 | 10.97 | 10.96 |
| K2O | 0.05 | 0.05 | 0.06 | 0.07 | 0.06 | 0.11 | 0.07 | 0.06 | 0.05 | 0.11 | 0.04 | 0.05 | 0.07 | 0.07 | 0.07 | 0.06 | 0.04 | 0.06 | 0.06 | 0.06 |
| Total | 99.34 | 100.35 | 99.26 | 98.67 | 99.18 | 98.69 | 99.58 | 99.40 | 99.59 | 99.13 | 99.28 | 99.10 | 99.19 | 99.18 | 99.23 | 98.19 | 98.97 | 99.13 | 99.10 | 99.05 |
| Number of cations on the basis of 8 oxygens: | | | | | | | | | | | | | | | | | | | | |
| Si | 3.004 | 3.002 | 3.001 | 2.992 | 3.006 | 2.967 | 2.989 | 2.997 | 3.013 | 2.994 | 3.006 | 2.997 | 2.996 | 2.996 | 2.996 | 2.942 | 2.996 | 2.993 | 2.993 | 2.991 |
| Al | 0.999 | 0.999 | 1.000 | 1.023 | 1.003 | 1.047 | 1.025 | 1.011 | 0.997 | 1.028 | 1.005 | 1.001 | 1.014 | 1.015 | 1.015 | 1.068 | 1.028 | 1.018 | 1.019 | 1.021 |
| Fe2+ | 0.005 | 0.011 | 0.003 | 0.007 | 0.003 | 0.002 | 0.005 | 0.000 | 0.000 | 0.007 | 0.000 | 0.000 | 0.003 | 0.003 | 0.002 | 0.004 | 0.001 | 0.002 | 0.002 | 0.002 |
| Mg | 0.000 | 0.000 | 0.000 | 0.000 | 0.000 | 0.000 | 0.000 | 0.000 | 0.000 | 0.000 | 0.000 | 0.000 | 0.000 | 0.000 | 0.000 | 0.000 | 0.000 | 0.000 | 0.000 | 0.000 |
| Ca | 0.003 | 0.002 | 0.021 | 0.007 | 0.004 | 0.028 | 0.007 | 0.010 | 0.006 | 0.005 | 0.004 | 0.009 | 0.010 | 0.009 | 0.009 | 0.054 | 0.012 | 0.013 | 0.013 | 0.014 |
| Na | 0.962 | 0.956 | 0.941 | 0.924 | 0.949 | 0.921 | 0.938 | 0.955 | 0.940 | 0.905 | 0.951 | 0.987 | 0.941 | 0.941 | 0.943 | 0.901 | 0.902 | 0.937 | 0.935 | 0.934 |
| K | 0.003 | 0.003 | 0.003 | 0.004 | 0.004 | 0.006 | 0.004 | 0.004 | 0.003 | 0.006 | 0.002 | 0.003 | 0.004 | 0.004 | 0.004 | 0.004 | 0.002 | 0.003 | 0.003 | 0.004 |
| Sum Catons | 4.976 | 4.973 | 4.969 | 4.957 | 4.968 | 4.972 | 4.967 | 4.977 | 4.959 | 4.944 | 4.968 | 4.997 | 4.968 | 4.968 | 4.969 | 4.973 | 4.942 | 4.966 | 4.965 | 4.966 |
| Molecular proportions of end-members: | | | | | | | | | | | | | | | | | | | | |
| An | 0.003 | 0.002 | 0.021 | 0.008 | 0.004 | 0.029 | 0.008 | 0.011 | 0.006 | 0.005 | 0.005 | 0.009 | 0.011 | 0.010 | 0.010 | 0.056 | 0.014 | 0.014 | 0.014 | 0.015 |
| Ab | 0.994 | 0.995 | 0.975 | 0.988 | 0.992 | 0.964 | 0.989 | 0.986 | 0.991 | 0.988 | 0.993 | 0.989 | 0.985 | 0.986 | 0.986 | 0.940 | 0.984 | 0.983 | 0.983 | 0.982 |
| Or | 0.003 | 0.003 | 0.003 | 0.004 | 0.004 | 0.006 | 0.004 | 0.004 | 0.003 | 0.007 | 0.002 | 0.003 | 0.004 | 0.004 | 0.004 | 0.004 | 0.003 | 0.004 | 0.004 | 0.004 |

* Total Fe as FeO

presence of albite in almost all of pelitic samples as well. The compositions of albite are listed in Table 5.2 (see Table B-1 in Appendix B for a complete data set).

**Muscovite :** Muscovite is present in about 70% of psammitic samples. It is a ubiquitous constituent of all pelitic samples. It occurs in two modes, i.e. detrital muscovite with very low celadonite content and fine-grained recrystallised phengitic muscovite with higher celadonite content. A modified AKF plot (following Coombs *et al.*, 1976) shown in Figure 5.3, indicates that muscovites in psammitic and pelitic samples are phengitic. The celadonite component ($K(Mg,Fe)AlSi_4O_{10}(OH)_2$) of muscovite, as expressed by the ratio (Mg+Fe)/(sum cations in octahedral sites), is between 0.07 and 0.34. This ratio corresponds to Si content of 3.03 to 3.52 as shown in Table 5.3 (see Table B-2 in Appendix B for a complete data set). The structural formula of muscovite was calculated on the basis of 11 oxygens (half unit cell) and by assuming total iron as FeO to avoid an arbitrary assumption on $Fe^{2+}$:$Fe^{3+}$ ratio. It is noted that muscovite composition is somewhat dependent on host rock chemistry. MgO/(MgO+FeO) ratios of muscovite and host rock are broadly correlated as shown in Figure 5.4. Paragonite component of muscovite in psammitic rocks is low, i.e. Na/(Na+K) in the range 0.005 to 0.125. However, paragonite component in pelitic samples is much higher than the psammitic samples, Na/(Na+K) ratio reaches 0.408 in sample 2/5291 and 0.574 in sample 3/9291 (Table 5.3). These high values of paragonite component exceed the solvus composition for any reasonable temperature and are best explained as due to submicroscopic intergrowth between muscovite and paragonite which is rather common in low-temperature pelitic rocks (e.g. Shau *et al.*, 1991). Such intergrowths can be directly imaged only by transmission electron microscopy which is beyond the attempt of this study.

**Chlorite :** Chlorite is green to light green in thin section. It has both brown and anomalous blue interference colours. Electron microprobe analyses of representative chlorites in the psammites and pelites are given in Table 5.4 (see Table B-3 in Appendix B for a complete data set). The structural formula of chlorite was calculated on the basis of 14 oxygens (half unit cell) and by assuming total iron as FeO. These chlorites are either ripidolite or brunsvigite according to Foster's classification (1962) shown in Figure 5.5. The compositional variation of chlorites in both psammites and pelites is rather small. Mg/(Mg+Fe) ratio varies in a narrow range from 0.347-0.562 and $Al^{iv}$ ranges between 1.029 and 1.438 (Table 5.4). It is noted that chlorite composition, like that of coexisting muscovite, is also dependent on host rock chemistry. MgO/(MgO+FeO) ratios of chlorite and host rock have a good correlation (Fig. 5.6).

Table 5.3 Representative electron microprobe analyses of phengitic muscovites in psammites and pelites of the Pha Som Metamorphic Complex.

| Sample no. | 2/5291 | 5/8291 | 3/9291 | 6/9291 | 3/8291 | SD-97 | 1/7291 | SD-60 | SD-99 | SD-193 | 1//6291 | 15/6291 | SD-42 | SD-64 | SD-104 | SD-165 | SD-198 | SD-211 | SD-213 | SD-217 | SD-221 | P-106 | P-107 |
|---|---|---|---|---|---|---|---|---|---|---|---|---|---|---|---|---|---|---|---|---|---|---|---|
| Point no. | Msm | Msm | Msm | Ms17 | Ms4 | C3-Ms5 | C4-Ms4 | C7-Ms4D | C5-Ms7 | Msm | Msm | Msm | Ms2 | C1-Ms3 | Msm | C2-Ms2 | Msm | C1-Ms2 | C5-Ms2 | C3-Ms2 | C2-Ms6 | Msm | Msm |
| SiO2 | 46.87 | 46.07 | 46.43 | 48.91 | 46.40 | 45.62 | 46.82 | 46.15 | 46.32 | 48.25 | 45.29 | 48.63 | 47.57 | 48.01 | 44.98 | 46.16 | 50.51 | 45.20 | 45.86 | 44.77 | 48.65 | 47.34 | 49.51 |
| TiO2 | 0.42 | 0.12 | 0.19 | 0.36 | 0.18 | 0.05 | 0.44 | 0.07 | 0.47 | 0.04 | 0.22 | 0.16 | 0.16 | 0.18 | 0.09 | 0.47 | 0.05 | 0.39 | 0.72 | 0.07 | 0.01 | 0.04 | 0.03 |
| Al2O3 | 35.43 | 35.12 | 37.57 | 30.44 | 33.04 | 31.55 | 32.63 | 34.38 | 34.78 | 30.93 | 33.39 | 31.55 | 28.35 | 29.95 | 34.92 | 34.03 | 21.73 | 31.68 | 30.23 | 29.47 | 32.33 | 26.09 | 29.52 |
| FeO* | 2.26 | 1.28 | 1.63 | 2.44 | 2.22 | 2.84 | 1.24 | 1.11 | 0.33 | 2.20 | 3.91 | 2.05 | 4.27 | 2.49 | 1.00 | 2.56 | 6.07 | 3.86 | 4.87 | 5.65 | 1.11 | 4.60 | 2.71 |
| MnO | 0.01 | 0.01 | 0.03 | 0.06 | 0.00 | 0.08 | 0.00 | 0.00 | 0.00 | 0.01 | 0.00 | 0.02 | 0.00 | 0.13 | 0.02 | 0.00 | 0.04 | 0.08 | 0.00 | 0.09 | 0.04 | 0.07 | 0.07 |
| MgO | 0.59 | 1.04 | 0.48 | 1.97 | 1.65 | 1.52 | 1.75 | 1.02 | 1.13 | 1.76 | 0.59 | 1.86 | 2.00 | 2.25 | 0.88 | 0.57 | 4.31 | 0.95 | 1.24 | 3.46 | 1.75 | 3.47 | 2.26 |
| CaO | 0.16 | 0.02 | 0.16 | 0.00 | 0.04 | 0.06 | 0.01 | 0.00 | 0.00 | 0.01 | 0.02 | 0.00 | 0.00 | 0.05 | 0.01 | 0.02 | 0.11 | 0.02 | 0.01 | 0.11 | 0.05 | 0.01 | 0.04 |
| Na2O | 2.64 | 0.81 | 3.84 | 0.62 | 0.47 | 0.03 | 0.41 | 0.37 | 0.55 | 0.23 | 0.32 | 0.20 | 0.10 | 0.17 | 0.63 | 0.80 | 0.03 | 0.28 | 0.29 | 0.12 | 0.26 | 0.08 | 0.13 |
| K2O | 5.83 | 8.59 | 4.33 | 9.44 | 9.32 | 10.89 | 9.23 | 10.78 | 10.65 | 10.81 | 11.14 | 9.09 | 10.81 | 10.34 | 10.54 | 10.10 | 10.37 | 10.93 | 10.92 | 8.16 | 9.58 | 11.27 | 11.24 |
| F | 0.00 | 0.00 | 0.00 | 0.00 | 0.00 | 0.51 | 0.00 | 0.05 | 0.22 | 0.29 | 0.05 | 0.00 | 0.19 | 0.00 | 0.00 | 0.00 | 0.00 | 0.00 | 0.08 | 0.08 | 0.13 | 0.26 | 0.12 |
| Cl | 0.01 | 0.02 | 0.02 | 0.00 | 0.00 | 0.01 | 0.00 | 0.01 | 0.02 | 0.01 | 0.01 | 0.00 | 0.00 | 0.02 | 0.01 | 0.02 | 0.04 | 0.00 | 0.01 | 0.00 | 0.03 | 0.01 | 0.01 |
| Total | 94.22 | 93.09 | 94.67 | 94.24 | 93.32 | 93.16 | 92.53 | 93.94 | 94.47 | 94.53 | 94.94 | 93.53 | 93.45 | 93.59 | 93.08 | 94.73 | 93.25 | 93.40 | 94.24 | 91.97 | 93.95 | 93.22 | 95.64 |
| O = F, Cl | 0.00 | 0.00 | -0.01 | 0.00 | 0.00 | -0.21 | 0.00 | -0.02 | -0.10 | -0.12 | -0.02 | 0.00 | -0.08 | 0.00 | 0.00 | -0.01 | 0.00 | 0.00 | -0.04 | -0.03 | -0.06 | -0.11 | -0.05 |
| Total | 94.21 | 93.09 | 94.67 | 94.24 | 93.32 | 92.94 | 92.53 | 93.91 | 94.37 | 94.41 | 94.92 | 93.53 | 93.37 | 93.58 | 93.08 | 94.73 | 93.25 | 93.40 | 94.21 | 91.93 | 93.88 | 93.11 | 95.59 |
| Number of cations on the basis of 11 oxygens: | | | | | | | | | | | | | | | | | | | | | | | |
| Si | 3.101 | 3.102 | 3.034 | 3.284 | 3.146 | 3.159 | 3.180 | 3.117 | 3.104 | 3.259 | 3.084 | 3.266 | 3.290 | 3.268 | 3.066 | 3.107 | 3.520 | 3.127 | 3.164 | 3.134 | 3.254 | 3.312 | 3.315 |
| Al iv | 0.899 | 0.898 | 0.966 | 0.716 | 0.854 | 0.841 | 0.820 | 0.883 | 0.896 | 0.741 | 0.916 | 0.734 | 0.710 | 0.732 | 0.934 | 0.893 | 0.480 | 0.873 | 0.836 | 0.866 | 0.746 | 0.688 | 0.685 |
| Sum T | 4.000 | 4.000 | 4.000 | 4.000 | 4.000 | 4.000 | 4.000 | 4.000 | 4.000 | 4.000 | 4.000 | 4.000 | 4.000 | 4.000 | 4.000 | 4.000 | 4.000 | 4.000 | 4.000 | 4.000 | 4.000 | 4.000 | 4.000 |
| Al vi | 1.865 | 1.890 | 1.928 | 1.693 | 1.786 | 1.734 | 1.793 | 1.854 | 1.852 | 1.722 | 1.764 | 1.765 | 1.601 | 1.671 | 1.873 | 1.807 | 1.305 | 1.711 | 1.622 | 1.566 | 1.803 | 1.464 | 1.644 |
| Ti | 0.021 | 0.006 | 0.009 | 0.018 | 0.009 | 0.003 | 0.022 | 0.003 | 0.024 | 0.002 | 0.011 | 0.008 | 0.008 | 0.009 | 0.005 | 0.024 | 0.002 | 0.020 | 0.037 | 0.004 | 0.001 | 0.002 | 0.001 |
| Fe2+ | 0.125 | 0.072 | 0.089 | 0.137 | 0.126 | 0.164 | 0.070 | 0.063 | 0.018 | 0.124 | 0.223 | 0.115 | 0.247 | 0.142 | 0.057 | 0.144 | 0.355 | 0.223 | 0.281 | 0.331 | 0.062 | 0.269 | 0.152 |
| Mn | 0.001 | 0.001 | 0.002 | 0.003 | 0.000 | 0.005 | 0.000 | 0.000 | 0.000 | 0.001 | 0.000 | 0.001 | 0.000 | 0.008 | 0.001 | 0.000 | 0.002 | 0.005 | 0.000 | 0.005 | 0.002 | 0.004 | 0.004 |
| Mg | 0.058 | 0.105 | 0.046 | 0.197 | 0.167 | 0.157 | 0.177 | 0.103 | 0.113 | 0.178 | 0.060 | 0.186 | 0.206 | 0.229 | 0.090 | 0.057 | 0.449 | 0.098 | 0.128 | 0.361 | 0.175 | 0.362 | 0.226 |
| Sum O | 2.070 | 2.074 | 2.074 | 2.049 | 2.088 | 2.063 | 2.063 | 2.023 | 2.007 | 2.026 | 2.058 | 2.074 | 2.063 | 2.058 | 2.025 | 2.032 | 2.114 | 2.058 | 2.069 | 2.266 | 2.042 | 2.101 | 2.028 |
| Ca | 0.011 | 0.002 | 0.011 | 0.000 | 0.003 | 0.004 | 0.000 | 0.000 | 0.000 | 0.001 | 0.001 | 0 000 | 0.000 | 0.003 | 0.001 | 0.002 | 0.008 | 0.002 | 0.001 | 0.008 | 0.003 | 0.001 | 0.003 |
| Na | 0.338 | 0.106 | 0.487 | 0.081 | 0.062 | 0.005 | 0.054 | 0.048 | 0.071 | 0.030 | 0.042 | 0.026 | 0.014 | 0.022 | 0.084 | 0.105 | 0.005 | 0.038 | 0.039 | 0.016 | 0.034 | 0.011 | 0.017 |
| K | 0.492 | 0.738 | 0.361 | 0.809 | 0.806 | 0.962 | 0.800 | 0.929 | 0.911 | 0.931 | 0.967 | 0.779 | 0.954 | 0.898 | 0.916 | 0.867 | 0.922 | 0.965 | 0.961 | 0.729 | 0.818 | 1.005 | 0.960 |
| Sum A | 0.841 | 0.846 | 0.859 | 0.889 | 0.871 | 0.971 | 0.855 | 0.976 | 0.982 | 0.962 | 1.011 | 0.805 | 0.967 | 0.923 | 1.001 | 0.974 | 0.934 | 1.004 | 1.001 | 0.753 | 0.855 | 1.017 | 0.980 |
| Sum Cations | 6.911 | 6.920 | 6.933 | 6.938 | 6.959 | 7.034 | 6.918 | 6.999 | 6.989 | 6.988 | 7.070 | 6.879 | 7.030 | 6.981 | 7.026 | 7.005 | 7.048 | 7.062 | 7.070 | 7.019 | 6.897 | 7.118 | 7.008 |
| Na/(Na+K) | 0.408 | 0.126 | 0.574 | 0.091 | 0.071 | 0.005 | 0.063 | 0.049 | 0.072 | 0.031 | 0.042 | 0.032 | 0.014 | 0.024 | 0.084 | 0.108 | 0.005 | 0 037 | 0.039 | 0.022 | 0.040 | 0 011 | 0.017 |

* Total Fe as FeO

Table 5.4 Representative electron microprobe analyses of chlorites in psammites and pelites of the Pha Som Metamorphic Complex.

| Sample no. | 2/5291 | 5/8291 | 3/9291 | 6/9291 | 3/8291 | SD-97 | 1/7291 | SD-60 | SD-99 | SD-193 | 15/6291 | SD-42 | SD-64 | SD-165 | SD-198 | SD-211 | SD-213 | SD-217 | SD-221 |
|---|---|---|---|---|---|---|---|---|---|---|---|---|---|---|---|---|---|---|---|
| Point no. | Chl1 | Chlm | Chlm | Chlm | Chl1 | Chlm | Chlm | Chlm | Chlm | Chlm | Chlm | Chlm | Ab3 | C5-Chl2 | Chlm | C3-Chl5 | Chlm | C1-Chl3 | C6-Chl4 |
| SiO2 | 25.31 | 24.07 | 23.81 | 26.79 | 26.54 | 25.57 | 27.47 | 24.71 | 25.05 | 25.48 | 27.00 | 24.89 | 25.23 | 24.76 | 26.92 | 24.36 | 25.55 | 25.04 | 24.60 |
| TiO2 | 0.00 | 0.05 | 0.00 | 0.05 | 0.09 | 0.07 | 0.87 | 0.03 | 0.24 | 0.16 | 0.01 | 0.04 | 0.06 | 0.04 | 0.01 | 0.04 | 0.06 | 0.19 | 0.00 |
| Al2O3 | 23.65 | 22.83 | 23.66 | 23.75 | 19.18 | 20.64 | 17.80 | 21.02 | 20.93 | 21.49 | 18.46 | 20.37 | 20.93 | 21.65 | 16.71 | 21.70 | 19.33 | 20.35 | 21.91 |
| Cr2O3 | 0.14 | 0.01 | 0.01 | 0.00 | 0.00 | 0.07 | 0.05 | 0.03 | 0.04 | 0.04 | 0.02 | 0.03 | 0.05 | 0.00 | 0.01 | 0.07 | 0.02 | 0.06 | 0.01 |
| FeO* | 30.27 | 26.42 | 26.13 | 20.41 | 27.89 | 23.26 | 24.62 | 25.79 | 26.64 | 25.71 | 25.97 | 27.46 | 28.00 | 27.54 | 24.33 | 26.92 | 26.36 | 27.56 | 25.55 |
| MnO | 0.01 | 0.44 | 0.12 | 0.32 | 0.57 | 0.33 | 0.22 | 0.24 | 0.21 | 0.27 | 0.23 | 0.12 | 0.24 | 0.24 | 0.37 | 0.12 | 0.23 | 0.38 | 0.31 |
| MgO | 9.04 | 12.05 | 12.35 | 14.64 | 12.74 | 16.18 | 13.96 | 13.56 | 13.45 | 13.11 | 14.44 | 13.81 | 12.76 | 12.99 | 17.54 | 12.53 | 13.02 | 12.01 | 13.41 |
| Total | 88.42 | 85.87 | 86.07 | 85.95 | 87.01 | 86.11 | 84.99 | 85.37 | 86.56 | 86.26 | 86.14 | 86.71 | 87.26 | 87.22 | 85.89 | 85.75 | 84.57 | 85.59 | 85.78 |
| Number of cations on the basis of 14 oxygens: | | | | | | | | | | | | | | | | | | | |
| Si | 2.696 | 2.612 | 2.562 | 2.782 | 2.858 | 2.719 | 2.971 | 2.689 | 2.695 | 2.732 | 2.905 | 2.689 | 2.710 | 2.655 | 2.893 | 2.652 | 2.813 | 2.741 | 2.654 |
| Al iv | 1.304 | 1.388 | 1.438 | 1.218 | 1.142 | 1.281 | 1.029 | 1.311 | 1.305 | 1.268 | 1.095 | 1.311 | 1.290 | 1.345 | 1.107 | 1.348 | 1.187 | 1.259 | 1.346 |
| Sum T | 4.000 | 4.000 | 4.000 | 4.000 | 4.000 | 4.000 | 4.000 | 4.000 | 4.000 | 4.000 | 4.000 | 4.000 | 4.000 | 4.000 | 4.000 | 4.000 | 4.000 | 4.000 | 4.000 |
| Al vi | 1.667 | 1.531 | 1.565 | 1.689 | 1.293 | 1.303 | 1.240 | 1.384 | 1.352 | 1.447 | 1.245 | 1.284 | 1.360 | 1.393 | 1.010 | 1.437 | 1.321 | 1.368 | 1.441 |
| Ti | 0.000 | 0.004 | 0.000 | 0.004 | 0.007 | 0.006 | 0.071 | 0.002 | 0.019 | 0.013 | 0.001 | 0.003 | 0.005 | 0.003 | 0.001 | 0.003 | 0.005 | 0.016 | 0.000 |
| Cr | 0.012 | 0.001 | 0.001 | 0.000 | 0.000 | 0.006 | 0.004 | 0.002 | 0.004 | 0.003 | 0.002 | 0.002 | 0.004 | 0.000 | 0.001 | 0.006 | 0.002 | 0.005 | 0.001 |
| Fe | 2.697 | 2.397 | 2.353 | 1.772 | 2.512 | 2.076 | 2.228 | 2.347 | 2.407 | 2.310 | 2.337 | 2.481 | 2.516 | 2.470 | 2.186 | 2.450 | 2.428 | 2.524 | 2.305 |
| Mn | 0.001 | 0.040 | 0.010 | 0.028 | 0.052 | 0.029 | 0.020 | 0.022 | 0.019 | 0.025 | 0.021 | 0.011 | 0.022 | 0.022 | 0.034 | 0.011 | 0.022 | 0.035 | 0.029 |
| Mg | 1.435 | 1.948 | 1.981 | 2.267 | 2.045 | 2.554 | 2.251 | 2.199 | 2.149 | 2.092 | 2.314 | 2.223 | 2.043 | 2.077 | 2.808 | 2.032 | 2.137 | 1.960 | 2.156 |
| Sum O | 5.811 | 5.922 | 5.910 | 5.760 | 5.909 | 5.974 | 5.814 | 5.956 | 5.949 | 5.890 | 5.920 | 6.005 | 5.950 | 5.965 | 6.041 | 5.940 | 5.915 | 5.907 | 5.931 |
| Sum Cations | 9.811 | 9.922 | 9.910 | 9.760 | 9.909 | 9.974 | 9.814 | 9.956 | 9.949 | 9.890 | 9.920 | 10.005 | 9.950 | 9.965 | 10.041 | 9.940 | 9.915 | 9.907 | 9.931 |
| Mg/(Mg+Fe2) | 0.347 | 0.448 | 0.457 | 0.561 | 0.449 | 0.552 | 0.503 | 0.484 | 0.472 | 0.475 | 0.498 | 0.473 | 0.448 | 0.457 | 0.562 | 0.453 | 0.468 | 0.437 | 0.483 |

* Total Fe as FeO

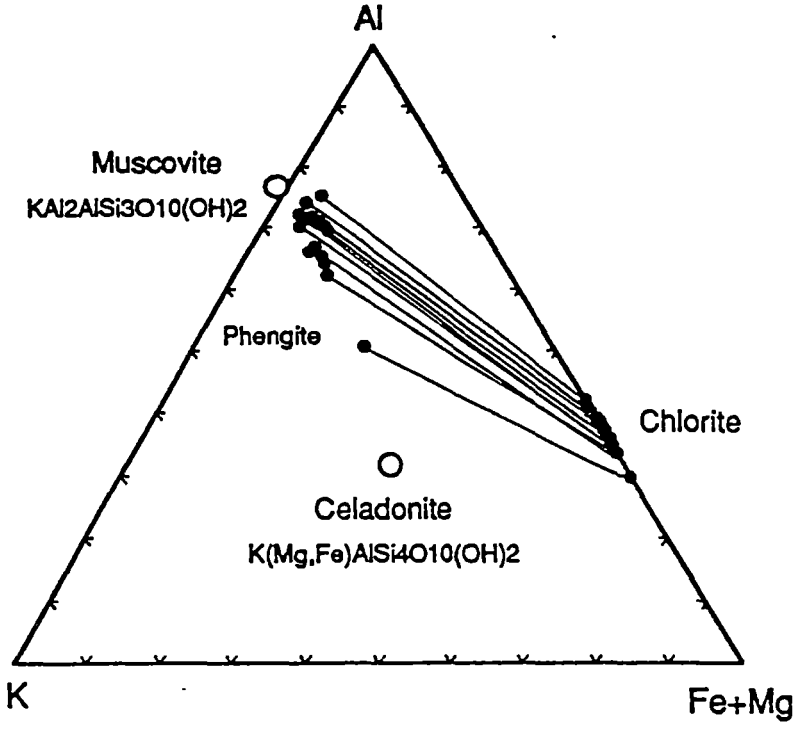


Figure 5.3 Modified AKF diagram (after Coombs *et al.*, 1976) showing compositional relationships between phengites and chlorites in the Pha Som M.C. psammites and pelites. Note parallel tie lines between the two phases. $SiO_2$ and $H_2O$ are saturated. Data from Tables 5.3 and 5.4.

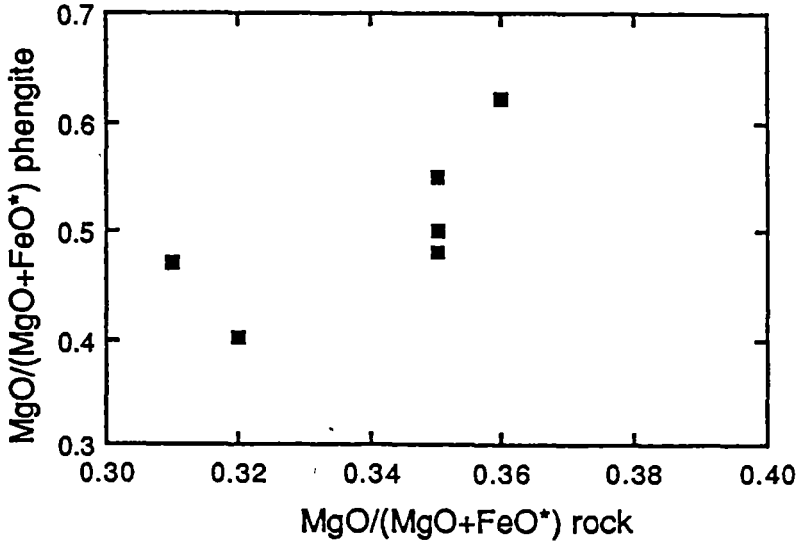


Figure 5.4 Plot of MgO/(MgO+FeO*) of phengites and MgO/(MgO+FeO*) of host rocks. Phengite compositions are from Table 5.3 and FeO* = 0.905 $Fe_2O_3$* is calculated for rocks on anhydrous basis from Table 7.3.

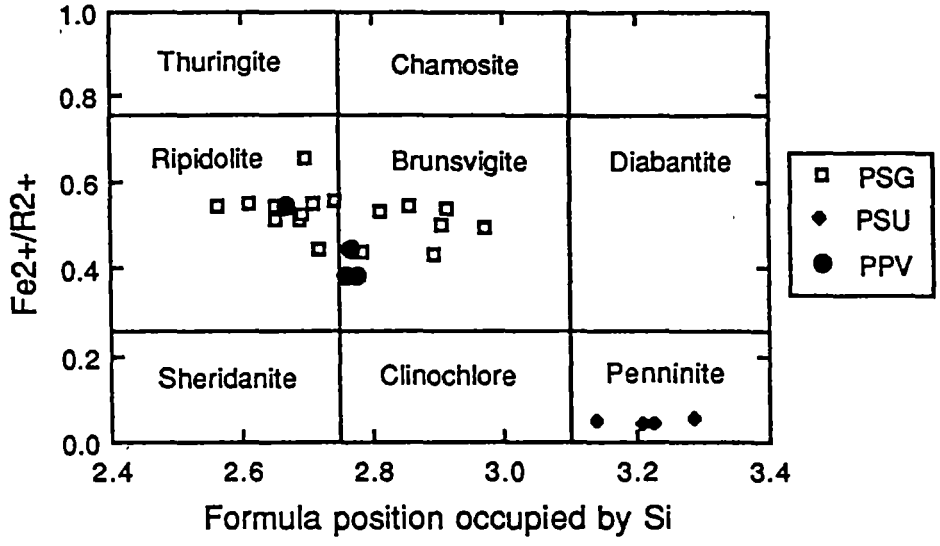


Figure 5.5 Chlorite compositions plotted on classification diagram of Foster (1962). PSG = the Pha Som M.C. (psammites and pelites), PSU = the Pha Som ophiolite association (serpentinites), PPV = the Pak Pat Volcanics.

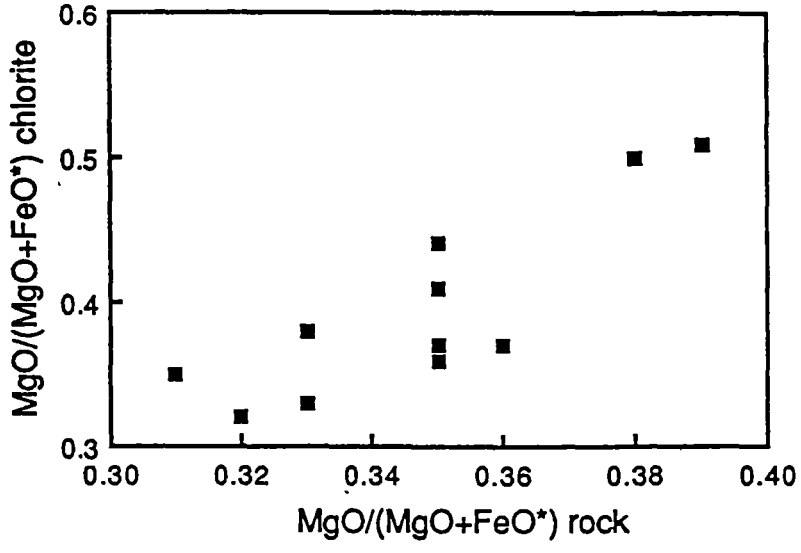


Figure 5.6 Plot of MgO/(MgO+FeO*) of chlorites and MgO/(MgO+FeO*) of host rocks. Chlorite compositions are from Table 5.4 and FeO* = 0.905 $Fe_2O_3$* is calculated for rocks on anhydrous basis from Table 7.4.

**Epidote :** Epidote is common in psammitic rocks throughout the Sirikit Dam area. It occurs as spongy grains or aggregates (Figs. 5.2c&d) as well as rare euhedral grains. Compositional data of epidotes in psammites and pelites are presented in Table B-4 (Appendix B). Structural formula of epidote was calculated on the basis of 12.5 oxygens and by assuming total iron as $Fe_2O_3$. Pistacite content, ($Ca_2FeAl_2Si_3O_{12}(OH)$), expressed as $Fe^{3+}/(Fe^{3+}+Al)$, varies from 0.18 to 0.34 with a mode of around 0.28 as shown in Figure 5.7. This modal value ($Ps_{28}$) is similar to the modal value ($Ps_{29}$) of epidotes in pumpellyite-actinolite facies metagreywackes from Upper Wakatipu district in the South Island of New Zealand (Kawachi, 1975). A variation in pistacite component of different epidote grains within the same thin section (e.g. Ps $_{18-32}$ in samples SD-225 and P-104) as well as a variation within the same grain were noted. However, electron microprobe traverse across a single epidote grain in sample P-104 (Table B-4) does not show a clear trend of systematic decrease in pistacite component from core to rim as has been noted previously (Bishop, 1972; Coombs *et al.*, 1976b; Baltatziz and Katagas, 1984). This observation suggests that the growth of clinozoisitic epidote does not necessarily follow a simple overgrowth pattern around a more pistacite-rich core of an epidote crystal. Nakajima *et al.* (1977) has also demonstrated a complex zoning in an epidote crystal from Sanbagawa metamorphic belt, Japan. Electron microprobe analysis revealed inclusions of pumpellyite in some epidote grains (e.g sample SD-104).

**Actinolite :** The amphibole in the psammites is actinolite according to the classification of Leake (1978). It occurs as colourless fine-grained needles in a matrix together with epidote and chlorite or pale green short prismatic grains which pseudomorph clastic hornblende. Compositional data of actinolite are given in Table B-5 (Appendix B). The actinolite structural formula was calculated on the basis of 23 oxygens and by normalising the number cations other than Ca, Na and K to 13 as recommended by Leake (1978). Actinolite in the Sirikit Dam area is rather uniform in composition. Mg/(Mg+Fe) ratio varies in a narrow range between 0.57-0.78. Si content, with only few exceptions, is always greater than 7.5. Overall, $Al_2O_3$ value is low (less than 2.5%) and $TiO_2$ content is also very low (less than 0.2% on average). In sample P-102, a transition from relict clastic hornblende core via actinolitic hornblende to actinolite rim is noted. This observation suggests incomplete pseudomorphism of actinolite after clastic hornblende.

**Pumpellyite :** Pumpellyite, a rare phase in the studied psammites, occurs as fine granules or small spongy aggregates together with epidote. It is colourless under microscope except in more basic samples (e.g. SD-198) in which typical blue-green pleochroism is seen. It is an Fe-rich variety (Table B-6 in Appendix B).

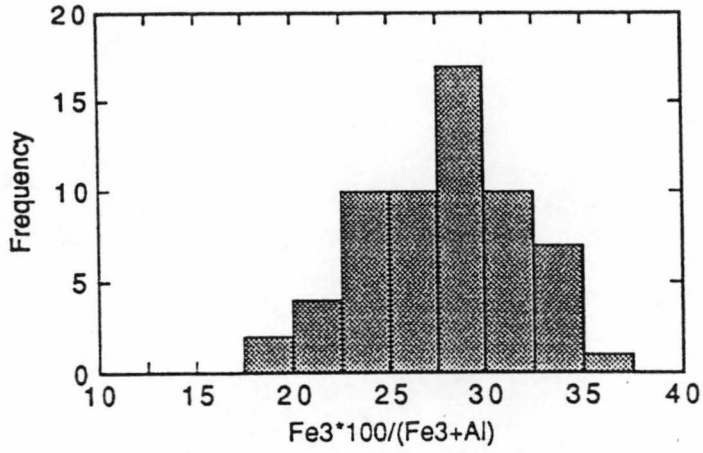


Fig. 5.7 Histogram of pistacite contents, expressed as $100*Fe^{3+}/(Fe^{3+}+Al)$, of epidotes in the Pha Som M.C. psammites.

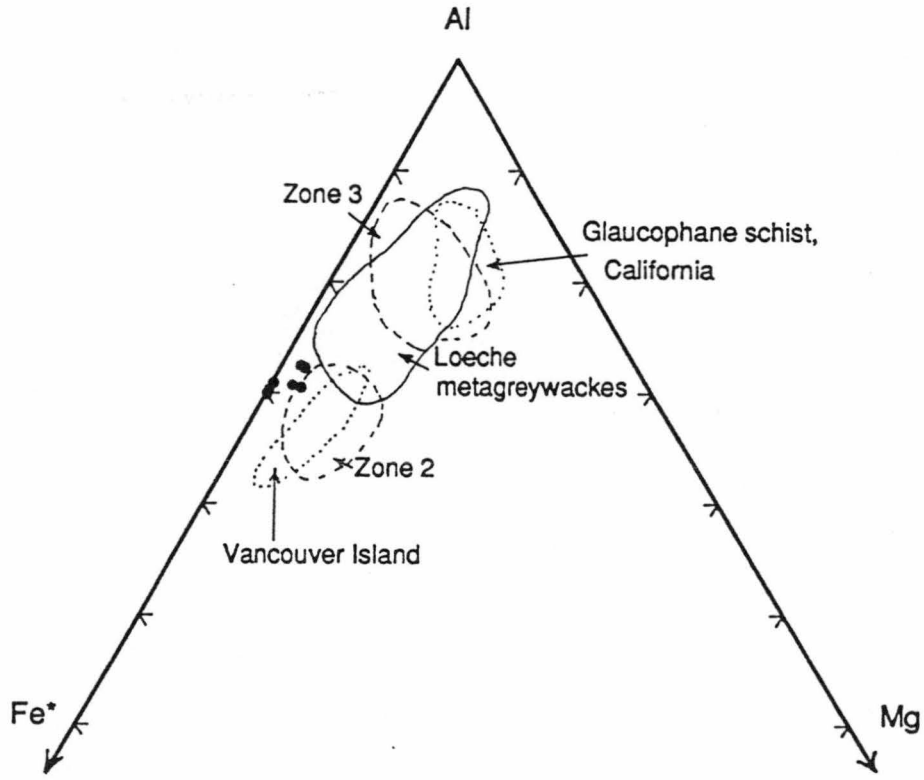


Figure 5.8 Compositional plot of pumpellyites in TZ3 fine-graine schists in terms of Al-Fe*-Mg (Fe* = total Fe). Compositional fields of analysed pumpellyites from Upper Wakatipu (zone2&3), New Zealand (Kawachi, 1975); Vancouver Island (Kunochi and Liou, 1976); glaucophane schist, California (Ernst *et al.*, 1970); and the Loeche metagreywackes (Coombs *et al.*, 1976) are shown for comparison.

$Fe^{3+}/(Fe^{3+}+Al)$ ratios, calculated assuming the ideal formula $Ca_4(Mg,Fe)(Fe^{3+},Al)_5Si_6O_{21}(OH)_7$ (Coombs *et al.*, 1976b; Nakajima *et al.*, 1977), vary from 0.15 to 0.19. The composition of pumpellyite in the Sirikit Dam area is similar to those from the prehnite-pumpellyite facies rocks (Coombs *et al.*, 1976; Cho *et al.*, 1986) as shown in Figure 5.8. It is suggested that this Fe-rich pumpellyite represents a relict phase crystallised at lower temperatures, the same conclusion drawn by Cho *et al.* (1987) for the transition from prehnite-pumpellyite to greenschist facies in the Karmutsen metabasites in British Columbia, Canada.

**Calcite :** Calcite occurs as sparry patches and is an abundant phase in some samples (e.g. SD-65). It is almost pure calcite with molecular proportions of $CaCO_3$ in the range 0.96 to 1.0 (Table B-7 in Appendix B).

**Ankerite :** Ankerite, $Ca(Mg_{0.5},Fe_{0.5})(CO_3)_2$, occurs in one pelitic rock (sample 2/5291) as rhomb-shaped crystals in pressure shadows of quartz porphyroclasts (Fig. 5.2h). The composition of the ankerite is given in Table B-7 (Appendix B).

**Sphene :** Sphene occurs as an accessory phase in psammitic rocks. In pelitic sample 2/5291, anatase is present instead of sphene. Compositional data of sphene are presented in Table B-8 (Appendix B). Structural formula of sphene was calculated after Coombs *et al.* (1976) by assuming 4 Si atoms per formula unit. By comparison with the end-member $CaTiSiO_5$, it is noted that the analysed sphenes show only little substitution of (OH,F) ion for oxygen atoms, i.e. the number of (OH,F) ion is less than 1.0 per formula unit. Sphene in pumpellyite-actinolite facies schists from Switzerland (Coombs *et al.*, 1976b) has a number of (OH,F) ion greater than 1.0.

**Other minerals :** Accessory pyrite, haematite, zircon and tourmaline are present in almost all psammitic rocks. A few electron microprobe analyses were carried out for these phases but discussion on their chemistry will not be attempted.

### 5.3.4 *P-T* conditions of metamorphism of the metasediments

The lack of low-variance assemblages limits the application of elaborate thermodynamic calculations (e.g. Powell and Holland, 1988 or Brown *et al.*, 1988) to determine metamorphic *P-T* conditions of the metasediments. The alternative approach is to use simple calibration such as phengite geobarometry (Massonne and Schreyer, 1987) and empirically-calibrated geothermometers such as phengite-chlorite geothermometer (Chapter 2), plagioclase-muscovite geothermometer (Green

and Usdansky, 1986) and chlorite geothermometer (Cathelineau and Nieva, 1985; Cathelineau, 1988).

## Geobarometry

The $b_0$ values of muscovite, demonstrably reflecting the celadonite contents, have been used to monitor the relative pressure at which the rocks formed (e.g. Sassi and Scolari, 1974; Padan *et al.*, 1982; Guidotti, 1984; Guidotti and Sassi, 1976, 1986; Offler *et al.*, 1987). Guidotti and Sassi (1986) noted that: (i) $b_0$ values progressively less than 9.000 Å reflect metamorphic facies series at pressure lower than Al-silicate triple point, i.e. 3.76 kbar at 501 °C (Holdaway, 1971); (ii) $b_0$ values greater than 9.000 Å and progressively ranging up to 9.040 Å reflect facies at successively higher pressure than 3.76 kbar; and (iii) $b_0$ values greater than 9.040 Å reflect facies series passing through the glaucophane stability field. The $b_0$ values of pelitic samples from the Sirikit Dam area (Table 5.5) range from 8.994 Å to 9.012 Å with a mean value of 9.002 Å indicating the low to medium pressure facies series according to the baric scale of Guidotti and Sassi (1986).

Table 5.5 Crystal lattice parameters ($b_0$ values) of muscovite in phyllites of the metasediments.

| Sample number | (060) | $b_0$ * |
|---|---|---|
| P-87 | 1.500 | 9.000 |
| P-92** | 1.499 | 8.994 |
| P-99 | 1.498 | 8.988 |
| P-100 | 1.499 | 8.994 |
| SD-85** | 1.499 | 8.994 |
| SD-96** | 1.501 | 9.006 |
| SD-151** | 1.501 | 9.006 |
| SD-219 | 1.502 | 9.012 |
| SD-222 | 1.501 | 9.006 |
| 5/8291 | 1.499 | 8.994 |
| 6/9291 | 1.499 | 8.994 |

* mean $b_0$ = 8.999, standard deviation = 0.007, n = 11

* *Calcite bearing sample

This value is different from the average value of 9.039 Å for similar semi-pelitic rocks from Otago, New Zealand (Sassi and Scolari, 1974). The metamorphism of Otago schists is similar to the Barrovian facies series but at somewhat higher pressure (Brown, 1974; Turner, 1981; Yardley, 1982; Kawachi *et al.*, 1983).

An attempt was made to determine metamorphic pressure in quantitative manner. The high-pressure minerals such as aragonite and jadeite are completely absent. The presence of crossite in association with epidote and actinolite in mafic schist within the metasediments (Barr *et al.*, 1985; Panjasawatwong, 1991) constrains the upper pressure limit to less than 7 kbar. The presence of Fe-pumpellyite in some samples together with the complete absence of prehnite suggest the pressure of greater than 3 kbar (Nitsch, 1971; Coombs *et al.*, 1976b). The phengite geobarometer of Massonne and Schreyer (1987) indicates a minimum pressure of 5±1 kbar at an assumed temperature of 350 °C for most of psammitic rocks of the metasediments (Table 5.6).

Table 5.6 Pressure estimates from phengitic muscovites in the Pha Som Metamorphic Complex psammites using phengite geobarometry (Massonne and Schreyer, 1987).

| Sample number | SD-193 | SD-42 | SD-64 | SD-198 | SD-221 | P-106 | P-107 |
|---|---|---|---|---|---|---|---|
| Si content | 3.26 | 3.29 | 3.27 | 3.52 | 3.25 | 3.31 | 3.32 |
| *P* (kbar) | 5±1 | 5±1 | 5±1 | 10±1 | 5±1 | 6±1 | 6±1 |

Because the analysed phengitic muscovites do not coexist with the limiting assemblage phengite + K-feldspar + phlogopite + quartz but contain Fe-Mg phases such as chlorite and/or actinolite, only minimum pressures could be determined (Massonne and Schreyer, 1987).

## Geothermometry

Illite crystallinity study was carried out for phyllites from the Sirikit Dam area. The illite crystallinity values of phyllites, expressed as $\Delta°2\theta$, are in the range 0.19 - 0.23 (Table 5.7) indicating an epizone (greenschist facies) to upper anchizone (sub-greenschist facies) metamorphic grade according to the illite crystallinity scale of Kisch (1980a, 1980b, 1990). It should be noted that these illite crystallinity values lie very close to the epizone/anchizone boundary ($\Delta°2\theta$ = 0.21).

Table 5.7 Illite crystallinity values of pelitic rocks from the Sirikit Dam area.

| Rock Unit | Sample No. | IC Value (Δ°2Ø) | Remarks |
|---|---|---|---|
| Pha Som M.C. metasediments | 5/8291 | 0.22 | |
| | 6/9291 | 0.22 | |
| | SD-54 | 0.21 | |
| | SD-56 | 0.20 | |
| | SD-59 | 0.21 | |
| | SD-85 | 0.23 | |
| | SD-96 | 0.22 | |
| | SD-98 | 0.22 | |
| | SD-105 | 0.22 | |
| | SD-107 | 0.22 | |
| | SD-150 | 0.20 | |
| | SD-163 | 0.20 | |
| | SD-166 | 0.20 | |
| | SD-195 | 0.21 | |
| | SD-207 | 0.20 | |
| | SD-212 | 0.20 | N* = 18 |
| | SD-216 | 0.20 | Mean* = 0.209 |
| | SD-219 | 0.19 | S.D.* = 0.009 |
| ophiolite association (Argillite blocks) | SD-168 | 0.25 | |
| | SD-174 | 0.28 | N = 4 |
| | SD-188 | 0.25 | Mean = 0.263 |
| | SD-191 | 0.27 | S.D. = 0.015 |
| Huai Bo Khong Formation | SD-7 | 0.35 | |
| | SD-16 | 0.41 | |
| | SD-19 | 0.41 | |
| | SD-23 | 0.41 | |
| | SD-31 | 0.30 | N = 7 |
| | SD-38 | 0.40 | Mean = 0.380 |
| | SD-40 | 0.38 | S.D. = 0.042 |

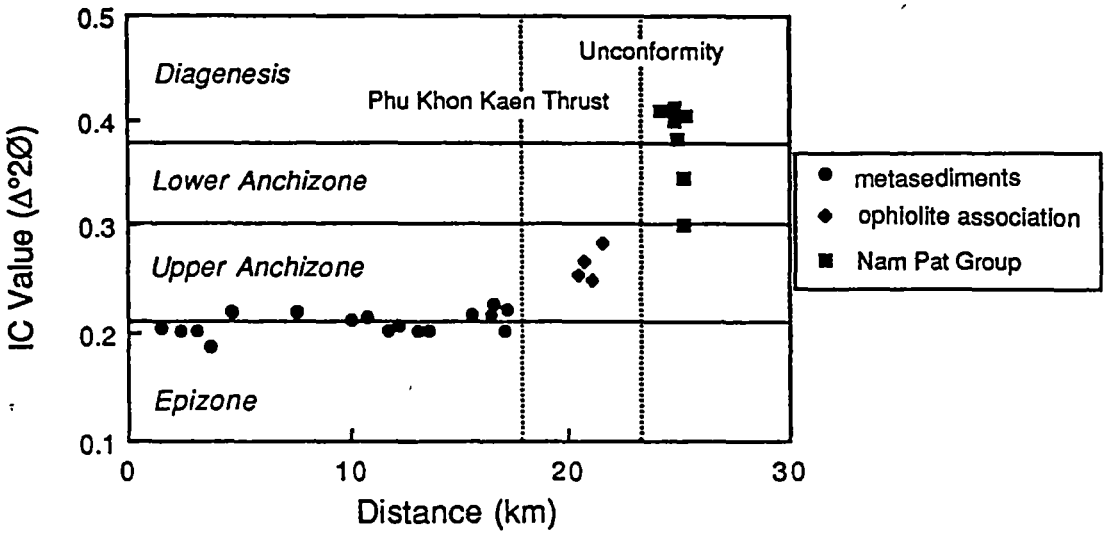


Figure 5.9 Plot showing variation of illite crystallinity of pelitic rocks across the Sirikit Dam area.

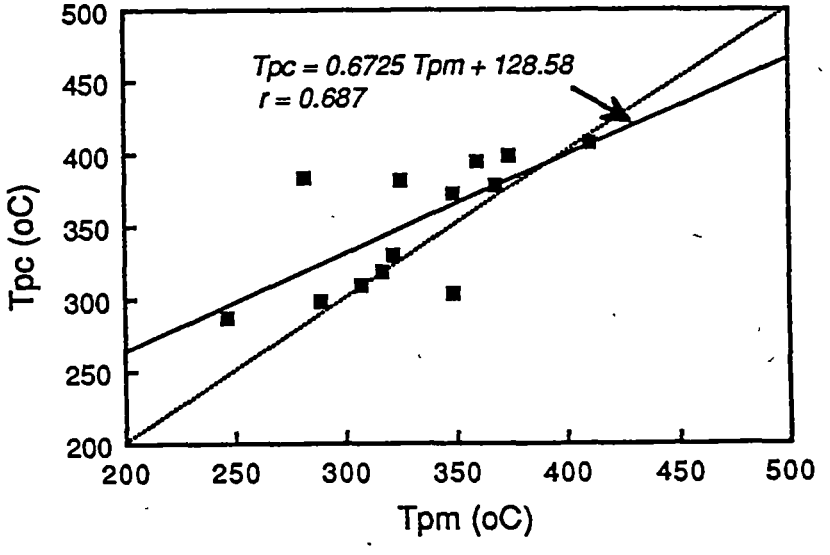


Figure 5.10 Plot comparing temperatures calculated using the phengite-chlorite geothermometer (Chapter 2) and plagioclase-muscovite geothermometer (Green and Usdansky, 1986) for the psammites and pelites. Data are from Table 5.8.

The illite crystallinity values of phyllites agree reasonably well with the estimated temperatures for pelitic and psammitic samples obtained from geothermometric calculations discussed below. The distribution of illite crystallinity values in the Sirikit Dam area is shown in Figures 5.1 and 5.9.

The metamorphic grade of psammites can also be deduced from univariant reactions involving solid-solution in epidote. Similar to metabasites, psammitic rocks of very-low grade may contain epidote, but it is invariably a pistacite-rich species (Winkler, 1976). With the prograde metamorphism passing from sub-greenschist to greenschist facies it is noticeable that the activity of clinozoisite component in epidote increases dramatically. Kawachi (1975), combining his own data with those of Brown (1967), concluded that pistacite content of epidote in Otago schists, New Zealand, decreases markedly from the pumpellyite zone (Chl 2 to lowest Chl 3) to pumpellyite-free zone (highest Chl 3 to Chl 4 and biotite zone), i.e. from $Ps_{29}$ to $Ps_{19}$. The pistacite content of epidote in the Sirikit Dam area ranges from $Ps_{34}$ to $Ps_{18}$ with the modal value of $Ps_{28}$ suggesting the transition from pumpellyite-actinolite to greenschist facies for these psammites. Liou (1979) and Schiffman and Liou (1983) proposed the simple reaction to delineate Fe-pumpellyite-epidote relations:

$2\ Ca_4Fe^{2+}Fe^{3+}Al_4Si_6O_{21}(OH)_7 + 1/2\ O_2$
Fe-pumpellyite
$= 4\ Ca_2Fe^{3+}Al_2Si_3O_{12}(OH) + 5\ H_2O$
epidote

This reaction was suggested to define the lower stability of epidote in relation to Fe-pumpellyite which is strongly affected by oxygen fugacity. The reaction curve was located at about 100 °C lower than that proposed by Nitsch (1971) for the reaction taken as the lower limit of greenschist facies in metabasites (*ca.* 350 ° ± 20 °C at 4 kbar):

$41\ Ca_4MgAl_5Si_6O_{21}(OH)_7 + 2\ Mg_7Al_4Si_4O_{15}(OH)_{12} + 47\ SiO_2$
pumpellyite + chlorite + quartz
$= 71\ Ca_2Al_3Si_3O_{12}(OH) + 11\ Ca_2Mg_5Si_8O_{22}(OH)_2 + 109\ H_2O$
= clinozoisite + actinolite + $H_2O$

The Fe-pumpellyite-epidote relation shown above can be applied for psammites in the Sirikit Dam area considering the Fe-rich nature of pumpellyites. Based on this reaction, the temperature range of around 250-350 °C would be appropriate for the formation of epidotes in the Sirikit Dam area.

For pelitic rocks which contain plagioclase and muscovite, Green and Usdansky (1986) have calibrated a geothermometer based on the K-Na exchange reaction between plagioclase and muscovite. Application of plagioclase-muscovite

Table 5.8 Data for phengite-chlorite assemblages in psammites and pelites of the Pha Som M.C. and comparison between the plagioclase-muscovite and phengite-chlorite temperatures.

| Sample no. | Phengite | | | | Chlorite | | | | P | T PlMs | T MsChl | T diff |
|---|---|---|---|---|---|---|---|---|---|---|---|---|
| | Mg | Fe | Alvi | Si | Mg | Fe | Alvi | Si | (kbar) | (oC) | (oC) | (oC) |
| 5/8291 | 0.105 | 0.073 | 1.890 | 3.102 | 1.949 | 2.398 | 1.532 | 2.612 | 5 | - | 349 | - |
| 6/9291 | 0.197 | 0.137 | 1.693 | 3.284 | 2.268 | 1.772 | 1.690 | 2.782 | 5 | 349 | 308 | -41 |
| 3/8291 | 0.167 | 0.126 | 1.787 | 3.146 | 2.045 | 2.512 | 1.293 | 2.858 | 5 | 349 | 358 | 9 |
| SD-97 | 0.157 | 0.165 | 1.735 | 3.159 | 2.555 | 2.076 | 1.303 | 2.719 | 5 | 369 | 372 | 3 |
| 1/7291 | 0.177 | 0.071 | 1.794 | 3.181 | 2.251 | 2.228 | 1.240 | 2.972 | 5 | 360 | 375 | 15 |
| SD-60 | 0.103 | 0.063 | 1.854 | 3.117 | 2.200 | 2.347 | 1.384 | 2.689 | 5 | 411 | 385 | -26 |
| SD-99 | 0.113 | 0.019 | 1.852 | 3.104 | 2.149 | 2.407 | 1.352 | 2.696 | 5 | 375 | 378 | 3 |
| SD-193 | 0.178 | 0.125 | 1.722 | 3.259 | 1.834 | 2.114 | 1.420 | 2.915 | 5 | 321 | 329 | 8 |
| 15/6291 | 0.186 | 0.115 | 1.765 | 3.267 | 2.314 | 2.347 | 1.246 | 2.905 | 5 | - | 353 | - |
| SD-42 | 0.206 | 0.247 | 1.602 | 3.290 | 2.223 | 2.481 | 1.298 | 2.689 | 5 | 307 | 322 | 15 |
| SD-64 | 0.229 | 0.142 | 1.671 | 3.268 | 2.044 | 2.517 | 1.360 | 2.710 | 5 | 289 | 303 | 14 |
| SD-198 | 0.449 | 0.355 | 1.306 | 3.520 | 2.809 | 2.187 | 1.010 | 2.894 | 5 | 246 | 303 | 57 |
| SD-211 | 0.098 | 0.224 | 1.711 | 3.127 | 2.033 | 2.450 | 1.437 | 2.652 | 5 | 325 | 385 | 60 |
| SD-217 | 0.128 | 0.281 | 1.623 | 3.164 | 2.138 | 2.428 | 1.322 | 2.813 | 5 | 281 | 393 | 112 |
| SD-221 | 0.175 | 0.062 | 1.803 | 3.254 | 2.156 | 2.305 | 1.441 | 2.654 | 5 | 316 | 309 | -7 |

P = estimated pressure in kbar,
T PlMs = plagioclase-muscovite temperature in oC (Green and Usdansky, 1986)
T MsChl = phengite-chlorite temperature in oC (Chapter 2)

geothermometer using the compositional data of plagioclase and muscovite in Table 5.2 and Table 5.3 respectively, gives the temperatures in the range 281-411 °C (Table 5.8). It is noted that this temperature is rather sensitive to mole fraction of orthoclase ($X_{or}$) which is always low in plagioclase of low-grade pelitic rocks, therefore a careful analysis of plagioclase was carried out. Long counting time (40-60 seconds) was used for $K_2O$ to reduce the component of analytical uncertainty. Samples containing plagioclases with $K_2O$ close to microprobe detection limit were not considered.

A newly developed calibration of the phengite-chlorite geothermometer (Chapter 2) applied to the same suite of rocks, using chlorite compositions in Table 5.4 and phengite compositions in Table 5.3, yields similar results (Table 5.8). The temperatures given by phengite-chlorite geothermometer (i.e. 303-393 °C) are similar to the temperatures calculated from Green and Usdansky's plagioclase-muscovite geothermometry (i.e. 281-411 °C) as shown in Table 5.8 and Figure 5.10. The textural evidence and parallel tie lines in AKF diagram (Fig. 5.3) indicate that phengite and chlorite pairs in these low-grade psammitic and pelitic rocks are in equilibrium, at least on a thin section scale.

Also shown are element partitionings between these two phases. Among these, Mg partitioning and the quotient $Al^{vi}.Al^{iv}/Mg.Si$ shows regular linear trends in contrast to Fe partitioning (Fig. 5.11). This supports the justification of calibrating the Tschermak substitution between phengite and chlorite as a practical geothermometer for low temperature metamorphism of pelites or semi-pelites.

Across the 20 Km of outcrop width no variation in metamorphic grade was detected within the metasedimentary package despite the large faults which cut through the study area.

### 5.3.5 Timing of metamorphism of the metasediments

The Pha Som Group is in thrust contact with the Permo-Triassic Pak Pat volcanics that are overlain by the Triassic turbidite sequence. From this field relationships, it is uncertain whether the timing of metamorphism of the metasediments within Pha Som Metamorphic Complex is pre-Permo-Triassic or younger. On the ground of microstructural evidence, the metamorphism is syn-$D_2$ which predates cleavage-forming event in the Triassic turbidites (Table 4.1). Barr and Macdonald (1987) interpreted a single Middle Permian K-Ar age (269±12 Ma) of actinolite from mafic schists of the Pha Som Group as a minimum age for the greenschist facies metamorphism. However, actinolite is strongly effected by inherited Ar, so it is difficult to accept this interpretation without a more extensive

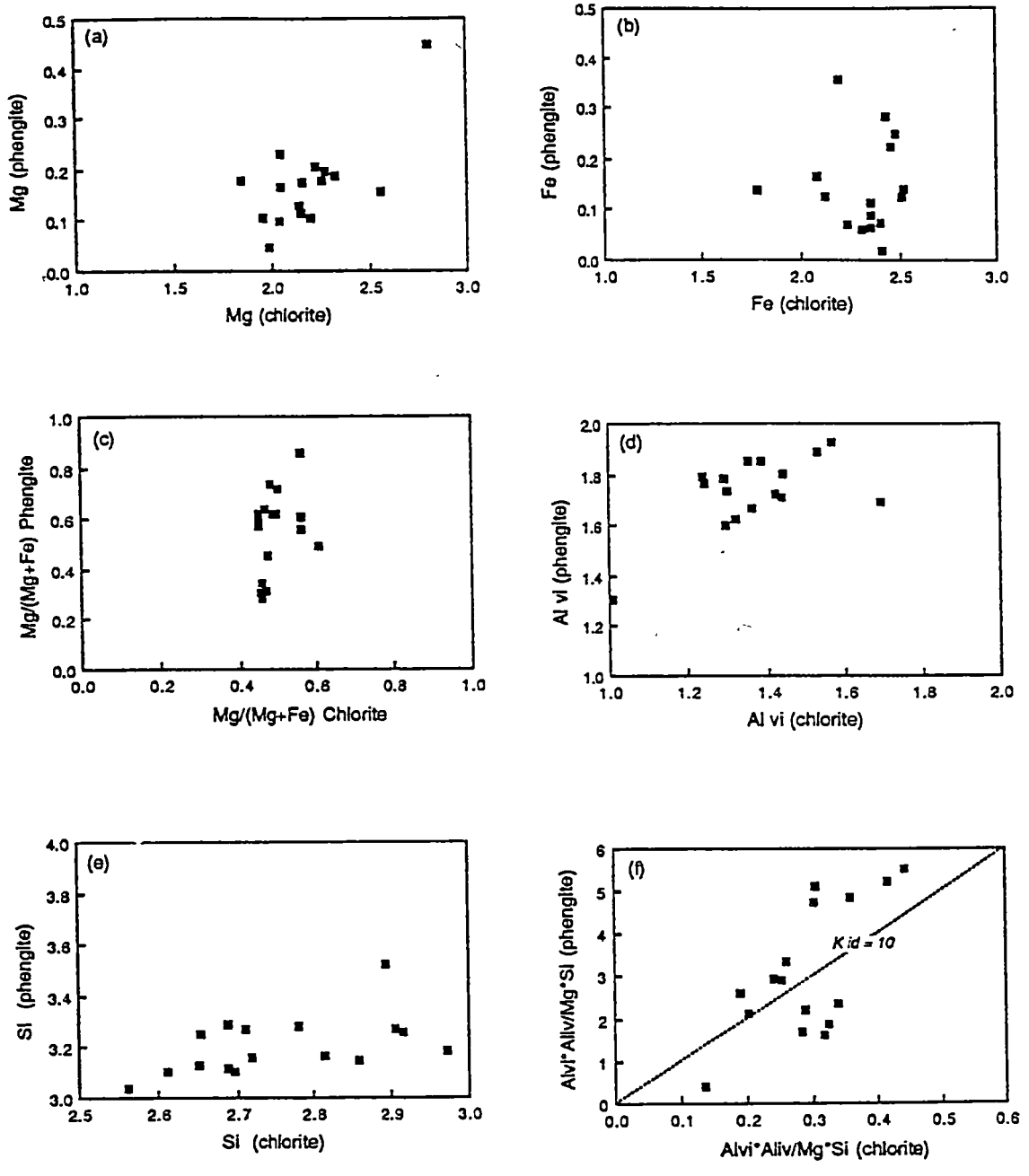


Figure 5.11 Plots showing element partitioning between coexisting phengites and chlorites in the Pha Sòm M.C. psammites and pelites: (a) Mg-Mg; (b) Fe-Fe, (c) Mg/(Mg+Fe) - Mg/(Mg+Fe); (d) $Al^{vi}$ - $Al^{vi}$, (e) Si-Si; (f) $Al^{iv}Al^{vi}$/MgSi - $Al^{iv}Al^{vi}$/MgSi with ideal partitioning coefficient (Kid) = 10 being shown.

dating program. On the basis of the existing constraints, the possible metamorphic age of the metasediments is between Carboniferous and Middle Triassic.

## 5.4 Metamorphism of the ophiolite association

The ophiolite association consists largely of fault-bounded blocks of a mixed variety of rocks ranging in size from less than 1 metre to a few kilometres. These blocks are enclosed in a sheared serpentinite matrix in several localities, thereby the term "serpentinite melange" was introduced (Hada,1990; Panjasawatwong, 1991). They include mainly mafic and ultramafic igneous rocks together with variable proportions of amphibolites, piemontite-bearing quartz schist, bedded chert, greywacke, argillite and limestone. The mafic and ultramafic igneous rocks which are the dominant lithologies include basalt, andesite, dolerite, gabbro, pyroxenite and peridotites. Amphibolitisation of clinopyroxenes in gabbros and pyroxenites together with serpentinisation of peridotites are common. The content of this section will focus specifically on the metamorphic history of amphibolites and piemontite-bearing quartz schist in which the prograde mineral assemblages are largely preserved. In addition, a brief account of the serpentinisation of peridotites is also presented as part of metamorphic history of the ophiolite association.

### 5.4.1 Amphibolites

Blocks of garnet amphibolite, zoisite amphibolite, and amphibolite are common within the serpentinite melange. Various geothermobarometric techniques were used in combination with available data on age-dating to decipher the *P-T* history of these amphibolite blocks.

#### Petrography

The studied amphibolites (Figs. 5.12a,b,c&d) consist mainly of amphibole with variable amounts of clinopyroxene, garnet, zoisite and plagioclase. Quartz occurs only as a retrograde mineral together with epidote, albite and rare prehnite in few samples, otherwise it is totally absent from the prograde assemblage. Texturally, the amphibolites range from medium-grained schistose rocks (e.g. sample 2/7291) to coarse-grained granoblastic rocks (e.g. sample 9/7291 shown in Figures 5.12a&b). The pronounced foliation developed in many samples is defined by the preferred orientation of prismatic crystals, particularly amphibole and to a

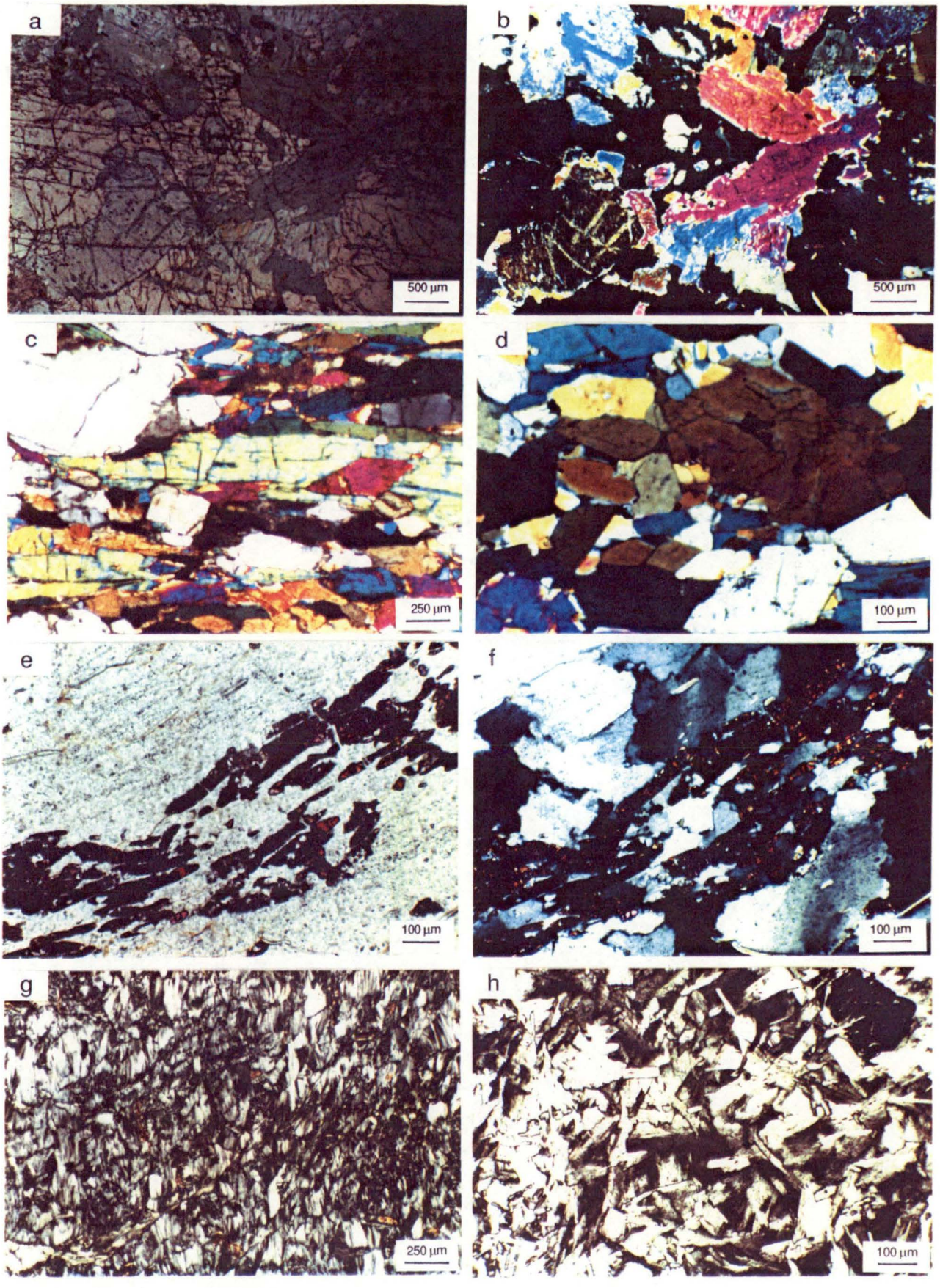
a
500 µm
b
500 µm
c
250 µm
d
100 µm
e
100 µm
f
100 µm
g
250 µm
h
100 µm

lesser extent zoisite (Fig. 5.12c). Poorly-defined differentiated layering between amphibole (dark) and zoisite (white) is common in zoisite amphibolites (e.g samples 4/7291 and 7/7291). Amphibole crystals commonly show straight grain-boundaries (Fig. 5.12d) indicating textural equilibrium.

## Mineralogy

The mineral assemblages in amphibolites are shown in Table 5.9. The most common assemblage is hornblende + clinopyroxene + zoisite.

Table 5.9 Mineral assemblages in amphibolites of the ophiolite association

| Sample no. | Hbl | Cpx | Grt | Zo | Pl |
|---|---|---|---|---|---|
| 5/6291 | X | X | | X | |
| 6/6291 | X | | | | |
| 2/7291 | X | | | | |
| 4/7291 | X | X | | X | |
| 7/7291 | X | | | X | |
| 8/7291 | X | X | | X | |
| 9/7291 | X | X | X | X | |
| 12/7291 | X | X | | X | X |

Sample 9/7291 is the only rock that contains the assemblage garnet+ hornblende + clinopyroxene.

**Amphibole :** Amphibole is the principal constituent of amphibolites, generally forming subhedral to euhedral crystals which commonly show sharp-straight grain boundaries. The amphibole analyses are given in Table C-1 (Appendix C). The structural formula of amphibole was calculated on the basis of 23 oxygens and by normalising the number of cations other than Ca, Na and K to 13 as recommended by Leake (1978). They are calcic amphiboles with relatively high Mg/(Mg+Fe) ratio (0.68-0.84). These calcic amphiboles can be classified into two subgroups according to Leake (1978): (i) those with $(Na+K)_A < 0.5$ include tschermakite, tschermakitic hornblende, magnesio-hornblende and actinolitic hornblende (samples 5/6291, 6/6291, 2/7291 and 9/7291); and (ii) those with

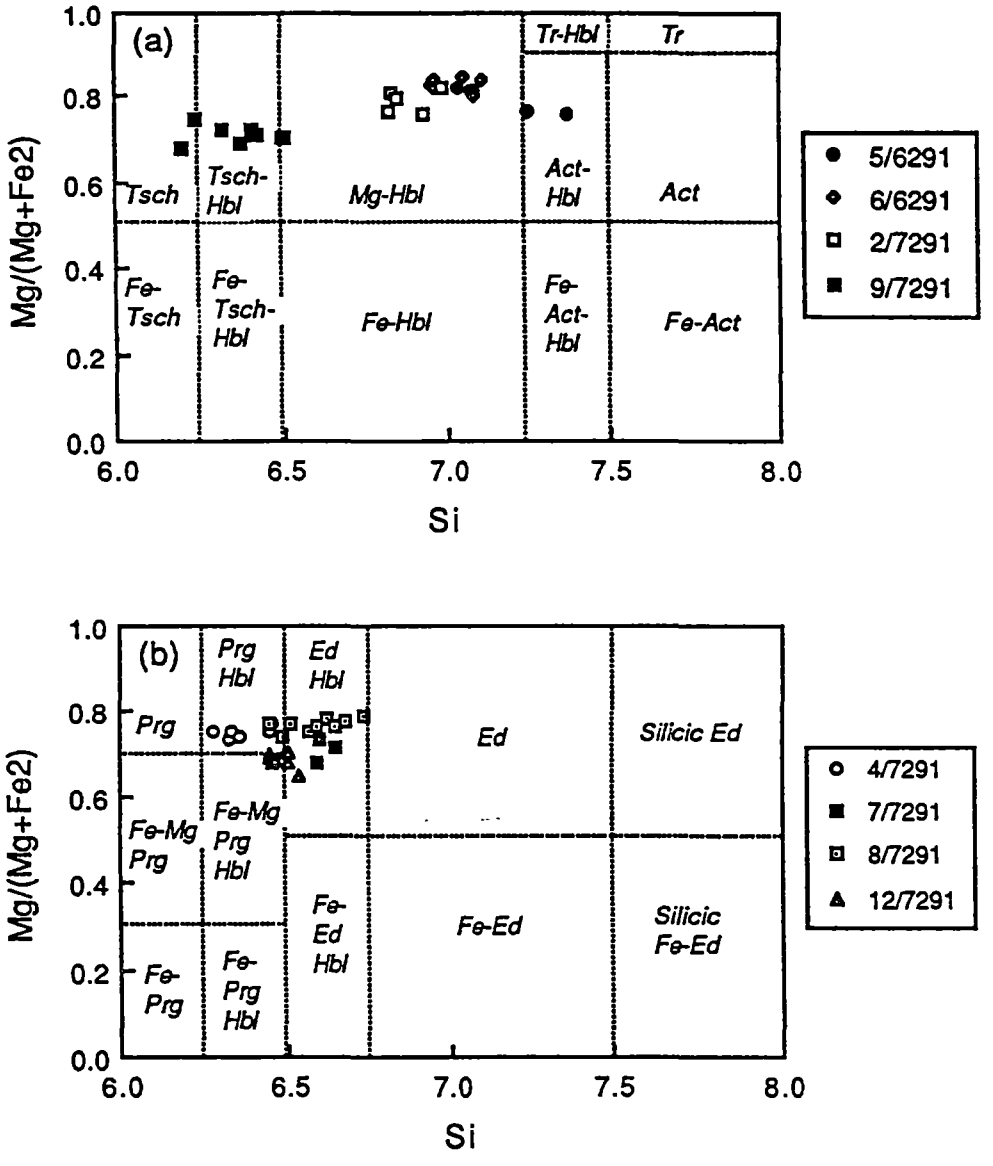


Figure 5.13 Amphibole compositions in the amphibolite blocks plotted on Mg/(Mg+Fe2) versus Si classification diagrams of Leake (1978): (a) amphiboles with (Na+K) in A sites less than 0.5, and (b) amphiboles with (Na+K) in A sites greater than 0.5. All are calcic amphiboles.

$(Na+K)_A \geq 0.5$ include pargasitic hornblende, edenitic hornblende and edenite (samples 4/7291, 7/7291, 8/7291 and 12/7291) as shown in Figure 5.13.

**Clinopyroxene :** Clinopyroxene crystals are anhedral to subhedral. In some samples (e.g. sample 9/7291) they have distinct exsolution lamellae and are commonly rimmed by or enclosed in amphibole crystals. Clinopyroxene is diopside (Table C-2 in Appendix C) with Mg/(Mg+Fe) ratio ranging between 0.78-0.90. The structural formula of clinopyroxene was calculated from the electron microprobe analyses assuming stoichiometry on the basis of 6 oxygens. The end-member components, wollastonite (Wo), enstatite (En) and ferrosilite (Fs), are calculated following the Subcommittee on Pyroxenes, International Mineralogical Association (1988).

**Garnet :** Garnet (sample 9/7291) occurs as large poikiloblastic grains enclosing clinopyroxene and amphibole crystals (Figs. 5.12a&b). It is almandine with high grossular component ($Alm_{46}Prp_{18}Sps_1Grs_{31}Adr_4$). The garnet analyses are listed in Table C-3 (Appendix C). The structural formula of garnet was calculated from the electron microprobe analyses assuming stoichiometry on the basis of 12 oxygens.

**Zoisite :** Zoisite occurs as euhedral-subhedral prismatic crystals in samples 4/7291, 7/7291 and 8/7291. It is virtually pure zoisite with uniform $Fe^{3+}/(Fe^{3+}+Al)$ ratio of about 0.05 (Table C-4 in Appendix C). Zoisite structural formula was calculated on the basis of 12.5 oxygens and by assuming total iron as $Fe_2O_3$. In sample 5/7291, clinozoisite occurs instead of zoisite. The composition of clinozoisite is also very uniform as indicated by a narrow range of $Fe^{3+}/(Fe^{3+}+Al)$ ratio between 0.14 and 0.16.

**Plagioclase :** Plagioclase is a rare phase in the studied amphibolites. If present, it has a turbid appearance due to alteration to epidote and Fe-oxide. In sample 12/7291, plagioclase is extremely calcic ($An_{87-97}$).

**Other minerals :** Some samples (e.g. 5/6291) contain the retrograde assemblage epidote + quartz + albite + prehnite which is probably associated with later deformation. The compositions of these retrograde phases will not be discussed any further.

## Amphibole composition as a qualitative indicator of metamorphic grade

The amphibole compositions vary systematically among the studied amphibolites. These compositional variations can be considered in terms of substitutions into the basic tremolite formula, $\diamond Ca_2Mg_5Si_8O_{22}(OH)_2$ (the symbol

◇ denotes a site vacancy) as suggested by Deer *et al.* (1966) and Spear (1981). The role of coupled substitutions has been shown to be much more important than that of simple substitutions (e.g. Fe-Mg or Fe-Mn exchange), these coupled substitutions include:

(i) ◇ (A) + Si = Na (A) + $Al^{iv}$, edenite substitution;

(ii) 2(Mg,Fe) + 2Si = 2$Al^{vi}$ + 2$Al^{iv}$, Tschermak substitution;

(iii) 2(Mg,Fe) + 2Si = 2$Fe^{3+}$ + 2$Al^{iv}$, ferri-Tschermak substitution;

(iv) ◇ (A) + (Mg,Fe) + 2Si = Na (A) +$Al^{vi}$ + $Al^{iv}$, pargasite substitution;

(v) 2Ca (M4) + 2(Mg,Fe) = 2Na (M4) + 2$Al^{vi}$ , glaucophane substitution;

(vi) ◇ (A) + (Mg,Fe) = 2$Al^{vi}$ + Ti, Ti-Tschermak substitution.

A plot of A-site occupancy (Na+K) versus $Al^{iv}$ (Fig. 5.14a) shows a broad linear relationship with a slope of about 0.5 that almost follows the trend of pargasite substitution. The intercept at approximately 0.5 $Al^{iv}$ for 0.0 A-site cations indicates that all A-site occupancy is compensated for by $Al^{iv}$ and the residual 0.5 $Al^{iv}$ requires additional substitution involving $Al^{iv}$, e.g. substitution (ii) or (iii) as suggested by Spear (1981).

A plot of $Al^{vi}$ versus $Al^{iv}$ (Fig. 5.14b) also indicates that an increase in Al-content of calcic-amphiboles is attributed to the combination between Tschermak and edenite substitutions that produce a pargasite substitution.

An excellent correlation between A-site occupancy+2Ti+$Al^{vi}$+$Fe^{3+}$ and $Al^{iv}$ shown in Figure 5.14c indicates that substitutions (i), (ii), (iii) and (vi) are combined to explain all the compositional variation.

No correlation is observed for Na (M4) and $Al^{vi}$ (Fig. 5.14d) which suggests that the compositional variation of the studied amphiboles does not significantly involve substitution (v).

Several workers (e.g. Brown, 1977; Laird and Albee, 1981a) have proposed that amphibole compositions, in particular the Al and Na contents, can be used (at least semi-qualitatively) as a pressure indicator. It has been noted that the glaucophane substitution dominates during high-pressure facies series metamorphism whereas edenite and Tschermak substitutions dominate during low-pressure facies series metamorphism. As shown above, the compositional variation of the studied amphiboles is accounted for largely by the edenite and Tschermak substitutions. In fact, their compositional field lies below 1:1 line (typical of medium-pressure facies series mafic schist) in a Na/(Na+Ca) and Al/(Al+Si) plot (Fig. 5.14e) and overlaps with the compositional fields of both medium and low-pressure facies series mafic schists from Vermont, U.S.A. (Laird and Albee, 1981b). These lines of evidence suggest that the amphibolites in the Sirikit Dam area belong to low to medium pressure facies series. The only problem may be related to

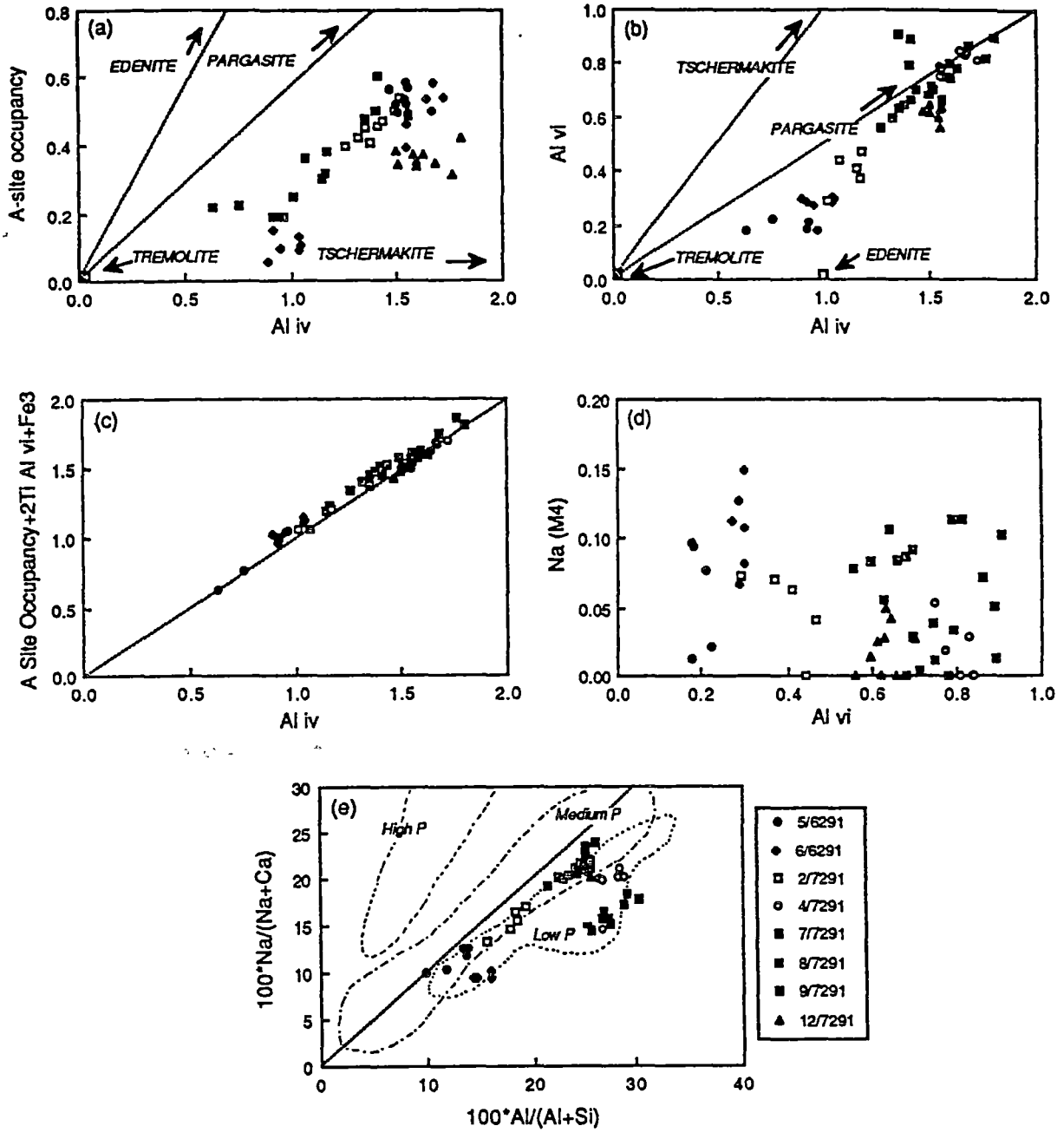


Figure 5.14 Plots showing compositional variations of amphiboles in amphibolite blocks: (a) A-site occupancy versus $Al^{iv}$; (b) $Al^{vi}$ versus $Al^{iv}$; (c) A-site occupancy $+2Ti+Al^{vi}+Fe^{3+}$ versus $Al^{iv}$; (d) Na(M4) versus $Al^{vi}$; and (e) 100Na/(Na+Ca) versus 100Al/(Al+Si).

the absence of quartz and low Na of these rocks which indicates they are not typical amphibolites.

## *P-T* conditions of metamorphism of amphibolites

Applications of garnet-hornblende geothermometry (Graham and Powell, 1985) and garnet-clinopyroxene geothermometry (Ellis and Green, 1979; Pattison and Newton, 1989; Yang, 1992) to sample 9/7291 (using mineral compositional data in Table 5.10) indicate that this rock has been equilibrated at the temperature of 690 °C, 720 °C, 570 °C and 659 °C respectively assuming a pressure of 6 kbar (Fig. 5.15). The geothermometers of Graham and Powell (1984) and Ellis and Green (1979) yield unlikely high temperatures whereas Pattison and Newton' geothermometer gives a very low value. The temperature of 659 °C given by the geothermometer of Yang (1992) is probably the best estimate because this thermometer has been calibrated to deal specifically with high grossular component of garnet in this rock ($X_{Ca}^{Grt} = 0.31$) and also to correct for the effect of Mg content of garnet ($X_{Mg}^{Grt}$) as well.

It was noted that the following Tschermak exchange reaction between coexisting clinopyroxene and hornblende:

$NaCa_2Mg_4AlSi_6Al_2O_{22}(OH)_2 + CaMgSi_2O_6 = CaAlSiAlO_6 + NaCa_2Mg_5Si_7AlO_{22}(OH)_2$

pargasite + diopside = Ca-Tschermak pyroxene + edenite

may be used as geothermometer. This reaction is not strongly dependent on pressure. The high uncertainties in the calculated activities of the end-member components, particularly Ca-Tschermak pyroxene and to a lesser extent edenite and pargasite, limit the usefulness of this potential thermometer. However, the temperatures computed from this reaction using thermodynamic data set of Holland and Powell (1990) are comparable to those obtained from garnet-hornblende geothermometer (Graham and Powell, 1984). Subsequently, an attempt was made to apply this reaction to the garnet-free amphibolites in the Sirikit Dam area. The ideal activity-composition relation (Powell and Holland, 1988) is used to calculate the activities of end-member components in clinopyroxene, amphibole and zoisite from the mineral compositional data in Table 5.10. Based on thermodynamic data set of Holland and Powell (1990), the reactions relevant to these phases can be calculated. The temperature of 600 °C, obtained when applied this technique to zoisite amphibolite (sample 4/7291), is in good agreement with that of garnet amphibolite (sample 9/7291). A calculated minimum equilibration pressure of this

Table 5.10 Representative electron microprobe analyses of minerals in amphibolites of the ophiolite association

| Sample no. | 9/7291 | | | | 4/7291 | | |
|---|---|---|---|---|---|---|---|
| Mineral | Grt(core) | Grt(rim) | Cpx | Hbl | Cpx | Hbl | Zo |
| SiO2 | 38.64 | 38.47 | 50.50 | 43.51 | 52.74 | 44.28 | 38.85 |
| TiO2 | 0.08 | 0.03 | 0.56 | 0.64 | 0.07 | 0.30 | 0.03 |
| Al2O3 | 21.41 | 21.45 | 4.28 | 14.59 | 3.04 | 13.92 | 31.45 |
| Cr2O3 | 0.02 | 0.03 | 0.00 | 0.03 | 0.06 | 0.09 | 0.04 |
| Fe2O3* | - | - | - | - | - | - | 2.47 |
| FeO# | 23.24 | 21.22 | 7.20 | 12.28 | 4.68 | 10.04 | - |
| MnO | 0.48 | 0.53 | 0.01 | 0.03 | 0.15 | 0.14 | 0.03 |
| MgO | 6.35 | 3.50 | 13.13 | 12.04 | 14.32 | 13.63 | 0.04 |
| CaO | 10.16 | 14.50 | 24.36 | 12.77 | 24.46 | 12.68 | 14.59 |
| Na2O | - | - | 0.20 | 1.37 | 0.20 | 1.78 | 0.01 |
| K2O | - | - | - | 0.02 | - | 0.10 | - |
| Total | 100.37 | 99.73 | 99.26 | 97.27 | 99.73 | 96.96 | 97.63 |
| Number of cations per formula unit$ | | | | | | | |
| Si | 2.97 | 3.00 | 1.90 | 6.32 | 1.95 | 6.61 | 2.98 |
| Ti | 0.01 | - | 0.02 | 0.07 | - | 0.04 | 0.02 |
| Al | 1.94 | 1.97 | 0.19 | 2.50 | 0.13 | 2.25 | 2.84 |
| Cr | 0.00 | - | - | - | - | - | - |
| Fe3+ | 0.12 | 0.04 | 0.06 | 0.34 | 0.00 | 0.02 | 0.14 |
| Fe2+ | 1.38 | 1.35 | 0.17 | 1.15 | 0.14 | 1.18 | - |
| Mn | 0.03 | 0.04 | - | - | 0.01 | 0.01 | - |
| Mg | 0.73 | 0.41 | 0.72 | 2.61 | 0.79 | 2.89 | 0.01 |
| Ca | 0.84 | 1.21 | 0.97 | 1.99 | 0.97 | 1.91 | 2.03 |
| Na | - | - | 0.01 | 0.39 | 0.01 | 0.58 | - |
| K | - | - | - | - | - | 0.04 | - |
| Total Cations | 8.00 | 8.00 | 4.00 | 15.38 | 4.00 | 15.52 | 8.01 |
| Oxygens | 12.00 | 12.00 | 6.00 | 23.00 | 6.00 | 23.00 | 12.50 |

* Total Fe as Fe2O3

# Total Fe as FeO

$ Calculated by stoichiometry for garnet and clinopyroxene and by normalising the number of cations other than Ca,Na, and K to 13 for hornblende.

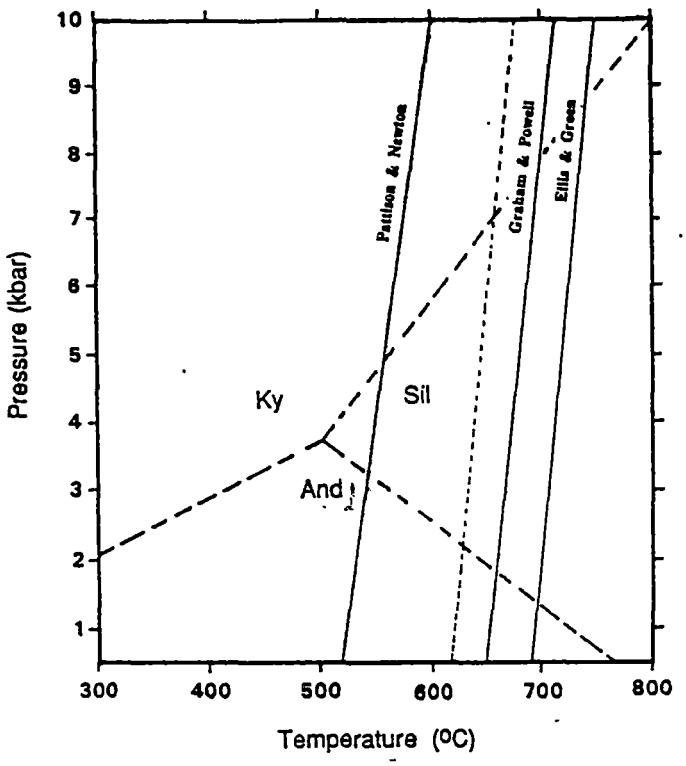


Figure 5.15 *P-T* diagram showing calculated temperatures for sample 9/7291 using garnet-clinopyroxene geothermometers of Ellis and Green (1979), Pattison and Newton (1989) and a new calibration of Yang (1992) (dashed line); and garnet-hornblende geothermometer of Graham and Powell (1984).

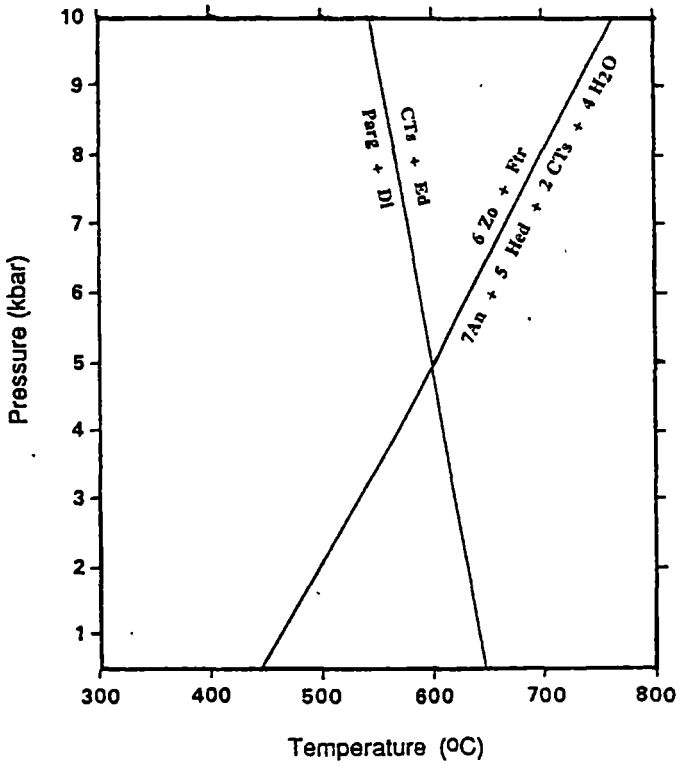


Figure 5.16 *P-T* diagram showing end-member reactions calculated from thermodynamic dataset of Holland and Powell (1990) for rock 4/7291. Note the steep slope of the Tschermak exchange reaction isopleth between coexisting clinopyroxene and amphibole.

rock is 5 kbar at the intersection with the reaction: zoisite + Fe-tremolite = anorthite + hedenbergite + Ca-Tschermak pyroxene + $H_2O$ (Fig. 5.16). Anorthite activity was assumed to be unity which is reasonable when considering a very calcic composition of plagioclase in these amphibolites.

### 5.4.2 Piemontite-bearing quartz schist

The piemontite-bearing quartz schist occurs probably as blocks together with amphibolites and ultramafic rocks of the opiolite association.

#### Petrography

Piemontite-bearing quartz schist consists chiefly of quartz (up to 95%) with subordinate phengitic white mica and small amount of chlorite and piemontite. Quartz grains are relatively flattened subparallel to the schistosity which is defined by alignment of slender prismatic piemontite and platy phengitic muscovite (Figs. 5.12e&f). Accessory minerals include haematite, magnetite and rutile.

#### Mineralogy

Piemontite-bearing quartz schist is characterised by the assemblage quartz + phengitic muscovite + chlorite + piemontite + haematite + magnetite + rutile.

**Quartz :** Quartz is an ubiquitous phase in piemontite-bearing quartz schist (e.g. sample 2/6291). Quartz crystals are about 500 μm in diameter on average. They commonly have undulatory extinction and sutured grain boundaries.

**Piemontite :** Piemontite occurs as fine-grained prismatic grains having distinctive pink, yellow and violet pleochroism. The average composition of this Mn-rich epidote mineral (sample 2/6291) is $Pm_{14}Ps_{19}Cz_{67}$, expressed in terms of clinozoisite ($Ca_2Al_3Si_3O_{12}(OH)$), pistacite ($Ca_2Fe^{3+}{}_3Si_3O_{12}(OH)$) and piemontite ($Ca_2Mn^{3+}{}_3Si_3O_{12}(OH)$) end-members. The piemontite analyses are listed in Table C-5 (Appendix C). The structural formula of piemontite was calculated after Smith and Albee (1967) and Kawachi *et al.* (1983).

**Muscovite :** Phengitic muscovite contains substantial proportion of celadonite component (Si = 3.25 -3. 47 atoms per 11 oxygens). A fairly high $Na_2O$ content (0.15-1.43 wt%) is similar to those occur in piemontite-bearing schist in western Otago, New Zealand (Kawachi, *et al.*, 1983). The paragonite component, expressed as Na/(Na+K), ranges from 0.02 to 0.189. The muscovite analyses are

given in Table C-6 (Appendix C). The structural formula of muscovite was calculated on the basis of 11 oxygens and by assuming total iron as FeO.

**Chlorite :** Chlorite, a minor phase in piemontite-bearing quartz schist, is virtually colourless in thin section. It is extremely high in MgO with the Mg/(Mg+Fe) ratio of up to 0.98 typical of chlorite coexisting with piemontite (Keskinen, 1981; Kawachi *et al.* , 1983). According to Foster (1962), this chlorite can be classified as clinochlore. The chlorite analyses are listed in Table C-7 (Appendix C). Chlorite structural formula was calculated on the basis of 14 oxygens and by assuming total iron as FeO.

**Other minerals :** Accessory haematite, magnetite and rutile occur as small disseminated grains of variable sizes (5-100 μm). Identification of these phases was aided by electron microprobe analyses.

## *P-T* conditions of metamorphism of piemontite-bearing quartz schist

The mineral assemblage of this rock type (sample 2/6291) does not allow for precise thermodynamic *P-T* calculation. However, the presence of Mg-chlorite instead of phlogopite in this rock suggests the temperature range in the lower end of greenschist facies (i.e. probably less than 450 °C).

The geobarometer of Massonne and Schreyer (1987) based on the Si content of phengitic muscovite (3.25 - 3.47 atoms per 11 oxygens) suggests the pressure of 7±1 kbar at an estimated temperature of 440 °C for this sample. This pressure estimate can be treated only as an approximation of a minimum pressure because the studied phengite does not occur in a limiting assemblage K-feldspar + quartz + phlogopite + phengite but coexists with only Mg-chlorite.

The phengite-chlorite geothermometry (Chapter 2) yields the temperature of 440 °C at a minimum pressure of 7 kbar for sample 2/6291.

Keskinen and Liou (1987) in their reversal study of the reaction:
Fe-piemontite ($Pm_{17}Ps_{17}Cz_{66}$) + quartz = garnet ($Grs_{33}Sps_{27}Adr_{40}$) + anorthite + fluid
at $P_{fluid}$ = 2 kbar, found that the breakdown of Fe-piemontite occurred at 365±10 °C for the haematite-magnetite buffer. The result of this experiment is potentially applicable to the occurrence of piemontite coexisting with haematite and magnetite from the Sirikit Dam area judging from the similarity in piemontite compositions and oxygen fugacity buffered by haematite and magnetite. The above piemontite breakdown reaction was shown not to be strongly affected by pressure in the experimental range (Keskinen and Liou, 1987). Unfortunately, their experimental

study did not extend to the higher pressure range where Langer, Anastasiou and Abs-Wurmbach (1976) suggested that the pressure effect on a piemontite breakdown temperature becomes more dramatic at 7-15 kbar.

In similar piemontite-bearing schists of the Haast Schist terrane in western Otago, New Zealand, *P-T* conditions of metamorphism have been correlated with those of the associated greenschists, i.e. temperatures in the range 363-422 °C and pressure of 6.4±0.4 kbar (Yardley, 1982; Kawachi *et al.* , 1983). This relatively high *P/T* metamorphism has largely been overprinted by regionally developed greenschist facies metamorphism (with estimated pressure of 4-5 kbar) that may result from thermal relaxation and/or decompression due to rapid uplift or tectonic unroofing (Kawachi *et al.* , 1983). However, the piemontite-bearing quartz schists in the Sirikit Dam area apparently preserve their high *P* - low*T* metamorphic assemblage without any significant greenschist facies overprint.

The presence of piemontite with haematite and magnetite in this rock suggests high oxygen fugacity ($fO_2$), low partial pressure of $CO_2$ in the fluid phase (Smith and Albee, 1967; Kawachi *et al.*, 1983; Keskinen and Liou, 1987). This highly oxidised condition is believed to be inherited from the oxidised protolith which is probably Mn-bearing siliceous pelagic/hemipelagic sediments.

### 5.4.3 Serpentinites

Serpentinisation of the peridotites, i.e. harzbergite, lherzolite and dunite, may be due to hydrothermal metamorphism at the ocean floor and/or lower greenschist-facies metamorphism during $D_2$ thrusting where water was able to percolate through faults or shear zones as evidence of high shear strain is always present in serpentinites.

### Petrography

Serpentine minerals in thin section were identified using the identification chart proposed by Wicks and Whittaker (1977). In some samples in which relic olivine or pyroxene grains are preserved, mesh-rim texture typical of lizardite make it distinct from fibrous chrysotile (Figs. 5.12g). Antigorite generally forms easily recognised interpenetrating (flame or thorn) textures composed of sharp distinct blades (Fig. 5.12h).

The mineral assemblage of the serpentinites is serpentine + chlorite ± talc ± garnet ± chromite ± magnetite ± magnesite ± calcite ± brucite.

## Mineralogy

**Serpentine :** The common varieties of serpentine in serpentinites from the Sirikit Dam area are lizardite and chrysotile. Antigorite is less common. The serpentine analyses are listed in Table C-8 (Appendix C). The structural formula of serpentine was calculated on the basis of 7 oxygens and assuming total iron as FeO.

**Chlorite :** Chlorite occurs as small colourless flakes in serpentinites. It has a very high Mg/(Mg+Fe) ratio, i.e. in the range 0.94-0.96 (Table C-9 in Appendix C). The structural formula of chlorite was calculated on the basis of 14 oxygens and assuming total iron as FeO. According to Foster's classification (1962), they can be classified as penninite (Fig. 5.4).

**Talc :** Talc (sample 206) appears as small colourless flakes with typical interference colour similar to muscovite. The Mg/(Mg+Fe) ratio is very high, ranging between 0.91 and 0.94.

**Garnet :** Garnet (sample 13/7291) occurs as poikiloblastic grains. Compositionally, it is andradite ($Grs_{10}Adr_{90}$).

**Other minerals :** Chromite occurs as disseminated grains having Cr/(Cr+Al) ratio of 0.81-0.83, Mg/(Mg+Fe) of 0.38-0.39. Disseminated magnetite is present in some samples. Carbonate mineral, occurring mostly in veinlets, is dolomite ($CaMg_{0.96}Fe_{0.04}(CO_3)_2$).

## *P-T* conditions of serpentinisation

Wenner and Taylor (1971, 1973, 1974) used the serpentine-magnetite thermometry to differentiate lizardite-chrysotile serpentinites ($T$ = 85-185 °C) and antigorite serpentinites ($T$ = 220-460 °C). Petrographic observation presented above indicate that the hydration of peridotites to form serpentine proceeds via a metastable reaction where lizardite pseudomorphs after olivine as suggested by O'Hanley (1991). This reaction is driven by the addition of water to the peridotite within the stability field of hydrous minerals such as chrysotile or antigorite. Serpentine recrystallisation occurs in the presence of a fluid rich in $X_{H_2O}$. This fluid is also a source of $SiO_2$ in the Sirikit Dam area where there is extensive silicification of serpentinite.

Alternatively, the *P-T* conditions of serpentinisation in the Sirikit Dam area may be approximated by the following univariant reactions, involving the assemblage serpentine + talc + magnesite + calcite + quartz:

(i) serpentine + 2 quartz = talc + $H_2O$

(ii) 2 serpentine + 3 $CO_2$ = 1 talc + 3 magnesite + 3 $H_2O$

(iii) serpentine + 3 $CO_2$ = 1 quartz + 3 magnesite + 2 $H_2O$

(iv) 4 quartz + 3 magnesite + $H_2O$ = talc + 3 $CO_2$

The invariant point is located at 340±10 °C and at $X_{CO_2}$ of about 0.01 (Winkler, 1976). Reaction (i) takes place only in $SiO_2$ rich ultramafic rocks and marks the boundary between very low- and low-grade metamorphism (Winkler, 1976).

In addition to the metamorphism discussed above, illite crystallinity study of argillite blocks indicates they have been subjected to very low-grade metamorphism. The illite crystallinity values of argillite (Table 5.8) fall in the range of upper anchimetamorphic grade ($\Delta°2\theta$ = 0.25-0.28) following the illite crystallinity scale of Kisch (1990).

### 5.4.4 Timing of metamorphism of the ophiolite association

An $^{40}Ar/^{39}Ar$ amphibole plateau date of 338 Ma was obtained for an amphibolite from the Nan River area (Drs. Y. Panjasawatwong and A.J. Crawford, pers. comm., 1993). This age probably represents the time of the amphibolite-facies metamorphism of blocks within the ophiolite association. Amphibolites in the Sirikit Dam area are chemically related to cumulate gabbros and associated ultramafics and chromitites which are chemically most like oceanic-island arc cumulates originated in a supra-subduction zone setting (Panjasawatwong, 1991). This implies that the amphibolites are probably the result of metamorphism of the oceanic-arc basement where high heat flow was supplied by invading magma.

The timing of metamorphism of piemontite-bearing quartz schist is not known. Possibly, it is pene-contemporaneous with the metamorphism of amphibolites. The highly oxidised condition of this rock type is taken as evidence for the oxidised protolith which is probably Mn-bearing siliceous pelagic/hemipelagic sediments subducted deeply beneath the volcanic arc/accretionary complex.

## 5.5 Metamorphism of the Pak Pat Volcanics

The metavolcanic rocks largely retain relict igneous textures. However, the original igneous mineralogy has extensively been replaced by secondary minerals probably the result of low-grade metamorphism. These secondary minerals include chlorite, epidote, calcite, albite and rare pumpellyite.

## Petrography

Most volcanic samples retain their original igneous texture, i.e. porphyritic to strongly porphyritic. The phenocryst and microphenocryst assemblage is strongly saussuritised plagioclase, clinopyroxene, chlorite and epidote. Plagioclase phenocrysts, generally shows glomero-porphyritic texture, are more abundant than their mafic counterparts. They are subhedral to anhedral and largely replaced by calcite, epidote, sericite and, to a lesser extent, pumpellyite and clinozoisite.

Groundmass constituents are predominantly lath-shaped albitised plagioclase with interstitial magnetite, dark cryptocrystalline materials and a small amount of microcrystalline quartz. Quartz and calcite veins are locally present.

## Mineralogy

**Chlorite :** Chlorite is pale green or green under microscope. Both brown and anomalous blue interference colours are present. Mg/(Mg+Fe) ratio of chlorite ranges from 0.45 to 0.62 (Table D-1 in Appendix D). Chlorite formula was calculated on the basis of 14 oxygens and by assuming total iron as FeO. Following Foster (1962), these chlorites are mainly brunsvigite with only minor ripidolite (Fig. 5.4).

**Epidote :** Epidote occurs as spongy grains or aggregates but rare broken grains are also present. It is easily identified by typical yellow pleochroic colour. Pistacite content of epidote is 0.23 for sample NZ-8.1 (Table D-2 in Appendix D). The structural formula of epidote was calculated on the basis of 12.5 oxygens and by assuming total iron as $Fe_2O_3$.

**Albite :** Plagioclase feldspar in volcanic samples is strongly turbid but polysynthetic twins are commonly preserved. Plagioclase grains are completely albitised as indicated by random electron microprobe analyses.

**Other minerals :** Calcite occurs as a vein or replacement mineral. It is almost pure calcite. Sericite, quartz, relic clinopyroxene, Fe-Ti oxides and sphene are also presented in these metavolcanic rocks.

## *P-T* conditions of metamorphism of the Pak Pat Volcanics

The lack of appropriate mineralogy limit the use of elaborate *P-T* calculations for metavolcanic rocks from the Sirikit Dam area. The only option is to use a chlorite geothermometer of Cathelineau (1988), an improved version of its

precursor (Cathelineau and Nieva, 1985). The results, listed in Table 5.12, were calculated from the regression equation proposed by Cathelineau (1988): $T$ (°C) = 321.98 $Al^{iv}$ - 69.92 (for chlorite formula based on 14 oxygens) using the chlorite composition in Table D-1 in Appendix D.

Table 5.11 Metamorphic temperatures calculated using a chlorite solid-solution geothermometer of Cathelineau (1988) for metavolcanic rocks of the Pak Pat Volcanics.

| Sample no. | NZ-1.1 | NZ-1.2 | NZ-1.3 | NZ-8.1 |
|---|---|---|---|---|
| $Al^{iv}$ | 2.613±0.118 | 2.440±0.108 | 2.448±0.060 | 2.467±0.111 |
| Temperature (°C) | 351±19 | 323±18 | 324±10 | 327±18 |

No conclusive evidence has been obtained as to the timing of metamorphism of the Pak Pat Volcanics. It is highly possible that the Pak Pat Volcanics were metamorphosed to sub-greenschist facies during cleavage formation in the Permian to Triassic turbidites to the west of the Sirikit Dam area (Chapters 8 and 9).

## 5.6 Metamorphism of the Nam Pat Group

The turbidite sequence of alternating sandstone and shale of the Nam Pat Group are virtually unaffected by very-low grade metamorphism. A brief account on the metamorphic aspect of this rock unit is presented so as to make a comparison with the low-grade metamorphism of the metasediments of the Pha Som Metamorphic Complex and the Pak Pat Volcanics.

The Nam Pat sandstone is characterised by high amount of volcanic rock fragments with respect to quartz and feldspar grains. Quartz and plagioclase feldspar show little sign of recrystallisation and/or alteration compared to unstable volcanic lithic grains. A matrix is made up of authigenic minerals, chiefly chlorite with minor amounts of calcite, sericite and epidote. In thin section, cleavage is difficult to recognise.

Shale is composed of illite, chlorite, calcite and quartz. Cleavage is not strongly developed as evident by the presence of pencil structure rather than penetrative slaty cleavage.

The metamorphic study of the Nam Pat Group has to rely solely on illite crystallinity technique due to the absence of recrystallised minerals. The illite

crystallinity values of shales (Table 5.8) fall in the range of diagenetic to lower anchimetamorphic grade ($\Delta°2\theta$ = 0.30-0.41) according to the illite crystallinity scale of Kisch (1980a,1980b,1990).

It is likely that this sedimentary sequence had been buried at a shallow depth before being folded and uplifted during collisional deformation.

# 5.7 Summary

## 5.7.1 Summary of metamorphism of the metasediments of the Pha Som Metamorphic Complex

The $b_0$ values of pelitic samples from the Sirikit Dam area range from 8.994 Å to 9.012 Å with a mean value of 9.002 Å indicating the low to medium pressure facies series. These $b_0$ values are different from the $b_0$ values of similar semi-pelitic rocks from Otago, New Zealand.

The absence of high-pressure minerals such as aragonite or jadeite and the presence of crossite in association with epidote and actinolite constrain the upper pressure limit to less than 7 kbar. The presence of Fe-pumpellyite in some samples together with the complete absence of prehnite suggest the pressure of greater than 3 kbar. The phengite geobarometry indicates a minimum pressure of 5±1 kbar at an assumed temperature of 350 °C for most of psammitic rocks of the metasediments.

A newly developed phengite-chlorite geothermometer (Chapter 2) applied to psammites and pelites from the Sirikit Dam area, northern Thailand yields the temperatures in the range 303-393 °C for psammites and pelites of the metasediments. These temperature are comparable to the temperature range of 281-411 °C obtained from Green and Usdansky's plagioclase - muscovite geothermometry.

Illite crystallinity values ($\Delta°2\theta$ = 0.19-0.23) indicate the epizone grade with minor upper anchizone grade for phyllites. These illite crystallinity values agree reasonably well with the estimated temperatures obtained from geothermometric calculations.

## 5.7.2 Summary of metamorphism of the ophiolite association of the Pha Som Metamorphic Complex

The amphibolites were metamorphosed to a temperature of around 600-700 °C and a pressure of about 5-6 kbar. This amphibolite-facies metamorphism

probably occurred about 338 Ma (Lower Carboniferous) prior to the final incorporation into the Pha Som Metamorphic Complex, probably during $D_2$ deformation. Amphibolites are chemically affiliated with gabbros and associated ultramafics which have the characteristics of the oceanic-island arc cumulates originated in a supra-subduction zone setting. This implies that the amphibolites are probably the result of metamorphism of the oceanic-arc basement where high heat flow was supplied by invading magma.

The piemontite-bearing quartz schists in the Sirikit Dam area were metamorphosed at the pressure of around 7±1 kbar and temperature of around 440 °C. This relatively high *P/T* metamorphism has not been strongly affected by later low-pressure metamorphism compared to the enclosing greenschist facies psammites and pelites.

### 5.7.3 Summary of metamorphism of the Pak Pat Volcanics

A chlorite geothermometry indicates the temperature of 320-350 °C for the regional metamorphism of the Pak Pat volcanics. The Pak Pat Volcanics had probably been undergone metamorphism during cleavage formation event during post-Middle Triassic regional folding and thrusting.

### 5.7.4 Summary of metamorphism of the Nam Pat Group

The illite crystallinity values of shales ($\Delta°2\theta$ = 0.30-0.41) indicate that the Nam Pat Group belong to diagenetic to lower anchimetamorphic grade. It is likely that this sedimentary sequence had been buried at a shallow depth before being folded and uplifted during the same event which uplfted the Pak Pat Volcanics.

# Chapter 6

# GEOCHEMISTRY AND TECTONIC SETTINGS OF IGNEOUS ROCKS IN THE SIRIKIT DAM AREA

## 6.1 Introduction

The igneous rocks and their metamorphic counterparts in the Sirikit Dam area have been grouped into two lithostratigraphic units, i.e. the Pak Pat Volcanics and the ophiolite association of the Pha Som Metamorphic Complex (Bunopas, 1969, 1981). The Pak Pat Volcanics are Permian-Triassic in age and are relatively coherent unit. The Pha Som Metamorphic Complex, largely Permo-Carboniferous in age, contain blocks of igneous and other rock types in serpentinite matrix and are referred to as a serpentinite melange unit (Panjasawatwong, 1991). The main body of mafic-ultramafic rocks of the Pha Som Metamorphic Complex is exposed further to the west and has been investigated in detail by Macdonald and Barr (1984) and Panjasawatwong (1991). These igneous rocks have been considered to have formed in a volcanic arc setting (Macdonald and Barr, 1984) and also as ophiolitic mafic and ultramafic suites formed in a backarc or interarc settings (Barr and Macdonald, 1987). A more detailed study by Panjasawatwong (1991), further showed that the Nan Suture is dominated by a serpentinite melange that contains blocks of at least three magmatic associations, i.e. ocean-island basalts (group A), backarc-basin suites (group B) and arc suites (group C).

In the present study, a geochemical approach was adopted to determine magmatic affinities and tectonic settings of eruption and/or emplacement of these two additional important igneous suites. The studied samples were collected from the Pak Pat Volcanics, and a thrust sliver of mafic volcanics and shallow intrusives (probably part of the Pha Som Metamorphic Complex) associated with serpentinite and chert along the Pat River. This study compliments the work of Panjasawatwong (1991), who gave a full account of the petrogenesis of the igneous rocks of the Nan Suture Zone including part of the Sirikit Dam area (the main serpentinite melange unit). However, the advantage of this additional study is that

the structural relationships between the Pak Pat Volcanics and the Pha Som Metamorphic Complex (including the ophiolite association) are better constrained.

## 6.2. The Pak Pat Volcanics

Seventeen representative samples of the Pak Pat Volcanics were analysed for major and some trace elements by XRF spectrometry (analytical details are given in Chapter 1) and two of these were analysed for rare earth elements using instrumental neutron activation analysis (INAA). The sample localities are shown in Figure 6.1. Among these samples, ten, preceded by NZ (abbreviation of the Nan Suture Zone), were collected by Dr. Yuenyong Panjasawatwong.

### 6.2.1 Occurrence and petrography

The Pak Pat Volcanics occur as a belt of volcanic rocks forming a high ridge between the Nan River valley in the west and Nam Pat Basin in the east (Fig. 6.1). This volcanic unit is overthrust on the west by metagreywacke-phyllite packets of the Pha Som Metamorphic Complex along the Phu Khon Kaen thrust and by the ophiolite association further to the north of the map area (a description of detailed stratigraphic relationships is given in Chapter 3). In the east, it is unconformably overlain by the conglomerate beds of the Nam Pat Group. The volcanic rocks are variably deformed. Cleavage is stronger in the tuffs than in lavas and generally dies out away from the Phu Khon Kaen thrust.

#### Petrography of lavas

The analysed samples are porphyritic to strongly porphyritic. The phenocryst and microphenocryst assemblage is strongly saussuritised plagioclase with chlorite and epidote probably replacing clinopyroxene. Plagioclase phenocrysts, locally with glomeroporphyritic texture, are more abundant than their mafic counterparts. They are subhedral to anhedral and largely replaced by calcite, epidote, sericite and, to a lesser extent, zoisite. Groundmass constituents are predominantly lath-shaped albitised plagioclase with interstitial magnetite, dark cryptocrystalline materials and a small amount of microcrystalline quartz. Quartz and calcite veins are locally present.

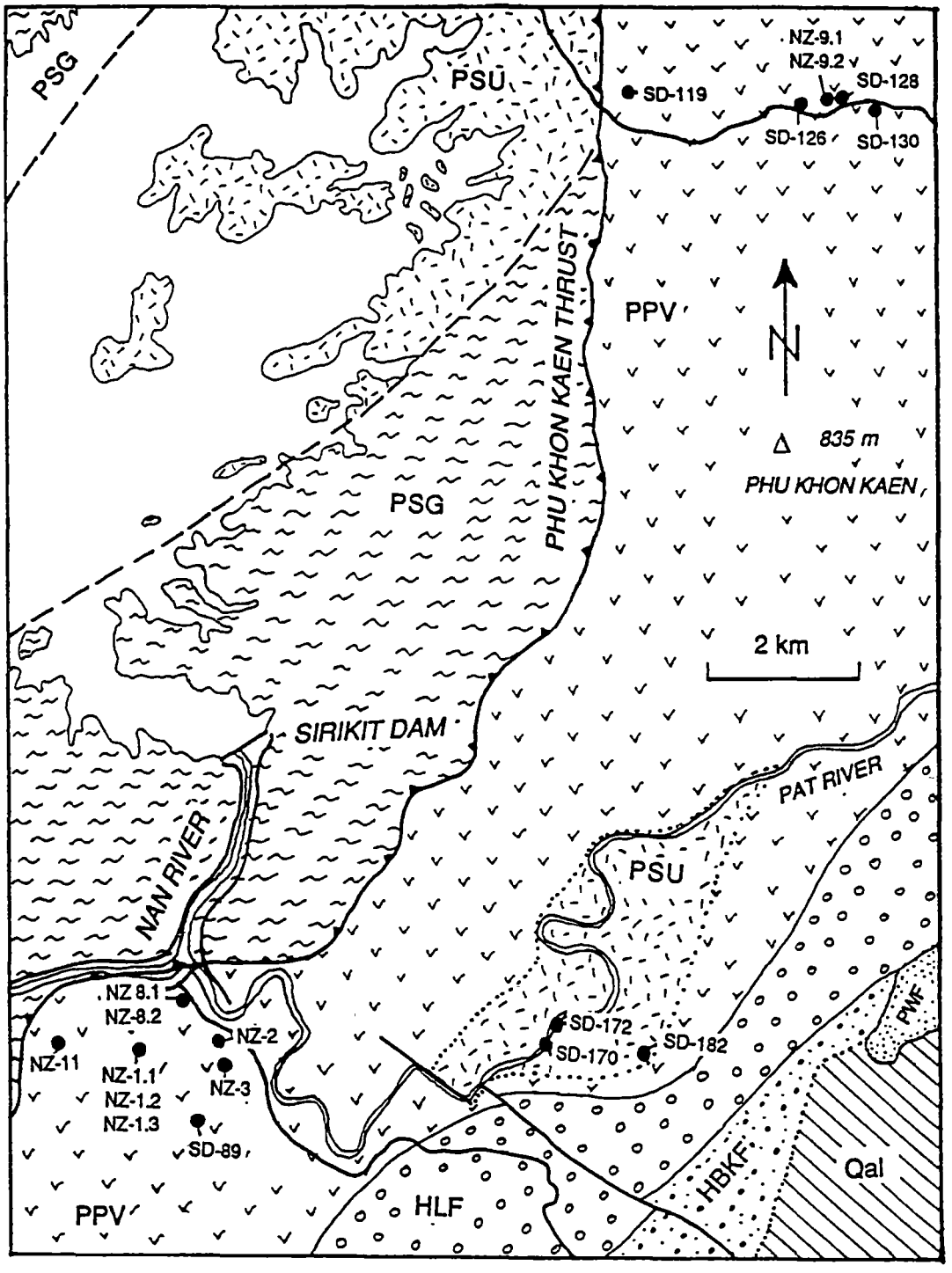


Figure 6.1 Location map of analysed samples. Lithostratigraphic units : PSU = ophiolite association of the Pha Som M.C., PSG = metasediments of the Pha Som M.C., PPV = Pak Pat volcanics, HLF = Huai Lat Formation, HBKF = Huai Bo Khong Formation, PWF = Phra Wihan Formation, Qal = Quaternary alluvium.

### 6.2.2 Alteration effects and element mobility

Petrographic examination suggested that these samples have experienced sub-greenschist facies regional metamorphism (see Chapter 5). Element mobility, especially for the alkalis, Ca and related trace elements (Ba, Rb, and Sr), during such alteration has been well documented (e.g. Vallance, 1960; 1969; Hart *et al.*, 1974). Therefore considerable caution was exercised in the selection of the relatively immobile elements used in the discrimination or interpretation of the original tectonic setting of the igneous suites. These elements include high field strength elements (HFSE) such as Ti, Nb, Zr, Y, and P. Many of the transitional metals (e.g. Ni, Cr, V, and Sc) are also considered to be immobile during very-low to low grade metamorphism (Pearce and Cann, 1973; Floyd and Winchester, 1976; Shervais, 1982). For the set of samples analysed in this study, petrographic examination showed an insignificant degree of silicification. Despite the fact that $SiO_2$ abundances of the rocks selected may be affected by limited silica mobility during alteration or metamorphism, $SiO_2$ (as well as Zr and FeO*/MgO) can be a very useful chemical discriminant and fractionation indicator when considered together with more immobile elements (e.g. Crawford *et al.*, 1992).

### 6.2.3 General chemical characteristics

The seventeen analysed rock samples of the Pak Pat Volcanics are basaltic to dacitic in composition (Table 6.1) as indicated by their major element compositions, especially $SiO_2$ abundances (51.75-68.83 %). In terms of the relatively immobile elements, these rocks are characterised by low abundances of $TiO_2$ (0.37-1.15 wt %), $P_2O_5$ (0.11-0.27 wt %), Nb (<1-4 ppm), Y (14-34 ppm), Ni (between 2 and 37 ppm), Cr (largely between 2 and 62 ppm) and relatively low values of Ti/Zr (20.1-87.2), Nb/Y (0.04-0.16). In contrast, they have high concentrations of Zr (55-141 ppm) and V (>200 ppm with few exceptions).

### 6.2.4 Geochemical affinities and tectonic setting

A set of binary diagrams of Winchester and Floyd (1976) in Figure 6.2 (a-c) shows that the Pak Pat Volcanics are a subalkaline magmatic suite with Ti-Y-Zr-Nb relationships strongly implying an origin in island arc setting (Figs. 6.3a&b; and 6.4). The majority of the samples plot within the basaltic andesite and andesite fields on the least-mobile element variation diagram $Zr/TiO_2$-Nb/Y (Fig. 6.3a).

Table 6.1 Whole-rock XRF analyses of volcanic and hypabyssal rocks from the Sirikit Dam area.

| Rock units | Pak Pat Volcanics | | | | | | | | | | | | | | | | | ophiolite association | | |
|---|---|---|---|---|---|---|---|---|---|---|---|---|---|---|---|---|---|---|---|---|
| Sample no. | SD-89 | SD-90.1 | SD-90.2 | SD-119 | SD-126 | SD-128 | SD-130 | NZ-1.1 | NZ-1.2 | NZ-1.3 | NZ-2 | NZ-3 | NZ-8 1 | NZ-8.2 | NZ-9.1 | NZ-9.2 | NZ-11 | SD-170 | SD-172 | SD-182 |
| *Major elements (wt %)* | | | | | | | | | | | | | | | | | | | | |
| SiO2 | 54.35 | 51.92 | 65.46 | 52.18 | 51.75 | 54.45 | 54.46 | 68.83 | 53.48 | 54.50 | 55.94 | 57.15 | 52.50 | 65.43 | 55.79 | 54.55 | 53.48 | 48.49 | 46.89 | 53.73 |
| TiO2 | 0.91 | 0.86 | 0.52 | 0.76 | 1.01 | 1.13 | 0.89 | 0.37 | 0.90 | 0.86 | 1.14 | 0.76 | 0.95 | 0.51 | 0.97 | 0.99 | 1.15 | 3.74 | 4.48 | 2.56 |
| Al2O3 | 22.64 | 22.12 | 17.74 | 21.79 | 19.76 | 19.88 | 18.09 | 16.20 | 19.69 | 19.23 | 21.24 | 18.90 | 21.35 | 17.40 | 20.09 | 19.57 | 17.84 | 15.25 | 15.67 | 13.34 |
| FeO* | 8.20 | 7.64 | 5.08 | 7.97 | 9.21 | 9.13 | 8.53 | 3.54 | 8.84 | 8.67 | 9.08 | 7.52 | 8.35 | 5.01 | 7.96 | 8.73 | 10.30 | 12.15 | 13.41 | 11.87 |
| MnO | 0.16 | 0.19 | 0.13 | 0.24 | 0.18 | 0.14 | 0.16 | 0.07 | 0.17 | 0.18 | 0.10 | 0.14 | 0.24 | 0.13 | 0.13 | 0.18 | 0.18 | 0.19 | 0.16 | 0.15 |
| MgO | 3.50 | 3.33 | 1.64 | 4.59 | 5.18 | 3.52 | 5.06 | 1.46 | 4.94 | 4.99 | 3.17 | 4.07 | 3.97 | 1.61 | 3.62 | 4.89 | 4.53 | 7.51 | 6.37 | 7.82 |
| CaO | 2.32 | 10.36 | 3.01 | 8.43 | 8.57 | 5.33 | 9.61 | 4.50 | 8.34 | 8.09 | 1.82 | 7.20 | 7.93 | 3.88 | 5.54 | 5.90 | 7.78 | 8.63 | 7.63 | 6.67 |
| Na2O | 6.52 | 3.14 | 4.37 | 3.20 | 3.50 | 3.06 | 2.87 | 3.40 | 3.16 | 3.04 | 6.12 | 3.78 | 3.89 | 4.52 | 4.54 | 4.37 | 3.75 | 3.47 | 3.78 | 3.23 |
| K2O | 1.25 | 0.30 | 1.79 | 0.71 | 0.64 | 3.10 | 0.14 | 1.51 | 0.33 | 0.27 | 1.16 | 0.35 | 0.67 | 1.27 | 1.14 | 0.60 | 0.80 | 0.05 | 0.66 | 0.25 |
| P2O5 | 0.16 | 0.15 | 0.25 | 0.14 | 0.19 | 0.27 | 0.19 | 0.11 | 0.16 | 0.16 | 0.21 | 0.15 | 0.15 | 0.24 | 0.22 | 0.21 | 0.20 | 0.51 | 0.95 | 0.40 |
| Total# | 100.00 | 100.00 | 100.00 | 100.00 | 100.00 | 100.00 | 100.00 | 100.00 | 100.00 | 100.00 | 100.00 | 100.00 | 100.00 | 100.00 | 100.00 | 100.00 | 100.00 | 100.00 | 100.00 | 100.00 |
| Total$ | 100.16 | 99.40 | 100.40 | 99.92 | 99.50 | 99.61 | 99.69 | 100.14 | 99.74 | 99.79 | 100.30 | 99.44 | 99.61 | 100.34 | 99.53 | 99.56 | 99.92 | 100.47 | 100.32 | 100.27 |
| LOI | 3.62 | 4.30 | 2.31 | 5.92 | 4.61 | 4.72 | 4.27 | 3.24 | 3.97 | 3.91 | 4.02 | 3.11 | 3.59 | 2.33 | 3.65 | 3.79 | 2.97 | 5.15 | 5.19 | 5.82 |
| FeO*/MgO | 2.34 | 2.30 | 3.10 | 1.74 | 1.78 | 2.59 | 1.68 | 2.43 | 1.79 | 1.74 | 2.87 | 1.85 | 2.10 | 3.11 | 2.20 | 1.79 | 2.28 | 1.62 | 2.10 | 1.52 |
| *Trace elements (ppm)* | | | | | | | | | | | | | | | | | | | | |
| Nb | 1 | 1 | 3 | 2 | 2 | 4 | 3 | 2 | 1 | 2 | 3 | 2 | 1 | 2 | 3 | 3 | 2 | 27 | 37 | 13 |
| Zr | 78 | 59 | 126 | 55 | 102 | 133 | 94 | 111 | 81 | 78 | 120 | 95 | 72 | 121 | 141 | 118 | 90 | 221 | 311 | 159 |
| Y | 22 | 20 | 27 | 29 | 26 | 28 | 20 | 14 | 24 | 23 | 34 | 20 | 24 | 27 | 26 | 24 | 27 | 34 | 46 | 29 |
| Ba | 324 | 78 | 353 | 110 | 156 | 639 | 43 | 332 | 120 | 106 | 254 | 129 | 136 | 236 | 298 | 173 | 188 | 50 | 159 | 116 |
| Sr | 569 | 447 | 179 | 451 | 463 | 334 | 654 | 233 | 465 | 459 | 318 | 552 | 377 | 343 | 373 | 473 | 329 | 304 | 198 | 340 |
| Rb | 41 | 6 | 38 | 22 | 10 | 70 | 2 | 33 | 5 | 6 | 28 | 7 | 15 | 30 | 22 | 12 | 13 | 1 | 16 | 5 |
| Pb | 7 | 2 | 3 | 6 | 5 | 4 | 6 | 4 | 3 | 2 | 7 | 5 | 1 | 5 | 3 | 4 | 5 | - | 2 | 1 |
| Th | 1 | - | 2 | 1 | 2 | 3 | 1 | 3 | 2 | 1 | 1 | 1 | 1 | 2 | 3 | 2 | 1 | 2 | 3 | 2 |
| Ni | 9 | 7 | 2 | 19 | 33 | 37 | 67 | 4 | 12 | 11 | 18 | 13 | 7 | 2 | 24 | 23 | 14 | 202 | 81 | 215 |
| Cr | 9 | 8 | 2 | 54 | 59 | 28 | 164 | 7 | 15 | 13 | 32 | 17 | 6 | 2 | 14 | 62 | 32 | 249 | 68 | 383 |
| V | 246 | 233 | 26 | 222 | 259 | 232 | 220 | 60 | 237 | 232 | 242 | 185 | 227 | 28 | 202 | 221 | 290 | 268 | 281 | 275 |
| Sc | 25 | 26 | 8 | 27 | 33 | 22 | 27 | 7 | 27 | 26 | 31 | 22 | 27 | 8 | 18 | 24 | 33 | 21 | 23 | 33 |
| La | 5 | 3 | 9 | 8 | 9 | 8 | 8 | 11 | 3 | 5 | 10 | 4 | 5 | 8 | 11 | 9 | 4 | 24 | 31 | 14 |
| Ce | 14 | 14 | 25 | 10 | 16 | 25 | 19 | 20 | 12 | 13 | 25 | 14 | 14 | 24 | 26 | 21 | 17 | 53 | 80 | 46 |
| Nd | 8 | 8 | 15 | 12 | 14 | 16 | 13 | 9 | 7 | 10 | 15 | 9 | 8 | 14 | 16 | 13 | 12 | 31 | 46 | 20 |
| Ti/Zr | 69.9 | 87.2 | 24.9 | 83.0 | 59.4 | 50.8 | 56.6 | 20.1 | 66.3 | 66.3 | 57.1 | 48.2 | 78.7 | 25.4 | 41.1 | 50.3 | 76.4 | 101.5 | 86.3 | 96.6 |
| Zr/Nb | 55.7 | 65.6 | 48.5 | 36.7 | 48.6 | 36.9 | 32.4 | 48.3 | 67.5 | 43.3 | 42.9 | 47.5 | 51.4 | 50.4 | 44.1 | 35.5 | 50.0 | 8.2 | 8.4 | 12.0 |
| Zr/Y | 3.5 | 2.9 | 4.8 | 1.9 | 3.9 | 4.8 | 4.7 | 8.0 | 3.3 | 3.3 | 3.6 | 4.7 | 3.0 | 4.5 | 5.4 | 4.9 | 3.3 | 6.5 | 6.8 | 5.6 |
| Y/Nb | 15.9 | 22.4 | 10.2 | 19.6 | 12.4 | 7.6 | 6.8 | 6.0 | 20.2 | 12.9 | 12.0 | 10.1 | 17.0 | 11.1 | 8.2 | 7.2 | 15.1 | 1.3 | 1.2 | 2.2 |

* Total Fe as FeO calculated as 0.905 Fe2O3 from the original analyses

# Analyses are recalculated and normalised to 100 % anhydrous

$ Original total; LOI = loss on ignition.

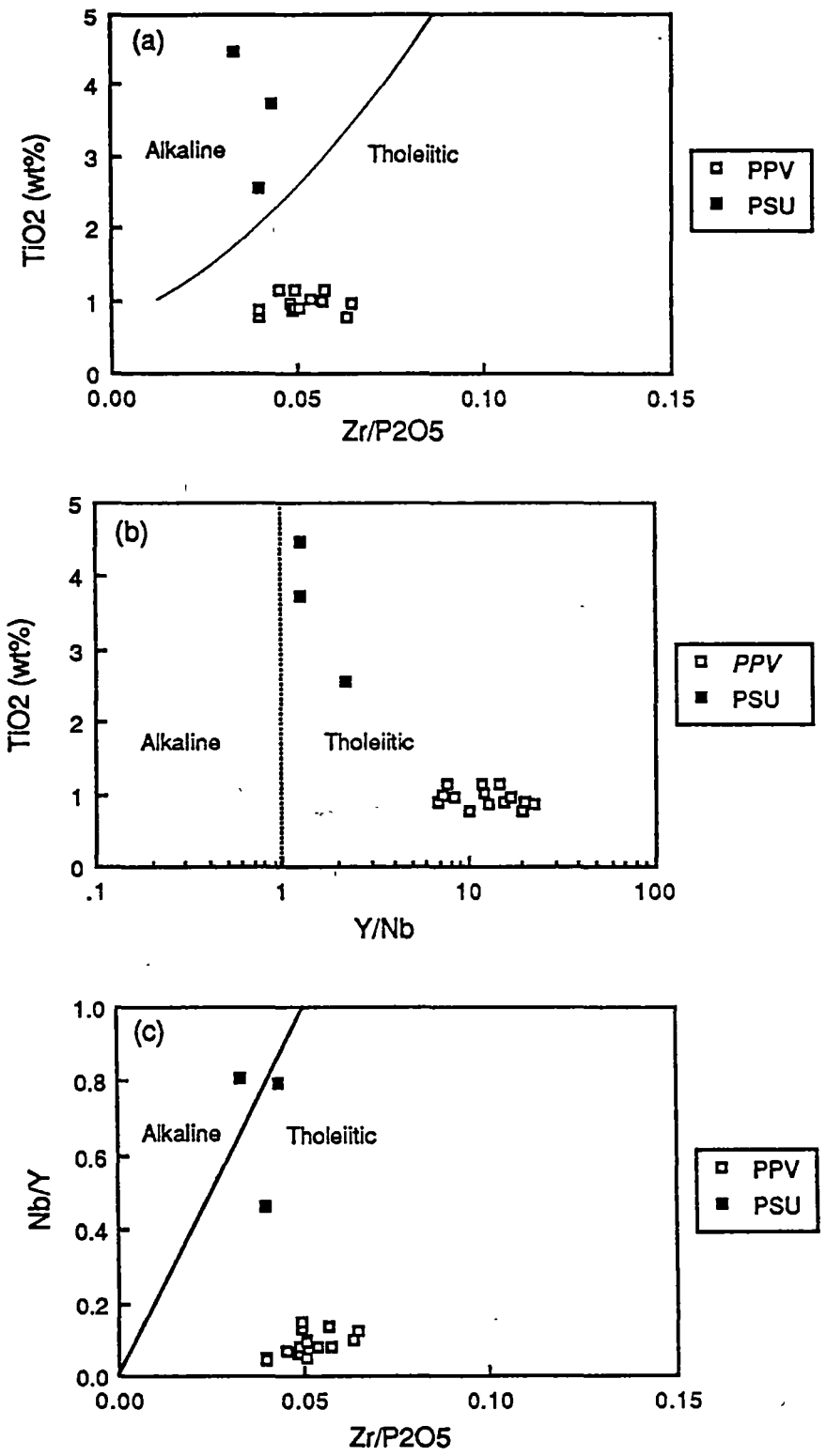


Figure 6.2 Plots of (a) $TiO_2$ versus $Zr/P_2O_5$, (b) $TiO_2$ versus Y/Nb, and (c) Nb/Y versus $Zr/P_2O_5$ (Winchester and Floyd, 1976) for samples from the Pak Pat volcanics (open squares) and ophiolite association (solid squares). Samples plotted on the diagrams are basalt and basaltic andesite exclusively.

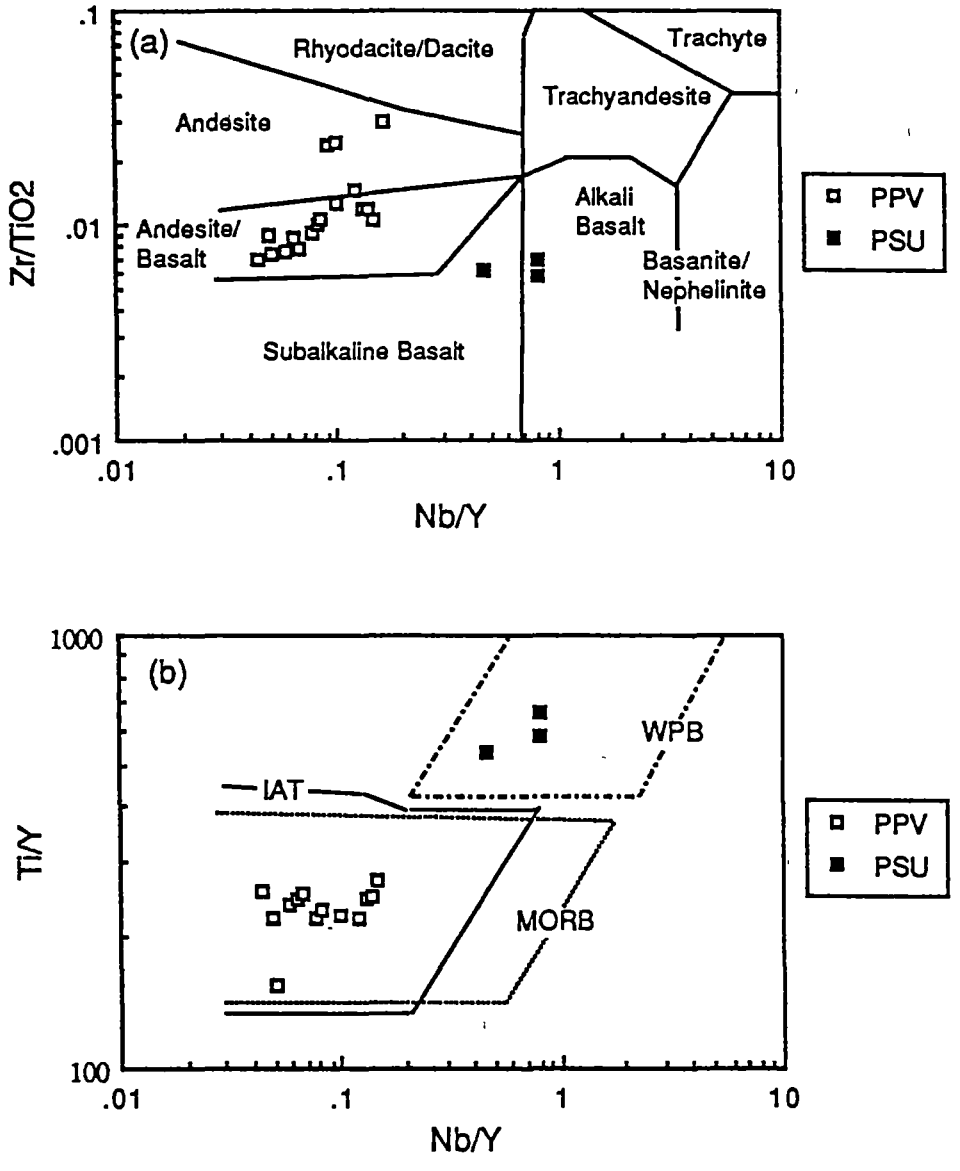


Figure 6.3 Plots of (a) $Zr/TiO_2$ versus Nb/Y (Winchester and Floyd, 1977) and (b) Ti/Y versus Nb/Y (Pearce, 1980) for samples from the Pak Pat volcanics (open squares) and ophiolite association of the Pha Som M.C. (solid squares).

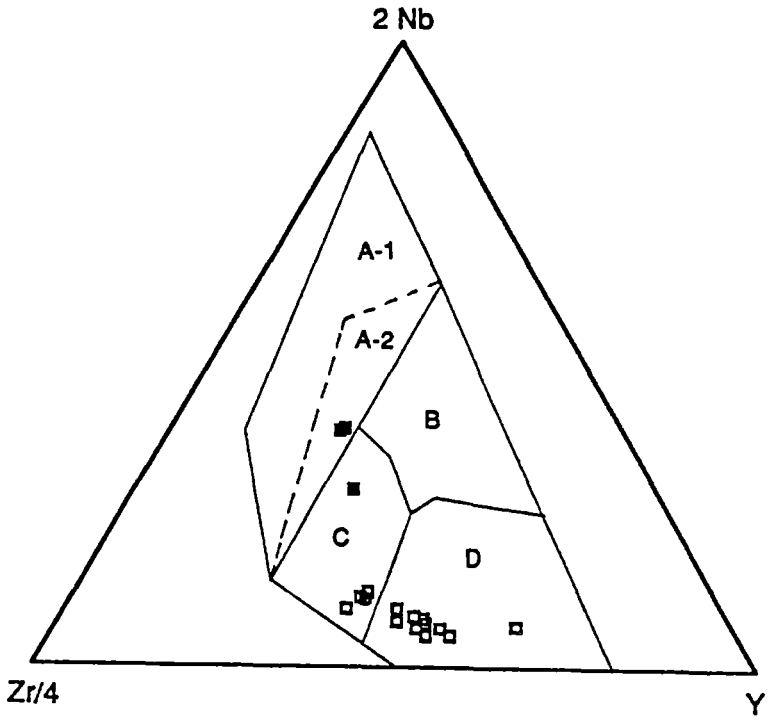


Figure 6.4 Discrimination diagram 2Nb-Zr/4-Y (Meschede, 1986) for samples from the Pak Pat Volcanics (open squares) and Pha Som Metamorphic Complex (solid squares). The plot fields are as follows: A-1 = alkali within-plate basalts; A-2 = tholeiitic within-plate basalts; B and D = mid-oceanic ridge basalts; and C and D = volcanic arc basalts.

Crawford *et al.* (1992) distinguished tholeiitic and calc-alkaline magma associations of the Mount Read Volcanics in Western Tasmania by defining that the samples showing a progressive decrease in FeO*, $TiO_2$, and Ti/Zr with increasing fractionation (i.e. increasing $SiO_2$ content or FeO*/MgO) belong to calc-alkaline series whereas tholeiitic suites are those that show a broad general increase in FeO* and $TiO_2$ with fractionation, especially in the basalt to andesite range. The same test may be applied to the Pak Pat volcanics considering the similar styles of alteration and/or metamorphism of these two volcanic suites. The FeO*/MgO values and MgO contents of the Pak Pat Volcanics samples are poorly correlated with $SiO_2$ contents (Fig. 6.5a&c). This probably reflects the variation of MgO due to alteration effects. A set of trial plots also reveal that the variations of the elements under consideration are more pronounced when plotted against SiO2 than FeO*/MgO. The coherence between $SiO_2$ content and other fractionation indicators such as Ti or Zr indicates that $SiO_2$ mobility has not been substantial in these rocks which were selected to be the freshest available. Therefore, $SiO_2$ content is adopted

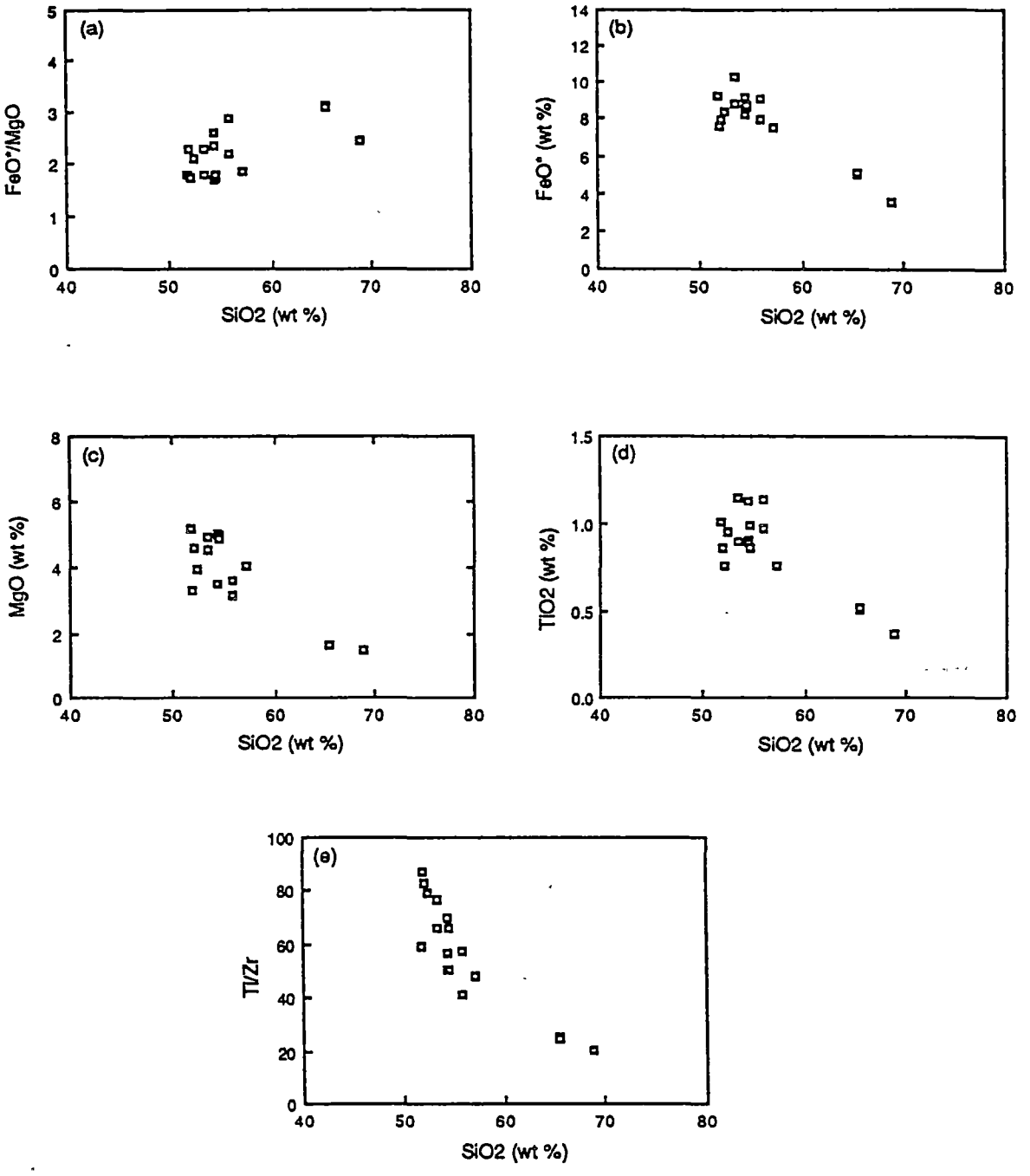


Figure 6.5 Plots of oxides and ratios versus $SiO_2$ for representative samples of the Pak Pat volcanics.

here as a fractionation index.The Pak Pat Volcanics samples display the calc-alkaline trend of decreasing FeO* and TiO2 with increasing differentiation index, here defined by $SiO_2$ contents (Fig. 6.5b&d). Ti/Zr values also decrease with increasing $SiO_2$ abundances (Fig. 6.5e). With progressive fractionation, V and Sc decrease smoothly (Fig. 6.6a&b). Similar trends are also noticeable on the FeO*/MgO variation diagrams (Figs. 6.6c&d) but are not as clear as those using $SiO_2$ contents as an index of fractionation.

Unaltered calc-alkaline volcanic rocks are usually classified using $K_2O$-$SiO_2$ variation diagrams for the major volcanic rock types (e.g. Peccirillo and Taylor, 1976; Gill, 1981; Basaltic Volcanism Study Project, 1981). However, due to $K_2O$ mobility, it is not a straight-forward exercise to apply such a classification scheme to altered or metamorphosed volcanic rocks. On a $K_2O$-$SiO_2$ variation diagram (Fig. 6.7), the $K_2O$ contents of the analysed Pak Pat volcanics are consistent with the low to medium-K basalts. Due to alkali mobility, it is uncertain how closely this variation reflects the original $K_2O$-$SiO_2$ relationships in these metavolcanics. However, the dominance of basalt to andesite over more evolved rocks evident in the Pak Pat volcanics, plus the absence of hornblende and dominance of clinopyroxene as a phenocryst phase, lends some support to this assignment, as younger arcs with typically low to medium-K lavas are dominated by basaltic to andesitic rocks (Gill, 1981) in which hornblende is rare or absent.

Rare earth element abundances of the studied Pak Pat volcanic rocks are listed in Table 6.2 below. The chondrite-normalised REE patterns of the Pak Pat volcanic rocks (Fig. 6.8) vary from relatively flat to slightly LREE enriched ($(La/Yb)_N$ = 1.41-1.96), typical of many low- to medium K arc lavas (Wheller *et al.*, 1987; Lin *et al.*, 1989; Barsdell and Berry, 1990). The REE patterns of some selected samples of modern oceanic arc basalts and andesites, e.g. from the Kaitoku Seamont in the northern Mariana Arc (Lin *et al.*, 1989) and western Epi in the Vanuatu Arc (Barsdell and Berry, 1990), show their strong compositional affinities with the Pak Pat basaltic andesites and andesites (Fig. 6.8). These are typical low- to medium-K arc basalt (sample 71047) and medium-K arc andesites (average Kaitoku samples).

It was also noted that the chondrite-normalised REE pattern of sample SD-90.1 (Fig. 6.8) is relatively flat, with REE abundances around 10 times chondrite, similar to subalkaline basalts from the Mundua Island (Witu Islands), on the western end of the actively spreading Manus basin (Johnson and Arculus, 1978). The Witu Island volcanic rocks were formed in a supra-subduction zone setting. They have compositions transitional between arc tholeiites and backarc basin tholeiites. From this comparison, it is considered possible that the Pak Pat volcanics

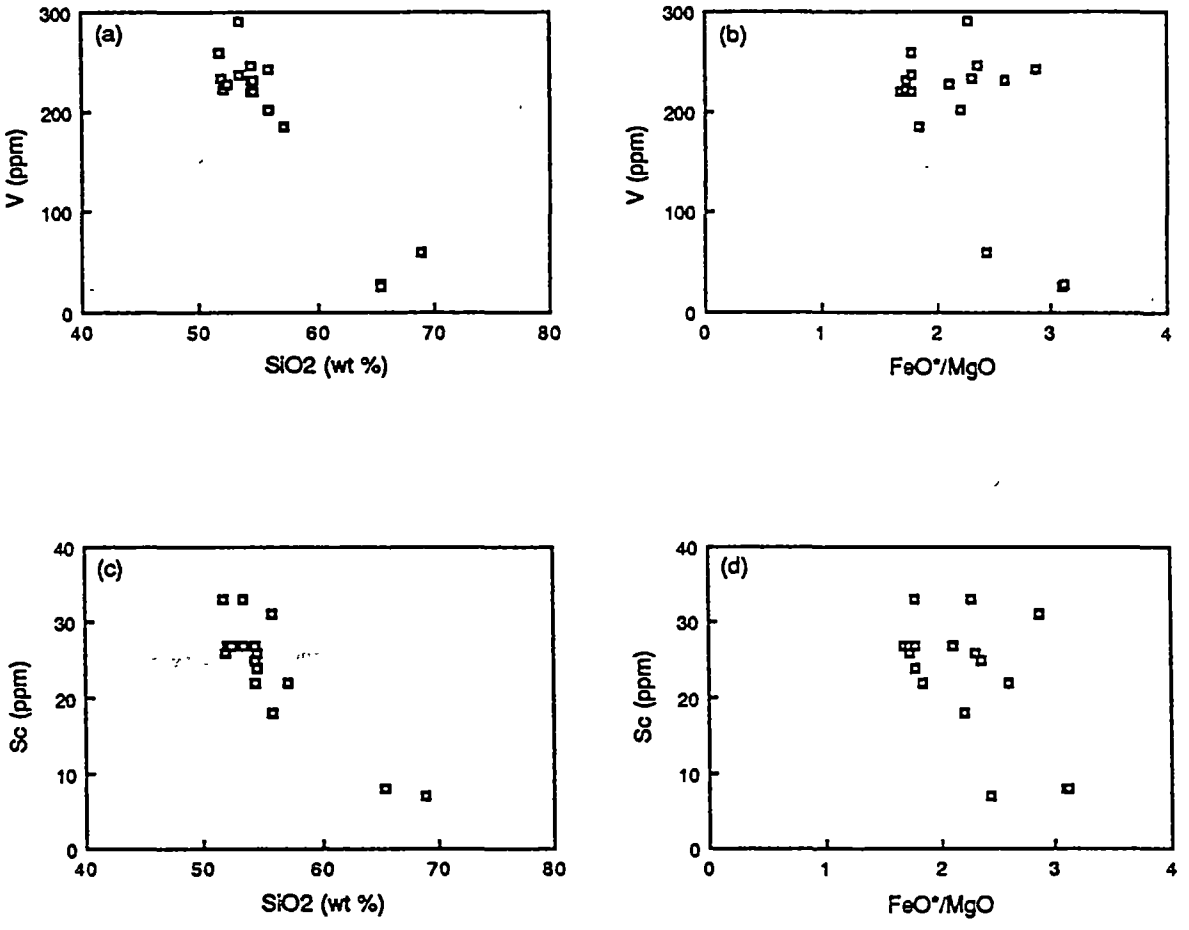


Figure 6.6 Plots of (a) V versus $SiO_2$, (b) V versus FeO*/MgO, (c) Sc versus $SiO_2$, and (d) Sc versus FeO*/MgO for representative samples of the Pak Pat volcanics.

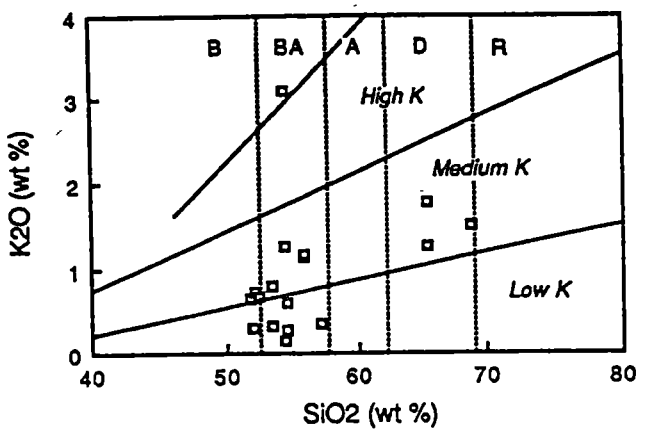


Figure 6.7 Plot of $K_2O$ versus $SiO_2$ for representative samples of the Pak Pat volcanics. The classification scheme is from Basaltic Volcanism Study Project (1981): B = basalts, BA = basaltic andesites, A = andesites, D = dacites, and R = rhyolites.

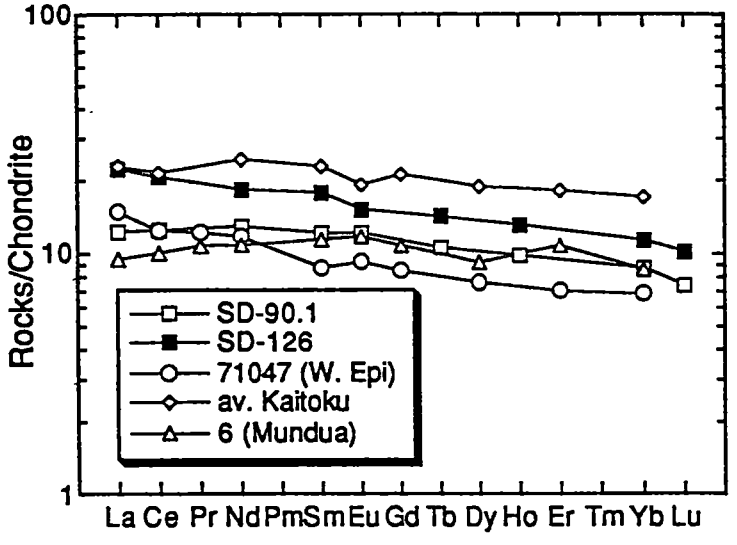


Figure 6.8 Chondrite-normalised REE patterns for selected basaltic samples of the Pak Pat volcanics (samples SD-90.1 and SD-126). Also shown are REE patterns of a western Epi tholeiite (sample 71047), Vanuatu (Barsdell and Berry, 1990), the average tholeiitic basalts of the Kaitoku Seamount (samples D75-4 and D77-1), northern Mariana Arc (Lin *et al.* 1989); and supra-subduction zone basalts, Mundua, Witu Islands (sample 6 of Johnson and Arculus, 1978).

originated in a similar setting as the Witu Island rocks, i.e. a supra-subduction zone environment with the initial stage of arc rifting and backarc-basin formation .

Table 6.2 Rare earth element analyses and selected chondrite normalised ratios for the studied igneous rocks. Chondrite normalisation values are: La = 0.315, Ce = 0.813, Nd = 0.597, Sm = 0.192, Eu = 0.88, Tb = 0.049, Ho = 0.073, Yb = 0.208, and Lu = 0.0323 (Taylor and Gorton, 1977).

| Sample no. | SD-90.1 | SD-126 | SD-170 | SD-182 |
|---|---|---|---|---|
| La | 3.89 | 7.05 | 20.40 | 12.90 |
| Ce | 10.20 | 16.90 | 48.40 | 31.00 |
| Nd | 7.75 | 11.00 | 27.90 | 19.60 |
| Sm | 2.34 | 3.43 | 7.51 | 5.20 |
| Eu | 0.88 | 1.10 | 2.48 | 1.75 |
| Tb | 0.52 | 0.70 | 1.25 | 0.82 |
| Ho | 0.72 | 0.96 | 1.35 | 0.96 |
| Yb | 1.82 | 2.37 | 2.28 | 1.89 |
| Lu | 0.24 | 0.33 | 0.29 | 0.23 |
| (La/Yb)N | 1.41 | 1.96 | 5.91 | 4.51 |
| (La/Sm)N | 1.01 | 1.25 | 1.66 | 1.51 |
| (Sm/Yb)N | 1.39 | 1.57 | 3.57 | 2.98 |

On the basis of geochemical and petrographic data discussed above, it is concluded that the Pak Pat volcanics belong to a subalkaline series with low- to medium-K affinities. The closest chemical analogues in modern settings are those that have been generated during rifting of an intra-oceanic arc to form a backarc basin.

## 6.3 The ophiolite association of the Pha Som Metamorphic Complex

Three samples of the ophiolite association were analysed for major and some trace elements by XRF spectrometry and two of these were analysed for rare earth elements using INAA. The sample localities are shown in Figure 6.1.

### 6.3.1 Occurrence and petrography

A small body of mafic igneous rocks and serpentinite associated with mafic tuffs and chert was found within the Pak Pat Volcanics along the Pat River in the northeastern part of the map area (Fig. 6.1). This is assigned to be part of the Pha Som Metamorphic Complex for which the main outcrop area was found further west in the Sirikit Reservoir and further north. To the north of the study area, the

ophiolite association was shown to be thrust over the Pak Pat Volcanics (Phromma *et al.*, 1991). Chert and marble blocks associated with the serpentinites are tightly folded whereas the mafic rocks themselves are strongly sheared and metamorphosed to sub-greenschist facies, as indicated by the metamorphic assemblage chlorite-epidote-calcite-pumpellyite. The actual contact between these two units has not been observed in the field, but a strong internal deformation of the ophiolite association point to tectonic rather than diapiric emplacement. Along the northward trend of the Pak Pat volcanics, several small bodies of mafic shallow intrusive rocks and serpentinites, similar to above, are common (Bunopas, 1981).

### Petrography of lavas

Specimen SD-182 is the only analysed lava. It is a fine-grained sheared rock made up of lenticular plagioclase porphyroclasts in a matrix of chlorite, pumpellyite and epidote. Original igneous texture is obliterated. This rock may originally have consisted of plagioclase and clinopyroxene phenocrysts, but the latter are completely replaced by chlorite and pumpellyite. Inclusion trains of epidote in plagioclase are common. Quartz and calcite veins are locally present.

### Petrography of dolerites

Specimens SD-170 and SD-172 are medium-grained rocks made up of plagioclase laths subophitically enclosed by subhedral clinopyroxene which is extensively pseudomorphed by amphibole. Original igneous textures are largely obliterated by deformation that produced poorly-defined schistosity. Chlorite, pumpellyite, calcite and quartz occur as alteration products. Fe-Ti oxide is an accessory mineral. Secondary quartz and calcite are not uncommon along cracks in clinopyroxene. Plagioclase is strongly altered to a very fine-grained mixture of chlorite and epidote minerals.

### Petrography of gabbros

Gabbros were not analysed in the present study but their petrography is included as additional data for the geochemical interpretation of the associated shallow intrusives and lavas. Sample SD-177 is a coarse-grained rock consisting of clinopyroxene and plagioclase. Clinopyroxene is largely pseudomorphed by amphibole, especially along the rim. Plagioclase is quite turbid, with alteration products made up of epidote, zoisite, and clinozoisite. Clinopyroxene is subhedral

to anhedral and commonly shows exsolution lamellae. A quartz-muscovite vein is also present. This gabbro is strongly sheared and has a cataclastic texture.

### 6.3.2 Pyroxene compositions

Clinopyroxene is the most abundant relict mafic mineral preserved in the dolerites of Pha Som Metamorphic Complex. Electron microprobe analyses of clinopyroxenes in specimens SD-170 and SD-172 are listed in Table 6.3. According to the nomenclature proposed by the Subcommittee on pyroxenes, IMA (1988), they are either diopside or augite (largely diopside) with Mg/(Mg+Fe) values in the range 0.69 to 0.76. These clinopyroxenes are Al- and Ti-rich but Si-poor (3.29%-4.99% $Al_2O_3$, 1.58%-2.65% $TiO_2$ and 46.96%-50.46% $SiO_2$ respectively), characteristic of clinopyroxenes from alkali basalts (Letterier *et al.*, 1982). The strong relationship between the analysed clinopyroxenes and alkali basalts is also indicated by a Ti versus Ca+Na plot (Fig. 6.9). On the conventional pyroxene quadrilateral (Fig. 6.10), they plot in the compositional field for Hawaiian alkali basalts.

### 6.3.3 General chemical characteristics

The three analysed samples of the Pha Som Metamorphic Complex are sub-alkaline (specimen SD-182) to alkali basaltic (SD-170 and SD-172) in composition as indicated by their major element compositions and by a variation diagram $Zr/TiO_2$-Nb/Y (Fig. 6.3a). Although $SiO_2$ abundances of the rocks may be affected by silica mobility during alteration/metamorphism, their $SiO_2$ contents (46.89-53.73 wt %) also lie within a range of unaltered basalts (Table 6.1). These basaltic rocks are characterised by high concentrations of $TiO_2$ (2.56-4.48 wt %), FeO* (11.87-13.41wt %), Nb (13-37 ppm), Zr (159-311 ppm), Ni (81-215 ppm), Cr (68-383 ppm), V (268-281 ppm) and high values of Ti/Zr (86.3-101.5), Nb/Y (0.45-0.83). The concentrations of $P_2O_5$ (0.40-0.95 wt %) and Y (29-46 ppm) are moderately high.

### 6.3.4 Geochemical affinities and tectonic setting

A set of binary diagrams of Winchester and Floyd (1976) in Figure 6.2 (a-c) suggests that the original magma is transitional between tholeiitic and alkali basalts with a stronger tendency towards the latter. The 2Nb-Zr/4-Y discrimination diagram (Fig. 6.4) further shows that they are transitional tholeiitic within-plate

Table 6.3 Electron microprobe analyses of clinopyroxenes in dolerites (samples SD-170 and SD-172) of the ophiolite association of the Pha Som M.C..

| Sample no. | SD-170 | | | | | | | SD-172 | | | | | |
|---|---|---|---|---|---|---|---|---|---|---|---|---|---|
| Analysis no. | 1 | 2 | 3 | 4 | 5 | 6 | 7 | 1 | 2 | 3 | 4 | 5 | 6 |
| Point no. | C4-Cpx1 | C1-Cpx1 | C1-Cpx2 | C1-Cpx3 | C2-Cpx5 | C3-Cpx6 | C4-Cpx7 | C4-Cpx1 | C4-Cpx2 | C4-Cpx4 | C4-Cpx5 | C5-Cpx8 | C5-Cpx9 |
| SiO2 | 49.74 | 49.80 | 49.84 | 49.14 | 49.08 | 49.83 | 50.46 | 47.63 | 47.58 | 46.96 | 47.82 | 47.63 | 47.21 |
| TiO2 | 2.11 | 1.70 | 1.75 | 1.94 | 2.27 | 1.58 | 1.83 | 2.37 | 2.24 | 2.65 | 2.31 | 2.09 | 2.51 |
| Al2O3 | 4.24 | 3.70 | 3.82 | 4.11 | 4.33 | 3.29 | 3.87 | 4.77 | 4.99 | 4.95 | 4.46 | 4.28 | 4.87 |
| Cr2O3 | 0.00 | 0.00 | 0.04 | 0.00 | 0.05 | 0.03 | 0.00 | 0.00 | 0.00 | 0.04 | 0.00 | 0.00 | 0.00 |
| Fe2O3* | 0.81 | 0.81 | 0.64 | 1.02 | 1.14 | 0.95 | 0.00 | 3.60 | 3.22 | 3.57 | 3.32 | 3.52 | 3.10 |
| FeO* | 9.15 | 9.15 | 9.28 | 8.84 | 9.15 | 8.56 | 10.05 | 6.89 | 7.30 | 7.31 | 6.91 | 6.82 | 7.14 |
| MnO | 0.31 | 0.20 | 0.22 | 0.26 | 0.27 | 0.29 | 0.38 | 0.29 | 0.36 | 0.32 | 0.17 | 0.14 | 0.11 |
| MgO | 12.94 | 12.78 | 12.75 | 12.57 | 12.60 | 12.99 | 12.65 | 12.29 | 12.58 | 11.65 | 12.25 | 12.06 | 12.14 |
| CaO | 21.24 | 21.33 | 21.31 | 21.24 | 20.90 | 21.20 | 20.72 | 21.73 | 20.85 | 21.34 | 21.97 | 22.14 | 21.67 |
| Na2O | 0.35 | 0.35 | 0.36 | 0.39 | 0.45 | 0.40 | 0.44 | 0.46 | 0.46 | 0.60 | 0.47 | 0.43 | 0.44 |
| Total | 100.88 | 99.82 | 100.00 | 99.51 | 100.24 | 99.11 | 100.40 | 100.04 | 99.57 | 99.41 | 99.67 | 99.11 | 99.20 |
| Number of cations on the basis of 6 oxygens: | | | | | | | | | | | | | |
| Si | 1.850 | 1.871 | 1.870 | 1.853 | 1.840 | 1.883 | 1.886 | 1.793 | 1.796 | 1.784 | 1.805 | 1.810 | 1.791 |
| Al iv | 0.150 | 0.129 | 0.130 | 0.147 | 0.160 | 0.117 | 0.114 | 0.207 | 0.204 | 0.216 | 0.195 | 0.190 | 0.209 |
| Fe3+ | 0.000 | 0.000 | 0.000 | 0.000 | 0.000 | 0.000 | 0.000 | 0.000 | 0.000 | 0.000 | 0.000 | 0.000 | 0.000 |
| Sum Tet. | 2.000 | 2.000 | 2.000 | 2.000 | 2.000 | 2.000 | 2.000 | 2.000 | 2.000 | 2.000 | 2.000 | 2.000 | 2.000 |
| Al vi | 0.035 | 0.035 | 0.038 | 0.036 | 0.031 | 0.029 | 0.056 | 0.005 | 0.018 | 0.006 | 0.004 | 0.002 | 0.009 |
| Ti | 0.059 | 0.048 | 0.049 | 0.055 | 0.064 | 0.045 | 0.051 | 0.067 | 0.063 | 0.076 | 0.066 | 0.060 | 0.072 |
| Cr | 0.000 | 0.000 | 0.001 | 0.000 | 0.001 | 0.001 | 0.000 | 0.000 | 0.000 | 0.001 | 0.000 | 0.000 | 0.000 |
| Fe3+ | 0.023 | 0.023 | 0.018 | 0.029 | 0.032 | 0.027 | 0.000 | 0.102 | 0.092 | 0.102 | 0.094 | 0.101 | 0.088 |
| Fe2+ | 0.285 | 0.288 | 0.291 | 0.279 | 0.287 | 0.270 | 0.314 | 0.217 | 0.230 | 0.232 | 0.218 | 0.217 | 0.227 |
| Mn | 0.010 | 0.006 | 0.007 | 0.008 | 0.008 | 0.009 | 0.012 | 0.009 | 0.011 | 0.010 | 0.006 | 0.004 | 0.004 |
| Mg | 0.717 | 0.716 | 0.713 | 0.706 | 0.704 | 0.731 | 0.704 | 0.690 | 0.708 | 0.659 | 0.689 | 0.683 | 0.687 |
| Sum Oct. | 1.128 | 1.116 | 1.117 | 1.113 | 1.128 | 1.113 | 1.139 | 1.090 | 1.123 | 1.087 | 1.077 | 1.066 | 1.086 |
| Ca | 0.846 | 0.859 | 0.857 | 0.858 | 0.839 | 0.858 | 0.830 | 0.876 | 0.843 | 0.869 | 0.889 | 0.902 | 0.881 |
| Na | 0.025 | 0.026 | 0.026 | 0.028 | 0.032 | 0.029 | 0.032 | 0.034 | 0.033 | 0.045 | 0.035 | 0.032 | 0.033 |
| Sum Cat. | 4.000 | 4.000 | 4.000 | 4.000 | 4.000 | 4.000 | 4.000 | 4.000 | 4.000 | 4.000 | 4.000 | 4.000 | 4.000 |
| Mg/(Mg+Fe2) | 0.716 | 0.713 | 0.710 | 0.717 | 0.710 | 0.730 | 0.692 | 0.761 | 0.754 | 0.739 | 0.760 | 0.759 | 0.752 |
| Molecular proportions of end-members# : | | | | | | | | | | | | | |
| Wo | 0.450 | 0.454 | 0.454 | 0.456 | 0.449 | 0.453 | 0.446 | 0.463 | 0.448 | 0.464 | 0.469 | 0.473 | 0.467 |
| En | 0.381 | 0.378 | 0.378 | 0.376 | 0.376 | 0.386 | 0.379 | 0.364 | 0.376 | 0.352 | 0.364 | 0.358 | 0.364 |
| Fs | 0.169 | 0.168 | 0.168 | 0.168 | 0.175 | 0.162 | 0.175 | 0.173 | 0.177 | 0.184 | 0.168 | 0.169 | 0.169 |

* FeO and Fe2O3 are calculated assuming stoichiometry on the basis of 4 cations and 6 oxygens.

# Pyroxene end-members are calculated after the Subcommittee on Pyroxenes. IMA (1988).

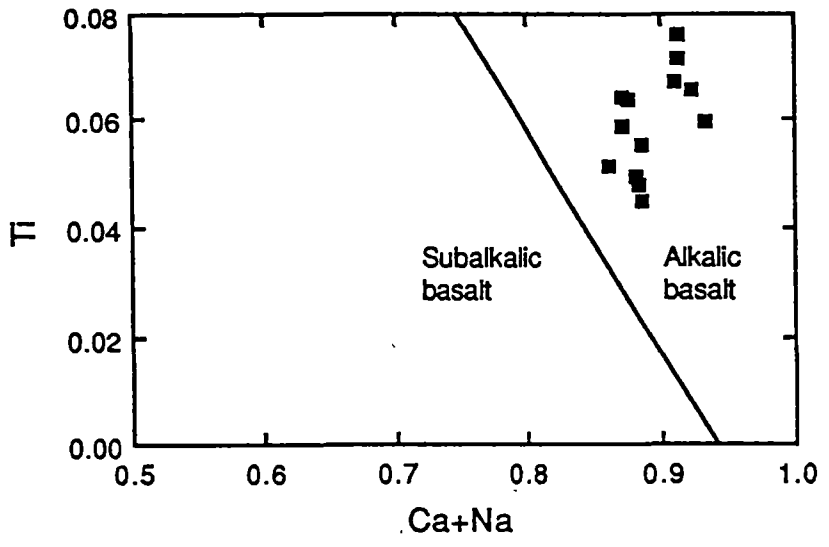


Figure 6.9 Tectonomagmatic discrimination diagram, Ti versus Ca+Na, based on clinopyroxene compositions (Latterrier *et al*, 1982). Data plotted from clinopyroxene analyses in Table 6.2 (samples SD-170 and SD-172 of the ophiolite association of the Pha Som M.C.).

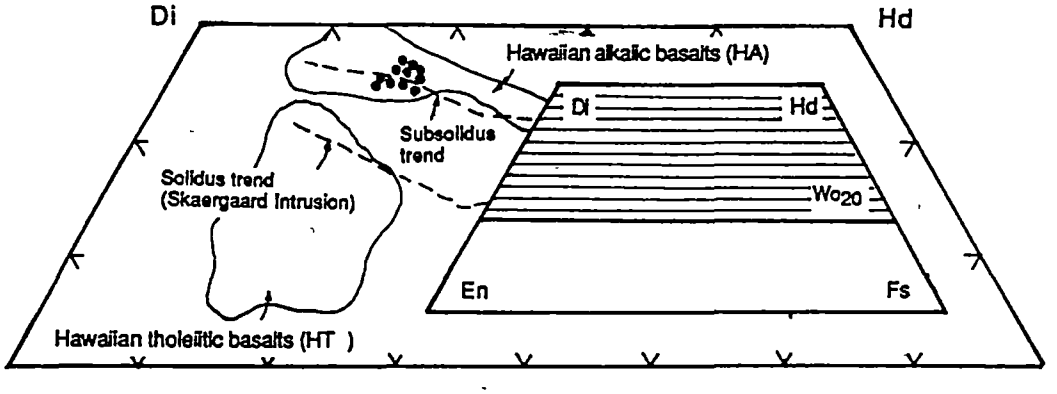


Figure 6.10 Wo-En-Fs diagram for clinopyroxenes in dolerites (samples SD-170 and SD-172) of the ophiolite association of the Pha Som M.C. Also shown are the compositional fields of clinopyroxenes in Hawaiian tholeiites and alkalic basalts (Basaltic Volcanism Study Project, 1981) and the solidus and subsolidus trends of the Skaergaard clinopyroxenes (Brown, 1967; Nwe, 1976).

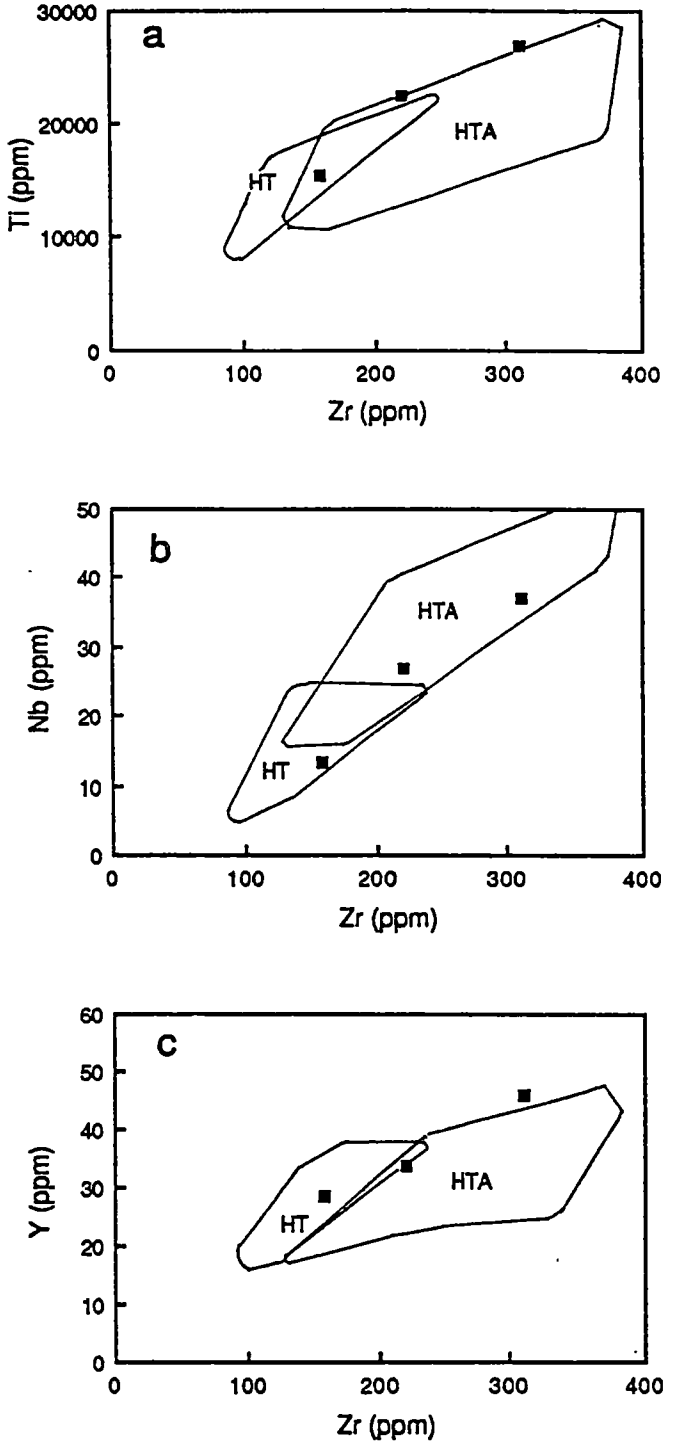


Figure 6.11 Binary plots of high-field-strength elements (HFSE) for the ophiolite association, showing the relationship between: (a) Ti and Zr, (b) Nb and Zr, and (c) Y and Zr. Compositional fields of Hawaiian tholeiites (HT) and Hawaiian transitional tholeiites and alkalic basalts (HTA) are from the Basaltic Volcanism Study Project (1981), Chen and Frey (1985), and Frey *et al.* (1990).

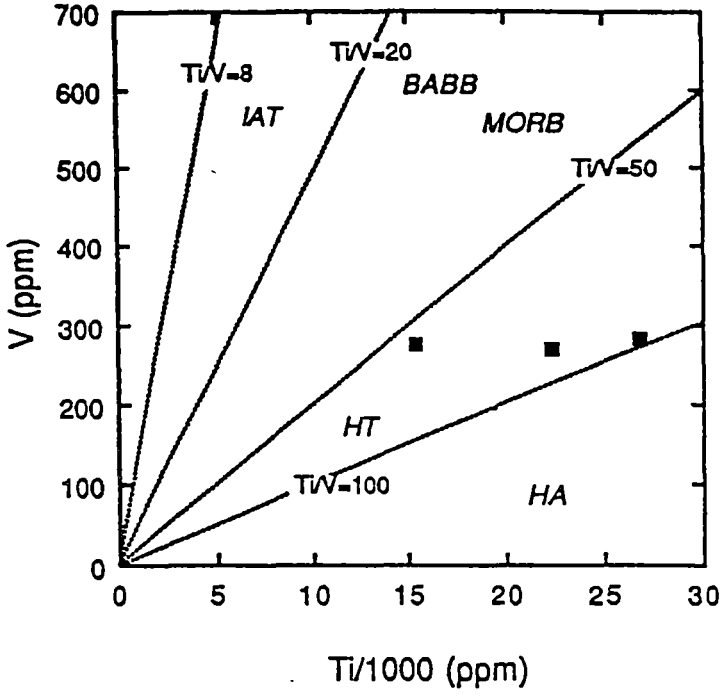


Figure 6.12 V-Ti plot (Shervais, 1982) for the ophiolite association of the Pha Som M.C. samples relative to the fields of island-arc tholeiites (IAT), backarc-basin basalts (BABB), mid-oceanic ridge basalts (MORB), Hawaiian tholeiites (HT) and Hawaiian alkalic basalts (HA).

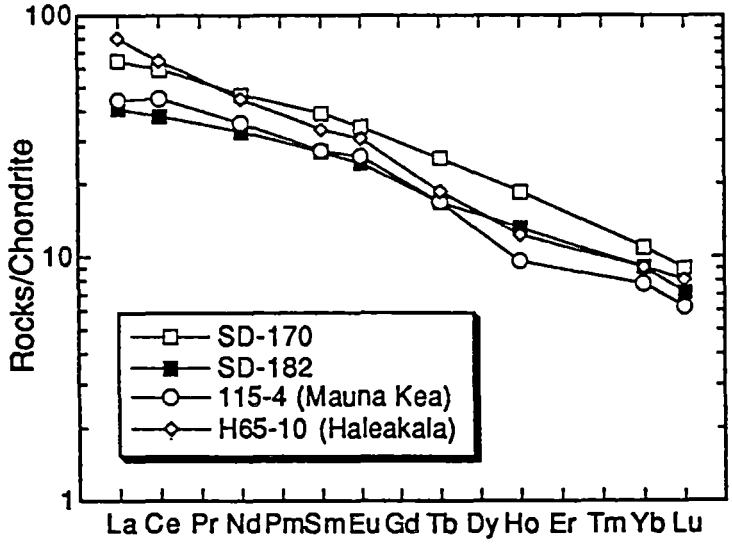


Figure 6.13 Chondrite-normalised REE patterns for the selected basaltic samples of the ophiolite association (samples SD-170 and SD-182). Also shown are the REE patterns for Hamakua transitional tholeiites and alkalic basalts, Mauna Kea Volcano, Hawaii (sample 115-4 of Frey *et al.* 1990) and alkalic basalts of Hana series, Haleakala Volcano, Maui (Chen and Frey, 1985).

basalts. The relationships between incompatible element pairs, such as Ti-Zr, Nb-Zr and Y-Zr (Figs. 6.11a,b&c) and Ti-V (Fig. 6.12), are linear and the compositional fields of these samples coincide with those of Hawaiian transitional tholeiites and alkali basalts.

Rare earth element abundances of two samples from the Pha Som Metamorphic Complex are given in Table 6.2. Their REE patterns show a marked enrichment of LREE relative to HREE. LREE abundances in these rocks range from 40-65 times chondrites and HREE abundances vary from 9-12 times chondrites (Fig. 6.13). The Pha Som transitional tholeiites and alkali basalts are comparable to the alkali basalts from the Hana volcanic series, Haleakala Volcano, Hawaii (Chen and Frey, 1985) and the Hamakua transitional tholeiites and alkali basalts, Mauna Kea Volcano, Hawaii that were considered to be the result of post-shield volcanism (Frey *et al.*, 1990).

From the geochemical and petrographic data discussed above, it is concluded that the original magma of the Pha Som Metamorphic Complex within the Pak Pat Volcanics is derived from the within-plate transitional tholeiitic and alkali basalts. They are confidently correlated with subgroup A-2 ocean-island transitional tholeiitic and alkali basalts of Panjasawatwong (1991). They show pronounced compositional similarities with the Hawaiian transitional tholeiites and alkali basalts (Frey *et al.*, 1990) suggesting that they formed in an intra-plate volcanic islands akin to modern Hawaiian islands.

## 6.4 Summary

The igneous rocks and their metamorphic equivalents in the Sirikit Dam area have been grouped into two lithostratigraphic units, i.e. the Pak Pat Volcanics and the Pha Som Metamorphic Complex. A small body of mafic volcanics and shallow intrusives, probably a thrust slice of the Pha Som Metamorphic Complex, is enclosed within the Pak Pat Volcanics.

The rocks of the Pak Pat Volcanics include lavas and tuffs ranging from basaltic to dacitic in compositions. Lavas are characterised by porphyritic texture with dominant albitised plagioclase phenocrysts and/or microphenocrysts. Tuffs are made up chiefly of basaltic rock fragments in fine-grained matrix. Chemically, these rocks are characterised by low abundances of $TiO_2$(0.37-1.15 wt %), $P_2O_5$ (0.11-0.27 wt %), Nb (<1-4 ppm), Y (14-34 ppm), Ni (mainly between 2 and 37 ppm), Cr (largely between 2 and 62 ppm) and relatively low values of Nb/Y (0.04-0.16). On the basis of geochemical and petrographic data discussed above, it is concluded that the Pak Pat volcanic rocks belong to the subalkaline arc basalt series and have

low- to medium-K affinities. They are similar in composition to some modern lavas erupted during incipient rifting of an oceanic island arc.

The rocks of the Pha Som Metamorphic Complex include altered gabbros, dolerites and basalts. The single lava studied is made up of lenticular plagioclase porphyroclasts in a matrix of chlorite, pumpellyite and epidote, of which the original igneous texture is largely obliterated. Dolerites are medium-grained rocks made up of plagioclase laths subophitically enclosed by subhedral clinopyroxene, which is extensively pseudomorphed by amphibole. A gabbro consists of plagioclase and clinopyroxene which is also largely pseudomorphed by amphibole. The analysed meta-basites are transitional tholeiitic to alkali within-plate basalts. They are characterised by high concentrations of $TiO_2$ (2.56-4.48 wt %), FeO* (11.87-13.41 wt %), Nb (13-37 ppm), Zr (159-311 ppm), Ni (81-215 ppm), Cr (68-383 ppm), V (268-281 ppm), Ti/Zr (86.3-101.5), Nb/Y (0.45-0.83) and moderately high concentrations of $P_2O_5$ (0.40-0.95 wt %) and Y (29-46 ppm). These basalts probably formed in an intra-plate volcanic islands akin to modern Hawaiian islands.

# Chapter 7

# PETROGRAPHY, GEOCHEMISTRY, PROVENANCE AND TECTONIC SETTINGS OF SANDSTONES AND METAGREYWACKES IN THE SIRIKIT DAM AREA

## 7.1 Introduction

The purpose of this chapter is to reconstruct provenances and tectonic settings for sandstones/metagreywackes of the Pha Som metasediments, and sandstones of the Nam Pat Group and Phra Wihan Formation in the Sirikit Dam area on the basis of petrographic and/or geochemical data.

Sandstone compositions have long been known to be influenced by the character of the sedimentary provenance, the nature of the sedimentary processes within the depositional basin, and the kind of dispersal paths that link the provenance to the basin (e.g. Dickinson and Suczek, 1979). The provenance of a particular sedimentary suite includes all aspects of the source area, such as source rocks, climate, and relief (Pettijohn *et al.*, 1972). In areas of intense tectonic and/or magmatic activity, a source-rock type has a stronger influence upon sediment compositions than climate and relief (Dickinson, 1970). The inter-relationships among these factors were probably best summed up by Dickinson and Suczek (1979) as follows: "detrital framework modes of sandstones from the different kind of basins are a function of provenance type governed by plate tectonics".

The compositional and chemical variations of sandstones have been utilised not only in the determination of the provenance of sedimentary suites but also in palaeotectonic and palaeogeographic reconstructions. On the basis of petrography, the use of a modal composition (detrital framework modes) of sandstones as an indicator of the provenance type has long been undertaken and has probably been well established (e.g. Dickinson, 1970; Crook, 1974; Dickinson and Suczek, 1979, Ingersoll and Suczek, 1979; Valloni and Maynard, 1981; Dickinson *et al.*, 1983; Marsaglia and Ingersoll, 1992). In contrast, the use of geochemistry of clastic sediments for a similar purpose has begun only recently (e.g. Bhatia and Taylor,

1981; Maynard *et al.*, 1982; Bhatia,1983) but the trend becomes increasingly prominent in the last few years (e.g. Bhatia and Crook, 1986; Roser and Korsch,1988; Roser and Cooper, 1990; McLennan and Taylor, 1991; Mortimer and Roser, 1992). On the basis of major element geochemistry, various discrimination diagrams have been derived for the determination of provenance of sandstones (Bhatia, 1983; Roser and Korsch, 1988). Likewise, some workers (e.g. Bhatia and Taylor, 1981; Bhatia and Crook, 1986) have utilised trace element geochemistry in the similar fashion as that used in the tectonic discrimination of volcanic rocks (e.g. Pearce and Cann, 1973; Winchester and Floyd, 1977). In addition, Roser and Cooper (1990) have demonstrated that immobile trace element geochemistry can also be applied in distinguishing metamorphosed sediments affiliated with different terrains in southern New Zealand.

## 7.2 Modal Analysis

As the character and amount of interstitial cement and matrix are largely a function of diagenesis, provenance studies have concentrated on proportions of framework grains (Dickinson, 1970; Dickinson and Suczek, 1979). The modal analyses of sandstone samples in this study used the Gazzi-Dickinson method of which the detailed procedure was given by Ingersoll *et al.* (1984). This method minimises variation in composition with grain size and therefore poorly-sorted samples of any sand size may be used. The unique aspects of the Gazzi-Dickinson method of point counting is the assignment of sand-sized crystals and grains within larger fragments to the category of the crystal or grain, rather than to the category of larger fragment.

In the present study, a minimum number of 400 points were counted on each thin section. Thin sections showing strong effects of diagenesis and metamorphism were excluded. The analysed samples were generally medium- to coarse-sand size, having mean grain sizes in the range 200 μm to 600 μm. However, samples of very coarse-grained sandstones (especially the Nam Pat Group) and fine-grained sandstones (especially the Pha Som metasediments) were also analysed because the medium-grained sandstones were not available in sufficient numbers. Sandstone samples with more than 20% matrix and/or carbonate cement, and those with grain size less than 60 μm were excluded from the analyses. The maximum spacing (about 350 μm) of the point counter was used in order to minimise the error caused by limitation of the identified area. More than 80% of the studied thin sections were stained to aid identification of K-feldspar.

The grain parameters used in this study are defined following the guidelines of Dickinson (1970), Graham *et al.* (1976) and Ingersoll and Suczek (1979). The useful criteria for recognition of detrital framework grains, modified from Ingersoll and Suczek (1979), are given in Table 7.1.

Table 7.1 Grain parameters (modified from Ingersoll and Suczek, 1979)

| | | | |
|---|---|---|---|
| (a) Q = Qm + Qp | where | Q = | total quartzose grains |
| | | Qm = | monocrystalline quartz grains |
| | | Qp = | polycrystalline aphanitic quartz grains |
| (b) F = P + K | where | F = | total feldspar grains |
| | | P = | plagioclase feldspar grains |
| | | K = | potassium feldspar grains |
| (c) Lt = L + Qp | where | Lt = | total aphanitic lithic grains |
| | | L = | unstable aphanitic lithic grains |
| (d) L = Lm+Lv+Ls | where | Lm = | metamorphic aphanitic lithic grains |
| | | Lv = | volcanic-hypabyssal aphanitic lithic grains |
| | | Ls = | sedimentary aphanitic lithic grains |
| (e) Lv + Lvm | where | Lvm = | volcanic-hypabyssal and metavolcanic aphanitic grains |
| (f) Lsm = Ls + Lm | where | Lsm = | sedimentary and metasedimentary aphanitic lithic grains |
| | and | M = | matrix and cementing materials |
| | | H = | heavy minerals |
| | | U = | miscellaneous and unidentified materials |

A brief description for each of grain types in Table 7.1 (modified from Ingersoll and Suczek, 1979) are as follows:

Recognition of monocrystalline quartz (Qm), plagioclase (P) and K-feldspar (K) is a straightforward exercise especially when facilitated by K-feldspar staining. Polycrystalline quartz (Qp), including chert, is microcrystalline aggregates of mono-mineralic quartz with most domains being less than 30 μm across. Volcanic-hypabyssal aphanitic lithic grains (Lv) are recognised by the presence of felsitic, microlitic or lathwork textures. Metamorphic aphanitic lithic grains (Lm) include quartz-mica tectonite with preferred planar fabric and quartz-mica or quartz-mica-feldspar aggregate without a preferred planar fabric. Sedimentary aphanitic lithic grains (Ls) are argillite and/or shale usually characterised by dark, semi-opaque, fine-grained detrital aggregates. Carbonate grains are not considered for the modal

analysis. Heavy minerals (H) are those clearly of detrital not diagenetic origin, e.g. epidote, sphene, rutile, tourmaline. Miscellaneous and unidentified grains (U) are those not clearly fitting into any of the above categories.

The point-count data were recalculated to 100% for each of the triangular QFL, QmFLt, QpLvmLsm and LmLvLs diagrams. The QFL and QmFLt plots are used in determining provenance of sediments which are classified into three main types: magmatic arc (undissected, transitional and dissected), continental block (craton interior, transitional continental and basement uplift) and recycled orogen (subduction complex, collision orogen and foreland uplift) provenances (Dickinson and Suczek, 1979; Dickinson *et al.*, 1983). The QpLvmLsm and LmLvLs diagrams are used to distinguish the provenance as well as the tectonic setting of deposition (Graham *et al.*, 1976; Ingersoll and Suczek, 1979). Moreover, the ratios of grain types such as plagioclase to total feldspar grains (P/F), polycrystalline aphanitic quartz to total quartz grains (Qp/Q) and volcanic aphanitic fragments to total lithic aphanitic fragments (Lv/L) have also been treated as criteria for the discrimination of provenance and tectonic setting (Dickinson, 1970; Valloni and Maynard, 1981; Ingersoll *et al.*, 1984; Dickinson, 1985).

In all, twenty-two thin sections of sandstone samples were point-counted. Five samples are from the Pha Som metasediments (only those which clearly retain sedimentary clastic textures), twelve from the Nam Pat Group and five from the Phra Wihan Formation (see Fig. 7.1 for sample locations). The small number of studied samples in the Pha Som metasediments was mainly due to widespread deformation and metamorphism. In spite of its extensive distribution across the study area, only a very small number of sandstone samples collected from the Pha Som metasediments were of use for provenance study via a petrographic technique. For most of the samples the framework clastic grains were too recrystallised for accurate point counting. Since these samples are unusual in retaining their texture, they may not be representative of the of the psammites as a whole. In this situation a geochemical approach to provenance and tectonic setting which can be applied to all the psammites regardless of level of recrystallisation, has many advantages.

## 7.3 Sandstone Petrography and Provenance

In this section, the important petrographic features and modal compositions of framework grains of the analysed sandstones are given. Subsequently, the interpretations of their provenances and tectonic settings of deposition are drawn based on various discrimination schemes discussed above.

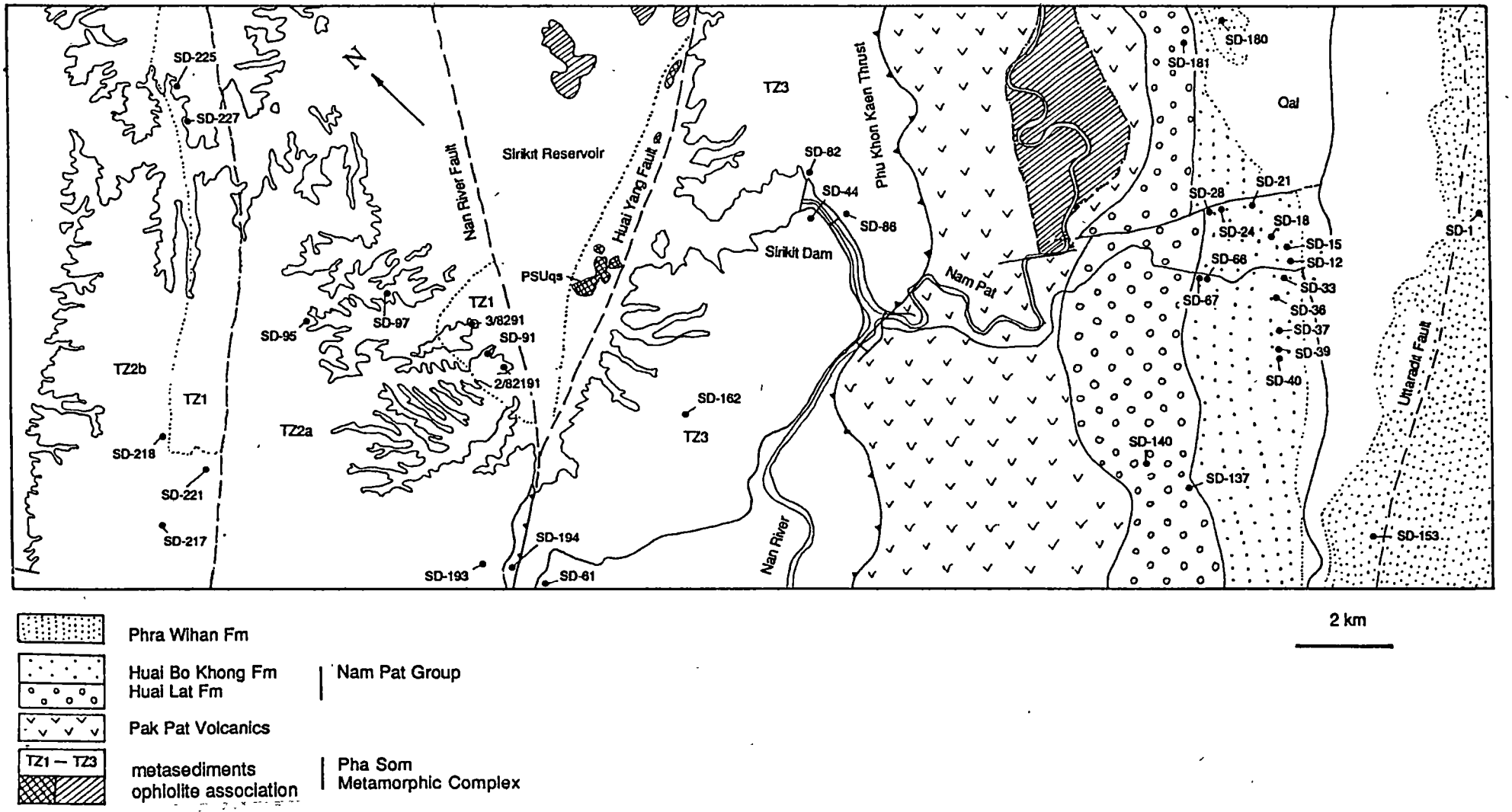


Figure 7.1 Sample location map (PSUqs = quartz schist and Qal = Quaternary alluvium).

### 7.3.1 Psammites of the Pha Som Metamorphic Complex

The dominant psammitic lithologies of the Pha Som metasediments are, in fact, metagreywackes whereas clastic sandstones are only minor components. Unfortunately, intense deformation together with recrystallisation of the original constituents render the metagreywackes of little use for modal analysis. The modal analysis relies on the clastic sandstones. Nonetheless, the petrographic features of metagreywackes are given in this section to outline the change in sandstone textures due to deformation and metamorphism and to provide an aid to the chemical interpretation of their provenances.

## Sandstones

Five samples of Pha Som sandstones showing little textural modification during deformation and recrystallisation were chosen for modal analysis. In addition, these samples show only a small degree of carbonate replacement during diagenesis/metamorphism. Sandstone samples of the Pha Som metasediments can be divided into two distinct types based on modal compositions of framework grains as follows:

**Quartz-rich greywackes:** The sandstones of this type are represented by samples 2/8291, 3/8291 and SD-91 and are classified as immature, fine- to medium-grained, slightly calcite cemented lithic greywackes (Pettijohn *et al.*, 1972). The framework grains consist chiefly of monocrystalline and polycrystalline quartz (>50%) with subordinate schist and phyllite fragments (20-30%), small amount of albitised plagioclase (10-15%) and few chert grains (<2%). Quartz is of volcanic origin and show either straight or slightly undulatory extinction. Polysynthetic twinning in albite is common. Tourmaline and pyrite are present as accessories. Grains are poorly- to moderately-sorted and angular to subangular with mean grain size of 250 μm to 500 μm. Grains are largely intact with little marginal granulation. Partially recrystallised matrix (5-10%) is made up of microcrystalline quartz, fine-grained white mica, chlorite and epidote. Grains are partly cemented by sparry calcite. The alignment of platy mica flakes is either random or subparallel. Schistosity has not developed in these samples.

The quartz-rich greywackes have the average composition $Q_{51}F_{14}L_{35}$ and $Qm_{33}F_{14}Lt_{53}$ (Table 7.2) which are comparable to those of modern and ancient subduction complex sands (Dickinson and Suczek, 1979) as tabulated in Table 7.3.

Table 7.2 Recalculated framework modes of sandstones from the Sirikit Dam area.

| Sample no. | QFL(%) | | | QmFLt(%) | | | QpLvmLsm(%) | | | LmLvLs(%) | | | Qp/Q | P/F | Lv/L | Grain |
|---|---|---|---|---|---|---|---|---|---|---|---|---|---|---|---|---|
| | Q | F | L | Qm | F | Lt | Qp | Lvm | Lsm | Lm | Lv | Ls | | | | size |
| *Pha Som* metasediments | | | | | | | | | | | | | | | | |
| 2/8291 | 50.7 | 8.5 | 40.8 | 29.7 | 8.5 | 61.8 | 34.0 | 8.3 | 57.7 | 87.4 | 12.6 | 0.0 | 0.41 | 1.00 | 0.13 | medium |
| 3/8291 | 47.0 | 17.7 | 35.3 | 31.0 | 17.7 | 51.4 | 31.2 | 27.1 | 41.7 | 59.4 | 39.4 | 1.2 | 0.34 | 1.00 | 0.39 | fine-medium |
| SD-91 | 55.8 | 15.1 | 29.1 | 38.8 | 15.1 | 46.2 | 36.9 | 18.2 | 44.9 | 66.9 | 28.8 | 4.2 | 0.31 | 1.00 | 0.29 | medium |
| Mean (n=3) | 51.2 | 13.7 | 35.1 | 33.1 | 13.7 | 53.1 | 34.0 | 17.9 | 48.1 | 71.3 | 26.9 | 1.8 | 0.35 | 1.00 | 0.27 | |
| SD | 4.4 | 4.7 | 5.8 | 4.9 | 4.7 | 8.0 | 2.9 | 9.4 | 8.5 | 14.5 | 13.5 | 2.2 | 0.06 | 0.00 | 0.14 | |
| SD-225 | 34.6 | 23.1 | 42.2 | 16.9 | 23.1 | 60.0 | 29.6 | 66.7 | 3.7 | 5.3 | 94.7 | 0.0 | 0.51 | 0.95 | 0.95 | coarse |
| SD-227 | 26.3 | 20.9 | 52.8 | 10.6 | 20.9 | 68.5 | 23.0 | 67.5 | 9.5 | 11.3 | 87.6 | 1.1 | 0.60 | 0.86 | 0.88 | coarse |
| Mean(n=2) | 30.5 | 22.0 | 47.5 | 13.7 | 22.0 | 64.3 | 26.3 | 67.1 | 6.6 | 8.3 | 91.2 | 0.5 | 0.56 | 0.91 | 0.91 | |
| SD | 5.9 | 1.6 | 7.5 | 4.5 | 1.6 | 6.0 | 4.7 | 0.6 | 4.1 | 4.2 | 5.0 | 0.8 | 0.06 | 0.06 | 0.05 | |
| *Nam Pat Group* | | | | | | | | | | | | | | | | |
| SD-12 | 26.3 | 27.1 | 46.6 | 9.4 | 27.1 | 63.5 | 26.6 | 66.2 | 7.2 | 6.3 | 90.2 | 3.5 | 0.64 | 1.00 | 0.90 | medium-coarse |
| SD-15 | 32.6 | 13.7 | 53.7 | 13.4 | 13.7 | 72.9 | 26.4 | 60.0 | 13.6 | 18.5 | 81.5 | 0.0 | 0.59 | 1.00 | 0.82 | very coarse |
| SD-24 | 29.0 | 28.6 | 42.4 | 15.4 | 28.6 | 56.1 | 24.4 | 70.1 | 5.5 | 7.3 | 92.7 | 0.0 | 0.47 | 1.00 | 0.93 | fine-medium |
| SD-28 | 22.9 | 23.9 | 53.2 | 11.3 | 23.9 | 64.8 | 18.0 | 78.3 | 3.7 | 4.3 | 95.4 | 0.3 | 0.51 | 1.00 | 0.95 | coarse |
| SD-33 | 27.4 | 26.0 | 46.6 | 16.6 | 26.0 | 57.4 | 18.9 | 69.7 | 11.4 | 12.3 | 86.0 | 1.7 | 0.40 | 1.00 | 0.86 | fine-medium |
| SD-36 | 22.4 | 20.9 | 56.8 | 15.0 | 20.9 | 64.1 | 11.5 | 79.9 | 8.6 | 9.1 | 90.3 | 0.6 | 0.33 | 1.00 | 0.90 | coarse |
| SD-37 | 49.5 | 19.5 | 31.0 | 25.2 | 19.5 | 55.3 | 43.9 | 43.2 | 12.9 | 23.0 | 77.0 | 0.0 | 0.49 | 1.00 | 0.77 | fine-medium |
| SD-39 | 26.6 | 21.1 | 52.2 | 13.7 | 21.1 | 65.1 | 19.8 | 73.3 | 6.9 | 8.0 | 91.4 | 0.5 | 0.48 | 0.98 | 0.91 | coarse |
| SD-40 | 40.1 | 28.4 | 31.5 | 25.7 | 28.4 | 45.9 | 31.4 | 44.0 | 24.6 | 33.6 | 64.1 | 2.3 | 0.36 | 1.00 | 0.64 | medium |
| SD-67 | 19.7 | 18.8 | 61.6 | 12.6 | 18.8 | 68.6 | 10.3 | 83.4 | 6.3 | 6.6 | 92.9 | 0.5 | 0.36 | 1.00 | 0.93 | medium-coarse |
| SD-140 | 25.6 | 22.2 | 52.3 | 17.4 | 22.2 | 60.4 | 13.5 | 80.1 | 6.4 | 7.4 | 92.6 | 0.0 | 0.32 | 0.95 | 0.93 | very coarse |
| SD-181 | 34.2 | 16.8 | 49.0 | 23.6 | 16.8 | 59.6 | 17.8 | 78.9 | 3.3 | 4.0 | 96.0 | 0.0 | 0.31 | 0.98 | 0.96 | very coarse |
| Mean(n=12) | 29.7 | 22.2 | 48.1 | 16.6 | 22.2 | 61.1 | 21.9 | 68.9 | 9.2 | 11.7 | 87.5 | 0.8 | 0.44 | 0.99 | 0.88 | |
| SD | 8,4 | 4.7 | 9.3 | 5.4 | 4.7 | 7.0 | 9.5 | 13.6 | 5.9 | 8.9 | 9.3 | 1.1 | 0.11 | 0.02 | 0.09 | |
| *Phra Wihan Formation* | | | | | | | | | | | | | | | | |
| SD-1 | 81.9 | 0.0 | 18.1 | 66.2 | 0.0 | 33.8 | 46.4 | 1.0 | 52.5 | 52.5 | 1.9 | 45.6 | 0.19 | | 0.02 | fine |
| SD-3 | 91.8 | 0.0 | 8.2 | 75.3 | 0.0 | 24.7 | 66.7 | 1.2 | 32.1 | 42.6 | 3.7 | 53.7 | 0.18 | | 0.04 | medium |
| SD-153 | 86.8 | 0.4 | 12.7 | 77.9 | 0.4 | 21.7 | 41.3 | 5.2 | 53.5 | 46.2 | 8.8 | 45.1 | 0.10 | | 0.09 | medium-coarse |
| SD-158 | 84.6 | 0.0 | 15.4 | 65.4 | 0.0 | 34.6 | 55.6 | 0.0 | 44.4 | 60.5 | 0.0 | 39.5 | 0.23 | | 0.00 | medium |
| SD-180 | 98.2 | 0.0 | 1.8 | 89.1 | 0.0 | 10.9 | 83.9 | 6.5 | 9.7 | 50.0 | 40.0 | 10.0 | 0.09 | | 0.40 | medium |
| Mean (n=5) | 88.7 | 0.1 | 11.3 | 74.8 | 0.1 | 25.2 | 58.8 | 2.8 | 38.5 | 50.4 | 10.9 | 38.8 | 0.16 | | 0.11 | |
| SD | 6.5 | 0.2 | 6.4 | 9.7 | 0.2 | 9.7 | 17.0 | 2.8 | 18.2 | 6.8 | 16.6 | 16.9 | 0.06 | | 0.17 | |

Table 7.3 Comparison of average values of framework grains between sandstones from the Sirikit Dam area and the discriminatory values. The average values with standard deviations for QFL, QmFLt and P/F are calculated from Dickinson and Suczek (1979) and Qp/Q and Lv/L ratios from Dickinson (1985) and * from Dickinson and Valloni (1980).

| Provenances | QFL% | | | QmFLt% | | | Grain ratios | | |
|---|---|---|---|---|---|---|---|---|---|
| | Q | F | L | Qm | F | Lt | Qp/Q | P/F | Lv/L |
| Continental block n=1700 | 75.1±20.2 | 21.8±17.9 | 3±2.9 | 70.4±21.3 | 21.8±17.9 | 7.8±6.7 | 0.07* | 0.25* | |
| Recycled orogen n=1955 | 65.2±18.3 | 9.7±8.0 | 25.1±16.3 | 48.3±24.4 | 9.7±8.0 | 42±24.1 | | 0.72 | |
| Collision orogen n=639 | 71±11.4 | 12.3±8.4 | 16.7±8.4 | 62.4±10.9 | 12.3±8.4 | 25.2±12.1 | 0.03 | 0.66 | 0.08 |
| Forelan uplift n=1136 | 59.2±24.5 | 8.1±6.5 | 24.5±15.4 | 44.1±24.6 | 8.1±6.5 | 39.3±22.9 | 0.3 | 0.49 | 0.8 |
| Subduction complex n=180 | 45.0±15.5 | 13.5±8.1 | 41.5±17.3 | 7.5±3.3 | 13.5±8.1 | 79.0±6.1 | 0.35 | 0.94 | 0.33 |
| Magmatic arc n=1667 | 22.6±12.6 | 32.3±8.6 | 45.0±17.0 | 20.0±12.2 | 32.3±8.6 | 47.7±16.7 | 0.07 | 0.83 | 0.98 |
| Undissected arc n=181 | 5.5±4.0 | 28.6±8.5 | 65.9±5.9 | 4.6±3.9 | 28.6±8.5 | 66.8±5.5 | | 0.97 | |
| Transitional arc n=224 | 18.7±2.6 | 28.2±7.0 | 53.0±6.8 | 14.7±4.5 | 28.2±7.0 | 57.1±6.9 | | 0.85 | |
| Dissected arc n=1262 | 33.4±6.3 | 36.5±7.9 | 30.1±8.2 | 30.7±5.7 | 36.5±7.9 | 32.8±8.5 | | 0.71 | |
| Pha Som metasediments (quartzose) n=3 | 51.2±4.4 | 13.7±4.7 | 35.1±5.8 | 33.1±4.9 | 13.7±4.7 | 53.1±8.0 | 0.35±.06 | 1 | 0.27±0.14 |
| Pha Som metasediments (quartz-poor) n=2 | 30.5±5.9 | 22.0±1.6 | 47.5±7.5 | 13.7±4.5 | 22.0±1.6 | 64.3±6.0 | 0.56±0.06 | 0.91±0.06 | 0.91±0.05 |
| Nam Pat Group n=12 | 29.7±8.4 | 22.0±4.7 | 48.1±9.3 | 16.6±5.4 | 22.0±4.7 | 61.1±7.0 | | 0.99 | 0.88 |
| Phra Wihan Formation n=5 | 88.7±6.5 | 0.1±0.2 | 11.3±6.4 | 74.8±9.7 | 0.1±0.2 | 25.2±9.7 | 0.16±.06 | | 0.11±0.17 |

The ratios of grain parameters, Qp/Q (0.35) and P/F (1.00) and Lv/L (0.27) are also very similar to the values given for the subduction complex sands (Dickinson, 1985). However, on the QFL triangular plot (Fig. 7.2a), they fall within a recycled orogenic provenance field; and on the QmFLt diagram (Fig. 7.2b), they occupy overlapping fields between the transitional recycled orogenic and the dissected arc provenance types of Dickinson *et al.* (1983). The QpLvmLsm plot of Ingersoll and Suczek (1979) indicates that these sandstone samples have come from either magmatic arcs or subduction complexes (Fig. 7.2c).

The compositional characteristics of the detrital framework modes of the three greywacke samples point towards the likelihood that they represent sediments derived from a subduction complex (accretionary complex) mixed with the detritus from a magmatic arc source.

**Quartz-poor greywackes:** Two representative samples of quartz-poor greywackes (samples SD-225 and SD-227) show strong affinity towards a volcanic source. Sample SD-225 is immature, coarse-grained grained, lithic greywacke. The framework grains consist chiefly of volcanic (microlithic and lathwork) lithic fragments and subordinate albitised plagioclase and monocrystalline and polycrystalline quartz. Haematite is present as an accessory mineral. Grains are moderately-sorted and subangular with mean grain size of 500 μm. Grains commonly show marginal granulation. Partially recrystallised matrix (<15 %) is made up of microcrystalline quartz, fine-grained white mica and chlorite. Plagioclase is largely replaced by epidote, calcite and to a lesser extent fine-grained white mica. Sample SD-227 is immature, coarse-grained, lithic greywacke. The framework grains consist mainly of lithic fragments with subordinate quartz and albitised plagioclase of almost equal amount. The volcanic (microlithic) lithic fragments are the dominant lithic grains together with small amounts of phyllite fragments. Sphene and haematite are present as accessories. Grains are moderately-sorted and subangular with mean grain size of 600 μm. Grains commonly show marginal granulation. Partially recrystallised matrix (<15 %) is made up of microcrystalline quartz, fine-grained white mica and chlorite. Plagioclase is largely replaced by epidote, calcite and to a lesser extent fine-grained white mica. Chloritisation of mafic minerals is common.

The quartz-poor greywackes have the average composition of $Q_{30}F_{22}L_{48}$ and $Qm_{14}F_{22}Lt_{64}$ (Table 7.2) which are comparable to transitional magmatic arc sandstones (Dickinson and Suczek, 1979) as tabulated in Table 7.3. The ratios of grain parameters, P/F (0.91) and Lv/L (0.91) are also very similar to the values for the magmatic arc sands (Dickinson, 1985). On the QFL triangular diagram (Fig.

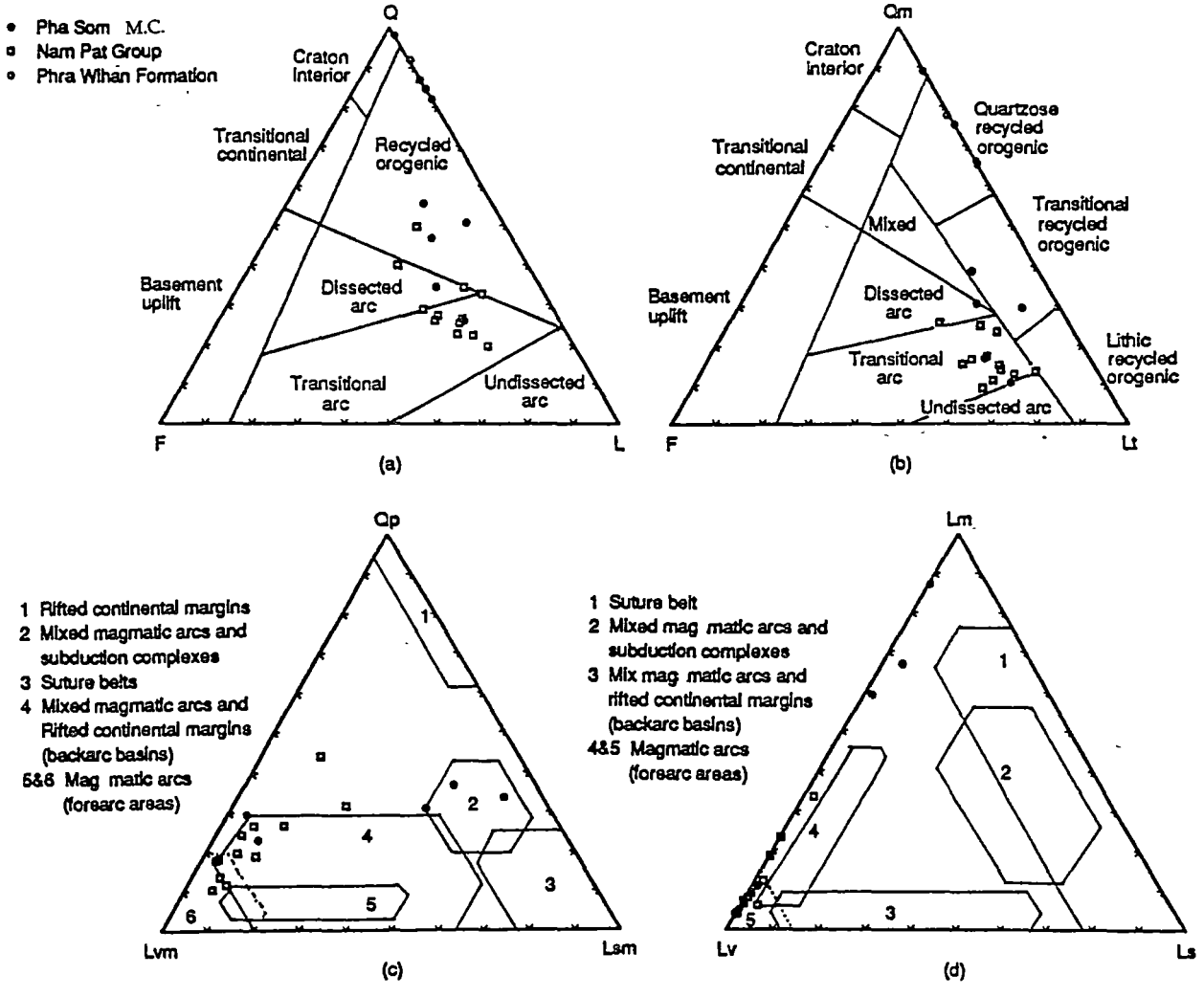


Figure 7.2 Ternary diagrams for sandstones from the Pha Som M.C., Nam Pat Group and Phra Wihan Formation. Provenance fields are after Dickinson *et al.* (1983) for QFL & QmFLt plots, Ingersoll and Suczek (1979) for QpLvmLsm & LmLvLs plots, and Dorsey (1988) for dashed boundary fields in QpLvmLsm & LmLvLs plots.

7.2a), they plot within transitional and dissected arc provenance fields; and on the QmFLt diagram (Fig. 7.2b), they occupy a transitional arc provenance field of Dickinson *et al.* (1983). The QpLvmLsm plot (Fig. 7.2c) of Ingersoll and Suczek (1979) indicates that these sandstone samples have a mixed provenance type between magmatic arcs and rifted continental margins (backarc basins) but they plot near the field for magmatic arc (forearc areas) on the LmLvLs diagram (Fig. 7.2d). From these discriminatory plots, it is can be strongly suggested that these samples were derived from a magmatic arc source.

The compositional characteristics of the detrital framework modes of these two greywacke samples are indicative of a magmatic arc source. This is further confirmed by the geochemical characteristics of sample SD-225 presented in section 7.4.1.

### Metagreywackes

There are two types of chlorite-zone metagreywackes of the Pha Som metasediments based on the degree of microstructural development. They are classified as semischists in one group and fine-grained schists in the other (using terminology of Spry, 1969). The semischists are metagreywackes that show only slight recrystallisation of the original grains and the fine-grained schists are those that develop more pronounced schistosity and have been subjected to intense recrystallisation. These two types of metagreywackes belong to the TZ2 and TZ3 textural zones discussed in full detail in Chapter 5.

## 7.3.2 Nam Pat Group sandstones

The sandstones of this group are characterised by high abundances of volcanic rock fragments with respect to quartz and feldspar. Their grain sizes vary from fine- to very coarse grained. The petrographic characteristics of the representative samples are as follows:

Sample SD-37 is submature, mud-cemented, fine-grained feldspathic litharenite. The framework grains consist chiefly of monocrystalline and polycrystalline quartz (49%) with minor amount of volcanic (microlithic) rock fragments (31%) and plagioclase (20%). Grains are moderately-sorted and subangular with mean grain size of 150 μm. The matrix is less than 5% and made up chiefly of chlorite with minor amount of calcite, white mica and epidote.

Sample SD-140 is classified as submature, mud-cemented, very coarse-grained feldspathic litharenite. The framework grains consist chiefly of volcanic (lathwork and microlithic) rock fragments (52%) with minor amounts of monocrystalline and polycrystalline quartz (26%) and plagioclase (22%). Grains are poorly-sorted and subangular with mean grain size of 2 mm. Matrix is less than 5% and made up of chlorite, white mica and epidote.

These sandstone samples are characterised by low abundances of quartz grains. The average compositions, $Q_{30}F_{22}L_{48}$ and $Qm_{17}F_{22}Lt_{61}$ (Table 7.2) are comparable to those of transitional magmatic arc sandstones (Dickinson and Suczek, 1979) as tabulated in Table 7.3. The ratios of grain parameters, P/F (0.99) and Lv/L (0.88) are also very similar to the values for the magmatic arc sandstones (Dickinson, 1985). On the QFL triangular diagram (Fig. 7.2a), they plot within transitional and dissected arc provenance fields and on the QmFLt diagram (Fig. 7.2b), they totally occupy the field for a transitional arc provenance of Dickinson *et al.* (1983). The QpLvmLsm plot of Ingersoll and Suczek (1979) shown in Figure 7.2c indicates that they have a mixed provenance between magmatic arcs and rifted continental margins (backarc basins) as well as magmatic arcs (forearc areas) but they exclusively plot within the field for magmatic (forearc areas) on the LmLvLs diagram (Fig. 7.2d). These discriminatory plots point to a magmatic arc source for the Nam Pat sandstones.

The compositional characteristics of the detrital framework grains and their immature textures indicate that the Nam Pat Group sandstones were derived from a nearby magmatic arc and were probably deposited in the forearc rather than the backarc basin. On the ground of compositions of the volcanic (lathwork and microlithic) lithic fragments and structural/stratigraphic relationships, it seems likely that the volcanic source is the volcanoes that generated the Pak Pat volcanics whose dominant rock types are basaltic andesites (see Chapter 6 for detailed discussion of the Pak Pat volcanics).

### 7.3.3 Phra Wihan sandstones

Sandstones of the Phra Wihan Formation are classified as mature to supermature, fine- to medium-grained, quartz-cemented quartzarenite (Mcbride, 1963). The framework grains consist chiefly of monocrystalline and subordinate polycrystalline quartz (85-97%) with minor amount of chert (3-10%). Muscovite is generally present in a very small amount but may be present up to 4% in some samples. Similarly, fine-grained schistose rock fragments which are a very minor

component may be up to 3% in some samples (e.g. samples SD-1 and SD-3). Tourmaline and zircon are present as accessories. Volcanic rock fragments have not been detected. Grains are well-sorted and subrounded to rounded with mean grain size of 150 μm to 300 μm. Clay matrix is practically absent and grains are cemented by authigenic quartz overgrowth. Quartz grains commonly exhibit undulatory extinction and possess either sharp or sutured grain boundaries.

The Phra Wihan sandstones are typically lithic-bearing mature sandstones. The detrital mode $Q_{89}F_0L_{11}$ and $Qm_{75}F_0Lt_{25}$ (Table 7.2) and the ratios Qp/Q (0.16) and Lv/L (<0.09) are similar to those derived from collision recycled orogenic provenance of Dickinson and Suczek (1979) as tabulated in Table 7.3. On the QFL triangular diagram (Fig. 7.2a), the majority of them plot within a recycled orogenic provenance field with one data point plot in a craton interior provenance field; and on the QmFLt diagram (Fig. 7.2b), they plot on a field for quartzose recycled orogenic provenance of Dickinson *et al.* (1983). Based on these discriminatory plots, it is suggested that the Phra Wihan sandstones were derived from a quartzose recycled orogenic source or from craton interior.

In the Khorat Plateau (northeastern Thailand), Phra Wihan sandstones have been interpreted as having been deposited by a braided stream or a major braided stream flanked by subsidiary meandering streams (Sattayarak, 1983) in a huge depositional basin known as the Indochina basin. The source rocks of the Phra Wihan Formation and probably other formations of the Khorat Group are thought to be the Chiang Saen massif near Chiang Rai, the Khun Tan granite west of Lampang, the concealed igneous rocks in the Central Plain, the Chon Buri massif, the Pailin massif in Cambodia, the Kontum, Rao Co and Song Ma massifs in Vietnam (Sattayarak,1983). These source rocks, largely basement gneisses and granites, correspond to continental block provenances of either craton interior and basement uplift type according to Dickinson and Suczek (1979).

Drumm *et al.* (1993) have shown that the Ms4 formation in northern Thailand, the probable equivalent of the Phra Wihan Formation in the study area and in the Khorat Plateau region, was characterised by fining-upward sequence typical of point-bar deposits of a meandering river. The proposed source rock area for the quartzose sandstones of the Ms4 formation is the Truong Son zone in north Vietnam based on K/Ar metamorphic age (350 Ma) of detrital mica and the palaeocurrent direction from ENE to WSW. However, they also suggested that the main sediment supply of the Ms4 formation might have been transported by rivers which originated in southwest China. Based on modal analysis, they concluded that the quartzose sandstones were reworked sediments eroded from an orogen.

Though there are some minor conflicting ideas among these workers, the general consensus is that; the Phra Wihan Formation were deposited in a large river basin, either by braided or meandering rivers, and received sediments from mainly crystalline basement (gneisses and granites) sources located along the basin margin.

The present study does not provide any further information on the depositional environment of the Phra Wihan Formation due to the limited extent of the study area and the scope of the study which focuses on the structure and metamorphism rather than sedimentology. However, additional knowledge on the source rocks of Phra Wihan sandstones was obtained by modal analysis of the framework grains. The quartz-rich and feldspar-poor character of Phra Wihan sandstones lead to the conclusion that the source rock area is mainly a quartzose recycled orogen rather than crystalline basements. This idea is in good agreement with that proposed by Drumm *et al.* (1993) but differs from the general opinions discussed above. Nevertheless, it should also be noted that the gradational relationships between quartzose recycled orogenic and craton interior provenances cannot be neglected. Dickinson *et al.* (1983) strongly expressed the idea that the quartzose variants of sands having orogenic provenances were recycled from sediments whose ultimate sources were cratonic. Sedimentological factors, notably the dispersal mechanism, may enhance the quartz content of sands by selective removal of lithic grains and feldspars. The Phra Wihan sandstones are texturally mature (in other words, they were transported from distant sources), therefore the influence of the source areas may be considerably obscured. This renders high uncertainty in the use of modal analysis as a mean to determine provenance. However, it is widely accepted that the framework modes of quartz-rich sandstones should still reflect the source rock compositions though they may be affected by other sedimentological factors (Dickinson *et al.*, 1983).

## 7.4 Geochemistry and Provenance

The major and trace element compositions of the Pha Som sandstones and metagreywackes (these will be referred to later as psammites for convenience) and the Nam Pat Group sandstones were determined by XRF spectrometry (the detailed procedures are given in Chapter 1). Particular care was exercised to avoid the samples with high carbonate cements (>5 modal%) as they may lead to incorrect interpretation of the tectonic setting and provenance of the sandstone suites. XRF analyses were not undertaken for samples from the Phra Wihan Formation as their provenance and depositional environment can be adequately treated via petrographic

and sedimentological approaches. In the following section, sixteen psammitic samples from the Pha Som metasediments and fourteen samples of the Nam Pat Group sandstones are considered in terms of their geochemical characteristics and provenance types. The sample locations are shown in Figure 7.1.

In the present study, various proposed schemes for discriminating provenances and tectonic settings of sediments and sedimentary rocks (e.g. Bhatia, 1983, Bhatia and Crook, 1986; Roser and Korsch, 1988) were applied. The basic concepts of these discrimination schemes were based on observations made from geochemical characteristics of several suites of sandstones with known provenances and tectonic settings.

Several studies, e.g. Bhatia (1983) and Roser and Korsch (1988), have led to recognition of major elements that are useful discriminating parameters. The parameters recognised by Bhatia (1983) include $TiO_2$, $Al_2O_3/SiO_2$, and $Fe_2O_3$*+MgO which decrease progressively from oceanic island arc to continental island arc to active continental margin to passive margin settings. Roser and Korsch (1988) proposed discriminant functions that give effective separation between four provenance group: P1 (primarily mafic and lesser intermediate igneous provenance), P2 (primarily intermediate igneous provenance), P3 (felsic igneous provenance), and P4 (recycled provenance). The proposed discriminant functions (F1 and F2) are as follows:

$$F1 = 1.773TiO_2 + 0.607Al_2O_3 + 0.76Fe_2O_3^* - 1.5MgO + 0.616CaO + 0.509Na_2O - 1.224K_2O - 9.09, \text{ and}$$

$$F2 = 0.445TiO_2 + 0.07Al_2O_3 - 0.25Fe_2O_3^* - 1.142MgO + 0.438CaO + 1.475Na_2O + 1.426K_2O - 6.681$$

Trace elements, especially the immobile elements, have also been used for the same purpose as the major elements. In general, it has been noted that there is a systematic increase in LREE (La, Ce, Nd), Th, Nb and the La/Y ratio and a decrease in V, Sc in greywackes from oceanic island arc to continental island arc to active continental margin to passive margin settings (Bhatia and Crook, 1986). On these grounds, the discrimination plots were proposed. Some useful plots which are adopted in the present study include ternary plots, La-Th-Sc and Th-Sc-Zr/10; and binary plots, La-Th, Ti/Zr-La/Sc. Roser and Cooper (1990) emphasised the use of immobile element ratios as guides to tectonic setting and provenance because the

dilution effects can be avoided. They applied discrimination plots, Ti/Zr-La/Sc and Y/Nb-Th/Sc, to distinguish lithologies from two different tectonic settings (i.e. the Torlesse and Caples terranes) in the Haast Schist terrane in New Zealand. The Torlesse terrane greywackes were interpreted as sediments derived from an active volcano-plutonic continental margin arc source and Caples terrane greywackes were derived from an intra-oceanic island arc (Coombs *et al.*, 1976; MacKinnon, 1983) with some input from a continental source area (Mortimer and Roser, 1992). In addition, Mortimer and Roser (1992) have proposed a ratio plot, Ce/V-La/Y, to delineate the Torlesse-Caples terrane boundary in the Otago Schist.

Application of these discrimination plots to sandstones and metagreywackes from the Sirikit Dam area, together with the discussion on their effectiveness and limitation are presented below (sections 7.4.1 and 7.4.2).

## 7.4.1 Psammites of the Pha Som Metamorphic Complex

Psammites of the Pha Som metasediments can be divided into two groups, PSG-1 and PSG-2, on the basis of their chemical characteristics. In the following sections, the average concentrations or ratios of elements are reported together with standard deviations ($1\sigma$).

### PSG-1

The PSG-1 group includes two greywackes (SD-61 and SD-97), two semischists (SD-95 and SD-193) and three fine-grained schists (SD-82, SD-162 and SD-194).

**Major elements:** PSG-1 samples are characterised by relatively low average concentrations of $TiO_2$ (0.57±0.07 wt%), $Al_2O_3$ (11.64±0.70 wt%), $Fe_2O_3$ (4.75±0.47 wt%) compared to those of PSG-2 samples as shown in Table 7.4 and Table 7.6. They plot within the felsic igneous rock provenance (P3) and the quartzose recycled provenance (P4) on the discrimination diagram of Roser and Korsch (1988) as shown in Figure 7.3. On the $TiO_2$ versus $Fe_2O_3$*+MgO diagram (Fig. 7.4a), they plot within the continental island arc field of Bhatia (1983). On the $Al_2O_3/SiO_2$ versus $Fe_2O_3$*+MgO plot of Bhatia (1983), the majority of them fall within the continental island arc but a few samples overlap into the field for active continental margin (Fig. 7.4b).

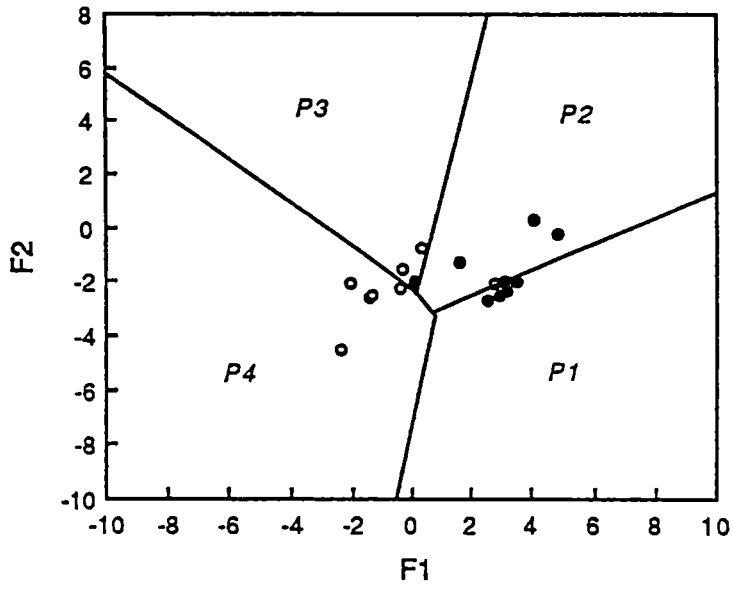


Figure 7.3 Major element discrimination plot for the Pha Som psammites. Symbols : open circles = PSG-1 and solid circles = PSG-2 (also applied for Figures 7.4, 7.5, 7.6 and 7.7). Discrimination functions (F1&F2) and provenance fields (P1 = mafic, P2 = intermediate, P3 = felsic, P4 = quartzose recycled) are after Roser and Korsch (1988). Sample scores are calculated from the anhydrous normalised data in Table 7.4, using the equations:
$F1 = 1.773TiO_2 + 0.607Al_2O_3 + 0.76Fe_2O_3^* - 1.5MgO + 0.616CaO + 0.509Na_2O - 1.224K_2O - 9.09,$
$F2 = 0.445TiO_2 + 0.07Al_2O_3 - 0.25Fe_2O_3^* - 1.142MgO + 0.438CaO + 1.475Na_2O + 1.426K_2O - 6.681.$

**Trace elements :** PSG-1 samples are characterised by relatively low average concentrations of V (88±8 ppm) and the ratios Zr/Th (16.0±2.2) and relatively high abundances of Pb (9±4 ppm), Th (12.1±3.0 ppm), LREE such as, La (26.6±3.4 ppm), Ce (51.6±8.0 ppm) and Nd (24.2±2.0 ppm) and the ratios Th/Sc (0.96±0.22) and Ce/V (0.59±0.05) compared to those of PSG-2 samples (Tables 7.4 and 7.6).

Absolute abundances and ratios of relatively immobile trace elements of PSG-1 samples were compared with greywackes from various tectonic settings from eastern Australia (Bhatia and Crook, 1986) in Table 7.6. PSG-1 samples are similar to greywackes derived from continental island arc settings, i.e. greywackes deposited in sedimentary basins (interarc, backarc and forearc) adjacent to felsic-dominated island arcs, where the arcs have formed on well-developed continental crust, e.g. the Lau Basin, Japan Sea (Bhatia, 1983; Bhatia and Crook, 1986). On the ternary plots La-Th-Sc (Fig. 7.5a) and Th-Sc-Zr/10 (Fig. 7.5b) of Bhatia and Crook (1986), they all plot within the continental island arc field. On the binary plot

Table 7.4 Whole-rock XRF analyses of the Pha Som M.C. psammites in the Sirikit Dam area.

| Chemical group | PSG-1 | | | | | | | PSG-1 | | PSG-2 | | | | | | | | | PSG-2 | |
|---|---|---|---|---|---|---|---|---|---|---|---|---|---|---|---|---|---|---|---|---|
| Sample no./ | SD-61 | SD-82 | SD-95 | SD-97 | SD-162 | SD-193 | SD-194 | Mean | SD | P-102 | P-104 | P-107 | SD-44 | SD-86 | SD-217 | SD-218 | SD-221 | SD-225 | Mean | SD |
| *Major elements (wt %)* | | | | | | | | | | | | | | | | | | | | |
| SiO2 | 71.00 | 70.73 | 74.31 | 73.73 | 73.30 | 76.20 | 71.01 | 72.90 | 2.06 | 66.11 | 67.04 | 64.14 | 65.34 | 62.73 | 70 21 | 62.60 | 58.10 | 68 57 | 64.98 | 3 62 |
| TiO2 | 0.59 | 0.53 | 0.49 | 0.51 | 0.58 | 0.60 | 0.69 | 0.57 | 0.07 | 0.78 | 0.73 | 0.83 | 0.85 | 0 87 | 0.56 | 0.70 | 0.77 | 0.65 | 0.75 | 0.10 |
| Al2O3 | 12.61 | 11.85 | 11.33 | 10.51 | 12.24 | 11.79 | 11.17 | 11.64 | 0.70 | 12.91 | 14 39 | 13.88 | 15.98 | 17.21 | 14.18 | 15.01 | 17.53 | 14.94 | 15.11 | 1.54 |
| Fe2O3* | 4.90 | 4.40 | 4.09 | 4.42 | 4.85 | 5.44 | 5.16 | 4.75 | 0.47 | 6.58 | 6 22 | 6.59 | 6.53 | 6.96 | 5.69 | 7.42 | 7.97 | 5.78 | 6.64 | 0.74 |
| MnO | 0.06 | 0.07 | 0.04 | 0.07 | 0.05 | 0.04 | 0.06 | 0.06 | 0.01 | 0.10 | 0 09 | 0.09 | 0.08 | 0 07 | 0 06 | 0.13 | 0.11 | 0 07 | 0.09 | 0.02 |
| MgO | 2.33 | 2.12 | 2.08 | 2.11 | 2.39 | 2.20 | 2.50 | 2.25 | 0.16 | 2.88 | 2.96 | 3.22 | 2.47 | 2.77 | 2.40 | 3.40 | 3.99 | 2.53 | 2.96 | 0.51 |
| CaO | 4.19 | 6.28 | 3.68 | 5.33 | 2.32 | 0.25 | 5.82 | 3.98 | 2.13 | 7.09 | 4.36 | 7.28 | 2.32 | 3.68 | 2 09 | 6 65 | 6.68 | 2.17 | 4.70 | 2.24 |
| Na2O | 2.57 | 2.23 | 2.22 | 1.81 | 2.93 | 2.26 | 2 04 | 2.30 | 0.36 | 2.96 | 3.91 | 3.16 | 6.06 | 4.87 | 3 23 | 2.78 | 2.77 | 4 36 | 3.79 | 1.13 |
| K2O | 1.58 | 1.64 | 1.63 | 1.37 | 1.20 | 1.09 | 1.35 | 1.41 | 0.22 | 0 46 | 0.13 | 0 65 | 0.23 | 0.67 | 1.50 | 1.16 | 1.88 | 0 83 | 0 83 | 0.58 |
| P2O5 | 0.15 | 0.14 | 0.13 | 0.14 | 0.14 | 0.13 | 0.17 | 0.14 | 0.01 | 0.15 | 0.16 | 0.16 | 0.16 | 0.18 | 0 08 | 0.16 | 0.20 | 0.10 | 0.15 | 0.04 |
| Total# | 100.00 | 100.00 | 100 00 | 100.00 | 100.00 | 100.00 | 100.00 | | | 100 00 | 100.00 | 100 00 | 100.00 | 100.00 | 100.00 | 100.00 | 100.00 | 100.00 | | |
| Total$ | 99.89 | 100.56 | 100.18 | 100.24 | 99.89 | 100.07 | 99.97 | | | 100.12 | 100.76 | 100.14 | 99.83 | 99.96 | 100 20 | 100.43 | 100.42 | 99.92 | | |
| LOI | 5.12 | 6.39 | 4.86 | 5.99 | 3.72 | 2.73 | 6 02 | 4.98 | 1.34 | 1.72 | 2.63 | 1.93 | 3.99 | 3.46 | 3.34 | 7.56 | 7.62 | 3.18 | | |
| *Trace elements (ppm)* | | | | | | | | | | | | | | | | | | | | |
| Nb | 10 | 8 | 8 | 8 | 9 | 9 | 10 | 9 | 1 | 5 | 6 | 5 | 5 | 5 | 3 | 3 | 2 | 3 | 4 | 1 |
| Zr | 172 | 162 | 165 | 166 | 212 | 176 | 290 | 192 | 46 | 147 | 167 | 155 | 144 | 153 | 105 | 107 | 86 | 116 | 131 | 28 |
| Y | 22 | 25 | 22 | 22 | 28 | 22 | 32 | 25 | 4 | 23 | 25 | 24 | 27 | 28 | 18 | 27 | 29 | 21 | 24 | 4 |
| Ba | 257 | 268 | 293 | 233 | 200 | 176 | 251 | 240 | 40 | 85 | 33 | 174 | 39 | 144 | 229 | 170 | 323 | 161 | 151 | 92 |
| Sr | 171 | 198 | 162 | 193 | 107 | 52 | 203 | 155 | 56 | 252 | 325 | 358 | 163 | 454 | 238 | 263 | 328 | 314 | 299 | 83 |
| Rb | 71 | 74 | 75 | 65 | 57 | 50 | 64 | 65 | 9 | 11 | 3 | 12 | 8 | 19 | 38 | 39 | 51 | 21 | 22 | 16 |
| Pb | 16 | 14 | 7 | 9 | 5 | 4 | 9 | 9 | 4 | 6 | 5 | 6 | 9 | 7 | 6 | 13 | 4 | 6 | 7 | 3 |
| Th | 12 | 10 | 11 | 12 | 12 | 9 | 18 | 12 | 3 | 5 | 5 | 5 | 4 | 5 | 3 | 3 | 2 | 3 | 4 | 1 |
| Ni | 28 | 24 | 23 | 23 | 22 | 29 | 26 | 25 | 3 | 25 | 25 | 29 | 15 | 18 | 16 | 35 | 54 | 16 | 26 | 13 |
| Cr | 64 | 57 | 56 | 61 | 62 | 67 | 78 | 64 | 7 | 72 | 59 | 80 | 45 | 58 | 49 | 103 | 213 | 59 | 82 | 52 |
| V | 92 | 84 | 79 | 81 | 88 | 87 | 103 | 88 | 8 | 136 | 109 | 138 | 152 | 161 | 117 | 166 | 227 | 145 | 150 | 34 |
| Sc | 14 | 13 | 11 | 12 | 13 | 12 | 13 | 13 | 1 | 16 | 15 | 17 | 18 | 18 | 14 | 23 | 34 | 16 | 19 | 6 |
| La | 28 | 26 | 21 | 28 | 27 | 24 | 32 | 27 | 3 | 17 | 12 | 14 | 13 | 12 | 7 | 12 | 12 | 10 | 12 | 3 |
| Ce | 55 | 48 | 43 | 53 | 51 | 44 | 67 | 52 | 8 | 26 | 29 | 29 | 30 | 32 | 16 | 29 | 22 | 20 | 26 | 5 |
| Nd | 24 | 25 | 21 | 25 | 25 | 23 | 28 | 24 | 2 | 15 | 17 | 18 | 17 | 18 | 10 | 16 | 15 | 11 | 15 | 3 |

* Total Fe as Fe2O3

# Analyses are recalculated and normalised to 100 % anhydrous

$ Original total; LOI = Loss on ignition

Table 7.4 (continued)

| Chemical group | PSG-1 | | | | | | | PSG-1 | | PSG-2 | | | | | | | | | PSG-2 | |
|---|---|---|---|---|---|---|---|---|---|---|---|---|---|---|---|---|---|---|---|---|
| Sample no. | SD-61 | SD-82 | SD-95 | SD-97 | SD-162 | SD-193 | SD-194 | Mean | SD | P-102 | P-104 | P-107 | SD-44 | SD-86 | SD-217 | SD-218 | SD-221 | SD-225 | Mean | SD |
| *Major element ratios* | | | | | | | | | | | | | | | | | | | | |
| Fe2O3*/MgO | 7.23 | 6.52 | 6.17 | 6.54 | 7.24 | 7.64 | 7.66 | 7.00 | 0.59 | 9.45 | 9.17 | 9 81 | 9.00 | 9.73 | 8.08 | 10 82 | 11.96 | 8 31 | 9.59 | 1.21 |
| Al2O3/SiO2 | 0.18 | 0.17 | 0.15 | 0.14 | 0.17 | 0.15 | 0.16 | 0.16 | 0 01 | 0.20 | 0.21 | 0.22 | 0 24 | 0 27 | 0.20 | 0.24 | 0.30 | 0.22 | 0.23 | 0.04 |
| K2O/Na2O | 0.61 | 0.73 | 0.73 | 0.75 | 0 41 | 0 48 | 0.66 | 0.63 | 0.13 | 0.15 | 0.03 | 0.21 | 0.04 | 0 14 | 0.46 | 0.42 | 0.68 | 0.19 | 0.26 | 0.22 |
| Al2O3/(Na2O+CaO) | 1.86 | 1.39 | 1.92 | 1.47 | 2.33 | 4.70 | 1.42 | 2.16 | 1.17 | 1.28 | 1.74 | 1.33 | 1.91 | 2 01 | 2.67 | 1.59 | 1.86 | 2.29 | 1.85 | 0.44 |
| *Trace element ratios* | | | | | | | | | | | | | | | | | | | | |
| Ti | 3542.5 | 3183.1 | 2956.0 | 3053.2 | 3490.9 | 3572.1 | 4147.7 | 3420.77 | 403.88 | 4691.2 | 4398.7 | 5005.5 | 5066.7 | 5218 4 | 3342.2 | 4195 9 | 4586.7 | 3904.1 | 4489.9 | 605.6 |
| Ti/Zr | 20.6 | 19.6 | 17.9 | 18.4 | 16.5 | 20.3 | 14.3 | 18.23 | 2.26 | 31.9 | 26.3 | 32.3 | 35.2 | 34.1 | 31.8 | 39.2 | 53.3 | 33.7 | 35.3 | 7.6 |
| Ti/V | 38.5 | 37.9 | 37.4 | 37.7 | 39.7 | 41.1 | 40.3 | 38.93 | 1.41 | 34.5 | 40.4 | 36.3 | 33.3 | 32.4 | 28.6 | 25.3 | 20.2 | 26.9 | 30.9 | 6.2 |
| Nb/Y | 0.4 | 0.3 | 0.4 | 0.4 | 0.3 | 0.4 | 0.3 | 0.36 | 0.04 | 0.2 | 0.2 | 0.2 | 0.2 | 0.2 | 0.2 | 0.1 | 0.1 | 0.1 | 0.2 | 0 0 |
| Zr/Nb | 17.7 | 19.5 | 20.6 | 21.3 | 23.0 | 20.2 | 28.7 | 21.59 | 3.53 | 30.6 | 30.4 | 29.8 | 32.0 | 31.9 | 36.2 | 35.7 | 39.1 | 40.0 | 34.0 | 3.9 |
| Zr/Y | 7.9 | 6 6 | 7.5 | 7.5 | 7.5 | 8.1 | 9.2 | 7.76 | 0.78 | 6.4 | 6.8 | 6 6 | 5.4 | 5.5 | 5.9 | 3.9 | 3.0 | 5.7 | 5.5 | 1.2 |
| Zr/Th | 13.9 | 15 5 | 15.3 | 14.0 | 17.2 | 20.2 | 15.8 | 15.99 | 2.17 | 27.0 | 34.4 | 33.3 | 35.1 | 31.5 | 35 0 | 38.2 | 39.1 | 36.3 | 34.4 | 3.6 |
| La/Y | 1.3 | 1.1 | 1.0 | 1.2 | 1.0 | 1.1 | 1.0 | 1.09 | 0.13 | 0.7 | 0.5 | 0.6 | 0.5 | 0.4 | 0.4 | 0.5 | 0.4 | 0.5 | 0.5 | 0.1 |
| La/Th | 2.3 | 2.5 | 1.9 | 2.3 | 2.2 | 2.8 | 1.7 | 2.25 | 0.34 | 3.0 | 2.5 | 3.0 | 3.1 | 2.5 | 2.4 | 4.4 | 5.5 | 3.0 | 3.3 | 1.0 |
| La/Sc | 2.0 | 2.0 | 1.9 | 2.3 | 2.1 | 2.0 | 2.5 | 2.11 | 0.20 | 1.0 | 0.8 | 0.8 | 0.7 | 0.7 | 0.5 | 0.5 | 0.4 | 0.6 | 0.7 | 0.2 |
| Th/Sc | 0.9 | 0.8 | 1.0 | 1.0 | 1.0 | 0.7 | 1.4 | 0.96 | 0.22 | 0.3 | 0.3 | 0.3 | 0.2 | 0.3 | 0.2 | 0.1 | 0.1 | 0.2 | 0.2 | 0.1 |
| Ce/V | 0.6 | 0.6 | 0.5 | 0.7 | 0.6 | 0.5 | 0.6 | 0.59 | 0 05 | 0.2 | 0.3 | 0.2 | 0.2 | 0.2 | 0.1 | 0 2 | 0.1 | 0.1 | 0.2 | 0.1 |

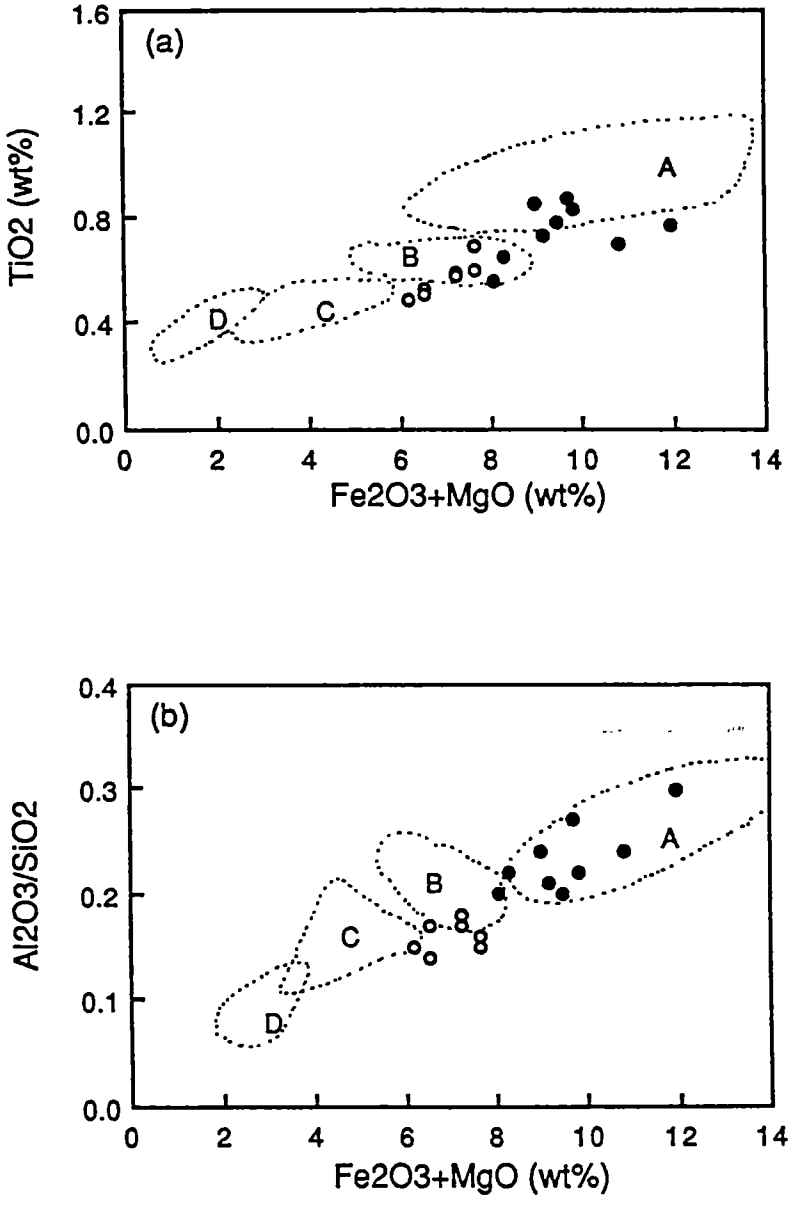


Figure 7.4 Discrimination plots: (a) $TiO_2$ versus $Fe_2O_3$*+MgO and (b) $Al_2O_3/SiO_2$ versus $Fe_2O_3$*+MgO for the Pha Som M.C. psammites. Fields: A = oceanic-island arc, B = continental island arc, C = active continental margin and D = passive margin (after Bhatia, 1983).

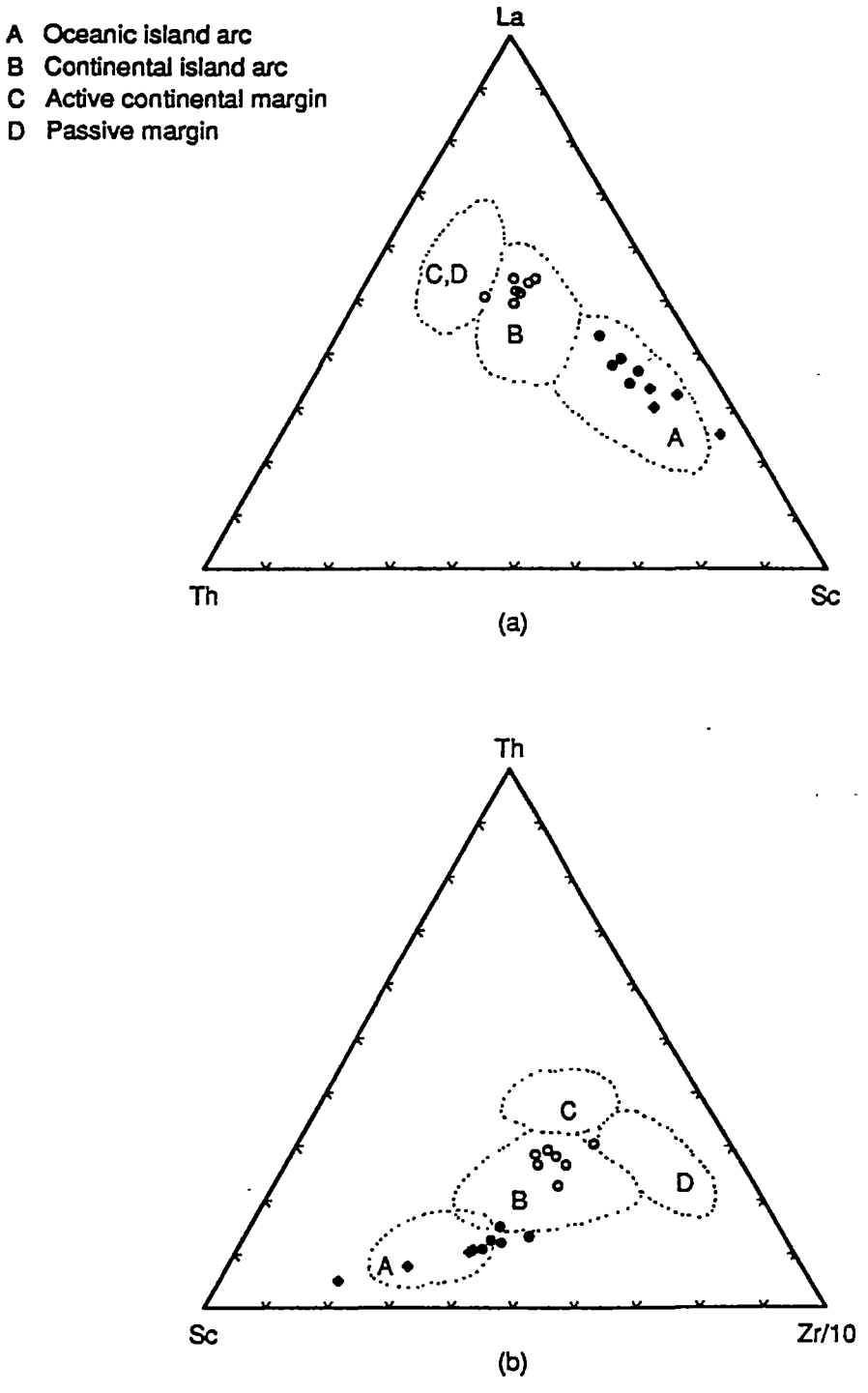


Figure 7.5 Discrimination plots: (a) La-Th-Sc and (b) Th-Sc-Zr/10 for the Pha Som M.C. psammites. Fields: A = oceanic-island arc, B = continental island arc, C = active continental margin and D = passive margin (after Bhatia and Crook, 1986).

La versus Th (Fig. 7.6), they almost exclusively fall within continental island arc setting of Bhatia and Crook (1986).

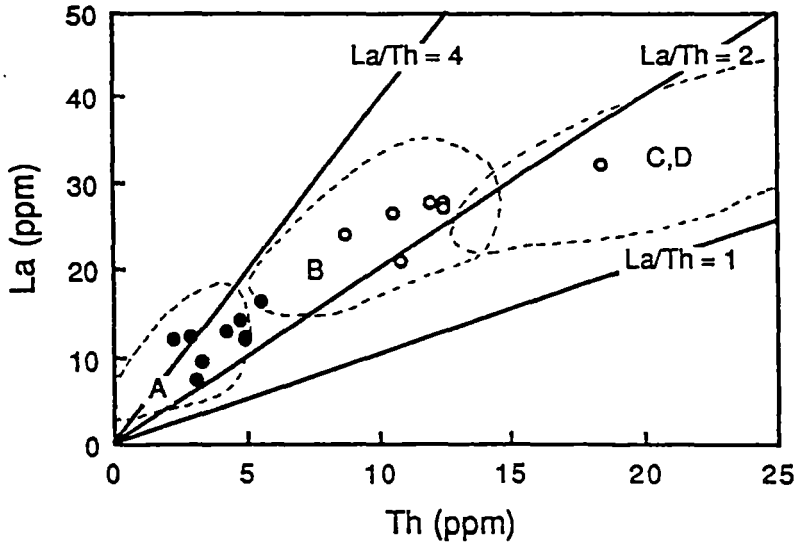


Figure 7.6 La-Th plot for the Pha Som psammites. Fields: A = oceanic-island arc, B = continental island arc, C = active continental margin and D = passive margin (after Bhatia and Crook, 1986).

On the Ti/Zr-La/Sc and Y/Nb-Th/Sc diagrams (Figs. 7.7a&b) of Roser and Cooper (1990), they plot within the fields for the Permian-Cretaceous Torlesse terrane in New Zealand which is dominated by quartzofeldspathic sediments considered to have been derived from an active continental magmatic arc and deposited in a trench or submarine fan setting at the subduction margin (MacKinnon, 1983; Roser and Korsch, 1988). The Ce/V-La/Y plot (Fig. 7.7c) of Mortimer and Roser (1992) also indicate the similarity between PSG-1 samples and those of the Torlesse terrane.

From the major element characteristics of the PSG-1 samples, a continental island arc or quartzose recycled terrain cannot be distinguished using the Roser and Korsch's diagram (Fig. 7.3). This is probably due to either the effect of metamorphism on some of the major elements (particularly Na, K, Ca and Si) or the limitation of this diagram. However, this limitation is not possible to assess in the present study. The Bhatia's diagrams (Figs. 7.4a&b), in contrast, clearly delineate the continental arc source of the PSG-1 psammites.

The immobile trace element characteristics (Figs. 7.5a&b and 7.6) clearly point to the continental island arc source for the PSG-1 psammites. The similarity in terms of trace element geochemistry between the PSG-1 samples and those of the

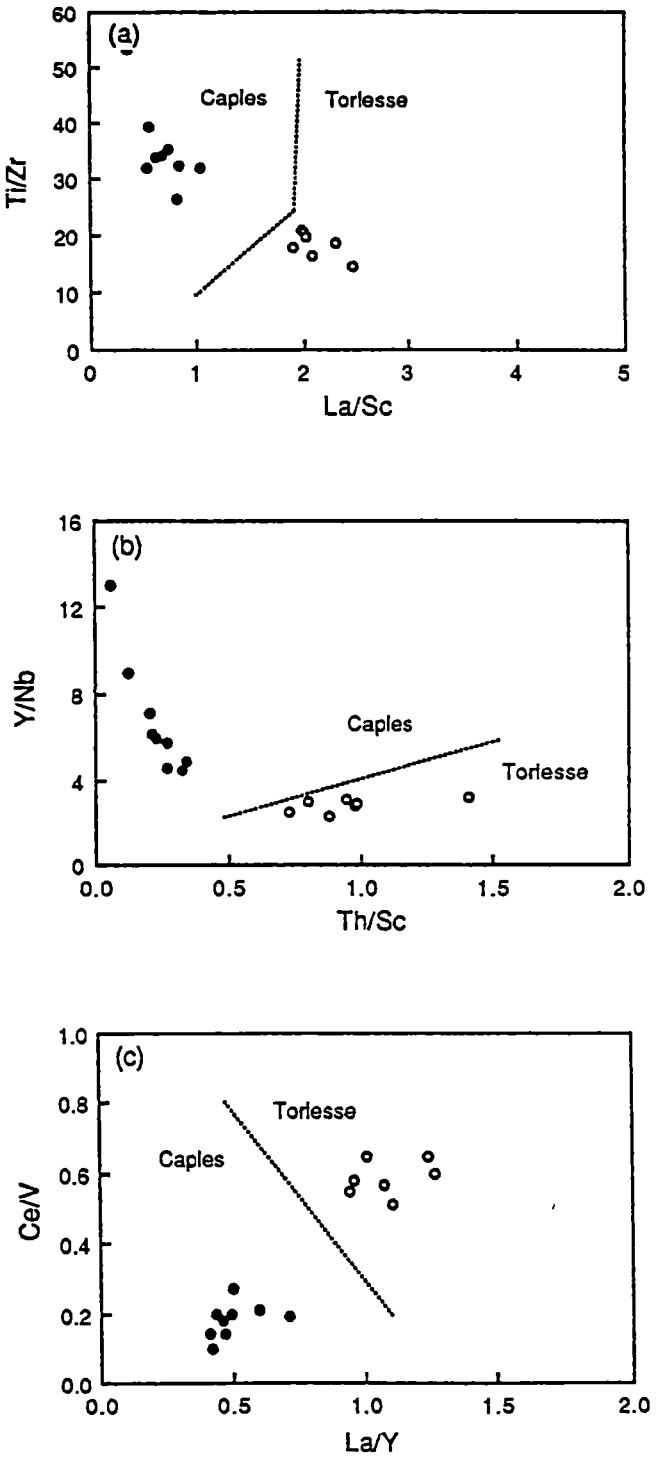


Figure 7.7 Plots: (a) Ti/Zr versus La/Sc, (b) Y/Nb versus Th/Sc, and (c) Ce/V versus La/Y for the Pha Som M.C. psammites. The lines separating the compositional fields of the Torlesse and Caples terrane rocks in New Zealand are after Roser and Cooper (1990) and Mortimer and Roser (1992).

Torlesse terrane in New Zealand strongly supports that PSG-1 samples represent sediments which were derived from an active continental magmatic arc as do the Torlesse sediments (MacKinnon, 1983). It is probable, despite the circumstantial nature of evidence, that these two suites were deposited in a similar setting, i.e. a trench or submarine fan setting at the subduction margin. In addition, the geochemical characteristics of the greywackes and metagreywackes of the PSG-1 group lend support to the interpretation that the quartz-rich greywackes (section 7.3.1) were probably deposited in a slope basin formed on top of and later incorporated into the accretionary complex by later deformation processes.

## PSG-2

The PSG-2 psammites include one greywacke (SD-225), three semischists (P-102, P-104 and P-107) and five fine-grained schists (SD-44, SD-86, SD-217, SD-218 and SD-221).

**Major elements:** PSG-2 samples are characterised by relatively high average concentrations of $TiO_2$ (0.75±0.1 wt%), $Al_2O_3$ (15.11±1.54 wt%), $Fe_2O_3$ (6.64±0.74 wt%) as shown in Table 7.4 and Table 7.6. They plot within the intermediate igneous rock provenance (P2) and overlap into the mafic igneous rock provenance (P1) on the discrimination diagram of Roser and Korsch (1988) shown in Figure 7.3. This suggests the provenance transitional between intermediate and mafic island arc. On the $TiO_2$ versus $Fe_2O_3$*+MgO and $Al_2O_3/SiO_2$ versus $Fe_2O_3$*+MgO plots of Bhatia (1983), they all fall within the fields for oceanic island arc (Figs. 7.4a &b).

**Trace elements:** PSG-2 psammites are characterised by relatively high average concentrations of V (131±28 ppm) and the ratios Zr/Th (34.4±3.6) and relatively low abundances of Pb (7±3 ppm), Th (4±1 ppm), LREE such as, La (12±3 ppm), Ce (26±5 ppm) and Nd (15±3 ppm) and the ratios Th/Sc (0.2±0.1) and Ce/V (0.2±0.1) as shown in Table 7.4 and Table 7.6.

Absolute abundances and ratios of relatively immobile trace elements between PSG-2 samples and greywackes from various tectonic settings from eastern Australia (Bhatia and Crook, 1986) are compared in Table 7.6. This group of metagreywackes have similar values as those of greywackes from the oceanic island arc setting, i.e. a sedimentary basin adjacent to an oceanic island arc (e.g. Marianas) or an island arc partly formed on thin continental crust (e.g. Aleutians) where sediments are mainly derived from subalkaline volcanics (Bhatia, 1983;

Bhatia and Crook, 1986). On the ternary plots La-Th-Sc (Fig. 7.5a) of Bhatia and Crook (1986), they plot within the oceanic island arc field but plot near the boundary between the oceanic island arc and continental island arc fields on the ternary plot Th-Sc-Zr/10 (Fig. 7.5b). On the binary plot, La versus Th (Fig. 7.6), they all plot within the oceanic island arc setting. On the Ti/Zr-La/Sc and Y/Nb-Th/Sc diagrams (Figs. 7.7a&b) of Roser and Cooper (1990), they plot within the fields for the Caples terrane in New Zealand which is dominated by volcanogenic sediments. The Ce/V-La/Y plot (Fig. 7.7c) of Mortimer and Roser (1992) also indicate the similarity between PSG-2 samples with those of the Caples terrane.

From their major and trace element characteristics, all discrimination plots show that the PSG-2 psammites represent sediments derived from the oceanic-island arc rocks. As with the PSG-1 samples, an intermediate or mafic igneous provenance of the PSG-2 samples cannot be distinguished using the Roser and Korsch's diagram (Fig. 7.3). This limitation render uncertainty in the general applicability of the diagram. The similarity between the PSG-2 metagreywackes and those of the Caples terrane in New Zealand lends strong support to the volcanic arc source for the PSG-2 psammites. The geochemical characteristics of sample SD-225 (a representative of quartz-poor greywackes in section 7.3.1) and equivalent metagreywackes of PSG-2 group suggest that the quartz-poor greywackes possibly represent the sediments of a slope basin formed on top of and later incorporated into the accretionary complex by later deformation processes. Alternatively, they may be sediments in the forearc basins deposited on top of and later incorporated into the accretionary complex in a similar manner as that of the slope-basin sediments.

## 7.4.2 Nam Pat Group sandstones

The Nam Pat Group sandstones includes three from the Huai Lat Formation (SD-137, SD-140 and SD-181) and eleven from the Huai Bo Khong Formation (SD-12, SD-15, SD-18, SD-21, SD-24, SD-33, SD-36, SD-37, SD-39 and SD-66) as shown in Figure 7.1.

**Major elements:** This group of sandstones is characterised by relatively high average concentrations of $TiO_2$ (0.78±0.13 wt%), $Al_2O_3$ (14.84±1.25 wt%), $Fe_2O_3$ (6.30±0.96 wt%) as shown in Table 7.5 and Table 7.6. The majority of them plot within the P2 field (intermediate igneous rock provenance) with slight overlap into the P3 field (felsic igneous rock provenance) on the discrimination diagram of Roser and Korsch (1988) shown in Figure 7.8.

Table 7.5 Whole-rock XRF analyses of the Nam Pat Group sandstones.

| Rock units | Huai Bo Khong Formation | | | | | | | | | | | Huai Lat Formation | | | Mean | SD |
|---|---|---|---|---|---|---|---|---|---|---|---|---|---|---|---|---|
| Sample no. | SD-12 | SD-15 | SD-18 | SD-21 | SD-24 | SD-28 | SD-33 | SD-36 | SD-37 | SD-39 | SD-66 | SD-137 | SD-140 | SD-181 | | |
| *Major elements (wt %)* | | | | | | | | | | | | | | | | |
| SiO2 | 64.02 | 67.60 | 68.58 | 73.17 | 69.37 | 67.83 | 66.14 | 63.83 | 68.66 | 68.55 | 63.87 | 70.12 | 70.03 | 73.39 | 68.23 | 3.05 |
| TiO2 | 0.86 | 0.76 | 0.65 | 0.70 | 0.64 | 0.94 | 0.72 | 0.95 | 0.72 | 0.71 | 1.05 | 0.84 | 0.75 | 0.65 | 0.78 | 0.13 |
| Al2O3 | 16.26 | 15.46 | 15.28 | 12.96 | 14.34 | 15.10 | 15.78 | 16.93 | 14.61 | 14.66 | 16.18 | 13.76 | 13.59 | 12.84 | 14.84 | 1.25 |
| Fe2O3* | 7.34 | 6.51 | 6.52 | 4.53 | 5.78 | 6.29 | 6.81 | 8.03 | 6.43 | 6.47 | 7.18 | 5.75 | 5.94 | 4.57 | 6.30 | 0.96 |
| MnO | 0.09 | 0.07 | 0.06 | 0.07 | 0.11 | 0.08 | 0.08 | 0.10 | 0.08 | 0.08 | 0.09 | 0.07 | 0.08 | 0.06 | 0.08 | 0.01 |
| MgO | 2.19 | 1.93 | 1.94 | 1.37 | 1.73 | 2.33 | 2.17 | 2.50 | 1.86 | 1.88 | 2.77 | 2.05 | 1.94 | 1.39 | 2.00 | 0.38 |
| CaO | 3.16 | 2.57 | 1.95 | 2.32 | 3.07 | 1.18 | 2.93 | 2.34 | 2.33 | 2.31 | 3.07 | 2.29 | 2.51 | 1.88 | 2.42 | 0.54 |
| Na2O | 4.88 | 3.67 | 3.66 | 3.87 | 3.55 | 4.19 | 4.17 | 3.68 | 4.36 | 4.39 | 4.63 | 3.37 | 3.23 | 3.34 | 3.93 | 0.51 |
| K2O | 0.93 | 1.24 | 1.24 | 0.91 | 1.30 | 1.94 | 1.04 | 1.45 | 0.78 | 0.76 | 0.89 | 1.58 | 1.79 | 1.75 | 1.26 | 0.39 |
| P2O5 | 0.25 | 0.20 | 0.12 | 0.10 | 0.12 | 0.12 | 0.14 | 0.19 | 0.18 | 0.18 | 0.26 | 0.17 | 0.13 | 0.12 | 0.16 | 0.05 |
| Total# | 100.00 | 100.00 | 100.00 | 100.00 | 100.00 | 100.00 | 100.00 | 100.00 | 100.00 | 100.00 | 100.00 | 100.00 | 100.00 | 100.00 | | |
| Total$ | 100.07 | 99.71 | 100.12 | 100.26 | 99.81 | 99.21 | 100.32 | 99.54 | 99.76 | 99.66 | 99.71 | 99.52 | 99.90 | 99.85 | | |
| LOI | 4.76 | 4.41 | 4.94 | 3.79 | 4.89 | 3.17 | 5.07 | 5.19 | 3.82 | 2.75 | 3.56 | 2.86 | 3.03 | 2.28 | | |
| *Trace elements (ppm)* | | | | | | | | | | | | | | | | |
| Nb | 5 | 6 | 6 | 6 | 6 | 6 | 5 | 7 | 5 | 6 | 6 | 6 | 5 | 6 | 6 | 0 |
| Zr | 156 | 152 | 180 | 161 | 178 | 170 | 151 | 169 | 146 | 168 | 187 | 163 | 146 | 151 | 163 | 13 |
| Y | 32 | 32 | 27 | 22 | 27 | 25 | 26 | 32 | 28 | 29 | 31 | 29 | 27 | 28 | 28 | 3 |
| Ba | 196 | 207 | 171 | 162 | 161 | 362 | 158 | 207 | 126 | 362 | 266 | 308 | 344 | 313 | 239 | 84 |
| Sr | 301 | 249 | 227 | 208 | 201 | 370 | 238 | 216 | 261 | 357 | 426 | 325 | 223 | 231 | 274 | 70 |
| Rb | 29 | 40 | 44 | 32 | 43 | 60 | 33 | 48 | 26 | 60 | 24 | 42 | 48 | 49 | 41 | 11 |
| Pb | 9 | 12 | 13 | 10 | 10 | 61 | 9 | 10 | 9 | 10 | 8 | 5 | 7 | 9 | 13 | 14 |
| Th | 4 | 6 | 6 | 6 | 6 | 5 | 4 | 6 | 5 | 6 | 6 | 6 | 5 | 5 | 5 | 1 |
| Ni | 14 | 17 | 17 | 10 | 13 | 16 | 14 | 19 | 11 | 11 | 15 | 23 | 11 | 15 | 15 | 4 |
| Cr | 34 | 40 | 34 | 31 | 27 | 47 | 31 | 40 | 28 | 26 | 41 | 55 | 40 | 27 | 36 | 8 |
| V | 130 | 121 | 99 | 101 | 86 | 124 | 111 | 133 | 101 | 103 | 162 | 119 | 126 | 94 | 115 | 20 |
| Sc | 20 | 19 | 16 | 15 | 15 | 19 | 19 | 22 | 17 | 15 | 21 | 18 | 15 | 12 | 17 | 3 |
| La | 14 | 18 | 15 | 16 | 32 | 15 | 14 | 15 | 13 | 15 | 18 | 12 | 12 | 16 | 16 | 5 |
| Ce | 34 | 39 | 27 | 34 | 64 | 35 | 28 | 34 | 33 | 30 | 38 | 34 | 31 | 31 | 35 | 9 |
| Nd | 20 | 22 | 15 | 18 | 32 | 18 | 17 | 21 | 19 | 18 | 21 | 19 | 16 | 17 | 19 | 4 |

* Total Fe as Fe2O3

\# Analyses are recalculated and normalised to 100 % anhydrous

$ Original total; LOI = Loss on ignition

Table 7.5 (continued)

| Rock units | Huai Bo Khong Formation | | | | | | | | | | | Huai Lat Formation | | | Mean | SD |
|---|---|---|---|---|---|---|---|---|---|---|---|---|---|---|---|---|
| Sample no. | SD-12 | SD-15 | SD-18 | SD-21 | SD-24 | SD-28 | SD-33 | SD-36 | SD-37 | SD-39 | SD-66 | SD-137 | SD-140 | SD-181 | | |
| *Major element ratios* | | | | | | | | | | | | | | | | |
| Fe2O3*/MgO | 9.54 | 8.44 | 8.47 | 5.90 | 7.51 | 8.62 | 8.99 | 10.54 | 8.29 | 8.35 | 9.94 | 7.80 | 7.88 | 5.96 | 8.30 | 1.30 |
| Al2O3/SiO2 | 0.25 | 0.23 | 0.22 | 0.18 | 0.21 | 0.22 | 0.24 | 0.27 | 0.21 | 0.21 | 0.25 | 0.20 | 0.19 | 0.17 | 0.22 | 0.03 |
| K2O/Na2O | 0.19 | 0.34 | 0.34 | 0.24 | 0.36 | 0.46 | 0.25 | 0.39 | 0.18 | 0.17 | 0.19 | 0.47 | 0.55 | 0.52 | 0.33 | 0.13 |
| Al2O3/(Na2O+CaO) | 2.02 | 2.48 | 2.72 | 2.09 | 2.17 | 2.82 | 2.22 | 2.81 | 2.18 | 2.19 | 2.10 | 2.43 | 2.37 | 2.46 | 2.36 | 0.27 |
| *Trace element ratios* | | | | | | | | | | | | | | | | |
| Ti | 5157.8 | 4529.3 | 3905.1 | 4225.8 | 3852.7 | 5618.0 | 4342.8 | 5718.6 | 4311.6 | 4268.4 | 6297.4 | 5023.7 | 4517.8 | 3870.9 | 4688.6 | 761.3 |
| Ti/Zr | 33.1 | 29.8 | 21.7 | 26.2 | 21.6 | 33.0 | 28.8 | 33.8 | 29.5 | 25.4 | 33.7 | 30.8 | 30.9 | 25.6 | 28.9 | 4.2 |
| Ti/V | 39.7 | 37.4 | 39.4 | 41.8 | 44.8 | 45.3 | 39.1 | 43.0 | 42.7 | 41.4 | 38.9 | 42.2 | 35.9 | 41.2 | 40.9 | 2.7 |
| Nb/Y | 0.2 | 0.2 | 0.2 | 0.3 | 0.2 | 0.3 | 0.2 | 0.2 | 0.2 | 0.2 | 0.2 | 0.2 | 0.2 | 0.2 | 0.2 | 0.0 |
| Zr/Nb | 29.4 | 25.8 | 29.0 | 26.4 | 28.7 | 26.6 | 29.6 | 26.0 | 27.5 | 27.1 | 29.2 | 26.7 | 28.1 | 27.0 | 27.7 | 1.3 |
| Zr/Y | 4.9 | 4.8 | 6.7 | 7.2 | 6.6 | 6.9 | 5.8 | 5.4 | 5.3 | 5.8 | 6.1 | 5.7 | 5.4 | 5.4 | 5.8 | 0.7 |
| Zr/Th | 39.5 | 27.6 | 30.8 | 28.2 | 28.7 | 31.2 | 36.4 | 30.2 | 26.8 | 27.5 | 33.4 | 27.9 | 27.5 | 31.5 | 30.5 | 3.7 |
| La/Y | 0.5 | 0.6 | 0.5 | 0.7 | 1.2 | 0.6 | 0.5 | 0.5 | 0.5 | 0.5 | 0.6 | 0.4 | 0.4 | 0.6 | 0.6 | 0.2 |
| La/Th | 3.6 | 3.3 | 2.5 | 2.8 | 5.1 | 2.8 | 3.3 | 2.7 | 2.4 | 2.5 | 3.2 | 2.1 | 2.2 | 3.4 | 3.0 | 0.8 |
| La/Sc | 0.7 | 0.9 | 0.9 | 1.1 | 2.1 | 0.8 | 0.7 | 0.7 | 0.8 | 1.0 | 0.9 | 0.7 | 0.8 | 1.3 | 1.0 | 0.4 |
| Th/Sc | 0.2 | 0.3 | 0.4 | 0.4 | 0.4 | 0.3 | 0.2 | 0.3 | 0.3 | 0.4 | 0.3 | 0.3 | 0.4 | 0.4 | 0.3 | 0.1 |
| Cc/V | 0.3 | 0.3 | 0.3 | 0.3 | 0.7 | 0.3 | 0.3 | 0.3 | 0.3 | 0.3 | 0.2 | 0.3 | 0.2 | 0.3 | 0.3 | 0.1 |

Table 7.6 Trace element characteristics of sandstones and metagreywackes from the Sirikit Dam area and greywackes from various tectonic settings in eastern Australia (after Bhatia and Crook, 1986).

| Geochemical group | PSG-1 (n=7) | | PSG-2 (n = 9) | | Nam Pat Group (n = 14) | | Oceanic island arc | | Continental island arc | | Active continental margin | | Passive margin | |
|---|---|---|---|---|---|---|---|---|---|---|---|---|---|---|
| | Mean | SD | Mean | SD | Mean | SD | Mean | SD | Mean | SD | Mean | SD | Mean | SD |
| *Trace elements (ppm)* | | | | | | | | | | | | | | |
| Ti | 3421 | 404 | 4490 | 606 | 4689 | 761 | 4800 | 1200 | 3900 | 600 | 2600 | 200 | 2200 | 600 |
| Nb | 9 | 1 | 4 | 1 | 6 | 0 | 2 | 0 | 9 | 1 | 11 | 1 | 8 | 2 |
| Zr | 192 | 46 | 131 | 28 | 163 | 13 | 96 | 20 | 229 | 27 | 179 | 33 | 298 | 80 |
| Y | 25 | 4 | 24 | 4 | 28 | 3 | 20 | 6 | 24 | 2 | 25 | 4 | 27 | 5 |
| Pb | 9 | 4 | 7 | 3 | 9 | 2 | 7 | 1 | 15 | 1 | 24 | 1 | 16 | 3 |
| Th | 12 | 3 | 4 | 1 | 5 | 1 | 2 | 1 | 11 | 1 | 19 | 3 | 17 | 4 |
| Ni | 25 | 3 | 26 | 13 | 15 | 4 | 11 | 5 | 13 | 2 | 10 | 3 | 8 | 4 |
| Cr | 64 | 7 | 82 | 52 | 36 | 8 | 37 | 13 | 51 | 7 | 26 | 5 | 39 | 9 |
| V | 88 | 8 | 150 | 34 | 11 | 15 | 131 | 40 | 89 | 14 | 48 | 6 | 31 | 10 |
| Sc | 13 | 1 | 19 | 6 | 17 | 3 | 20 | 5 | 15 | 2 | 8 | 1 | 6 | 1 |
| La | 27 | 3 | 12 | 3 | 15 | 2 | 9 | 3 | 24 | 2 | 33 | 5 | 34 | 6 |
| Ce | 52 | 8 | 26 | 5 | 33 | 4 | 23 | 6 | 51 | 4 | 73 | 10 | 72 | 12 |
| Nd | 24 | 2 | 15 | 3 | 19 | 4 | 11 | 3 | 21 | 2 | 25 | 3 | 29 | 5 |
| *Trace element ratios* | | | | | | | | | | | | | | |
| Ti/Zr | 18.2 | 2.3 | 35.3 | 7.6 | 28.9 | 4.2 | 56.8 | 21.4 | 19.7 | 4.3 | 15.3 | 2.4 | 6.7 | 0.9 |
| Ti/V | 38.9 | 1.4 | 30.9 | 6.2 | 40.9 | 2.7 | | | | | | | | |
| Nb/Y | 0.4 | 0.0 | 0.2 | 0.0 | 0.2 | 0.0 | 0.1 | 0.0 | 0.4 | 0.0 | 0.4 | 0.0 | 0.3 | 0.1 |
| Zr/Nb | 21.6 | 3.5 | 34.0 | 3.9 | 27.7 | 1.3 | 49.3 | 10.2 | 31.5 | 9.9 | 16.7 | 1.8 | 37.2 | 8.0 |
| Zr/Y | 7.8 | 0.8 | 5.5 | 1.2 | 5.8 | 0.7 | 5.7 | 1.9 | 9.6 | 0.8 | 7.2 | 0.4 | 12.4 | 4.0 |
| Zr/Th | 16.0 | 2.2 | 34.4 | 3.6 | 30.5 | 3.7 | 48.0 | 13.4 | 21.5 | 2.4 | 9.5 | 0.7 | 19.1 | 5.8 |
| La/Y | 1.1 | 0.1 | 0.5 | 0.1 | 0.5 | 0.1 | 0.5 | 0.1 | 1.0 | 0.1 | 1.3 | 0.1 | 1.3 | 0.3 |
| La/Th | 2.3 | 0.3 | 3.3 | 1.0 | 2.8 | 0.5 | 4.3 | 1.2 | 2.4 | 0.3 | 1.8 | 0.1 | 2.2 | 0.5 |
| La/Sc | 2.1 | 0.2 | 0.7 | 0.2 | 0.9 | 0.2 | 0.6 | 0.2 | 1.8 | 0.3 | 4.6 | 0.8 | 6.3 | 1.4 |
| Th/Sc | 1.0 | 0.2 | 0.2 | 0.1 | 0.3 | 0.1 | 0.2 | 0.1 | 0.9 | 0.1 | 2.6 | 0.5 | 3.1 | 0.8 |
| Cc/V | 0.6 | 0.1 | 0.2 | 0.1 | 0.3 | 0.0 | | | | | | | | |

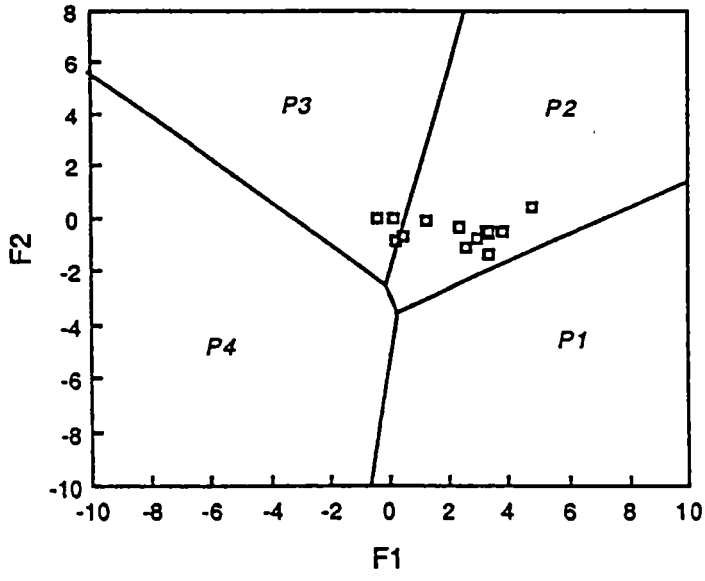


Figure 7.8 Major element discrimination plot for the Nam Pat Group sandstones. Discrimination functions (F1&F2) and provenance fields (P1, P2, P3, P4) are after Roser and Korsch (1988). Sample scores are calculated from anhydrous normalised data in Table 7.5, using the same equations as Figure 7.3.

On the $TiO_2$ versus $Fe_2O_3$*+MgO and $Al_2O_3/SiO_2$ versus $Fe_2O_3$*+MgO diagrams of Bhatia (1983), they plot both within the fields for oceanic island arc and continental island arc (Figs. 7.9a&b).

**Trace elements:** The Nam Pat sandstones are characterised by relatively high average concentrations of V (111±15 ppm) and the ratios Zr/Th (30.5±3.7) and relatively low abundances of Th (5±1 ppm) and the ratios Th/Sc (0.3±0.1) and Ce/V (0.3±0.1) as shown in Table 7.5 and Table 7.6.

Absolute abundances and ratios of relatively immobile trace elements of the Nam Pat sandstones and greywackes from various tectonic settings from eastern Australia (Bhatia and Crook, 1986) are shown in Table 7.6. Nam Pat sandstones have similar values to those of greywackes from the oceanic island arc setting (Bhatia, 1983; Bhatia and Crook, 1986). On the ternary plot, La-Th-Sc (Fig. 7.10a) they plot in the oceanic island arc field but on the Th-Sc-Zr/10 diagram (Fig. 7.10b) of Bhatia and Crook (1986), they both plot within oceanic island arc and continental island arc fields. On the binary plot La versus Th (Fig. 7.11), their compositions also overlap between the oceanic island arc and continental island arc settings of Bhatia and Crook (1986).

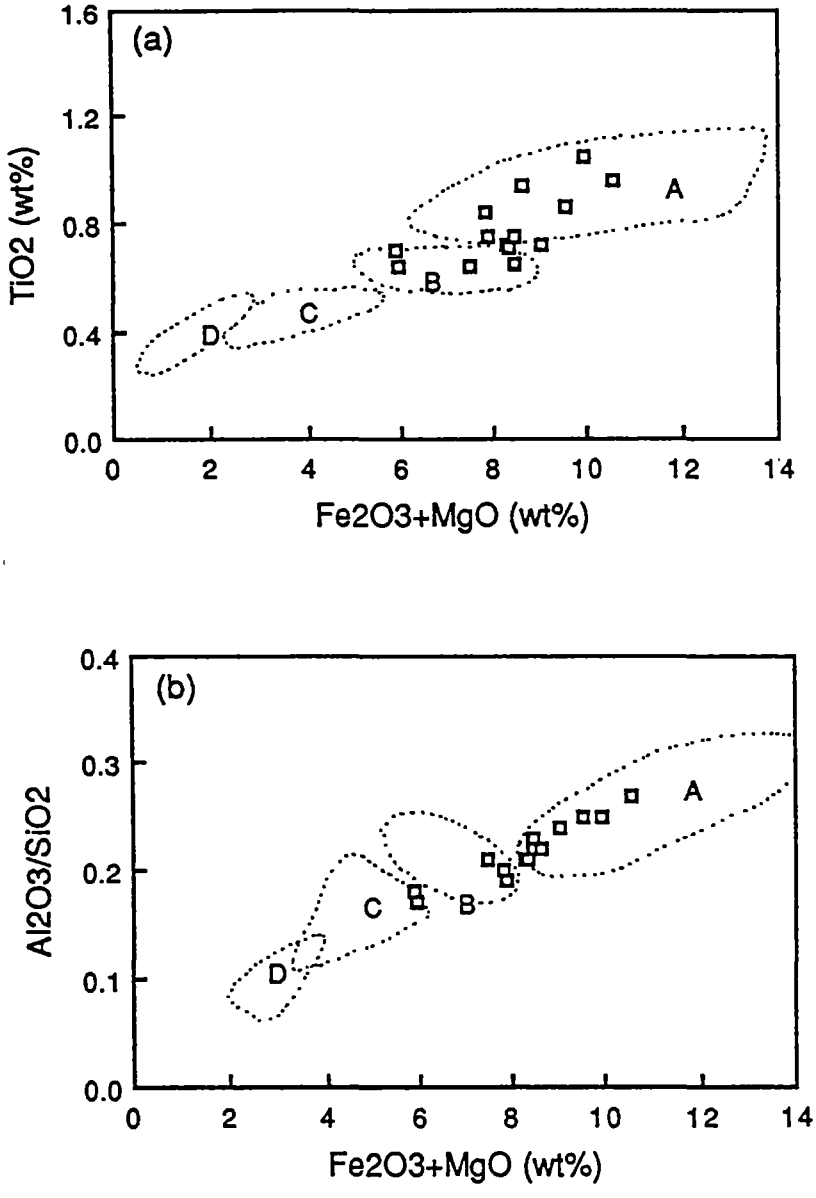


Figure 7.9 Discrimination plots: (a) $TiO_2$ versus $Fe_2O_3$*+MgO and (b) $Al_2O_3/SiO_2$ versus $Fe_2O_3$*+MgO for the Nam Pat Group sandstones. Fields: A = oceanic-island arc, B = continental island arc, C = active continental margin and D = passive margin (after Bhatia, 1983).

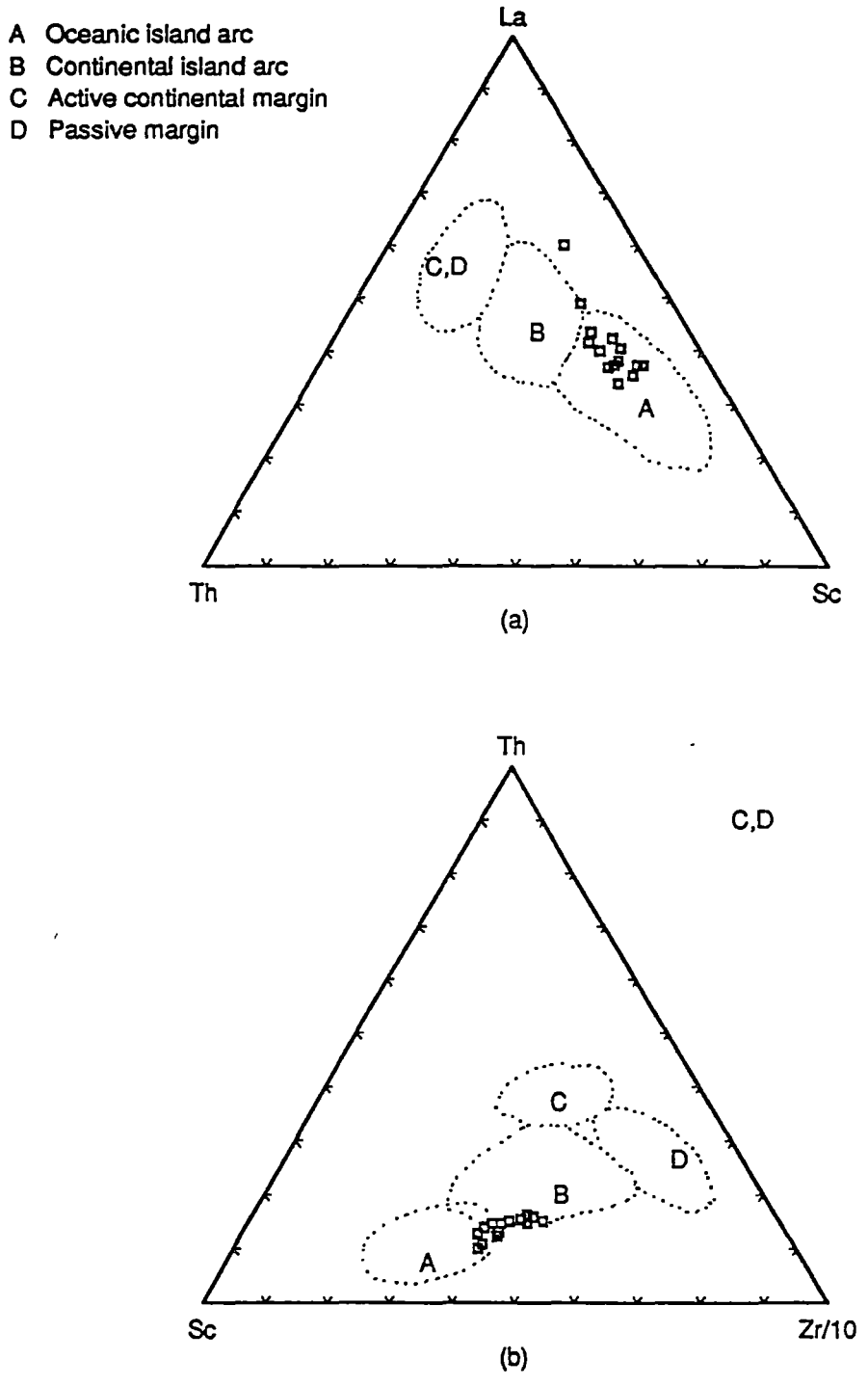


Figure 7.10 Discrimination plots: (a) La-Th-Sc and (b) Th-Sc-Zr/10 for the Nam Pat Group sandstones. Fields: A = oceanic-island arc, B = continental island arc, C = active continental margin and D = passive margin (after Bhatia and Crook, 1986).

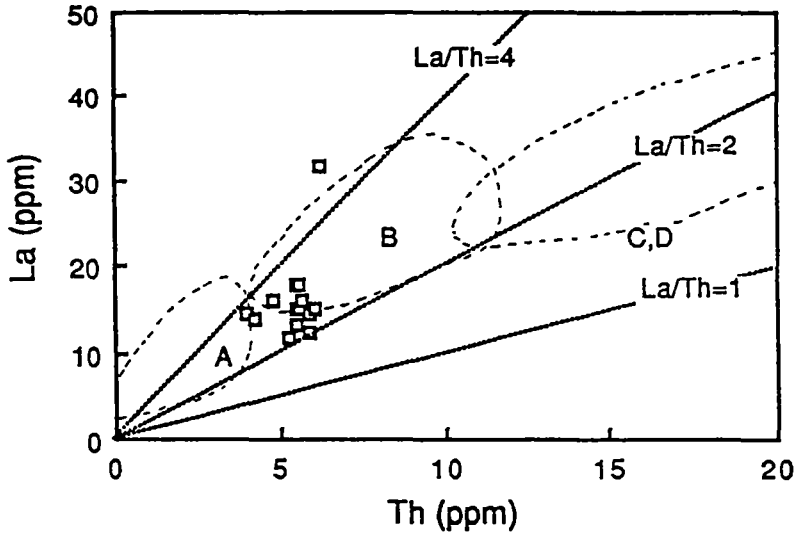


Figure 7.11 La-Th plot for the Nam Pat Group sandstones. Fields: A = oceanic-island arc, B = continental island arc, C = active continental margin and D = passive margin (after Bhatia and Crook, 1986).

On the Ti/Zr-La/Sc and Y/Nb-Th/Sc diagrams (Figs. 7.12a&b) of Roser and Cooper (1990) as well as on the Ce/V-La/Y plot (Fig. 7.12c) of Mortimer and Roser (1992), they plot well within the fields for the Caples terrane in New Zealand.

From the major and trace element characteristics of the Nam Pat Group samples, the volcanic source was an oceanic island arc or a continental island arc setting. The compositional similarities between the Nam Pat Group samples and the Caples terrane in New Zealand, however lend strong support for the oceanic arc source for the Nam Pat sandstones.

On the basis of other geological data, an oceanic arc source for the Nam Pat Group seems unlikely. The Pak Pat volcanics are a likely source and have an oceanic arc signature but they are correlated with continental arc volcanics 20 km to the west and are deposited unconformably on an accretionary complex (c.f. Java) which is not typical of oceanic arcs. A much larger database for sandstones from a range of tectonic environments is needed to test the discriminant diagrams before they have sufficient reliability to ignore the regional geology when interpreting the geochemistry.

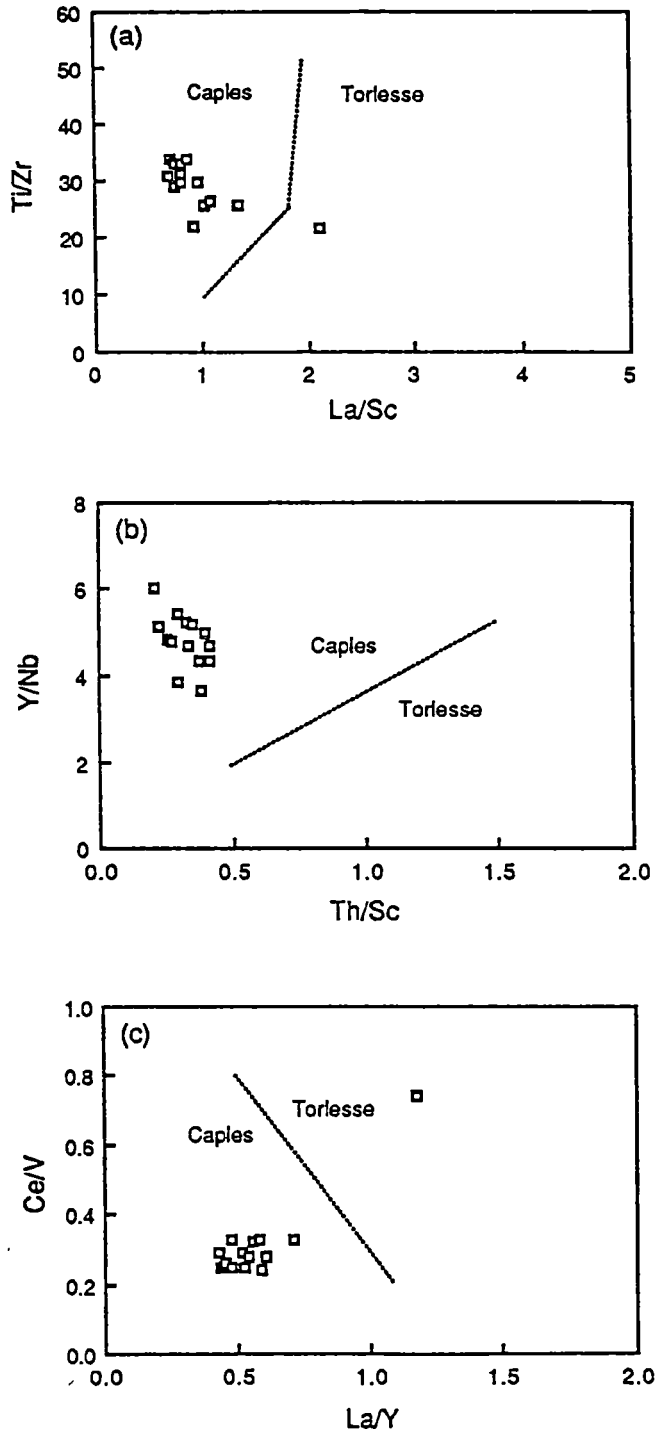


Figure 7.12 Plots: (a) Ti/Zr versus La/Sc, (b) Y/Nb versus Th/Sc, and (c) Ce/V versus La/Y for the Nam Pat Group sandstones. The lines separating the compositional fields of the Torlesse and Caples terrane rocks in New Zealand are after Roser and Cooper (1990) and Mortimer and Roser (1992).

# 7.5 Summary

## 7.5.1 Psammites of the Pha Som Metamorphic Complex

**Petrography:** Sandstone samples of the Pha Som metasediments are divided into two distinct types based on modal compositions of framework grains as follows:

(1) The quartz-rich greywackes have the average composition of $Q_{51}F_{14}L_{35}$ and $Qm_{33}F_{14}Lt_{53}$ and grain parameter ratios, Qp/Q (0.35), P/F (1.00) and Lv/L (0.27) similar to those of modern and ancient subduction complex. The compositional characteristics of the detrital framework modes suggest that the quartz-rich greywackes were derived from a subduction complex (accretionary complex) mixed with the detritus from a magmatic arc source.

(2) The quartz-poor greywackes showing strong affinity towards a volcanic source have the average composition of $Q_{30}F_{22}L_{48}$ and $Qm_{14}F_{22}Lt_{64}$ and grain parameter ratios, P/F (0.91) and Lv/L (0.91) comparable to transitional magmatic arc. The compositional characteristics of the detrital framework modes indicate that the quartz-poor greywackes were derived from a magmatic arc source.

**Geochemistry:** On the basis of major and trace element geochemistry, sandstones and metagreywackes of the Pha Som metasediments are divided into two categories as follows:

(1) PSG-1 group is characterised by relatively low average concentrations of $TiO_2$ (0.57±0.07 wt%), $Al_2O_3$ (11.64±0.70 wt%), $Fe_2O_3$ (4.75±0.47 wt%), V (88±8 ppm) and the ratios Zr/Th (16.0±2.2) and relatively high abundances of Pb (9±4 ppm), Th (12±3 ppm), LREE such as, La (27±3 ppm), Ce (52±8 ppm) and Nd (24±2 ppm) and the ratios Th/Sc (1.0±0.2) and Ce/V (0.6±0.1). The major element geochemistry of the PSG-1 samples alone cannot distinguish whether they represent sediments derived from the continental island arc or recycled provenance. However, the immobile trace element characteristics strongly suggest that they are more likely to be derived from continental island arc source. The PSG-1 samples are compositionally similar to those of the Torlesse terrane in New Zealand suggesting that they were probably derived from a similar source, i.e. an active continental magmatic arc and deposited in a trench or submarine fan setting at the subduction margin .

(2) PSG-2 group is characterised by relatively high average concentrations of $TiO_2$ (0.75±0.10 wt%), $Al_2O_3$ (15.11±1.54 wt%), $Fe_2O_3$ (6.64±0.74 wt%), V (150±34 ppm) and the ratios Zr/Th (34.4±3.6) and relatively low abundances of Pb

(7±3 ppm), Th (4±1 ppm), LREE such as La (12±3 ppm), Ce (26±5 ppm) and Nd (15±3 ppm) and the ratios Th/Sc (0.2±0.1) and Ce/V (0.2±0.1). The major and trace element characteristics suggest that the PSG-2 samples represent sediments derived mainly from the oceanic island arc source. There are strong similarities between the PSG-2 samples and those of the Caples terrane in New Zealand which have been considered to have derived from intra-oceanic arc terrane (Mackinnon, 1983).

### 7.5.2 Nam Pat Group sandstones

**Petrography:** The sandstones of this group are characterised by high amount of volcanic rock fragments. The average composition, $Q_{30}F_{22}L_{48}$ and $Qm_{17}F_{22}Lt_{61}$ is comparable to those of transitional magmatic arc sandstones. The ratios of grain parameters, P/F (0.99) and Lv/L (0.88) are also very similar to the values for the magmatic arc sandstones. The compositional characteristics of the detrital framework grains and their immature textures indicate that the Nam Pat sandstones were derived from a nearby magmatic arc. The andesitic volcanoes that generated the Pak Pat Volcanics are a suitable source.

**Geochemistry:** The Nam Pat Group sandstones have high average concentrations of $TiO_2$ (0.78±0.13 wt%), $Al_2O_3$ (14.84±1.25 wt%), $Fe_2O_3$ (6.30±0.96 wt%). They have relatively high concentrations of V (115±20 ppm) and the ratios Zr/Th (30.5±3.7) and relatively low abundances of Th (5±1 ppm) and the ratios Th/Sc (0.3±0.1) and Ce/V (0.3±0.1). They represent sediments derived from the volcanic rocks of mainly intermediate compositions. This volcanic source may be an oceanic island arc or a continental island arc setting. The Nam Pat Group samples are very similar those of the Caples terrane in New Zealand.

### 7.5.3 Phra Wihan sandstones

The quartzose sandstones of the Phra Wihan Formation are typically lithic-bearing mature sandstones. They have the detrital mode $Q_{89}F_0L_{11}$ and $Qm_{75}F_0Lt_{25}$ and the ratios Qp/Q (0.16) and Lv/L (<0.09) which are similar to those derived from collision recycled orogenic provenance. The compositional characteristics of the detrital framework modes indicate that the sandstone samples of the Phra Wihan Formation were derived from a quartzose recycled orogenic source or from craton interior. They have been interpreted as having been laid down by a braided stream or a major braided stream flanked by subsidiary meandering streams.

# Chapter 8

# STRUCTURE AND METAMORPHISM OF ROCKS ALONG THE PHRAE - SIRIKIT DAM TRANSECT

## 8.1 Introduction

A geological transect across the area between Phrae and the Sirikit Dam was undertaken along the 50 km long unpaved road (Highway 1022) from Ban Pa Daeng, 8 km east of Phrae, to Ban Nam Phra on the bank of the Sirikit Reservoir. This transect is almost normal to the regional trend of the stratigraphic units in the area.

Previous studies provide only a broad account of the stratigraphy of the area (see Table 1.1 for summarised stratigraphic schemes of the area). The rock units presented in a 1:250,000 geological map by Piyasin (1972) include (i) the "Silurian-Devonian" Donchai Group consisting of low-grade metasedimentary rocks, (ii) the Carboniferous Mae Tha Group composed of sandstone, shale and chert, (iii) the Permian Kiu Lom Formation (tuffaceous shale and sandstone) and Pha Huat Formation (mainly massive limestone), and (iv) the Middle Triassic Hong Hoi Formation comprising greenish-grey sandstone and shale.

The stratigraphy of the area was later modified by Bunopas (1981) who proposed the name Phrae Group for a sedimentary sequence previously mapped as the Carboniferous Mae Tha Formation and the Permian Kiu Lom and Huai Thak Formations by Piyasin (1972). The Phrae Group was subdivided into the Rong Kwang Formation (upper unit) and the Mae Sai Formation (lower unit). The base of the Mae Sai Formation was reported to rest unconformably on the metasedimentary unit of the Pha Som Metamorphic Complex which is equivalent to the Donchai Group of Piyasin (1972). The lithologies of the Phrae Group include conglomerate and volcanic breccia of the Mae Sai Formation grading upwards into greywacke, slate and crystalline limestone of the Rong Kwang Formation (Bunopas, 1981).

This area has been re-investigated by geologists from the Royal Thai Department of Mineral Resources. The data relevant to the present study is the finding of additional Middle-Upper Permian fossils from limestone and slate of the

Rong Kwang Formation (Maranate *et al.*, 1987). Concurrently, Charoenpravat *et al.* (1987) reported Triassic bivalves found in the Hong Hoi Formation of Piyasin (1972). According to Chaodumrong (1992), turbiditic mudrocks in the Phrae area previously classified as the Middle Triassic Hong Hoi Formation should be referred to by the new name, the Wang Chin Formation of Upper Triassic based on the presence of middle Carnian to lowermost Norian bivalves. This latest proposal is adopted in the present study on the grounds of compatible lithofacies characteristics.

Like most of Thailand, the structures of rocks across the Phrae-Sirikit Reservoir area have not been studied in detail. The purpose of this chapter is to document structure and metamorphism in this area. The detailed structures of the metasedimentary unit of the Pha Som Metamorphic Complex, the Rong Kwang Formation and the Wang Chin Formation along the transect, are used to place constraints on the regional structure. In addition, the outline of structural and metamorphic history of this area is discussed.

## 8.2 Lithostratigraphy and Petrography

Rocks exposed along the transect from Phrae to the Sirikit Reservoir (Fig. 8.1) include Permo-Carboniferous (?) low-grade metasedimentary rocks, Permian and Triassic sedimentary sequences. The low-grade metasedimentary rocks along this transect can be traced to the Pha Som Metamorphic Complex in the Sirikit Dam area (see Chapter 3 for comparison). The Permian strata in this area belong to the Rong Kwang Formation, the upper unit of the Phrae Group of Bunopas (1981). The Triassic sequence in the study area is probably correlated with the Upper Triassic Wang Chin Formation in the area between Phrae and Lampang which was described by Chaodumrong (1992). The lithostratigraphic characteristics of these rocks are described below.

### 8.2.1 The Pha Som Metamorphic Complex

The low-grade metasedimentary rocks along the Phrae-Sirikit Reservoir transect (Fig. 8.1) is the continuation of the metasedimentary unit of the Pha Som Metamorphic Complex which is best exposed in the Sirikit Dam area to the southeast. Like most of the low-grade metasedimentary rocks in the Sirikit Dam area, the combination of recrystallisation and complex deformation has almost completely destroyed the sedimentary features and hence restricts meaningful sedimentological interpretations. Detailed stratigraphic subdivision is also hindered

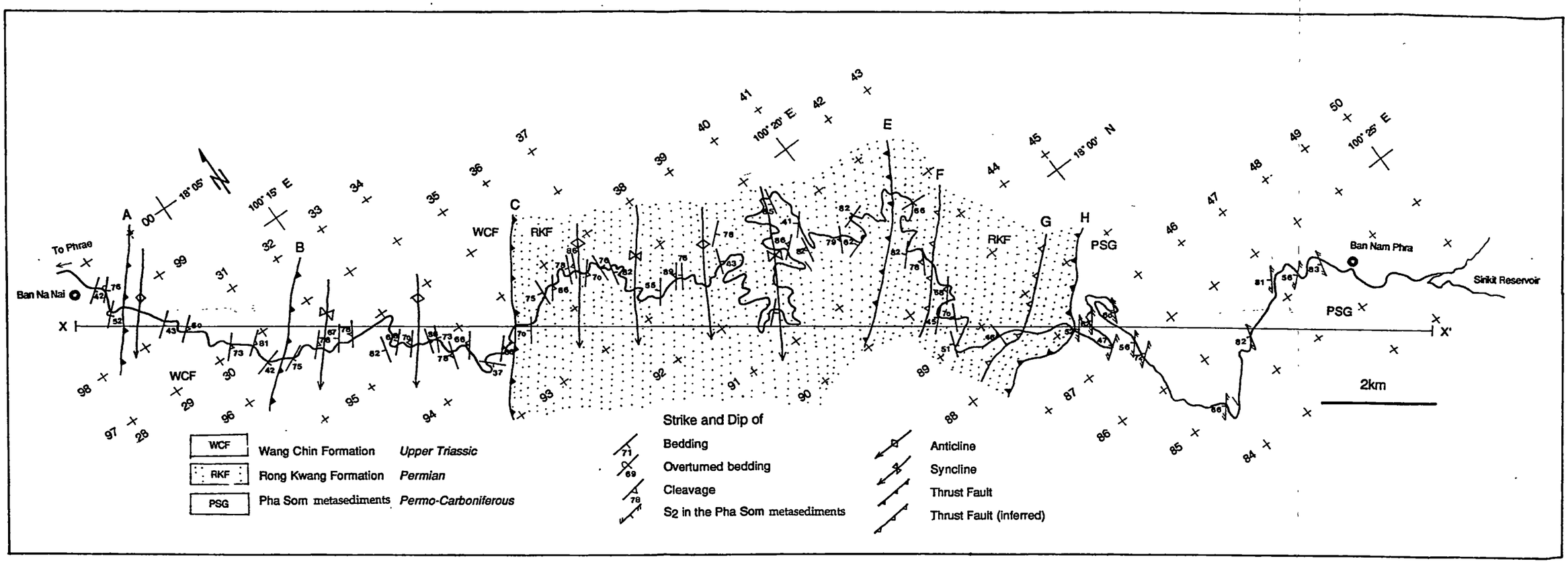


Figure 8.1 Structural map of the Phrae-Sirikit Reservoir transect.

by the structural complexity, the scarcity of the marker horizons and the poor outcrops.

**Lithology:** In contrast to the Sirikit Dam area, the dominant rock type of the Pha Som Metamorphic Complex along the Phrae-Sirikit Reservoir transect is a pelitic rock (phyllite) instead of a psammitic rock (metagreywacke). Phyllite constitutes more than 80% of the exposed part of this rock unit. It is dark grey to light greenish grey in colour and commonly has crenulations and mineral stretching lineations markedly displayed on shiny cleavage surfaces.

Metagreywackes largely occur as lenticular blocks in phyllites probably as a result of structural disruption (Figs. 8.2a&b). Locally, they also occur in a coherent layer together with phyllites. A micaceous sheen on the foliation surface is common.

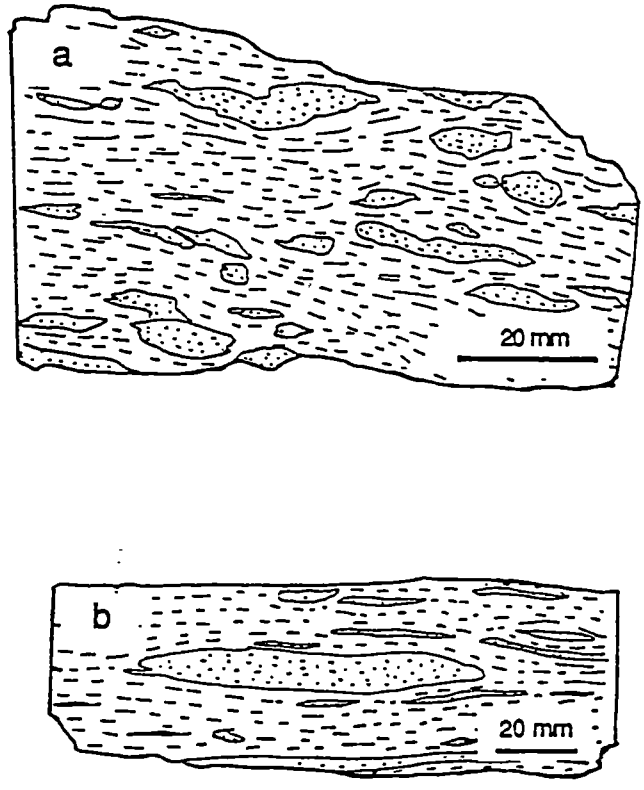


Figure 8.2 Line drawings reproduced from photographs of hand specimens showing lenticular blocks of greywackes in a phyllitic matrix. The polished surfaces in both specimens (a&b) are perpendicular to phyllitic cleavage and parallel to stretching lineation.

**Petrography:** The phyllites along this transect are too fine-grained for optical study. However, as part of $b_0$ and illite crystallinity studies, identification and semi-quantitative estimation of the minerals present in phyllite samples were attempted. On the basis of XRD analysis, the phyllite consists mainly of white mica, quartz, chlorite with subordinate plagioclase but is devoid of K-feldspar. A small amount of calcite is detected in one sample (sample P-92).

The complete absence of biotite in metagreywackes and phyllites in the Phrae-Sirikit Reservoir area indicates that they were recrystallised in the chlorite zone of the greenschist facies. Texturally, the metagreywackes from the Phrae-Sirikit Reservoir area can be classified as slightly-sheared greywackes (TZ1 metagreywackes) and semischists (TZ2 metagreywackes) following the textural zones proposed by Turner (1938) and Bishop (1972). The fine-grained schists (TZ3 metagreywackes) which are common in the Sirikit Dam area were not observed in this transect.

Quartz-poor metagreywackes (samples P-102, P-104, P-106 and P-107) show strong influence of a volcanic source. They can be classified as immature, medium-grained, feldspathic greywackes based on Pettijohn *et al.* (1973). The framework grains consist of monocrystalline and polycrystalline quartz (30-40%), albitised plagioclase (30-45%) and lithic fragments (10-30%) set in a fine-grained matrix (10-20%). Grains are poorly- to moderately-sorted and angular to subangular with mean grain sizes of 250-300 μm. Quartz shows slightly undulatory extinction. Straight extinction typical of volcanic quartz is rare. Plagioclase occurs as broken euhedral, twinned grains; largely replaced by epidote, calcite and to a lesser extent sericite. Lithic fragments, mainly microlitic volcanic rock fragments with small amounts of phyllite and quartz-schist, are highly deformed and indistinct from the matrix. A partially recrystallised matrix includes microcrystalline quartz, sericite and chlorite. In samples P-102, P-106 and P-107, colourless to light green actinolite occurs as radiating acicular aggregates in a matrix as well as around detrital hornblende. Epidote occurs as irregular patches in plagioclase or subhedral grains in a matrix. Quartz-phengite veins are locally present in sample P-106 and P-107. Sphene and zircon are present as accessory minerals.

**Thickness:** Determining of the stratigraphic thickness of the Pha Som Metamorphic Complex is impracticable due to a complex deformation of the rocks. Nevertheless, it should be noted that the present apparent thickness may be much larger than the original stratigraphic thickness due to the repetition of the sequence by thrust stacking.

**Contact:** The base of the metasedimentary unit of the Pha Som Metamorphic Complex has not been seen. This rock unit continues towards the

Sirikit Dam area where it tectonically encloses the ophiolite association. The contact with a pelite-dominated sequence of the Rong Kwang Formation in the west has not been directly observed. Whether the contact is an unconformity or a fault is uncertain. In this transect, a fault contact is more likely considering the increase in cleavage intensity in the Rong Kwang Formation towards the contact. The conformable contact between the Pha Som Metamorphic Complex and the Rong Kwang Formation, reported by Bunopas (1981), was not supported by the present investigation.

**Age and correlation:** The age of the metasedimentary units of the Pha Som Metamorphic Complex remains debatable. No fossil has been found in this rock unit. On the basis of the regional stratigraphy, Bunopas (1981) regarded this rock unit as pre-Permo-Carboniferous and suggested a Silurian-Devonian age. Hess and Koch (1975), on the same grounds, assigned a Permo-Carboniferous age. Barr and Macdonald (1987) later suggested Middle Permian (269± 12 Ma) as a minimum metamorphic age based on a K-Ar date of actinolite in quartz schist. However, a Middle Cretaceous metamorphic age of phyllite based on a K-Ar date of muscovite has recently been reported (Ahrendt *et al.*, 1993). This young age is best considered as a result of resetting. It is very likely that the depositional age of sedimentary rocks within the Pha Som Metamorphic Complex is Carboniferous to Middle Permian or younger, rather than Silurian-Devonian (see detailed discussion in section 3.5 of Chapter 3).

**Environment of deposition:** The siliciclastic component of the Pha Som Metamorphic Complex was inferred to represent the sediments of the inner-trench slope on the grounds of metamorphism, deformation style and chaotic stratigraphy (Bunopas, 1981). On the basis of major and trace element geochemistry, psammitic samples P-102, P-104 and P-107 of the Pha Som Metamorphic Complex are interpreted to represent sediments derived from the volcanic source terrane and probably deposited in the trench (see more detailed discussion in Chapter 7).

### 8.2.2 The Rong Kwang Formation

The Rong Kwang Formation crops out in the middle part of the transect (Fig. 8.1).

**Lithology:** The Rong Kwang Formation consists typically of dark grey to black shale (grading to slate) and massive limestones. Interbeds of sandstone and shale are rare. The shale is generally massive, occasionally laminated, with moderately- to strongly-developed cleavage. Light grey to grey, finely crystalline, massive limestone is common across the area. Limestones characteristically have

irregular, dark stylolite seams and their outcrops are characterised by cliffs or steep-sided ridges in contrast to surrounding shale outcrops. The rare sandstone is grey, fine- to coarse-grained and 20-200 mm thick.

Interbeds of dark grey shale and dark grey to grey, medium-bedded to massive limestone occur in the middle part of the section. These interbeds grade into massive limestone which commonly forms steep-sided ridges.

The lower part of this formation is characterised by calcareous black slate with common lenticular limestone clasts. Pyrite crystals in slate are more common than in the upper part of the formation. A slaty cleavage is very pronounced. A splintery fracture is also a marked feature of the black slate. Rare sandstone beds are intercalated with slate.

At grid reference 418898 (map sheet 5044 I), calcareous black slate has been cut by a 4 m wide aplite dyke.

**Petrography:** No petrographic study is carried out for shale/slate due to a very fine-grained size of these pelitic rocks. However, as part of $b_0$ and illite crystallinity studies, identification and semi-quantitative estimation of the minerals present in shale/slate were attempted. On the basis of XRD analysis, the slate consists mainly of illite, chlorite, quartz with subordinate plagioclase and K-feldspar. Small amounts of calcite and siderite are also detected in a few samples (i.e. samples P-72 and P-73).

The limestones are largely recrystallised lime mudstone according to Dunham's classification (1962). They consist chiefly of calcite microspar (equant-polyhedral grains of 4-10 μm in diameter) and pseudospar (10-50 μm in diameter) and are characterised by dark irregular stylolite seams with associated degrading neomorphism. A broken fossil coral (sample P-48), crinoid ossicles and brachiopod shells (sample P-56: bioclastic wackestone) are sporadically present within micrite (5-10 μm). Drusy calcite veins are common in these samples. Silt-size or fine-sand-size quartz grains are present in sample P-65.1. A peloidal packstone (sample P-65.2) consists of subparallel peloids in calcite microspar (10-30 μm) matrix. A sheared arenaceous limestone (sample P-67) is composed of deformed sparry calcite patches and detrital quartz grains in calcite microspar matrix. A bioclastic lime mudstone (sample P-49) consists of fossil fragments of very coarse sand-size (0.5-2 mm) in a matrix of calcite microspar in which numerous rhombs of probably siderite are present. Most of the bioclasts are echinoderm fragments with a few compound rugose coral clasts. A few fusulinids are also present and there are possibly a few dasyclad algae. Stylolites filled with yellowish brown clay are common and the rock is cut by several calcite veinlets.

Sandstones (e.g. sample P-78) are immature, medium-grained, calcareous greywackes according to the classification of Pettijohn *et al.* (1972). The framework grains consist of monocrystalline quartz (20%), polycrystalline quartz (30%), twinned and untwinned plagioclase feldspar (25%) and microlitic volcanic rock fragment (10%). Quartz grains commonly exhibit straight extinction. Grains are moderately-sorted, subangular, medium grained with mean grain size of 200 μm and are cemented by clay matrix (15%) and sparry calcite.

**Thickness:** Lithological monotony and complex folding and thrusting preclude an accurate measurement of the thickness of the Rong Kwang Formation. Bunopas (1981) estimated the total thickness of this rock unit to be in the range 1500 to 2500 m. The apparent thickness along the transect is about 2000 m.

**Contacts:** The contact between the Rong Kwang Formation and the Pha Som Metamorphic Complex has not been directly observed during this study. The sudden changes in metamorphic grade and structural style suggest that the contact is either an unconformity or a fault. A fault contact is favoured here based on an increase in cleavage intensity towards the contact. In the west, the Rong Kwang Formation overthrusts the Wang Chin Formation. The thrust contact between these two rock units was also reported from the Wang Chin area further south, between Phrae and Sukhothai (Wolfart, 1987). Elsewhere, the Rong Kwang Formation is reported to be underlain conformably by the Mae Sai Formation which in turn rests unconformably on the Pha Som Metamorphic Complex (Bunopas, 1981).

**Age and correlation:** Disarticulated and fragmentary bivalves of unknown age were collected from shale beds in the present study. These bivalves are deformed and are probably pectinoids (identified by Dr. M. R. Banks). Elsewhere, the fusulinids *Paraschwagerina sp.* (Middle Permian) and *Orthoceras sp.* (identified by R. Ingavat-Helmcke) were found in the upper part of the Rong Kwang Formation (Bunopas, 1981). The lower age limit of this rock unit was suggested as Lower Carboniferous based on the presumed conformable contact with the underlying "Silurian-Devonian" Pha Som Metamorphic Complex (Bunopas, 1981). Both conformable contact and the Silurian-Devonian age of the Pha Som Metamorphic Complex have not been supported by the present study. Therefore, the lower age limit of the Rong Kwang Formation is still debatable. The contact between the Rong Kwang Formation and the Carboniferous (?) Mae Sai Formation was considered to be time-transgressive (Bunopas, 1981). Again, the Carboniferous age of the Mae Sai Formation is inferred from the stratigraphic position between the underlying Pha Som Metamorphic Complex and the overlying Rong Kwang Formation.

**Environment of deposition:** The pelite-dominated lithological characteristics of the Rong Kwang Formation suggest a quiet, low-energy environment of deposition with distant terrigeneous source. The dark colour of the pelitic rocks and the common occurrence of pyrite crystals suggest a depositional basin with restricted water-circulation or presumably reducing condition. Moreover, the dominant recrystallised lime-mudstone suggests a low-energy, restricted marine environment (Tucker and Wright, 1990). The presence of localised peloidal wackestone and recrystallised bioclastic lime mudstone with fossil rugose corals and echinoderms further point towards a localised warm water, shallow marine environment. The thinness and fine-ribbing of the valves of fossil pectinoids suggest a growth in deep water (close to or below wave base; Dr.M.R Banks, pers. comm., 1993). The fossil evidence for shallow water contrasts with the clastic evidence for a below wavebase low energy setting. The fossils may have been transported from their living area to the depositional area by turbidity currents.

### 8.2.3 The Wang Chin Formation

The Wang Chin Formation crops out in the western part of the section (Fig. 8.1). Most of the outcrops are observed along a series of road-cuttings and the Nam Mae Khon which flows across the main strike of the strata.

**Lithology:** The Wang Chin Formation dominantly consists of massive dark grey shale/slate. Laminations or thin beds of grey to greenish grey, calcareous siltstone and fine to medium-grained sandstone are locally present. Limestone, in general, occurs as small massive bodies forming small cliffs locally. Rectangular to lenticular clasts or blocks of dark grey finely crystalline limestone, ranging from a few centimetres to a few metres in length, enclosed within slate are common in many localities. Bedding is generally obscured by moderately to strongly-developed cleavage coupled with low arenite to pelite ratio (usually less than 1: 10) of the entire unit.

Interbeds of sandstone and shale/slate are more common towards the lower part of the sequence. Arenite to pelite ratio is also higher. The thickness of sandstone beds ranges from thin to medium and never reaches 300 mm. Primary sedimentary structures, e.g. graded bedding, are rare.

Intercalation of medium to thickly-bedded, dark grey limestone and very thinly-bedded, dark grey shale occurs in the middle part of the sequence.

**Petrography:** No petrographic study has been carried out for shale due to a very fine-grained size of this rock type. However, as part of illite crystallinity studies, identification and semi-quantitative estimation of the minerals present in

shale were attempted. On the basis of XRD analysis, shale consists mainly of illite, chlorite, quartz with subordinate plagioclase and K-feldspar. A small amount of calcite was also detected.

Sandstone (sample P-30) is immature, very-fine-grained calcareous litharenite. The framework grains consist mainly of monocrystalline quartz (80%) with minor amounts of polycrystalline quartz (10%) and twinned plagioclase feldspar (5%). Few muscovite flakes are present as detrital grains. Quartz grains commonly exhibit undulatory extinction possibly inherited from the source rocks. Grains are moderately-sorted and subrounded with mean grain size of 80 μm. Grains are cemented partly by clay matrix (5%) and partly by sparry calcite.

Limestones of the Wang Chin Formation can largely be classified as lime mudstone following Dunham (1962). Sample P-2 is a lime mudstone consisting almost entirely of calcite microspar (10-20 μm) matrix with few patches of sparry calcite. This sparry calcite is presumably recrystallised fossil fragments. Samples P-12, 12.1 and 19.1 are also lime mudstones. They are composed largely of microspar (5-15 μm) matrix with few patches of sparry calcite that may represent original bioclasts. Few silt-size (30-40 μm) detrital quartz grains are also present within the sparry calcite. Stylolite seams are common and pyrite cubes are present.

**Thickness:** The exact thickness of the Wang Chin Formation cannot be measured along this traverse due to the incompleteness of the studied section and the scatter of the outcrops. Based on vertical facies relations, the approximate thickness is close to 1000 m. In the area between Phrae and Lampang, it has been estimated to be 600-1000 m thick (Chaodumrong, 1992).

**Contacts:** The contact between the Wang Chin Formation and the Rong Kwang Formation is a thrust fault (Fig. 8.1). The Wang Chin Formation is concealed beneath the Quaternary alluvium in the west.

**Age and correlation:** Charoenpravat *et al.* (1987) reported the presence of Triassic bivalves *Halobia sp.*, *Daonella sp.*, and *Posidonia sp.* in shale beds of the Wang Chin Formation. Pelecypod, ammonite and gastropod were also reported from interbedded shale, sandstone and limestone of this formation by Maranate *et al.* (1987). In the area between Phrae and Lampang, this formation was inferred to be middle Carnian to lower Norian on the basis of middle Carnian bivalves *Halobia styriaca* and *Halobia cassiana* together with lowermost Norian bivalves (Chaodumrong, 1992). Conodonts of Norian age (identified by Dr. C. F. Burrett) were collected from a road cutting on Highway 1022 (grid reference 330953).

**Environment of deposition:** The Wang Chin Formation in the area west of Phrae (especially along the Lampang-Denchai Highway) is a mud-rich turbidite succession. It has been thought to represent the turbiditic sediments accumulated

within the forearc basin (Bunopas, 1981, Sengör, 1984). On the basis of facies association and vertical facies sequences, it was interpreted to have been deposited as a mud-dominated submarine fan with detached sand bodies (Chaodumrong, 1992). The lithology and lithofacies of the mud-dominated turbidite sequence along the Phrae-Sirikit Reservoir transect are consistent with this latest interpretation.

## 8.3 Structural Analysis

Field observation indicates that the Pha Som Metamorphic Complex and the cover sequence (the Rong Kwang and Wang Chin Formations) have different deformation style and history. The structures recognised in the Pha Som Metamorphic Complex along this transect are comparable with $D_1$ to $D_3$ structures in the Sirikit Dam area. Kink and angular folds ($D_4$ structures) common in the Pha Som Metamorphic Complex in the Sirikit Dam area were not observed on this transect. The structures in the Rong Kwang and Wang Chin Formations, i.e. folds and cleavage, are similar in style and orientation. They are correlated here with the $F_3$ folds and related structures in the Pha Som Metamorphic Complex.

The mesoscopic structures developed in each of these rock units are described separately. The geometrical relationships of the mesoscopic structures of each rock unit are used to place constraints on the interpretation of the macroscopic structure and structural development along the transect.

### 8.3.1 Structure of the metasediments of the Pha Som Metamorphic Complex

#### Folds

A small-scale tight fold, correlated with $F_2$ folds in the Sirikit Dam area, was observed in phyllite at grid reference 432878 (map sheet 5044 I). This fold is asymmetrical with eastward vergence. The scarcity of folds precludes meaningful detailed analysis of folding in this rock unit. This is probably due to the lack of competent layers or, alternatively, folds may have been obliterated by transposed foliation defined by strongly-developed cleavage ($S_2$)

#### Cleavage

A cleavage ($S_2$) is strongly developed and generally obliterates the older structure (e.g. quartz veins, $S_1$ and bedding, $S_0$). Lenticular blocks of psammitic

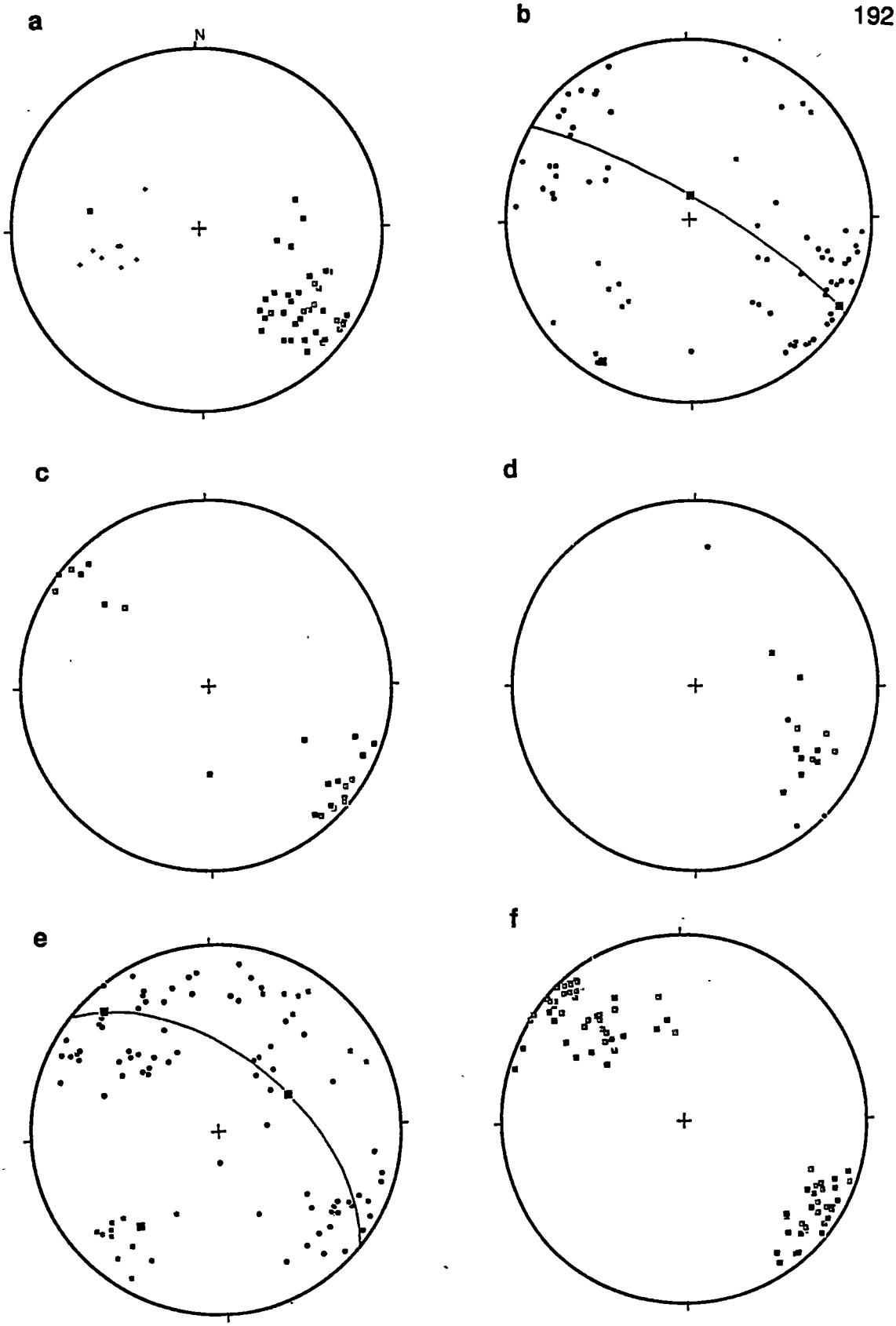
a
N
b
c
d
e
f

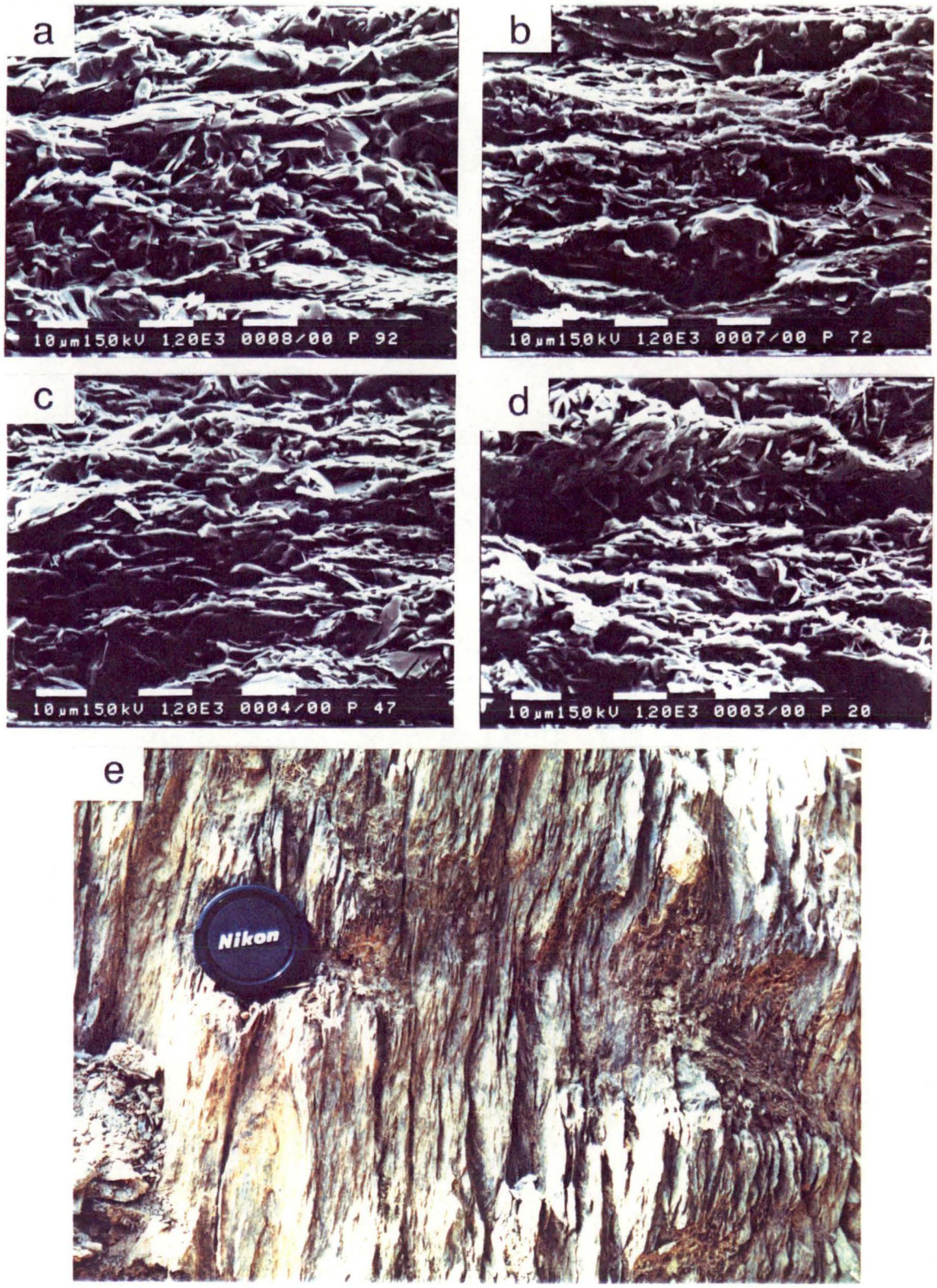
a
10µm15.0kV 1.20E3 0008/00 P 92
b
10µm15.0kV 1.20E3 0007/00 P 72
c
10µm15.0kV 1.20E3 0004/00 P 47
d
10µm15.0kV 1.20E3 0003/00 P 20
e
Nikon

rocks are abundant in a matrix of pelites creating a fabric which is similar to tectonic melanges. $S_2$ cleavage dips uniformly towards the northwest (Fig. 8.3a). Microstructurally, a cleavage in phyllite is similar to that in the Rong Kwang slate but phyllosilicate grains are slightly larger in size. (Fig. 8.4a). In a few localities, quartz veins have been deformed in such a manner that they suggest east-directed thrusting (Fig. 8.5).

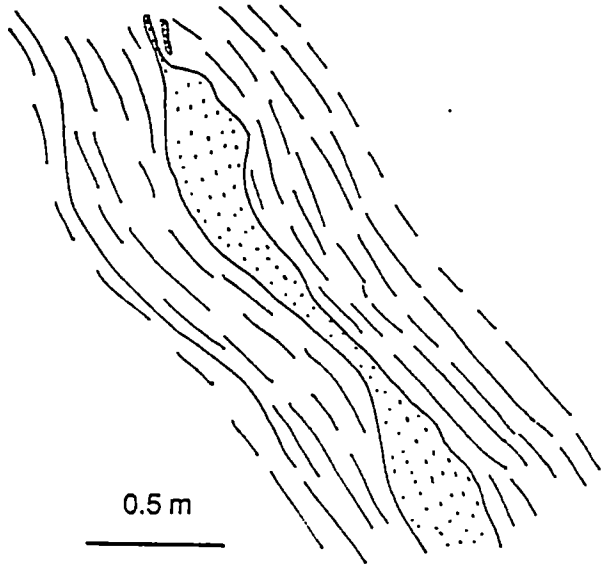


Figure 8.5 Line drawing from photograph of pinch and swell structure in quartz veins in the Pha Som Metamorphic Complex phyllite (looking southwest at grid reference 448850). Asymmetry (foliation boudinage) of this quartz vein supports top-to-the-southeast sense of shear.

## Stretching lineations

One of the marked feature of the pelitic rock of the Pha Som Metamorphic Complex on this traverse is the mineral stretching lineation which is correlatable with the $L_2$ stretching lineation in the Sirikit Dam area. The stretching lineation is defined by alignment of deformed quartz grains. A streak of light coloured stretched

mineral grains on a background of dark coloured pelitic matrix is unique in appearance. Alignment of lenticular psammitic blocks enhances the lineated feature in this rock type rendering them a melange-like character. The stretching lineation uniformly plunges to the west-southwest (Fig. 8.3a).

### Crenulations

Crenulations in phyllite on this transect are as common as those in the Sirikit Dam area. However, crenulation cleavage was not observed. The orientation data of these structures are insufficient for meaningful geometrical analysis. The crenulations observed in phyllite along this transect are correlated with the $D_3$ crenulations in the Sirikit Dam area.

## 8.3.2 Structure of the Rong Kwang Formation

The Rong Kwang Formation has a relatively simple pattern of deformation, compared with the Pha Som Metamorphic Complex. The mesoscopic structures in this rock unit are characterised by a series of open to tight chevron folds and numerous associated thrust faults.

### Folds

The outcrop-scale folds in the Rong Kwang Formation are characterised by chevron-style, open to tight folds (Fig. 8.6a&b) with amplitude between 1 to 2 m and wavelength of less than 1 m. Across the whole section of the Rong Kwang Formation, fold closures are very rare whereas long straight beds probably representing fold limbs are more common. A single measurement of fold axis, at grid reference 390914 (map sheet 5045 II), indicates a steep plunge (60°/045°). However, a more common cleavage-bedding intersection lineation ($L_1$), statistically parallel to local macroscopic fold-axis, plunges shallowly to the northeast and southwest (Fig. 8.3b).

### Cleavage

A cleavage ($S_1$), moderately to strongly developed, is demonstrably axial-planar to folds in the interbeds of shale and sandstone or limestone. The cleavage dips steeply to the northwest and southeast (Fig. 8.3c). Cleavage fanning is common. Convergent fanning occurs in competent beds (limestone and sandstone)

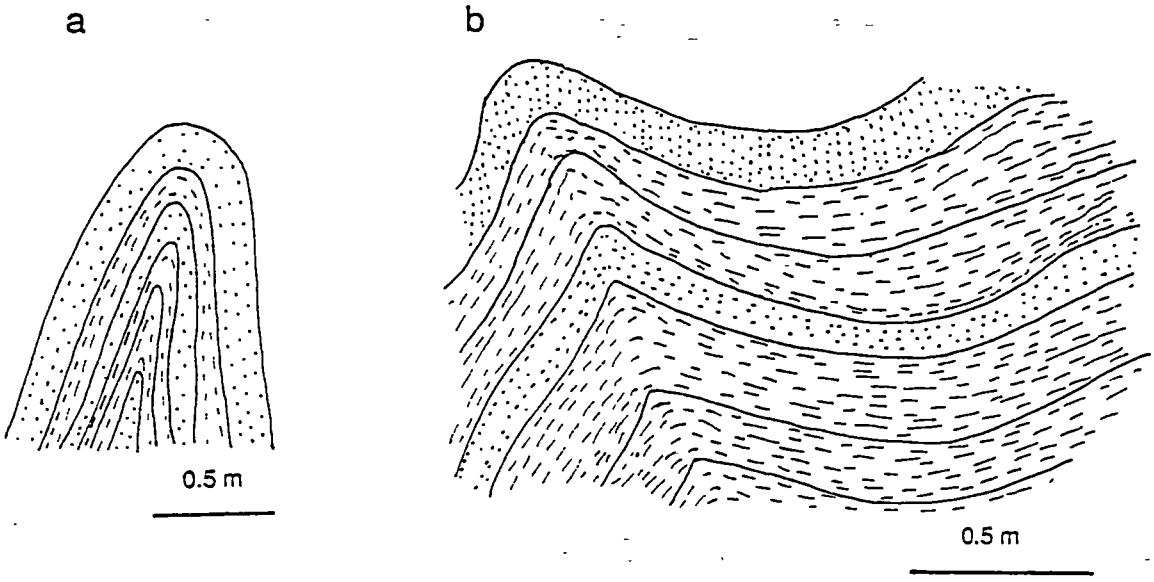


Fig. 8.6 Line drawings from photographs showing fold style of the Rong Kwang Formation: (a) chevron close fold in interbedded slate and fine-grained sandstone, grid reference 390914, looking SW; (b) angular open fold in interbedded shale and sandstone, grid reference 403935, looking S.

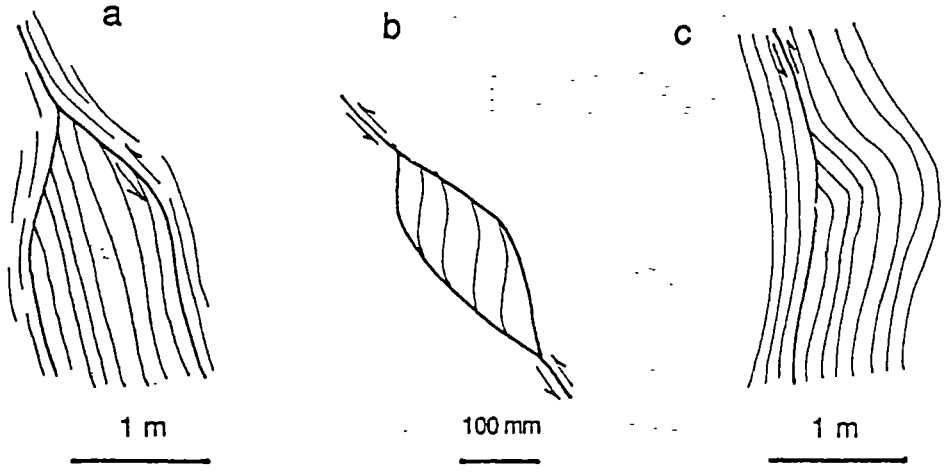


Fig 8.7 Outcrop sketches showing geometry of small-scale thrust faults in the Rong Kwang Formation. Grid reference 350943, looking S.See text for details.

and divergent fanning is common in weaker/softer beds (shale/slate). The strong cleavage development almost completely obliterates the bedding ($S_0$) in many localities, especially in laminations or thin interbeds of shale/slate and sandstone or limestone. Cleavage in the Rong Kwang slate is better developed than the cleavage in the Wang Chin slate (Fig. 8.4b,c&d). In the lower part of the section (eastern subdomain), the structure is characterised by abundant lenticular clasts of limestone enclosed by strongly cleaved slate. The cleavage ($S_1$) invariably dips to the west or northwest (Fig. 8.3d).

## Faults

Faults are not easily recognised in the Rong Kwang Formation due to lithological monotony of this unit. However, small-scale thrust faults were observed in interbeds of shale/slate and limestone in a few places. Thrust geometry dominates these outcrops. The thrusting is dominantly east-directed (Fig. 8.7a). A small-scale horse outlined by roof thrust and floor thrust (Fig. 8.7b) was recognised at grid reference 350943 (map sheet 5045 III). Fault-bend folds are also observed (Fig. 8.7c).These thrusts were seen to shear off bedding and cleavage. Bedding and cleavage are dragged in the narrow zones close to the thrust surfaces. This suggests that thrusting is synchronous with or postdates folding and cleavage formation.

### 8.3.3 Structure of the Wang Chin Formation

The mesoscopic structures in the Wang Chin Formation are characterised by a series of upright to overturned chevron folds with axial-plane cleavage. They are similar in style and orientation to those observed in the Rong Kwang Formation. All available data supports a direct correlation between the structures in these two units. The $D_3$ structures in the metasediments of the Pha Som Metamorphic Complex are different in style but similar in orientation. A provisional correlation is made here between $D_3$ in the Pha Som Metamorphic Complex and the folds in the cover sequence.

## Folds

The mesoscopic folds recognised along the traverse are mainly of upright chevron fold-style with steeply-dipping axial plane cleavage. Overturned folds are

present in the western part of the transect. Folds are best developed in the well-bedded sequence of alternating shale and sandstone or minor limestone beds. Upright, close to tight folds are the most common style of structure in the Wang Chin Formation (Fig. 8.8a&b). The mesoscopic fold amplitude is in the range 1 to 2 m with wavelength of about 0.5 to 1 m. The major fold axis determined from stereographic projection technique (Fig. 8.3e) plunges shallowly to the south-southwest (22°/218°). The cleavage-bedding intersection lineation ($L_1$) is statistically parallel to major fold-axis and plunges shallowly to the northeast and southwest (Fig. 8.3e).

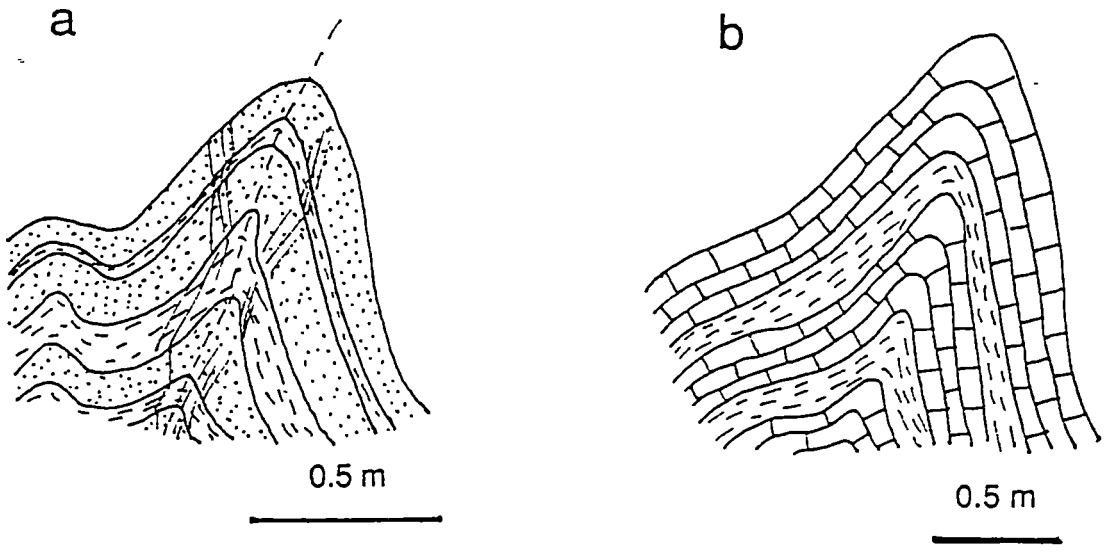


Figure 8.8 Profile sketches of folds in the Wang Chin Formation: (a) fold in interbedded sandstone (stippled) and shale (dashed) at grid reference 327955 (looking south); (b) fold in interbedded limestone (brick) and shale (dashed) at grid reference 332952 (looking south).

## Cleavage

Cleavage intensity is variable depending on the lithology, nature of stratification, tightness of fold and position of rocks in the fold structure. Cleavage in interbeds of shale and sandstone or limestone displays refraction when passing from shale into sandstone or limestone. Cleavage dips steeply to the northwest and southeast (Fig. 8.3f). Cleavage fanning is common. The strong cleavage development almost completely obliterates the bedding ($S_0$) in many places, especially in laminations or thin interbeds of shale/slate and sandstone or limestone. This causes difficulties in recognising bedding. In the slates, the cleavage is

moderately to strongly developed (Figs. 8.4d&e). Cleavage intensity increases towards the faults.

### Faults

At grid reference 320960 of map sheet 5045 III, a northeast-striking high-angle fault (040°/88°W) with right-lateral normal slip (30°/038°) is exposed on a road cutting. The amount of displacement cannot be determined due to the absence of marker layers. In addition, bedding-plane and fold-limb thrusts are common within interbedded slate, limestone and sandstone of the Wang Chin Formation.

## 8.4 Structural Interpretation

### 8.4.1 Basic concepts and limitations

Some important points of the basic concepts for structural interpretation adopted in the present study are discussed below:

(i) The fundamental concept for the macroscopic interpretation is that folds of a given generation commonly have a very similar appearance in profile whatever their size (Hobbs *et al.*, 1976). Therefore, the geometry of a major or macroscopic fold can be reasonably approximated by the shape of mesoscopic folds of the same generation. The presence of a major fold with the same plunge as the group of outcrop-scale folds in the same area is indicated by the orientation diagrams of the folded bedding.

(ii) In drawing a structural cross section, the kink method (Suppe, 1983; 1985) is preferable to the Busk method (Busk, 1929) . This is because the style of folding in the study area is characterised by chevron folds with straight limbs and sharp-angular hinges not by concentric folds with rounded-hinges. Thickening of the fold hinge zone and associated thinning of the fold limbs do occur but not extensively. This variation in geometry has to be taken into account in the construction of the balanced cross-section across the study area.

(iii) A cross-section was drawn following the technique of section balancing of Dahlstrom (1969), Suppe (1983), Boyer and Elliot (1982) and Woodward *et al.* (1989). The detachment surface is inferred to be located in the upper part of the Pha Som Metamorphic Complex just below the base of the Rong Kwang Formation. Due to the complex deformation history and the metamorphism where volume change is likely to be significant, the reconstruction method commonly used for

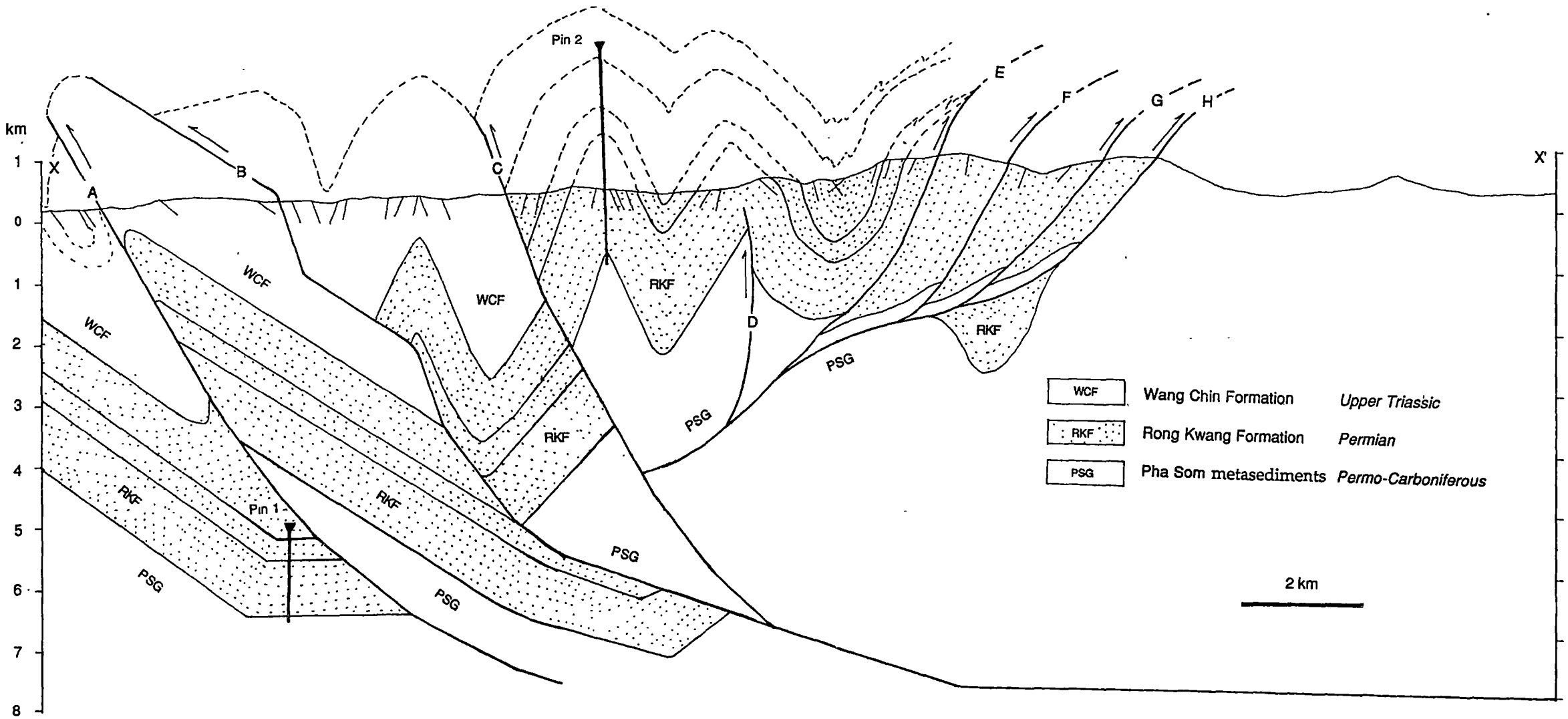


Figure 8.9 Interpretive cross-section of the Phrae-Sirikit Reservoir transect (along line XX' in Figure 8.1) including a restored template (on the opposite page).

balanced cross-section is not applicable for the Pha Som Metamorphic Complex. This limits the interpretation of the structure in the deeper level below the exposures of the Pha Som Metamorphic Complex. Further, the presence of cleavage in the Rong Kwang and Wang Chin Formations may introduce errors in the reconstruction, however, the cleavage development is weak except locally on faults until about half way across the section (see Fig 8.9). The cleavage intensity is comparable to those observed in many slate belts where a similar style of reconstruction has been applied, e.g. the Slate Belt in central Victoria, Australia (Cox *et al.*, 1991; Gray and Willman, 1991). The section presented here is a first attempt to put the structure of this transect into a modern perspective. With the present level of data no accurate reconstruction is possible. The section can only be drawn on the assumption of parallel folding. This approximation becomes untenable towards the east of the section and cannot be applied to the Pha Son Metamorphic Complex.

Across the study area, outcrop-scale folds are rare and stratigraphic facing of bedding was mainly deduced from the angular relationship between bedding and axial plane cleavage. Sedimentary structures are scarce but were used to support the structural facing.

## 8.4.2 Macroscopic structure

A series of macroscopic folds and associated thrust faults were recognised on the basis of field evidence and mesoscopic analysis. The interpretive structural cross-section (Fig. 8.9) was done with the aid of FAULT II computer program (Wilkerson, 1990). The input data includes the thickness of lithostratigraphic units (i.e. the Rong Kwang and the Wang Chin Formations) and the fold and thrust fault geometry. The gross geometry of the final cross-section is very similar to the output from this program but the fine-scale details have been adjusted to comply with the observed structures. Macroscopic faults and related structures are discussed starting from the eastern end of the section.

In the eastern part of the cross-section (Fig. 8.9), the Permian Rong Kwang Formation is shown here to have a thrust contact with the metasedimentary rocks of the Pha Som Metamorphic Complex (fault H). There is no direct field evidence for this fault but it is inferred from the contrasting lithology, metamorphic grade and structural style of these two rock units. The cleavage in the Rong Kwang Formation increases in intensity towards this boundary. That the younger unit is thrust over the older unit may be explained by a transecting thrust cutting down section in the transported direction analogous to Figure 2d of McClay and Buchanan (1991). A

hidden syncline below fault H is required for this interpretation. An imbricate zone (represented by faults E, F and G) is modelled to account for the excessive apparent thickness of the Rong Kwang black slate (about double the best estimate for the thickness of the Rong Kwang Formation in section 8.2.2). The amount of displacement is unconstrained. These imbricate faults probably splay off the main thrust surface within the Pha Som Metamorphic Complex at depth. Within and near this zone, the cleavages in both rock units consistently dip to the northwest and becomes shallower in orientation than the regional cleavage. This is probably due to the shear effect which causes rotation of the cleavages into parallelism with the faults (e.g. Ramsay, 1980). This geometry lend some support to the interpretation that imbricate zone is northwest-dipping with east-directed transport direction. In contrast, no evidence was found for normal fault movement in this part of the section.

A blind thrust (fault D) is interpreted to splay off the main fault (fault H) and shear off anticlinal hinge. The position of fault D is placed to maintain the thickness of the Rong Kwang Formation around the anticline.

Fault C marks the boundary between the Permian Rong Kwang Formation and the Upper Triassic Wang Chin Formation. This fault can be recognised from aerial photographs and it is marked by a narrow brecciated zone. However, the sense of movement along this fault is not clearly evident due to poor exposure. It is shown here as a high-angle reverse fault based on the geometrical relationships of the bedding of both rock units and the east-side-up motion required by the stratigraphy. Like other faults to the west, it is interpreted to branch off the main west-directed detachment fault at depth (Fig. 8.9). Fault C is shown to have offset fault H as the hanging wall block moved up. To the east of fault C, the Rong Kwang Formation is folded into open to close folds about the steeply southeast-dipping axial surfaces. The fold wavelengths are more than 1 km and amplitudes are about 1 km. In this part of the cross-section, the fold geometry is a mixture of class 1a and 1c of Ramsay (1967). The position of anticlines and synclines are interpreted from the bedding orientation.

Fault B is modelled to account for the excessive outcrop width of the Triassic strata. The position of this fault is based on the fact that folds located close to the fault are tighter than those located further away. Folding of the Triassic strata between fault B and fault C is characterised by upright close fold. Syncline and anticline are interpreted from bedding orientation with an indication from bedding-cleavage relationships. The anticline is interpreted as ramp anticline which requires the kink at the upper portion of fault B.

In the westernmost part of the section, fault A is shown as a west-directed thrust coincident with a sheared off overturned anticline. Overturning of bedding west of this fault is indicated by the fact that bedding dips steeper towards the southeast than the cleavage. Cleavage intensity in the Wang Chin slate increases towards this fault.

It should be noted that the concept of section balancing is strictly applied only to the section between pin 1 and pin 2. The eastern part of the section beyond pin 2 was not restored. The present length of the restored section (between pin 1 and pin 2) is 5.35 km and the original length is 15 km indicating a shortening of 9.65 km or 64% for this section. The amount of the overall shortening is consistent with the fold tightness and cleavage intensity in the Rong Kwang and Wang Chin Formations.

### 8.4.3 Structural development

The structural development of the Phrae-Sirikit Reservoir area is dominated by thrusting. Two generations of thrusting were recognised. The early east-directed thrusting (i.e. fault H) involves the Pha Som Metamorphic Complex and the Middle Permian Rong Kwang Formation suggesting that the age of thrusting is post-Middle Permian. Since the associated folds buckle the Upper Triassic Wang Chin Formation (Fig. 8.9), it is likely that these faults postdated the deposition of the Wang Chin Formation. This means faulting occurred in the Upper Triassic or later. The west-directed thrusting (i.e. faults A, B and C) is associated with folding of the Permian Rong Kwang and the Upper Triassic Wang Chin Formations. The relative age of this thrusting event is inferred from the cross-section where it offset the early thrust (e.g. fault H). However, this is not well-constrained. The west-directed faulting postdates early east-directed thrusting but these two faulting events probably occurred during the same deformation in the Late Triassic.

## 8.5 Metamorphism

Metamorphism of the rocks along the traverse was studied via the use of the $b_0$ and illite crystallinity for diagenetic to low grade pelitic rocks. In addition, the mineral assemblages of metagreywackes constrain their metamorphic grade to lower-greenschist facies.

### 8.5.1 Metamorphism of the Pha Som Metamorphic Complex

Table 8.1 Illite crystallinity values of pelitic rocks from the Phrae-Sirikit Reservoir Road.

| Sample no. | Grid reference/map sheet | IC (EG) Δo2Θ |
|---|---|---|
| | *Wang Chin Formation* | |
| P-1 | 288990/5045III | 0.23 |
| P-4 | 313963/5045III | 0.21 |
| P-7 | 289994/5045III | 0.25 |
| P-10 | 297979/5045III | 0.21 |
| P-13 | 306969/5045III | 0.24 |
| P-15 | 317960/5045III | 0.20 |
| P-22 | 322959/5045II | 0.21 |
| P-26 | 327955/5045II | 0.22 |
| P-27 | 332952/5045II | 0.20 |
| P-35 | 336946/5045II | 0.22 |
| P-38 | 339953/5045II | 0.21 |
| | *Rong Kwang Formation* | |
| P-42 | 343941/5045II | 0.22 |
| P-44 | 346942/5045II | 0.22 |
| P-47 | 350943/5045II | 0.22 |
| P-50 | 357947/5045II | 0.26 |
| P-52 | 361947/5045II | 0.25 |
| P-55 | 366945/5045II | 0.24 |
| P-58 | 374933/5045II | 0.26 |
| P-60 | 385915/5045II | 0.26 |
| P-61 | 390914/5045II | 0.23 |
| P-63 | 403923/5045II | 0.24 |
| P-66 | 412923/5045II | 0.22 |
| P-69 | 417914/5045II | 0.20 |
| P-72 | 419906/5045II | 0.20 |
| P-73 | 418898/5044I | 0.21 |
| P-77 | 417894/5044I | 0.21 |
| P-80 | 414888/5044I | 0.20 |
| P-82 | 422886/5044I | 0.20 |
| P-84 | 424886/5044I | 0.24 |
| | *Pha Som Metamorphic Complex* | |
| P-87 | 437871/5044I | 0.19 |
| P-92 | 437878/5044I | 0.19 |
| P-96 | 438882/5044I | 0.19 |
| P-97 | 442870/5044I | 0.20 |
| P-99 | 447851/5044I | 0.19 |
| P-100 | 448850/5044I | 0.19 |
| P-105 | 469858/5044I | 0.19 |

The metamorphism of the Pha Som Metamorphic Complex is discussed in more detail in Chapter 5. This chapter focuses on the $b_o$ and illite crystallinity study of pelitic rocks. Only a brief account on the metamorphism of metagreywackes is presented.

This $b_o$ values of pelitic rocks in along the Phrae-Sirikit Reservoir transect range from 8.988Å to 9.012Å with the average of 8.999Å (see Table 5.6 in Chapter 5). This average $b_o$ value places them in a low to medium pressure metamorphic facies series (Guidotti and Sassi, 1986).

Illite crystallinity study was carried out for phyllites from the Phrae-Sirikit Reservoir transect. The illite crystallinity values of phyllites are in the range 0.191-0.203 Δ°2θ (Table 8.1) indicating an epizone (greenschist facies) metamorphic grade according to the Kisch's scale (1990). The illite crystallinity values of phyllites agree reasonably well with the estimated temperatures for psammitic samples obtained from geothermometric calculations discussed in Chapter 5. A plot of illite crystallinity values versus a distance along the Phrae-Sirikit Reservoir transect (starting from the western end) is shown in Figure 8.10.

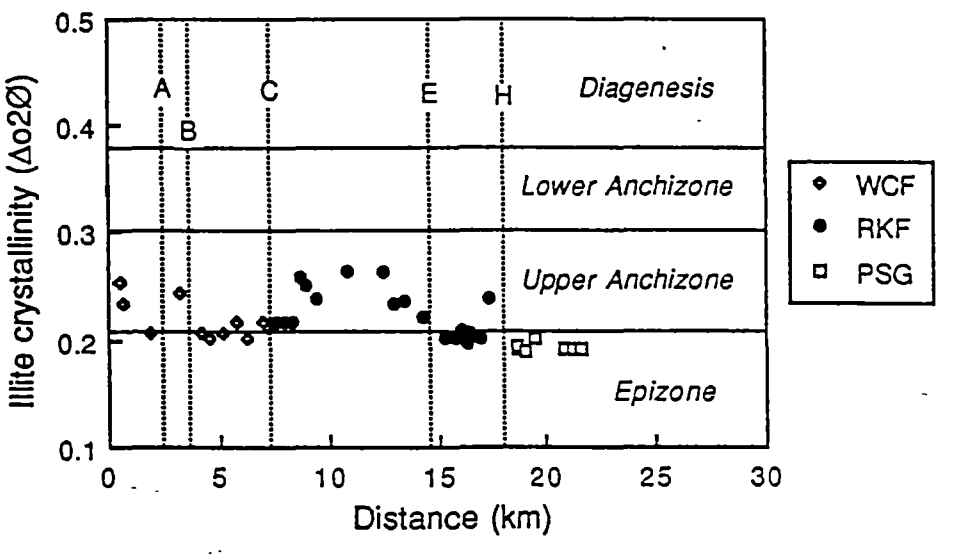


Figure 8.10 Plot of illite crystallinity values versus distance along the Phrae-Sirikit Reservoir transect. Also shown are the positions of faults (see also Figure 8.9)

Slightly sheared greywacke is restricted to blocks in a pelitic matrix in the transect. It consist largely of quartz, albite, muscovite, chlorite, actinolite, epidote and calcite. The plagioclase-muscovite geothermometer of Green and Usdansky

(1986) applied to sample P-102 gives the temperature of 333 °C. The phengite geobarometer of Massonne and Schreyer (1987) yield a pressure of 5 kbar for sample P-104.

Metamorphism of the metasediments of the Pha Som Metamorphic Complex may have reached its peak during the formation of phyllitic cleavage (correlated with $S_2$ in the Sirikit Dam area). The peak conditions probably occurred in the Middle Permian (i.e. 269±12 Ma) as indicated by Barr and Macdonald (1987).

## 8.5.2 Metamorphism of the Rong Kwang Formation

Slate is the dominant lithology of the Rong Kwang Formation in this area. The $b_0$ values of muscovite in pelitic samples of the Rong Kwang Formation along the Phrae-Sirikit Reservoir transect (Table 8.2) range from 8.988 Å to 9.012 Å with a mean value of 8.996 Å indicating the low to medium pressure facies series according to the baric scale of Guidotti and Sassi (1986).

Table 8.2 Crystal lattice parameters ($b_0$ values) of muscovite in pelites of the Rong Kwang Formation along the Phrae-Sirikit Reservoir transect.

| Sample number | (060) | $b_0$ * |
|---|---|---|
| P-55 | 1.499 | 8.994 |
| P-58 | 1.498 | 8.988 |
| P-60 | 1.499 | 8.994 |
| P-61 | 1.499 | 8.994 |
| P-72 | 1.502 | 9.012 |
| P-73** | 1.502 | 9.012 |
| P-77 | 1.498 | 8.988 |
| P-80 | 1.499 | 8.994 |
| P-84 | 1.498 | 8.988 |

* mean $b_0$ = 8.996, standard deviation = 0.009, n = 9; ** Calcite-bearing sample

The illite crystallinity values of the slate samples (except sample P-58) of the Rong Kwang Formation, are in the range of 0.198-0.260 Δ°2θ (Table 8.1) with the average value of 0.224 Δ°2θ (n = 17). A value of 0.360 for sample P-58 could be due to localised kinetic effect. The illite crystallinity values indicate that they belong to the upper anchizone grade (sub-greenschist facies). A plot of illite crystallinity values of the Rong Kwang slate versus distance is shown in Figure 8.10.

The metamorphism of the Rong Kwang Formation sediments is contemporaneous with the Late Triassic deformation that produced slaty cleavage in slate.

### 8.5.3 Metamorphism of the Wang Chin Formation

The illite crystallinity values of the pelitic rocks of the Wang Chin Formation are in the range of 0.203 - 0.253 $\Delta°2\theta$ (Table 8.1) with the average value of 0.215 $\Delta°2\theta$ (n = 11). The illite crystallinity values indicate that they belong to upper anchizone metamorphic grade (sub-greenschist facies) transitional to the epizone grade (greenschist facies). The low illite crystallinity values (reflecting better crystallinity of illite) of the Wang Chin Formation shale/slate compared to slates of the Rong Kwang Formation are probably related to the higher strain associated with the late west-directed thrusting. A plot of illite crystallinity values versus distance is shown in Figure 8.10.

The metamorphism of the Wang Chin Formation sediments, like the Rong Kwang Formation, is contemporaneous with the Late Triassic deformation that produced slaty cleavage in slate.

## 8.6 Summary

### 8.6.1 Summary of structure

The rocks exposed along the Phrae-Sirikit Reservoir traverse include the Permo-Carboniferous Pha Som Metamorphic Complex, the Permian Rong Kwang Formation and the Upper Triassic Wang Chin Formation.

The Pha Som Metamorphic Complex is more complexly deformed than the overlying rock units in the study area. The structures in this rock unit are comparable to $D_1$-$D_3$ structures in the Sirikit Dam area. The dominant structure along this transect is strongly-developed phyllitic cleavage which is equivalent to $S_2$ in the Sirikit dam area. Lenticular blocks of psammitic rocks are abundant in the matrix of pelites creating a fabric which is similar to that in tectonic melanges. The marked feature of the pelitic rock is the mineral stretching lineation which plunges consistently to the west-southwest. Crenulations in phyllite along this transect are very common and are correlated with $D_3$ crenulation in the Sirikit Dam area.

Structures in the Rong Kwang Formation are correlated with the $D_3$ structures in the Pha Som Metamorphic Complex in the Sirikit dam area. The cleavage-bedding intersection lineation, sub-parallel to the fold-axis, plunges

shallowly to the northeast and southwest. The cleavage is axial-planar to folds in interbedded of shale and sandstone or limestone. The cleavage dips steeply to the northwest and southeast. In the lower part of the rock unit, the structure is characterised by abundant lenticular clasts of limestone in strongly cleaved slate. Small-scale thrust faults are dominantly east-directed.

Structures in the Wang Chin Formation are correlated with those in the Rong Kwang Formation. The mesoscopic folds recognised along the transect are mainly of upright chevron folds with steeply-dipping axial plane cleavage. The strong cleavage development largely obliterates the bedding in most outcrops. Bedding-plane thrusts are common within interbedded slate, limestone and sandstone.

A cross-section was drawn from the available structural and stratigraphic data. Shortening of about 64% is suggested on the basis of the restored section. The amount of the shortening is consistent with the fold tightness and cleavage intensity in the Rong Kwang and Wang Chin Formations.

The Late Triassic structural development of the Phrae-Sirikit Reservoir area is relatively simple. Two generations of thrusting were recognised. The early east-directed thrusting involves the Pha Som Metamorphic Complex and the Middle Permian Rong Kwang Formation. The late west-directed thrusting, associated with folding of the Rong Kwang and the Upper Triassic Wang Chin Formations.

### 8.6.2 Summary of metamorphism

The Pha Som Metamorphic Complex along the Phrae-Sirikit Reservoir transect reached its peak during the formation of phyllitic cleavage, probably in Middle Permian. This peak was epizone (greenschist facies) metamorphic grade in a low to medium pressure metamorphic facies series.

The Rong Kwang Formation was metamorphosed to upper anchizone (sub-greenschist facies) grade in a low to medium pressure facies series. The metamorphism was apparently contemporaneous with the deformation that produced slaty cleavage, probably in the Late Triassic.

Wang Chin Formation was metamorphosed to upper anchizone metamorphic grade (sub-greenschist facies) transitional to the epizone grade (greenschist facies). The metamorphism was contemporaneous with the deformation that produced the slaty cleavage probably in the Late Triassic.

# Chapter 9

# STRUCTURE AND METAMORPHISM OF ROCKS ALONG THE LAMPANG-DENCHAI TRANSECT

## 9.1 Introduction

The cross-sectional study across the Lampang-Phrae area, was carried out between km 6.00 and km 75.00 on Highway 11 from Lampang to Denchai, a small town 25 km south-southwest of Phrae (Fig 9.1). However, the main outcrops of interest start from km 30.00. Between km 9.00 and 30.00, Highway 11 crosses the southern part of the Tertiary Mae Moh basin where most of the rocks of interest are concealed beneath Pleistocene basalts and Quaternary deposits. In general, this highway crosses the strike of the major rock units in the Lampang-Phrae area. Road-cuttings along this highway provide excellent exposures for a detailed structural study. The traverse was carried out on 1:25,000 scale with further detailed mapping (1:1000 scale) being done on a few excellent outcrops to obtain detailed structural data. For convenience, kilometre numbers referred to in the text are those applied for this highway unless it is indicated otherwise.

The general geology and stratigraphy of the Lampang-Phrae area is relatively well documented (e.g. Piyasin, 1972; Chonglakmani, 1981, 1983; Bunopas, 1981; Chaodumrong, 1992). The mapped rock units in this area include Permian sedimentary strata, Permo-Triassic volcaniclastic and volcanic rocks, Triassic sedimentary sequences, small intrusive bodies of Upper Triassic-Lower Jurassic granitic rocks and Pleistocene basalts (Fig. 9.1 and see also Fig. 1.2).

The Permian strata were mapped as the Huai Thak Formation (Piyasin, 1972). They consist dominantly of shale and tuffaceous sandstones. The felsic to intermediate volcanic rocks and volcaniclastic rocks have been commonly referred to as the Permo-Triassic volcanics by most workers (e.g. Bunopas, 1981, Chaodumrong, 1992). The Triassic strata were formally named as the Lampang Group (Piyasin, 1972) and its stratigraphic definition and classification have been modified or revised by later workers (i.e. Chonglakmani, 1981, 1983; Wolfrat, 1987; Chaodumrong, 1992). Granitic rocks in this area have not been fully

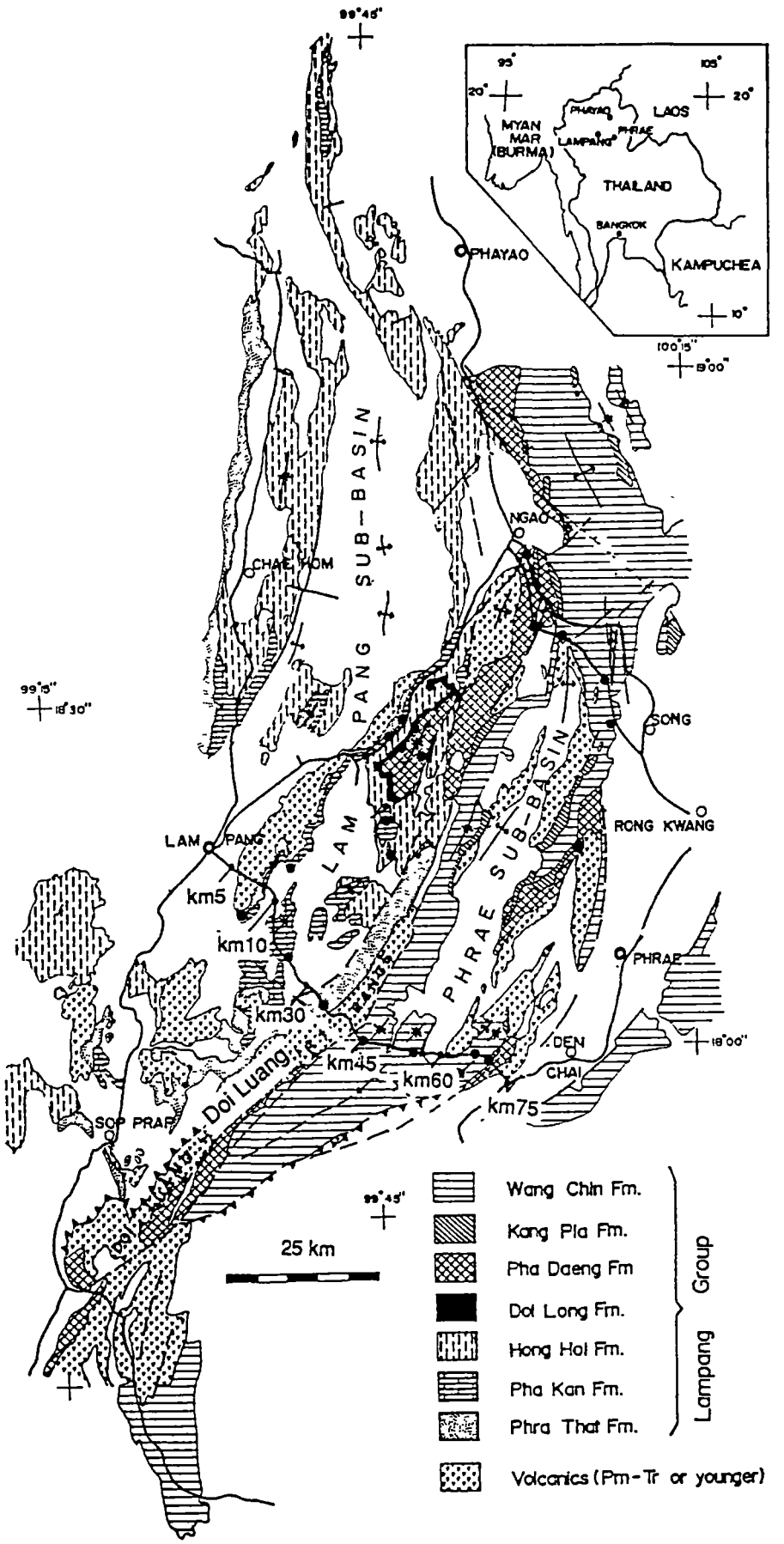


Figure 9.1 Simplified geological map of the Lampang-Phrae area showing distribution of the Triassic sequences and the Permo-Triassic volcanics (after Chaodumrong, 1992). Unfilled area is Tertiary and Quaternary cover.

documented possibly because they occur merely as small stocks compared to larger batholiths elsewhere. The Pleistocene basalts are restricted to two small areas near Lampang and Denchai (Piyasin, 1972). They belong to the alkali basalt series typical of a continental basaltic province (Barr and Macdonald, 1978, 1981).

Most previous workers have paid little attention to the detailed structure and deformation in the Lampang-Phrae area. It is the purpose of this chapter to document the structure and metamorphism in this area. The detailed mesoscopic (outcrop-scale) structures of the rock units along the traverse are used to place constraints on the interpretation of the regional structures and the structural history of this part of northern Thailand.

## 9.2 Lithostratigraphy and Petrography

The lithostratigraphic details of the rock units exposed along the Lampang-Denchai Highway (Figs. 9.1 and 9.2) are discussed in the following sections. Other rock units exposed elsewhere are also included to give complete information.

### 9.2.1 The Huai Thak Formation

The Huai Thak Formation is the upper-most rock unit of the Permian Ratburi Group in northern Thailand which has been divided into three formations, in ascending order, as the Kiu Lom, Pha Huat and Huai Thak Formations respectively (Piyasin, 1972). Bunopas (1981) renamed this rock group as the Ngao Group (equivalent to the Phrae Group in Chapter 8) and used it for a Permian sequence in the Lampang-Ngao area but restricted the use of the Ratburi Group to limestones and associated clastic rocks of the Permian age in peninsular Thailand only.

The Huai Thak Formation is exposed between km 56.00 and km 60.00. Piyasin (1972) previously mapped the sedimentary unit at this interval and adjacent area as the Pha Huat Formation which is typically a massive limestone unit. Lithologically, the sequence is more likely to belong to the overlying Huai Thak Formation which is characterised by a sequence of dark grey to brownish grey shale interbedded with thinly bedded, light grey to brown tuffaceous sandstones. Hence, the name Huai Thak Formation is more appropriate for the Permian rocks observed along this traverse.

**Lithology:** The Huai Thak Formation consists of very thinly to thinly bedded light grey to grey shale with minor interbedded thinly- to medium-bedded tuffaceous sandstones. The shale has moderately to well-developed bedding-plane

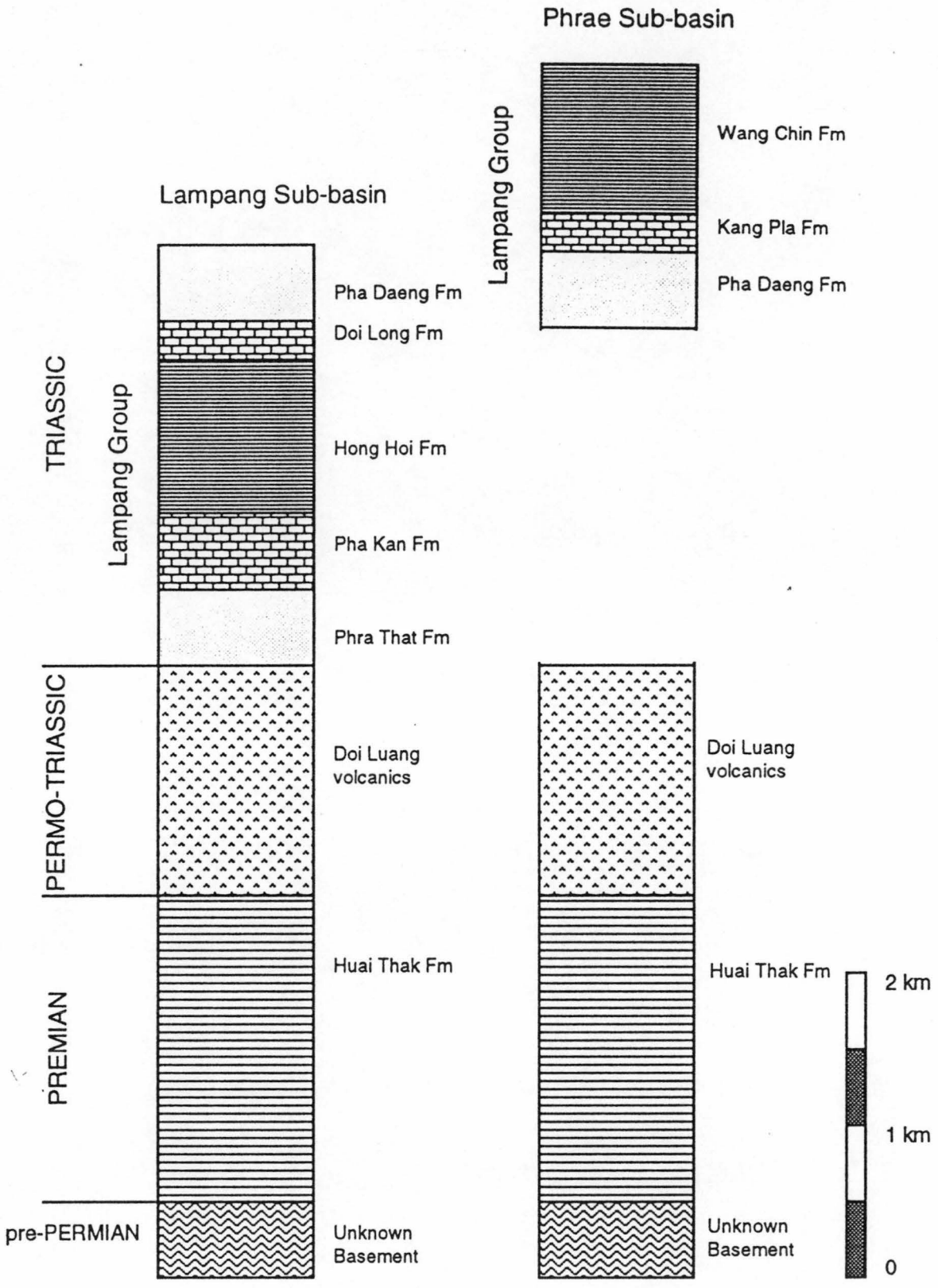


Figure 9.2 Generalised stratigraphic columns of lithostratigraphic units in the Lampang-Denchai area. See detailed discussion in text.

fissility. The sandstones are fine- to coarse-grained and contain appreciable amounts of weathered feldspar. These rocks are more deeply weathered than the adjacent Triassic strata along the same traverse. This is probably due to the higher contents of feldspar and volcanic lithic fragments which are more susceptible to weathering than detrital quartz, clay mineral and other types of lithic fragments in these rocks. This weathering effect hinders a detailed petrographic examination of the rocks.

**Thickness:** The Huai Thak Formation is folded and repeatedly faulted. An accurate measurement of its thickness is therefore impracticable. At the type locality, the thickness of the incomplete section was measured at 762 m, and hence, the total thickness of this formation was estimated to be somewhere between 1000 m and 1500 m (Piyasin, 1972).

**Contacts:** The base of the Huai Thak Formation is not exposed on this traverse whereas its upper part is faulted against the Permo-Triassic Doi Luang volcanics. Elsewhere in the Lampang area, it conformably overlies the massive limestone of the Pha Huat Formation and unconformably underlies the Permo-Triassic volcanics or the lowest part of the Lampang Group wherever the volcanics are absent (Piyasin, 1972).

**Fossils and age:** No fossils have been found on this traverse. At the type locality, the Huai Thak Formation contains brachiopods, pelecypods and bryozoans. The age of this rock unit was suggested as Upper Permian (Kungarian to Kazanian) on the basis of the brachiopods *Leptodus sp.* and *Orthotetes sp.* (Piyasin, 1972).

**Depositional environment:** The marine fauna indicate a marine environment of deposition for the sediments of the Huai Thak Formation. The high content of volcanic fragments of the rocks suggests the depositional basin proximal to a volcanic arc source, but no direct evidence for this suggestion was observed.

### 9.2.2 The Doi Luang volcanics

No formal name has been established for the volcanic and volcaniclastic rocks distributed throughout the central part of northern Thailand (i.e. the region between Lampang and Phrae). The name Volcanic Group was informally used by Piyasin (1972) for a sequence of volcanic rocks which usually unconformably underlies the Triassic Lampang Group and unconformably overlies the Upper Permian Huai Thak Formation. In this study, the informal name, the Doi Luang volcanics, will be used for convenience. The name of this rock unit is derived from Doi Luang (meaning a great mountain), a dividing range between Lampang and

Phrae where the volcanic and volcaniclastic rocks are extensively exposed. To date, no detailed investigation of the petrogenesis of the Doi Luang volcanics has been carried out probably due to the high degree of weathering and the scarcity of lavas.

The Doi Luang volcanics crops out in four separate intervals along the Lampang-Denchai highway, i.e. km 5.75-9.30, km 32.10-41.30, km 60.45-63.70 and km 69.00-74.00.

**Lithology:** The Doi Luang volcanics are characterised by a massive unit of volcaniclastic rocks with minor volcanic rocks. In general, the volcaniclastic rocks are strongly cleaved with respect to their volcanic counterparts. The dominant rock types are grey to green tuffs with minor green to reddish purple volcanic breccias. Rhyolite and dacite are restricted to thin layers within these massive volcaniclastics. The volcaniclastics are largely of rhyolitic to dacitic composition. Bedding is rare, but is recognisable in some localities where interbeds of mudstone and tuffaceous sandstone are present.

Between km 5.75 and km 9.30, the Doi Luang volcanics consists of massive dacite, rhyolite, tuff, lapilli tuff, volcanic breccia with intervening thin interbeds of mudstone and tuffaceous sandstone. Dacite is green, fine-grained, massive and fractured. Disseminated pyrite is common. Rhyolite is grey, fine-grained and massive. Tuff is pale green to green, medium-grained, massive. Lapilli tuff is purplish red to green, coarse-grained, massive and contains quartz and abundant feldspar fragments in a sandy matrix. Volcanic breccia is green, massive, grain-supported and composed of large angular to subangular fragments of dacite and rhyolite with smaller quartz and feldspar grains in a finer-grained green matrix. In the middle of the section, steeply-dipping, interbedded tuffaceous sandstone and mudstone are present. Tuffaceous sandstone is grey to pale green, medium grained, very thickly bedded to massive. The mudstone is dark grey to black, carbonaceous, slightly cleaved and very thinly to thinly bedded.

The section between km 32.10 and km 41.30 is characterised by massive dacitic tuff. A zone of cataclastic tuff, carbonaceous shale and tuffaceous sandstones occur between km 32.10 and km 33.80. Towards the top of the shear zone, near the contact with the Phra That Formation at km 32.10, grey to black shale with white stretched minerals on the cleavage contains black lenticular chert clasts. Fine- to medium-grained tuffaceous sandstone is light grey with abundant white feldspar fragments. The bedding is planar and is commonly medium thick. Graded bedding, convoluted lamination and flame structures are also present. Shale is light grey to black, laminated to very thinly bedded and has characteristically dark and white colour bands. Towards the bottom of this shear zone at km 33.80, where the rocks grade into the less deformed and more massive dacitic tuff, reddish purple

to greenish grey lineated phyllonitic tuff becomes more abundant.

Massive tuff and volcanic breccia are the principal rock types that crop out between km 60.45 and km 63.70. A volcanic breccia unit overlies a tuff unit at km 61.87. Towards the base and the top of the sequence, they grade into medium to thickly bedded tuffaceous sandstone alternating with thinly bedded shale. Tuff is green with disseminated dark-green chlorite spots, medium-grained and has weakly-developed cleavage. Green to reddish-purple volcanic breccia comprises pebble to cobble-size clasts of mainly red rhyolitic tuff and green dacitic tuff set in a green tuffaceous sandy matrix. Tuffaceous sandstone is light grey, fine to medium-grained. Shale is light grey, with well-developed cleavage.

Between km 69.00 and km 73.00, massive tuff and minor volcanic breccia are the dominant rock types as in the other section along this traverse. East-dipping interbeds of shale with minor siltstone are exposed at km 69.70. Massive tuff is green, weathered to brown or reddish-brown. Volcanic breccia is green containing clasts of mainly dacite and rhyolite. Part of these volcanics are reddish purple, probably due to oxidation during diagenesis and/or very-low grade metamorphism.

**Petrography:** Dacite (sample 21/151290) consists of idiomorphic phenocrysts of chiefly plagioclase with polysynthetic twins set in a groundmass of feldspar microlites together with quartz and fine-grained white mica. Plagioclase is partly altered to sericite, calcite and chlorite. Chlorite and sparry calcite totally replace former crystals of probable plagioclase.

Dacitic tuff (sample 22/151290) consists of broken feldspar crystals (totally replaced by sericite and microcrystalline quartz and calcite) in the matrix of microcrystalline quartz, fibrous white mica, chlorite, clay minerals and opaque material.

Lithic tuff (samples 2/161290 and 1/151290) is composed of framework grains of monocrystalline quartz, rock fragments and minor feldspars in a fine-grained matrix of microcrystalline quartz, feldspar microlaths with patches of sparry calcite and fibrous white mica veinlets. Quartz grains have straight extinction and are embayed with glassy materials. Feldspar is partially altered to sericite and calcite.

Lapilli tuffs (samples 2/151290, 3/151290 and 4/151290) have framework grains consisting of volcanic rock fragment, K-feldspar, zoned plagioclase and quartz set in a matrix of green-brown chloritised glassy or chloritised feldspar microlite and microcrystalline quartz. Volcanic lithic grains are characterised by numerous feldspar microlites. K-feldspar grains are largely broken, turbid and sericitised. Chloritisation is common. Plagioclase is extensively replaced by sparry calcite which also replaces some part of the matrix. One large fragment of volcanic

rock contains abundant pyrite.

Silicified tuffs (samples 6/161290, 7/161290, 31/161290, 32/161290 and 18/161290) consist of framework grains of chiefly monocrystalline quartz, feldspar and rock fragments set in silicified ash. Quartz grains are commonly embayed with volcanic glass. Some plagioclase grains are zoned and partially altered to calcite. Lithic grains are made up of siltstone, volcanic rocks, quartzite, recrystallised limestone and slate. Faint subgrains are commonly developed in relic quartz grains of some samples (e.g. sample 18/161290).

Sheared tuff (sample 1/111290) is composed of alkali feldspar (completely replaced by fibrous sericite) and clear quartz grains set in an altered matrix. Sericitised alkali feldspar grains are up to 3.5 mm in diameter. A weakly-developed foliation is defined by subparallel to parallel alignment of minute fibrous white mica. Secondary calcite and chlorite occur as replacement grains.

Tuffaceous lithic subarkose (sample 4/161290) is very fine- to medium grained, subangular to subrounded and poorly to moderately sorted framework grains of monocrystalline quartz, plagioclase and rock fragments set in a silicified matrix. Quartz grains having typical bipyramidal form invariably have straight extinction and glassy embayment. Plagioclase grains with polysynthetic twins are partly altered to calcite and minute fibrous white mica. Patches of sparry calcite in the matrix are common.

**Thickness:** The exact thickness of the unit is not known because of the poor stratification but it is estimated to be between 1000 m and 1500 m judging from the apparent thickness measured from the outcrops along the traverse. However, it is very likely that the thickness of this volcanic unit varies markedly. The accumulation of volcanic detritus would have been thickest close to the volcanoes and thin rapidly outwards.

**Contacts:** The Doi Luang volcanics is usually unconformably underlain by or is in fault contact with the Permian strata. Throughout the entire section it is unconformably overlain by or in fault contact with the lower part of the Lampang Group.

**Fossils and age:** No fossils have been found in the Doi Luang volcanics. Based on the fact that it commonly overlies the Upper Permian Huai Thak Formation and underlies the Lower Triassic Phra That Formation or the Pha Kan Formation, the age of the Doi Luang volcanics can be bracketed between Upper Permian and Lower Triassic.

**Tectonic setting of eruption:** Since there has been no petrochemical study for these volcanics, it is not possible at this stage to interpret their tectonic settings of eruption with confidence. The predominance of volcaniclastics over the

lavas and the acid to intermediate composition suggest that the Doi Luang volcanics may have erupted along the continental arc (e.g. the Sumatra arc in Indonesia) rather than in the oceanic island arc setting. The presence of black shale and tuffaceous sandstone in the upper part of this volcanic unit indicates subaqueous deposition probably in a shallow marine environment.

### 9.2.3 The Lampang Group

The Triassic sedimentary succession in northern Thailand has been assigned as the Lampang Group by Piyasin (1972). He divided the Lampang Group into five formations, in ascending order, as the Phra That, Pha Kan, Hong Hoi, Doi Chang and Pha Daeng Formations. Later, Chonglakmani (1981, 1983) revised the stratigraphy of the Lampang Group and proposed a new classification scheme. This new scheme includes only those formations which are essentially marine in origin. Some formations were redefined or replaced by a new name, i.e. the Phra That, Doi Chang, Hong Hoi and Doi Long Formations. The Pha Daeng Formation of Piyasin (1972) was excluded from the Lampang Group because of its non-marine characteristics. Chaodumrong (1992) reclassified the Lampang Group as follows: the Phra That, Pha Kan, Hong Hoi, Doi Long, Pha Daeng, Kang Pla and Wang Chin Formations respectively.

The sediments of the Lampang Group were considered as having been deposited in a large basin with eastward migration of the depocenter through time (Chonglakmani, 1981). Chaodumrong (1992) proposed a two-adjacent basins model, i.e. the Lampang sub-basin and Phrae sub-basin. Sediments of the Lampang sub-basin are considered to be older than those in the Phrae sub-basin based on fossil assemblages.

The overall thickness of the Lampang Group has been given by various workers at approximately 3000 m or greater (Piyasin, 1972; Chonglakmani, 1981) or between 2400 m and 3700 m (Bunopas, 1981). Chaodumrong (1992) with his two-basins model estimated the total thickness of the Lampang Group at 3000 m and 2000 m in the Lampang subbasin and Phrae subbasin respectively.

The Lampang Group almost everywhere unconformably overlies the Doi Luang volcanics and is conformably or unconformably underlain by the Permian sequence. It is to be noted, however, that The Lampang Group is also in fault contact with the older rocks in some places.

The Lampang Group commonly contains a diverse bivalve fauna and a few brachiopods with very few ammonoids indicating the age range from Scythian to middle Carnian or to probably lower Norian (Chonglakmani, 1981, 1983).

The following lithostratigraphic discussion of the Lampang Group is based on the stratigraphic classification scheme currently proposed by Chaodumrong (1992).

## The Phra That Formation

The Phra That Formation crops out between km 30.50 and km 32.10. This formation was named by Piyasin (1972).

**Lithology:** The Phra That Formation consists of a sequence of medium to thick beds of medium to coarse-grained sandstone and pebbly sandstone with minor siltstone and mudstone in its lower part and interbeds of siltstone, mudstone and minor very fine- to fine-grained sandstone in the upper part. Sandstone is white to grey, medium to thickly bedded. Siltstone is light green to maroon, laminated to very thinly bedded. Small-scale ripple marks, current bedding and cross laminations are common sedimentary structures in siltstone and fine-grained sandstone beds. Mudstone is maroon, moderately cleaved and medium to thickly bedded. Some mudstone beds, near the top of the sequence, contain flattened ellipsoidal carbonate nodules. Fining-upward sequences are common.

**Petrography:** Siltstones (samples 20/161290 and 21/161290), are laminated rocks consisting largely of silt-grade equant quartz grains (40-90 μm range with a mean of 60 μm) and minor amount of detrital white mica flakes (2x10 μm to 30x120 μm). Quartz grains are subangular to subrounded and occasionally have undulatory extinction. Interstitial finer-grained materials are a mixture of chlorite with minor white mica and other clay minerals and microcrystalline quartz and calcite. Pressure shadows around quartz grains are common and are composed of recrystallised microcrystalline quartz mixed with very fine fibrous white mica and chlorite. Weakly developed anastomosing-spaced cleavage defined by dark laminae of aligned white mica, chlorite and opaque material wraps around quartz grains with an angle of 20-30° to the lamination. Silt-size tourmaline and opaque minerals are accessory components.

Quartz arenite (sample 32/151290) is made up chiefly of fine to medium-grained, subangular to subrounded, and well-sorted monocrystalline quartz (100-400 μm range with a mean of 250 μm) framework grains. Quartz grains commonly have undulatory extinction and authigenic overgrowth. Fibrous overgrowth and recrystallised matrix of microcrystalline quartz and very fine-grained white mica form beards around framework grains. Strong parallelism of white mica defines foliation of the rock. Haematite occurs as either grain-coating or very fine dissemination (1-2 μm) throughout the rock. A few tourmaline and zircon grains

are also present.

Sheared sandstone (sample 2/121290) is very fine- to fine-grained and consists of clear monocrystalline quartz grains (40-200 μm range with a mean of 100 μm) and detrital white mica flakes in a microcrystalline mixture of fibrous white mica and quartz. Few lithic fragments are detrital quartzite. Some quartz grains have small irregular cracks filled largely with fine-grained fibrous white mica. A weakly-developed S-C fabric is common. Quartz grains commonly show pressure solution effect expressed by recrystallised microcrystalline quartz in the pressure shadows. Accessory tourmaline is also present in a sand-size fraction.

**Thickness:** In the type area at Ban Tha Si, 40 km north of Lampang, the measured thickness of the Phra That Formation has been reported to be 200 m (Piyasin, 1972) and 650 m (Chonglakmani, 1972). This difference is probably due to the different traverses chosen by these workers. Elsewhere, the thickness of this formation ranges from 100 to 840 m (Chonglakmani, 1981) or 90 to 650 m (Chaodumrong, 1992). The incomplete section exposed between km 30.50 and km 32.10 was measured at 500 m in this study.

**Contacts:** On this traverse, the boundary between the base of the Phra That Formation and the top of the Doi Luang volcanics is marked by a shear zone at km 32.10. Elsewhere, this formation unconformably overlies the Doi Luang volcanics or the Permian strata and is conformably overlain by limestones of the Pha Kan Formation.

**Fossils and age:** No fossils have been found in the present study. However, in the other localities, this formation contains bivalves, ammonoids, and brachiopods which indicate the age range from Lower Triassic (Scythian) to middle Carnian. At Ban Tha Si, a limestone bed in the lower part of the formation contains *Eumorphotis multiformis* which is the characteristic form of the Scythian age whereas the middle part contains a *Costatoria* assemblage of lower Anisian age (Chonglakmani, 1981). The conodont *Neospathodus pakistanensis* of uppermost Dienerian to lowermost Smithian age (Lower Triassic) was reported from an interbedded limestone cropping out near Pra Tu Pha limestone quarry, 50 km north of Lampang (Chaodumrong, 1992).

**Depositional environment:** Sediments of the Phra That Formation are thought to have been deposited in a near-shore fan-delta type environments (Chonglakmani, 1983). On the basis of facies analysis and sandstone petrography, these sediments were interpreted as having been deposited in tidal environments where quartzose detritus were derived from sedimentary or volcanic sources (Chaodumrong, 1992).

## The Pha Kan Formation

The Pha Kan Formation has been found as isolated inliers within Pleistocene basalt flows along the traverse between km 9.50 and km 22.00. The formation name was proposed by Piyasin (1972). Chonglakmani (1981) renamed this formation as the Doi Chang Formation. However, the original name is used in this study.

**Lithology:** The Pha Kan Formation consists dominantly of carbonates characterised by interbeds of lime mudstone, peloidal packstone, wackestone and oolitic grainstone with minor intercalated shale and sandstone. The limestones are generally grey to dark grey and well-bedded to massive. Stylolitic seams are common post-depositional features in massive limestones. Medium-bedded calcareous sandstones are occasionally interbedded with medium to thickly bedded oolitic grainstone.

**Petrography:** Dolomitic wackestone (sample 35/161290) consists of oncoids, ooids and bioclasts in a matrix of dolomitised pseudospar. The main skeletal components are bivalve and crinoid fragments. Rhombic dolomite crystals are common.

Dolomitic lime mudstone (sample 37/161290) consists almost entirely of dolomitised pseudospar with few scattered fragments of bivalves and echinoderms (crinoids). Rhombic dolomite crystals are common.

Peloidal packstone (sample 38/161290) consists chiefly of peloids with scattered fragments of bivalves, crinoids and foraminifera in a micrite matrix.

Oolitic grainstones (samples 28/161290 and 29/161290) consist of ooids (75-80%), oncoids (0-5%) and skeletal fragments (5%) cemented by drusy sparite (15%). Rounded ooids (0.5-2 mm in diameter) having either skeletal fragments or peloids as the nuclei are of layered concentric types and some are composite ooids. Spherical to subspherical oncoids, ranging from 5 to 8 mm in diameter, have a dense fabric composed mainly of spongiostromate with rare algal laminae (porostromate). Bioclasts consist of gastropod and bivalve fragments together with a few relics of foraminifera.

Calcareous subarkose (sample 30/161290) consists of mainly monocrystalline quartz and minor polycrystalline quartz together with feldspar grains (predominantly plagioclase) cemented by drusy sparite. The framework grains are subangular to subrounded, moderately sorted, ranging in size between 30 and 600 μm with a mean of 100 μm. Grains appear to float in the calcite cement. Quartz grains are often corroded and etched at their margins. The other mineral

grains present are chlorite, opaque materials, white mica and volcanic lithic fragments.

**Thickness:** The thickness of this formation cannot be measured due to the scatter of the outcrops but elsewhere it has been shown to be in the range of 80 to 500 m (Chonglakmani, 1981) and 400 to 640 m (Chaodumrong, 1992).

**Contacts:** The Pha Kan Formation conformably overlies the Phra That Formation and underlies the Hong Hoi Formation.

**Fossils and age:** No fossils have been discovered in this study but a large number of fossils have previously been found in this formation. The characteristic fauna of ammonoids, bivalves and brachiopods indicate an age range from upper Anisian to upper Carnian (Chonglakmani, 1981). The conodont *Neospathodus pakistanensis* of the Lower Triassic (uppermost Dienerian to lowermost Smithian) was reported from a limestone bed at km 9.60 (Chaodumrong, 1992).

**Depositional environment:** The lack of an elongate barrier-reef, fore-reef deposits and a marked slope-break typical of rimmed shelf together with a small areal extent of this carbonate unit, led Chaodumrong (1992) to conclude that the Pha Kan Formation probably represents a drowned carbonate ramp platform. This carbonate ramp platform facies grades from the landward part towards the basinal facies (i.e. the Hong Hoi Formation).

## The Hong Hoi Formation

The Hong Hoi Formation is not exposed along the traverse but a few outcrops were studied particularly in the Mae Moh areas, 15 km north of the traverse and also an isolated outcrop at km 577.00 on the Phaholyothin Highway (Highway 1), approximately 20 km south of Lampang. This formation is the most widespread rock unit of the Lampang Group in the Lampang area.

**Lithology:** The Hong Hoi Formation is characterised by a sequence of thinly bedded grey shale interbedded with thin to medium beds of greenish grey sandstone and minor limestone. At km 577.00 on the Phaholyothin Highway, this formation consists of an alternating sequence of thinly-bedded grey limestone and shale. The basal part of this formation exposed at Mae Chang canal is dominated by an olistrostrome-like unit. Large blocks of limestone, conglomerate and sandstone up to 5 m in diameter in a sandy to shaly matrix are the marked features.

**Petrography:** The sandstone of the Hong Hoi Formation are mainly lithic arkose and feldspathic litharenite characterised by abundant plagioclase feldspar and volcanic rock fragments with minor quartz and plutonic rock and rare sedimentary

rock fragments (Chaodumrong, 1992).

**Thickness:** The thickness of the Hong Hoi Formation cannot be measured due to the scatter of the outcrops. At Ban Tha Si, 35 km north of Lampang, a complete section was measured at 1200 m by Piyasin (1972) and 1900 m by Chonglakmani (1972).

**Contacts:** This formation conformably overlies the Pha Kan Formation and underlies the Doi Long Formation.

**Fossils and age:** An unidentified fossil ammonoid was discovered in this study near the Mae Chang Dam. Elsewhere, the Hong Hoi Formation contains numerous marine fauna. Fossil bivalves and ammonoids indicate an age range from Scythian (upper Griesbachian) to lower Norian (Chonglakmani, 1981).

**Depositional environment:** The Hong Hoi sediments were interpreted, based on facies associations and vertical facies sequences, as mud-dominated submarine fan deposits (overbank and channel-levee deposits) with detached sand bodies (Chaodumrong, 1992).

## The Doi Long Formation

The Doi Long Formation is not exposed along the traverse. The formation name was proposed by Chonglakmani (1981) to replace the Doi Chang Formation of Piyasin (1972) and is followed by Chaodumrong (1992).

**Lithology:** This unit is basically carbonate-dominated, consisting chiefly of light grey, massively-bedded, finely crystalline limestone and occasional dolomitic limestone (Chonglakmani, 1981; 1983).

**Petrography:** The limestones vary in texture from packstone to grainstone of peloids, oncoids and algal debris with minor bioclasts, ooids and stromatolite beds or lenses (Chaodumrong, 1992).

**Thickness:** The thickness of the Doi Long Formation has not been measured in the present study because the section is not exposed in the study area but elsewhere it was measured at 230 m by Chonglakmani (1981) at Doi Huai Long on the western limb of Tha Si syncline near Ban Tha Si. In addition, it has been noted that this formation has a limited geographic distribution and probably has lensoidal shape (Chaodumrong, 1992).

**Contacts:** This formation has a gradational contact with the underlying Hong Hoi Formation. Its upper boundary has been placed at the top of a limestone bed below a basal limestone conglomerate at the base of the Pha Daeng Formation (Chonglakmani, 1981; 1983).

**Fossils and age:** The Doi Long Formation contains an indeterminate

fauna of bivalves and brachiopods and gastropods (Piyasin, 1972; Chonglakmani, 1972). However, it is considered to be middle Carnian age on the stratigraphic grounds (Chonglakmani, 1981; 1983).

**Depositional environment:** Sediments of the Doi Long Formation were interpreted as a carbonate sequence of a regressive ramp platform grading from clastic turbidites of the Hong Hoi Formation (Chaodumrong, 1992).

## The Pha Daeng Formation

The Pha Daeng Formation is not exposed in the study area. This formation was considered to be the uppermost unit of the Lampang Group by Piyasin (1972). Later, Chonglakmani (1981) excluded the Pha Daeng Formation from the Lampang Group on account of its redbed characteristic but he also noted that it has the same deformation style as the other formations of the Lampang Group unlike the younger redbeds of the Jurassic-Cretaceous Khorat Group. However, the Pha Daeng Formation has been reinstated in the Lampang Group by Chaodumrong (1992).

**Lithology:** This unit consists mainly of red to maroon sandstone, siltstone, shale and conglomerate with subordinate limestone conglomerate and grey sandstones (Chonglakmani, 1981; Chaodumrong, 1992).

**Petrography:** The sandstones of the Pha Daeng Formation are lithic arkose and feldspathic litharenite with increasing quartz content and decreasing grain size up the sequence (Chaodumrong, 1992).

**Thickness:** The thickness of this formation ranges from 200 to 700 m (Chaodumrong, 1992). At the type locality at Doi Pha Daeng (meaning a red-cliff hill), 4 km east of Ban Tha Si, various authors have given the estimated thickness of 500 m (Piyasin, 1972), 600 m (Chonglakmani, 1981), 400-500 m (Bunopas, 1981) and 700 m (Chaodumrong, 1992).

**Contacts:** The Pha Daeng Formation is shown to have distributed in both the Lampang and Phrae sub-basins (Chaodumrong, 1992). It has a conformable contact with the underlying Doi Long Formation in the Lampang sub-basin. However, it also unconformably overlies the Permo-Triassic Doi Luang volcanics where the lower part of the Lampang Group is absent, especailly in the Phrae sub-basin (Chaodumrong, 1992). This formation is conformably overlain by the Kang Pla Formation.

**Fossils and age:** No fossils have been discovered in this study. A lower middle Carnian assemblage including *Halobia styriaca*, *Halobia cassiana*, *Palaeocardita singularis* and *Cassianella tenuistria* of the *Halobia styriaca* zone has been reported from the upper part of the formation along the Rong Kwang-Ngao

Highway (Chonglakmani, 1981).

**Depositional environment:** The Pha Daeng redbeds are interpreted to represent fan-delta type sediments deposited in a shallow-marine environment (Chaodumrong, 1992).

## The Kang Pla Formation

The name Kang Pla Formation was first proposed by Chonglakmani and Tiyapun (1985) and later adopted by Chaodumrong (1992) for the limestone sequence overlying the Pha Daeng Formation in the Phrae sub-basin. This formation is exposed at km 69.00 on the Lampang-Denchai Highway. It can be traced along strike from the road-cutting section northwards to Doi Pha Lak Muen where a large limestone quarry provides an excellent exposure of this formation.

**Lithology:** The Kang Pla Formation consists mainly of limestone with minor sandstone and mudstone. The limestone is grey, thinly bedded to massively bedded.

**Petrography:** In thin section, the grainstone (sample 8/151290) consists of ooids and skeletal grains cemented by calcite sparite. Minor amount of detrital grains of medium- to coarse-grained, subangular to subrounded quartz and rock fragments are also present. Lithic grains are chiefly volcanic rocks with minor chert.

The peloidal packstone (sample 5/151290) consists chiefly of flattened peloids and few bioclasts in a microspar (10-30 μm) matrix. Bioclasts are entirely rounded crinoid ossicles having a micrite envelope. Silt-size detrital grains of quartz are also present.

Lithic subarkose (sample 6/151290) contains fine-grained monocrystalline quartz, plagioclase and lithic fragments cemented by cryptocrystalline to microcrystalline quartz with patches of sparry calcite. Dolomite rhombs and calcite veinlets are common. A few zircon grains are present.

**Thickness:** The thickness of this formation at km 69.00 was measured in this study at 40 m but it apparently becomes much thicker northwards from the road cutting. Chonglakmani (1981) reported the thickness of about 500 m at Ban Kaeng Luang, 20 km northeast of Long while Chaodumrong (1992) measured a 76 m thick section at km 45.50 on the Ngao-Song Highway which was designated as the type locality.

**Contacts:** The Kang Pla Formation conformably underlies Wang Chin Formation and disconformably overlies the Doi Luang volcanics at km 69.00 on the Lampang-Denchai highway. It has been reported to conformably overlie the Pha

Daeng Formation at km 45.50 on the Ngao-Song Highway (Chaodumrong, 1992) and disconformably overlies the Doi Luang volcanics at Ban Pha Kho, 15 km north of Long (Chonglakmani, 1981).

**Fossils and age:** This formation ranges in age from middle Carnian to lower Norian. Chaodumrong (1992) found the lower Norian conodont *Epigondodella abneptis* in a limestone bed at km 69.00. The middle Carnian *Halobia comata* and *Spiriferina sp.* were reported from the grey limestone at Ban Pha Kho, 15 km north of Long (Chonglakmani, 1981).

**Depositional environment:** The Kang Pla Formation was interpreted to have the same type of depositional environment as the Pha Kan Formation, i.e. it probably represents a drowned carbonate ramp platform (Chaodumrong, 1992). This carbonate ramp platform facies grades from the landward facies towards the basinal facies (the Wang Chin Formation).

## The Wang Chin Formation

The name of this unit was first adopted by Wolfrat (1987) for a sequence of mudrock and sandstone in the Wang Chin area, 65 km southeast of Lampang which is equivalent to the Hong Hoi Formation. Chaodumrong (1992) disagreed with Wolfart's correlation but still retained the original name and re-defined it as a new formation.

**Lithology:** The Wang Chin Formation is lithologically very similar to the Hong Hoi Formation. The major part of this formation is made up predominantly of mudstone with subordinate sandstone. This is marked by the massive appearance of the mudstone that occasionally contain laminated to very thinly-bedded fine-grained sandstone or siltstone. The other part of this formation also contains, though in a minor proportion, a sequence of alternating beds of mudstone and sandstone which have the distinct characteristics of a turbidite sequence. Continuous, planar, and parallel bedding is a characteristic feature of this sequence. It is also noted that, in many localities, massively-bedded mudstones apparently contain large lensoid to irregular blocks of calcareous sandstone or limestone. Mudstone has poorly- to well-developed cleavage. In the latter case, mudstone approaches slate in appearance. Sandstone is thinly to medium bedded and occasionally thickly-bedded.

**Petrography:** In thin section, the calcareous subarkose (sample 4/61290) consists of poorly to moderately sorted, very fine-grained, subangular quartz (70%) together with plagioclase grains (10%) in a fine-grained matrix of microcrystalline quartz, clay minerals, white mica and opaque materials. Calcite occurs as a

ubiquitous cement.

Calcareous litharenites (samples 5/6290 and 16/15290) are made up of fine- to medium-grained (100-400 μm), subangular to subrounded grains of monocrystalline and polycrystalline quartz (30-35%), rock fragments (8-15%), plagioclase feldspar (0-7%), bioclasts and ooids (0-10 %) cemented by sparry calcite (40-50%). Lithic grains include volcanic rock fragments and fine-grained mica schist. Bioclasts are entirely bivalve shells. Accessory minerals are zircon, tourmaline and white mica.

**Thickness:** The thickness of the Wang Chin Formation was not measured due to the incompleteness of the section. However, it has been estimated to be in the range of 600 m to over 1000 m (Chaodumrong, 1992).

**Contacts:** The upper boundary of the Wang Chin Formation is not present on this traverse. Elsewhere, it has been reported to be conformably overlain by the clastic rocks of possibly Jurassic age. The base of this unit is faulted against the Huai Thak Formation at km 56.05. At Ban Thung Laeng, about 22 km northeast of Wang Chin, it disconformably overlies a Permian limestone and shale possibly comparable to the Huai Thak Formation (Chonglakmani, 1981).

**Fossils and age:** Middle Carnian to lowermost Norian fossils have been reported from the Wang Chin Formation. At Ban Thung Laeng, the middle Carnian bivalves *Halobia styriaca* and *Halobia cassiana* were discovered in a bed of grey mudrock 150 m above the base of this formation and the lowermost Norian bivalves were reported from elsewhere in Ngao, Song and Thoen areas (Chonglakmani, 1981). The middle Carnian *Halobia styriaca* was also found at km 55.54 (Chaodumrong, 1992).

**Depositional environment:** The sediments of the Wang Chin Formation were interpreted to have been deposited in the same type of environment as the Hong Hoi sediments, i.e. they are mud-dominated submarine fan deposits (overbank and channel-levee deposits) with detached sand bodies (Chaodumrong, 1992).

### 9.2.4 Granitic and hornfelsic rocks

A small body of granitic rocks has intruded the Doi Luang volcanics and developed a contact aureole around its margin. It has also been reported to intrude a sandstone-shale sequence of the Wang Chin Formation further north of the traverse (Piyasin, 1972; Wannakasem, 1980). Along the traverse this granitic stock crops out between km 42.50 to km 43.25. It has a chilled margin and a contact metamorphic aureole on its eastern boundary.

## Granitic rocks

**Lithology:** The granitic rocks are leucogranitoids on the basis of their colour and mineralogy. They are medium-grained, non-porphyritic and consist essentially of quartz, feldspar with a small amount of muscovite. Many small-scale high-angle faults and veins cross cut this granitic stock.

**Petrography:** Granitic rocks (samples 2/111290, 12/161290 and 13/161290) are medium-grained, non-porphyritic rocks with typical hypidiomorphic-granular texture. The major mineral constituents include quartz (30-40%), K-feldspar (40-50%) and sodic plagioclase (20-30%). Identification of K-feldspar and sodic plagioclase was aided by staining. Based on electron microprobe analysis, K-feldspar composition is almost pure orthoclase ($An_0Ab_2Or_{98}$) and sodic plagioclase is albite ($An_{1-4}Ab_{90-99}Or_{0-7}$). Perthite and graphic intergrowth of quartz and K-feldspar are common. These granitic rocks are virtually devoid of ferromagnesian minerals except chlorite which is probably an alteration product of biotite. The structural formula of chlorite calculated from electron microprobe data assuming total iron as FeO is $[(Mg_{2.32}Fe_{2.35}Al_{1.15})(Al_{1.11}Si_{2.89})O_{10}(OH)_8]$ and can be classified as brunsvigite according to Foster 's classification (Foster, 1962). Muscovite is present in a very small amount and apparently occurs in two modes, i.e. as a primary mineral and as a fine-grained alteration product of K-feldspar. The structural formula of muscovite calculated from electron microprobe data assuming total iron as FeO is $[(K_{.81}Na_{.02})(Mg_{.08}Fe_{.06}Al_{1.88})\ (Al_{.76}Si_{3.24})O_{10}(OH)_2]$. Irregular networks of veinlets filled with epidote, calcite and chlorite are common. Epidote has average pistacite content of 18%. Accessory minerals include magnetite, zircon, sphene and apatite.

**Contact:** This granite stock has intruded volcanic rocks of the Doi Luang volcanics. Elsewhere, similar granitic stocks have been reported to intrude the Permian sedimentary sequence and the Triassic Lampang Group (Piyasin, 1972; Wannakasem, 1980).

**Age:** No radiometric age dating has been done for the granitic rocks in this area, but the cross-cutting relationship with the country rocks indicates that they are younger than the Wang Chin Formation which has an Upper Triassic (middle Carnian to lower Norian) age. Granitic bodies of this composition have not been seen to intrude any Jurassic redbeds in the northern Thailand region. On these grounds, the age of this granite stock can probably be bracketed as Upper Triassic-Lower Jurassic. Wannakasem (1980) also suggested the age of the leucogranitoids

and granitoids in the Doi Ngom area, Amphoe Long (approximately 20 km north of the studied granite stock) as Upper Triassic-Lower Jurassic.

**Tectonic setting of intrusion:** Apart from minor faulting and brecciation, the granitic rocks and the hornfelsic rocks in the contact aureole are relatively undeformed compared to the folded and faulted country rocks. From these observations, it is likely that this granite stock as well as the neighbouring granitic bodies are the result of post-tectonic intrusion.

## Hornfelsic rocks

The hornfelsic rocks occur in a narrow zone on the eastern margin of the granite stock. These rocks grade into the volcanic and volcaniclastic rocks of the Doi Luang volcanics further away from the contact zone.

**Lithology:** In the outcrop and hand specimen, these granoblastic hornfelses are characterised by dense and dark rocks. They are massive, lacking well-defined planar structure. The small-scale high-angle faults and veins commonly cross cut these hornfelsic rocks.

**Petrography:** In thin section, hornfelsic rocks (samples 4/111290 and 7/111290) consist chiefly of brownish green to bluish green amphibole (hastingsite) in either prismatic or nematoblastic form. Hedenbergitic pyroxene and andradite-grossular garnet occur as small granoblastic aggregates. Poikiloblastic crystals of garnet are present locally. The representative compositions of amphibole, clinopyroxene, garnet and other minerals are listed in Table 9.1 (see complete analyses in Appendix E). Interstitial quartz and plagioclase grains are anhedral. Quartz grains have straight extinction and occasionally have polygonal triple junction. Polysynthetic twins in plagioclase crystals and twin lamellae in granoblastic calcite crystals are common. Clinozoisite and epidote are also present. Accessory magnetite and sphene are scattered throughout the rocks.

**Contact:** These hornfelsic rocks are found only in a narrow zone on the eastern side the granite stock. They grade outwards to unmetamorphosed volcanic and volcaniclastic rocks of the Doi Luang volcanics.

**Metamorphism and age:** The presence of abundant hastingsitic amphibole indicates that these hornfelsic rocks have been thermally metamorphosed to hornblende-hornfels facies. As these contact metamorphic rocks are formed by granitic intrusion into the surrounding Doi Luang volcanics, the metamorphic age should be the same as the age of the intrusion, i.e. Late Triassic-Early Jurassic.

Table 9.1 Representative electron microprobe analyses of minerals in hornfelsic rocks.

| Mineral | Amph | Amph | | Cpx | Cpx | | Grt | | Ep | Ep |
|---|---|---|---|---|---|---|---|---|---|---|
| Sample no. | 4/111290 | 7/111290 | | 4/111290 | 7/111290 | | 4/111290 | | 4/111290 | 7/111290 |
| n | 11 | 12 | | 9 | 7 | | 10 | | 4 | 3 |
| SiO2 | 37.78 | 36.97 | SiO2 | 51.30 | 49.89 | SiO2 | 36.87 | SiO2 | 37 50 | 37.70 |
| TiO2 | 0.39 | 0.31 | TiO2 | 0.04 | 0.03 | TiO2 | 0.37 | TiO2 | 0.02 | 0.03 |
| Al2O3 | 11.49 | 10.46 | Al2O3 | 0.60 | 0.55 | Al2O3 | 6 64 | Al2O3 | 21.77 | 24.44 |
| Cr2O3 | 0.01 | 0.03 | Cr2O3 | 0.01 | 0.03 | Cr2O3 | 0.02 | Fe2O3$ | 15.15 | 11.63 |
| FeO* | 28.81 | 30.63 | Fe2O3# | 1.70 | 2.66 | Fe2O3# | 21.88 | MnO | 0.36 | 0.15 |
| MnO | 0.46 | 0.47 | FeO# | 9.74 | 16.36 | FeO# | 0.01 | MgO | 0.00 | 0.03 |
| MgO | 2.77 | 2.14 | MnO | 1.44 | 0.83 | MnO | 0.76 | CaO | 23.52 | 23.93 |
| CaO | 11.67 | 11.58 | MgO | 10.18 | 6.07 | MgO | 0.03 | Total | 98.33 | 97.92 |
| Na2O | 1.62 | 1.51 | CaO | 24.52 | 24.05 | CaO | 34.69 | | | |
| K2O | 1.66 | 1.78 | Na2O | 0.14 | 0.18 | Total | 101.27 | | | |
| F | 0.00 | 0.00 | Total | 99.67 | 100.65 | | | | | |
| Cl | 1.07 | 1.38 | | | | | | | | |
| Total | 97.72 | 97.26 | | | | | | | | |
| O = F, Cl | -0.24 | -0.31 | | | | | | | | |
| Total | 97.48 | 96.95 | | | | | | | | |
| | | | | | | | | | | |
| Oxygens | 23 | 23 | | 6 | 6 | | 12 | | 12.50 | 12.50 |
| | | | | | | | | | | |
| Si | 6.120 | 6.103 | Si | 1.965 | 1.954 | Si | 2.970 | Si | 3 002 | 2.990 |
| Al iv | 1.880 | 1.897 | Al iv | 0.026 | 0 025 | Al iv | 0 030 | Al iv | 0.006 | 0.016 |
| Sum Z | 8.000 | 8.000 | Fe3+ | 0.009 | 0.021 | Al vi | 0.599 | Sum Z | 3.007 | 3.006 |
| Al vi | 0.316 | 0.138 | Sum Tet. | 2.000 | 2.000 | Ti | 0.022 | Al vi | 2.049 | 2.269 |
| Ti | 0.047 | 0.038 | Al vi | 0.001 | 0.000 | Cr | 0.001 | Ti | 0.001 | 0.002 |
| Cr | 0.001 | 0.004 | Ti | 0.001 | 0.001 | Fe3+ | 1.327 | Fe3+ | 0.913 | 0.694 |
| Fe3+ | 0.566 | 0.724 | Cr | 0.000 | 0.001 | Fe2+ | 0.001 | Sum Y | 2.963 | 2.964 |
| Mg | 0.667 | 0.524 | Fe3+ | 0.041 | 0.057 | Mn | 0.052 | Fe2+ | 0.000 | 0.000 |
| Fe2+ | 3.340 | 3.506 | Fe2+ | 0.317 | 0 536 | Mg | 0.004 | Mn | 0.024 | 0.010 |
| Mn | 0.063 | 0.065 | Mn | 0.047 | 0.027 | Ca | 2.994 | Mg | 0.000 | 0.004 |
| Ca | 0.000 | 0.000 | Mg | 0.576 | 0.354 | Sum Cat. | 8.000 | Ca | 2.018 | 2.034 |
| Sum Y | 5.000 | 5.000 | Sum Oct. | 0.983 | 0.977 | | | Sum W | 2.042 | 2.048 |
| Fe2+ | 0.000 | 0.000 | Ca | 1.006 | 1.009 | | | Sum Cat. | 8.013 | 8.019 |
| Mn | 0.000 | 0.000 | Na | 0.010 | 0.014 | | | | | |
| Ca | 1.994 | 1.996 | Sum Cat. | 4.000 | 4.000 | | | | | |
| Na | 0.006 | 0.004 | | | | | | | | |
| Sum X | 2.000 | 2.000 | | | | | | | | |
| Ca | 0.031 | 0.053 | | | | | | | | |
| Na | 0.502 | 0.478 | | | | | | | | |
| K | 0.343 | 0.375 | | | | | | | | |
| Sum A | 0.876 | 0.906 | | | | | | | | |
| Sum Cat. | 15.876 | 15.906 | | | | | | | | |
| | | | | | | | | | | |
| Mg/Mg+Fe2 | 0.167 | 0.130 | Mg/Mg+Fe2 | 0.641 | 0.398 | Mg/Mg+Fe2 | 0.936 | Fe3/Fe3+Al | 0.308 | 0 233 |
| | | | | | | | | | | |
| | | | Wo | 0.507 | 0.509 | Alm | 0.000 | | | |
| | | | En | 0.289 | 0.178 | Py | 0.001 | | | |
| | | | Fs | 0 204 | 0.313 | Sp | 0.017 | | | |
| | | | | | | Gr | 0.329 | | | |
| | | | | | | Adr | 0.653 | | | |

* Total Fe as FeO.

# Calculated from stoichiometry.

$ Total Fe as Fe2O3

Note : Amphibole formulae are calculated by normalising the number of cations other than Ca, Na and K to 13.

# 9.3 Structural Analysis

The Upper Permian Huai Thak Formation and the Triassic Lampang Group have similar deformation style and history. On the basis of style and orientation, structures recognised in both rock units can be correlated. However, the mesoscopic structures developed in each of these rock units are discussed separately for convenience.

## 9.3.1 Structure of the Huai Thak Formation

The mesoscopic structures in the Huai Thak Formation are characterised by a series of close to open chevron folds with associated thrust faults.

### Folds

The outcrop-scale folds in the Huai Thak Formation are dominantly upright to inclined, close angular folds (interlimb angle between 30°-50°) with amplitude and wavelength of less than 1 m (Fig. 9.3a). Locally, folds with rounded hinge zones are also present, e.g. at km 59.78 on the Lampang-Denchai Highway (Fig. 9.3b). Minor fold axes plunge shallowly to the southwest parallel to cleavage-bedding intersection lineation (Fig. 9.4a). The axial planes of minor folds strike northeasterly and dip to the northwest (Fig. 9.4b).

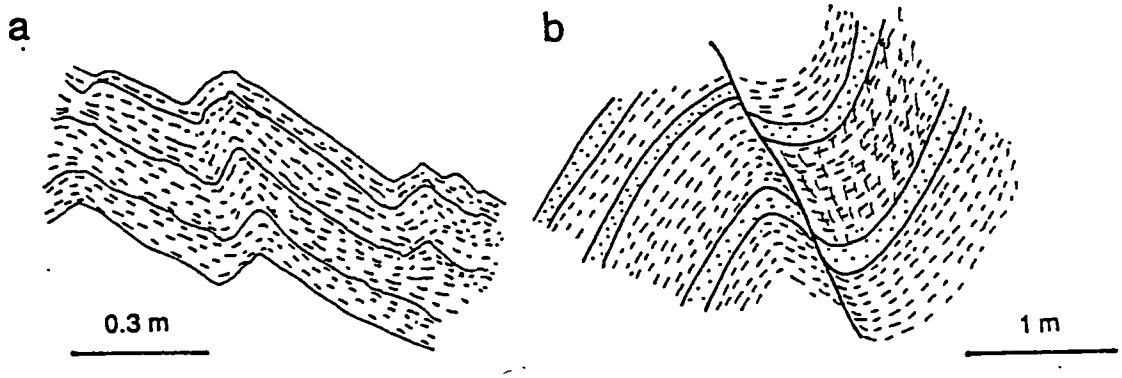


Figure 9.3 Line drawings from photographs of folds in the Upper Permian Huai Thak Formation. (a) Asymmetrical angular folds in shale at km 58.25 (looking south). (b) Cylindrical fold with rounded hinge in interbedded shale (dashed) and sandstone (stippled) at km 59.78 (looking south). Fold limb is truncated by a normal fault.

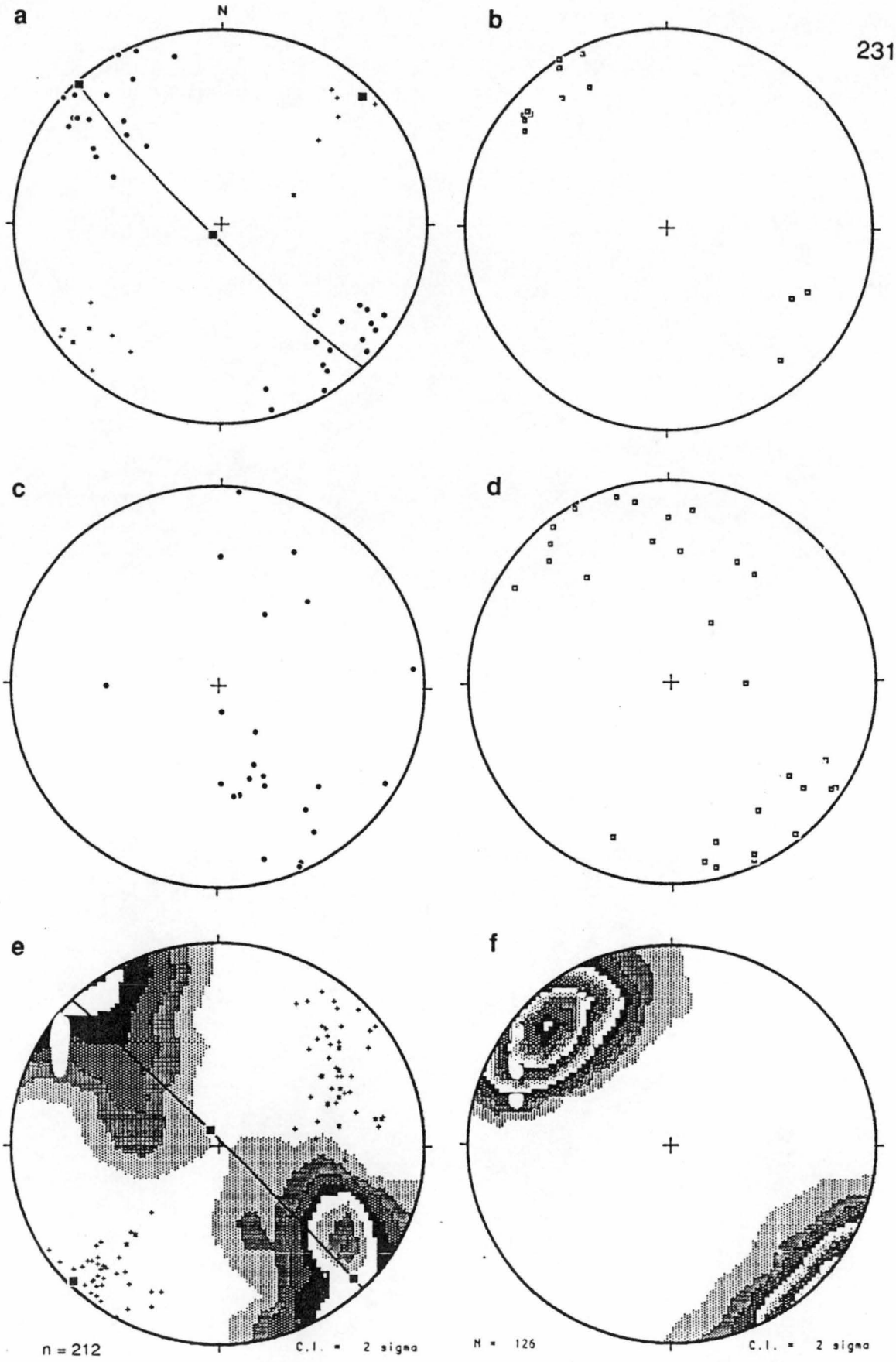
a
N
b
c
d
e
f
n = 212
C.I. = 2 sigma
N = 126
C.I. = 2 sigma

### Cleavage

The cleavage in the Huai Thak Formation is moderately to strongly developed and is axial-planar to mesoscopic folds in the interbedded shale and sandstone. This cleavage is subvertical and strikes northeasterly (Fig. 9.4b).

### Thrust faults

Outcrop-scale thrust faults are common in the Huai Thak Formation. The thrusting is dominantly east-directed (Figs. 9.5a, b&c). These thrusts were seen to truncate bedding and cleavage surfaces. Normal drag affects bedding and cleavage in narrow zones close to the thrust surfaces (Fig. 9.5b&c).

## 9.3.2 Structure of the Doi Luang volcanics

The structural features in the Doi Luang volcanics are not as clear as those developed in the other rock units. The dominant outcrop-scale structures are mainly joints and faults. In the bedded volcaniclastic sequence, folds were locally recognised. Narrow shear zones displaying intense deformation marked by strongly-cleaved rocks also occur within this rock unit.

### Folds

Outcrop-scale folds in the volcaniclastic part of Doi Luang volcanics are rare. Folds observed in the volcaniclastic layers are strongly variable in style and orientation suggesting distortion of bedding due to complex movement along local faults (Figs. 9.6a and 9.4c). At km 32.60 an open, inclined, rounded fold with an amplitude of about 1 m occurs in interbedded tuffaceous sandstone and shale. There is an axial-plane spaced cleavage associated with this rounded fold. A small-scale fault-bend fold occurs on its limb (Fig. 9.6b).

### Cleavage

A weakly to strongly-developed cleavage is common in the Doi Luang volcanics especially in the volcaniclastic facies (Figs. 9.6c&d). It is disjunctive cleavage according to the classification of Powell (1979). The orientation of cleavage varies considerably (Fig. 9.4d) possibly due to the effect of local faults as in the case of bedding.

### High-angle faults

Faults are easily recognised in the Doi Luang volcanics. At km 70.60, the

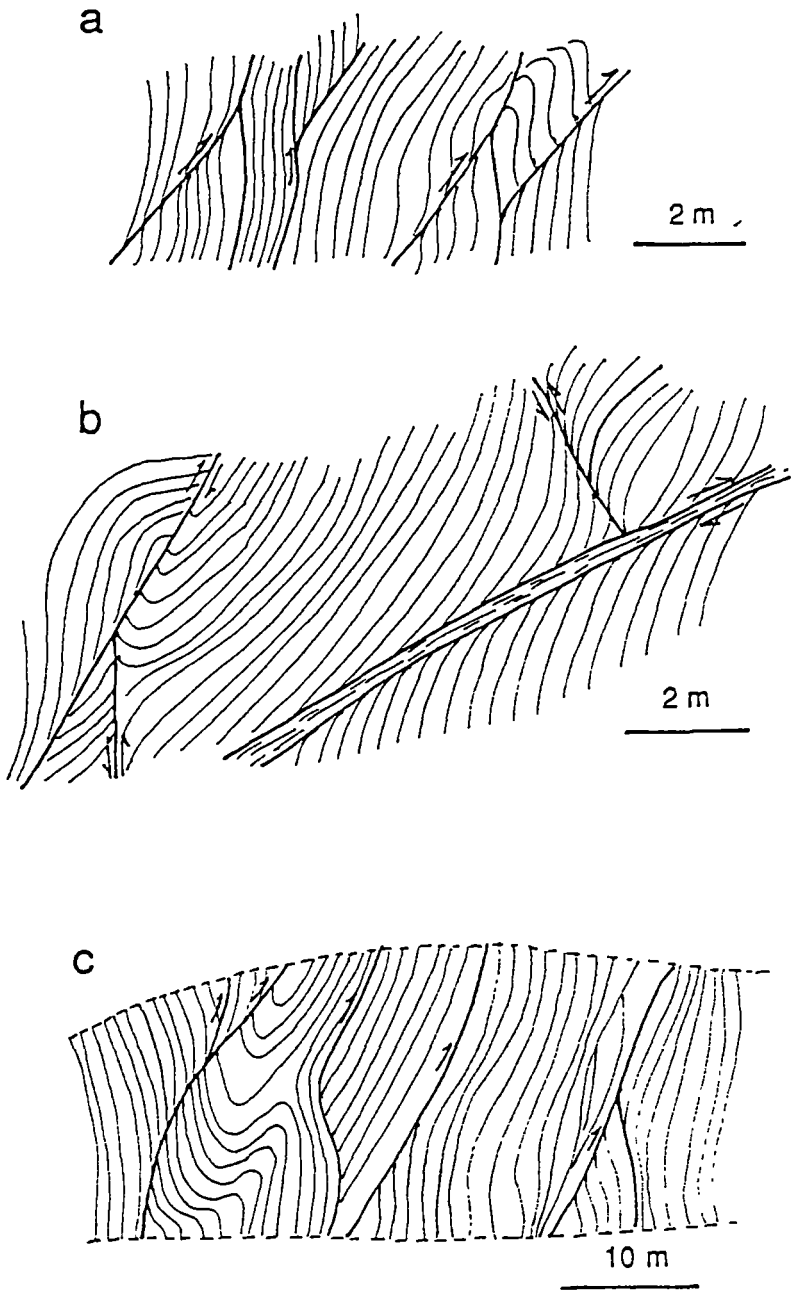


Figure 9.5 Outcrop sketches showing geometry of reverse faults (heavy lines) in the Huai Thak Formation (bedding traces are shown as light lines). (a) km 63.50 (looking south). (b) km 59.75 (looking northeast). (c) km 57.40 (looking north). The arrows show sense of shear determined from cleavage drag in narrow high strain zones adjacent to the faults.

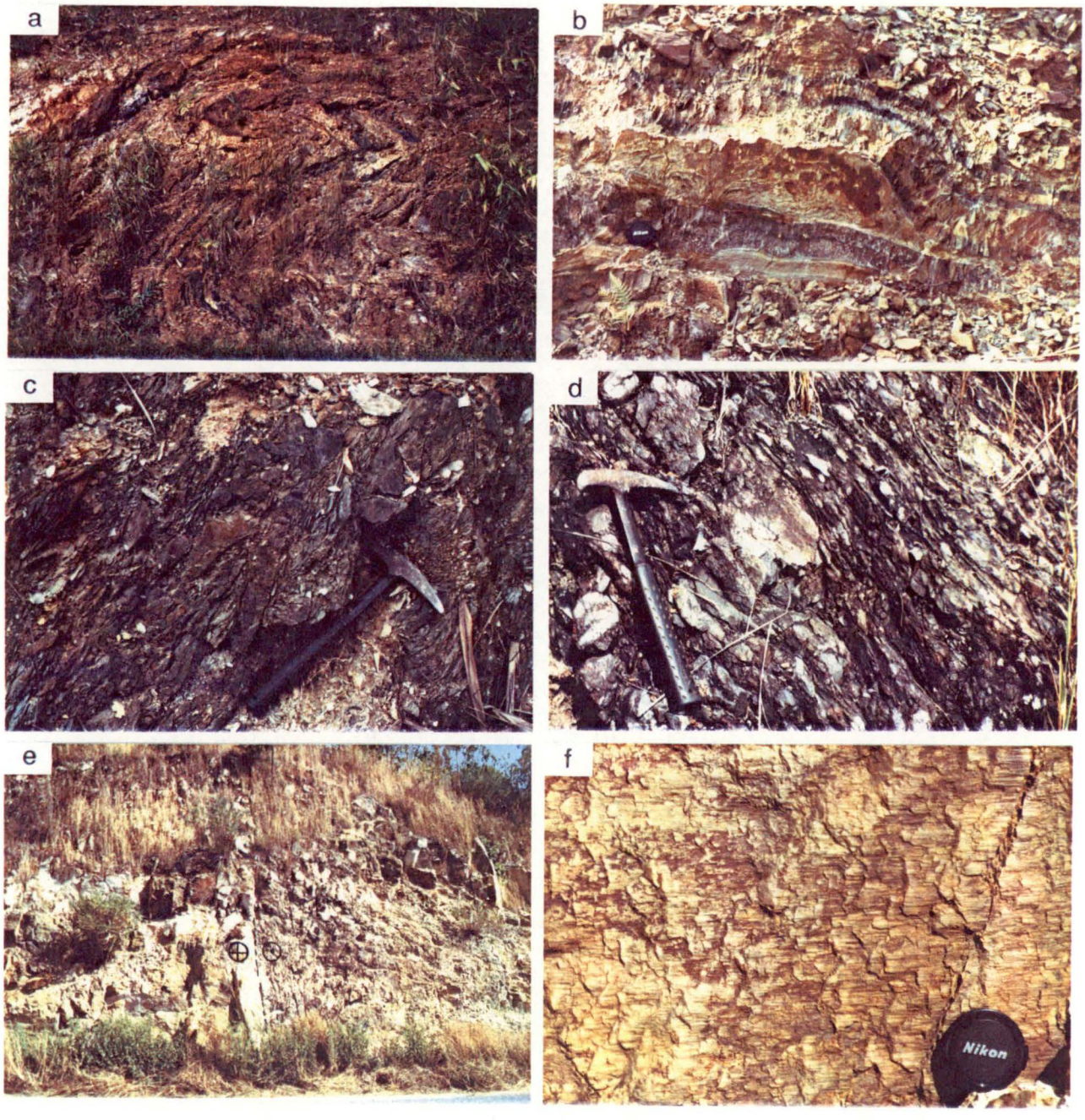


Figure 9.6 Photographs of structures in the Doi Luang volcanics. (a) Distorted beds in the volcaniclastics probably due to strong local thrust faulting at km 32.80 (looking southwest). (b) Small-scale fault-bend fold in the volcaniclastics at km 32.60 (looking southwest). (c) Cleavage in the shear zone at km 33.25. (d) Cleavage in volcanic breccia at km 60.85. (e) Dextral wrench fault in silicified volcaniclastics at km 70.60 (looking north). (f) Close-up view of the fault surface in (e) showing quartz fibres that indicate dextral movement (looking west). Scale: hammer is 280 mm long; lens cap is 52 mm in diameter.

main dextral strike-slip fault (Fig 9.6e), with the orientation of a fault plane of 035°/86°SE, cuts through silicified tuff. This strike-slip fault is marked by a narrow zone (2-3 m in width) of brecciated rocks. The dextral sense of movement on this strike-slip fault is indicated by quartz fibres on the fault plane (Fig. 9.6f). This fault cross-cuts two sets of earlier strike-slip faults. A sinistral set has a fault-plane attitude of 335°/80°NE and a dextral set has a fault-plane attitude of 285°/84°S. At km 7.00, a series of normal faults striking north-south and dipping steeply to the west and east are common. Thrust faults have not been observed in the Doi Luang volcanics.

### 9.3.3 Structure of the Lampang Group

The mesoscopic folds recognised along the traverse are mainly of upright chevron fold-style with steeply-dipping axial plane cleavage. Folds are best developed in the sequence of interbedded shale and sandstone or minor limestone. Cleavage intensity is variable depending on the lithology, nature of stratification, tightness of fold and position of rocks in the fold structure. Stratigraphic facing of bedding is mainly deduced from the angular relationship between bedding and axial plane cleavage because sedimentary structures, e.g. graded bedding or current ripples, which may be helpful in delineating stratigraphic facing are rather uncommon.

#### Folds

The outcrop-scale folds in the Lampang Group are open to close, upright to inclined angular folds with amplitude and wavelength of less than 2 m (Figs. 9.7a,b,c&d). Folds with bulbous angular hinge zones are present locally, e.g. at km 52.00 (Figs. 9.7e&f). Poles to bedding surfaces are broadly distributed along a great-circle girdle but two maxima are quite distinct (Fig. 9.4e). β-axis defined by the pole to the great-circle passing through these two maxima, is SW-trending and subhorizontal. Minor fold axes plunge shallowly to the northeast or southwest, and are approximately parallel to the cleavage-bedding intersection lineation (Fig. 9.4e). Steeply-plunging minor fold axes and cleavage-bedding intersection lineation occur locally, probably due to the effect of small faults.

#### Cleavage

The cleavage is weakly to strongly developed and is axial-planar to mesoscopic folds in the interbedded shale and sandstone or limestone (Figs. 9.7b&f). The cleavage dips steeply to the northwest and southeast (Fig. 9.4f). At

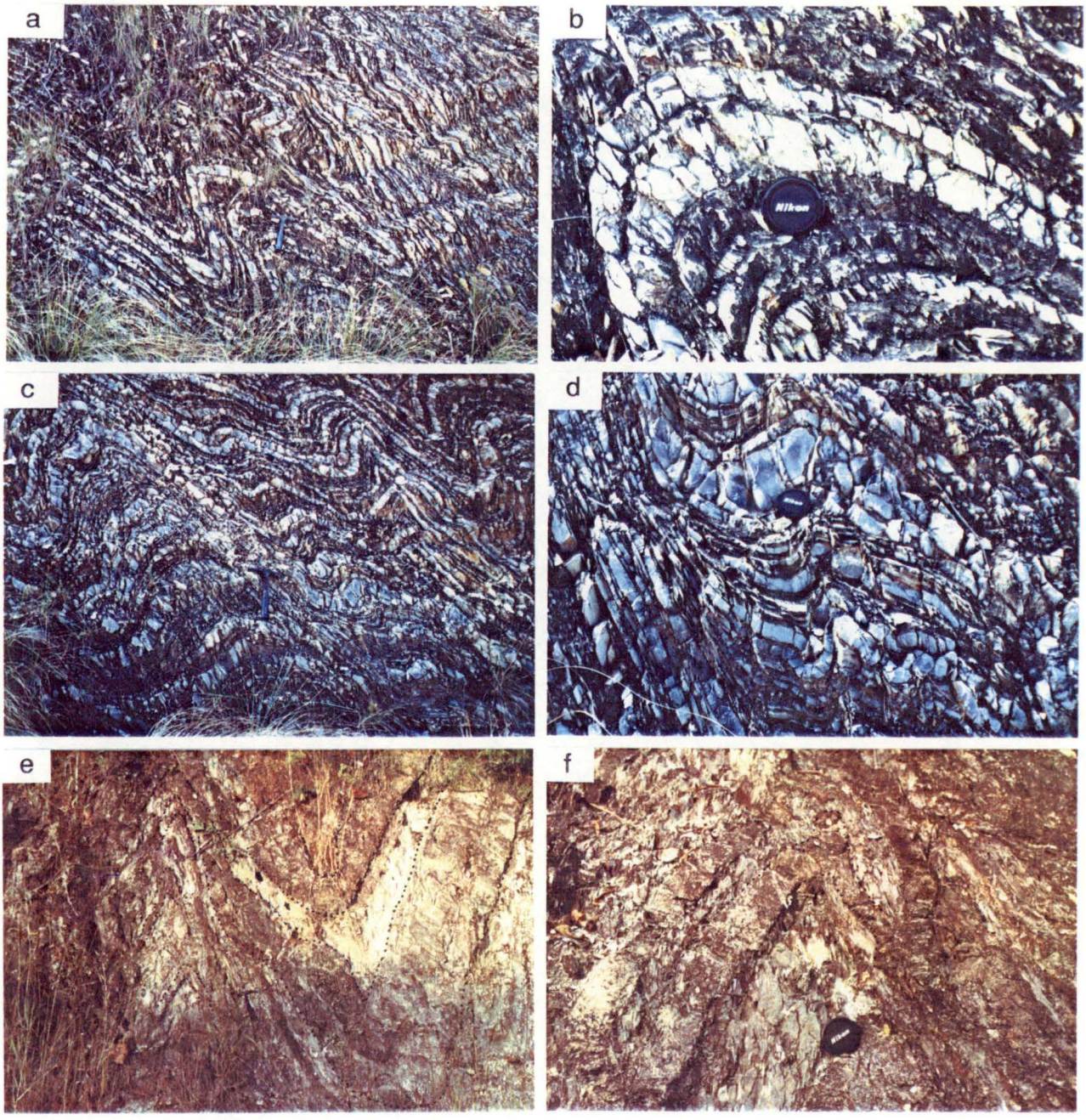


Figure 9.7 Photographs of outcrop-scale folds in the Lampang Group turbidites. (a)-(d) Inclined close folds in interbedded shale (dark) and limestone (light) of the Hong Hoi Formation at km 577.00 on the Phaholyothin Highway, about 15 km south of Lampang (looking southwest). Note the difference in cleavage spacing between limestone and shale in (b). (e)-(f) Upright close angular folds in interbedded shale (cleaved) and sandstone (uncleaved) of the Wang Chin Formation at km 52.00 on the Lampang-Denchai Highway. Note the bulbous fold hinge in (e). Scale: hammer is 280 mm long; lens cap is 52 mm in diameter. (e - f looking north.)

km 67.87 to km 67.91, cleavage is strongest in thin units of pebbly mudstone in which clasts of variable size of limestone and sandstone are abundant (Figs. 9.8a&b). The cleavage in adjacent interbedded shale and sandstone is weaker (Figs. 9.8c&d). The cleavage is slightly stronger in the hinge zone than in the limb (Fig. 9.8c&d). In interbedded fine-grained sandstone and mudstone at km 54.80, a moderately developed cleavage intersects bedding at high angle resulting in an anastomosing cleavage-bedding intersection lineation which are markedly displayed on bedding surfaces (Fig. 9.8e). On a plane normal to the intersection lineation, it is apparent that the cleavage domain coincides with the thinned sandstone beds which are in turn gently folded (Fig. 9.8f). The cleavage in the studied section is not the true slaty cleavage but rather pencil cleavage (e.g. Crook, 1964; Engelder and Geiser, 1979; Reks and Gray, 1982; Ramsay and Huber, 1983; Engelder and Marshak, 1985). This is consistent with the amount of shortening calculated for this particular section. Folds between km 63.70 and 68.80 are tighter than those between km 45.00 and 56.00. Cleavage intensity is apparently stronger in the former section than on the latter. The calculated amount of shortening of the folded strata (assuming that the error introduced by volume change is minimal) between km 63.70 and km 68.80 is 31% compared to the value of 21% for the latter section. Reks and Gray (1982) showed that the pencil structure commonly occurs where shortening is in the range of 9-26% whereas the slaty cleavage start to form beyond this range. Kisch (1991) showed that slaty cleavage developed at the strain around 50% and the good commercial slate are formed at higher strain (60-75%).

Microstructural features clearly demonstrate the differences in the degree of parallelism of phyllosilicates in strongly-cleaved and weakly-cleaved mudstones. Phyllosilicates in weakly to moderately developed cleavage (Figs. 9.9a,b&c) show only slight parallelism compared to strong parallel alignment in strongly-developed cleavage (Fig. 9.9d).

## Thrust faults

Small-scale thrust faults were observed locally in interbedded mudstone and sandstone. The thrust faults are mostly parallel to bedding, e.g. at km 55.82 (Fig. 9.10a&b) or cut across bedding at low angle forming a ramp geometry, e.g. at km 55.25 (Fig. 9.10c). In a few locations, bedding is truncated by steep thrust surfaces which shear off the hinge zones of synclines or anticlines, e.g. at km 52.00 (Fig. 9.10d). These thrusts are invariably southeast-directed.

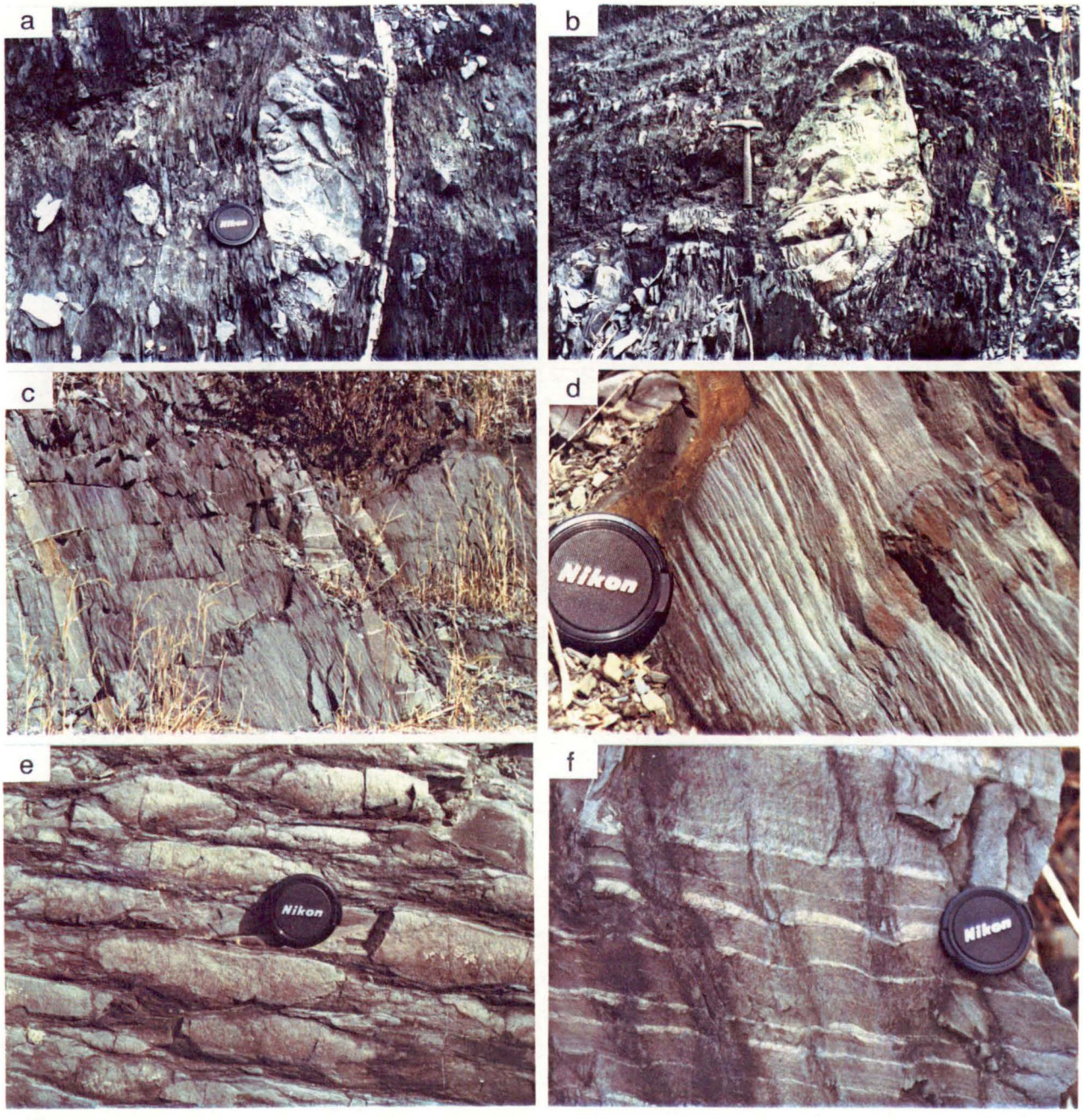


Figure 9.8 Photographs of cleavage in shale/slate of the Wang Chin Formation. (a)-(b) Lenticular clast of limestone (a) and sandstone (b) in strongly cleaved matrix in pebbly shale/slate at km 67.90. (c)-(d) moderately-developed cleavage in mudstone in the fold limb (c) and in the fold hinge (d) at km 67.20. (e) Anastomosed cleavage-bedding intersection lineation on the bedding plane and (f) section perpendicular to the lineation. Note the cleavage domain coincides with thinned sandstone layers. Scale: hammer is 280 mm long; lens cap is 52 mm in diameter.

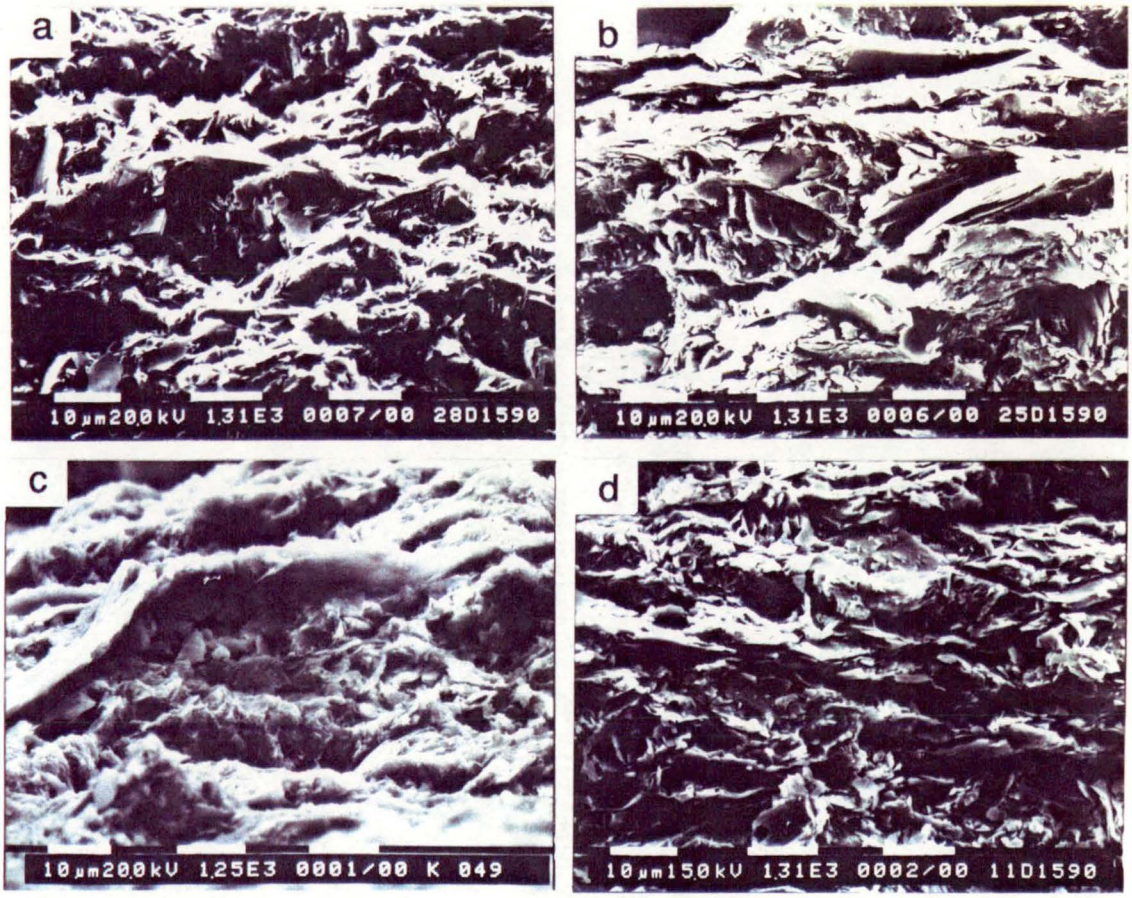


Figure 9.9 Scanning electron micrographs of cleavage in shale/slate of the Wang Chin Formation: (a) sample 28/151290; (b) sample 25/151290; (c) sample 24/151290; (d) sample 11/151290. Note the strong parallelism of phyllosilicates in (d) compared to (a)-(c). Scale bar is 10 µm long.


a

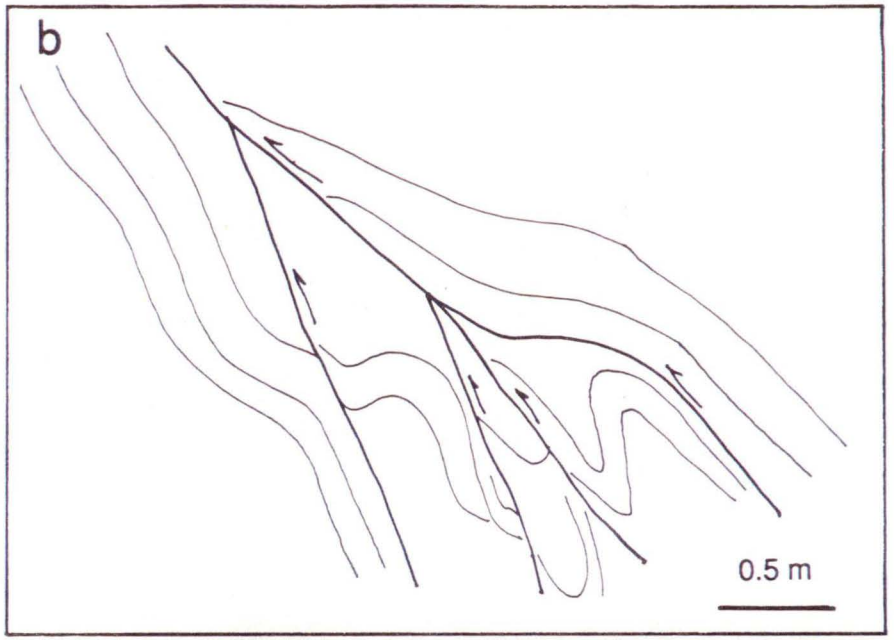
b
0.5 m

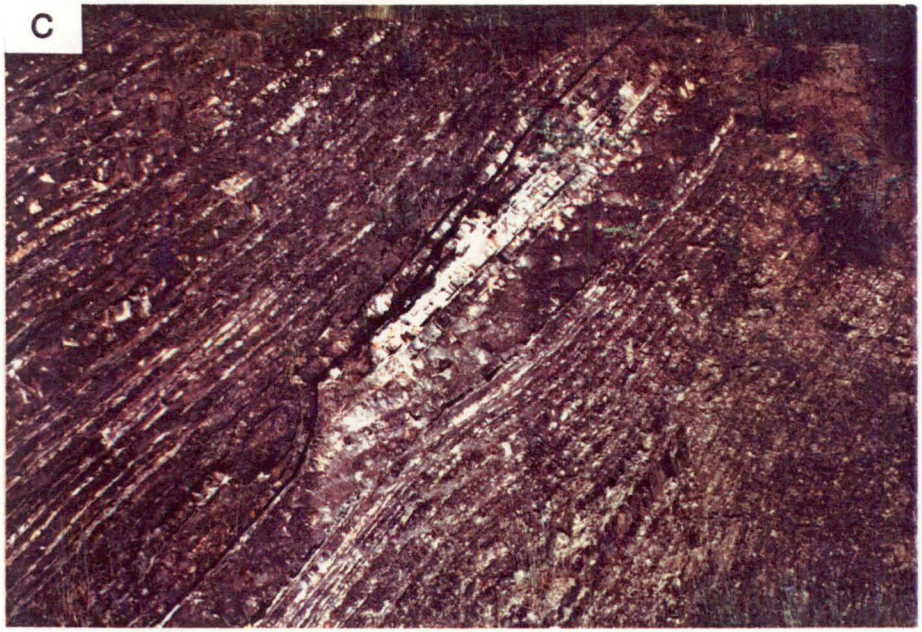
c


d

### 9.3.4 Structure of granitic and hornfelsic rocks

Granitic and hornfelsic rocks are massive unstratified rocks. The structural features commonly observed in these rocks are fractures and faults. The fault geometry in these rocks are similar to those observed in the Permo-Triassic Doi Luang volcanics.

## High-angle faults

Fractures and faults are common in the granitic and hornfelsic rocks. Faults are invariable high-angle with dominant strike-slip movement. Normal faults are associated with strike-slip faults. Three sets of faults are recognised (Fig. 9.11). The first set is N-S trending with dominant strike-slip component. The second set is NW-SE to WNW-ESE-striking with normal slip. The third set is NE-SW-trending with strong normal slip.

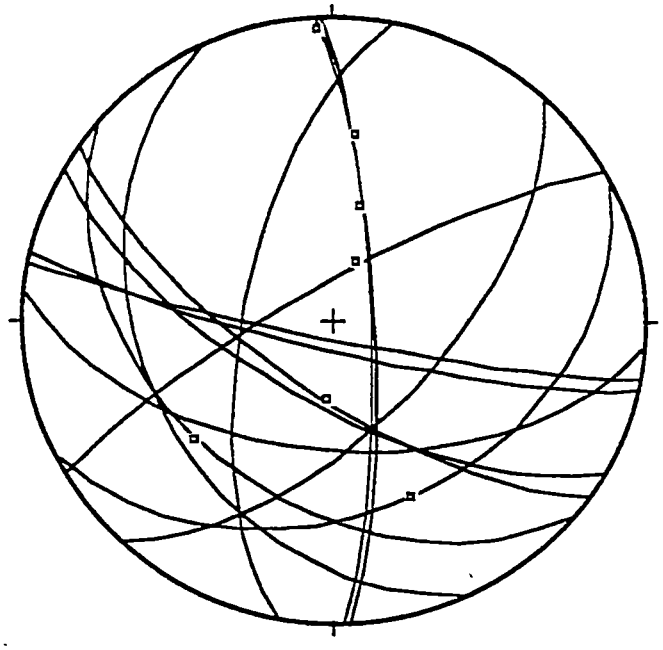

Figure 9.11 Lower-hemisphere equal-area stereographic projection of fault surfaces and fault striations in the granite and associated hornfelsic rocks.

# 9.4 Structural Interpretation

## 9.4.1 Basic concepts and limitations

The basic concepts and limitations in the structural interpretation have previously been discussed in Chapter 8. However, some additional points will be discussed as follows:

1. This section was drawn assuming thin-skinned deformation. One supporting line of evidence for thin-skinned style is that no older or basement rocks have been brought to the surface along any of the thrusts (Fig. 9.12). The basement is presumably a sequence of metasedimentary rocks of the Don Chai Group (equivalent to the Pha Som Metamorphic Complex). The detachment surface is inferred to be located within the basement or along the base of the Huai Thak Formation. This allows the depth to the detachment to be estimated but there is no independent data to support this depth estimate. A seismic survey may help resolve this problem in the future.

2. The thickness of the Permian sequence (including the Huai Thak Formation) used in drawing the cross-section is 2000 m.

3. The thickness of the Permo-Triassic Doi Luang volcanics is uncertain. This could vary markedly. However, the estimated thickness of 1500 m is used in the construction of the structural cross-section.

4. The thickness of the Triassic Lampang Group used for the construction of the structural cross-section is 3000 m in the Lampang sub-basin and 2000 m in the Phrae sub-basin following Piyasin (1972) and Chaodumrong (1992). Though the sedimentary sequence in the Lampang and Phrae sub-basins are not entirely time-equivalent, strong similarities in lithofacies and lithostratigraphic sequence suggest that they are facies-equivalent. To enable the construction of the cross-section, the Phra That, Pha Kan, Hong Hoi, Doi Long Formations (in the Lampang sub-basin) are treated as the equivalents of the Pha Daeng, Kang Pla and Wang Chin Formations (in the Phrae sub-basin).

5. In balancing the cross-section, local pins (pin 1 to pin 6) were used on folds to isolate problems in the section (Fig 9.13). It should be noted that some of these pins are not exactly vertical but rather used as a guide throughout the section.

## 9.4.2 Regional section

Discussion of the structures starts from the western end of the section (Fig.

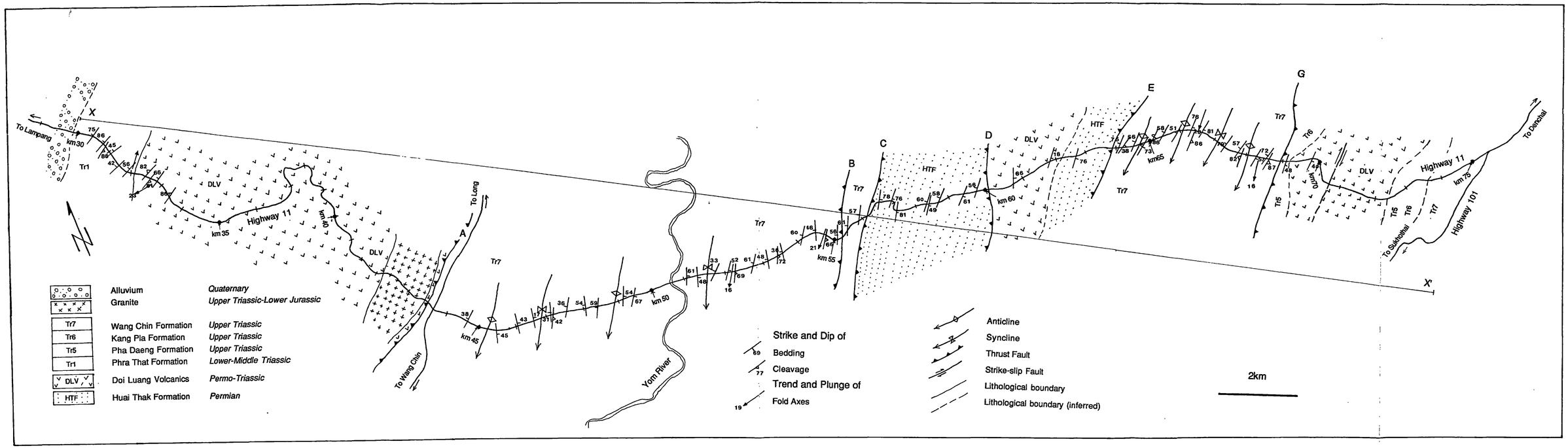


Figure 9.12 Structural map of the Lampang-Denchai transect.

9.13). For convenience, faults are labelled as A, B, C, D, E, F and G without any chronological connotation.

A fault shown in the westernmost part of the section (Figs. 9.12&9.13) is a thrust fault (fault A). The outcrop evidence of this fault is located near the spillway of the small dam, about 2 km north of km 44.50 on the Lampang-Denchai Highway. Thrust fault A branches off the main detachment fault located within the inferred basement. The depth of 7-8 km to the basement is estimated from the overall thickness of Permian-Triassic sequences (including the Permian Ngao Group, the Permo-Triassic Doi Luang volcanics and the Triassic Lampang Group). This thrust fault cuts through the Lampang Group sedimentary sequence down to the basement and brought the volcanic rocks of the Doi Luang volcanics in contact with the Wang Chin Formation. In addition, the lower part of the Lampang Group including the Phra That, Pha Kan and Hong Hoi Formations (shown as eroded part of the section on the hanging wall of fault A) may have been tectonically transported by this fault to rest on top of the Wang Chin Formation. However, the amount of fault throw is not constrained. It is estimated from the section to be about 10 km (Fig. 9.13). This fault is shown to be cross-cut by the Upper Triassic-Lower Jurassic granite stock as there is no structural evidence to suggest that the granite and associated hornfels have been affected by this fault. The granite is also shown as stoping into the section based on the lack of evidence for forceful intrusion in the exposed contacts.

Thrust fault B is modelled to account for the excessive apparent thickness of the Wang Chin Formation. The position of this fault at the surface is deduced from the outcrop-scale thrust faults in the Wang Chin Formation (e.g. Figs. 9.10a, b&c). Projection of this fault to depth is based on the geometry of major folds in the Wang Chin Formation (on the hanging wall of fault B). The position of cut-off, flat and ramp are interpreted corresponding to the anticline and syncline following Woodward *et al.* (1989). This thrust ramps through the lower part of the Lampang Group causing the repetition of the Wang Chin Formation. From the section, the estimated displacement along this fault is 5 km. This is poorly constrained.

Fault C is not directly evident from field observation. The position of this fault is interpreted from the contrast in bedding orientation of the Wang Chin Formation and the Huai Thak Formation. Fault C, analogous to an antithetic back thrust (e.g. Butler, 1982), is required to compensate for the movement along fault D (frontal ramp) which causes the back rotation of the Permian Huai Thak Formation. The steepening of bedding and tightening of folds in the Wang Chin Formation may be the results of this faulting. The displacement along fault C is uncertain.

Fault D is shown on the section as a branch from fault E (Fig. 9.13). The

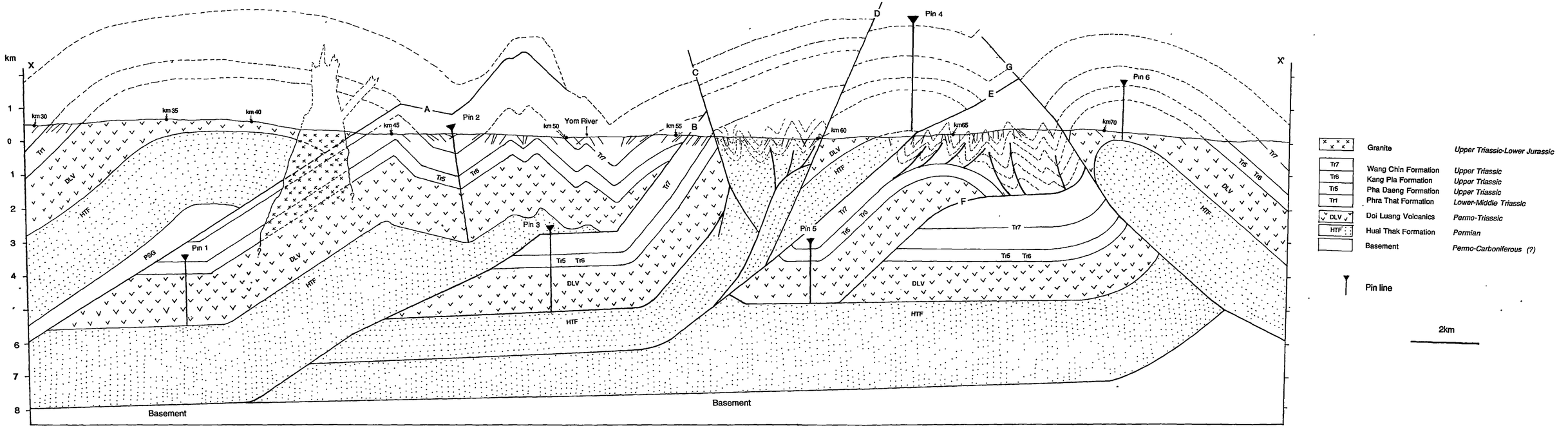


Figure 9.13 Interpretive cross-section of the Lampang-Denchai transect (along line XX' in Figure 9.12) including a restored template (on the opposite page).

surface expression of fault D is indicative of high-angle fault. The outcrop-scale thrust faults in the Huai Thak Formation near fault D (e.g. Figs. 9.5a, b&c) consistently indicates top-to-the-east sense of movement of this fault. The blind duplex at depth (located between the branching point and the topographic surface) is required to maintain the thickness of the Huai Thak Formation. The blind imbricate thrusts near the tip of this duplex are shown to terminate at the cores of the anticlines, the scenario similar to the fault-propagation folds (e.g. Suppe, 1983; Suppe, 1985). This fault is responsible for the back rotation of the hanging wall block and the uplift of the Permian strata reminiscent of inverted structure. The possible displacement along fault D is 3 km.

Fault E is shown to cut through the Permian sequence as a flat and then ramped through the sequence of the Doi Luang volcanics and the Lampang Group creating the triangular zone when combined with late west-directed thrust G. This fault crops out at km 63.70 as a narrow west-dipping zone (about 1-2 m wide) of cataclasites. However, the evidence of slip direction (e.g. fault striations) is obscured by intense weathering. The Wang Chin Formation within the triangular zone is greatly shortened as indicated by fold tightening and strongly developed axial-plane cleavage compared to the other part of the section. In addition, illite crystallinity values of shale/slate in this triangular zone, particularly close to faults E and G, indicate the higher metamorphic grade compared to the rest of the regional section (see detailed discussion in section 9.5). The shortening across this particular interval is estimated to be 6 km from the interpretive cross-section (Fig. 9.13) with the probable original length of 16 km. The displacement along fault E is not well constrained, it is estimated to be 7.5 km.

A blind duplex on top of the ramp (fault F) is shown within the triangular zone between fault E and fault G. Fault F is drawn to satisfy the assumption of thin skinned deformation. The position of the ramp at depth is not well constrained. The estimated displacement along fault F is shown here as 3 km, but this is rather speculative.

In the eastern end of the section, a west-directed thrust (fault G) is modelled. There is no direct field evidence of this fault, but the contrast in bedding orientations and the missing stratigraphy lend support to this interpretation. The east-dipping bedding and cleavage in the Kang Pla limestone and the Doi Luang volcaniclastic rocks on the eastern side of fault G suggests the easterly dip of this fault. This fault appears to occur late in the deformation event of the Permian-Triassic sequences across the section as suggested by the cross-cutting relationships with other thrust faults west of it. The movement of this late thrusting is probably responsible for the tightening of folds in the Wang Chin Formation between km

63.70 and km 68.80. It brought the Triassic package and Permo-Triassic Doi Luang volcanics from lower structural level into contact with the Wang Chin Formation. The amount of throw of fault G is estimated at 5 km.

The restored section length between pin 1 and pin 6 (Fig. 9.13) is 51.6 km and the present length is 27.7 km indicating an overall shortening of 23.9 km (46%). Much of the shortening is accommodated by thrust faulting at depth and only minor portion by folding at the shallow level. It should be noted that the shortening is not evenly distributed. Some parts are shortened more than the others and it can be seen that the style of structure varies according to the amount of shortening of the rocks (Fig 9.13). The fold tightness and cleavage intensity increase near the major faults.

### 9.4.3 Structural development

The structural development of the Lampang-Denchai area is relatively simple. Only a single folding event with associated thrusting was recognised in the Permian-Triassic sequences. The cleavage in these sedimentary sequences is axial planar to the folds, and thus both folds and cleavage are most likely to represent the same deformation event. The timing of folding and thrusting is constrained by the age of the youngest unit in the section affected by this deformation (i.e. the lower Norian Wang Chin Formation) and the age of post-kinematic granite and associated hornfelsic rocks (Upper Triassic-Lower Jurassic). Recent K-Ar dating of fine mineral fractions of shale/slate indicates that the cleavage formed between 188-220 Ma (Ahrendt *et al.*, 1993). The radiometric age and the structural relationships consistently point to an Upper Triassic age for the deformation in this region. This deformation event is proposed here to be the result of the collision between the Shan-Thai and Indochina terranes (detailed discussion is given in Chapter 11).

## 9.5 Metamorphism

Metamorphism of rocks along the Lampang-Denchai transect was studied via the illite crystallinity of pelitic rocks (see Chapter 1 for the technique of illite crystallinity measurement).

The illite crystallinity values of the pelitic rocks (shale/slate) of the Triassic Lampang Group are in the range of 0.25-0.36 $\Delta^\circ 2\theta$ (Table 9.2) indicating that they belong to lower to upper anchimetamorphic zones according to the scale of Kisch (1980a, 1980b, 1990). Unfortunately, the pelitic samples collected from the Permian Huai Thak Formation are rather weathered so they are not appropriate for

Table 9.2 Illite crystallinity values of pelitic rocks from the Lampang-Denchai Highway.

| Sample no. | Location | IC $\Delta o2\Theta$ |
|---|---|---|
| | *Wang Chin Formation* | |
| 30/151290 | km48.50 | 0.29 |
| 29/251290 | km52.32 | 0.36 |
| 28/151290 | km53.05 | 0.32 |
| 27/151290 | km54.40 | 0.29 |
| 24/151290 | km55.85 | 0.32 |
| 18/151290 | km64.53 | 0.25 |
| 17/151290 | km65.80 | 0.30 |
| 2/71290 | km66.40 | 0.28 |
| 6/61290 | km67.20 | 0.31 |
| 12/151290 | km67.90 | 0.32 |
| 3/6290 | km68.47 | 0.28 |
| 11/151290 | km68.47 | 0.25 |
| 2/6290 | km68.53 | 0.26 |
| LP-3 | km65.00 | 0.26 |
| LP-4 | km66.00 | 0.25 |
| LP-8 | km55.22 | 0.27 |
| LP-9 | km54.00 | 0.27 |
| LP-10 | km52.00 | 0.28 |
| LP-11 | km49.00 | 0.30 |
| LP-13 | km47.80 | 0.27 |
| LP-14 | km46.60 | 0.29 |
| LP-24 | km44.00 | 0.34 |
| | *Phra That Formation* | |
| 35/151290 | km31.61 | 0.32 |
| LP-22 | km30.60 | 0.27 |
| LP-23 | km32.05 | 0.26 |
| | *Huai Thak Formation* | |
| LP-18 | km59.75 | 0.32 |
| LP-20 | km57.37 | 0.32 |

illite crystallinity study. For comparison, the illite crystallinity measurements were carried out on the least weathered samples and the values of 0.33 Δ°2θ (sample LP-18) and 0.32 Δ°2θ (sample LP-20) indicate the lower anchimetamorphic grade of this formation. The plot of illite crystallinity on a transect broadly reflects the relationship between metamorphic grade and structural level, position of rocks in the major structures and the amount of strain involved (Fig 9.14). However, the strongly-cleaved rocks yield lower illite crystallinity values (i.e. higher grade) than the poorly- to moderately-cleaved rocks. For instance, slate between km 63.70-68.80 have lower illite crystallinity values than the rest of the section (Figs. 9.13 and 9.14). The axial plane cleavage in shale/slate is defined by parallel alignment of illite and other phyllosilicate phases. The parallelism of the phyllosilicates in slates is largely due to mechanical rotation which has also been accompanied by syntectonic crystallisation and preferred growth of new phyllosilicates (White and Knipe, 1978; White and Johnson, 1981). On this ground, the K-Ar ages of 188-220 Ma for the formation of the cleavage in section 9.4.3, would also represent the metamorphic age of these pelitic rocks. As there is no major granite batholith in this area, it is unlikely that the granitic intrusions in the Late Triassic-Early Jurassic could have a regionally extensive thermal reset of the K-Ar ages in the shale/slate.

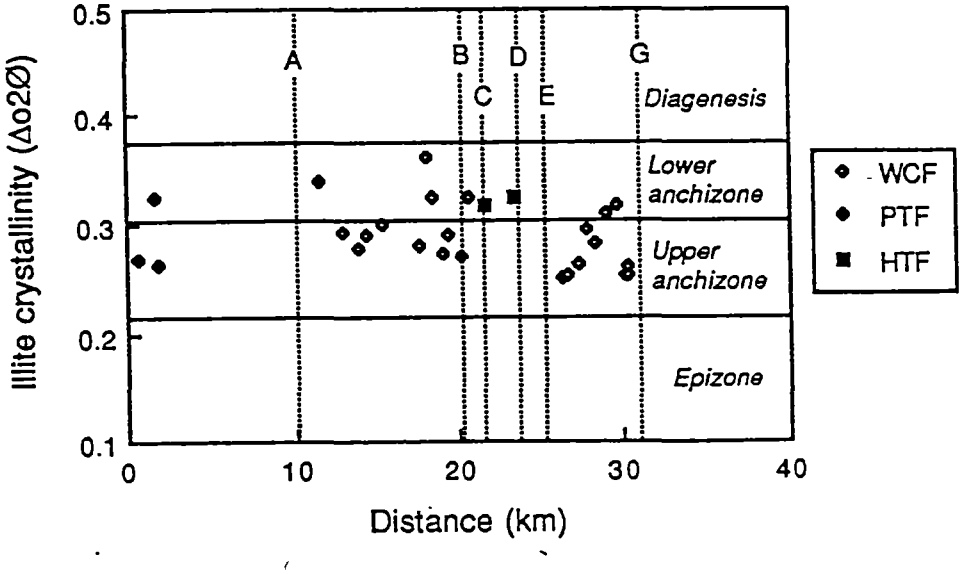


Figure 9.14 Illite crystallinity values of pelitic rocks along the Lampang-Denchai transect. Also shown are position of thrust faults from Figure 9.13.

## 9.6 Summary

From the data and the interpretations discussed in the previous sections, the stratigraphy, structure and metamorphism of the rocks along the Lampang-Denchai transect can be summarised as follows:

The exposed rock units along the transect include the Permian Huai Thak Formation (the upper rock unit of the Permian sequence), the Permo-Triassic Doi Luang volcanics, the Triassic Lampang Group, and a small intrusive body of Upper Triassic-Lower Jurassic granite. The exposed Permian strata consist dominantly of shale and tuffaceous sandstones of probable forearc setting. The Doi Luang volcanics includes felsic to intermediate volcanic rocks and volcaniclastic rocks. The Triassic Lampang Group consisting of turbidite sequence and carbonates deposited in the forearc basin.

The structural styles of the Huai Thak Formation and the Triassic Lampang Group are very similar though thrust faults are more common in the former. Mesoscopic structures are characterised by upright to inclined open to close folds with variably-developed axial plane cleavage. Overall shortening of 23.9 km (46% shortening) was estimated for the Permian-Triassic sequences shown in the regional cross-section. Much of the shortening is accommodated by thrust faulting and only minor portion by folding. This relationship arises from the assumptions of a thin skinned style for the thrusting. The shortening estimated here is probably a maximum value.

Only a single folding event with associated thrusting was recognised in the Permian and Triassic sequences. The cleavage in these sedimentary sequences is axial planar to the folds, and thus both folds and cleavage are most likely to represent the same deformation event. The timing of folding and thrusting is constrained by the age of the youngest unit in the section affected by this deformation (i.e. the lower Norian Wang Chin Formation) and the age of post-kinematic granite and associated hornfelsic rocks (Upper Triassic-Early Jurassic). Recent K-Ar ages of 188-220 Ma for the cleavage have been suggested for the deformation by Ahrendt *et al.* (1993). The radiometric age and the relative age consistently point to the Upper Triassic age of the deformation in this region.

The Triassic Lampang Group was metamorphosed to lower to upper anchimetamorphic zone. The Permian Huai Thak Formation have the lower anchizone grade illite crystallinity values. Metamorphism of these sedimentary sequences are closely related to the deformation (folding and thrusting) which produced the cleavage in shale/slate.

# Chapter 10

# THE METAMORPHISM AND STRUCTURE OF THE DOI INTHANON METAMORPHIC COMPLEX

## 10.1 Introduction

The Doi Inthanon metamorphic complex occupies a northern portion of a continuous belt of middle to upper amphibolite facies gneissic rocks which extends over 400 km along the western mountain range of Thailand from Mae Hong Son in northern Thailand to Uthai Thani in central Thailand (Fig. 10.1). This gneiss belt has generally been inferred to represent a Precambrian basement of the Shan-Thai terrane based on its higher metamorphic grade, more complex internal deformation history and lower structural and/or stratigraphic level compared to the overlying Lower Palaeozoic cover sequence.

Baum *et al.* (1970) regarded the high-grade gneissic rocks in this gneiss belt as Precambrian paragneisses which formed the core of a N-S trending anticlinorium and have been subjected to anatexis or migmatisation during Lower Carboniferous orogeny. However, this view has been disproved by the radiometric dating of granitic rocks in northern Thailand, especially those in close spatial relation with the gneisses. All the radiometric dates indicate Permo-Triassic or younger ages for the intrusions (Teggin, 1975; von Braun *et al.*, 1976; Macdonald *et al.*, 1993). These granitic rocks have characteristics of S-type granites (Cobbing *et al.*, 1986).

Barr and Macdonald (1991) suggested that the gneiss belt formed in the Early Mesozoic as a series of metamorphic core complexes in response to collisional underthrusting of the Shan-Thai cratonic margin beneath the amalgamated Sukhothai and Indosinian (Indochina) terranes. Recently, Macdonald *et al.* (1993) noted that the belt has many features similar to the Cordilleran metamorphic core complexes and proposed that it is a result of Late Cretaceous high-grade metamorphism of Late Precambrian-Early Cambrian sediments and Late Triassic-Early Jurassic granites and was subjected to uplift and tectonic unroofing in Tertiary time. These events were considered to be related to crustal thinning some 300 km behind the Cretaceous-Eocene east-dipping subduction zone, represented by the

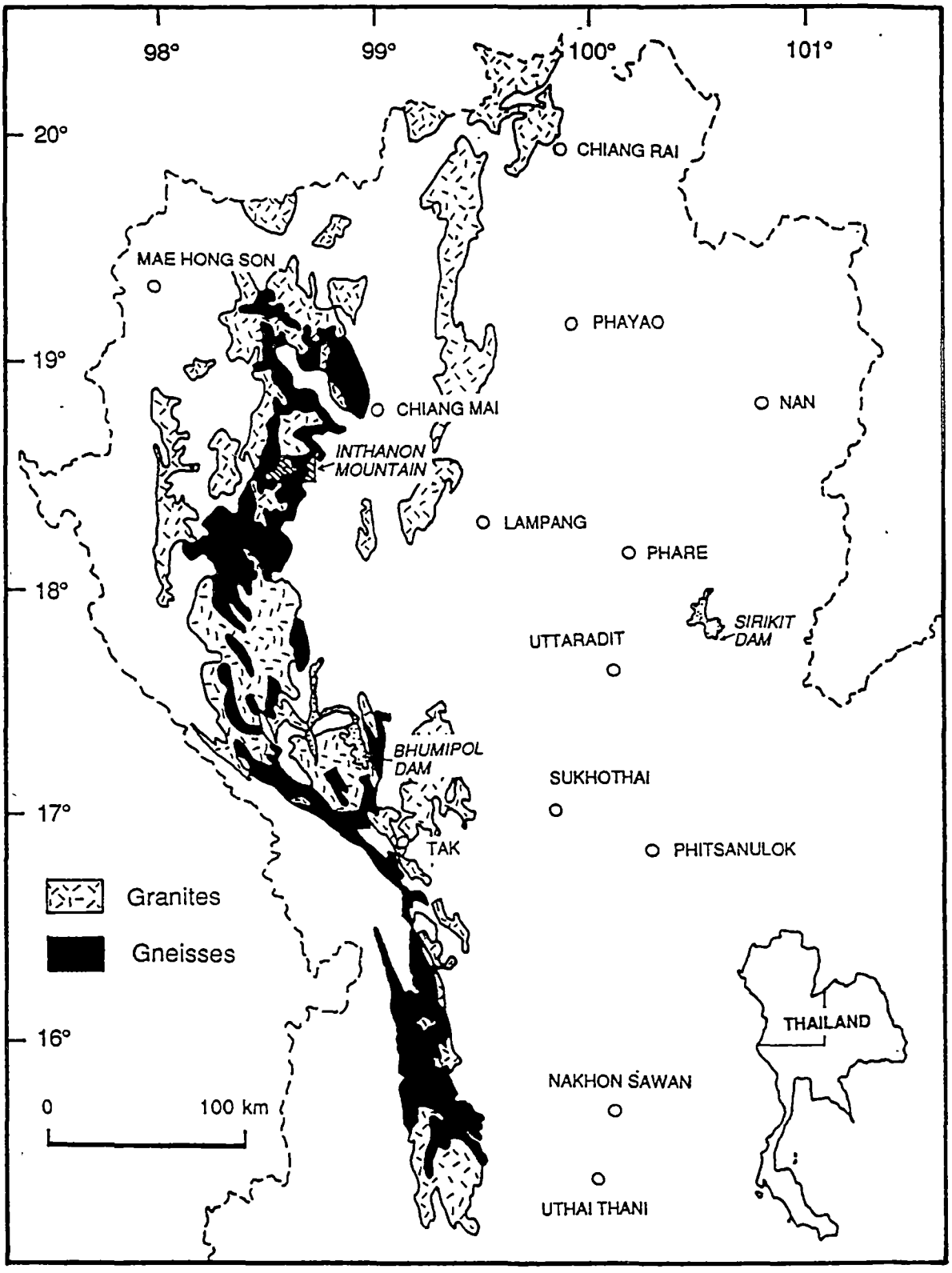


Figure 10.1 Map showing distribution of gneissic rocks and granitic plutons in the western part of northern Thailand (modified after Department of Mineral Resources, 1987). Also shown are the locations of major towns in northern Thailand. The shaded rectangle indicates the Doi Intanon area shown in Figure 10.2.

Burma magmatic arc of Mitchell (1977). This magmatic arc is now located in the central part of the West Burma terrane (Fig. 1.1).

Given the diverse tectonic interpretations of this high-grade metamorphic terrain, a re-evaluation of existing data (especially the age dating of gneisses and granites) is required. As part of this revision, further metamorphic and structural study of the gneisses has been carried out to test the tectonic models and to reconcile the current contrasting views. Of equal importance is an attempt to determine the relationship between the evolution this metamorphic complex and that of the Sukhothai fold belt further east. No quantitative thermobarometric study of these high-grade gneisses has been reported before. A brief study of the complexes has been included to determine the *P-T* conditions and fluid characteristics during metamorphism of these high-grade rocks.

## 10.2 Lithology and Age

The geological map of the Inthanon Mountain metamorphic complex presented recently by Macdonald *et al.* (1993) was used in the present study as a guideline in the subdivision of rock types within this metamorphic complex. The modified version of this map is shown in Figure 10.2 and a brief description of important lithologies is given below.

### Gneissic rocks

The gneissic rocks of the Inthanon Mountain metamorphic complex are divided into core orthogneisses and mantling paragneisses (Fig. 10.2).

The core orthogneisses consist of two main lithological units: sillimanite-bearing muscovite-biotite-K-feldspar gneiss and muscovite-biotite-K-feldspar megacrystic gneiss. Migmatitic segregation banding within the gneissic foliation together with concordant aplite and pegmatite sheets are common. The U-Pb zircon radiometric age of megacrystic gneiss is 207 ± 3 Ma (Late Triassic) and the monazite age is 72±1 Ma (Late Cretaceous). These were interpreted to represent the age of crystallisation of the protolith and the age of high-grade metamorphism respectively (Macdonald *et al.*, 1993).

The paragneisses which mantle the core zone on the eastern flank of the Inthanon Mountain are composed chiefly of fine- to medium-grained biotite-plagioclase gneiss with rare thin-layered biotite schist. Towards the upper part, thin layers of medium- to very-coarse grained calc-silicate rocks occur within much thicker layers of biotite-plagioclase gneiss. Small multiple sills and dykes of aplite

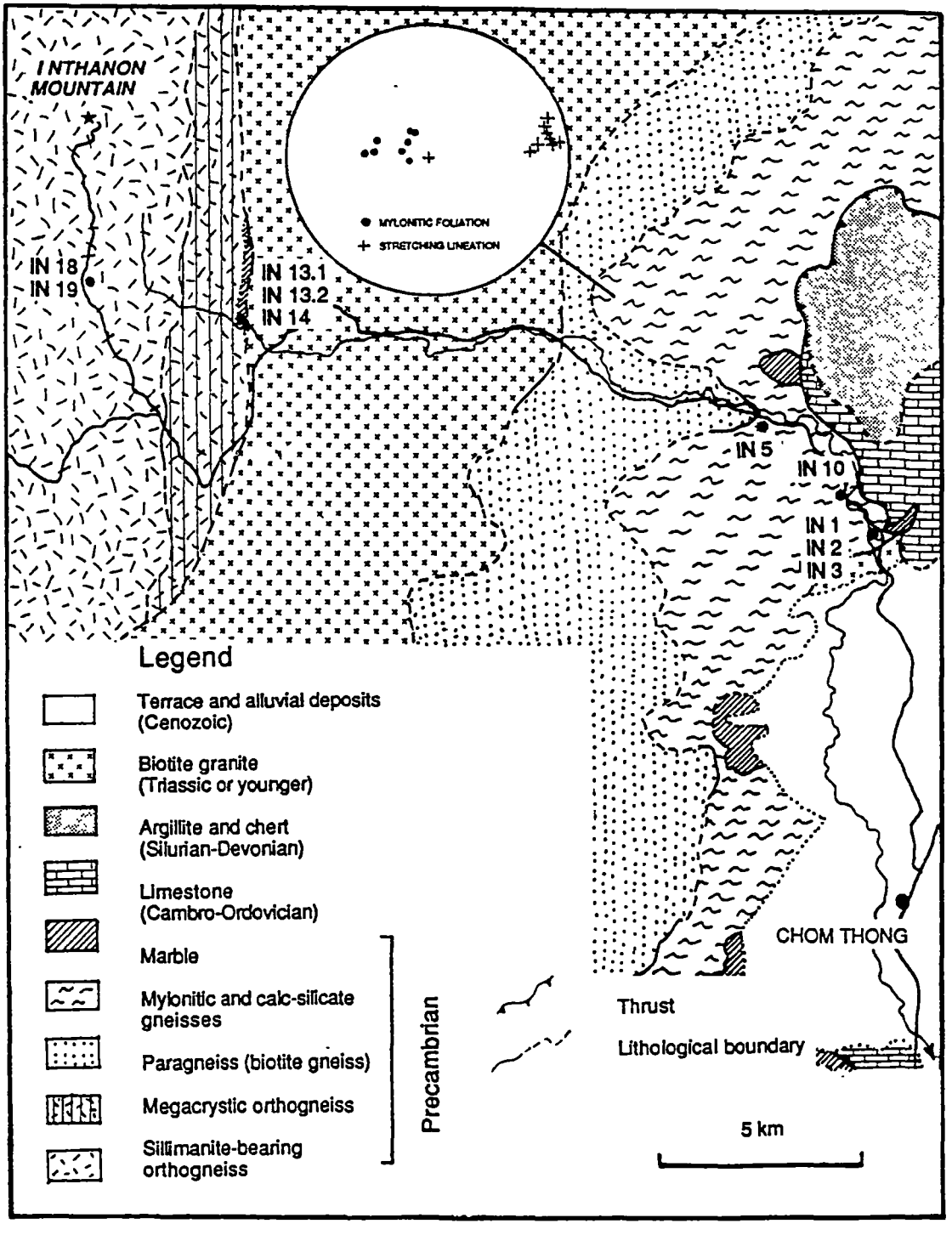


Figure 10.2 Geological map of the Doi Inthanon area showing distribution of major lithological units and sample locations. Also shown is an equal area lower-hemisphere stereographic projection of mylonitic foliation and stretching lineation in mylonitic gneiss (geology after Macdonald *et al.*, 1993).

and pegmatite are common within these gneisses. The protolithic age of a paragneissic unit is not known but has been inferred to be Late Precambrian - Early Cambrian by Macdonald *et al.* (1993). This inference is based on the assumption that the detachment faults have not exploited a major unconformity at the base of the Lower Palaeozoic stratigraphic section which is generally inferred to be Cambro-Ordovician in age (Baum *et al.*, 1970). It is noted that the protoliths of this paragneissic unit are very different in composition from the Cambro-Ordovician rocks which comprise thick quartzose sandstone and shelf-carbonate sequences.

### Cover rocks

The cover rocks are separated from the gneissic basement by a surface of low-angle fault which is thought to be the detachment fault by Macdonald *et al.* (1993). A thick sequence of fine-grained marble gradational to limestone of Ordovician age lies directly on a fault. On top of the carbonate sequence is a succession of grey to black argillite, sandstone and chert considered to be Silurian-Devonian in age (Baum *et al.*, 1970).

### Granites

The foliated granite plutons have intruded both core and mantling gneisses (Fig. 10.2) with crudely concordant contact with adjacent gneisses and were suggested to be tabular in shape (Macdonald *et al.*, 1993). The granite varies from fine- to medium-grained biotite granite to medium-grained leucogranite. The texture is generally equigranular but may be sub-porphyritic locally. Mylonitisation of this granitic pluton developed locally. A U-Pb monazite age of 25 ± 1 Ma (latest Oligocene) was interpreted as crystallisation age for this pluton (Macdonald *et al.*, 1993).

## 10.3 Deformation History

In a broad sense, the Inthanon metamorphic complex can be classified as a mantled gneiss dome of Eskola, a structure comprises a core of granitic migmatites or gneisses overlain by a layered metasedimentary or metavolcanic cover or mantle (Hobbs *et al.*, 1976). The gneissic core of the Doi Inthanon complex forms a broad dome towering over the nearby Tertiary Chiang Mai basin (Fig 10.3a).

The deformation events recorded in the gneissic rocks have been studied by a few workers (e.g. Mongkolthip, 1986; Macdonald *et al.*, 1993). Mongkolthip

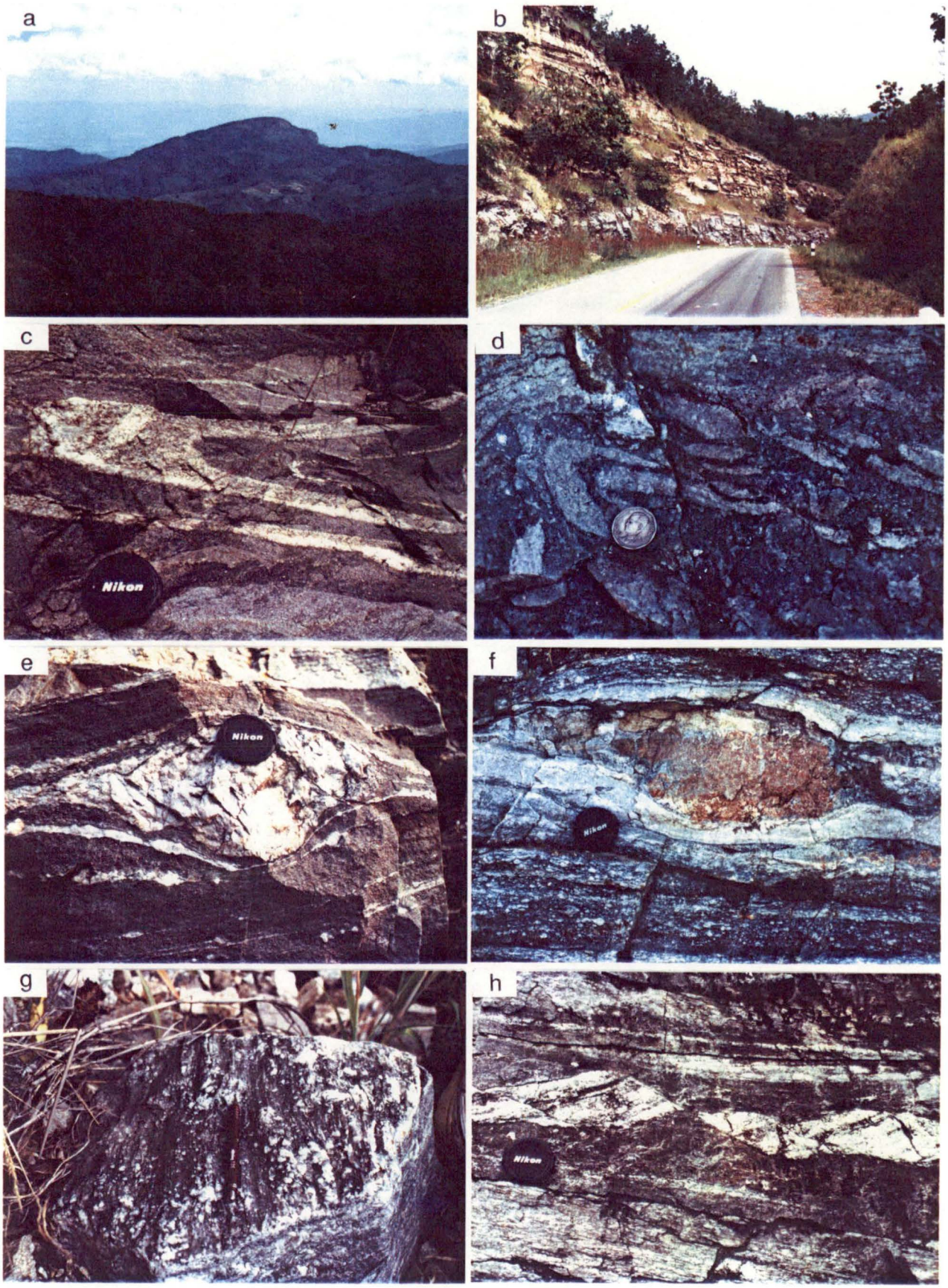
a
b
c
Nikon
d
e
Nikon
f
Nikon
g
h
Nikon

(1986) recognised only two folding phases in the gneisses whereas Macdonald *et al.* (1993) recognised three folding phases ($F_1$, $F_2$ and $F_3$) and late mylonitic fabrics (mylonitic shear foliation, $S_m$ and stretching lineation, $L_m$). A brief account of these deformation episodes observed in the gneisses is given below.

From field observations in the present study, the earliest deformation ($D_1$) produced a prominent gneissic foliation which is the dominant structural element of the Inthanon complex. The gneissic foliation is characterised by differentiated layering enhanced by migmatitic segregation banding and layer-parallel intrusion of aplite and pegmatite sheets (Fig.10.3b). Rootless intrafolial folds are seen locally within both biotite-plagioclase gneiss (Fig. 10.3c) and calc-silicate rocks (Fig 10.3d) and are probably $F_1$ recumbent folds of Macdonald *et al.* (1993). Large porphyroclasts of feldspars (Fig. 10.3e) and blocks of grossular-rich calc-silicate rocks (Fig. 10.3f) are common within biotite-plagioclase gneiss and calc-silicate rocks respectively. $D_2$ and $D_3$ deformation phases are represented by W-plunging $F_2$ overturned folds and SSE-plunging $F_3$ chevron folds of Macdonald *et al.* (1993) respectively. $D_4$ deformation phase is characterised by the formation of mylonitic fabrics (Fig. 10.3g) which consist of mylonitic foliation ($S_m$) and mineral stretching lineation ($L_s$) subparallel to or at low-angle to gneissic layering. The small-scale boudinage at km 8.6 on the highway to Inthanon Mountain summit (Fig. 10.3h), is part of this mylonitic fabrics. The mylonitic fabric elements are remarkably uniform in orientation. From Figure 10.2, it can be seen that $S_m$ strikes northeasterly and dips shallowly to the southeast whereas $L_s$ plunges shallowly to the southeast.

The last structural event recognised in the Doi Inthanon metamorphic complex is a series of N-S-trending high angle normal faults which are probably related to the formation of the adjacent extensional basin during Middle Tertiary (early Miocene) time.

## 10.4 Mineral Assemblages and Microfabrics

Gneissic rocks from the Inthanon Mountain area which were selected for petrographic and electron-microprobe studies include sillimanite-bearing muscovite-biotite-feldspathic gneiss, muscovite-biotite-feldspar megacrystic gneiss, biotite-plagioclase gneiss and calc-silicate rocks. The mineral assemblages in these samples are shown in Table 10.1 and their petrographic features are described below.

Table 10.1 Mineral assemblages in quartzofeldspathic gneisses and calc-silicate rocks of the Doi Inthanon metamorphic complex.

| Sample no. | Mineral assemblages | | | | | | | | | | |
|---|---|---|---|---|---|---|---|---|---|---|---|
| | Sil | Qtz | Kfs | Pl | Bt | Ms | Cpx | Amph | Grt | Cal | Zo |
| *Quartzo-feldspathic gneisses* | | | | | | | | | | | |
| IN-19 | X | X | X | X | X | X | | | | | |
| IN-18 | X | X | X | X | X | X | | | | | |
| IN-14 | | X | X | X | X | X | | | | | |
| IN-1 | | X | | X | X | | | | | | |
| IN-5 | | X | X | | X | | | | | | |
| IN-10 | | X | X | X | X | X | | | | | |
| *Calc-silicate gneisses* | | | | | | | | | | | |
| IN-13.1 | | X | X | X | | | X | | X | | |
| IN-13.2 | | X | X | X | X | | X | | | | |
| IN-2 | | X | | X | | | X | X | X | X | |
| IN-3 | | X | X | X | | | X | | X | | X |

**Sillimanite-bearing muscovite-biotite gneiss:** This rock type is represented by samples IN-18 and IN-19 which are medium- to coarse-grained gneissic rocks. They consist of quartz, K-feldspar, plagioclase, biotite, muscovite with sillimanite, apatite and zircon as accessory minerals. The representative compositions of coexisting minerals in these two samples are given in Table 10.2 (see complete analyses in Appendix F).

K-feldspar, mainly orthoclase, occurs as porphyroblastic grains which commonly shows microperthitic texture and some grains show cross-hatched twin of microcline. Perthitic orthoclase commonly contain inclusions of quartz, biotite and muscovite. Plagioclase is more or less equal in amount to K-feldspar and ranges in composition from albite ($An_{3-8}$) in sample IN-18 to oligoclase ($An_{11-14}$) in sample IN-19. Many plagioclase grains contain inclusions of quartz, biotite and muscovite as does the K-feldspar. Sericitisation in feldspars is moderately developed giving rise to a slightly turbid appearance.

Quartz grains have serrated grain boundaries. Biotite locally encloses zircon and possesses pleochroic halos. Fluorine contents in biotites are characteristically high (1.95% in sample IN-18 and 2.14% in sample IN-19). Muscovite occurs as large flakes intergrown with biotite and contains high amount of fluorine (0.70% in sample IN-18 and 0.86% in sample IN-19).

Sillimanite occurs as fibrolitic mats enclosed within porphyroblastic muscovite (Fig. 10.4a&b). The sillimanite contains a small amount of iron (total

Table 10.2 Representative electron microprobe analyses of minerals in quartzo feldspathic gneisses.

| Mineral | Bt | Bt | Bt | Bt | Bt | Bt | Bt | Ms | Ms | Ms | Ms | | Kfs | Kfs | Kfs | Kfs | Kfs | Pl | Pl | Pl | Pl | Pl | Pl | | Sil | Sil |
|---|---|---|---|---|---|---|---|---|---|---|---|---|---|---|---|---|---|---|---|---|---|---|---|---|---|---|
| Sample no. | IN-19 | IN-18 | IN-14 | IN-1 | IN-5 | IN-10 | IN-13.2 | IN-19 | IN-18 | IN-14 | IN-10 | | IN-19 | IN-18 | IN-14 | IN-5 | IN-10 | IN-19 | IN-18 | IN-14 | IN-1 | IN-5 | IN-10 | | IN-19 | IN-18 |
| N | 8 | 10 | 10 | 7 | 7 | 6 | 7 | 9 | 12 | 2 | 6 | | 8 | 6 | 6 | 5 | 6 | 7 | 10 | 6 | 7 | 7 | 4 | | 1 | 1 |
| SiO2 | 36.09 | 36.49 | 35.91 | 36.21 | 34.90 | 33.86 | 36.77 | 46.40 | 46.71 | 45.85 | 45.38 | SiO2 | 64.77 | 64.50 | 64.47 | 64.15 | 64.30 | 65.56 | 67.19 | 63.31 | 59.59 | 59.59 | 62.77 | SiO2 | 36.45 | 36.84 |
| TiO2 | 2.22 | 2.32 | 3.40 | 3.26 | 3.96 | 2.58 | 3.01 | 1.10 | 0.83 | 1.97 | 0.68 | Al2O3 | 18.58 | 18.37 | 18.17 | 18.60 | 18.73 | 21.29 | 20.11 | 23.11 | 25.64 | 25.64 | 23.35 | TiO2 | 0.02 | 0.04 |
| Al2O3 | 16.98 | 17.13 | 17.66 | 15.11 | 15.39 | 18.97 | 13.09 | 32.92 | 34.17 | 32.60 | 35.30 | FeO* | 0.02 | 0.02 | 0.03 | 0.02 | 0.03 | 0.02 | 0.01 | 0.06 | 0.05 | 0.05 | 0.02 | Al2O3 | 63.01 | 63.14 |
| FeO* | 22.02 | 21.36 | 20.07 | 19.35 | 21.75 | 23.36 | 21.25 | 1.88 | 1.65 | 1.71 | 1.37 | MgO | 0.00 | 0.00 | 0.01 | 0.00 | 0.02 | 0.01 | 0.15 | 0.01 | 0.00 | 0.00 | 0.00 | Cr2O3 | 0.00 | 0.00 |
| MnO | 0.50 | 0.39 | 0.38 | 0.52 | 0.17 | 0.44 | 0.31 | 0.03 | 0.04 | 0.00 | 0.09 | CaO | 0.02 | 0.00 | 0.02 | 0.02 | 0.02 | 2.48 | 0.94 | 4.64 | 7.20 | 7.20 | 4.38 | Fe2O3# | 0.25 | 0.16 |
| MgO | 8.15 | 8.51 | 8.66 | 11.14 | 8.70 | 5.96 | 10.84 | 1.29 | 1.04 | 1.00 | 0.64 | Na2O | 1.16 | 0.84 | 1.33 | 1.49 | 1.27 | 9.74 | 10.81 | 8.50 | 7.00 | 7.00 | 8.63 | MnO | 0.00 | 0.00 |
| CaO | 0.01 | 0.01 | 0.00 | 0.05 | 0.00 | 0.05 | 0.00 | 0.00 | 0.01 | 0.01 | 0.00 | K2O | 15.33 | 15.53 | 15.15 | 14.34 | 14.78 | 0.24 | 0.10 | 0.35 | 0.37 | 0.37 | 0.31 | MgO | 0.01 | 0.00 |
| Na2O | 0.09 | 0.08 | 0.08 | 0.07 | 0.10 | 0.10 | 0.03 | 0.34 | 0.38 | 0.26 | 0.57 | | | | | | | | | | | | | CaO | 0.01 | 0.00 |
| K2O | 9.72 | 9.80 | 9.80 | 9.66 | 9.65 | 9.47 | 9.82 | 11.14 | 11.08 | 10.27 | 10.65 | | | | | | | | | | | | | | | |
| F | 2.14 | 1.95 | 0.65 | 0.30 | 1.01 | 0.71 | 1.00 | 0.86 | 0.70 | 0.09 | 0.22 | | | | | | | | | | | | | | | |
| Cl | 0.05 | 0.04 | 0.03 | 0.00 | 0.00 | 0.04 | 0.03 | 0.00 | 0.00 | 0.01 | 0.03 | | | | | | | | | | | | | | | |
| Total | 97.97 | 98.07 | 96.65 | 95.68 | 95.62 | 95.54 | 96.15 | 95.96 | 96.60 | 93.79 | 94.92 | | | | | | | | | | | | | | | |
| O = F, Cl | -0.91 | -0.83 | -0.28 | -0.14 | -0.43 | -0.31 | -0.43 | -0.36 | -0.29 | -0.04 | -0.10 | | | | | | | | | | | | | | | |
| Total | 97.06 | 97.24 | 96.37 | 95.54 | 95.19 | 95.23 | 95.72 | 95.60 | 96.30 | 93.75 | 94.82 | Total | 99.87 | 99.27 | 99.18 | 98.62 | 99.15 | 99.34 | 99.31 | 99.98 | 99.86 | 99.86 | 99.47 | Total | 99.75 | 100.18 |
| Si | 5.558 | 5.575 | 5.466 | 5.551 | 5.464 | 5.316 | 5.709 | 6.239 | 6.209 | 6.224 | 6.098 | Si | 2.989 | 2.995 | 2.997 | 2.986 | 2.982 | 2.896 | 2.959 | 2.797 | 2.657 | 2.657 | 2.788 | Si | 0.987 | 0.993 |
| Al iv | 2.442 | 2.425 | 2.534 | 2.449 | 2.536 | 2.684 | 2.291 | 1.761 | 1.791 | 1.776 | 1.902 | Al | 1.011 | 1.006 | 0.995 | 1.021 | 1.024 | 1.109 | 1.044 | 1.204 | 1.348 | 1.348 | 1.223 | Ti | 0.000 | 0.001 |
| Al vi | 0.641 | 0.662 | 0.636 | 0.282 | 0.305 | 0.828 | 0.105 | 3.457 | 3.565 | 3.442 | 3.690 | Fe2+ | 0.002 | 0.002 | 0.002 | 0.001 | 0.003 | 0.002 | 0.001 | 0.004 | 0.004 | 0.004 | 0.001 | Al | 2.011 | 2.006 |
| Ti | 0.257 | 0.267 | 0.389 | 0.376 | 0.466 | 0.304 | 0.351 | 0.111 | 0.083 | 0.201 | 0.068 | Mg | 0.000 | 0.000 | 0.000 | 0.000 | 0.000 | 0.000 | 0.000 | 0.000 | 0.000 | 0.000 | 0.000 | Cr | 0.000 | 0.000 |
| Fe2+ | 2.837 | 2.730 | 2.555 | 2.480 | 2.848 | 3.067 | 2.758 | 0.211 | 0.183 | 0.194 | 0.154 | Ca | 0.001 | 0.000 | 0.001 | 0.001 | 0.001 | 0.117 | 0.044 | 0.219 | 0.344 | 0.344 | 0.208 | Fe3+ | 0.005 | 0.003 |
| Mn | 0.065 | 0.050 | 0.049 | 0.067 | 0.022 | 0.058 | 0.041 | 0.004 | 0.004 | 0.000 | 0.010 | Na | 0.103 | 0.076 | 0.120 | 0.134 | 0.114 | 0.834 | 0.923 | 0.728 | 0.606 | 0.606 | 0.743 | Mn | 0.000 | 0.000 |
| Mg | 1.872 | 1.938 | 1.965 | 2.545 | 2.030 | 1.395 | 2.509 | 0.258 | 0.206 | 0.203 | 0.128 | K | 0.903 | 0.920 | 0.899 | 0.852 | 0.875 | 0.014 | 0.005 | 0.020 | 0.021 | 0.021 | 0.018 | Mg | 0.000 | 0.000 |
| Ca | 0.002 | 0.001 | 0.000 | 0.008 | 0.000 | 0.008 | 0.001 | 0.000 | 0.001 | 0.001 | 0.001 | | | | | | | | | | | | | Ca | 0.000 | 0.000 |
| Na | 0.027 | 0.023 | 0.024 | 0.021 | 0.029 | 0.030 | 0.009 | 0.089 | 0.099 | 0.069 | 0.148 | | | | | | | | | | | | | | | |
| K | 1.911 | 1.910 | 1.903 | 1.890 | 1.927 | 1.898 | 1.945 | 1.911 | 1.879 | 1.779 | 1.826 | | | | | | | | | | | | | | | |
| Sum cations | 15.612 | 15.581 | 15.523 | 15.670 | 15.628 | 15.588 | 15.719 | 14.041 | 14.019 | 13.890 | 14.024 | | 5.008 | 4.999 | 5.014 | 4.996 | 4.998 | 4.972 | 4.977 | 4.973 | 4.980 | 4.980 | 4.981 | | 3.004 | 3.002 |
| Oxygens | 22.0 | 22.0 | 22.0 | 22.0 | 22.0 | 22.0 | 22.0 | 22.0 | 22.0 | 22.0 | 22.0 | | 8.0 | 8.0 | 8.0 | 8.0 | 8.0 | 8.0 | 8.0 | 8.0 | 8.0 | 8.0 | 8.0 | | 5.0 | 5.0 |
| Mg/(Mg+Fe2) | 0.398 | 0.415 | 0.435 | 0.506 | 0.416 | 0.313 | 0.476 | 0.550 | 0.526 | 0.511 | 0.454 | | | | | | | | | | | | | | | |
| | | | | | | | | | | | | An | 0.001 | 0.000 | 0.001 | 0.001 | 0.001 | 0.122 | 0.046 | 0.227 | 0.355 | 0.355 | 0.215 | | | |
| | | | | | | | | | | | | Ab | 0.103 | 0.076 | 0.118 | 0.136 | 0.115 | 0.864 | 0.949 | 0.753 | 0.624 | 0.624 | 0.767 | | | |
| | | | | | | | | | | | | Or | 0.896 | 0.924 | 0.881 | 0.863 | 0.884 | 0.014 | 0.006 | 0.020 | 0.021 | 0.021 | 0.018 | | | |

* Total Fe as FeO
# Total Fe as Fe2O3

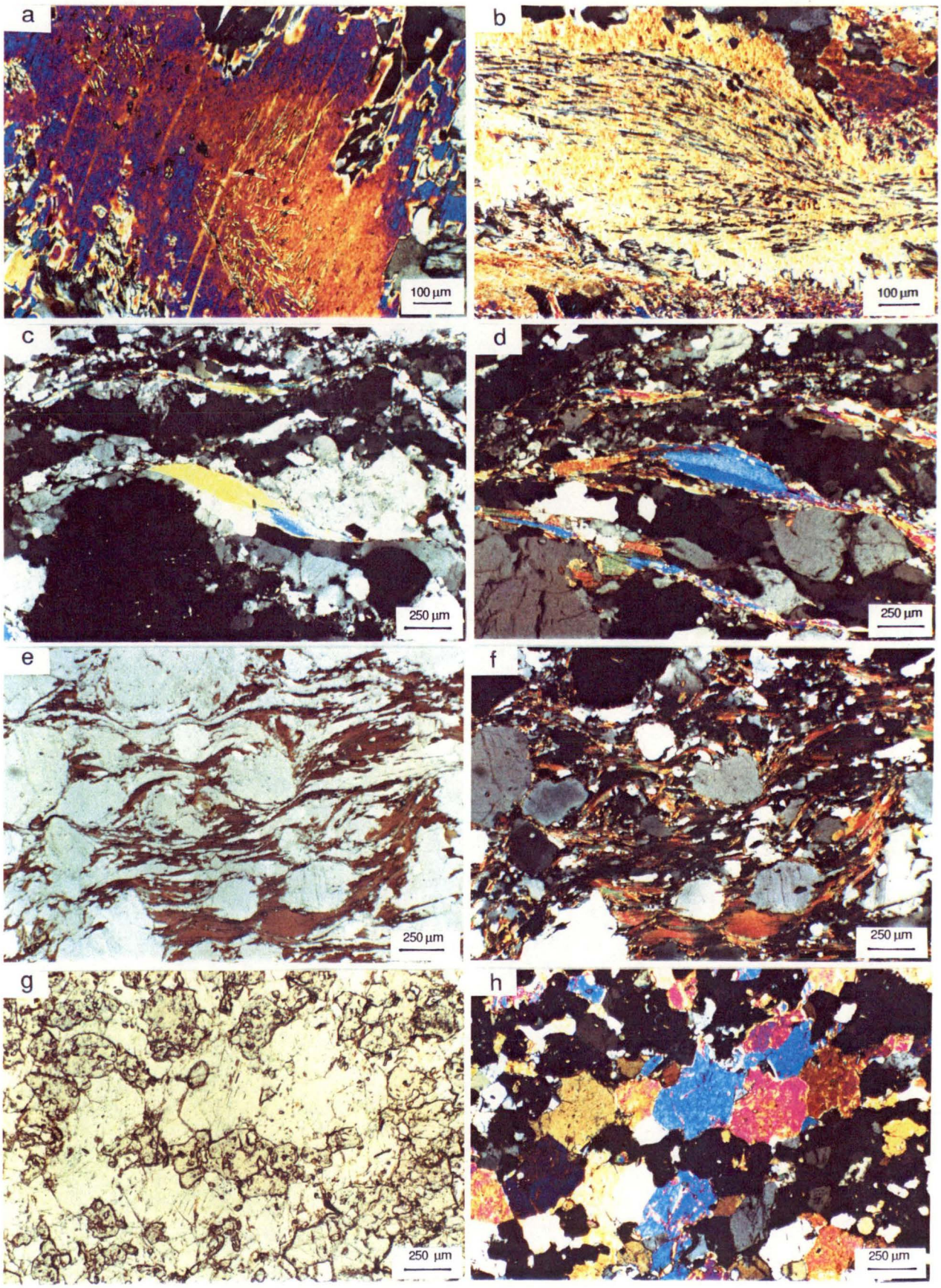
a
100 µm
b
100 µm
c
250 µm
d
250 µm
e
250 µm
f
250 µm
g
250 µm
h
250 µm

iron as $Fe_2O_3$) in the structure (0.16% in sample IN-18.1 and 0.25% in sample IN-19).

**Biotite megacrystic gneiss:** This rock type, represented by sample IN-14, consists of quartz, K-feldspar, biotite, muscovite and plagioclase. The compositions of the constituent minerals are given in Table 10.2.

K-feldspar (orthoclase) occurs as porphyroblasts and commonly show microperthitic texture. Myrmekitic texture produced by quartz-alkali feldspar intergrowth is also common. Perthitic orthoclase commonly contain inclusions of quartz and biotite. Plagioclase ($An_{22-24}$) is less abundant than K-feldspar. Inclusions of quartz and biotite are common in plagioclase.

Quartz grains have serrated grain boundaries. Biotite occurs as a large flakes and is replaced by fine-grained chlorite locally. This mineral contains lower amount of F (0.65%) than those in sillimanite-bearing samples. Subparallel alignment of biotite crudely defines the gneissic foliation of the rock. Muscovite occurs as a small flakes within larger biotite flakes and contains much lower amount of F (0.09%) than those in sillimanite-bearing samples. Ilmenite, apatite and zircon are accessory minerals.

**Biotite gneiss:** The representative samples of this rock type (samples IN-1, IN-5, IN-8 and IN-10) consist mainly of quartz, plagioclase and biotite with subordinate amounts of K-feldspar and muscovite. The compositions of the constituent minerals are given in Table 10.2.

Plagioclase occurs as porphyroblastic grains and ranges in composition from oligoclase ($An_{20-25}$) in IN-10 to andesine ($An_{35-36}$) in IN-5. Myrmekitic texture is common.

Biotite contains high amount of F (0.71% in IN-10 and 1.01% in IN-5) but lower than those in sillimanite-bearing samples. Muscovite contains lower amount of F (0.22%) than those in sillimanite-bearing samples.

These samples are characterised by mylonitic fabrics. In thin section, sample IN-10 have pronounced mylonitic fabrics including asymmetrical plagioclase porphyroclast, asymmetrical muscovite porphyroclast or mica fish (Figs. 10.4c&d), quartz ribbons and S-C fabrics. Sample IN-1, a fine-grained mylonitic gneiss, contains abundant plagioclase porphyroclasts embedded in a biotite-rich matrix with an incipiently developed mylonitic fabric (Figs. 10.4e&f).

**Calc-silicate rocks:** This rock type is invariably interlayered with biotite gneiss and are medium- to very coarse-grained granoblastic rocks. In thin section (samples IN-2, IN-3, IN-13.1 and IN-13.2), it is characterised by abundant porphyroblasts of clinopyroxene and garnet (Figs. 10.4g&h) and, to a lesser extent, amphibole (sample IN-2) associated with finer-grained quartz and calcite. The

representative electron-microprobe analyses of the constituent minerals of these calc-silicates are given in Table 10.3 (see complete analyses in Appendix F).

Garnet is chiefly grossular-andradite solid-solution with insignificant mole fraction of other end-members (Table 10.3). Poikiloblastic garnet grains commonly contain small inclusions probably of quartz. Clinopyroxene is diopside-rich in composition. Poikiloblastic clinopyroxene grains commonly contain small inclusions of quartz. Amphiboles are ferroan-pargasitic hornblende to edenitic hornblende according to classification of Leake (1978). This mineral coexists stably with grossular garnet and diopsidic clinopyroxene. Plagioclase together with K-feldspar are present in all analysed thin section. The composition of plagioclase ranges from oligoclase ($An_{25}$) in sample IN-13.2 to anorthite ($An_{91}$) in sample IN-13.1. Zoisite (IN-3) occurs as anhedral crystals between garnet and plagioclase, apparently as a retrograde mineral. Biotite is a trace component in sample IN-13.2 and contains relatively high F content (1.00%). Sphene and apatite are accessory minerals.

## 10.5 Geothermobarometry

In the present study, quantitative approach is adopted to achieve better *P-T* constraints on peak conditions of metamorphism of the Doi Inthanon metamorphic complex. Various geothermometers based on exchanged reactions between coexisting mineral pairs, e.g. biotite-muscovite geothermometer (Hoisch, 1989), two-feldspar geothermometers (Stromer, 1975; Ghiorso, 1984; Price, 1985; Fuhrman and Lindsley, 1988) and plagioclase-muscovite geothermometer (Green and Usdansky, 1986), were applied. In terms of geobarometry, the Si contents of muscovite was used to approximate the metamorphic pressure of gneisses. In addition, thermodynamic calculations, i.e. Holland and Powell (1990) and Brown *et al.* (1988), based on phase equilibria among the end-members of coexisting phases (though not a critical assemblage) were also employed to provide better constraints for metamorphic *P-T* estimates.

Compositionally, the gneissic rocks in the present study can be divided into quartzofeldspathic gneisses (semi-pelites) and calc-silicate rocks and they are treated separately in the following sections.

Table 10.3 Representative electron microprobe analyses of minerals in calc-silicate rocks.

| Mineral | Grt | Grt | Grt | | Cpx | Cpx | Cpx | Cpx | | Hbl$ | | Bt | | Kfs | Kfs | Kfs | Pl | Pl | Pl | Pl | | Zo |
|---|---|---|---|---|---|---|---|---|---|---|---|---|---|---|---|---|---|---|---|---|---|---|
| Sample no. | IN-13.1 | IN-2 | IN-3 | | IN-13.1 | IN-13.2 | IN-2 | IN-3 | | | | IN-13.2 | | IN-13.1 | IN13.2 | IN-3 | IN-13.1 | IN13.2 | IN-2 | IN-3 | | |
| N | | 8 | 25 | | 9 | 6 | 7 | 7 | | | | 7 | | 6 | 5 | 4 | 5 | 6 | 5 | 5 | | |
| SiO2 | 37.82 | 38.32 | 38.47 | SiO2 | 51.78 | 51.38 | 51.28 | 51.99 | SiO2 | 44.37 | SiO2 | 36.77 | SiO2 | 64.27 | 64.46 | 64.43 | 44.97 | 62.19 | 59.17 | 47.41 | SiO2 | 38.50 |
| TiO2 | 0.61 | 0.30 | 0.21 | TiO2 | 0.02 | 0.05 | 0.03 | 0.01 | TiO2 | 0.47 | TiO2 | 3.01 | Al2O3 | 18.19 | 18.82 | 18.35 | 34.28 | 23.66 | 25.27 | 33.27 | TiO2 | 0.05 |
| Al2O3 | 18.42 | 20.33 | 20.46 | Al2O3 | 0.54 | 0.46 | 0.36 | 0.38 | Al2O3 | 12.49 | Al2O3 | 13.09 | FeO# | 0.03 | 0.04 | 0.01 | 0.11 | 0.03 | 0.07 | 0.05 | Al2O3 | 28.83 |
| Cr2O3 | 0.03 | 0.10 | 0.01 | Cr2O3 | 0.01 | 0.03 | 0.03 | 0.04 | Cr2O3 | 0.05 | FeO# | 21.25 | MgO | 0.00 | 0.00 | 0.00 | 0.00 | 0.00 | 0.00 | 0.00 | Fe2O3§ | 6.45 |
| Fe2O3* | 6.86 | 4.32 | 4.71 | Fe2O3* | 2.23 | 2.06 | 2.03 | 1.81 | FeO# | 12.69 | MnO | 0.31 | CaO | 0.01 | 0.02 | 0.02 | 18.82 | 4.88 | 6.91 | 16.90 | MnO | 0.53 |
| FeO* | 0.04 | 0.03 | 0.51 | FeO* | 9.41 | 12.85 | 10.02 | 10.72 | MnO | 0.18 | MgO | 10.84 | Na2O | 0.79 | 1.55 | 0.99 | 0.97 | 8.03 | 7.08 | 1.85 | MgO | 0.01 |
| MnO | 0.26 | 0.91 | 0.78 | MnO | 0.30 | 0.61 | 0.74 | 0.66 | MgO | 12.62 | CaO | 0.00 | K2O | 16.08 | 14.37 | 15.30 | 0.03 | 0.33 | 0.35 | 0.03 | CaO | 24.14 |
| MgO | 0.07 | 0.07 | 0.07 | MgO | 10.97 | 9.07 | 10.33 | 10.31 | CaO | 12.66 | Na2O | 0.03 | | | | | | | | | | |
| CaO | 36.30 | 35.56 | 34.94 | CaO | 25.04 | 23.98 | 24.56 | 24.89 | Na2O | 1.85 | K2O | 9.82 | | | | | | | | | | |
| | | | | Na2O | 0.13 | 0.24 | 0.15 | 0.11 | K2O | 0.13 | F | 1.00 | | | | | | | | | | |
| | | | | | | | | | F | 0.00 | Cl | 0.03 | | | | | | | | | | |
| | | | | | | | | | Cl | 0.03 | Total | 96.15 | | | | | | | | | | |
| | | | | | | | | | Total | 97.54 | O = F, Cl | -0.43 | | | | | | | | | | |
| | | | | | | | | | O = F, Cl | -0.01 | | | | | | | | | | | | |
| Total | 100.40 | 99.94 | 100.17 | Total | 100.44 | 100.74 | 99.51 | 100.92 | Total | 97.54 | Total | 95.72 | Total | 99.37 | 99.26 | 99.10 | 99.18 | 99.13 | 98.86 | 99.51 | Total | 98.51 |
| Si | 2.898 | 2.924 | 2.933 | Si | 1.960 | 1.967 | 1.967 | 1.969 | Si | 6.477 | Si | 5.709 | Si | 2.992 | 2.981 | 2.995 | 2.092 | 2.771 | 2.664 | 2.184 | Si | 2.977 |
| Al iv | 0.102 | 0.076 | 0.067 | Al iv | 0.023 | 0.019 | 0.016 | 0.017 | Al iv | 1.523 | Al iv | 2.291 | Al | 0.998 | 1.026 | 1.006 | 1.880 | 1.243 | 1.341 | 1.806 | Al iv | 0.023 |
| Al vi | 1.561 | 1.753 | 1.772 | Fe3+ | 0.017 | 0.014 | 0.017 | 0.014 | Al vi | 0.626 | Al vi | 0.105 | Fe2+ | 0.003 | 0.003 | 0.001 | 0.009 | 0.002 | 0.006 | 0.004 | Al vi | 2.605 |
| Ti | 0.035 | 0.017 | 0.012 | Al vi | 0.001 | 0.002 | 0.000 | 0.000 | Ti | 0.051 | Ti | 0.351 | Mg | 0.000 | 0.000 | 0.000 | 0.000 | 0.000 | 0.000 | 0.000 | Ti | 0.003 |
| Cr | 0.002 | 0.006 | 0.001 | Ti | 0.001 | 0.001 | 0.001 | 0.000 | Cr | 0.006 | Fe2+ | 2.758 | Ca | 0.001 | 0.001 | 0.001 | 0.938 | 0.233 | 0.333 | 0.834 | Fe3+ | 0.375 |
| Fe3+ | 0.396 | 0.248 | 0.270 | Cr | 0.000 | 0.001 | 0.001 | 0.001 | Fe3+ | 0.279 | Mn | 0.041 | Na | 0.072 | 0.139 | 0.089 | 0.087 | 0.694 | 0.618 | 0.165 | Fe2+ | 0.000 |
| Fe2+ | 0.002 | 0.002 | 0.033 | Fe3+ | 0.047 | 0.045 | 0.042 | 0.038 | Mg | 2.745 | Mg | 2.509 | K | 0.955 | 0.848 | 0.908 | 0.002 | 0.019 | 0.020 | 0.002 | Mn | 0.034 |
| Mn | 0.017 | 0.059 | 0.051 | Fe2+ | 0.299 | 0.412 | 0.321 | 0.340 | Fe2+ | 1.271 | Ca | 0.001 | | | | | | | | | Mg | 0.001 |
| Mg | 0.008 | 0.008 | 0.008 | Mn | 0.009 | 0.020 | 0.024 | 0.021 | Mn | 0.023 | Na | 0.009 | | | | | | | | | Ca | 2.000 |
| Ca | 2.980 | 2.907 | 2.854 | Mg | 0.618 | 0.518 | 0.590 | 0.582 | Ca | 1.978 | K | 1.945 | | | | | | | | | | |
| | | | | Ca | 1.016 | 0.984 | 1.010 | 1.010 | Na | 0.022 | | | | | | | | | | | | |
| | | | | Na | 0.009 | 0.018 | 0.011 | 0.008 | Ca | 0.003 | | | | | | | | | | | | |
| | | | | | | | | | Na | 0.502 | | | | | | | | | | | | |
| | | | | | | | | | K | 0.025 | | | | | | | | | | | | |
| Sum cations | 8.000 | 8.000 | 8.000 | | 4.000 | 4.000 | 4.000 | 4.000 | | 15.530 | | 15.719 | | 5.020 | 4.998 | 5.000 | 5.008 | 4.962 | 4.982 | 4.995 | | 8.019 |
| Oxygens | 12.0 | 12.0 | 12.0 | | 6.0 | 6.0 | 6.0 | 6.0 | | 23.0 | | 22.0 | | 8.0 | 8.0 | 8.0 | 8.0 | 8.0 | 8.0 | 8.0 | | 12.5 |
| Mg/Mg+Fe2 | 0.903 | 0.908 | 3.010 | | 0.674 | 0.557 | 0.647 | 0.632 | | 0.684 | | 0.476 | | | | | | | | | Fe3/(Fe3+al) | 0.125 |
| Alm | 0.001 | 0.001 | 0.011 | Wo | 0.511 | 0.497 | 0.508 | 0.508 | | | | | An | 0.001 | 0.001 | 0.001 | 0.913 | 0.247 | 0.343 | 0.833 | | |
| Py | 0.003 | 0.003 | 0.003 | En | 0.311 | 0.262 | 0.297 | 0.292 | | | | | Ab | 0.070 | 0.141 | 0.089 | 0.085 | 0.734 | 0.636 | 0.165 | | |
| Sp | 0.006 | 0.020 | 0.017 | Fs | 0.178 | 0.241 | 0.195 | 0.200 | | | | | Or | 0.930 | 0.858 | 0.910 | 0.002 | 0.020 | 0.021 | 0.002 | | |
| Gr | 0.793 | 0.852 | 0.831 | | | | | | | | | | | | | | | | | | | |
| Adr | 0.198 | 0.125 | 0.138 | | | | | | | | | | | | | | | | | | | |

* Calculated from stoichiometry

# Total Fe as FeO.

§ Total Fe as Fe2O3.

Note : End-members are expressed in terms of molecular proportions; pyroxene end-members calculated after the Subcommittee on Pyroxenes (IMA, 1988); and hornblende structural formula are calculated by normalising the number of cations other than Ca, Na and K to 13.

## *P-T* conditions for quartzofeldspathic gneisses

Quartzofeldspathic gneisses include sillimanite-bearing muscovite-biotite gneiss, biotite megacrystic gneiss and biotite gneiss. They can be divided into two types according to the mineral assemblages, i.e. (i) sillimanite + K-feldspar + plagioclase + biotite + muscovite + quartz and (ii) K-feldspar + plagioclase + biotite + quartz ± muscovite .

A number of geothermometers applied to the gneissic rocks (samples IN-18.1, IN-19, IN-14, IN-1, IN-5 and IN-10) yield somewhat different results as shown in Table 10.4.

Table 10.4 Calculated temperatures for quartzofeldspathic gneisses using two-feldspars (Price, 1985), plagioclase-muscovite (Green and Usdansky, 1986) and biotite-muscovite (Hoisch, 1989) geothermometers. All temperatures are calculated at an assumed pressure of 4 kbar.

| Geothermometer | Two-feldspars (Price, 1985) | Plagioclase-muscovite Green and Usdansky, 1986) | Biotite-muscovite (Hoisch, 1989) |
|---|---|---|---|
| Sample no. | T (°C) | T (°C) | T (°C) |
| IN-18 | 346 | 389 | 713 |
| IN-19 | 415 | 485 | 728 |
| IN-14 | 483 | 562 | 669 |
| IN-5 | 579 | - | - |
| IN-10 | 472 | 626 | 577 |

Two-feldspars geothermometer (Price, 1985) yields unrealistic peak temperatures for these gneisses (346-579 °C), especially for the sillimanite-bearing rocks (samples IN-18 and IN-19). This is probably due to the exsolution of albite from K-feldspar to form perthite or re-equilibration of plagioclase and K-feldspar during slow cooling period of the gneisses. This illustrates the problem in application of two-feldspar geothermometer to upper-amphibolite facies rocks though it may have been proven to be useful for granulite-facies rocks (Stormer, 1975; Fuhrman and Lindsley, 1988).

The temperatures obtained from the plagioclase-muscovite geothermometer of Green and Usdansky (1986) are similar though somewhat higher than those given by the two-feldspar thermometer. A number of reasons for the low calculated temperatures are probably: (i) the re-equilibration of muscovite and plagioclase to lower temperature range, (ii) the low An content of plagioclase (which exerts a

strong influence on the calculated temperature) due to exsolution of albite from K-feldspar and, to the less degree, and (iii) uncertainties in microprobe analyses.

Biotite-muscovite thermometer (Hoisch, 1989) which has been calibrated against garnet-biotite thermometer (Ferry and Spear, 1978; Hodges and Spear, 1982) yields more realistic values, allowing for analytical uncertainties, than the other thermometers. However, it should be noted that the compositions of muscovite and biotite in the studied gneisses fall slightly outside the compositional ranges of micas used in the calibration of this thermometer. This difference may cause an additional degree of inaccuracy but the calculated temperatures agree well with petrogenetic grids and thus are accepted here.

The studied gneisses do not contain pressure-sensitive minerals, such as garnet or kyanite that may be used to determine pressure of equilibration. Therefore, metamorphic pressure of the gneisses can only be approximated via the use of Si content of muscovite. The numbers of Si atoms in muscovites from the studied gneisses are in the range 3.10 - 3.12 on the basis of 11 oxygens (Table 10.2). Using phengite geobarometry based on the limiting assemblage phengite + phlogopite + K-feldspar + quartz of Massonne and Schreyer (1987), the minimum pressure of about 4 kbar at preferred temperature of 700 °C was obtained.

If the oxidation state of iron in phengite is taken into account, the result would be a lower estimated pressure because a decrease in $Fe^{2+}$: $Fe^{3+}$ leads to a lower Si content of phengite. However, this effect is not considered to be significant because of the low absolute abundance of Fe (total Fe as FeO) in the studied phengites (FeO < 2%). For instance, if $Fe^{2+}$: $Fe^{3+}$ decreases from 1 : 0 to 0.5 : 0.5, the Si content will decrease by only 0.01 p.f.u. (p.f.u. = per formula unit). Additionally, the substitutions of $Fe^{2+}$ for Mg and $Fe^{3+}$ for Al in phengite lower the Si content of phengite in comparison with MgAl phengite used in the calibration of Massonne and Schreyer (1987). This effect is probably moderate because Mg/(Mg+$Fe^{2+}$) values of the studied phengites are rather high (0.45-0.55) and, also because the low absolute abundance of iron in the studied phengite as pointed out earlier.

An antipathy between Fe-Mg substitution in the octahedral sites and Na occupancy of neighbouring interlayer sites of white micas has been noted (Bailey, 1984; Guidotti, 1984, Green and Usdansky, 1986). The consequence of this relationship is that the introduction of Na for K into the white mica interlayer as a paragonite component would reduce the phengite Si content. Since the studied phengites contain very low Na contents (0.035-0.075 Na p.f.u.), this effect is very limited.

Nemec (1980) and Massonne and Schreyer (1987) showed that fluorine content of phengite causes an increase in Si content of phengite by 0.625 Si p.f.u./$X_F$ ($X_F$ = F/F+OH). This would result in the overestimation of equilibration pressure. The $X_F$ values of the studied phengites are in the range 0.03-0.09 (Table 10.2) which lead to an increase in Si content by 0.02-0.06 Si p.f.u. (equivalent to an increase in pressure estimate of about 0.5-1 kbar).

Massonne and Schreyer (1987) has also pointed out that the Si isopleths would shift towards the higher pressures with the reduction of water activity, $a_{H2O}$, e.g. a reduction of $a_{H2O}$ from 1.0 to 0.6 leads to a pressure increase of about 3 kbar. In the present study, this effect can not be evaluated.

Taking into account all factors that may affect the Si contents of phengite, it may be concluded that a pressure of around 4 kbar or less, based on phengite geobarometry of Massonne and Schreyer (1987), would be an appropriate estimate for the Doi Inthanon metamorphic complex.

The phase diagrams calculated by the THERMOCAL program of Holland and Powell (1990) for samples IN-18 and IN-19 (Figs. 10.5a&b) suggest that the peak temperature and pressure are 700±50 °C and 4±1 kbar respectively. In these phase diagrams, the granite (system $Na_2O$-$K_2O$-CaO-$Al_2O_3$-$SiO_2$-$H_2O$) minimum melting curve (for $An_0$) under water saturated condition of Johannes (1984) was used instead of Wyllie (1977). The melting curve should be displaced towards the higher temperature side with lowering $a_{H2O}$ but should not be affected significantly by the small variation in An content of plagioclase feldspar, e.g. the difference in solidus temperature between $An_{10}$ and $An_{40}$ is less than 10 °C according to Johannes (1984).

The *P-T* condition calculated using muscovite-biotite geothermometer (Hoisch, 1989) and phengite geobarometer (Massonne and Schreyer, 1987) in this study agree well with that of Mongkolthip (1986) who, based on a petrogenetic grid involving the breakdown reaction of muscovite in the presence of quartz: muscovite + quartz = K-feldspar + sillimanite + $H_2O$ (Chatterjee and Johannes, 1974) and granite melting curve (Wyllie, 1977), estimated the metamorphic pressure and temperature of sillimanite-bearing gneisses and migmatites in the Inthanon Mountain area to be more than 3 kbar and 650 °C respectively. Macdonald *et al.* (1993), using the phase diagram of Yardley (1989), suggest that the metamorphism of the high-grade gneisses took place under the pressure of about 2.8 ± 0.6 kbar and the temperatures in the range 600-700 °C which is slightly lower than the values obtained in this study. The peak metamorphism (M1) of the Doi Inthanon metamorphic complex is confirmed by this study to take place under low pressure

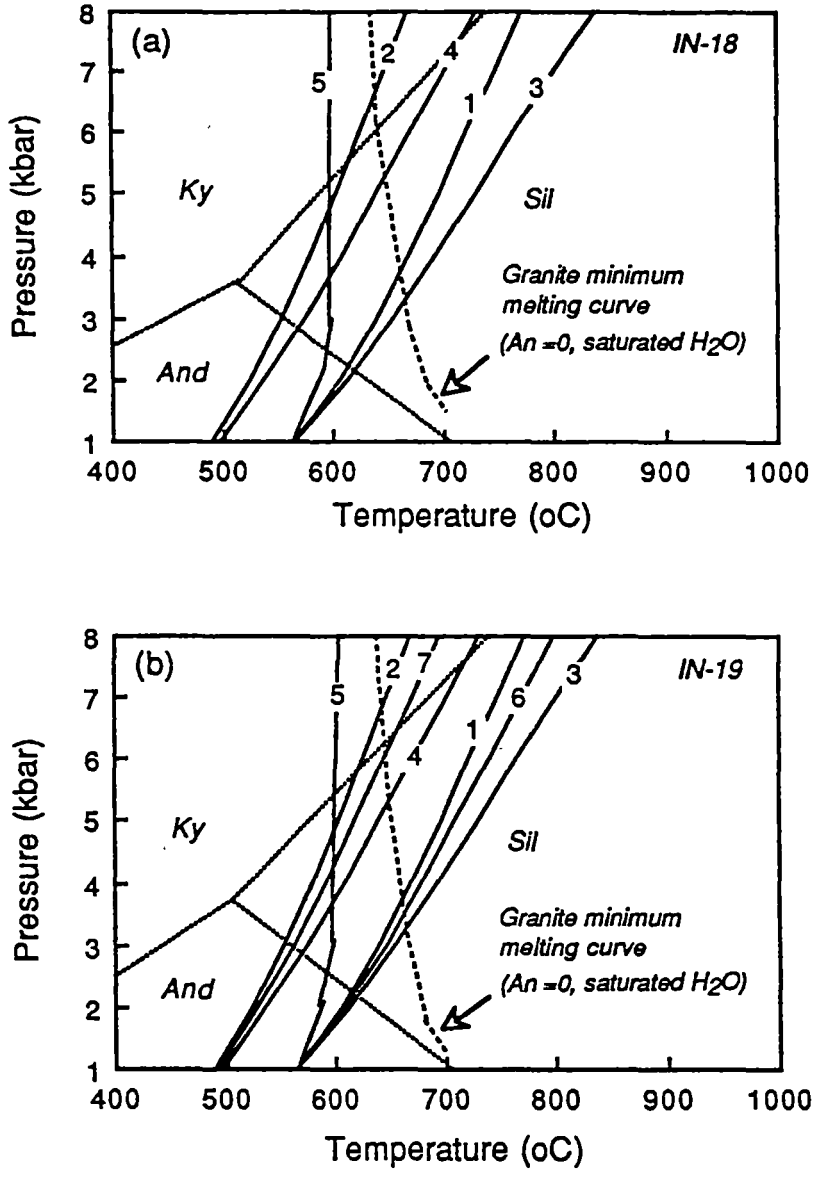


(1) Ms + Qtz = Kfs + Sil + $H_2O$
(2) Pg + Qtz = Ab + Sil + $H_2O$
(3) 3Ms + 3Phl = 3East + 2Kfs + 3Qtz + $2H_2O$
(4) Ms + 2Pg + 2Phl = 3East + 2Ab + 3Qtz+ $2H_2O$
(5) 3East + 6Qtz = 2Phl + Kfs + 3Sil + $H_2O$
(6) 6Ms + 2Phl = 3East + 5Kfs +3Sil + $5H_2O$
(7) Ms + 5Pg + 2Phl = 3East + 5Ab + 3Sil + $5H_2O$

Figure 10.5 Pressure-temperature diagrams showing the end-member reactions for sillimanite-bearing muscovite-biotite gneisses: (a) sample IN-18 and (b) sample IN-19. Reaction isopleths are calculated using the THERMOCAL program and the dataset of Holland and Powell (1990). A granite minimum melting curve is from Johannes (1984).

and high temperature condition, i.e. under a pressure of 4±1 kbar (corresponding to the depth of around 13 ±3 km) and a temperature of 700±50 °C.

### *P-T* conditions for calc-silicate rocks

The mineral assemblages in the studied calc-silicates do not allow for pressure estimation. Judging from their present structural relationships, it is believed that the equilibration pressure for the prograde metamorphic assemblage of the calc-silicates is probably less than 1 kbar lower than that of their quartzofeldspathic counterparts, i.e. in the order of 3±1 kbar.

Calc-silicates contain the assemblage clinopyroxene + plagioclase + quartz ± K-feldspar ± garnet ± hornblende ± calcite ± zoisite. Figures 10.6a&b show the *P-T* and *T* -$X_{CO2}$ diagrams calculated from the thermodynamic data set of Holland and Powell (1990) for sample IN-2 which contains the assemblage clinopyroxene + plagioclase + garnet + hornblende + quartz + calcite. The reaction Qtz + 2 Cal + An = Grs + CO2 (Fig. 10.6a) yields the temperature of about 700 °C at an estimated pressure of 3 kbar.*T* -$X_{CO2}$ diagram (Fig. 10.6c) for the assemblage containing wollastonite was calculated using GeØ-Calc program of Brown *et al.* (1988) and the Berman (1988) data base. From this diagram the peak temperature of around 680 °C was obtained and, in the similar manner, it is inferred that the retrograde metamorphism involving the formation of zoisite in sample IN-3 probably took place at about 520 °C.

The compositions of fluids during metamorphism have been studied from calc-silicate rocks, especially in granulite facies terrains (e.g. Nichols and Berry, 1991; Harley and Buick, 1992). At a preferred temperature of 700 °C and 3 kbar, the calc-silicates in this study suggest the $a_{CO2}$ was about 0.3 (Fig. 10.6b).

The calculated peak temperature (700 °C) and fluid activity ($a_{CO2} \approx 0.3$) during prograde metamorphism of calc-silicates obtained in the present study generally agree with but are better constrained than the values suggested by Macdonald *et al.* (1993) who, using the isobaric ($P_f$ = 2 kbar)*T* -$X_{CO2}$ diagram of Winkler (1976), inferred that the calc-silicates have been metamorphosed at a temperature greater than 600 °C under low $CO_2$ partial pressure.

## 10.6 Timing of Deformation and Metamorphism

Macdonald *et al.* (1993) suggested that $F_1$ and $F_2$ in the basement gneisses correspond to the folding phases in the cover rocks. However, this suggestion is not well-demonstrated and the structural correlation between the basement and the

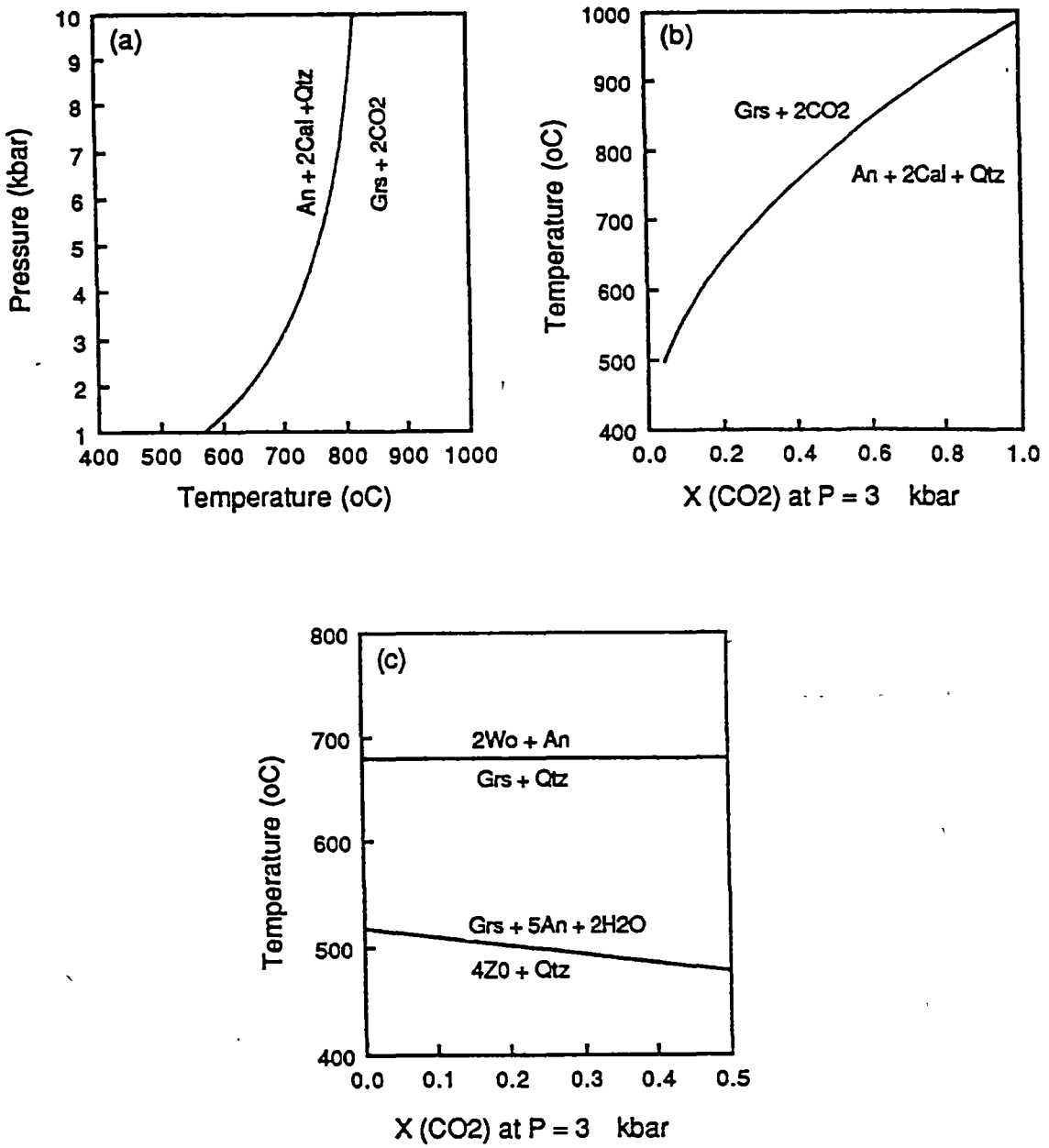


Figure 10.6 Phase diagrams: (a) pressure-temperature diagram showing the isopleth of the end-member reaction An+2Cal+Qtz = Grs+2$CO_2$ for sample IN-2; (b) T-$X_{CO2}$ diagram showing the same reaction in (a), based on the data set of Holland and Powell (1990); and (c) T-$X_{CO2}$ diagram (based on GeØ-Calc program (Brown *et al.*, 1988) and Berman (1988) data base) showing the end-member reactions involving wollastonite for calc-silicate rocks (sample IN-3).

cover sequence is still inconclusive at this stage. Further detailed study is required. Within the basement gneisses, the microstructural relationships clearly show that the earlier formed gneissic foliation/ compositional layering is overprinted by incipient to moderately developed mylonitic fabrics.

In the Bhumipol Dam area, north of Tak (see Figure 10.1 for the location), two folding periods were recognised in the gneissic complex similar to the Doi Inthanon area. The first folding event is characterised by the N-S trending upright to inclined isoclinal folds with associated schistosity and the second folding resulted in southerly-plunging recumbent isoclinal folds with axial-plane crenulation cleavage (Nutalaya, 1974). The peak metamorphism (amphibolite-facies) was inferred to be synchronous with the first folding phase and the retrograde metamorphism (upper greenschist-facies) was in part synchronous with and in part postdates the second folding phase. In the Lansang area, about 20 km west of Tak, two deformation phases were also recognised in the gneiss belt (Chantaramee, 1978). These two deformation phases are both characterised by tight to isoclinal folds and are coaxial to each other. The stretching lineations parallel to the fold axes have a gentle plunge. However, the gneissic rocks from these two areas lack strong late mylonitic overprint as in the case of the Doi Inthanon complex.

Based on U-Pb data from the biotite-muscovite orthogneiss (section 10.2), Macdonald *et al.* (1993) proposed that prograde metamorphism that associated with the gneiss dome of the Doi Inthanon metamorphic complex took place around 72±1 Ma (Late Cretaceous) and the granitic protolith crystallised around 207±3 Ma. Microstructural evidence indicate that peak metamorphism was attained during $D_1$ deformation. The later deformation episodes were not accompanied by the growth of the peak mineral assemblages. It is more likely that the peak metamorphism ($M_1$) and the synchronous $D_1$ deformation occurred contemporaneously with the Late Triassic-Early Jurassic granites (i.e. around 200-210 Ma). Ahrendt *et al.* (1993) suggested that the U-Pb date of zircon (around 200 Ma), in porphyroblastic feldspar-biotite gneiss from the Lansang area (around 15 km west of Tak), represents the amphibolite facies in the area. The mylonitic fabrics were accompanied by retrograde greenschist facies minerals, e.g. zoisite, biotite and chlorite (during retrograde metamorphism). K/Ar dating of micas from the mylonites (Ahrendt *et al.*, 1993) suggests this movement took place in Late Cretaceous to Middle Tertiary during uplift and cooling of the gneissic complex.

## 10.7 Tectonic Implications

Several tectonic models have been put forward to explain the formation of the gneiss belt in northwestern Thailand including the Doi Inthanon metamorphic complex. The petrology, metamorphic and deformation history discussed above place constraints on models for the tectonic evolution of this important high-grade terrain and are used as the basis for testing these models as follows:

**The Lower Carboniferous orogenic model:** Baum *et al.* (1970) regarded the high-grade gneissic rocks of the gneiss belt west of the Sukhothai fold belt as Precambrian paragneisses which formed the core of a north-south-trending anticlinorium and have been subjected to anatexis or migmatisation during Lower Carboniferous orogeny.

This view is not supported by the radiometric dating of granitic rocks in northern Thailand, especially those in close spatial relation with the gneisses, all indicate Permo-Triassic or younger ages of the intrusions (Teggin, 1975; Braun *et al.*, 1976; Macdonald *et al.*, 1993).

**The Triassic orogenic model**: Cobbing *et al.*, (1986) suggested the gneiss belt with the characteristic migmatites formed in the Triassic due to the thermal effect of the extensive S-type granites. Later Barr and Macdonald (1991) inferred the occurrence of S-type granites to be indicative of Triassic metamorphism and crustal melting and suggested that the gneiss belt formed as a series of metamorphic core complexes in response to collisional underthrusting of the Shan-Thai cratonic margin beneath the amalgamated Sukhothai and Indosinian (Indochina) terranes.

This model is most consistent with the observations made of the structure and metamorphism of the gneissic rocks. The S-type granites have high $^{87}Sr/^{86}Sr$ ratios (Hutchison, 1983) suggesting that they probably formed by anatexis of mid-crustal rocks. Moreover, the syn-tectonic nature of most Triassic granitic plutons in association with the gneisses lends strong support to this model as well. It should also noted that the zircon ages in both granites and the gneisses are restricted to around 200-210 Ma which suggest the major thermal events, the granitic intrusions and the high-grade metamorphism/migmatisation, were at the end of the Triassic.

**The Cretaceous metamorphic-core complex model**: Macdonald *et al.* (1993) noted that the gneiss belt has many features similar to those of the Cordilleran metamorphic core complexes and proposed that it was the result of Late Cretaceous high-grade metamorphism of Late Precambrian - Early Cambrian sediments and Late Triassic-Early Jurassic granites and was subjected to uplift,

detachment and unroofing in Tertiary time. These events are considered to be related to crustal thinning some 300 km behind the east-dipping subduction zone of Cretaceous-Eocene age, represented by Burma magmatic arc of Mitchell (1977).

This model emphasises the importance of the Cretaceous-Tertiary thermal activity in the development of the gneissic belt of western Thailand. However, the the dominance of the Late Triassic S-type granites in the gneiss belt rather than the Cretaceous granites does not support this model, particularly the timing of the high-grade metamorphism. The fact that the metamorphism of high-grade gneissic rocks along this belt requires an extensive and prolong heat sources favours the thermal event that was also responsible for the voluminous Triassic granitic intrusions. Many of the Triassic granitic plutons have syn-tectonic relationships with the enclosing gneissic rocks (Cobbing *et al.*, 1986).

The extensional regime required to produce the metamorphic core complex in this model, was ascribed to the a crustal thinning 300 km behind the Cretaceous-Eocene east-dipping subduction zone (which is now part of the West Burma terrane shown in Figure 1.1). This implies that the metamorphic core complexes occupied the axis of the backarc region during that time. This scenario is possible but fails to account for the lack of coeval volcanic counterparts of backarc affinities in western Thailand.

**Present view:** Among the models discussed above, the Triassic orogenic model is most consistent with the observed data, either the high $T$ /low $P$ metamorphism of the gneisses or the extensive Triassic granitic intrusions in the gneiss belt. The formation of mylonitic fabrics is probably related to uplift during the Late Cretaceous to Middle Tertiary.

At the present stage of the knowledge, it is not possible to confidently suggest the relationships between the Doi Inthanon metamorphic complex and the Sukhothai fold belt to the east. A further detailed study of deformation history of the Lower-Middle Palaeozoic shelf sequences (lying between the gneiss belt and the Sukhothai fold belt) is needed to place constraints on the correlation of these two tectonic elements as well as the structural correlation between the gneissic basement and the Lower Palaeozoic cover rocks.

## 10.8 Summary

The gneissic rocks of the Doi Inthanon metamorphic complex are divided into core orthogneisses and mantling paragneisses separated from the Lower Palaeozoic cover rocks by a low-angle fault which is thought to be the detachment

fault. Both core and mantling gneisses have been intruded by the foliated granitic plutons with crudely concordant contacts.

In general, the Doi Inthanon metamorphic complex is a mantled gneiss dome. Four deformation episodes have been recognised in the gneisses. $D_1$ deformation produced a prominent gneissic foliation with local rootless intrafolial folds. $D_2$ and $D_3$ deformation phases are probably represented by $F_2$ overturned folds and $F_3$ chevron folds of Macdonald *et al.* (1993) respectively. $D_4$ deformation phase is characterised by the formation of mylonitic fabrics which consist of mylonitic foliation and mineral stretching lineation subparallel to or at low-angle to gneissic layering. A series of N-S-striking high angle normal faults are common in the gneisses and are probably related to the formation of the nearby Middle Tertiary extensional basin.

The *P-T* conditions of peak metamorphism of quartzofeldspathic gneisses were calculated using muscovite-biotite geothermometer, phengite geobarometer together with thermodynamic calculations. It is suggested that the peak metamorphism of the Doi Inthanon metamorphic complex occurred under low pressure and high temperature conditions, i.e. under a pressure of 4±1 kbar (corresponding to the depth of around 13 ±3 km) and a temperature of 700±50 °C. In addition, the *P-T* conditions for calc-silicate rocks were determined by thermodynamic calculations. The peak temperature of 700 °C was obtained and the equilibration pressure was inferred to be 3±1 kbar based on structural relationship with the quartzofeldspathic gneisses. The $CO_2$ activity, during metamorphism was inferred to be around 0.3. Retrograde metamorphism involving the formation of zoisite took place at about 520 °C.

The peak metamorphic episode ($M_1$) was probably attained during $D_1$ deformation in the Late Triassic-Early Jurassic due to crustal thickening as a result of the collision between Shan-Thai and Indochina terranes and the retrograde metamorphic event ($M_2$) was contemporaneous with the formation of mylonitic fabrics probably during Cretaceous to Middle Tertiary.

Among the models proposed to explain the development of the Doi Inthanon metamorphic complex, the Triassic orogenic model is most consistent with the observed data, either the high *T* /low *P* metamorphism of the gneisses or the extensive Triassic granitic intrusions in the gneiss belt. The formation of mylonitic fabrics is more probably related to uplift during the Late Cretaceous to Middle Tertiary.

# Chapter 11

# TECTONIC IMPLICATIONS OF THE SUKHOTHAI FOLD BELT

## 11.1 Introduction

The tectonic evolution of the northern Thailand region has been a subject of interest and controversy in the recent years. Much of the debate has centred on the geometry and timing of terrane accretion in this part of Southeast Asia. As the Sukhothai fold belt constitutes a major part of the region, the evolution of this fold belt could be significant in determining the evolution of the whole of northern Thailand.

In this chapter, the structural and metamorphic evolution of key rock units within the Sukhothai fold belt will be discussed in the context of plate tectonics. Various existing tectonic models for this part of Southeast Asia are tested in the light of the new structural and metamorphic data. Additional stratigraphic, sedimentological and petrochemical data also make some contribution to discussion. A tectonic model for the Sukhothai fold belt is proposed.

## 11.2 The Current Tectonic Models

The common view among geoscientists concerned with the tectonic evolution of Southeast Asia is that mainland Southeast Asia (south of the Red River in Vietnam) was created by the amalgamation of the Shan-Thai and Indochina terranes (Fig. 11.1). These two terranes have been thought to be part of Gondwana in Early Palaeozoic (Ridd, 1971; Burrett, 1974; Audley-Charles, 1983; Burrett and Stait, 1985, 1986). After the break-up of Gondwana in Middle Palaeozoic, the Shan-Thai and Indochina terranes drifted northwards during Late Palaeozoic (Ridd, 1980) and collided with each other prior to the final collision with mainland Asia in Late Triassic (Bunopas and Vella, 1978; Ridd, 1980). At this stage, discussion will centre on the interaction between the Shan-Thai and Indochina terranes only. The data obtained from this study does not contribute to discussion whether the Shan-

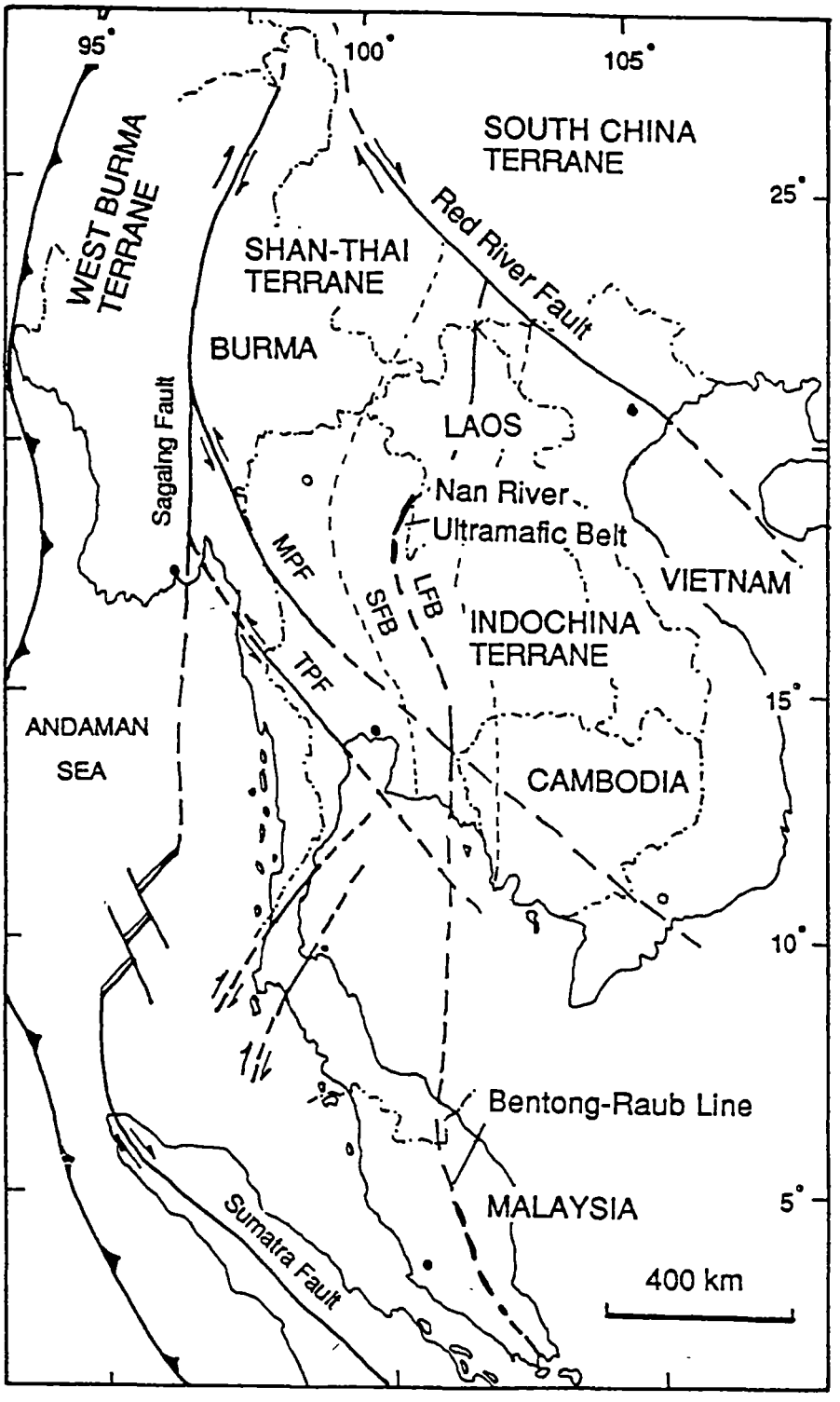


Figure 11.1 Tectonic map showing tectono-stratigraphic terranes of mainland Southeast Asia. SFB = Sukhothai fold belt, LFB = Loei fold belt, MPF = Mae Ping fault, TPF = Three Pagoda fault (modified after Bunopas, 1981; Metcalfe, 1986; Mitchell, 1992).

Thai and Indochina terranes were once part of the Gondwana or when and how the fusion of these two terranes and the mainland Asia continent occurred.

Plate tectonic models accounting for the collision between the Shan-Thai and Indochina terranes have been proposed by a number of workers. The general agreement among these models is that there exist a palaeo-ocean basin between the two terranes in the Late Palaeozoic time. Nevertheless, the geometry and timing of collision remain controversial due to the lack of detailed structural information, biostratigraphic data and radiometric age dating of the key lithological units.

The geometry of plate convergence prior to collision has been viewed in three different perspectives as follows:

(i) Westward subduction of the Indochina terrane beneath the Shan-Thai terrane (Fig. 11.2a) has been proposed by Stauffer (1974), Hutchison (1975), Asnachinda (1978), Bunopas and Vella (1978), Chantaramee (1978), Macdonald and Barr (1978), Hamilton (1979), Ridd (1980), Suensilpong *et al.* (1983), Barr and Macdonald (1987), Hayashi (1989) and Hada (1990).

(ii) Eastward subduction of the Shan-Thai terrane under the Indochina terrane (Fig. 11.2b) has been suggested by Mitchell (1977, 1986) and Beckinsale *et al.* (1979).

(iii) A pair of subduction zones dipping in the opposite directions, i.e. towards both the west and the east (Fig. 9.12c), has also been suggested by several workers (Gatinsky *et al.*, 1978; Thanasuthipitak, 1978; Bunopas, 1981; Bunopas and Vella, 1983; Cooper *et al.*, 1989, Hutchison, 1989).

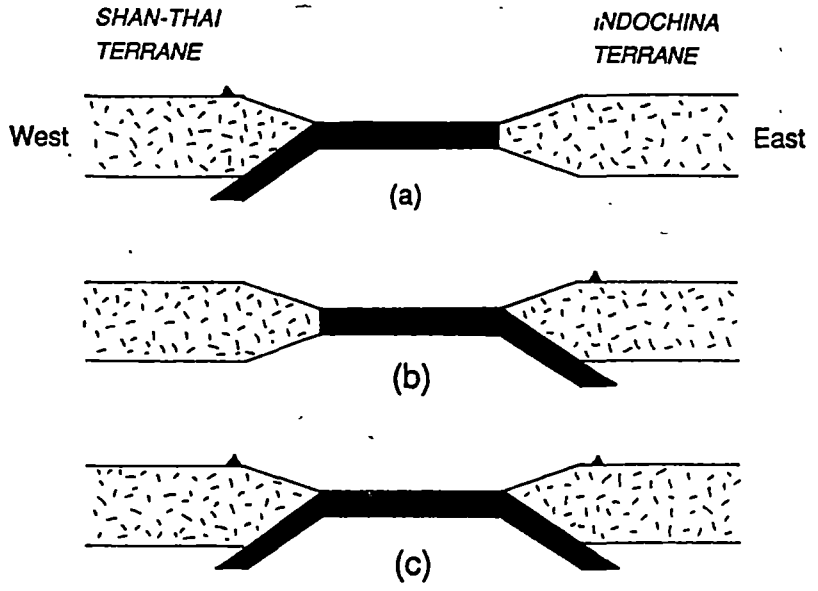


Figure 11.2 Schematic diagrams showing three different views of plate configuration of northern Thailand prior to the amalgamation of the Shan-Thai and Indochina terranes.

As to the timing of collision of these two terranes, three major different opinions have been noted:

(i) Late Triassic (Hutchison, 1975, 1983, 1989; Mitchell, 1977, 1986, 1992; Asnachinda, 1978; Chantaramee, 1978; Gatinsky *et al.*, 1978; Macdonald and Barr, 1978; Bunopas and Vella, 1978, 1983; Bunopas, 1981; Panjasawatwong, 1991),

(ii) Late Permian-Early Triassic (Stauffer, 1974; Thanasuthipitak, 1978; Ridd, 1980; Metcalfe, 1986; Hayachi, 1989; Cooper *et al.*, 1989), and

(iii) Middle Permian (Helmcke, 1982, 1985, 1986; Helmcke and Kraikhong, 1982; Helmcke and Lindenberg, 1983; Burton, 1984; Sengör,1984; Hahn, 1985; Barr and Macdonald, 1991).

The suture between these two terranes is usually drawn along the "Nan River ophiolite belt". This belt is thought to extend southwards across the Gulf of Thailand and possibly into Peninsular Malaysia where a similar feature known as the Bentong-Raub ophiolite line (Fig. 11.1) has been recognised (Stauffer, 1974; Bunopas, 1981). Tan and Khoo (1981) and Tan (1984) questioned whether the Bentong-Raub serpentinised ultramafics represent true ophiolite. They cast doubts on the prevailing idea that the emplacement of these mafic-ultramafic rocks was subduction-related. Instead, Tan (1984) proposed that the serpentinised ultramafics have been intruded along deep-seated extensional fracture zones.

This wide diversity of interpretation reflects not only the complicated tectonic evolution of this region but also the lack of sufficient detailed geological knowledge that may help distinguish between the different views.

## 11.3 Requirements for the Tectonic Model

Any tectonic model attempting to explain the geological evolution of northern Thailand, and the Sukhothai fold belt in particular, has to take into account the following critical observations which have been discussed in detail in the previous chapters.

(i) The multiple deformation of the Permo-Carboniferous Pha Som Metamorphic Complex, especially the metasedimentary rocks. This complex bears strong similarities to many ancient accretionary complexes around the world, e.g. the Kodiak Complex in Alaska and Calaveras Complex in California (Paterson and Sample, 1988), Shimanto Complex in Japan (Needham and MacKenzie, 1988), Torlesse terrane in New Zealand (MacKinnon, 1983), New England fold belt in eastern Australia (Fergusson *et al.*, 1990), Southern Uplands of Scotland (Knipe and Needham, 1986) and the Dunnage Zone in Newfoundland (van der Pluijm,

1987). Since the internal evidence is for east directed thrusting as the dominant mechanism for the formation of this accretionary complex the data presented here supports models suggesting a west-dipping subduction zone under the Shan-Thai block in the Carboniferous and early Permian.

(ii) The presence of a Permo-Triassic volcanic and volcaniclastic sequence within the Sukhothai fold belt.

(iii) The presence of turbidite and carbonate sequences having the character of forearc deposits, i.e. the Permian sequence (the Phrae or Ngao Group) and Triassic sequence (the Lampang Group).

(iv) The similarity in structural style and structural succession between the Permian sequence (the Phrae or Ngao Group) and Triassic sequence (the Lampang Group).

(v) The difference in structural and sedimentological styles between the Permian-Triassic sequences within the Sukhothai fold belt and the Jurassic-Cretaceous redbed sequences.

Apart from these critical observations, some other well-documented information has to be considered as well. These include:

(i) The occurrences of Late Permian-Middle Triassic I-type granitoids and Late Triassic-Early Jurassic S-type granitoids in the western part of the Sukhothai fold belt (e.g. Mitchell, 1977; Beckinsale *et al.*, 1979; Hutchison, 1983; Cobbing *et al.*, 1986; Mahawat *et al.*, 1990) .

(ii) The occurrence of crossite-bearing blueschists in the Permo-Carboniferous metasedimentary rocks in the eastern part of the Sukhothai fold belt (Barr *et al.*, 1985; Barr and Macdonald, 1987; Panjasawatwong, 1991).

## 11.4 The evidence

A summary of the critical evidence used to test the validity of each tectonic model (section 11.2) is given below. Detailed discussion is presented in the previous chapters.

### 11.4.1 Accretionary complex

The multiply deformed Pha Som Metamorphic Complex is located on the eastern limit of the Sukhothai fold belt. This metamorphic complex encompasses an ophiolite association and a metasedimentary unit. These two units though lithologically different from each other but both have compositions and deformation histories commonly reported from accretionary complexes.

(i) Modal compositions of framework grains suggest that the greywackes of the Pha Som Metamorphic Complex were derived from two main sources, an accretionary complex/magmatic arc source and a volcanic arc source. Geochemical studies of the metagreywackes of the Pha Som Metamorphic Complex suggest that some part of the metagreywackes were derived from the continental arc source as well as the oceanic volcanic arc source. The geochemical similarities between the Pha Som metagreywackes and the Torlesse and Caples terranes in New Zealand (see details in Chapter 7) suggest that they were derived from the active continental magmatic arc as well as the oceanic volcanic sources and deposited in a trench or submarine fan setting at the subduction margin as do the Torlesse and Caples sediments (MacKinnon, 1983; Roser and Cooper, 1990; Mortimer and Roser, 1992).

(ii) Four deformation phases ($D_1$ - $D_4$) have been recognised in the metasediments of the Pha Som Metamorphic Complex (detailed discussion is presented in Chapter 4). The structural vergence and other kinematic criteria, especially during $D_2$ event, indicate eastward tectonic transport. The $D_1$ to $D_2$ deformation events in the Pha Som Group are consistent with the deformation processes in the well-studied accretionary prisms, e.g. the Kodiak Complex in Alaska (Sample and Fisher, 1986; Sample and Moore, 1987; Paterson and Sample, 1988). Since $S_2$ is dominant foliation that has a style typical of accretionary complexes, the eastward transport associated with this structure is correlated with a normal convergent margin setting and indicates a west dipping subduction zone. $D_3$ and the $D_4$ thrusts and asymmetrical angular folds in this complex probably represents the collision stage.

(iii) Metamorphism of the accretionary complexes is commonly characterised by the high *P* /low *T* type, i.e. blueschist-facies metamorphism. However, many accretionary complexes have greenschist facies rather than blueschist facies metamorphism, e.g the Kodiak Complex in Alaska and the Calaveras Complex in California (Paterson and Sample, 1988). The metamorphism of the Pha Som metasedimentary rocks occurred under greenschist facies conditions, i.e. the pressure of 3-6 kbar and the temperature in the range 300-400 °C. The occurrence of crossite-bearing epidote-quartz schist (Barr and Macdonald, 1987) within the metamorphic complex is indicative of relatively high-pressure metamorphism (probably up to 7 kbar). This greenschist facies metamorphism is contemporaneous with $D_2$ deformation. Blocks in a serpentinite melange (the ophiolite association) have somewhat different metamorphic history. Amphibolite blocks are the result of amphibolite facies metamorphism before incorporation in the accretionary complex. The piemontite-bearing quartz schists may represent the

blueschist facies metamorphism (at a pressure of around 7 kbar and a temperature of 400-450 °C) of the hemipelagic or pelagic chert with high-Mn contents.

(iv) The age of the Pha Som Metamorphic Complex is probably Permo-Carboniferous. The Ar-Ar amphibole ages of the amphibolite blocks (the Pha Som Ultramafics) range from 356 to 256 Ma (Drs. Y. Panjasawatwong and A.J. Crawford, pers. comm., 1993). A Permo-Carboniferous age was reported by Hahn (1985), on basis of fossils foraminifera and bryozoan in a calcareous cement of a volcanic breccia within the ophiolite association. These age data suggest that the probable age range of blocks within the ophiolite association is the Carboniferous-Middle Permian. The age of the Pha Som metasediments was suggested by Bunopas (1981) as a Silurian-Devonian age but this age is not consistent with the stratigraphy of the region and recent radiometric dating. Hess and Koch (1975) proposed a Permo-Carboniferous age on the basis of regional stratigraphy. A minimum metamorphic age of 269 Ma (Middle Permian), based on a K-Ar date of actinolite-quartz schist, was suggested by Barr and Macdonald (1987). A Carboniferous-Middle Permian age for the assembly of the Pha Som Metamorphic Complex is suggested. The Upper Cretaceous K-Ar date on white mica recently reported (Ahrendt *et al.*, 1993) is not consistent with the deformation history and structural relationships of the Pha Som Metamorphic Complex and it is best considered as a later thermal overprint unrelated to the formation of this metamorphic complex.

## 11.4.2 Volcanic arcs

Permo-Carboniferous basaltic volcanic rocks occur within the sedimentary sequences in the western part of the Sukhothai fold belt, 20 km east of Chiang Mai. Previously these volcanic rocks were thought to have been generated in an island arc environment (Macdonald and Barr, 1978). However, pyroxene compositions and whole-rock geochemistry indicate that the volcanics rocks formed mainly in an extensional continental setting not in a subduction zone environment (Barr *et al.*, 1990). They suggested that these volcanic rocks, which extend in a N-S trend, may represent a zone of backarc continental extension within the Shan-Thai craton behind a west-dipping Permo-Carboniferous subduction zone. Their interpretation, though speculative, is consistent with stratigraphic and sedimentation pattern in the central part of the Sukhothai fold belt (i.e. in the Lampang-Phrae area).

The Permo-Triassic volcanic rocks observed close to the boundary between the Sukhothai and the Loei fold belts (the Pak Pat volcanics) belong to subalkali

series with probable medium to low-K affinities suggesting an oceanic island arc affinities (see Chapter 6 for details). The age of these volcanic rocks is in the range Middle Permian to Early Triassic

The tectonic setting of eruption of the Permo-Triassic volcanics in Lampang-Phrae area (i.e. the central part of the Sukhothai fold belt) has not been documented. On the basis of field observations and petrography, it is likely that the felsic to intermediate volcanic rocks (rhyolite to dacite with rare andesite) and associated volcaniclastic rocks formed in continental arc environment.

Preliminary geochemical data of volcanic rocks from the Loei fold belt, to the east of the inferred suture, suggesting a subduction-related arc volcanism in that area (Dr. A.J. Crawford, pers. comm., 1993). Recent studies by Intasopa and Dunn (1994) showed that these volcanic rocks have diverse tectonic settings of eruption and range in age from Late Devonian and Triassic. The present evidence suggests most of the volcanic rocks in the Loei volcanic province are older than the Sukhothai fold belt.

### 11.4.3 Turbidite sequences

The Permian turbidites and limestone (the Rong Kwang Formation) have thrust or unconformable contacts with the Permo-Carboniferous Pha Som Metamorphic Complex. This sedimentary sequence (see Chapter 8) has a character of sediments that are accumulated in the forearc basin.

The Triassic turbidite sequences (the Lampang Group) in Lampang and Phrae areas both unconformably and conformably overlie the Permo-Triassic volcanic sequence and the Permian turbidite sequence. In the eastern part of the Sukhothai fold belt, the contact between the Triassic and Permian sequence is conformable indicating continuous deposition through the Permian-Triassic boundary. This observation agrees well with the previous report that there was more or less continuous marine sedimentation from the Permian into the Triassic (Junhavat and Piyasin, 1978; Hahn, 1985). Chonglakmani and Helmcke (1989) argued against the idea that the sediments of the Triassic Lampang Group are forearc-basin fills in a pre-collisional setting which, in their view, are characterised by deep marine flysch strata. They interpreted that these sediments have been deposited in post-collisional shallow intramontane molasse basins. Chaodumrong (1992), citing examples of many forearc basins around the world, demonstrated that forearc basins are not necessarily deep, many of them are shallow and filled with continental sediments. Chaodumrong (1992) re-affirmed the idea that the Lampang Group sediments have been deposited in a shallow forearc basin prior to

the collision. These sediments lack characteristic features of pull-apart or successor basins and were shown to be derived from the volcanic source terrain.

The sediments of the Triassic Nam Pat Group in the east of the Sirikit Dam are very similar to the Lampang Group sediments and they were probably derived from a volcanic source and were deposited in the nearby basin. They sit on top of the conglomerate unit which is thought to be reworked volcaniclastic sediment and re-deposited by turbidity current. Lüddecke *et al.* (1991) analysed pebble associations in the lower conglomerate unit (the Huai Lat Formation) and suggested that the source area was the Triassic andesitic continental volcanic arc not the shallowing trench as implied by Bunopas (1981). The compositional characteristics of the detrital framework grains and their immature textures indicate that the Nam Pat sandstones were derived from a nearby magmatic arc. The volcanic source is possibly the andesitic volcanoes that generated the Pak Pat volcanics. The major and trace element characteristics, suggest that they represent sediments derived from the volcanic rocks of mainly intermediate in compositions.

### 11.4.4 Deformation and metamorphism of the turbidite sequences

The deformation of the Permian and Triassic sequences is characterised by the upright open folds and thrusts. These strata were subjected to a single phase of folding with associated northeast-striking regional cleavage. The folding is associated with thrusting.

The metamorphic grade of the Permian and Triassic sequences increases from west to east. In the eastern part of the Sukhothai fold belt, the metamorphic grades of the Permian and Triassic pelites range from upper anchizone to epizone. In the west, the pelitic rocks of the Triassic sequence belong to diagenetic to lower-anchizone grade. This metamorphic event is related to the single cleavage-forming event in the Permian and Triassic sequences.

Recent K-Ar dating of fine mineral fractions of shale/slate of the Triassic Lampang Group indicates that the cleavage formed between 188-220 Ma (Ahrendt *et al.*, 1993). The radiometric age and the relative age consistently point to the Late Triassic age of the deformation and metamorphism in northern Thailand. This is consistent with the presence of this cleavage in Middle Triassic sedimentary rocks and its absence from Middle Jurassic sedimentary rocks

## 11.4.5 Post-orogenic granites and continental red beds

### Granitic intrusions

The granitic intrusions in Thailand are shown by Beckinsale *et al.* (1979) to have occurred at around 240 Ma (Lower Triassic), 210 Ma (Upper Triassic), 130 Ma (Lower Cretaceous) and 90 Ma (Middle Cretaceous). Only the first two magmatic events are relevant to the evolution of the Sukhothai fold belt. There is a general consensus among the several studies (Mitchell, 1977; Beckinsale *et al.*, 1979; Hutchison, 1983; Cobbing *et al.*, 1986; Mahawat *et al.*, 1990) that the granitoids in Thailand can be divided into three provinces that extend into peninsular Malaysia (Fig. 11.3).

The Eastern province is well-defined in Peninsular Malaysia and southeastern Thailand but includes only scattered plutons in northern Thailand. Throughout the belt the granitoids develop very narrow thermal aureoles and some have miarolitic cavities indicating high-level emplacement (Cobbing *et al.*, 1986). The granitoids, dominantly monzogranite in composition, are mainly I-type (Hutchison, 1977, Beckinsale *et al.*, 1979). The granitoids of the Eastern province have been noted to be associated with the Permo-Triassic volcanic rocks in northern Thailand (Mahawat *et al.*, 1990). These granitoids have been inferred to have formed in an Andean-type continental margin of the Shan-Thai terrane (Hutchison, 1983; Mahawat *et al.*, 1990). This model is supportive of the Permo-Triassic subduction zone.

The central province is the Northern Thailand and Migmatite Complex province which is geographically continuous with the Main Range province in Peninsular Malaysia (Cobbing *et al.*, 1986). The granitoids of this province have the characteristics of S-type granites and are of Middle to Late Triassic age. The granitoids in the Migmatite Complex (e.g. the Doi Inthanon metamorphic complex discussed in Chapter 10) are highly deformed with strong sub-horizontal foliation interlayered with orthogneisses and paragneisses. Other types of granitoids occur as larger batholiths and associated smaller plutons intruding the Palaeozoic-Lower Mesozoic sedimentary sequences and the Migmatite zone. The S-type granites usually have very high $^{87}Sr/^{86}Sr$ ratios (commonly in the range 0.722 to 0.734) indicating upper crustal origin (Hutchison, 1983). These granites have of a post-kinematic character with respect to the deformed sedimentary country rocks.

The Western province is characterised by Cretaceous plutons of mixed I- and S-type character. These granitoids intruded Permo-Carboniferous marine tillites

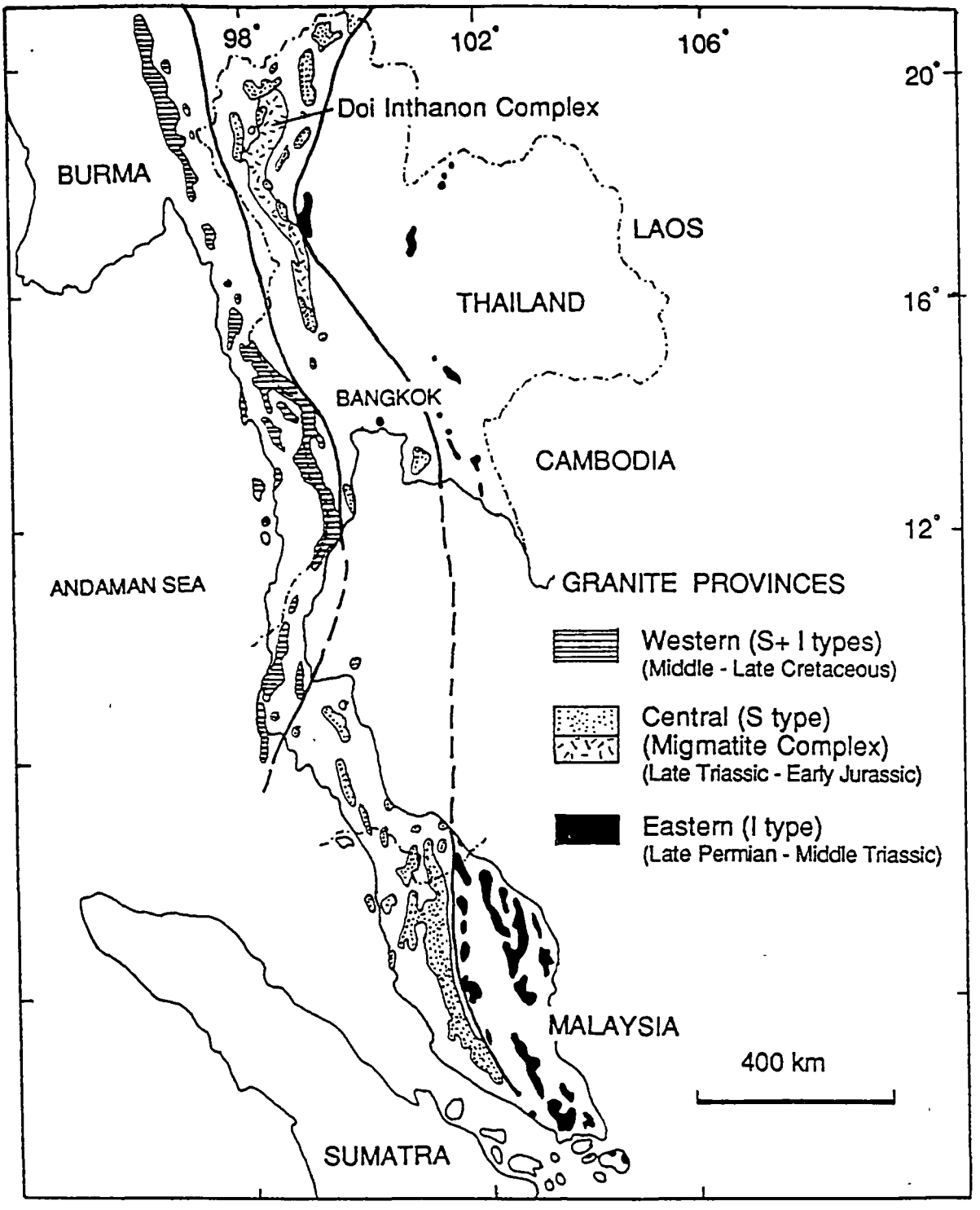


Figure 11.3 Distribution of granite provinces of mainland Southeast Asia (modified after Mitchell, 1977; Beckinsale *et al.*, 1979; Cobbing *et al.*, 1986).

along Peninsular Thailand and Burma. This Cretaceous Western province is probably related to the subduction of Indian plate beneath the West Burma and Shan-Thai terranes (Mitchell, 1977; Hutchison, 1983; Barr and Macdonald, 1991).

**Jurassic redbeds**

In the Sirikit Dam area, the open-folded Jurassic continental redbeds (the Phra Wihan Formation) unconformably overlie the close-folded Triassic Nam Pat turbidites. Elsewhere in northern Thailand, the Jurassic-Cretaceous continental redbeds (including the Phra Wihan Formation) unconformably overlie the Triassic Lampang Group and the Permian Phrae Group (e.g. the 1:2,500,000 geological map of the Department of Mineral Resources, 1987). The compositional characteristics of the detrital framework modes indicate that the quartzose sandstones of the Phra Wihan Formation were derived from a quartzose recycled orogenic source or from the craton interior suggesting post-orogenic deposition. These sediments were laid down in a braided stream environment.

## 11.5 Testing of the Current Tectonic Models

Validity and applicability of each of the tectonic models described in section 11.2 can be tested on the basis of several lines of evidence discussed above. However, greater emphasis is placed on the structure and metamorphism of the key lithostratigraphic units studied.

### 11.5.1 Geometry of plate convergence

There are three different views of plate configuration of northern Thailand prior to the amalgamation of the Shan-Thai and Indochina terranes (Figure 11.2). The west-dipping subduction zone model (hereafter referred to as model A, Fig. 11.2a) has been proposed mainly to account for the presence of volcanic arc in the Sukhothai fold belt and, later, the paired-subduction zone (hereafter referred to as model C, Fig. 11.2c) has been proposed to account for the presence of similar volcanic arc in the Loei fold belt as well. In contrast, the east-dipping subduction zone model (hereafter referred to as model B, Fig. 11.2b) was mainly developed to explain the I-type granites in mainland Southeast Asia by Mitchell (1977) and followed by Beckinsale *et al.* (1979).

Model A, with a west-dipping subduction zone beneath the eastern margin of the Shan-Thai block and a passive margin on the western edge of the Indochina

block, is consistent with the presence of the east-facing accretionary complex (the Permo-Carboniferous Pha Som Metamorphic Complex) and the Permo-Triassic volcanic arc (e.g. the Doi Luang volcanics in the Lampang-Phrae area). In addition, it explains the absence of an accretionary complex and the presence of extensive Middle-Late Permian platform-carbonates on the western edge of the Indochina block. However, model A does not account for the presence of the Loei volcanic province. The volcanism in this province has a complex tectonic history starting from the Late Devonian to Permo-Triassic and it has recently been interpreted as the result of interaction between the Indochina and South China terranes (Intasopa and Dunn, 1994). The significance of the Loei volcanic belt is not directly relevant to the tectonic history of the Sukhothai fold belt and it is beyond the scope of the present study to discuss this volcanic belt in detail.

According to Beckinsale *et al.* (1979), eastward subduction in the Late Permian (Model B) would account for the Permo-Triassic volcanic arc and the known porphyry copper deposit at Loei and the Eastern Belt granites of Mitchell (1977). Model B envisages the eastern margin of the Shan-Thai terrane (i.e. the Sukhothai fold belt) as a passive margin citing the widespread Late Permian-Early Triassic carbonate platform facies (Mitchell, 1977). This is in contrast with the recent study (i.e. Chaodumrong, 1992) which showed that the Triassic turbidites and carbonates have many features of forearc sediments. In addition, model B fails to explain the presence of an east-facing accretionary complex (the Permo-Carboniferous Pha Som Metamorphic Complex). Model B requires the Permo-Triassic volcanic arc (e.g. the Doi Luang volcanics) and all of the related arc derived sediments to be allochthonous elements thrust over the Shan Thai terrane. This is inconsistent with the dominantly east directed thrusting in the Sukothai Fold Belt and is improbable on the present field data.

Model C combines the basic elements of both models A and B and suggests that the arc volcanics in the Sukhothai and Loei fold belts formed above a pair of subduction zones (e.g. Thanasuthipitak, 1978). This model, however, predicts an accretionary complex in the western side of the Indochina terrane which has not been recognised. As the deformation history of the Loei fold belt is not well constrained, further structural study of the Loei fold belt is required to properly test model C.

The data from the Sukhothai fold belt are most consistent with model A and may be compatible with model C but are inconsistent with the passive margin suggested in model B.

### 11.5.2 Timing of the collision

The timing of the collision between the Shan-Thai and Indochina terranes is a subject of much debate. The three major different views concerning the timing of collision, i.e. the Middle Permian, Late Permian-Early Triassic and Late Triassic collision times, are discussed below.

The Middle Permian collision time has been proposed based mainly on the sedimentological and stratigraphical evidence from the Permian sequence in the Loei fold belt (e.g. Helmcke and Kraikhong, 1982; Helmcke and Lindenberg, 1983; Helmcke, 1986). These studies emphasise the contrast in fold styles between the "Lower Permian pelagic and flysch sediments" and the "Middle-Upper Permian molasse sequence" (e.g. Helmcke and Lindenberg, 1983). This collision time is consistent with the age of low-grade metasedimentary rocks in the Pha Som accretionary complex, i.e. the K-Ar age of 269 Ma for actinolite in the Pha Som metasediments (Barr and Macdonald, 1987). The direct corollary is that the Triassic Lampang Group sediments (probably including the Upper Permian part of the Rong Kwang Formation as well) are post-collisional. The problems with the Middle Permian collision time are: (i) it fails to account for the presence of the Late Permian-Early Triassic arc volcanics in the Sukhothai fold belt; (ii) it does not explain the similarities in the deformation and metamorphism of the Permian and Triassic sequences; (iii) there are no syn-collision deformation features visible through the cover sequence; (iv) the requirement that all the plagioclase-dominated turbidites of the Permian Rong Kwang Formation and the Triassic Lampang Group are post-collisional leads to the question that why post-collisional sediments are mainly derived from a volcanic arc with very little or no contribution from continental sources, and why they are entirely marine in origin.

The Late Permian-Triassic collision time matches with the stratigraphic break in the Loei fold belt where Early to Middle Triassic strata are missing. The Permian marine strata in this fold belt are unconformably overlain by largely lacustrine, deltaic and fluvial clastic sediments of the Upper Triassic (Norian) Huai Hin Lat Formation (Chonglakmani and Sattayarak, 1978). However, it does not account for the presence of Late Permian-Early Triassic arc volcanics in the Sukhothai fold belt. Nor does this model explain the continuous stratigraphic succession from Late Permian to Early Triassic in the study area (Junhavat and Piyasin, 1978; Hahn, 1982). As with the Middle Permian collision time, no explanation is provided for the similarities in the deformation and metamorphism of the Permian and Triassic sequences

A Late Triassic age for the collision is most consistent with the evidence presented above. In particular, this collision time is consistent with the similarities in the deformation and metamorphism of the Permian and Triassic sequences, the Late Triassic-Early Jurassic post-orogenic granite intrusions and the distribution of the Jurassic continental redbeds across the Shan-Thai and Indochina terrane boundary. The problems with this model are: (i) the lack of direct evidence for the Middle Triassic arc volcanics apart from the volcanic-derived turbidites; (ii) the exposed parts of the accretionary complex do not include Triassic material.

## 11.6 The Proposed Model

A tectonic model explaining the evolution of the Sukhothai fold belt is described below. This model has been developed to satisfy the requirements and structural constraints discussed in the preceding sections. The proposed model incorporates a model based on the geometry of modern forearc environments (Fig. 11.4). The evolution of the accretionary complex and forearc basin is considered here to be the most important stage during the evolution of the Sukhothai fold belt. The present model also incorporates the important features of the previous models (e.g. Bunopas and Vella, 1983; Barr *et al.*, 1990; Panjasawatwong, 1991) that are consistent with the evidence discussed above.

In the Late Carboniferous, an accretionary complex was accumulating at the margin of the Shan-Thai terrane above a west-dipping subduction zone (Fig. 11.5a). The position of the Carboniferous-Permian arc is uncertain because no outcrops have been proven but the arc can be inferred from abundant volcanic components being eroded into the Pha Som Metamorphic Complex. The complex was mainly composed from accreted trench turbidites and pelagic sediments. No proven forarc basin sediments are known for the age range Late Carboniferous to Early Permian, but the Phrae Group may have started to onlap the Phae Som Metamorphic Complex by the Early Permian.

This scenario continued until Middle Permian when an oceanic arc together with oceanic islands and back-arc basin (represented by the serpentinite melange of the Pha Som Metamorphic Complex) were scraped off and accreted into the accretionary complex (represented by the Pha Som metasedimentary rocks). The volcanic arcs migrated oceanwards (Fig. 11.5b) through time possibly in response to the accretion of arc material. The migration is required to produced the unconformable relationship between the forearc basin sediments and the accretionary prism, and especially because of the volume of arc volcanics within this succession suggests a very near arc setting. The processes continued from Late

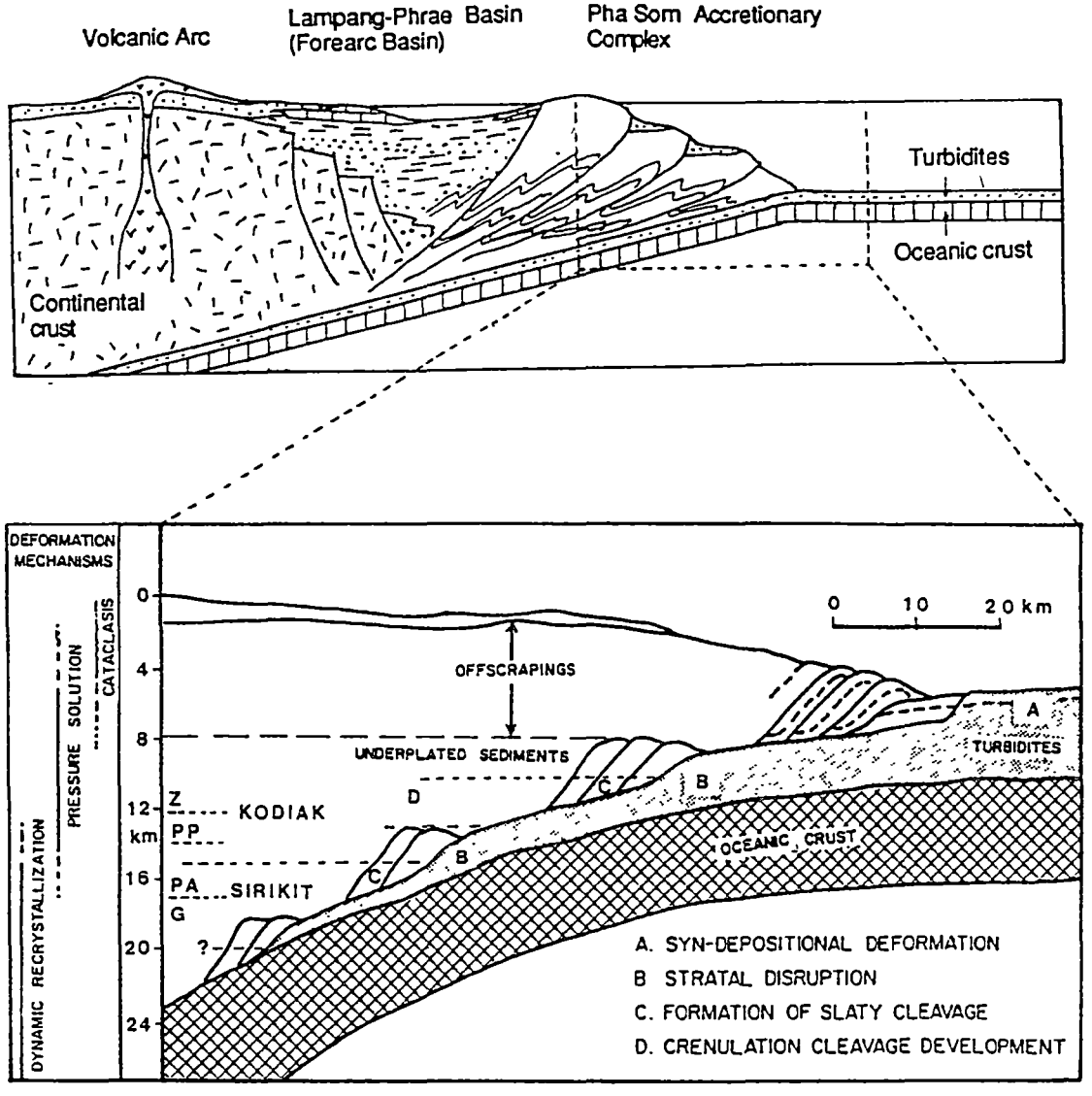


Figure 11.4 Schematic model illustrating a tectonic scenario of northern Thailand during an accretionary stage (upper diagram). The lower diagram represents the accretionary model for the Kodiak Island, Alaska (after Sample and Moore, 1987; Paterson and Sample, 1988).

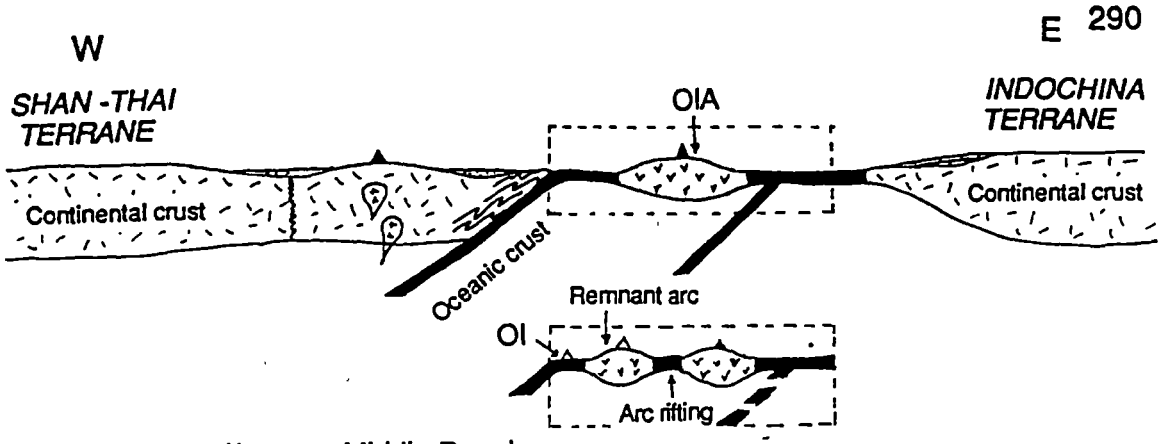


(a) Late Carboniferous - Middle Permian

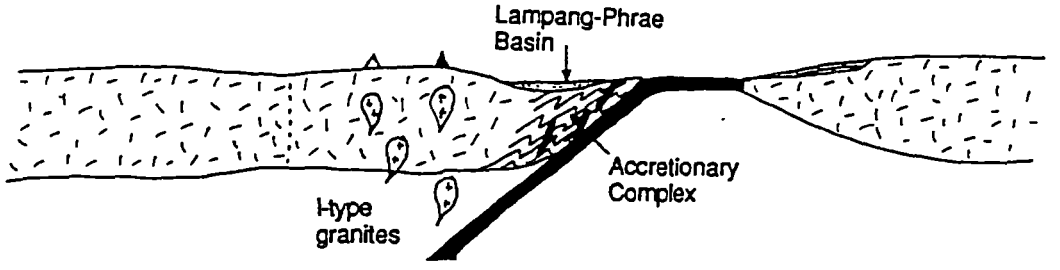


(b) Late Permian - Middle Triassic

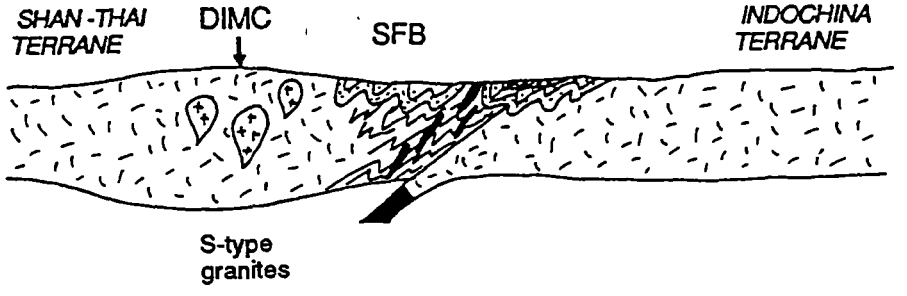


(c) Late Triassic - Early Jurassic

Figure 11.5 Schematic model for tectonic evolution of the Sukhothai fold belt and adjacent region in northern Thailand during Late Carboniferous to Early Jurassic times. SFB = Sukhothai fold belt, DIMC = Doi Inthanon Metamorphic Complex, OI = Ocean island, OIA = oceanic-island arc.

Permian into Early or Middle Triassic. During this period, there were scattered intrusions of I-type granitoids and associated eruptions of felsic to intermediate volcanic arcs in northern Thailand. The sedimentation in the forearc basin has many internal local unconformities due to the eastward migration of volcanic arc closer to the depositional basin. This is evident in the Lampang basin where the lower part of the Triassic succession, i.e. the Phra That Formation, sits unconformably on the Permo-Triassic volcanics and also conformably overlies the shale beds of the Permian sequence that contains fossil *Leptodus sp.* (Piyasin, 1972; Junhavat and Piyasin, 1978).

This model ignores the geochemical evidence for oceanic arc rocks within the Permian and in the source area for the Pha Som Metamorphic Complex. The Pak Pat Volcanics are part of a continental arc succession despite their chemistry. It is a common feature of arcs effected by additional stress, such as the accretion of an oceanic plateau, that a volcanoes are more primitive, more typical of oceanic arcs. This may explain the Pak Pat Volcanics. Not enough is known about the source area of the Pha Som metasediments to identify possible reasons for the anomalous chemistry.

Further east, the margin of the Indochina terrane was moving towards the subduction zone. It is beyond the scope of this thesis to debate whether the margin of the Indochina terrane is passive or active type. For simplicity, the passive margin (Atlantic-type) is shown.

The sedimentation in the Lampang basin continued until Late Triassic (early Norian) when the basin started to fill up probably due to tectonic uplift that mark the main collision period. During Late Triassic, both Permian and Triassic sequences were folded and thrust forming the Sukhothai fold and thrust belt. As collision proceeded the thrusting changes from east-directed to west-directed probably in response to uplift in the east associated with the full crustal section entering the collision zone. At the same time, the Permian sequence on the western margin of the Indochina terrane suffered the same deformation phase. This collision period was followed shortly afterwards by the widespread intrusions of S-type granites. These granitic intrusions occurred on the Shan-Thai terrane only (Fig. 11.3) suggesting that the crust in this region was thickened by underthrusting of the Indochina terrane. The formation of the Doi Inthanon metamorphic complex (Fig. 11.5c) which is characterised by low pressure-high temperature metamorphism may have been related to high heat influx supplied by these Triassic intrusions.

In Early Jurassic, the accumulation of the continental redbeds began and these redbed sequences expanded across the Sukhothai and Loei fold belts until Cretaceous. The main depositional basin for these continental sediments is the

Khorat basin which occupies the entire northeastern Thailand and part of Laos (Fig. 11.1).

The entire region experienced another major tectonic event starting at the Cretaceous-Tertiary boundary due to the approaching Indian subcontinent. This deformation event folded the Jurassic-Cretaceous redbeds into large wavelength NE-trending open to gentle folds along the discrete zones possibly related to reactivation of older faults such as along the Nan River - Uttaradit zone. At the same time, the other major strike-slip faults, e.g. the Mae Ping fault (Fig. 11.1) were also active. The formation of widespread extensional basins in northern Thailand occurred later in Early to Middle Tertiary probably related to movement of these major strike-slip faults (Polachan and Sattayarak, 1989).

## 11.7 Summary

The tectonic evolution of the Sukhothai fold belt in northern Thailand region can be summarised as follows:

The northern Thailand region, during Carboniferous to Permian, is dominated by subduction-accretion and arc volcanism. The accretion of trench and ocean basin sediments and igneous rocks took place during this time interval and eventually culminated in the collision between the Shan-Thai and the Indochina terranes in Late Triassic. The collision phase is best exemplified by folding and thrusting of the Triassic turbiditic sequences followed by extensive intrusions of Late Triassic-Early Jurassic granitoids and post-orogenic Jurassic-Cretaceous continental redbeds. There has been extensive Tertiary faulting which results in the formation of widespread extensional basins in northern Thailand and uplift of horsts of Upper Palaeozoic and Mesozoic rocks.

# Chapter 12

# CONCLUSIONS

A cross-sectional study across the Sukhothai fold belt in Northern Thailand provides additional data for testing many of the tectonic models currently used to explained the geological evolution of this part of Southeast Asia. The data also include the result of a brief study of the Doi Inthanon metamorphic complex west of the fold belt. These results are summarised below.

## 12.1 Stratigraphy

The oldest rocks recognised in the Sukhothai fold belt, particularly the eastern part, are arc volcanics and a subduction-accretion complex sequence represented by the Permo-Carboniferous Pha Som Metamorphic Complex. This complex consists of a metasedimentary unit and a serpentinite melange unit (ophiolite association).

The metasediments consist of metagreywackes with minor phyllites. Texturally, the metagreywackes can be divided into three textural groups, i.e. sheared greywacke, semischist and fine-grained schist belonging to TZ1-, TZ2- and TZ3 textural zone respectively. The metamorphic age of the Pha Som metasediments is probably Permo-Carboniferous based on regional stratigraphy (Hess and Koch, 1975) and the K-Ar age (269 Ma) of actinolite (Barr and Macdonald, 1987).

The ophiolite association is tectonically enclosed in the metasedimentary packages. It is composed of blocks of mafic-ultramafic rocks and minor sedimentary rocks in sheared serpentinite matrix. Radiometric dating of the amphibolite and gabbroic blocks indicate an Early Carboniferous to Late Permian age (Drs. Y. Panjasawatwong and A.J. Crawford, pers. comm., 1993), which agrees with the reported Permo-Carboniferous age for sedimentary blocks (Hahn, 1985).

The Permian turbidites and limestone (the Phrae or Ngao Group) are distributed mainly in the central and eastern part of the Sukhothai fold belt. Along

the Phrae-Sirikit Reservoir transect, the Rong Kwang Formation (the upper unit of the Phrae Group) is probably in thrust contact with the Permo-Carboniferous Pha Som Metamorphic Complex.

The Permo-Triassic volcanic and volcaniclastic rocks occur in two areas. In the Lampang-Phrae area (i.e. the central part of the Sukhothai fold belt) they are characterised by felsic to intermediate volcanic rocks (the Doi Luang volcanics). In the Sirikit Dam area close to the boundary between the Sukhothai and the Loei fold belts they include basaltic andesite with minor basalt, dacite and volcaniclastic rocks (the Pak Pat volcanics) .

The Triassic turbidite sequences (the Lampang Group) in Lampang and Phrae areas both unconformably and conformably overlie the Permo-Triassic volcanics and the Permian turbidite sequence. In the eastern part of the Sukhothai fold belt, the contact between the Triassic and Permian sequence is conformable indicating continuous deposition through the Permian-Triassic boundary. In the Sirikit Dam area, the Triassic successions (the Nam Pat Group) are characterised by a thick conglomerate unit (the Huai Lat Formation) grading upwards to the turbidite sequence (the Huai Bo Khong Formation). The conglomerate unit has unconformable contact with the underlying Permo-Triassic Pak Pat Volcanics but the fault contact is also present locally.

Granitic rocks in the Lampang-Denchai transect have intruded into the Permo-Triassic volcanics and the Upper Triassic sedimentary strata. The age of the granites is probably Upper Triassic to Lower Jurassic.

In the Sirikit Dam area, the continental redbeds of Middle Jurassic age (the Phra Wihan Formation) unconformably overlies the folded Triassic turbidites (the upper part of the Nam Pat Group).

## 12.2 Sedimentary Provenance and Tectonic Setting

Modal analysis of the framework grains of the greywackes suggests that the metasediments of the Pha Som Metamorphic Complex were derived from two main sources, i.e. an accretionary complex/magmatic arc source and a volcanic arc source. Geochemical study suggests that the metagreywackes were derived mainly from the continental arc terrain and minor intermediate oceanic-arc rocks. In terms of trace element geochemistry, the Pha Som metagreywackes are similar to those of the Torlesse and Caples terranes in New Zealand (e.g. MacKinnon, 1983). This suggests that they were derived from a similar type of sources (i.e a continental magmatic arc source for the Torlesse terrane and an oceanic island arc source for the

Caples terrane) and probably deposited in a similar environment (i.e. trench or submarine fan setting at the subduction margin).

The Permian Rong Kwang Formation which is characterised by turbiditic mudrocks and minor limestones has a character of sediments that are accumulated in the forearc basin .

Chaodumrong (1992) demonstrated that the Lampang Group sediments were deposited in a shallow forearc basin prior to the collision. The sediments of the Triassic Nam Pat Group in the east of the Sukhothai fold belt are markedly similar to the Lampang Group sediments. They were derived from a volcanic source and were deposited in the adjacent basin. They sit on top of the conglomerate unit which has pebble associations indicating that the source area was the andesitic continental volcanic arc. The compositional characteristics of the detrital framework grains and their immature textures indicate that the Nam Pat sandstones were derived from a nearby magmatic arc and were probably deposited in the forearc basin. The major and trace element characteristics, suggest that they represent sediments derived from the volcanic rocks of mainly intermediate compositions.

The compositions of the detrital framework modes indicate that the sandstones of the Middle Jurassic Phra Wihan Formation were derived from a quartzose recycled orogenic source or from the craton interior. These sediments were laid down in a braided stream environment.

## 12.3 Magmatic Affinity and Granite Intrusion

Three volcanic suites were recognised in the ophiolite association of the Pha Som Metamorphic Complex. These include ocean island basalts, immature backarc basin basalts and andesites and island arc basalts and andesites together with mafic plutonic blocks formed in supra-subduction zone environment (Panjasawatwong, 1991). Whole-rock geochemistry and pyroxene compositions indicate that the small body of the ophiolite association found within the Permo-Triassic Pak Pat volcanics (Chapter 6) belong to ocean-island transitional tholeiitic and alkali basaltic suites.

The Permo-Triassic Pak Pat volcanics are subalkaline with probable medium to low K affinities. These volcanic rocks have an oceanic arc signature inconsistent with their present setting. The tectonic setting of eruption of the Permo-Triassic felsic to intermediate volcanic rocks in Lampang-Phrae area (the Doi Luang volcanics) was inferred, on the basis of field observations and petrography, to have formed in continental arc environment.

The Upper Triassic-Lower Jurassic granites probably belong to the Northern Thailand granite province of Cobbing *et al.* (1986). The granites of this province have the characteristics of S-type granites and are of Middle to Upper Triassic age. The granitoids in the migmatite complex (e.g. the Doi Inthanon metamorphic complex discussed in Chapter 10) are highly deformed with strong sub-horizontal foliation. The complex is composed of interlayered orthogneisses and paragneisses. Other types of granites occur as larger batholiths and associated smaller plutons intruding the Palaeozoic-Lower Mesozoic sedimentary sequences and the migmatite complex. The distribution of S-type granites in northern Thailand has been inferred to be indicative of widespread Triassic metamorphism and crustal melting related to the collision of the Shan-Thai and Indochina terranes in the Late Triassic-Early Jurassic (Barr and Macdonald, 1990).

## 12.4 Deformation

Deformation history of key rock units provide the best constraints for timing and geometry of plate interaction in this part of northern Thailand. These rock units include the coherent metasediments of the Pha Som Metamorphic Complex, the Permian sequence (the Phrae or Ngao Group), The Triassic Lampang Group and the Jurassic continental redbeds (the Phra Wihan Formation). The deformation history of these rock units is discussed below.

### Deformation during accretion

Four structural phases were recognised in the coherent metasedimentary unit of the Pha Som Metamorphic Complex. The earliest recognisable structure is compositional layering ($S_1$). $D_2$ structures are characterised by $F_2$ close to tight folds, differentiated layering/phyllitic cleavage ($S_2$) and a stretching lineation ($L_2$). The $D_1$ and $D_2$ structures are interpreted to be the results of deformation in a thrust environment during which diffusional mass transfer was the dominant deformation mechanism. $D_1$-$D_2$ events are consistent with subduction-accretion models based on modern analogues observed in the Kodiak Island, Alaska (e.g. Paterson and Sample, 1988).

### Post-accretion or collisional deformation

$D_3$ in the Pha Som metasediments produced open folds with associated crenulations and crenulation cleavage. This cleavage is correlated with the regional

cleavage in the Permian and Triassic units. $D_4$ angular folds and kinks are probably related to thrusting.

Upright open folds and thrusts in the Permian and Triassic sequences probably represent the main collisional structures. These rocks have been subjected to only a single phase of folding and associated northeast-striking regional cleavage. The timing of folding and thrusting is Late Triassic based on the age of the youngest formation being folded (middle Carnian-lower Norian) and the age of post-kinematic granites (Late Triassic-Early Jurassic).

### Post-collisional deformation

High angle faults, common in the Permo-Triassic volcanics, have normal displacement that are partly overprinted by strike slip movements and are regarded here as Tertiary structures postdating the collision. An alternative interpretation is that the normal faults were formed as the result of extension related to relaxation after the main collision and were reactivated by later Tertiary strike-slip faults.

## 12.5 Metamorphism

To enable quantitative estimate of metamorphic temperatures of low-grade metasedimentary rocks, a new geothermometer based on Mg-Tschermak substitution between phengite and chlorite was calibrated. This geothermometer is expressed as follows:

$$T = \frac{539.5242 + 0.01334P + 135.4304\,[(X_{Mg}^{Ms})^2 - (X_{Al}^{Ms})^2]}{1 - 0.01507\,R\,\ln K_X}$$

where $T$ = temperature (°K), $P$ = pressure (bars), $(X_{Mg}^{Ms})$ and $(X_{Al}^{Ms})$ = mole fraction of Mg and Al in phengite, $R$ = universal gas constant and $K_X$ = ideal equilibrium constant. For the end-member reaction ($\ln K_X = 0$), $dT/dP$ = 0.01334 °K/bar, indicating that 1 kbar uncertainty in assumed pressure causes a 13 °K uncertainty in temperature. The phengite-chlorite geothermometer was tested on rocks from low-grade terranes and the results showed that reasonable estimates can be obtained. Application of this geothermometer to low-grade metasedimentary rock in the Sirikit Dam area yields similar results to those obtained from the plagioclase-muscovite geothermometer of Green and Usdansky (1986). This geothermometer may also be applied to pelitic or semi-pelitic rocks elsewhere which formed under

the conditions of high-temperature diagenesis to lower greenschist and blueschist facies metamorphism. However, the application of this geothermometer should be restricted to white micas and chlorites which have the composition ranges similar to those used in the calibration.

## Metamorphism of the Pha Som Metamorphic Complex

A single metamorphic episode was recognised for the coherent metasedimentary unit. The peak conditions were probably attained during $D_2$ event. The $b_0$ values of pelitic rocks indicate the low to medium pressure facies series for this unit. However, the occurrence of crossite-bearing blueschist within the complex is indicative of relatively high-pressure metamorphism (i.e. 3-7 kbar).

The serpentinite melange unit contains blocks of medium-pressure amphibolites, metamorphosed around Lower Carboniferous prior to the final incorporation into the Pha Som Metamorphic Complex probably during $D_2$ deformation. The amphibolite blocks are chemically affiliated with gabbros and associated ultramafics which have the characteristics of the oceanic-island arc cumulates originated in a supra-subduction zone setting. This implies that metamorphism of the amphibolites probably took place in the oceanic-arc basement. The piemontite-bearing quartz schists, metamorphosed at the pressure of around 7 kbar and temperature of 400-450 °C, may represent blueschist facies metamorphism of the hemipelagic or pelagic chert with high-Mn contents.

## Metamorphism of the Permo-Triassic volcanics

The metamorphic and/or alteration effects observed in the Permo-Triassic volcanics are either sericitisation or chloritisation. In the eastern margin of the Sukhothai fold belt, the Permo-Triassic Pak Pat Volcanics were regionally metamorphosed to prehnite-pumpellyite facies probably related to folding and faulting during the collisional deformation.

## Metamorphism of the Permian and Triassic sequences

The metamorphic grade of the Permian and Triassic sequences increases from the western to the eastern part of the Sukhothai fold belt (i.e. from diagenetic-lower anchizone grade to upper anchizone-epizone grade). This metamorphic event is likely to be related to the single cleavage-forming event in these forearc sequences

in Late Triassic. Illite crystallinity study indicates that the Nam Pat Group has a diagenetic to lower anchimetamorphic grade.

## 12.6 Tectonic Implications

Plate tectonic models accounting for the amalgamation of the Shan-Thai and Indochina terranes have been proposed by a number of workers. The general agreement among these models is that there exist a palaeo-ocean basin between the two terranes in the Late Palaeozoic time. Nevertheless, the geometry and timing of collision remains controversial. The geometry of plate convergence prior to collision has been viewed in three different perspectives as follows: (i) westward subduction of the Indochina terrane beneath the Shan-Thai terrane; (ii) eastward subduction of the Shan-Thai terrane under the Indochina terrane; (iii) a pair of subduction zones dipping in the opposite directions. As to the timing of collision of these two terranes, three major different opinions have been noted: (i) Late Triassic collision; (ii) Late-Permian-Early Triassic collision; (iii) Middle Permian collision.

Any tectonic model attempting to explain the geological evolution of northern Thailand, and the Sukhothai fold belt in particular, has to take into account the following critical observations: (i) the multiple deformation of the Permo-Carboniferous Pha Som Metamorphic Complex, especially the metasedimentary rocks which bear strong similarities to many ancient accretionary complexes around the world; (ii) the similarity in structural style and structural succession between the Permian sequence and Triassic sequence which have the characters of forearc deposits; (iii) the difference in structural and sedimentological styles between the Permian-Triassic sequences and the Jurassic-Cretaceous redbeds sequences. In addition, some other well-documented data which have to be considered includes: (i) the occurrences of Late Permian-Middle Triassic I-type granitoids and Late Triassic-Early Jurassic S-type granitoids in the western part of the Sukhothai fold belt; (ii) the occurrence of crossite-bearing blueschists in the Permo-Carboniferous metasedimentary rocks in the eastern part of the Sukhothai fold belt.

The model that envisages the passive margin of the Shan-Thai terrane (i.e. the eastward subduction model) does not fit the above observations. The west-dipping subduction zone and the paired-subduction zone models are most consistent with the above observations but further study is needed to test the paired-subduction zone model.

The timing of collision remains debatable. The Middle Permian time for collision agrees well with the age of the accretionary complex but fails to account for the Permo-Triassic arc volcanics and the Upper Permian and Triassic marine-

forearc turbidites which are exclusively derived from a volcanic source. The Late Permian-Early Triassic collision matches the age break (i.e between Late Permian and Late Triassic) in the Loei fold belt but is not consistent with the continuous deposition of Late Permian and Triassic sediments in the Sukhothai fold belt and the presence of the Permo-Triassic arc volcanics. The Late Triassic time of collision accounts well for almost every aspect of the above observations. However, the problems with this model are the lack of evidence for a component within the arc volcanics of Middle Triassic age and the absence of Triassic blocks or matrix within the exposed section of the accretionary complex.

A tectonic model which best fits the existing data is proposed below.

In the Late Carboniferous, arc volcanism occurred at the margin of the Shan-Thai terrane above the west-dipping subduction zone. Trench turbidites and pelagic sediments were accreted to the margin of the Shan-Thai terrane in response to the westward subduction of oceanic crust. In the Middle Permian, an oceanic arc together with oceanic islands and back-arc basin were scraped off and accreted into the accretionary complex. The continental volcanic arc migrated oceanwards through time with the forearc basin sediments onlapping the older inactive part of the accretionary complex. This process continued from Late Permian until Early or Middle Triassic. During this period, there were scattered intrusions of I-type granitoids and associated eruptions of felsic to intermediate volcanic arcs in northern Thailand.

The sedimentation in the Lampang basin continued until Late Triassic when the basin started to fill up probably due to tectonic uplift that mark the main collision period. During Late Triassic, both Permian and Triassic sequence were folded and thrust forming the Sukhothai fold and thrust belt. At the same time, the Permian sequence on the western margin of the Indochina terrane was also deformed. This collision period was followed shortly afterwards by the widespread intrusions of S-type granites. These granitic intrusions occurred on the Shan-Thai terrane only suggesting that the crust in this region was thickened by underthrusting of the Indochina terrane. The formation of the Doi Inthanon metamorphic complex which is characterised by low pressure-high temperature metamorphism may have been related to high heat influx supplied by these Triassic intrusions.

In the Early Jurassic, the accumulation of the continental redbeds began. These redbeds sequences expanded across the Sukhothai and Loei fold belt until Cretaceous.

The entire region experienced another major tectonic event at the Cretaceous-Tertiary boundary due to the Indian plate approaching mainland Asia. This deformation event folded the Jurassic-Cretaceous redbeds sequences into large

wavelength open to gentle folds and activated major strike-slip faults, e.g. the Mae Ping fault. The formation of widespread extensional basins in northern Thailand occurred later in Early to Middle Tertiary possibly related to dextral strike-slip faulting.

# REFERENCES

Aagaard, P. and Jahren, J.S., 1992, Diagenetic illite-chlorite assemblages in arenites II. Thermodynamic relations, Clays and Clay Minerals, v. 40, p. 547-554.

Ahrendt, H., Chonglakmani, C., Hansen, B.T. and Helmcke D., 1993, Geochronological cross section through northern Thailand, Journal of Southeast Asian Earth Sciences, v. 8, p. 207-214.

Almendinger, R.W., 1987, STEREONET version 2.6: a plotting program for orientation data for the Macintosh Computer.

Asnachinda, P., 1978, The mineralisation in the Burmese-Malayan Peninsula-a plate tectonic model, *in* : Nutalaya, P., ed., Proceedings of the Third Regional Conference on Geology and Mineral Resources of Southeast Asia, Bangkok, p. 293-299.

Audley-Charles, M., 1983, Reconstruction of eastern Gondwanaland, Nature, v. 306, p. 48-50.

Bailey, S.W., 1984, Crystal chemistry of true micas, *in* : Bailey S.W., ed., Reviews in Mineralogy Volume 13 (Micas), Mineralogical Society of America, p. 13-60.

Baltatzis, E.G. and Katagas, 1984, The pumpellyite-actinolite and contiguous facies in part of the Phyllite-Quartzite Series, central Northern Peloponnesus, Greece, Journal of Metamorphic Geology, v. 2, p. 349-363.

Barr, S.M. and Macdonald, A.S., 1978, Geochemistry and petrogenesis of Late Cenozoic alkaline basalts of Thailand, Geological Society of Malasia Bulletin, v. 10, p.25-52.

Barr, S.M. and Macdonald, A.S., 1981, Geochemistry and geochronology of Late Cenozoic basalts of Southeast Asia, Geological Society of America Bulletin, v. 92, p. 1096-1142.

Barr, S.M., MacDonald, A.S., Yaowanoiyothin, W., Panjasawatwong, Y.,1985, Occurrence of blueschist in the Nan River mafic-ultramafic belt, northern Thailand, Warta Geologi, v. 11, p. 47-50.

Barr, S.M. and MacDonald, A.S.,1987, Nan River suture zone, northern Thailand, Geology, v. 15, p. 907-910.

Barr, S.M., Tantisukrit, C., Yaowanoiyothin, W. and Macdonald, A.S., 1990, Petrology and tectonic implications of upper Palaeozoic volcanic rocks of the Chiang Mai belt, northern Thailand, Journal of Southeast Asian Earth Sciences, v. 4, p. 37-47.

Barr, S.M., and MacDonald, A.S., 1991, Toward a late Paleozoic-early Mesozoic tectonic model for Thailand, Journal of Thai Geosciences, v. 1, p. 11-22.

Barsdell, M. and Berry, R.F., 1990, Origin and evolution of primitive island arc ankaramites from western Epi, Vanuatu, Journal of Petrology, v.31, p. 747-777.

Basaltic Volcanism Study Project, 1981, Basaltic volcanism on the terrestrial planets, Pergamon Press, New York, 1286 p.

Baum, F., von Braun, E., Hahn, L., Hess, A., Koch, K.E., Kruse, G., Quarch, H., and Seebenhuner, M., 1970, On the geology of northern Thailand, Beih. Geologische Jahrbuch, v. 102, p. 1-24.

Beckinsale, R.D., Suensilpong, S., and Nakapádungrat, S., 1979, Geochronology and geochemistry of granite magmatism in Thailand in relation to plate tectonic model, Journal of Geological Society, London, v. 136, p. 529-540.

Berman, R.G., 1988, Internally-consistent thermodynamic data for minerals in the system $Na_2O$-$K_2O$-CaO-MgO-FeO-$Fe_2O_3$-$Al_2O_3$-$SiO_2$-$TiO_2$-$H_2O$-$CO_2$, Journal of Petrology, v. 29, p. 445-522.

Berry, R.F. and Grady, 1981, Deformation and Metamorphism of the Aileu Formation, north coast, East Timor and its tectonic implications, Journal of Structural Geology, v. 3, p. 143-167

Bhatia, M.R., 1983, Plate tectonics and geochemical composition of sandstones, Journal of Geology, v. 91, p. 611-627.

Bhatia, M.R. and Taylor, S.R., 1981, Trace-element geochemistry and sedimentary provinces: A study from the Tasman geosyncline, Australia, Chemical Geology, v. 33, p. 115-1125.

Bhatia, M.R. and Crook, K.A.W., 1986, Trace elment characteristics of graywackes and tectonic setting discrimination of sedimentary basins, Contributions to Mineralogy and Petrology, v. 92, p. 181-193.

Bishop, D.G., 1972, Progressive metamorphism from prehnite-pumpellyite to greenschist facies in the Dancey Pass area, Otago, New Zealand, Geological Society of America Bulletin, v. 83, p. 3177-3198.

Black, P.M., 1975, Mineralogy of new Caledonian metamorphic rocks IV. Sheet silicates from the Ouegoa district, Contributions to Mineralogy and Petrology, v. 49, p. 269-284.

Blake, M.C., Irwin, W.P. and Coleman, R.G., 1967, Upside-down metamorphic zonation, blueschist facies, along a regional thrust fault in California and Oregon, United States Geological Survey Professional Paper 575-C, p.1-9.

Blenkinsop, T.G., 1988, Definition of low-grade metamorphic zones using illite crystallinity, Journal of Metamorphic Petrology, v. 6, p. 623-636.

Borradaile, G.J., Bayly, M.B., and Powell, C. McA., eds., 1982, Atlas of Deformational and Metamorphic Rock Fabrics, Springer-Verlag, Berlin, 551 p.

Boyer, S.E. and Elliott, D. 1982, Thrust systems, American Association of Petroleum Geologists Bulletin, v. 66, p. 1196-1230.

Brown, E.H., 1967, The greenschist facies in part of eastern Otago, New Zealand, Contributions to Mineralogy and Petrology, v. 14, p. 259-292.

Brown, E.H., 1974, Comparison of the mineralogy and phase relations of blueschists from the North Cascades, Washington, and Greenschists from Otago, New Zealand, Geological Society of America Bulletin, v. 85, p. 333-344.

Brown, E.H., 1977, The crossite content of Ca-amphibole as a guide to pressure of metamorphism, Journal of Petrology, v. 18, p. 53-72.

Brown, E.H. and Ghent, E.D., 1983, Mineralogic and phase relations in the blueschist facies of the Black Butte and Bull Rock areas, northern California Coast Ranges, American Mineralogist, v. 68, p. 365-372.

Brown, G.M., 1964, Mineralogy of basaltic rocks, *in* : Hess, H.H. and Poldervaart, A., eds., Basalts, the Poldervaart treatise of rocks of basaltic compositions, v. 1, p. 103-162.

Brown, T.H., Berman, R.G., and Perkins, E.H., 1988, GeO-Calc: Software package for calculation and display of pressure-temperature-composition phase diagrams using an IBM or compatible personal computer, Computers and Geosciences, v. 14, p. 279-289.

Bunopas, S., 1969, Geology of Amphoe Tha Pla-Nam Pat (47Q/EB19) and Pha Som Dam (47Q/EC14), unpublished report, Department of Mineral Resources, Bangkok.

Bunopas, S., 1981, Paleogeographic History of Western Thailand and Adjacent Parts of South-East Asia - A Plate Tectonic Interpretation, unpublished PhD thesis, Victoria University of Wellinton, 810 p.(Reprinted 1982, Geological Survey Paper No. 5, Geological Survey Division, Department of Mineral Resources, Thailand).

Bunopas, S. and Vella, P., 1978, Late Palaeozoic and Mesozoic structural evolution of northern Thailand: a plate tectonic model , *in* : Nutalaya, P., ed., Proceedings of the Third Regional Conference on Geology and Mineral Resources of Southeast Asia, Bangkok, p. 133-140.

Bunopas, S. and Vella, P., 1983, Tectonic and geologic evolution of Thailand, *in* : Nutalaya, P., ed., Proceedings of the Workshop on Stratigraphic Correlation of Thailand and Malaysia, Haad Yai, p. 307-322.

Burrett, C.F., 1974, Plate tectonics and the fusion of Asia, Earth and Planetary Science Letters, v. 21, p. 181-189.

Burrett, C. and Stait, B., 1985, South East Asia as a part of an Ordovician Gondwanaland- a palaeobiogeographic test of a tectonic hypothesis, Earth and Planetary Science Letters, v. 75, p. 184-190.

Burrett, C. and Stait, B., 1986, Southeast Asia as a part of an early Palaeozoic Gondwanaland, Geological Society of Malaysia Bulletin, v. 19, p. 103-107.

Burton, C.K., 1984, The tectonic framework of mainland Southeast Asia, *in* : Proceedings of the Conference on Applications of Geology and the National Development, Chulalonkorn University, Bangkok, p. 255-266.

Busk, H.G., 1929, Earth Flexures, Cambridge University Press, 106 p.

Butler, R.W.H., 1982, The terminology of structures in thrust belts, Journal of Structural Geology, v. 4, p. 239-245.

Cathelineau, M., 1988, Cation site occupancy in chlorites and illites as a function of temperature, Clay Minerals, v. 23, p. 471-485.

Cathelineau, M. and Nieva, D. 1985, A chlorite solid solution geothermometer: The Los Azufres (Mexico) geothermal system, Contributions to Mineralogy and Petrology, v. 91, p. 235-244.

Chairangsee, C., Bhavabhutanonda, R. and Kosuwan, S., 1989, Geological map of Amphoe Nam Pat quadrangle (1:50,000), Department of Mineral Resources, Bangkok.

Chantaramee, S., 1978, Tectonic synthesis of Lansang area and discussion of regional tectonic evolution, *in* : Nutalaya, P., ed., Proceedings of the Third Regional Conference on Geology and Mineral Resources of Southeast Asia, Bangkok, p. 177-186.

Chaodumrong, P., Sedimentology of Triassic Lampang Group, northern Thailand, unpublished PhD thesis, University of Tasmania, 230 p.

Charoenpravat, A., Wongwanich, T., Tantiwanit, W. and Theetiparivatra, U., 1976, Geological Map of Loei (1:250,000), Department of Mineral Resources, Bangkok.

Charoenpravat, A., Phuanda, J. and Maneenai, D., 1987, Geological map of the Phrae quadrangle (1 : 50,000), Department of Mineral Resources, Bangkok.

Charungrum, B., Wongdenrungruang, W and Thamboonya, S., 1991, Geology of Ban Pak Pat and Ban Huai See Siat area, Amphoe Nam Pat, Changwat Uttaradit, unpublished BSc report, Chiang Mai University.

Chatterjee, N.D. and Johannes, W., 1974, Thermal stability and standard thermodynamic properties of synthetic 2M-muscovite, $KAl_2AlSi_3O_{10}(OH)_2$, Contributions to Mineralogy and Petrology, v. 48, p. 89-114.

Chen, C.Y. and Frey, F.A., 1985, Trace element and isotopic geochemistry of lavas from Haleakala volcano, East Maui, Hawaii - Implications for the origin of Hawaiian basalts, Journal of Geophysical Research, v. 90, p. 8743-8768.

Cho, M., Liou, J.G., and Maruyama, S., 1986, Transition from the zeolite to prehnite-pumpellyite facies in the Karmutsen metabasites, Vancouver Island, British Columbia, Journal of Petrology, v. 27, p. 467-494.

Chonglakmani, C., 1972, Stratigraphy of the Triassic Lampang Group in Northern Thailand, Geological Society of Thailand Newsletter, v. 5, p. 33-36.

Chonglakmani, C., 1981, The systemmatics and biostratigraphy of Triassic bivalves and ammonoids of Thailand, unpublished PhD thesis, University of Auckland, 504 p.

Chonglakmani, C., 1983, The marine Mesozoic stratigraphy of Thailand, *in* : Nutalaya, P., ed., Proceedings of the Workshop on Stratigraphic Correlation of Thailand and Malaysia, Haad Yai, p. 105-126.

Chonglakmani, C. and Sattayarak, N., 1978, Stratigraphy of the Huai Hin Lat Formation (Upper Triassic) in northeastern Thailand, *in* : Nutalaya, P., ed., Proceedings of the Third Regional Conference on Geology and Mineral Resources of Southeast Asia, Bangkok, p. 739-762.

Chonglakmani, C., and Helmcke, D., 1989, The Triassic Lampang Group of Northern Thailand - Fore-arc basin deposits or sediment of intramontane basins, *in* : Thanasuthipitak, T. and Ounchanum, P., eds., Proceedings of the International Symposium on Intermontane Basins: Geology and Resources, Chiang Mai, p. 265-275.

Chopin, C., 1981, Talc-phengite: a widespread assemblage in high-grade pelitic blueschists of the Western Alps, Journal of Petrology, v. 22, p. 628-650.

Cobbing, E.J., Mallick, D.I.J., Pitfield, P.E.J., and Teoh, L.H., 1986, The granites of the Southeast Asian Tin Belt, Journal of Geological Society, London, v. 143, p. 537-550.

Coombs, D.S., Landis, C.A., Norris, R.J., Sinton, J.M., Borns, D.J. and Craw, D., 1976a, The Dunn Mountain Ophiolite Belt, New Zealand, its tectonic setting, constitution, and origin, with special reference to the southern portion, American Journal of Science, v. 276, p. 561-603.

Coombs, D.S., Nakamura, Y, and Vuagnat, M., 1976b, Pumpellyite-actinolite facies schists of the Taveyanne Formation near Loeche, Valais, Switzerland, Journal of Petrology, v. 17, p. 440-471.

Cooper, M.A., Herbert, R., and Hill, G.S., 1989, The structural evolution of Triassic intermontane basin in northeastern Thailand, *in* : Thanasuttipitak, T. and Ounchanum, P., eds., Proceedings of the International Symposium on Intermontane Basins: Geology and Resources, Chiang Mai, p. 231-242

Cox, S.F., Etheridge, M.A., Cas, R.A.F. and Clifford, B.A., 1991, Deformation style of the Castlemaine area, Bendigo-Ballarat Zone: Implications for evolution of crustal structure in central Victoria, Australian Journal of Earth Sciences, v. 38, p. 151-170.

Crawford, A.J., Corbett, K.D. and Everard, J.L., 1992, Geochemistry of the Cambrian volcanic-hosted massive sulphide-rich Mount Read Volcanics, Tasmania and some tectonic implications, Economic Geology, v. 87, p. 597-619.

Crook, K.A.W., 1964, Cleavage in weakly deformed mudstones, American Journal of Science, v. 262, p. 523-531.

Crook, K.A.W., 1974, Lithogenesis and geotectonics: The significance of compositional variation in flysch arenites (greywackes), *in* : Dott, R.H. and Shaver, R.H., eds., Modern and Ancient Geosynclinal Sedimentation, Society of Economic Paleontology and Mineralogy Special Publication No. 19, p. 304-310.

Dahlstrom, C.D.A., 1969, Balanced cross sections, Canadian Journal of Earth Sciences, v. 6, p. 743-57.

Davis, J.C., 1973, Statistics and Data Analysis in Geology, John Wiley & Sons, New York, 550 p.

Deer, W.A., Howie, R.A., and Zussman, J. 1966, An Introduction to the Rock Forming Minerals, Longman Scientific and Technical, London, 528 p.

Department of Mineral Resources, 1987, Geological Map of Thailand (1: 2,500,000), Department of Mineral Resources, Bangkok.

Dickinson, W.R., 1970, Interpreting detrital modes of greywacke and arkose, Journal of Sedimentary Petrology, v. 40, p. 695-707.

Dickinson, W.R., 1985, Interpreting provenance relations from detrital modes of sandstones, *in* : Zuffa, G.G., ed., Provenance of Arenites, NATO Advanced Study Institute Series, D. Reidel, p. 331-361.

Dickinson, W.R., and Suczek, C.A., 1979, Plate tectonics and sandstone compositions, American Association of Petroleum Geologists Bulletin, v. 63, p. 2164-2182.

Dickinson, W.R., Beard, L.S., Brakenridge, G.R., Erjavec, J.L., Ferguson, R.C., Inman, K.F., Knepp, R.A., Lindberg, F.A., and Ryberg, P.T., 1983, Provenance of North American Phenerozoic sandstones in relation to tectonic setting, Geological Society of America Bulletin, v. 94, p. 222-235.

Drumm, A., Heggemann, H. and Helmcke, D., 1993, Contribution to the sedimentology and sedimentary petrology of the non-marine Mesozoic sediments in northern Thailand (Phrae and Nan Provinces), *in* : Thanasuthipitak, T., ed., Proceedings of the International Symposium on Biostratigraphy of Mainland Southeast Asia: Facies and Palaeontology, Chiang Mai, p.299-318.

Dunham, R.J., 1962, Classification of carbonate rocks according to depositional texture, *in* : Ham, W.E., ed., Classification of Carbonate Rocks, American Association of Petroleum Geologists Memoir 1, p. 108-121.

Ellis, D.J., and Green, D.H., 1979, An experimental study of the effect of Ca upon garnet-clinopyroxene Fe-Mg exchange equilibria, Contributions to Mineralogy and Petrology, v. 71, p. 13-22.

Engelder, T., and Geiser, P., 1979, The relationship between pencil cleavage and lateral shortening within the Devonian section of the Appalachian Plateau, New York, Geology, v. 7, p. 460-464.

Engelder, T. and Marshak, S., 1985, Disjunctive cleavage formed at shallow depths in sedimentary rocks, Journal of Structural Geology, v. 7, p. 327-343.

Ernst, W.G., Seki, Y., Onuki, H., and Gilbert, M.C., 1970, Comparative study of low-grade metamorphism in the California Coast Ranges and the outer metamorphic belt of Japan, Geological Society of America Memoir 124.

Essene, E.J., 1989, The current status of thermobarometry in metamorphic rocks, *in* : Daly, J.S., Cliff, R.A. and Yardley, R.W.D., eds., Evolution of Metamorphic Belts, Geological Society Special Publication No. 43, p.1-44.

Fergusson, C.L., Handerson, R.A., and Leitch, E.C., 1990, Subduction complex melange of the Wandilla terrane, Paleozoic New England Orogen, central Queensland, Australia, Journal of Structural Geology, v. 12, p. 591-599.

Ferry, J.M., and Spear, F.S., 1978, Experimental calibration of the partitioning of Fe and Mg between biotite and garnet, Contributions to Mineralogy and Petrology, v. 66, p. 113-117.

Fleuty, M.J., 1964, The description of folds, Proceedings of the Geological Association of England, v. 75, p. 461-489.

Foster, M.D., 1962, Interpretation of the Composition and a Classification of the Chlorites, Geological Survey Professional Paper 414-A, United States Government Printing Office, Washington, 33 p.

Frey, F.A., Wise, W.S., Garcia, M.O., West, H., Kwon, S.T. and Kennedy, A., 1990, Evolution of Mauna Kea volcano, Hawaii - Petrologic and geochemical constraints on postshield volcanism, Journal of Geophysical Research, v. 95, p. 1271-1300.

Frey, M., De Capitani, C., and Liou, J.G., 1991, A new petrogenetic grid for low-grade metabasites, Journal of Metamorphic Geology, v. 9, p. 497-509.

Fuhrman, M.L., and Lindsley, 1988, Ternary-feldspar modelling and thermometry, American Mineralogist, v. 73, p. 201-215.

Gatinsky, Y.G., Mischina, A.V., Vinogradov, I.V., and Kovalev, A.A., 1978, The main metallogenic belts of Southeast Asia as the result of different geodynamic conditions interference, *in* : Nutalaya, P., ed., Proceedings of the Third Regional Conference on Geology and Mineral Resources of Southeast Asia, Bangkok, p. 313-318.

Ghent, E.D., 1965, Glaucophane-schist facies metamorphism in the Black Butte area, Northern Coast Ranges, California, American Journal of Science, v. 263, p. 385-400.

Ghiorso, M.S., 1984, Activity-composition relations in the ternary feldspars, Contributions to Mineralogy and Petroplogy, v. 87, p. 282-296.

Gill, 1981, J.B., Orogenic andesites and plate tectonics, Springer Verlag, Berlin, 390 p.

Gottschalk, R.R., 1990, Structural evolution of the schist belt, south-central Brooks Range fold and thrust belt, Alaska, Journal of Structural Geology, v. 12, p. 453-469.

Graham, S.A., Ingersoll, R.V. and Dickinson, W.R., 1976, Common provenance for lithic grains in Carboniferous sandstones from Ouachita Mountains and Black Warrior basin, Journal of Sedimentary Petrology, v. 46, p. 620-632.

Graham, C.M., and Powell, R., 1984, A garnet-hornblende geothermometer: calibration, testing, and application to the Pelona Schist, Southern California, Journal of Metamorphic Geology, v. 2, p. 13-31.

Gray, D.R., 1977, Morphological classification of crenulation cleavage, Journal of Geology, v. 85, p. 229-235.

Gray, D.R., 1979, Geometry of crenulation-folds and their relatiopnships to crenulation cleavage, Journal of Structural Geology, v. 1, p. 187-205.

Gray, D.R. and Willman, C.E., 1991, Thrust-related strain gradients and thrusting mechanisms in a chevron folded sequence, southeastern Australia, Journal of Structural Geology, v. 13, p. 691-710.

Green, N.L. and Usdansky, S.I., 1986, Toward a practical plagioclase-muscovite thermometer, American Mineralogist, v. 71, p. 1109-1117.

Guidotti, C.V., 1984, Micas in metamorphic rocks, *in* : Bailey S.W., ed., Reviews in Mineralogy Volume 13 (Micas), Mineralogical Society of America, p. 357-467.

Guidotti, C.V. and Sassi, F.P., 1976, Muscovite as a petrogenetic indicator mineral in pelitic schist, Neues Jahrbuch fur Mineralogie Abhandlungen, v. 27, p. 97-142.

Guidotti, C.V., and Sassi, F.P., 1986, Classification and correlation of metamorphic facies series by means of muscovite $b_0$ data from low-grade metapelites, Neues Jahrbuch fur Mineralogie Abhandlungen, v. 153, p. 363-380.

Hada, S. and Suzuki, T., 1983, Tectonic environments and crustal section of the Outer Zone of southwest Japan, *in* : Hashimoto, M. and Uyeda, S., eds., Accretion Tectonics in the Circum-Pacific Regions, Terra, Tokyo, p. 207-218.

Hada, S., 1990, Geology of the Nan-Chantha Buri suture zone(I)-stratigraphy and geolgic structure, *in* : Proceedings of the Symposium on Development Geology for Thailand into the Year 2000 (Abstract), Chulalongkorn University, Bangkok, p. 9-10.

Hahn, L., 1976, The stratigraphy and palaeogeography of the nonmarine Mesozoic deposits in northern Thailand, Geologische Jahrburch, B21, Hannover, p. 155-169.

Hahn, L., 1982, The Triassic in Thailand, Geologiche Rundschau, v. 71, p. 1041-1056.

Hahn, L., 1985, The Indosinian orogeny in Thailand and adjacent areas, Memoires de la Societe Geologique de France 147, p. 71-82.

Harley, S.L. and Buick, I.S., 1992, Wollastonite-scapolite assemblages as indicators of granulite pressure-temperature-fluid histories: The Rauer Group, East Antarctica, Journal of Petrology, v. 33, p. 693-728

Hart, S.R., Erlank, A.J. and Kable, E.J.D., 1974, Sea floor basalt alteration: some chemical and Sr isotopic effects, Contributions to Mineralogy and Petrology, v. 44, p. 219-230.

Hayashi, M., 1989, The hydrocarbon potential and tectonics of Indochina, Geological Society of Malaysia Bulletin, v. 225, p. 65-78.

Helmcke, D., 1982, On the Variscan evolution of central mainland Southeast Asia, Earth Evolution Sciences, v. 4, p. 309-319.

Helmcke, D., 1985, The Permo-Triassic Paleotethys in mainland Southeast -Asia and adjacent parts of China, Geologiche Rundschau, v. 74, p. 215-228.

Helmcke, D., 1986, On the geology of Petchabun Fold Belt (Central Thailand)-implications for the geodynamic evolution of Mainland S.E. Asia, Geological Society of Malaysia Bulletin, v. 19, p. 79-85.

Helmcke, D. and Kraikhong, C., 1982, On the geosynclineal and geological evolution of central and northeastern Thailand, Journal of the Geological Society of Thailand, v. 5, no. 1, p. 52-74.

Helmcke, D. and Lindenberg, H.G., 1983, New data on the Indosinian orogeny from Central Thailand, Geologische Rundschau, band 72, p. 317-328.

Hess, A. and Koch, K.E., 1975, Geological Map of Nan (1:250,000), Federal Institute of Geosciences and Natural Resources, Hannover.

Hobbs, B.E., Means, W.D., and Williams, P.F., 1976, An Outline of Structural Geology, John Wiley & Sons, New York, 571 p.

Hodges, K.V., and Spear, F.S., 1982, Geothermometry, geobarometry, and the $Al_2SiO_5$ triple point at Mt. Moosilauke, New Hampshire, American Mineralogist, v. 67, p. 1118-1134.

Hoisch, T.D., 1989, A muscovite-biotite geothermometer, American Mineralogist, v. 74, p. 565-572.

Holdaway, M.J., 1971, Stability of andalusite and the aluminum silicate phase diagram, American Journal of Science, v. 271, p. 97-131.

Holland, T.J.B., and Powell, R., 1990, An enlarged and updated internally consistent thermodynamic dataset with uncertainties and correlations: the system $K_2O$-$Na_2O$-CaO-MgO-MnO-FeO-$Fe_2O_3$-$Al_2O_3$-$TiO_2$-$SiO_2$-C-$H_2$-$O_2$, Journal of Metamorphic Geology, v. 8, p. 89-124.

Huddleston, P.J., 1973, Fold morphology and some geometrical implications of theories of fold development, Tectonophysics, v.16, p.1-46.

Hutchison, C.S.,1975, Ophiolite in Southeast Asia, Geological Society of America Bulletin, v. 86, p. 797-806.

Hutchison, C.S., 1977, Granite emplacement and tectonic subdivision of Peninsular Malaya, Geological Society of Malaysia Bulletin, v. 9, p. 187-207.

Hutchison, C.S., 1983, Multiple Mesozoic Sn-W-Sb granitoids of Southeast Asia, *in* : Roddick, J.A., ed., Circum-Pacific Plutonic Terranes, Geological Society of America Memoir 159, p. 35-60.

Hutchison, C.S., 1989, Geological Evolution of Southeast Asia, Clarendon Press, Oxford, 368 p.

Ingersoll, R.V., and Suczek, C.A., 1979, Petrology and provenance of Neogene sand from Nicobar and Bengal fans, DSDP sites 211 and 218, Journal of Sedimentary Petrology, v. 49, p. 1217-1228.

Ingersoll, R.V., Bullard, T.F., Ford, R.L., Grimm, J.P., Pickle, J.D. and Sares, S.W., 1984, The effect of grain size on detrital modes : A test of the Gazzi-Dickinson point-counting method, Journal of Sedimentary Petrology, v. 54, p. 103-116.

Intasopa, S. and Dunn, T., 1990, Petrology and geochronology of Loei province volcanics, central Thailand volcanic belt, Transactions American Geophysical Union EOS, v. 71, p. 1700.

Intasopa, S. and Dunn, T. and Lux, D.R., 1990, $^{40}Ar/^{39}Ar$ geochronology of central Thailand volcanic belt, Transactions American Geophysical Union EOS, v. 71, p. 1700.

Intasopa, S. and Dunn, T., 1994, Petrology and Sr-Nd isotopic systems of the basalts and rhyolites, Loei, Thailand, Journal of Southeast Asian Earth Sciences, v. 9, p. 167-180.

Iwai, J., Asama, K., Veeraburus, M. and Hongnusonthi, A, 1966, Stratigraphy of the so-called Khorat Series and a note on the fossil plant-bearing Palaeozoic strata in Thailand, Geology and Palaeontology of Southeast Asia, Tokyo University Press, v. 2, p. 179-196.

Jahren, J.S.and Aagaard, P., 1992, Diagenetic illite-chlorite assemblages in arenites I. Chemical evolution, Clays and Clay Minerals, v. 40, p. 540-546.

Jayko, A.S., Blake Jr., M.C., and Brothers, R.N., 1986, Blueschist metamorphism of the eastern Franciscan belt, Northern California, Geological Society of America Memoir 164, p. 107-123.

Jayko, A.S. and Blake Jr., M.C., 1989, Deformation of the Eastern Franciscan Belt, northern California, Journal of Structural Geology, v. 11, p. 375-390.

Johannes, W., 1984, Beginning of melting in the granite system Qz-Or-Ab-An-$H_2O$, Contributions to Mineralogy and Petrology, v. 86, p. 264-273.

Johnson, R.S. and Arculus, R.J., 1978, Volcanic rocks of the Vitu Islands, Papua New Guinea - The origin of magma above the deepest part of the New Britain Benioff zone, Bulletin of Volcanology, v. 41, p. 609-655.

Junhavat, S. and Piyasin, S., 1978, Triassic rocks of Thailand, *in* : Nutalaya, P., ed., Proceedings of the Third Regional Conference on Geology and Mineral Resources of Southeast Asia, Bangkok, p. 735-737.

Kawachi, Y., 1975, Pumpellyite-actinolite and contiguous facies metamorphism in part of Upper Wakatipu district, South Island, New Zealand, New Zealand Journal of Geology and Geophysics, v. 18, p. 401-441.

Kawachi, Y., Grapes, R.H., Coombs, D.S., and Dowse, M., 1983, Mineralogy and petrology of a piemontite-bearing schist, western Otago, New Zealand, Journal of Metamorphic Petrology, v. 1, p. 353-372.

Kemp, A.E.S., Oliver, G.H.J., and Baldwin, J.R., 1985, Low-grade metamorphism and accretion tectonics: Southern Uplands terrane, Scotland, Mineralogical Magazine, v. 49, p. 335-344.

Keskinen, M., 1981, Petrochemical investigation of the Shadow Lake Piemontite Zone, eastern Sierra Nevada, California, American Journal of Science, v. 281, p. 896-921.

Keskinen, M.,and Liou, J.G., 1987, Stability relations of Mn-Fe-Al piemontite, Journal of Metamorphic Geology, v. 5, p. 495-507.

Kisch, H.J., 1980a, Incipient metamorphism of Cambro-Silurian clastic rocks from the Jamtland Supergroup, central Scandinavian Caledonides, western Sweden: illite crystallinity and vitrinite reflectance, Journal of Geological Society, London, v. 137, p. 271-288.

Kisch, H.J., 1980b, Illite crystallinity and coal rank associated with lowest-grade metamorphism of the Taveyanne greywacke in the Helvitic zone of the Swiss Alps, Eclogae Geologische Helvitae, v. 73, p. 753-777.

Kisch, H.J., 1987, Correlation between indicators of very low-grade metamorphism, *in* : Frey, M., ed., Low Temperature Metamorphism, Blackie & Son Ltd, Glasgow, p. 227-304.

Kisch, H.J., 1990, Calibration of the anchizone: a critical comparison of illite crystallinity scales used for definition, Journal of Metamorphic Geology, v. 8, p. 31-46.

Kisch, H.J., 1991, Development of slaty cleavage and degree of very-low-grade metamorphism: a review, Journal of Metamorphic Geology, v. 9, p. 735-750.

Knipe, R.J., and Needham, D.T., 1986, Deformation processes in accretionary wedges -examples from the SW margin of the Southern Uplands, Scotland, *in* : Coward, M.P., and Ries, A.C., eds., Collision Tectonics, Geological Socity Special Publication No. 19,, p. 51-65.

Kotov. N.V., 1975, Muscovite-chlorite paleothermometer, Doklady Akademii Nauk SSSR, v. 222, p. 701-704.

Kretz, R., 1983, Symbols for rock-forming minerals, American Mineralogist, v. 68, p. 277-279.

Kubler, B., 1967, La crystallinite de l'illite et les zones tout a fait superieures du metamorphisme. *in* : Etages tectoniques, Colloque de Neuchatel 1966, A la Baconniere, Neuchatel, Suisse, p. 105-121.

Kuniyoshi, S. and Liou, J.G., 1976, Contact metamorphism of the Karmutsen volcanics, Vancouver Island, British Columbia, Journal of Petrology, v. 17, p. 73-99.

Laird, J., and Albee, A.L., 1981a, High-pressure metamorphism in mafic schist from northern Vermont, American Journal of Science, v. 281, p. 97-126.

Laird, J., and Albee, A.L., 1981b, Pressure, temperature, and time indicators in mafic schist: their application to reconstructing the polymetamorphic history of Vermont, American Journal of Science, v. 281, p. 127-175.

Langer, K., Anastasiou, P. and Abs-Wurmbbach, I., 1976, Synthesis, stability, and physical properties of $Mn^{3+}$- bearing silicate minerals, 25th International Geological Congress, Sydney (Abstracts), v. 2, p. 578-579.

Leake, B.E., 1978, Nomenclature of amphiboles, Canadian Mineralogist, v. 16, p. 501-520.

Leterrier, J., Maury, R.C., Thonon, P., Girard, D. and Marchal, M., 1982, Clinopyroxene composition as a method of identification of magmatic affinities of paleo-volcanic series, Earth and Planetary Science Letter, v. 59, p. 139-154.

Lin, P.N., Stern, R.J. and Bloomer, S.H., 1989, Shoshonitic volcanism in the northern Mariana Arc-2. Large-ion-lithophile and rare earth element abundances - evidence for the source of incompatible element enrichments in intraoceanic arcs, Journal of Geophysical Research, v. 94, p. 4497-4514.

Liou, J.G., 1979, Zeolite facies metamorphism of basaltic rocks from the East Taiwan Ophiolite, American Mineralogist, v. 64, p. 1-14.

Lüddecke, S., Chonglakmani, C. and Helmcke, D., 1991, Analysis of pebble associations from the marine Triassic of northern Thailand, Journal of Thai Geosciences, v.2, p. 91-101.

Lumchuan, A., and Sinpoonanant, S., 1987, Geology of Khuen Sirikit (map sheet 5144 IV) and Amphoe Tha Pla (map sheet 5044 I), unpublished report, Department of Mineral Resources, Bangkok.

Macdonald, A.S. and Barr, S.M., 1978, Tectonic significance of a Late Carboniferous volcanic arc in northern Thailand, *in* : Nutalaya, P., ed., Proceedings of the Third Regional Conference on Geology and Mineral Resources of Southeast Asia, Bangkok, p. 151-156.

Macdonald , A.S., and Barr, S.M., 1984, The Nan River mafic-ultramafic belt, northern Thailand: Geochemistry and tectonic significance, Geological Society of Malaysia Bulletin, v.17, p. 209-224.

Macdonald, A.S., Barr, S.M., Dunning, G.R. and Yaowanoiyothin, W., 1993, The Doi Inthanon metamorphic core complex in SW Thailand: age and tectonic significance, Journal of Southeast Asian Earth Sciences, v. 8, p. 117-125.

MacKinnon, T.C., 1983, Origin of the Torlesse terrane and coeval rocks, south Island, New Zealand, Geological Society of America Bulletin, v. 94, p. 967-985.

Mahawat, C., Atherton, M.P., and Brotherton, M.S., 1990, The Tak Batholith, Thailand: the evolution of contrasting granite types and implications for tectonic setting, Journal of Southeast Asian Earth Sciences, v. 4, p. 11-27.

Maranate, S., Butmuang, C. and Karnjano, B., 1987, Geological map of Ban Wiang Nua quadrangle (1: 50,000), Department of Mineral Resources, Bangkok.

Marsaglia, K.M. and Ingersoll, R.V., 1992, Compositional trends in arc-related, deep-marine sand and sandstone: A reassessment of magmartic provenance, Geological Society of America Bulletin, v. 104, p. 1637-1649.

Massonne, H.J., and Schreyer, W., 1987, Phengite geobarometry based on the limiting assemblage with K-feldspar, phlogopite, and quartz, Contributions to Mineralogy and Petrology, v. 96, p. 212-224.

Massonne, H.J. and Chopin, C., 1989, *P-T* history of the Gran Paradiso (western Alps) metagranites based on phengite geobarometry, *in* : Daly, J.S., Cliff, R.A. and Yardley, B.W.D., eds., Evolutions of Metamorphic Belts, Geological Society Special Publication No. 43, p. 545-549.

Mather, J.D., 1970, The biotite isograd and the lower greenschist facies in the Dalradian Rocks of Scotland, Journal of Petrology, v. 11, p. 253-275.

Maynard, J.B., Valloni, R and Yu, H.S., 1982, Composition of modern deep-sea sands from arc related basins, *in* : Legget, J.K., ed., Trench-Forearc Geology: Sedimentation and Tectonics on Modern and Ancient Active Plate Margins, Geological Society Special Publication No. 10, p. 551-561.

McBride, E.F., 1963, A classification of common sandstones, Journal of Sedimentary Petrology, v. 33, p. 664-669.

McClay, K.R. and Buchanan, P.G., 1992, Thrust faults in inverted extensional basins, *in* : McClay, K.R., ed., Thrust Tectonics, Chapman-Hall, London, p. 93-104.

McDowell, S.D. and Elders, W.A., 1980, Authigenic layer silicate minerals in borehole Elmore 1, Salton Sea geothermal field, California, USA, Contributions to Mineralogy and Petrology, v. 74, p. 293-310.

McLennan, S.M. and Taylor, S.R., 1991, Sedimentary rocks and crustal evolution: tectonic setting and secular trends, Journal of Geology, v. 99, p. 1-21.

Meschede, M., 1986, A method of discriminating between different types of mid-ocean ridge basalts and continental tholeiites with the Nb-Zr-Y diagram, Chemical Geology, v. 56, p. 207-218.

Metcalfe, I., 1986, Late Palaeozoic palaeogeography of Southeast Asia: some stratigraphical and palaeomagnetic constraints, Geological Society of Malaysia Bulletin, v. 19, p. 153-164.

Mitchell, A.H.G., 1977, Tectonic settings for emplacement of Southeast Asian tin granites, Geological Society of Malaysia Bulletin, v. 9, p. 123-140.

Mitchell, A.H.G., 1986, Mesozoic and Cenozoic regional tectonics and metallogenesis in Mainland SE Asia, Geological Society of Malaysia Bulletin, v. 20, p. 221-239.

Mitchell, A.H.G., 1992, Late Permian-Mesozoic events and the Mergui Group nappe in Myanmar and Thailand, Journal of Southeast Asian Earth Sciences, v. 7, p. 165-178.

Miyashiro, A. and Shido, F., 1985, Tschermak substitution in low- and middle-grade pelitic schists, Journal of Petrology, v. 26, p. 449-487.

Mongkoltip, P., 1986, Metamorphic mineral assemblages of gneiss along Doi Inthanon highway, Northern Thailand, Geological Society of Malaysia Bulletin, v. 20, p. 473-485.

Mortimer, N. and Roser, B.P., 1992, Geochemical evidence for the position of the Caples-Torlesse boundary in the Otago Schist, New Zealand, Journal of the Geological Society, London, v. 149, p. 967-977.

Nakajima, T., Banno, S., and Suzuki, T., 1977, Reactions leading to the disappearance of pumpellyite in low-grade metamorphic rocks of the Sanbagawa metamorphic belt in Central Shikoku, Japan, Journal of Petrology, v. 18, p. 263-284.

Needham, D.T., and MacKenzie, J.S., 1988, Structural evolution of the Shimanto Belt accretionary complex in the area of the Gokase River, Kyushu, SW Japan, Journal of the Geological Society, London, v. 145, p. 85-94.

Nemec, D., 1980, Fluorine phengites from tin-bearing orthogneisses of the Bohemian-Marovian Heights, Czechoslovakia, Neues Jahrbuch fur Mineralogie Abhandlungen, v.139, p. 155-169.

Nichols, G.T. and Berry, R.F., 1991, A decompressional *P-T* path, Reinbolt Hills, East Antarctica, Journal of Metamorphic Geology, v. 9, p. 257-266.

Nitsch, K.H., 1971, Stabilitatsbeziehungen von prehnit und pumpellyit-haltigen paragenesen, Contributions to Mineralogy and Petrology, v. 30, p. 240-260.

Norrish, K. and Chappell, B.W., 1967, X-ray fluorescence spectrography, *in* : Zussman, J., ed., Physical Methods in Determinative Mineralogy, Acadamic Press, London, p. 161-214.

Norrish, K. and Hutton, J.T., 1969, An accurate X-ray spectrographic method for the analysis of a wide range of geological samples, Geochemica et Cosmochimica Acta, v. 33, p. 431-455.

Nutalaya, P., 1974, Geology of the Bhumipol Dam area, Tak Province, Thailand, *in* : Proceedings of the Conference on the Geology of Thailand, Department of Geological Sciences, Chiang Mai University.

Nutpeerean, D., Puvapan, S. and Chartree, S., 1991, Geology of Phu Khon Kaen area, Amphoe Nam Pat, Changwat Uttaradit, unpublished Bsc report, Chiang Mai University.

Nwe, Y.Y., 1976, Electron-probe studies of the earlier pyroxenes and olivines from the Skaergaard Intrusion, East Grrenland, Contributions to Mineralogy and Petrology, v. 55, p. 105-126.

Offler, R., Hand, M., and Bale, R., 1987, $b_o$ and illite crystallinity studies of K-white micas in rocks from forearc basin and accretionary complex sequences, Southern New England fold belt, New South Wales, Australia, Sci. Geol. Bull., v.40, p. 245-254.

O'Hanley, D.S., 1991, Fault-related phenomena associated with hydration and serpentine recrystallisation during serpentinisation, Canadian Mineralogist, v. 29, p. 21-35.

Padan, A., Kisch, H.J., and Shagam, R., 1982, Use of the lattice parameter $b_o$ of dioctahedral illite/muscovite for the characterization of *P/T* gradients of incipient metamorphism, Contributions to Mineralogy and Petrology, v. 79, p. 85-95.

Panjasawatwong, Y., 1991, Petrology, geochemistry and tectonic implicatins of igneous rocks in the Nan suture, Thailand and an empirical study of the effects of Ca/Na, Al/Si and $H_2O$ on plagioclase-melt equilibria at 5-10 kb pressure, unpublished PhD thesis, University of Tasmania, 239 p.

Paterson, S.R., and Sample, J.C., 1988, The development of folds and cleavages in slate belts by underplating in accretionary complexes: A comparison of the Kodiak Formation, Alaska and the Calveras Complex, California, Tectonics, v. 7, p. 859-874.

Pattison, D.R.M., and Newton, R.C., 1989, Reversed experimental calibration of the garnet-clinopyroxene Fe-Mg exchange thermometer, Contributions to Mineralogy and Petrology, v. 101, p. 87-103.

Pearce, J.A., 1980, Geochemical evidence for the genesis and eruptive setting of lavas from Tethyan ophiolites, *in* : Proceedings of the International Ophiolite Symposium, Cyprus Geological Survey Department, p. 261-272.

Pearce, J.A. and Cann, J.R., 1973, Tectonic setting of basic volcanic rocks determined using trace element analyses, Earth and Planetary Science Letter, v. 19, p. 290-300.

Peccirillo, A. and Taylor, S.R., 1976, Geochemistry of Eocene calc-alkaline volcanic rocks from the Kastamonu area, Northern Turkey, Contributions to Mineralogy and Petrology, v. 58, p. 63-81.

Petit, J.P., 1987, Criteria for the sense of movement on fault surfaces in brittle rocks, Journal of Structural Geology, v. 9, p. 597-608.

Pettijohn, F.J., Potter, P.E. and Siever, R., 1972, Sand and Sandstone, Springer-Verlag, New York, 618 p.

Piyasin, S., 1972, Geology of Lampang, Report of Investigation No. 14, Department of Mineral Resources, Bangkok, 98 p.

Piyasin, S., 1975, Geology of Uttaradit, Report of Investigation No. 15, Department of Mineral Resources, Bangkok, 66 p.

Piyasin, S., 1991, Tectonic events and radiometric dating of the basement rocks of Phitsanulok Basin, Journal of Thai Geosciences, v.1, p. 41-48.

Platt, J.P., and Vissers, R.L.M., 1980, Extension structures in anisotropic rocks, Journal of Structural Geology, v. 2, p. 397-410.

Polachan, S., and Sattayarak, N., 1989, Strike-slip tectonics and the development of Tertiary basins in Thailand, *in* : Thanasuthipitak, T. and Ounchanum, P., eds., Proceedings of the International Symposium on Intermontane Basins: Geology and Resources, Chiang Mai University, Chiang Mai, p. 243-253.

Powell, C. McA., 1979, A morphological classification of rock cleavage, Tectonophysics, v. 58, p. 21-34.

Powell, R., 1978, Equilibrium Thermodynamics in Petrology, Harper and Row, London, 284 p.

Powell, R., and Holland, T.J.B., 1988, An internally consistent dataset with uncertainties and correlations: 3. Applications to geobarometry, work examples and a computer program, Journal of Metamorphic Geology, v.6, p. 173-204.

Press, W.H., Flannery, B.P., Teukolsky, S.A., and Vettering, W.T., 1986, Numerical Recipes: The Art of Scientific Computing, Cambridge University Press, Cambridge, 818 p.

Price, J.G., 1985, Ideal site mixing in solid solutions, with application to two-feldspar geothermometry, American Mineralogist, v. 70, p. 696-701.

Promma, K., Jittichai, T. and Khongtiph, P., 1991, Geology of Huai Yang Area, Tha Pla, Uttaradit , unpublished BSc report, Chiang Mai University.

Ramsay, J.G., 1967, Folding and Fracturing of Rocks, McGraw-Hill, New York, 568 p.

Ramsay, J.G., 1980, Shear zone geometry: a review, Journal of Structural Geology, v. 2, p. 83-99.

Ramsay, J.G. and Huber, M.I., 1983, The Techniques of Modern Structural Geology, volume 2: Folds and Fractures, Academic Press, London.

Rao, T.R., 1977, Distribution of elements between coexisting phengite and chlorite from the greenschist facies of the Tennant Creek area, Central Australia, Lithos, v. 10, p. 103-112.

Reks, I.J. and Gray, D.R., 1982, Pencil structure and strain in weakly deformed mudstone and siltstone, Journal of Structural Geology, v. 4, p. 161-176.

Ridd, M.F., 1971, South-East Asia as a part of Gondwanaland, Nature, v.234, p. 531-533.

Ridd, M.F., 1980, Possible Palaeozoic drift of SE Asia and Triassic collision with China, Journal of the Geological Society, London, v. 137, p. 635-640.

Robinson, D., Warr, L.N., and Bevins, R.E., 1990, The illite crystallinity technique: a critical appraisal of its precision, Journal of Metamorphic Petrology, v. 8, p. 333-344.

Roser, B.P. and Korsch, R.J., 1988, Provenance signatures of sandstone-mudstone suites determined using discriminant function analysis of major-element data, Chemical Geology, v. 67, p. 119-139.

Roser, B.P. and Cooper, A.F., 1990, Geochemistry and terrane affiliation of Haast Schist from the western Southern Alps, New Zealand, New Zealand Journal of Geology and Geophysics, v. 33, p. 1-10.

Sample, J.C., and Fisher, D.M., 1986, Duplex accretion and underplating in an accretionary complex, Kodiak islands, Alaska, Geology, v. 14, p. 160-163.

Sample, J.C., and Moore, J.C., 1987, Structural styles and kinematics of an under plated slate belt, Kodiak and adjacent islands, Geological Society of America Bulletin, v. 99, p. 191-213.

Sassi, F.P., and Scolari, A., 1974, The $b_o$ value of the potassic white micas as a barometric indicator in low-grade metamorphism of pelitic schists, Contributions to Mineralogy and Petrology, v. 45, p. 143-152.

Sattayarak, N., 1983, Review of the continental Mesozoic stratigraphy of Thailand, *in* : Nutalaya, P., ed., Proceedings of the Workshop on Stratigraphic Correlation of Thailand and Malaysia, Haad Yai, p. 127-148.

Schiffman, P. and Liou, J.G., 1983, Synthesis of Fe-pumpellyite and its stability relations with epidote, Journal of Metamorphic Geology, v. 1, p. 91-101.

Sengör, A.M.C., 1984, The Cimmeride orogenic system and the tectonics of Eurasia, Geological Society of America Special Paper 195.

Shau,Y.H., Feather, M.E., Essene, E.,and Peacor, D.R., 1991, Genesis and solvus relations of submicroscopically intergrown paragonite and phengite in a blueschist from northern California, Contributions to Mineralogy and Petrology, v. 106, p. 367-378.

Shervais, J.W., 1982, Ti-V plots and the petrogenesis of modern and ophiolitic lavas, Earth and Planetary Science Letters, v. 59, p. 101-118.

Simpson, C., and Schmid, S.M., 1983, An evaluation of criteria to deduce the sense of movement in sheared rocks, Geological Society of America Bulletin, v. 94, p. 1281-1288.

Simpson, C., 1986, Determination of the movement sense in mylonitè, Journal of Geological Education, v. 34, p. 246-261.

Singharajwarapan, S. and Berry, R.F., 1993, Structural analysis of the accretionary complex in Sirikit Dam area, Uttaradit, Northern Thailand, Journal of Southeast Asian Earth Sciences, v. 8, p. 233-245.

Smith, D. and Albee, A., 1967, Petrology of a piemontite-bearing gneiss, San Gorgonio Pass, California, Contributions to Mineralogy and Petrology, v. 16, p. 189-203.

Spear, F., 1981, An experimental study of hornblende stability and compositional variability in amphibolite, American Journal of Science, v. 281, p. 697-734.

Spry, A., 1969, Metamorphic Textures, Pergamon Press, Oxford, 350 p.

Stauffer, P.H., 1974, Malaya and Southeast Asia in the pattern of continental drift, Geological Society of Malaysia Bulletin, v. 7, p. 89-138.

Storey, B.C. and Meneilly, A.W., 1985, Petrology of metamorphic rocks within a subduction-accretion terrane, Signy Island, South Orkney Islands, Journal of Metamorphic Geology, v. 3, p. 21-42.

Streckeisen, A., 1976, To each plutonic rocks its proper name, Earth and Planetary Science Letters, v. 12, p. 1-33.

Stormer, J.C., 1975, A practical two-feldspar geothermometer, American Mineralogist, v. 60, p. 667-674.

Subcommittee on Pyroxenes, International Mineralogical Association, 1988, Nomenclature of pyroxenes, American Mineralogist, v. 73, p. 1123-1133.

Suensilpong, S., Putthapiban, P., and Mantajit, N., 1983, Some aspects of tin granite and its relationship to tectonic setting, Geological Society of America Memoir 159, p. 77-85.

Suensilpong, S., Nakornsri, N., Dheeradilok, P., Lumjuan, A., Tansathien, W., and Vimuktanandana, S., 1984, Geological Map of Thailand 1:1,000,000, Department of Mineral Resources, Bangkok.

Suppe, J., 1983, Geometry and kinematics of fault-bend folding, American Journal of Science, v. 283, p. 684-721.

Suppe, J., 1985, Principles of Structural Geology, Prentice-Hall, Englewood Cliffs, 537 p.

Tan, B.K. and Khoo, T.T., 1981, Ultramafic rocks in Peninsular Malaysia and their tectonic implications, *in* : Fernando, T., ed., Proceedings of the Fourth Regional Ronference on Geology and Mineral Resources of Southeast Asia, Manila, the Philipines, p. 259-264.

Tan, B.K., 1984, The tectonic framework and evolution of the Central Belt and its margins, Peninsular Malaysia, Geological Society of Malaysia Bulletin, v. 17, p. 307-322.

Taylor, S.R. and Gorton, M.K., 1977, Geochemical application of spark-source mass spectrometry III : element sensitivity, precision and accuracy, Geochimica et Cosmochimica Acta, v. 41, p. 1375-1380.

Teggin, D.E., 1975, The granites of Northern Thailand, unpublished PhD thesis, University of Manchester.

Thanasuthipitak, T., 1978, Geology of Uttaradit area and its implications on tectonic history history of Thailand, *in* : Nutalaya, P., ed., Proceedings of the Third Regional Conference on Geology and Mineral Resources of Southeast Asia, Bangkok, p. 187-197.

Tucker, M.E., 1981, Sedimentary Petrology: An Introduction, Blackwell Scientific Publications, London, 252 p.

Tucker, M.E. and Wright, V.P., 1990, Carbonate Sedimentology, Blackwell Scientific Publications, Melbourne, 482 p.

Tullis, T.E., 1976, Experiments on the origin of slaty cleavage and schistosity, v. 87, p. 745-753.

Turner, F.J., 1938, Progressive regional metamorphism in Southern New Zealand, Geological Magazine, v. 75, p. 160-174.

Turner, F.J., 1981, Metamorphic Petrology, 2nd ed., McGraw-Hill, New York, 524 p.

Turner, F.J. and Weiss, L.E., 1963, Structural Analysis of Metamorphic Tectonites, McGraw-Hill, New York, 543 p.

Vallance, T.G., 1960, Concerning spilites, Proceedings of the Linnean Society of New South Wales 85, p. 8-52.

Vallance, T.G., 1969, Spilites again: some consequences of the degradation of basalts, Proceedings of the Linnean Society of New South Wales 94, p. 8-53.

Valloni, R. and Maynard, J.B., 1981, Detrital modes of recent deep-sea sands and their relation to tectonic setting: a first approximation, Sedimentology, v. 84, p. 195-212.

van der Pluijm, B.A., 1986, Geology of eastern New World Island, New Foundland: An accretionary terrane in the northeastern Appalachians, Geological Society of America Bulletin, v. 97, p. 932-945.

von Braun, E., Besang, C., Eberle, W., Harre, W., Kreuzer, H., Muller, P. and Wendt, I., 1976, Radiometric age determinations of granites in northern Thailand, Geologische Jahrbuch, Reihe R. Heft 21, p. 171-204.

Wang, G.F., and Banno, S., 1987, Non-stoichiometry of interlayer cations in micas from low- to middle-grade metamorphic rocks in the Ryoke and the Sanbagawa belts, Japan, Contributions to Mineralogy and Petrology, v. 97, p. 313-319.

Wannakasem, S., 1980, Geochemistry and genesis of the Doi Ngom wolfram deposits, Amphoe Long, Phrae, unpublished MSc thesis, Chiang Mai University, 165 p.

Ward, D.E. and Bunnag, D., 1964, Stratigraphy of the Mesozoic Khorat Group in northeastern Thailand, Report of Investigation No. 6, Department of Mineral Resources, Bangkok, 95 p.

Weaver, C.E., 1960, Possible uses of clay minerals in search for oil, American Association of Petroleum Geologists Bulletin, v. 44, p. 1505-1518.

Wenner, D.B. and Taylor, H.P., Jr., 1971, Temperatures of serpentinisation of ultramafic rocks based on $O^{18}/O^{16}$ fractionation between coexisting serpentinite and magnetite, Contributions to Mineralogy and Petrology, v. 32, p. 165-185.

Wenner, D.B. and Taylor, H.P., Jr., 1973, Oxygen and hydrogen isotope studies of the serpentinisation of ultramafic rocks in oceanic environments and continental ophiolite complexes, American Journal of Science, v. 273, p. 207-239.

Wenner, D.B. and Taylor, H.P., Jr., 1971, D/H and $O^{18}/O^{16}$ studies of serpentinisation ultramafic rocks, Geochimica et Cosmochimica Acta, v. 38, p. 1255-1286.

Wheller, G.E., Varne, R., Foden, J.D. and Abbot, M.J., 1987, Geochemistry of Quaternary volcanism in the Sunda-Bunda arc, Indonesia, and three components genesis of island arc basaltic magmas, Journal of Volcanology and Geothermal Research, v. 32, p. 137-160.

White, S.H., and Knipe, R.J., 1978, Microstructure and cleavage decelopment in selected slates, Contributions to Mineralogy and Petrology, v. 66, p. 165-174.

White, S.H., and Johnson, D.C., 1981, A microstructural and microchemical study of cleavage lamellae in a slate, Journal of Structural Geology, v.3, p. 279-290.

Whitten, E.H.T., 1966, Structural Geology of Folded Rocks, Rand McNally, Chicago, 663 p.

Wilkerson, M.S., 1990, FAULT II - A cross-section modelling program for the Macintosh, Wilkerson and Associates.

Williams, P.F., 1985, Multiply deformed terrains-problems of correlation, Journal of Structural Geology, v. 7, p. 269-280.

Winchester, J.A., and Floyd, P.A., 1976, Geochemical magma type discrimination: application to altered and metamorphosed basic igneous rocks, Earth and Planetary Science Letters, v. 28, p. 459-469.

Winchester, J.A., and Floyd, P.A., 1977, Geochemical discrimination of different magma series and their differentiation products using immobile elements, Chemical Geology, v. 20, p. 325-343.

Winkler, H.G.F., 1976, Petrogenesis of Metamorphic Rocks, 4th ed., Springer-Verlag, New York, 348 p.

Wicks, F.J. and Whittaker, E.J.W., 1977, Serpentine textures and serpentinisation, Canadian Mineralogist, v. 15, p. 459-488.

Wise, D.U., Dunn, D.E., Engelder, J.T., Geiser, P.A., Hatcher, R.D., Kish, S.A., Odom, A.L., and Schamel, S., 1984, Fault-related rocks: Suggestions for terminology, Geology, v. 12, p. 391-394.

Wohl, K., 1946, Thermodynamic evaluation of binary and ternary liquid systems, Transactions of American Institute of Chemical Engineering, v. 42, p. 1-15.

Wolfart, R., 1987, Geology of Amphoe Sop Prap and Amphoe Wang Chin, Thailand, Geologisches Jahrbuch Reihe B, Federal Institute for Geosciences and Natural Resources, Hannover, 52 p.

Woodward, N.B., Boyer, S.E. and Suppe, J., 1989, Balanced cross-sections: an essential technique in geological research and exploration, Short Course 6 (International Geological Congress), American Geophysical Union Publication, Washinton DC, 132 p.

Wyllie, P.J., 1977, Crustal anatexis: an experimental review, Tectonophysics, v. 43, p. 41-71.

Yang, A., 1992, Major and minor element systematics in the lherzolite system: a petrologic and experimental study, unpublished PhD thesis, University of Tasmania, 171 p.

Yardley, B.W.D., 1982, The early metamorphic history of the Haast Schists and related rocks of New Zealand, Contributions to Mineralogy and Petrology, v. 81, p. 317-327.

Yardley, B.W.D., 1989, An Introduction to Metamorphic Petrology, Longman Scientific and Technical, Singapore, 248 p.

# Appendix A

## Catalogue of Rock Specimens

(R = Hand specimen, T = Thin section, TS = Polished thin section, and C = Crushed specimen)

| CATALOG# | FIELD# | DESCRIPTION | FORMATION | AGE | LOCALITY | CO-ORDS | PREPARATION |
|---|---|---|---|---|---|---|---|
| 78611 | SD-42 | Metagreywacke | Pha Som metasediments | Permo-Carb. | Sirikit Dam | 657644/5144IV | R,PT |
| 78612 | SD-44 | " | " | " | " | 658640/5144IV | C |
| 78613 | SD-52 | " | " | " | Ban Hat Ngui | 586618/5044II | R |
| 78614 | SD-54 | Phyllite | " | " | " | 582619/5044II | C |
| 78615 | SD-56 | " | " | " | " | 578621/5044II | C |
| 78616 | SD-59 | " | " | " | " | 572629/5044II | C |
| 78617 | SD-60 | Metagreywacke | " | " | " | " | R,PT |
| 78618 | SD-61 | " | " | " | " | 565626/5044II | R,T |
| 78619 | SD-64 | " | " | " | " | 559629/5044II | R,PT |
| 78620 | SD-65 | " | " | " | " | 473598/5044II | R,PT |
| 78621 | SD-82 | " | " | " | Sirikit Dam | 663647/5144IV | R,PT |
| 78622 | SD-85 | Phyllite | " | " | " | 662636/5144IV | R,C |
| 78623 | SD-86 | " | " | " | " | 662634/5144IV | R,C |
| 78624 | SD-91 | Metagreywacke | " | " | " | 594661/5144IV | R,PT |
| 78625 | SD-92 | " | " | " | Tha Pla | 569710/5044I | R,C |
| 78626 | SD-95 | " | " | " | " | 566698/5044I | C |
| 78627 | SD-96 | Phyllite | " | " | " | 559703/5044I | C |
| 78628 | SD-97 | Metagreywacke | " | " | " | 587690/5044I | R,PT |
| 78629 | SD-98 | Phyllite | " | " | " | " | C |
| 78630 | SD-99 | Metagreywacke | " | " | " | 572685/5044I | R,PT |
| 78631 | SD-100 | " | " | " | Sirikit Dam | 644660/5144IV | R,PT |
| 78632 | SD-104 | " | " | " | " | 661659/5144IV | R,PT |
| 78633 | SD-105 | Phyllite | " | " | " | 672657/5144IV | C |
| 78634 | SD-107 | " | " | " | " | 685649/5144IV | C |
| 78635 | SD-148 | " | " | " | " | 631597/5144III | R,PT |
| 78636 | SD-148.1 | Metagreywacke | " | " | " | " | R,PT |
| 78637 | SD-150 | " | " | " | " | 628596/5144III | R,PT |
| 78638 | SD-151 | Phyllite | " | " | " | " | R,PT |
| 78639 | SD-156 | Metagreywacke | " | " | " | 627623/5144III | R,PT |
| 78640 | SD-162 | " | " | " | " | 627623/5144III | C |
| 78641 | SD-163 | Phyllite | " | " | " | 613630/5144III | C |
| 78642 | SD-165 | Metagreywacke | " | " | Sirikit Dam | 610634/5144IV | R,PT |
| 78643 | SD-193 | " | " | " | Tha Pla | 560635/5044I | R,PT |
| 78644 | SD-194 | " | " | " | " | 563633/5044I | R,C |
| 78645 | SD-195 | Phyllite | " | " | " | 565632/5044I | C |
| 78646 | SD-198 | Metagreywacke | " | " | " | 570638/5044I | R,PT |
| 78647 | SD-207 | Phyllite | " | " | " | 503694/5044I | C |
| 78648 | SD-209 | Metagreywacke | " | " | " | 509694/5044I | R,PT |
| 78649 | SD-211 | " | " | " | " | 516693/5044I | R,PT |
| 78650 | SD-212 | Phyllite | " | " | " | " | C |
| 78651 | SD-213 | Metagreywacke | " | " | " | 518692/5044I | R,PT |
| 78652 | SD-216 | Phyllite | " | " | " | 528694/5044I | C |
| 78653 | SD-217 | Metagreywacke | " | " | " | 526689/5044I | R,PT |
| 78654 | SD-218 | " | " | " | " | 537701/5044I | R,C |
| 78655 | SD-219 | Slate | " | " | " | 534692/5044I | C |
| 78656 | SD-221 | Metagreywacke | " | " | " | 536692/5044I | R,PT |
| 78657 | SD-222 | Slate | " | " | " | 538692/5044I | C |
| 78658 | SD-224 | Metagreywacke | " | " | " | 518722/5044I | R,PT |
| 78659 | SD-225 | " | " | " | " | 588748/5044I | R,PT |
| 78660 | SD-227 | " | " | " | " | 587745/5044I | R,PT |
| 78661 | 2/5291 | Phyllite | " | " | Nam Pat | 6576095144III | R,PT |
| 78662 | 1/6291 | Metagreywacke | " | " | Sirikit Dam | 660658/5144IV | R,PT |
| 78663 | 15/6291 | " | " | " | " | 644654/5144IV | R,PT |
| 78664 | 17/6291 | " | " | " | " | 662649/5144IV | R,PT |
| 78665 | 1/7291 | " | " | " | " | 662762/5144IV | R,PT |
| 78666 | 2/8291 | " | " | " | " | 594661/5144IV | R,PT |
| 78667 | 3/8291 | " | " | " | " | 597673/5144IV | R,PT |
| 78668 | 5/8291 | Phyllite | " | " | " | " | R,PT |
| 78669 | 3/9291 | " | " | " | Nam Pat | 650610/5144III | R,PT |
| 78670 | 6/9291 | " | " | " | " | 625614/5144III | R,PT |
| 78671 | 7/9291 | " | " | " | " | " | R,PT |

| | | | | | | | |
|---|---|---|---|---|---|---|---|
| 78672 | SD-168 | Slate | Pha Som ophiolite association | Permo-Carb. | " | 697606/5144III | C |
| 78673 | SD-170 | Metabasalt | " | " | " | 699608/5144III | R,PT |
| 78674 | SD-172 | " | " | " | " | " | R,PT |
| 78675 | SD-174 | Phyllite | " | " | " | 708614/5144III | C |
| 78676 | SD-176 | Serpentinite | " | " | " | 709608/5144III | R,PT |
| 78677 | SD-177 | Gabbro | " | " | " | " | R,PT |
| 78678 | SD-178 | Serpentinite | " | " | " | " | R,PT |
| 78679 | SD-179.2 | " | " | " | " | " | PT |
| 78680 | SD-182 | Metabasalt | " | " | " | 717603/5144III | R,PT |
| 78681 | SD-188 | Phyllite | " | " | " | " | C |
| 78682 | SD-189 | Greywacke | " | " | " | 707622/5144III | R,PT |
| 78683 | SD-191 | Phyllite | " | " | " | 705622/5144III | C |
| 78684 | 5/6291 | Amphibolite | " | " | Sirikit Dam | 646694/5144IV | R,PT |
| 78685 | 6/6291 | " | " | " | " | " | R,PT |
| 78686 | 2/7291 | " | " | " | " | 663756/5144IV | R,PT |
| 78687 | 4/7291 | " | " | " | " | " | R,PT |
| 78688 | 5/7291 | " | " | " | " | " | R,PT |
| 78689 | 7/7291 | " | " | " | " | " | R,PT |
| 78690 | 8/7291 | " | " | " | " | " | R,PT |
| 78691 | 9/7291 | Garnet Amphibolite | " | " | " | " | R,PT |
| 78692 | 12/7291 | Amphibolite | " | " | " | 668757/5144IV | R,PT |
| 78693 | 13/7291 | Serpentinite | " | " | " | " | R,PT |
| 78694 | 15/7291 | Chromitite | " | " | " | 664752/5144IV | R,PT |
| 78695 | 2/6291 | Piemontite-quartz schist | " | " | " | 648674/5144IV | R,PT |
| 78696 | 1/8291 | Quartz schist | " | " | " | 615663/5144IV | R |
| 78697 | SD-89 | Basalt | Pak Pat Volcanics | Permo-Triassic | Nam Pat | 653598/5144III | R,PT |
| 78698 | SD-90.1 | " | " | " | " | 650612/5144III | R,T |
| 78699 | SD-90.2 | Dacite | " | " | " | " | R,T |
| 78700 | SD-119 | Basalt | " | " | Sirikit Dam | 710728/5144IV | R,PT |
| 78701 | SD-126 | " | " | " | " | 733727/5144IV | R,PT |
| 78702 | SD-128 | " | " | " | " | 737728/5144IV | R,PT |
| 78703 | SD-130 | " | " | " | " | 742727/5144IV | R,PT |
| 78704 | NZ-1.1 | Dacite | " | " | Nam Pat | 647607/5144III | PT |
| 78705 | NZ-1.2 | Basalt | " | " | " | 647607/5144III | PT |
| 78706 | NZ-1.3 | " | " | " | " | 647607/5144III | PT |
| 78707 | NZ-2 | Andesite | " | " | " | 656608/5144III | T |
| 78708 | NZ-3 | " | " | " | " | 658605/5144III | T |
| 78709 | NZ-8.1 | Basalt | " | " | " | 653614/5144III | PT |
| 78710 | NZ-8.2 | Dacite | " | " | " | 653614/5144III | PT |
| 78711 | NZ-9.1 | Andesite | " | " | Sirikit dam | 7335728/5144IV | T |
| 78712 | NZ-9.2 | " | " | " | " | 735728/5144IV | T |
| 78713 | NZ-11 | " | " | " | Nam Pat | 636607/5144III | T |
| 78714 | SD-137 | Greywacke | Huai Lat Fm | Triassic | " | 674544/5144III | C |
| 78715 | SD-140 | " | " | " | " | 668557/5144III | R,PT |
| 78716 | SD-181 | " | " | " | " | 737612/5144III | PT |
| 78717 | SD-7 | Shale | Huai Bo Khong Fm | Triassic | Huai Bo Khong | 717567/5144III | C |
| 78718 | SD-12 | Greywacke | " | " | " | 720570/5144III | R,PT |
| 78719 | SD-15 | " | " | " | " | 720572/5144III | R,PT |
| 78720 | SD-16 | Shale | " | " | " | 720572/5144III | C |
| 78721 | SD-18 | Greywacke | " | " | " | 719574/5144III | R,PT |
| 78722 | SD-19 | Shale | " | " | " | 721578/5144III | C |
| 78723 | SD-21 | Greywacke | " | " | " | 721582/5144III | R,PT |
| 78724 | SD-23 | Shale | " | " | " | 717584/5144III | C |
| 78725 | SD-24 | Greywacke | " | " | " | 716586/5144III | R,PT |
| 78726 | SD-28 | " | " | " | " | 714587/5144III | R,PT |
| 78727 | SD-31 | Shale | " | " | " | 716566/5144III | C |
| 78728 | SD-33 | Greywacke | " | " | " | 714565/5144III | R,PT |
| 78729 | SD-36 | " | " | " | " | 710564/5144III | R,PT |
| 78730 | SD-37 | " | " | " | " | 705561/5144III | R,T |
| 78731 | SD-38 | Slate | " | " | " | 705561/5144III | C |
| 78732 | SD-39 | Greywacke | " | " | " | 703558/5144III | R,PT |
| 78733 | SD-40 | Slate | " | " | " | 703558/5144III | C |
| 78734 | SD-66 | Greywacke | " | " | " | 705576/5144III | R,C |
| 78735 | SD-67 | " | " | " | " | 704578/5144III | R,PT |
| 78736 | SD-1 | Quartzose sandstone | Phra Wihan Fm | Middle Jurassic | Nam Pat | 757546/5144III | R,T |
| 78737 | SD-3 | " | " | " | " | 833578/5144III | R,T |
| 78738 | SD-153 | " | " | " | " | 689516/5144III | R,T |
| 78739 | SD-158 | " | " | " | " | 818575/5144III | R,T |
| 78740 | SD-180 | " | " | " | " | 745610/5144III | R,T |
| 78741 | P-1 | Shale | Wang Chin Fm | Triassic | Phrae-Nam Phra | 288990/5045III | C |
| 78742 | P-2 | Limestone | " | " | " | " | R,T |

| | | | | | | | |
|---|---|---|---|---|---|---|---|
| 78743 | P-4 | Shale | " | " | " | 3132963/5045III | C |
| 78744 | P-7 | " | " | " | " | 287995/5045III | C |
| 78745 | P-10 | " | " | " | " | 300977/5045III | C |
| 78746 | P-11 | Greywacke | " | " | " | " | T |
| 78747 | P-12 | Limestone | " | " | " | 302973/5045III | R,T |
| 78748 | P-12.1 | " | " | " | " | " | R,T |
| 78749 | P-13 | Shale | " | " | " | 306969/5045III | C |
| 78750 | P-15 | Slate | " | " | " | 317960/5045III | C |
| 78751 | P-16 | Limestone | " | " | " | " | R,T |
| 78752 | P-19 | Greywacke | " | " | " | 320960/5045III | R,T |
| 78753 | P-19.1 | Limestone | " | " | " | " | T |
| 78754 | P-20 | Slate | " | " | " | 322959/5045III | C |
| 78755 | P-21 | Greywacke | " | " | " | " | R,PT |
| 78756 | P-22 | Shale | " | " | " | " | C |
| 78757 | P-25 | Greywacke | " | " | " | 329956/5045II | R,T |
| 78758 | P-26 | Shale | " | " | " | 327955/5045II | C |
| 78759 | P-27 | " | " | " | " | 332952/5045II | C |
| 78760 | P-30 | Limestone | " | " | " | 336953/5045II | T |
| 78761 | P-34 | " | " | " | " | 336946/5045II | R,T |
| 78762 | P-35 | Shale | " | " | " | " | C |
| 78763 | P-38 | " | " | " | " | 338943/5045II | C |
| 78764 | P-42 | " | Rong Kwang Fm | Permian | " | 341942/5045II | C |
| 78765 | P-44 | " | " | " | " | 346942/5045II | C |
| 78766 | P-47 | " | " | " | " | 350944/5045II | C |
| 78767 | P-48 | Limestone | " | " | " | 352942/5045II | T |
| 78768 | P-49 | " | " | " | " | 357947/5045II | R,T |
| 78769 | P-50 | Shale | " | " | " | " | C |
| 78770 | P-52 | " | " | " | " | 361947/5045II | C |
| 78771 | P-55 | " | " | " | " | 366945/5045II | C |
| 78772 | P-56 | Limestone | " | " | " | 370940/5045II | R,T |
| 78773 | P-58 | Shale | " | " | " | 374933/5045II | C |
| 78774 | P-60 | " | " | " | " | 385915/5045II | C |
| 78775 | P-61 | " | " | " | " | 390914/5045II | C |
| 78776 | P-63 | " | " | " | " | 403923/5045II | C |
| 78777 | P-65 | Limestone | " | " | " | 412922/5045II | R,T |
| 78778 | P-66 | Shale | " | " | " | 412923/5045II | C |
| 78779 | P-69 | Slate | " | " | " | 417914/5045II | C |
| 78780 | P-72 | " | " | " | " | 419906/5045II | C |
| 78781 | P-73 | " | " | " | " | 418898/5044I | C |
| 78782 | P-77 | " | " | " | " | 417894/5044I | C |
| 78783 | P-78 | Greywacke | " | " | " | " | R,PT |
| 78784 | P-80 | Slate | " | " | " | 414888/5044I | C |
| 78785 | P-82 | " | " | " | " | 422886/5044I | C |
| 78786 | P-84 | " | " | " | " | 424886/5044I | C |
| 78787 | P-87 | Phyllite | Pha Som metasediments | Permo-Carb | " | 437872/5044I | C |
| 78788 | P-92 | " | " | " | " | 836948/5044I | C |
| 78789 | P-96 | " | " | " | " | 438882/5044I | C |
| 78790 | P-99 | " | " | " | " | 447851/5044I | C |
| 78791 | P-100 | " | " | " | " | 448850/5044I | C |
| 78792 | P-102 | Metagreywacke | " | " | " | 452850/5044I | R,PT |
| 78793 | P-104 | " | " | " | " | 456856/5044I | R,PT |
| 78794 | P-105 | Phyllite | " | " | " | 460858/5044I | C |
| 78795 | P-106 | Metagreywacke | " | " | " | 464860/5044I | R,PT |
| 78796 | P-107 | " | " | " | " | 474862/5044I | R,PT |
| 78797 | LP-18 | Shale | Huai Thak Fm | Permian | Lampang-Denchai | km59.75/H11 | C |
| 78798 | LP-20 | " | " | " | " | km57.37/H11 | C |
| 78799 | 2/161290 | Dacitic tuff | Doi Luang volcanics | Permo-Triassic | " | km7.83/H11 | R,T |
| 78800 | 4/161290 | Volcanic sandstone | " | " | " | " | R,PT |
| 78801 | 6/161290 | Lapilli tuff | " | " | " | km8.00/H11 | T |
| 78802 | 7/161290 | " | " | " | " | " | R,T |
| 78803 | 31/161290 | Conglomerate | " | " | " | km8.30/H11 | R,T |
| 78804 | 32/161290 | Tuff | " | " | " | " | R,Y |
| 78805 | 18/161290 | Shale | " | " | " | km32.60/H11 | R,T |
| 78806 | 1/111290 | ShearedtTuff | " | " | " | km33.25/H11 | R,T |
| 78807 | 22/151290 | Dacitic tuff | " | " | " | km60.70/H11 | T |
| 78808 | 1/151290 | Lithic tuff | " | " | " | km61.83/H11 | T |
| 78809 | 21/151290 | Crystal tuff | " | " | " | km61.87/H11 | R,PT |
| 78810 | 4/151290 | Conglomerate | " | " | " | km70.00/H11 | R,T |
| 78811 | 3/151290 | " | " | " | " | " | R,T |
| 78812 | 2/151290 | " | " | " | " | " | R,T |
| 78813 | 20/161290 | Laminated siltstone | Phra That Fm | Tnassic | " | km30.80/H11 | R,T |

| | | | | | | | |
|---|---|---|---|---|---|---|---|
| 78814 | 21/161290 | " | " | " | " | " | R,T |
| 78815 | 32/151290 | Sandstone | " | " | " | km31.61/H11 | R,PT |
| 78816 | 33/151290 | Shale | " | " | " | " | R |
| 78817 | 2/121290 | Sheared Tuff | " | " | " | km32.10/H11 | R,T |
| 78818 | LP-22 | Shale | " | " | " | km30.60/H11 | C |
| 78819 | LP-23 | " | " | " | " | km32.05/H11 | C |
| 78820 | 28/161290 | Limestone | Pha Kan Fm | " | " | km22.80/H11 | R,T |
| 78821 | 29/161290 | " | " | " | " | km22.81/H11 | R,T |
| 78822 | 30/161290 | " | " | " | " | km22.86/H11 | R,T |
| 78823 | 35/161290 | " | " | " | " | km16.40/H11 | R,T |
| 78824 | 37/161290 | " | " | " | " | km19.37/H11 | R,T |
| 78825 | 38/161290 | " | " | " | " | km22.10/H11 | R,T |
| 78826 | 8/151290 | " | Kang Pla Fm | " | " | km68.96/H11 | R,T |
| 78827 | 6/151290 | " | " | " | " | km68.98/H11 | R,T |
| 78828 | 5/151290 | " | " | " | " | " | R,T |
| 78829 | 30/151290 | Shale | Wang Chin Fm | " | " | km48.50/H11 | R |
| 78830 | 29/151290 | " | " | " | " | km52.32/H11 | R |
| 78831 | 28/151290 | " | " | " | " | km53.05/H11 | R |
| 78832 | 27/151290 | " | " | " | " | km54.00/H11 | R |
| 78833 | 25/151290 | " | " | " | " | km54.80/H11 | R |
| 78834 | 24/151290 | " | " | " | " | km55.85/H11 | R |
| 78835 | 18/151290 | " | " | " | " | km64.35/H11 | R |
| 78836 | 17/151290 | " | " | " | " | km65.80/H11 | R |
| 78837 | 2/71290 | " | " | " | " | km66.50/H11 | R |
| 78838 | 4/61290 | Sandstone | " | " | " | km67.10/H11 | R,PT |
| 78839 | 16/151290 | " | " | " | " | km67.17/H11 | T |
| 78840 | 6/61290 | Shale | " | " | " | km67.20/H11 | R |
| 78841 | 12/151290 | " | " | " | " | km67.90/H11 | R |
| 78842 | 5/61290 | Limestone | " | " | " | km67.91/H11 | T |
| 78843 | 3/61290 | " | " | " | " | km68.47/H11 | R |
| 78844 | 11/151290 | " | " | " | " | " | R |
| 78845 | 2/61290 | Shale | " | " | " | km68 52/H11 | R |
| 78846 | LP-3 | " | " | " | " | km65.00/H11 | C |
| 78847 | LP-4 | " | " | " | " | km64.00/H11 | C |
| 78848 | LP-8 | " | " | " | " | km55.22/H11 | C |
| 78849 | LP-9 | " | " | " | " | km54.00/H11 | C |
| 78850 | LP-10 | " | " | " | " | km52.00/H11 | C |
| 78851 | LP-11 | " | " | " | " | km49.00/H11 | C |
| 78852 | LP-13 | " | " | " | " | km47.80/H11 | C |
| 78853 | LP-14 | " | " | " | " | km46.60/H11 | C |
| 78854 | LP-24 | " | " | " | " | km44.80/H11 | C |
| 78855 | 13/161290 | Granite | Granite | Upper Triassic | " | km43.10/H11 | PT |
| 78856 | 12/161290 | " | " | " | " | " | R,PT |
| 78857 | 2/111290 | " | " | " | " | km43.25/H11 | R,PT |
| 78858 | 4/111290 | Hornfels | Hornfels | " | " | km43.50/H11 | R,PT |
| 78859 | 7/111290 | " | " | " | " | " | R,PT |
| 78860 | IN-1 | Quartzofeldspathic gneiss | Doi Inthanon Complex | Triassic(?) | Doi Inthanon | 655454/4745IV | PT |
| 78861 | IN-2 | Calc-silicate rock | " | " | " | " | PT |
| 78862 | IN-3 | " | " | " | " | " | R,PT |
| 78863 | IN-5 | Quartzofeldspathic gneiss | " | " | " | 627474/4746II | PT |
| 78864 | IN-8 | " | " | " | " | 643460/4746II | R,PT |
| 78865 | IN-10 | " | " | " | " | " | PT |
| 78866 | IN-12 | Calc-silicate rock | " | " | " | 655454/4745IV | R,PT |
| 78867 | IN-13.1 | " | " | " | " | 492506/4746II | R,PT |
| 78868 | IN-13.2 | " | " | " | " | " | PT |
| 78869 | IN-14 | Quartzofeldspathic gneiss | " | " | " | " | R,PT |
| 78870 | IN-16 | Marble | " | " | " | 592472/4746II | R,PT |
| 78871 | IN-18 | Quartzofeldspathic gneiss | " | " | " | 456513/4746III | R,PT |
| 78872 | IN-19 | " | " | " | " | " | R,PT |

# Appendix B

Table B-1 Electron microprobe analyses of albites (metasediments of the Pha Som Metamorphic Complex).

| Sample no. | 2/5291 | | | | 5/8291 | 6/9291 | | | | | 3/8291 | | | | SD-97 |
|---|---|---|---|---|---|---|---|---|---|---|---|---|---|---|---|
| Analysis no. | 1 | 2 | 3 | 4 | 1 | 1 | 2 | 3 | 4 | 5 | 1 | 2 | 3 | 4 | 1 |
| | | | | | | C2-Ab1 | C2-Ab2 | C2-Ab4 | C2-Ab5 | C2-Ab6 | | | | | C3-Ab2 |
| SiO2 | 68 52 | 68.94 | 68.75 | 68.82 | 68 59 | 68.46 | 68.70 | 69 46 | 68.57 | 69.20 | 68.50 | 68.35 | 68.41 | 68.41 | 66.88 |
| Al2O3 | 19.33 | 19.59 | 19.53 | 19.68 | 19.49 | 19.51 | 19.58 | 19.68 | 19 61 | 19.53 | 19.49 | 19 32 | 19.55 | 19 84 | 20 37 |
| FeO* | 0 07 | 0 06 | 0.00 | 0.16 | 0 21 | 0.21 | 0.27 | 0.25 | 0.20 | 0.15 | 0.07 | 0.04 | 0.00 | 0.02 | 0.01 |
| MgO | 0.00 | 0 02 | 0.00 | 0.01 | 0 01 | 0.00 | 0.07 | 0.00 | 0.01 | 0.00 | 0 00 | 0 00 | 0 00 | 0 00 | 0 00 |
| CaO | 0 07 | 0.05 | 0.00 | 0 04 | 0.03 | 0.10 | 0.08 | 0.06 | 0 06 | 0.05 | 0.33 | 0.44 | 0.45 | 0 07 | 0.99 |
| Na2O | 11.31 | 10.96 | 11.22 | 10.72 | 11.14 | 11.33 | 11.11 | 11.38 | 11.36 | 11.37 | 11.12 | 11 05 | 10.99 | 11.19 | 10.51 |
| K2O | 0.05 | 0 02 | 0.03 | 0.02 | 0.67 | 0.02 | 0.04 | 0.04 | 0.03 | 0.05 | 0.03 | 0.06 | 0 03 | 0 02 | 0.16 |
| Total | 99.34 | 99.64 | 99 53 | 99 45 | 100.144 | 99.63 | 99.85 | 100.87 | 99 84 | 100.35 | 99.54 | 99.26 | 99.43 | 99.55 | 98.90 |
| Number of cations on the basis of 8 oxygens: | | | | | | | | | | | | | | | |
| Si | 3.004 | 3.008 | 3.007 | 3.004 | 2.991 | 2.992 | 2.993 | 2.996 | 2.991 | 3.002 | 2.998 | 3.001 | 2.998 | 2 992 | 2.954 |
| Al | 0.999 | 1 008 | 1.007 | 1.013 | 1.002 | 1.005 | 1.006 | 1.001 | 1.008 | 0.999 | 1.006 | 1.000 | 1.010 | 1.023 | 1.060 |
| Fe2+ | 0.005 | 0 004 | 0.000 | 0 012 | 0.015 | 0.015 | 0 020 | 0.018 | 0.015 | 0.011 | 0.005 | 0.003 | 0.000 | 0.001 | 0.001 |
| Mg | 0.000 | 0.000 | 0.000 | 0.000 | 0.000 | 0.000 | 0.000 | 0.000 | 0.000 | 0.000 | 0.000 | 0.000 | 0.000 | 0 000 | 0.000 |
| Ca | 0.003 | 0.002 | 0.000 | 0 002 | 0.001 | 0.005 | 0.004 | 0.003 | 0.003 | 0.002 | 0.015 | 0.021 | 0 021 | 0 003 | 0.047 |
| Na | 0 962 | 0.927 | 0.951 | 0.907 | 0.942 | 0.960 | 0.938 | 0.952 | 0.961 | 0 956 | 0.944 | 0.941 | 0.934 | 0.949 | 0.900 |
| K | 0.003 | 0.001 | 0.002 | 0.001 | 0.037 | 0 001 | 0.002 | 0.002 | 0.002 | 0.003 | 0 002 | 0.003 | 0.002 | 0 001 | 0.009 |
| Sum Cations | 4.976 | 4.950 | 4.967 | 4.938 | 4.989 | 4.978 | 4.962 | 4.972 | 4 979 | 4.973 | 4.969 | 4 969 | 4.965 | 4.970 | 4.970 |
| Molecular proportions of end-members: | | | | | | | | | | | | | | | |
| An | 0 003 | 0.003 | 0.000 | 0 002 | 0.002 | 0.005 | 0.004 | 0.003 | 0.003 | 0.002 | 0.016 | 0 021 | 0 022 | 0.003 | 0.049 |
| Ab | 0.994 | 0.996 | 0.998 | 0.997 | 0.960 | 0.994 | 0.994 | 0.995 | 0.995 | 0.995 | 0.982 | 0.975 | 0.976 | 0.995 | 0.942 |
| Or | 0.003 | 0.001 | 0.002 | 0 001 | 0.038 | 0.001 | 0.002 | 0.002 | 0 002 | 0.003 | 0.002 | 0 003 | 0.002 | 0 001 | 0.009 |

Table B-1 (continued)

| Sample no. | SD-97 | | | | SD-225 | | | | | | SD-227 | | | | 1/7291 |
|---|---|---|---|---|---|---|---|---|---|---|---|---|---|---|---|
| Analysis no. | 2 | 3 | 4 | 5 | 1 | 2 | 3 | 4 | 5 | 6 | 1 | 2 | 3 | 4 | 1 |
| | C3-Ab3 | C3-Ab4 | C4-Ab6 | C4-Ab7 | C4-Ab1 | C4-Ab2 | C4-Ab3 | C4-Ab4 | C4-Ab6 | C5-Ab7 | C5-Ab1 | C5-Ab2 | C5-Ab3 | C5-Ab4 | C1-Ab1 |
| SiO2 | 67.10 | 66.94 | 68.51 | 67.85 | 68.42 | 68.19 | 68.24 | 68.41 | 68.30 | 67.98 | 68.27 | 67.07 | 67.30 | 67.53 | 68.47 |
| Al2O3 | 20.57 | 20.42 | 20 02 | 19.68 | 19.77 | 19.75 | 19.36 | 19.95 | 19.23 | 19.91 | 19.94 | 20.43 | 20.51 | 20.58 | 19.38 |
| FeO* | 0.06 | 0.00 | 0.02 | 0.10 | 0.12 | 0.00 | 0.05 | 0.07 | 0.06 | 0 04 | 0.01 | 0.19 | 0.13 | 0 04 | 0.04 |
| MgO | 0.00 | 0.00 | 0.02 | 0.00 | 0.00 | 0 02 | 0.00 | 0.00 | 0 00 | 0.04 | 0.02 | 0.03 | 0 04 | 0 00 | 0.00 |
| CaO | 0.94 | 0.70 | 0.14 | 0.16 | 0.15 | 0.41 | 0.20 | 0 23 | 0.15 | 0.14 | 0.19 | 0.20 | 0.19 | 0.29 | 0.08 |
| Na2O | 10.49 | 10 69 | 11.01 | 10.81 | 10.96 | 10.73 | 10.82 | 10.90 | 11.10 | 10.95 | 11.29 | 10.90 | 10.80 | 10.87 | 11.15 |
| K2O | 0.15 | 0.08 | 0.05 | 0.07 | 0.03 | 0.01 | 0.02 | 0.04 | 0 02 | 0.00 | 0.08 | 0.49 | 0.54 | 0 28 | 0.06 |
| Total | 99.31 | 98.84 | 99.77 | 98.67 | 99.45 | 99.12 | 98.70 | 99.60 | 98.86 | 97.07 | 99.80 | 99.32 | 99.52 | 99.57 | 99.18 |
| Number of cations on the basis of 8 oxygens: | | | | | | | | | | | | | | | |
| Si | 2.949 | 2.956 | 2.989 | 2.992 | 2.993 | 2.994 | 3.007 | 2.989 | 3.007 | 2.987 | 2.984 | 2.950 | 2.954 | 2.959 | 3.006 |
| Al | 1.066 | 1.063 | 1.030 | 1 023 | 1.019 | 1.023 | 1.006 | 1.028 | 0.998 | 1.031 | 1.027 | 1.059 | 1.061 | 1.063 | 1.003 |
| Fe2+ | 0.004 | 0.000 | 0.001 | 0.007 | 0.009 | 0.000 | 0.004 | 0.005 | 0.005 | 0.003 | 0.001 | 0.014 | 0.010 | 0.003 | 0 003 |
| Mg | 0.000 | 0.000 | 0.000 | 0.000 | 0.000 | 0.000 | 0.000 | 0.000 | 0 000 | 0.000 | 0 000 | 0.000 | 0.000 | 0.000 | 0.000 |
| Ca | 0.044 | 0.033 | 0.006 | 0.007 | 0.007 | 0.019 | 0.010 | 0.011 | 0 007 | 0.007 | 0.009 | 0.010 | 0.009 | 0.013 | 0.004 |
| Na | 0 894 | 0.916 | 0.932 | 0.924 | 0.930 | 0.914 | 0.924 | 0.923 | 0.947 | 0.933 | 0.957 | 0.930 | 0.919 | 0.923 | 0.949 |
| K | 0.009 | 0.004 | 0.003 | 0.004 | 0.002 | 0.001 | 0.001 | 0.002 | 0.001 | 0.000 | 0.004 | 0.028 | 0.030 | 0.015 | 0.004 |
| Sum Cations | 4.967 | 4.972 | 4.961 | 4.957 | 4.959 | 4.951 | 4.951 | 4.958 | 4.966 | 4.961 | 4.982 | 4.991 | 4.983 | 4.977 | 4.968 |
| Molecular proportions of end-members: | | | | | | | | | | | | | | | |
| An | 0.047 | 0.035 | 0.007 | 0 008 | 0.007 | 0.021 | 0.010 | 0.012 | 0 007 | 0.007 | 0.009 | 0.010 | 0.009 | 0.014 | 0 004 |
| Ab | 0.944 | 0.960 | 0.990 | 0.988 | 0.991 | 0.979 | 0.988 | 0.986 | 0.991 | 0.993 | 0.986 | 0.961 | 0.959 | 0.970 | 0.992 |
| Or | 0 009 | 0.005 | 0.003 | 0.004 | 0.002 | 0.001 | 0 001 | 0.002 | 0 002 | 0.000 | 0 004 | 0.029 | 0 031 | 0 016 | 0 004 |

* Total Fe as FeO

Table B-1 (Continued)

| Sample no. | SD-60 | | | | | SD-99 | | | | | |
|---|---|---|---|---|---|---|---|---|---|---|---|
| Analysis no. | 1 | 2 | 3 | 4 | 5 | 1 | 2 | 3 | 4 | 5 | 6 |
| | C1-Ab1 | C1-Ab2 | C1-Ab3 | C2-Ab4 | C2-Ab5 | C3-Ab1 | C3-Ab2 | C3-Ab3 | C3-Ab4 | C3-Ab5 | C3-Ab6 |
| SiO2 | 69.04 | 67.58 | 67.88 | 67.11 | 67 68 | 68.14 | 68.04 | 68.77 | 68.58 | 68.16 | 68.35 |
| Al2O3 | 0.04 | 19.58 | 19.48 | 20.09 | 19.70 | 20.23 | 19.77 | 19.73 | 19.82 | 19.93 | 19.77 |
| FeO* | 19.67 | 0.05 | 0.01 | 0.03 | 0.03 | 0.18 | 0.05 | 0.08 | 0.00 | 0 00 | 0.11 |
| MgO | 0.02 | 0.01 | 0.02 | 0.01 | 0.01 | 0.04 | 0.01 | 0.00 | 0.00 | 0.03 | 0.00 |
| CaO | 0.03 | 0.06 | 0.17 | 0.59 | 0.35 | 0.11 | 0.15 | 0.14 | 0.17 | 0.17 | 0.17 |
| Na2O | 11.01 | 11.13 | 11.32 | 10.75 | 11.06 | 10.85 | 11.07 | 11.15 | 11.22 | 11.05 | 11.01 |
| K2O | 0.03 | 0.02 | 0.02 | 0.11 | 0.03 | 0.21 | 0.03 | 0.04 | 0.04 | 0 03 | 0.06 |
| Total | 99.85 | 98.42 | 98.89 | 98.69 | 98.87 | 99.74 | 99.12 | 99.91 | 99.84 | 99.37 | 99.48 |
| Number of cations on the basis of 8 oxygens: | | | | | | | | | | | |
| Si | 2.786 | 2.991 | 2.993 | 2.967 | 2.985 | 2.974 | 2.990 | 2.996 | 2.993 | 2.988 | 2.991 |
| Al | 0.002 | 1.022 | 1.013 | 1 047 | 1.024 | 1.041 | 1.024 | 1.014 | 1.020 | 1.030 | 1.020 |
| Fe2+ | 1.328 | 0.003 | 0.001 | 0.002 | 0.002 | 0.013 | 0.003 | 0.006 | 0.000 | 0.000 | 0.008 |
| Mg | 0.000 | 0.000 | 0.000 | 0.000 | 0.000 | 0.000 | 0.000 | 0.000 | 0.000 | 0.000 | 0.000 |
| Ca | 0.001 | 0.003 | 0.008 | 0.028 | 0.017 | 0.005 | 0 007 | 0.007 | 0.008 | 0.008 | 0.008 |
| Na | 0.862 | 0.955 | 0.968 | 0.921 | 0.946 | 0.918 | 0.943 | 0.942 | 0.950 | 0.939 | 0.934 |
| K | 0.001 | 0 001 | 0.001 | 0.006 | 0.002 | 0.011 | 0.002 | 0.002 | 0.002 | 0.002 | 0.003 |
| Sum Cations | 4.980 | 4.975 | 4.984 | 4.972 | 4.975 | 4.962 | 4.969 | 4.966 | 4.973 | 4 967 | 4.964 |
| Molecular proportions of end-members: | | | | | | | | | | | |
| An | 0.002 | 0.003 | 0.008 | 0.029 | 0.017 | 0.005 | 0.007 | 0.007 | 0.008 | 0.009 | 0.008 |
| Ab | 0.997 | 0.996 | 0.991 | 0.964 | 0.981 | 0.982 | 0.991 | 0.991 | 0.989 | 0.990 | 0.988 |
| Or | 0.002 | 0 001 | 0.001 | 0.006 | 0.002 | 0.012 | 0.002 | 0.002 | 0.002 | 0.002 | 0.003 |

Table B-1 (continued)

| Sample no. | SD-193 | | | | | 1/6291 | SD-42 | | | | | |
|---|---|---|---|---|---|---|---|---|---|---|---|---|
| Analysis no. | 1 | 2 | 3 | 4 | 5 | 1 | 1 | 2 | 3 | 4 | 5 | 6 |
| | C2-Ab1 | C2-Ab2 | C4-Ab3 | C4-Ab5 | C4-Ab6 | C7-Ab | C2-Ab1 | C2-Ab2 | C2-Ab3 | Ab5/Ms3 | Ab6/Ms5 | Ab8/Ms7 |
| SiO2 | 68.58 | 68.14 | 68.32 | 68.60 | 67.24 | 68.96 | 68 62 | 68.53 | 68.65 | 68.52 | 68.78 | 68.51 |
| Al2O3 | 19.77 | 19.85 | 19.54 | 19.51 | 19.76 | 19.36 | 19 80 | 19.74 | 19 90 | 20.13 | 19.96 | 20.19 |
| FeO* | 0.02 | 0.05 | 0.00 | 0 04 | 0.06 | 0.00 | 0.03 | 0.02 | 0 00 | 0.13 | 0.09 | 0.06 |
| MgO | 0.00 | 0 00 | 0.02 | 0.00 | 0.00 | 0.00 | 0.00 | 0.00 | 0.00 | 0.00 | 0 01 | 0.02 |
| CaO | 0.07 | 0.08 | 0.22 | 0.21 | 0.47 | 0.13 | 0.05 | 0.05 | 0.21 | 0.13 | 0.00 | 0 08 |
| Na2O | 11.01 | 10.86 | 11.23 | 11.05 | 11.01 | 11.09 | 10.87 | 10.86 | 10.90 | 10.91 | 11 09 | 11 03 |
| K2O | 0.01 | 0.02 | 0.06 | 0.04 | 0.03 | 0.05 | 0 01 | 0.03 | 0.04 | 0.01 | 0.03 | 0.06 |
| Total | 99.45 | 99.00 | 99.40 | 99.45 | 98.56 | 99.59 | 99.38 | 99.24 | 99.70 | 99 84 | 99.95 | 99.95 |
| Number of cations on the basis of 8 oxygens: | | | | | | | | | | | | |
| Si | 2.999 | 2.993 | 2.997 | 3.003 | 2.976 | 3.013 | 3.001 | 3.002 | 2.996 | 2.984 | 2.993 | 2.983 |
| Al | 1.019 | 1.028 | 1.011 | 1.007 | 1.031 | 0.997 | 1.021 | 1.020 | 1.024 | 1.034 | 1.024 | 1.036 |
| Fe2+ | 0.001 | 0.003 | 0.000 | 0.003 | 0.004 | 0.000 | 0.002 | 0 001 | 0.000 | 0.010 | 0.006 | 0.005 |
| Mg | 0.000 | 0.000 | 0.000 | 0.000 | 0.000 | 0.000 | 0.000 | 0.000 | 0.000 | 0.000 | 0.000 | 0.000 |
| Ca | 0.003 | 0.004 | 0.010 | 0.010 | 0.023 | 0.006 | 0.002 | 0.002 | 0.010 | 0.006 | 0.000 | 0.004 |
| Na | 0.934 | 0.925 | 0.955 | 0.938 | 0.945 | 0.940 | 0.922 | 0.923 | 0.922 | 0.921 | 0.935 | 0.932 |
| K | 0.001 | 0.001 | 0.004 | 0.002 | 0.002 | 0.003 | 0.001 | 0 002 | 0.002 | 0.001 | 0.002 | 0.003 |
| Sum Cations | 4.958 | 4.955 | 4.977 | 4.962 | 4.980 | 4.959 | 4.949 | 4.950 | 4.954 | 4.955 | 4.960 | 4.963 |
| Molecular proportions of end-members: | | | | | | | | | | | | |
| An | 0.003 | 0.004 | 0.011 | 0 010 | 0.023 | 0.006 | 0.002 | 0 003 | 0.011 | 0.007 | 0 000 | 0.004 |
| Ab | 0.996 | 0.994 | 0.986 | 0.987 | 0 975 | 0.991 | 0.997 | 0.996 | 0.987 | 0.993 | 0.998 | 0.993 |
| Or | 0.001 | 0.001 | 0.004 | 0.002 | 0.002 | 0 003 | 0.001 | 0 002 | 0.002 | 0.001 | 0.002 | 0 003 |

* Total Fe as FeO

Table B-1 (continued)

| Sample no. | SD-64 | | | | | SD-104 | | | | | SD-148.1 | | | | SD-150 | |
|---|---|---|---|---|---|---|---|---|---|---|---|---|---|---|---|---|
| Analysis no. | 1 | 2 | 3 | 4 | 5 | 1 | 2 | 3 | 4 | 5 | 1 | 2 | 3 | 4 | 1 | 2 |
| | C8-Ab1 | C8-Ab2 | C1-Ab3 | C1-Ab4 | C1-Ab5 | C1-Ab1 | C1-Ab2 | C1-Ab4 | C1-Ab5 | C1-Ab6 | C1-Ab2 | C1-Ab3 | C3-Ab4 | C3-Ab5 | C3-Ab1 | C3-Ab2 |
| SiO2 | 68.81 | 68.45 | 68.53 | 68.49 | 68.39 | 68.33 | 68.02 | 68.49 | 68.23 | 68.46 | 68.48 | 68.15 | 68.55 | 68.39 | 68.49 | 68.57 |
| Al2O3 | 19.40 | 19.35 | 19.43 | 19.35 | 19.34 | 19.39 | 19.27 | 19.48 | 19.23 | 19.55 | 19.55 | 19.33 | 19.32 | 19.38 | 19.61 | 19.39 |
| FeO* | 0.00 | 0.00 | 0.00 | 0.01 | 0.04 | 0.00 | 0.00 | 0.13 | 0 06 | 0.02 | 0.06 | 0.17 | 0.02 | 0.03 | 0.03 | 0.06 |
| MgO | 0.02 | 0.00 | 0.00 | 0 00 | 0.03 | 0.00 | 0.02 | 0.08 | 0.01 | 0.00 | 0.00 | 0.03 | 0.00 | 0 00 | 0.01 | 0.02 |
| CaO | 0.09 | 0.09 | 0.09 | 0.12 | 0.18 | 0.07 | 0.19 | 0.17 | 0.32 | 0.27 | 0.07 | 0.09 | 0 09 | 0 02 | 0.23 | 0 21 |
| Na2O | 10.95 | 11.23 | 11.18 | 11.18 | 11.05 | 11.38 | 11.55 | 11.43 | 11.54 | 11.42 | 11.36 | 11.41 | 11.49 | 11.28 | 11.21 | 11.33 |
| K2O | 0.03 | 0.00 | 0.04 | 0.01 | 0.02 | 0.02 | 0.05 | 0.01 | 0.04 | 0.02 | 0.13 | 0.04 | 0.02 | 0 03 | 0 01 | 0.01 |
| Total | 99.29 | 99.13 | 99.28 | 99.17 | 99.05 | 99.20 | 99.10 | 99.79 | 99.41 | 99.76 | 99.66 | 99.22 | 99.50 | 99.14 | 99.58 | 99.58 |
| Number of cations on the basis of 8 oxygens: | | | | | | | | | | | | | | | | |
| Si | 3.014 | 3.007 | 3.006 | 3.007 | 3 006 | 3.002 | 2.997 | 2.993 | 2.996 | 2.994 | 2.996 | 2.994 | 3.004 | 3 004 | 2.997 | 3.001 |
| Al | 1.002 | 1.002 | 1.005 | 1 002 | 1.002 | 1.005 | 1.001 | 1.003 | 0.995 | 1.008 | 1 008 | 1.001 | 0.998 | 1.004 | 1.011 | 1.000 |
| Fe2+ | 0.000 | 0.000 | 0.000 | 0.001 | 0.003 | 0.000 | 0.000 | 0.009 | 0.005 | 0.002 | 0.005 | 0 012 | 0.002 | 0.002 | 0.002 | 0 004 |
| Mg | 0.000 | 0.000 | 0.000 | 0.000 | 0.000 | 0.000 | 0.000 | 0.000 | 0.000 | 0.000 | 0.000 | 0.000 | 0.000 | 0.000 | 0.000 | 0.000 |
| Ca | 0.004 | 0.004 | 0.004 | 0.006 | 0.009 | 0.003 | 0.009 | 0.008 | 0.015 | 0.013 | 0 003 | 0 004 | 0 004 | 0.001 | 0.011 | 0 010 |
| Na | 0.929 | 0.957 | 0.951 | 0.952 | 0.942 | 0.970 | 0.987 | 0.968 | 0.982 | 0.969 | 0.964 | 0.972 | 0 976 | 0.961 | 0.951 | 0.961 |
| K | 0.001 | 0.000 | 0.002 | 0.000 | 0.001 | 0.001 | 0.003 | 0.001 | 0.002 | 0.001 | 0.007 | 0.002 | 0 001 | 0.002 | 0.000 | 0.001 |
| Sum Cations | 4.950 | 4.970 | 4.968 | 4.968 | 4.962 | 4.981 | 4.997 | 4.982 | 4.996 | 4.986 | 4.983 | 4.986 | 4.985 | 4.974 | 4.972 | 4.977 |
| Molecular proportions of end-members: | | | | | | | | | | | | | | | | |
| An | 0.004 | 0.005 | 0.005 | 0.006 | 0.009 | 0.003 | 0.009 | 0.008 | 0.015 | 0.013 | 0 003 | 0 004 | 0.004 | 0.001 | 0 011 | 0.010 |
| Ab | 0.994 | 0.995 | 0.993 | 0.994 | 0.990 | 0.995 | 0.989 | 0.991 | 0.983 | 0.985 | 0.989 | 0.993 | 0.995 | 0.997 | 0.988 | 0.989 |
| Or | 0.002 | 0.000 | 0.002 | 0.000 | 0.001 | 0.001 | 0.003 | 0 001 | 0.002 | 0 001 | 0.007 | 0.002 | 0.001 | 0 002 | 0.000 | 0.001 |

Table B-1 (continued)

| Sample no. | SD-150 | SD-165 | | | | | SD-198 | | | | SD-209 | | | | | |
|---|---|---|---|---|---|---|---|---|---|---|---|---|---|---|---|---|
| Analysis no. | 3 | 1 | 2 | 3 | 4 | 5 | 1 | 2 | 3 | 4 | 1 | 2 | 3 | 4 | 5 | 6 |
| | C3-Ab3 | C1-Ab1 | C1-Ab3 | C1-Ab4 | C1-Ab5 | C1-Ab6 | C5-Ab1/1 | C5-Ab1 | C5-Ab2 | C5-Ab4 | C7-Ab1 | C1-Ab4 | C1-Ab5 | C8-Ab6 | C8-Ab7 | C3-Kfs2 |
| SiO2 | 68.68 | 68.53 | 68.32 | 68.30 | 68.05 | 68.49 | 68.49 | 68.28 | 68.13 | 68.11 | 68.50 | 68.23 | 68.40 | 68.28 | 68.36 | 67.94 |
| Al2O3 | 19.59 | 19.50 | 19.47 | 19.39 | 19.35 | 19.22 | 19.52 | 19.24 | 19.33 | 19.28 | 19.58 | 19.27 | 19.24 | 19.49 | 19.09 | 19.32 |
| FeO* | 0.04 | 0.09 | 0.09 | 0.05 | 0.09 | 0.03 | 0.08 | 0.00 | 0.06 | 0.00 | 0.00 | 0.20 | 0.18 | 0.04 | 0.16 | 0.08 |
| MgO | 0.01 | 0.01 | 0.00 | 0.00 | 0.00 | 0.02 | 0.05 | 0.02 | 0.00 | 0.00 | 0.03 | 0.06 | 0.07 | 0.01 | 0.04 | 0.02 |
| CaO | 0.24 | 0.20 | 0.08 | 0.19 | 0.19 | 0.10 | 0.21 | 0.17 | 0.36 | 0.24 | 0.25 | 0.10 | 0.20 | 0.56 | 0.92 | 0.25 |
| Na2O | 11.27 | 11.24 | 11.13 | 11.44 | 11.54 | 11.49 | 11.33 | 11.43 | 11.09 | 11.30 | 10.80 | 10.86 | 10.23 | 11.34 | 10.55 | 11.43 |
| K2O | 0.02 | 0.19 | 0.01 | 0.01 | 0.01 | 0.02 | 0.22 | 0.16 | 0.07 | 0.08 | 0.07 | 1.27 | 1.83 | 0.21 | 0.51 | 0.14 |
| Total | 99 85 | 99.75 | 99.10 | 99.39 | 99.23 | 99.37 | 99.89 | 99.30 | 99.03 | 99.01 | 99.23 | 99.98 | 100.15 | 99.93 | 99.64 | 99.18 |
| Number of cations on the basis of 8 oxygens: | | | | | | | | | | | | | | | | |
| Si | 2.997 | 2.996 | 3.000 | 2.997 | 2.992 | 3.00503 | 2.993 | 3.002 | 2.999 | 3.001 | 3.004 | 2.991 | 2.996 | 2.987 | 2.997 | 2.991 |
| Al | 1.008 | 1.005 | 1.008 | 1.003 | 1.003 | 0.994 | 1.006 | 0.997 | 1.003 | 1.002 | 1.012 | 0.996 | 0.993 | 1.005 | 0.987 | 1.003 |
| Fe2+ | 0 003 | 0 006 | 0.007 | 0.004 | 0.007 | 0.003 | 0.006 | 0.000 | 0.005 | 0.000 | 0.000 | 0.015 | 0.013 | 0 003 | 0.012 | 0.006 |
| Mg | 0.000 | 0.000 | 0.000 | 0.000 | 0.000 | 0.000 | 0.000 | 0.000 | 0.000 | 0.000 | 0.000 | 0.000 | 0.000 | 0.000 | 0.000 | 0.000 |
| Ca | 0.011 | 0.010 | 0.004 | 0.009 | 0.009 | 0.005 | 0.010 | 0.008 | 0.017 | 0.011 | 0.012 | 0.005 | 0.009 | 0.026 | 0 043 | 0.012 |
| Na | 0.954 | 0.953 | 0.947 | 0.974 | 0.984 | 0.978 | 0.960 | 0.974 | 0.946 | 0.965 | 0.918 | 0.923 | 0 868 | 0.962 | 0 897 | 0.975 |
| K | 0.001 | 0.010 | 0.001 | 0.001 | 0 001 | 0.001 | 0.012 | 0.009 | 0.004 | 0.005 | 0.004 | 0.071 | 0.102 | 0 012 | 0 029 | 0.008 |
| Sum Cations | 4.974 | 4.980 | 4.967 | 4.987 | 4.995 | 4.985 | 4.986 | 4.990 | 4.973 | 4.983 | 4.950 | 4.999 | 4.983 | 4.995 | 4.965 | 4.995 |
| Molecular proportions of end-members: | | | | | | | | | | | | | | | | |
| An | 0.012 | 0.010 | 0.004 | 0.009 | 0.009 | 0.005 | 0.010 | 0.008 | 0.017 | 0.011 | 0.012 | 0 005 | 0.010 | 0.026 | 0 045 | 0.012 |
| Ab | 0.987 | 0.979 | 0.995 | 0.990 | 0.990 | 0.994 | 0.977 | 0.983 | 0.979 | 0.984 | 0.983 | 0 924 | 0.886 | 0.962 | 0.926 | 0.980 |
| Or | 0.001 | 0 011 | 0.001 | 0.001 | 0.001 | 0.001 | 0.012 | 0.009 | 0.004 | 0.005 | 0.004 | 0.071 | 0.104 | 0 012 | 0 030 | 0.008 |

* Total Fe as FeO

Table B-1 (continued)

| Sample no. | SD-211 | | | | SD-213 | | | | | | SD-217 | | | SD-221 | |
|---|---|---|---|---|---|---|---|---|---|---|---|---|---|---|---|
| Analysis no. | 1 | 2 | 3 | 4 | 1 | 2 | 3 | 4 | 5 | 6 | 1 | 2 | 3 | 1 | 2 |
| | C4-Ab2 | C4-Ab3 | C4-Ab4 | C4-Ab6 | C5-Ab1 | C5-Ab2 | C5-Ab3 | C2-Ab4 | C2-Ab5 | C1-Ab6 | C1-Ab2 | C5- Ab3 | C5-Ab4 | C3-Ab1 | C3-Ab2 |
| SiO2 | 68.28 | 68 06 | 67.50 | 67.51 | 66.92 | 67 62 | 67.18 | 66.12 | 66.57 | 66.49 | 67.71 | 68 01 | 67.94 | 68.13 | 67.16 |
| Al2O3 | 20.10 | 19.84 | 20.08 | 20.38 | 20.28 | 19.74 | 19 89 | 20.36 | 20.57 | 20.43 | 20.10 | 19.45 | 19.75 | 20.34 | 20.79 |
| FeO* | 0.09 | 0.00 | 0.11 | 0.00 | 0.06 | 0.04 | 0.00 | 0.05 | 0.04 | 0.02 | 0 04 | 0.18 | 0.19 | 0.03 | 0.08 |
| MgO | 0.00 | 0.00 | 0.00 | 0.00 | 0.05 | 0.02 | 0.00 | 0.02 | 0 00 | 0.02 | 0.01 | 0.06 | 0.02 | 0.00 | 0.04 |
| CaO | 0.38 | 0.35 | 0.47 | 0.38 | 0.22 | 0.14 | 0.51 | 1.13 | 1 20 | 1.30 | 0.50 | 0.22 | 0.19 | 0.30 | 0.23 |
| Na2O | 11.06 | 10.77 | 10.86 | 10.75 | 10.58 | 11.16 | 10.71 | 10.44 | 10.49 | 10.71 | 10.85 | 11.02 | 10.96 | 10 95 | 10.72 |
| K2O | 0 03 | 0.03 | 0.01 | 0 13 | 0.27 | 0.03 | 0 05 | 0.06 | 0 04 | 0.03 | 0.04 | 0 00 | 0.03 | 0 03 | 0.16 |
| Total | 99.94 | 99 05 | 99.02 | 99.14 | 98.39 | 98.73 | 98.32 | 98.19 | 98.90 | 99.00 | 99.26 | 98.94 | 99.08 | 99.79 | 99.18 |
| Number of cations on the basis of 8 oxygens: | | | | | | | | | | | | | | | |
| Si | 2.977 | 2.991 | 2.970 | 2.968 | 2.965 | 2.985 | 2.978 | 2.942 | 2.941 | 2.939 | 2.973 | 2.992 | 2.984 | 2.974 | 2 951 |
| Al | 1.033 | 1.028 | 1.042 | 1.056 | 1.059 | 1 027 | 1.039 | 1.068 | 1.071 | 1.065 | 1 041 | 1.009 | 1.023 | 1.047 | 1 077 |
| Fe2+ | 0.007 | 0.000 | 0.008 | 0.000 | 0.005 | 0 003 | 0.000 | 0 004 | 0.003 | 0.002 | 0.003 | 0 014 | 0 014 | 0.002 | 0.006 |
| Mg | 0.000 | 0 000 | 0.000 | 0.000 | 0 000 | 0.000 | 0.000 | 0.000 | 0.000 | 0.000 | 0.000 | 0.000 | 0.000 | 0.000 | 0.000 |
| Ca | 0.018 | 0.016 | 0.022 | 0.018 | 0 011 | 0.006 | 0.024 | 0.054 | 0.057 | 0.061 | 0.024 | 0.010 | 0 009 | 0.014 | 0.011 |
| Na | 0.935 | 0.917 | 0.926 | 0.916 | 0.909 | 0.955 | 0.920 | 0 901 | 0 899 | 0.918 | 0 924 | 0 940 | 0.933 | 0.927 | 0.913 |
| K | 0.002 | 0.002 | 0.001 | 0.007 | 0.015 | 0 001 | 0.003 | 0.004 | 0.002 | 0.002 | 0.002 | 0.000 | 0.002 | 0.002 | 0.009 |
| Sum Cations | 4.972 | 4.954 | 4.969 | 4.965 | 4.963 | 4.978 | 4.964 | 4.973 | 4.973 | 4.987 | 4.967 | 4.965 | 4.964 | 4.966 | 4.967 |
| Molecular proportions of end-members: | | | | | | | | | | | | | | | |
| An | 0.019 | 0.017 | 0.023 | 0 019 | 0.011 | 0.007 | 0.025 | 0.056 | 0 059 | 0.063 | 0 025 | 0.011 | 0 010 | 0 015 | 0 012 |
| Ab | 0.980 | 0.981 | 0.976 | 0 974 | 0.972 | 0.992 | 0.972 | 0.940 | 0.938 | 0.936 | 0.973 | 0.989 | 0.989 | 0.983 | 0.979 |
| Or | 0.002 | 0.002 | 0.001 | 0.008 | 0.017 | 0 001 | 0.003 | 0 004 | 0.003 | 0.002 | 0.002 | 0.000 | 0.002 | 0.002 | 0.010 |

Table B-1 (continued)

| Sample no. | SD-221 | | | | P-102 | | | | | | | P-104 | | | | |
|---|---|---|---|---|---|---|---|---|---|---|---|---|---|---|---|---|
| Analysis no. | 3 | 4 | 5 | 6 | 1 | 2 | 3 | 4 | 5 | 6 | 7 | 1 | 2 | 3 | 4 | 5 |
| | C3-Ab3 | C3-Ab4 | C5-Ab5 | C5-Ab6 | C4-Ab1 | C4-Ab2 | C4-Ab3 | C4-Ab4 | C4-Ab5 | C4-Ab6/1 | C5-Ab10 | C4-Ab2 | C4-Ab3 | C5-Ab4 | C5-Ab5 | C7-Ab6 |
| SiO2 | 66.89 | 66.91 | 68.22 | 68.72 | 68.17 | 68.55 | 67.83 | 67.89 | 68.30 | 68.52 | 68.63 | 68.55 | 68.41 | 68.37 | 68.42 | 68.53 |
| Al2O3 | 21.00 | 20.88 | 19.88 | 19.96 | 19.21 | 19.15 | 19.55 | 19.35 | 19.16 | 19.22 | 19.32 | 19.18 | 19.48 | 19.40 | 19.41 | 19.37 |
| FeO* | 0.08 | 0.04 | 0.00 | 0.02 | 0.10 | 0.63 | 0.00 | 0.00 | 0.03 | 0.00 | 0.05 | 0.01 | 0.04 | 0.16 | 0.08 | 0.11 |
| MgO | 0.01 | 0.02 | 0.00 | 0.00 | 0.00 | 0.26 | 0.01 | 0.00 | 0.00 | 0.03 | 0.00 | 0.02 | 0.01 | 0.02 | 0.00 | 0.03 |
| CaO | 0.35 | 0.25 | 0.08 | 0.09 | 0.19 | 0.24 | 0.17 | 0.18 | 0.10 | 0.50 | 0.20 | 0.58 | 0.43 | 0.42 | 0.41 | 0.13 |
| Na2O | 10.47 | 10.74 | 10.83 | 10.95 | 11.44 | 10.40 | 11.79 | 11.49 | 10.79 | 11.20 | 11.08 | 11.34 | 11.21 | 11.28 | 11.40 | 11.44 |
| K2O | 0.03 | 0.03 | 0.01 | 0.01 | 0.06 | 1.10 | 0.06 | 0.05 | 1.11 | 0.27 | 0.16 | 0.06 | 0.04 | 0.12 | 0.08 | 0.04 |
| Total | 98.84 | 98.87 | 99.02 | 99.75 | 99.17 | 100.33 | 99.40 | 98.96 | 99.48 | 99.74 | 99.44 | 99.76 | 99.63 | 99.76 | 99.79 | 99.65 |
| Number of cations on the basis of 8 oxygens: | | | | | | | | | | | | | | | | |
| Si | 2.945 | 2.948 | 2.996 | 2.996 | 2.998 | 2.983 | 2.983 | 2.995 | 3.005 | 3.002 | 3.007 | 3.001 | 2.995 | 2.990 | 2.993 | 2.998 |
| Al | 1.090 | 1.085 | 1.029 | 1.026 | 0.996 | 0.983 | 1.014 | 1.006 | 0.994 | 0.993 | 0.998 | 0.990 | 1.006 | 1.000 | 1.001 | 0.999 |
| Fe2+ | 0.006 | 0.003 | 0.000 | 0.002 | 0.007 | 0.046 | 0.000 | 0.000 | 0.002 | 0.000 | 0.004 | 0.001 | 0.003 | 0.012 | 0.006 | 0.008 |
| Mg | 0.000 | 0.000 | 0.000 | 0.000 | 0 000 | 0.000 | 0.000 | 0.000 | 0.000 | 0.000 | 0.000 | 0.000 | 0.000 | 0.000 | 0.000 | 0.000 |
| Ca | 0.017 | 0.012 | 0 004 | 0.004 | 0.009 | 0.011 | 0.008 | 0.008 | 0.005 | 0.024 | 0 010 | 0.027 | 0.020 | 0.019 | 0.019 | 0.006 |
| Na | 0 894 | 0.917 | 0.922 | 0.926 | 0.975 | 0.878 | 1.005 | 0.982 | 0.921 | 0.952 | 0.942 | 0.963 | 0.952 | 0.956 | 0.967 | 0.971 |
| K | 0.002 | 0.002 | 0.001 | 0.001 | 0.003 | 0.061 | 0.003 | 0.003 | 0.063 | 0.015 | 0.009 | 0.004 | 0.002 | 0.006 | 0.004 | 0.002 |
| Sum Cations | 4.954 | 4.967 | 4.951 | 4.954 | 4.989 | 4.962 | 5.013 | 4.995 | 4.989 | 4.985 | 4.968 | 4.986 | 4.978 | 4.985 | 4.989 | 4.984 |
| Molecular proportions of end-members: | | | | | | | | | | | | | | | | |
| An | 0.018 | 0.013 | 0.004 | 0.004 | 0.009 | 0.012 | 0.008 | 0.009 | 0.005 | 0.024 | 0 010 | 0.027 | 0.021 | 0.020 | 0.019 | 0.006 |
| Ab | 0.980 | 0 985 | 0.995 | 0.995 | 0.988 | 0.924 | 0.989 | 0.988 | 0.932 | 0.961 | 0.981 | 0.969 | 0.977 | 0.974 | 0.977 | 0.992 |
| Or | 0.002 | 0 002 | 0.001 | 0.001 | 0.003 | 0 064 | 0.003 | 0 003 | 0.063 | 0.015 | 0 009 | 0.004 | 0.003 | 0 007 | 0.004 | 0 002 |

* Total Fe as FeO

Table B-1 (continued)

| Sample no. | P-104 | | | P-106 | | | | P-107 | | | |
|---|---|---|---|---|---|---|---|---|---|---|---|
| Analysis no. | 6 | 7 | 8 | 1 | 2 | 3 | 4 | 1 | 2 | 3 | 4 |
| | C7-Ab7 | C7-Ab8 | C14-Ab9 | C4-Ab2 | C4-Ab3 | C5-Ab5 | C5-Ab6 | C5-Ab1 | C6-Ab4 | C11-Ab8 | C14-Ab10 |
| SiO2 | 68.47 | 68.50 | 68.20 | 68.99 | 68.57 | 68.00 | 67.58 | 68.38 | 68.13 | 68.73 | 68.46 |
| Al2O3 | 19.45 | 19.41 | 19.38 | 19.87 | 20.34 | 20.18 | 20.27 | 19.58 | 19.56 | 19.52 | 19.49 |
| FeO* | 0.03 | 0.01 | 0.00 | 0.07 | 0.06 | 0.09 | 0.00 | 0.00 | 0.11 | 0.11 | 0.01 |
| MgO | 0.00 | 0.00 | 0.00 | 0.00 | 0.01 | 0.00 | 0.02 | 0.00 | 0.02 | 0.00 | 0.00 |
| CaO | 0.28 | 0.12 | 0.48 | 0.23 | 0.28 | 0.45 | 0.25 | 0.31 | 0.25 | 0.12 | 0.26 |
| Na2O | 11.53 | 11.59 | 11.51 | 11.10 | 11.03 | 11.63 | 10.97 | 10.94 | 10.79 | 10.94 | 10.82 |
| K2O | 0.03 | 0.04 | 0.07 | 0.12 | 0.25 | 0.08 | 0.19 | 0.06 | 0.14 | 0.05 | 0.14 |
| Total | 99.78 | 99.68 | 99.64 | 100.39 | 100.53 | 100.42 | 99.27 | 99.27 | 99.00 | 99.48 | 99.18 |
| Number of cations on the basis of 8 oxygens: | | | | | | | | | | | |
| Si | 2.995 | 2.999 | 2.991 | 2.993 | 2.975 | 2.961 | 2.970 | 3.000 | 2.995 | 3.004 | 3.005 |
| Al | 1.003 | 1.002 | 1.002 | 1.017 | 1.040 | 1.036 | 1.050 | 1.013 | 1.014 | 1.006 | 1.008 |
| Fe2+ | 0.002 | 0.001 | 0.000 | 0.005 | 0.004 | 0.006 | 0.000 | 0.000 | 0.008 | 0.008 | 0.001 |
| Mg | 0.000 | 0.000 | 0.000 | 0.000 | 0.000 | 0.000 | 0.000 | 0.000 | 0.000 | 0.000 | 0.000 |
| Ca | 0.013 | 0.005 | 0.023 | 0.011 | 0.013 | 0.021 | 0.012 | 0.014 | 0.012 | 0.005 | 0.012 |
| Na | 0.978 | 0.984 | 0.979 | 0.934 | 0.927 | 0.982 | 0.934 | 0.931 | 0.920 | 0.927 | 0.920 |
| K | 0.001 | 0.002 | 0.004 | 0.007 | 0.014 | 0.005 | 0.011 | 0.004 | 0.008 | 0.003 | 0.008 |
| Sum Cations | 4.992 | 4.993 | 4.999 | 4.967 | 4.974 | 5.011 | 4.977 | 4.961 | 4.957 | 4.954 | 4.955 |
| Molecular proportions of end-members: | | | | | | | | | | | |
| An | 0.013 | 0.006 | 0.023 | 0.011 | 0.014 | 0.021 | 0.012 | 0.015 | 0.013 | 0.006 | 0.013 |
| Ab | 0.986 | 0.992 | 0.973 | 0.981 | 0.972 | 0.975 | 0.976 | 0.981 | 0.979 | 0.991 | 0.978 |
| Or | 0.001 | 0.002 | 0.004 | 0.007 | 0.014 | 0.004 | 0.011 | 0.004 | 0.008 | 0.003 | 0.009 |

* Total Fe as FeO

Table B-2 Electron microprobe analyses of muscovites (metasediments of the Pha Som Metamorphic Complex).

| Sample no. | 2/5291 | | | | | | | 5/8291 | | | | | |
|---|---|---|---|---|---|---|---|---|---|---|---|---|---|
| Analysis no. | 1 | 2 | 3 | 4 | 5 | 6 | 7 | 1 | 2 | 3 | 4 | 5 | 6 |
| SiO2 | 46.99 | 47.16 | 48.38 | 47.24 | 47.34 | 47.32 | 46.95 | 46.30 | 46.09 | 46.41 | 45.44 | 45.58 | 46.52 |
| TiO2 | 0.08 | 0.07 | 0.04 | 0.06 | 0.01 | 0.31 | 0.08 | 0.09 | 0.21 | 0.13 | 0.06 | 0.15 | 0.08 |
| Al2O3 | 36.53 | 36.64 | 35.41 | 34.92 | 35.86 | 35.64 | 33.59 | 35.80 | 34.19 | 35.35 | 35.18 | 35.34 | 35.09 |
| FeO* | 1.60 | 1.60 | 2.24 | 1.74 | 1.80 | 2.46 | 3.99 | 1.34 | 0.76 | 0.62 | 1.52 | 0.97 | 0.89 |
| MnO | 0.00 | 0.00 | 0.00 | 0.00 | 0.00 | 0.02 | 0.07 | 0.01 | 0.00 | 0.01 | 0.09 | 0.00 | 0.00 |
| MgO | 0.35 | 0.30 | 0.71 | 0.44 | 0.48 | 0.65 | 1.12 | 1.01 | 1.22 | 0.76 | 1.04 | 0.72 | 0.92 |
| CaO | 0.12 | 0.13 | 0.11 | 0.08 | 0.16 | 0.15 | 0.19 | 0.01 | 0.04 | 0.05 | 0.01 | 0.02 | 0.01 |
| Na2O | 2.95 | 2.67 | 1.64 | 2.46 | 2.43 | 2.86 | 2.70 | 1.11 | 0.67 | 0.87 | 0.82 | 0.88 | 0.74 |
| K2O | 6.25 | 6.38 | 6.38 | 6.25 | 6.37 | 5.18 | 4.94 | 7.53 | 8.83 | 8.27 | 8.77 | 9.31 | 9.12 |
| F | 0.00 | 0.00 | 0.00 | 0.00 | 0.00 | 0.00 | 0.00 | 0.00 | 0.00 | 0.00 | 0.00 | 0.00 | 0.00 |
| Cl | 0.00 | 0.03 | 0.00 | 0.00 | 0.02 | 0.00 | 0.02 | 0.00 | 0.00 | 0.00 | 0.03 | 0.10 | 0.00 |
| Total | 94.87 | 94.98 | 94.91 | 93.19 | 94.47 | 94.58 | 93.65 | 93.20 | 92.01 | 92.47 | 92.96 | 93.07 | 93.37 |
| O = F, Cl | 0.00 | -0.01 | 0.00 | 0.00 | -0.01 | 0.00 | 0.00 | 0.00 | 0.00 | 0.00 | -0.01 | -0.02 | 0.00 |
| Total | 94.87 | 94.98 | 94.91 | 93.19 | 94.47 | 94.58 | 93.65 | 93.20 | 92.01 | 92.47 | 92.95 | 93.05 | 93.37 |
| Number of cations on the basis of 11 oxygens: | | | | | | | | | | | | | |
| Si | 3.085 | 3.092 | 3.165 | 3.151 | 3.120 | 3.109 | 3.140 | 3.095 | 3.135 | 3.125 | 3.076 | 3.084 | 3.123 |
| Al iv | 0.915 | 0.908 | 0.835 | 0.849 | 0.880 | 0.891 | 0.860 | 0.905 | 0.865 | 0.875 | 0.924 | 0.916 | 0.877 |
| Sum T | 4.000 | 4.000 | 4.000 | 4.000 | 4.000 | 4.000 | 4.000 | 4.000 | 4.000 | 4.000 | 4.000 | 4.000 | 4.000 |
| Al vi | 1.913 | 1.923 | 1.896 | 1.898 | 1.906 | 1.870 | 1.789 | 1.916 | 1.876 | 1.931 | 1.884 | 1.903 | 1.899 |
| Ti | 0.004 | 0.003 | 0.002 | 0.003 | 0.001 | 0.015 | 0.004 | 0.005 | 0.011 | 0.007 | 0.003 | 0.008 | 0.004 |
| Fe2+ | 0.088 | 0.088 | 0.123 | 0.097 | 0.099 | 0.135 | 0.223 | 0.075 | 0.043 | 0.035 | 0.086 | 0.055 | 0.050 |
| Mn | 0.000 | 0.000 | 0.000 | 0.000 | 0.000 | 0.001 | 0.004 | 0.001 | 0.000 | 0.001 | 0.005 | 0.000 | 0.000 |
| Mg | 0.034 | 0.029 | 0.069 | 0.044 | 0.047 | 0.063 | 0.111 | 0.101 | 0.124 | 0.076 | 0.105 | 0.073 | 0.092 |
| Sum O | 2.039 | 2.044 | 2.090 | 2.042 | 2.053 | 2.085 | 2.131 | 2.096 | 2.054 | 2.050 | 2.083 | 2.038 | 2.046 |
| Ca | 0.008 | 0.009 | 0.008 | 0.006 | 0.011 | 0.010 | 0.014 | 0.001 | 0.003 | 0.004 | 0.001 | 0.001 | 0.001 |
| Na | 0.376 | 0.339 | 0.208 | 0.318 | 0.310 | 0.364 | 0.351 | 0.144 | 0.088 | 0.114 | 0.108 | 0.115 | 0.096 |
| K | 0.524 | 0.534 | 0.532 | 0.532 | 0.536 | 0.434 | 0.422 | 0.642 | 0.766 | 0.710 | 0.757 | 0.804 | 0.781 |
| Sum A | 0.908 | 0.882 | 0.748 | 0.856 | 0.857 | 0.809 | 0.786 | 0.787 | 0.857 | 0.828 | 0.866 | 0.921 | 0.878 |
| Sum Cations | 6.947 | 6.926 | 6.838 | 6.897 | 6.910 | 6.894 | 6.918 | 6.883 | 6.911 | 6.877 | 6.949 | 6.959 | 6.924 |

* Total Fe as FeO

Table B-2 (continued)

| Sample no. | 5/8291 | | | 3/9291 | | | | 6/9291 | | | | | | | | |
|---|---|---|---|---|---|---|---|---|---|---|---|---|---|---|---|---|
| Analysis no. | 7 | 8 | 9 | 1 | 2 | 3 | 4 | 1 | 2 | 3 | 4 | 5 | 6 | 7 | 8 | 9 |
| | | | | | | | | s1 fold | s1 fold | large gr | bent s3 | s2 | s2 | s2 | s2 | s2 |
| SiO2 | 47.05 | 46.23 | 44.99 | 45.86 | 45.58 | 46.21 | 48.07 | 46.22 | 45.86 | 48.59 | 44.66 | 46.80 | 46.81 | 45.10 | 45.87 | 46.02 |
| TiO2 | 0.12 | 0.11 | 0.16 | 0.00 | 0.03 | 0.50 | 0.24 | 0.24 | 0.26 | 0.05 | 0.43 | 0.18 | 0.32 | 0.03 | 0.30 | 1.50 |
| Al2O3 | 35.76 | 35.45 | 33.95 | 38.39 | 37.61 | 37.88 | 36.40 | 36.03 | 35.74 | 35.72 | 34.01 | 34.09 | 33.90 | 35.39 | 35.07 | 32.85 |
| FeO* | 0.93 | 0.92 | 3.60 | 0.99 | 2.85 | 1.14 | 1.52 | 1.04 | 1.92 | 0.69 | 2.70 | 1.65 | 1.37 | 1.23 | 0.98 | 2 07 |
| MnO | 0.00 | 0.00 | 0.00 | 0.07 | 0.03 | 0.00 | 0.01 | 0.00 | 0.02 | 0.00 | 0.00 | 0.01 | 0.00 | 0.00 | 0.12 | 0 00 |
| MgO | 0.86 | 0.78 | 2.08 | 0.22 | 1.07 | 0.21 | 0.41 | 0.69 | 1.09 | 0.90 | 1.62 | 1.05 | 1.20 | 0.59 | 1.05 | 1.70 |
| CaO | 0.02 | 0.04 | 0.00 | 0.07 | 0.19 | 0.24 | 0.15 | 0.02 | 0.01 | 0.03 | 0.02 | 0 06 | 0.00 | 0.01 | 0.09 | 0.05 |
| Na2O | 0.74 | 0.90 | 0.58 | 3.84 | 4.21 | 3.77 | 3.54 | 1.46 | 1.90 | 1.12 | 0.55 | 0.96 | 0.54 | 0.51 | 0 86 | 0 62 |
| K2O | 8.90 | 8.43 | 8.14 | 4.59 | 3.69 | 4.49 | 4.55 | 8.32 | 7.55 | 8.35 | 9.43 | 8.65 | 9.90 | 10 09 | 8.82 | 8.95 |
| F | 0.00 | 0.00 | 0.00 | 0.00 | 0.00 | 0.00 | 0.00 | 0.00 | 0.00 | 0.00 | 0 00 | 0.00 | 0.00 | 0.00 | 0.00 | 0.00 |
| Cl | 0.03 | 0.00 | 0.00 | 0.07 | 0.00 | 0.00 | 0.00 | 0.00 | 0.00 | 0.00 | 0 00 | 0.00 | 0.00 | 0 00 | 0.00 | 0.00 |
| Total | 94.41 | 92.86 | 93.50 | 94.10 | 95.26 | 94.44 | 94.89 | 94.02 | 94.35 | 95.45 | 93.42 | 93.45 | 94.04 | 92.95 | 93.16 | 93.76 |
| O = F, Cl | -0.01 | 0.00 | 0.00 | -0 03 | 0.00 | 0.00 | 0.00 | 0.00 | 0.00 | 0.00 | 0.00 | 0.00 | 0.00 | 0.00 | 0.00 | 0.00 |
| Total | 94.40 | 92.86 | 93.50 | 94.07 | 95.26 | 94.44 | 94.89 | 94.02 | 94.35 | 95.45 | 93.42 | 93.45 | 94.04 | 92.95 | 93.16 | 93.76 |
| Number of cations on the basis of 11 oxygens: | | | | | | | | | | | | | | | | |
| Si | 3.118 | 3.110 | 3.052 | 3.011 | 2.978 | 3.022 | 3.124 | 3.078 | 3.053 | 3.167 | 3.045 | 3.146 | 3.143 | 3.068 | 3.091 | 3.105 |
| Al iv | 0.882 | 0.890 | 0.948 | 0.989 | 1.022 | 0.978 | 0.876 | 0.922 | 0.947 | 0.833 | 0.955 | 0.854 | 0.857 | 0.932 | 0.909 | 0.895 |
| Sum T | 4.000 | 4.000 | 4.000 | 4.000 | 4.000 | 4.000 | 4.000 | 4.000 | 4.000 | 4.000 | 4.000 | 4.000 | 4.000 | 4.000 | 4.000 | 4.000 |
| Al vi | 1.912 | 1.921 | 1.768 | 1.982 | 1.875 | 1.943 | 1.913 | 1.907 | 1 858 | 1.911 | 1.778 | 1.848 | 1.827 | 1.907 | 1.877 | 1.719 |
| Ti | 0 006 | 0.006 | 0.008 | 0.000 | 0.001 | 0.025 | 0.012 | 0.012 | 0 013 | 0.002 | 0.022 | 0.009 | 0.016 | 0 002 | 0.015 | 0.076 |
| Fe2+ | 0.052 | 0.052 | 0.204 | 0.054 | 0.156 | 0.062 | 0.083 | 0.058 | 0.107 | 0.038 | 0.154 | 0.093 | 0.077 | 0.070 | 0.055 | 0.117 |
| Mn | 0.000 | 0.000 | 0.000 | 0.004 | 0.002 | 0.000 | 0.001 | 0.000 | 0.001 | 0.000 | 0 000 | 0.001 | 0.000 | 0.000 | 0.007 | 0.000 |
| Mg | 0.085 | 0.078 | 0.211 | 0.022 | 0.104 | 0.020 | 0.040 | 0.068 | 0.108 | 0.087 | 0.165 | 0.105 | 0.120 | 0.060 | 0.105 | 0.171 |
| Sum O | 2.054 | 2.056 | 2.191 | 2.062 | 2.138 | 2.050 | 2.048 | 2.046 | 2.087 | 2.039 | 2.119 | 2.056 | 2.040 | 2.038 | 2.059 | 2.082 |
| Ca | 0.001 | 0.003 | 0 000 | 0.005 | 0.013 | 0.017 | 0.010 | 0.001 | 0.001 | 0.002 | 0.001 | 0.004 | 0.000 | 0.001 | 0.006 | 0.004 |
| Na | 0 095 | 0.117 | 0.076 | 0.489 | 0.533 | 0.478 | 0.446 | 0 189 | 0.245 | 0.142 | 0.073 | 0.125 | 0.070 | 0.067 | 0.112 | 0.081 |
| K | 0.752 | 0.723 | 0.705 | 0.384 | 0.308 | 0.375 | 0.377 | 0.707 | 0.641 | 0.694 | 0.820 | 0.742 | 0.848 | 0.876 | 0.758 | 0.770 |
| Sum A | 0.849 | 0.844 | 0.781 | 0.878 | 0.854 | 0.869 | 0.834 | 0.897 | 0.887 | 0.838 | 0.894 | 0.871 | 0.918 | 0.944 | 0.877 | 0.855 |
| Sum Cations | 6.903 | 6.900 | 6.972 | 6.940 | 6.992 | 6.919 | 6 881 | 6 943 | 6.975 | 6.877 | 7.013 | 6.927 | 6.958 | 6.982 | 6.936 | 6.938 |

Table B-2 (continued)

| Sample no. | 6/9291 | | | | | | | | | 3/8291 | | | | | SD-97 | |
|---|---|---|---|---|---|---|---|---|---|---|---|---|---|---|---|---|
| Analysis no. | 10 | 11 | 12 | 13 | 14 | 15 | 16 | 17 | 18 | 1 | 2 | 3 | 4 | 5 | 1 | 2 |
| | s2 | s2 | s2 | s2 | s2 | s2 | s2 | s2 | s2 | | | | | | C2-Ms1 | C2-Ms2 |
| SiO2 | 44.47 | 45.78 | 46.58 | 44.73 | 46.45 | 46.77 | 44.26 | 48.91 | 47 64 | 45.88 | 46.33 | 46.02 | 46.40 | 45.93 | 46.02 | 46.43 |
| TiO2 | 1.13 | 1.95 | 1.65 | 1.45 | 0.07 | 0.08 | 0.33 | 0.36 | 0.57 | 0.48 | 0.48 | 0.44 | 0.18 | 0.68 | 0.29 | 0.32 |
| Al2O3 | 33.24 | 33.29 | 33.32 | 32.86 | 32.59 | 31.69 | 31.77 | 30.44 | 31.30 | 36.20 | 36.08 | 35.58 | 33.04 | 35 65 | 33.65 | 33.02 |
| FeO* | 4.10 | 1.28 | 1.34 | 4.00 | 2.49 | 3.37 | 5.44 | 2.44 | 2.80 | 1.01 | 0.89 | 0.97 | 2.22 | 1.14 | 2.27 | 2.49 |
| MnO | 0.00 | 0.03 | 0.00 | 0.02 | 0.11 | 0.02 | 0.00 | 0.06 | 0.03 | 0.00 | 0.00 | 0.00 | 0.00 | 0.00 | 0.00 | 0.00 |
| MgO | 1.04 | 1.32 | 1.48 | 2.14 | 2.11 | 1.91 | 2.64 | 1.97 | 2.78 | 0.64 | 0.57 | 0.62 | 1.65 | 0.68 | 0.89 | 1.02 |
| CaO | 0.00 | 0.02 | 0.04 | 0.02 | 0.04 | 0.00 | 0.02 | 0.00 | 0.00 | 0.04 | 0.00 | 0.00 | 0.04 | 0.00 | 0.01 | 0.00 |
| Na2O | 0.65 | 0.73 | 0.72 | 0.61 | 0.37 | 0.70 | 0.48 | 0.62 | 0.76 | 1.02 | 1.11 | 1.09 | 0.47 | 0.59 | 1.11 | 1.13 |
| K2O | 9.70 | 8.88 | 8.79 | 8.92 | 9.10 | 8.83 | 8.43 | 9.44 | 8.35 | 8.83 | 8 83 | 8.70 | 9.32 | 9.56 | 9.96 | 9.39 |
| F | 0.00 | 0.00 | 0.00 | 0 00 | 0.00 | 0.00 | 0.00 | 0.00 | 0.00 | 0.00 | 0.01 | 0.00 | 0.00 | 0.00 | 0.34 | 0.29 |
| Cl | 0.00 | 0.00 | 0.00 | 0.00 | 0.00 | 0.00 | 0.00 | 0.00 | 0.00 | 0.00 | 0.01 | 0.00 | 0.00 | 0.01 | 0.00 | 0.00 |
| Total | 94.33 | 93.28 | 93.92 | 94 55 | 93.33 | 93.37 | 93.37 | 94.24 | 94.23 | 94.10 | 94.31 | 93.42 | 93.32 | 94.24 | 94.53 | 94.11 |
| O = F, Cl | 0.00 | 0.00 | 0.00 | 0.00 | 0.00 | 0.00 | 0.00 | 0.00 | 0.00 | 0.00 | 0.00 | 0.00 | 0.00 | 0.00 | -0.15 | -0.12 |
| Total | 94.33 | 93.28 | 93.92 | 94.55 | 93.33 | 93.37 | 93.37 | 94.24 | 94.23 | 94.10 | 94.31 | 93.42 | 93.32 | 94.24 | 94.39 | 93.98 |
| Number of cations on the basis of 11 oxygens: | | | | | | | | | | | | | | | | |
| Si | 3.034 | 3.093 | 3.120 | 3.030 | 3.151 | 3.182 | 3.052 | 3.284 | 3.194 | 3.059 | 3.080 | 3.087 | 3.146 | 3.070 | 3.112 | 3.144 |
| Al iv | 0.966 | 0.907 | 0.880 | 0.970 | 0.849 | 0.818 | 0.948 | 0.716 | 0.806 | 0.941 | 0.920 | 0.913 | 0.854 | 0.930 | 0.888 | 0.856 |
| Sum T | 4.000 | 4.000 | 4.000 | 4.000 | 4.000 | 4.000 | 4.000 | 4.000 | 4.000 | 4.000 | 4.000 | 4.000 | 4.000 | 4 000 | 4.000 | 4.000 |
| Al vi | 1.708 | 1.744 | 1.751 | 1.653 | 1.757 | 1.723 | 1.634 | 1.693 | 1.668 | 1.905 | 1.907 | 1.902 | 1.786 | 1.879 | 1.795 | 1.781 |
| Ti | 0.058 | 0.099 | 0.083 | 0.074 | 0.004 | 0.004 | 0.017 | 0.018 | 0.029 | 0.024 | 0.024 | 0.022 | 0.009 | 0.034 | 0.015 | 0.016 |
| Fe2+ | 0.234 | 0.072 | 0.075 | 0.227 | 0.141 | 0.192 | 0.314 | 0.137 | 0.157 | 0.056 | 0.049 | 0.054 | 0.126 | 0.064 | 0.128 | 0.141 |
| Mn | 0 000 | 0 002 | 0.000 | 0.001 | 0.006 | 0 001 | 0.000 | 0.003 | 0.002 | 0.000 | 0.000 | 0.000 | 0.000 | 0.000 | 0.000 | 0.000 |
| Mg | 0.106 | 0.133 | 0.148 | 0.216 | 0.213 | 0.194 | 0.271 | 0.197 | 0.278 | 0 064 | 0.056 | 0.062 | 0.167 | 0 068 | 0.089 | 0.103 |
| Sum O | 2.106 | 2.050 | 2.057 | 2.171 | 2.121 | 2.114 | 2.236 | 2.049 | 2.134 | 2.049 | 2.037 | 2.040 | 2.088 | 2.045 | 2.028 | 2.041 |
| Ca | 0.000 | 0.001 | 0.003 | 0.001 | 0.003 | 0.000 | 0.001 | 0 000 | 0.000 | 0.003 | 0.000 | 0.000 | 0.003 | 0.000 | 0.001 | 0.000 |
| Na | 0.086 | 0.096 | 0 094 | 0 054 | 0.049 | 0.092 | 0.064 | 0.081 | 0.099 | 0.132 | 0.143 | 0.142 | 0.062 | 0.076 | 0.146 | 0.149 |
| K | 0.844 | 0.765 | 0.751 | 0.771 | 0.788 | 0.766 | 0.742 | 0.809 | 0.714 | 0.751 | 0.749 | 0.745 | 0.806 | 0.815 | 0.859 | 0.811 |
| Sum A | 0.930 | 0.862 | 0.847 | 0.826 | 0.839 | 0 859 | 0.807 | 0.889 | 0.813 | 0.886 | 0.892 | 0.886 | 0.871 | 0.892 | 1.006 | 0.960 |
| Sum Cations | 7.036 | 6.913 | 6.904 | 6.997 | 6.961 | 6.973 | 7.043 | 6.938 | 6.947 | 6.935 | 6.929 | 6.927 | 6.959 | 6.937 | 7.034 | 7.001 |

* Total Fe as FeO

Table B-2 (continued)

| Sample no. | SD-97 | | | | | 1/7291 | | | | | | SD-60 | | | | |
|---|---|---|---|---|---|---|---|---|---|---|---|---|---|---|---|---|
| Analysis no. | 3 | 4 | 5 | 6 | 7 | 1 | 2 | 3 | 4 | 5 | 6 | 1 | 2 | 3 | 4 | 5 |
| | C2-Ms3 | C3-Ms4 | C3-Ms5 | C3-Ms6 | C3-Ms7 | C2-Ms1 | C2-Ms2 | C4-Ms3- | C4-Ms4-1 | C10-Ms5 | C10-Ms6 | C7-Ms1I | C7-Ms3I | C7-Ms4I | C1-Ms5I | C2-Ms7N |
| SiO2 | 46.97 | 45.53 | 45.62 | 44.78 | 45.96 | 45.48 | 45.02 | 47.45 | 46.82 | 47.09 | 46.73 | 44.98 | 45.48 | 46.15 | 47.63 | 45.44 |
| TiO2 | 0.37 | 0.32 | 0.05 | 0.00 | 0.01 | 0.83 | 0.93 | 0.35 | 0.44 | 0.31 | 0.36 | 0.07 | 0.03 | 0.07 | 0.00 | 0.88 |
| Al2O3 | 32.78 | 33.04 | 31.55 | 33.68 | 34.33 | 34.19 | 33.82 | 31.38 | 32.63 | 31.20 | 30.48 | 35.05 | 34.95 | 34.38 | 31.47 | 34.79 |
| FeO* | 2.26 | 3.29 | 2.84 | 1.70 | 1.54 | 1.25 | 1.26 | 1.48 | 1.24 | 3.07 | 3.48 | 1.04 | 0.81 | 1.11 | 1.92 | 0.93 |
| MnO | 0.00 | 0.12 | 0.08 | 0.00 | 0.00 | 0.02 | 0.05 | 0.02 | 0.00 | 0.03 | 0.00 | 0.00 | 0.00 | 0.00 | 0.00 | 0.02 |
| MgO | 0.98 | 1.33 | 1.52 | 1.16 | 1.09 | 0.90 | 0.91 | 2.01 | 1.75 | 1.53 | 1.54 | 0.82 | 0.73 | 1 02 | 1.92 | 0.75 |
| CaO | 0.01 | 0.00 | 0.06 | 0.06 | 0.06 | 0.00 | 0.00 | 0.02 | 0.01 | 0.00 | 0 05 | 0.00 | 0.00 | 0 00 | 0.04 | 0.02 |
| Na2O | 1.15 | 1.07 | 0.03 | 0.48 | 0.56 | 0.49 | 0.57 | 0.30 | 0.41 | 0.44 | 0.38 | 0.44 | 0.53 | 0.37 | 0.17 | 0.56 |
| K2O | 9.66 | 9.38 | 10.89 | 10.56 | 10.54 | 9.60 | 9.51 | 9.05 | 9.23 | 9.36 | 9.82 | 10.42 | 10.54 | 10.78 | 11.02 | 9.95 |
| F | 0.37 | 0.21 | 0.51 | 0.08 | 0.00 | 0.00 | 0.00 | 0.00 | 0.00 | 0.00 | 0 00 | 0.14 | 0.14 | 0.05 | 0.08 | 0.30 |
| Cl | 0.03 | 0.00 | 0.01 | 0.00 | 0.01 | 0.05 | 0.00 | 0.00 | 0.00 | 0.03 | 0 00 | 0.03 | 0.00 | 0.01 | 0.00 | 0.03 |
| Total | 94.58 | 94.30 | 93.16 | 92.49 | 94.12 | 92.81 | 92.07 | 92.07 | 92.53 | 93.08 | 92.84 | 92.99 | 93.20 | 93 94 | 94.24 | 93 66 |
| O = F, Cl | -0.16 | -0 09 | -0.21 | -0.03 | 0.00 | -0.01 | 0.00 | 0.00 | 0.00 | -0.01 | 0.00 | -0.06 | -0 06 | -0 02 | -0.03 | -0.13 |
| Total | 94.42 | 94.21 | 92.94 | 92.46 | 94.12 | 92.79 | 92.07 | 92.07 | 92.53 | 93.08 | 92.84 | 92.92 | 93.14 | 93.91 | 94.20 | 93.53 |
| Number of cations on the basis of 11 oxygens: | | | | | | | | | | | | | | | | |
| Si | 3.168 | 3.095 | 3.159 | 3 088 | 3.104 | 3.094 | 3.089 | 3.237 | 3.180 | 3.215 | 3.217 | 3.069 | 3 092 | 3.117 | 3.222 | 3.075 |
| Al iv | 0.832 | 0.905 | 0.841 | 0.912 | 0.896 | 0.906 | 0.911 | 0.763 | 0.820 | 0.785 | 0.783 | 0.931 | 0.908 | 0.883 | 0.778 | 0.925 |
| Sum T | 4.000 | 4.000 | 4.000 | 4.000 | 4.000 | 4.000 | 4.000 | 4.000 | 4.000 | 4.000 | 4.000 | 4.000 | 4.000 | 4.000 | 4.000 | 4.000 |
| Al vi | 1.774 | 1.742 | 1.734 | 1.826 | 1.836 | 1.837 | 1.825 | 1.761 | 1.793 | 1.727 | 1.690 | 1.889 | 1.893 | 1.854 | 1.732 | 1.851 |
| Ti | 0.019 | 0.017 | 0.003 | 0.000 | 0.001 | 0.043 | 0.048 | 0.018 | 0.022 | 0.016 | 0 019 | 0 004 | 0.001 | 0.003 | 0.000 | 0.045 |
| Fe2+ | 0.127 | 0.187 | 0.164 | 0.098 | 0.087 | 0.071 | 0.072 | 0.084 | 0.070 | 0.175 | 0.200 | 0.059 | 0 046 | 0.063 | 0.108 | 0.053 |
| Mn | 0.000 | 0.007 | 0.005 | 0.000 | 0.000 | 0.001 | 0.003 | 0.001 | 0.000 | 0.002 | 0.000 | 0.000 | 0.000 | 0.000 | 0.000 | 0.001 |
| Mg | 0.099 | 0.135 | 0.157 | 0.119 | 0.110 | 0.091 | 0.093 | 0.204 | 0.177 | 0.156 | 0.158 | 0.083 | 0 074 | 0.103 | 0.193 | 0.076 |
| Sum O | 2.019 | 2.088 | 2.063 | 2.043 | 2.034 | 2.043 | 2.041 | 2.068 | 2.063 | 2.076 | 2.067 | 2.035 | 2.014 | 2.023 | 2.034 | 2 025 |
| Ca | 0.001 | 0.000 | 0.004 | 0.004 | 0 004 | 0.000 | 0.000 | 0.002 | 0 000 | 0.000 | 0.004 | 0.000 | 0 000 | 0.000 | 0.003 | 0.002 |
| Na | 0.150 | 0.141 | 0.005 | 0.064 | 0 073 | 0.065 | 0.076 | 0.039 | 0.054 | 0.058 | 0.051 | 0.058 | 0 069 | 0.048 | 0.023 | 0.073 |
| K | 0.831 | 0.814 | 0.962 | 0.929 | 0.908 | 0.833 | 0.833 | 0.788 | 0.800 | 0.815 | 0.863 | 0.907 | 0.914 | 0.929 | 0.951 | 0 859 |
| Sum A | 0.982 | 0.955 | 0.971 | 0.997 | 0.986 | 0 898 | 0.909 | 0.829 | 0.855 | 0.874 | 0.918 | 0.965 | 0.984 | 0.976 | 0.976 | 0.934 |
| Sum Cations | 7 001 | 7 043 | 7.034 | 7.040 | 7.020 | 6.941 | 6.949 | 6.897 | 6.918 | 6.950 | 6.985 | 7 000 | 6 998 | 6.999 | 7 010 | 6.959 |

Table B-2 (continued)

| Sample no. | SD-60 | SD-99 | | | | | | | | SD-193 | | | | | 1/6291 | |
|---|---|---|---|---|---|---|---|---|---|---|---|---|---|---|---|---|
| Analysis no. | 6 | 1 | 2 | 3 | 4 | 5 | 6 | 7 | 8 | 1 | 2 | 3 | 4 | 5 | 1 | 2 |
| | C2-Ms8N | C1-Ms1 | C1-Ms2 | C1-Ms3 | C1-Ms4 | C2-Ms5 | C2-Ms6 | C5-Ms7 | C5-Ms8 | C2-Ms3 | C8-Ms4 | C8-Ms5 | C8-Ms6 | C8-Ms7 | C5-Ms1 | C5-Ms2 |
| SiO2 | 45.30 | 46.18 | 45.61 | 45.57 | 45.67 | 45.67 | 46.09 | 46.32 | 46.16 | 47.38 | 47.95 | 48.92 | 48.95 | 48.02 | 45.33 | 45.51 |
| TiO2 | 0.80 | 0.24 | 0.38 | 0.11 | 0.04 | 0.90 | 0.59 | 0.47 | 0.39 | 0.13 | 0.00 | 0.03 | 0.01 | 0.03 | 0.23 | 0.23 |
| Al2O3 | 34.64 | 35.63 | 35.54 | 35.13 | 35.61 | 34.46 | 34.52 | 34.78 | 34.89 | 31.36 | 31.21 | 30.23 | 30.86 | 31 00 | 33.15 | 33.27 |
| FeO* | 0.76 | 0.87 | 0.93 | 0.99 | 0.83 | 1.14 | 1 09 | 0.33 | 0.43 | 3.70 | 1.87 | 1 86 | 1.87 | 1.70 | 4.02 | 3.94 |
| MnO | 0.02 | 0.00 | 0.00 | 0.10 | 0.00 | 0.03 | 0.00 | 0.00 | 0.00 | 0.00 | 0.00 | 0.04 | 0.00 | 0.00 | 0.00 | 0 00 |
| MgO | 0.71 | 0.86 | 0.77 | 0.84 | 0.85 | 0.70 | 0.86 | 1.13 | 1.19 | 1.56 | 1.87 | 1 89 | 1.87 | 1.63 | 0.64 | 0.69 |
| CaO | 0.02 | 0.03 | 0.00 | 0.01 | 0.00 | 0.00 | 0.02 | 0.00 | 0.03 | 0.04 | 0.00 | 0.00 | 0.00 | 0.01 | 0.02 | 0.04 |
| Na2O | 0.51 | 0.73 | 0.67 | 0.72 | 0.43 | 0 67 | 0.63 | 0.55 | 0.60 | 0.60 | 0.12 | 0.23 | 0.06 | 0.12 | 0.33 | 0.29 |
| K2O | 9.81 | 10.40 | 10.53 | 10.74 | 10.94 | 10.60 | 10.24 | 10.65 | 10.35 | 9.95 | 11.31 | 10.60 | 11.25 | 10.93 | 11.28 | 11.18 |
| F | 0.03 | 0.08 | 0.22 | 0.03 | 0.32 | 0.16 | 0.35 | 0.22 | 0.00 | 0.24 | 0.45 | 0.35 | 0.32 | 0.08 | 0.03 | 0.10 |
| Cl | 0.00 | 0.02 | 0.00 | 0.02 | 0 03 | 0.00 | 0 00 | 0.02 | 0.00 | 0.03 | 0.01 | 0.00 | 0.02 | 0.01 | 0 00 | 0.00 |
| Total | 92.58 | 95.03 | 94.64 | 94.25 | 94.72 | 94.34 | 94.40 | 94.47 | 94.04 | 94.98 | 94.80 | 94.14 | 95.22 | 93.53 | 95.02 | 95.25 |
| O = F, Cl | -0.01 | -0.03 | -0.09 | -0.02 | -0.14 | -0.07 | -0.15 | -0.10 | 0.00 | -0.11 | -0.19 | -0.15 | -0.14 | -0.04 | -0.01 | -0.04 |
| Total | 92.56 | 95.00 | 94.55 | 94.24 | 94.58. | 94.27 | 94.25 | 94.37 | 94.04 | 94.88 | 94.60 | 94.00 | 95.08 | 93.49 | 95.00 | 95.21 |
| Number of cations on the basis of 11 oxygens: | | | | | | | | | | | | | | | | |
| Si | 3.085 | 3 077 | 3.061 | 3.072 | 3.068 | 3.080 | 3.101 | 3.104 | 3.097 | 3.201 | 3.241 | 3.307 | 3.282 | 3.264 | 3.088 | 3.091 |
| Al iv | 0.915 | 0.923 | 0.939 | 0.928 | 0.932 | 0.920 | 0.899 | 0.896 | 0.903 | 0.799 | 0.759 | 0.693 | 0.718 | 0.736 | 0.912 | 0.909 |
| Sum T | 4.000 | 4.000 | 4.000 | 4.000 | 4.000 | 4.000 | 4.000 | 4.000 | 4.000 | 4.000 | 4.000 | 4.000 | 4.000 | 4 000 | 4.000 | 4 000 |
| Al vi | 1.866 | 1.875 | 1.872 | 1.865 | 1.889 | 1.821 | 1.840 | 1.852 | 1.857 | 1.699 | 1.727 | 1.716 | 1.721 | 1.747 | 1.750 | 1.754 |
| Ti | 0.041 | 0.012 | 0.019 | 0.006 | 0.002 | 0.045 | 0.030 | 0.024 | 0.019 | 0.007 | 0.000 | 0.001 | 0 000 | 0.001 | 0.012 | 0.012 |
| Fe2+ | 0.043 | 0.048 | 0.052 | 0.056 | 0.047 | 0.064 | 0.061 | 0 018 | 0.024 | 0.209 | 0.106 | 0.105 | 0.105 | 0.097 | 0.229 | 0.224 |
| Mn | 0.001 | 0.000 | 0.000 | 0.006 | 0.000 | 0.002 | 0.000 | 0.000 | 0.000 | 0.000 | 0.000 | 0.002 | 0 000 | 0.000 | 0.000 | 0.000 |
| Mg | 0 072 | 0 085 | 0.077 | 0.084 | 0 085 | 0 071 | 0.086 | 0.113 | 0.119 | 0.157 | 0.188 | 0.191 | 0.187 | 0.165 | 0.065 | 0.070 |
| Sum O | 2.023 | 2.021 | 2.020 | 2.016 | 2.023 | 2.003 | 2.017 | 2.007 | 2.019 | 2.072 | 2.021 | 2.015 | 2 013 | 2.010 | 2.056 | 2.060 |
| Ca | 0.001 | 0.002 | 0.000 | 0.001 | 0.000 | 0.000 | 0.001 | 0.000 | 0.002 | 0 003 | 0 000 | 0.000 | 0 000 | 0 001 | 0.001 | 0.003 |
| Na | 0.068 | 0.095 | 0.087 | 0.094 | 0.056 | 0.088 | 0.083 | 0.071 | 0.078 | 0.079 | 0.015 | 0.030 | 0.008 | 0 016 | 0.043 | 0.038 |
| K | 0 852 | 0.884 | 0.901 | 0.924 | 0.937 | 0.913 | 0.879 | 0.911 | 0.886 | 0.858 | 0.975 | 0 914 | 0.962 | 0.948 | 0.980 | 0.968 |
| Sum A | 0.921 | 0.981 | 0.989 | 1.019 | 0.993 | 1.001 | 0.963 | 0.982 | 0.966 | 0.939 | 0.991 | 0.944 | 0.970 | 0.965 | 1.025 | 1.010 |
| Sum Cations | 6.944 | 7.002 | 7.009 | 7.035 | 7.016 | 7.004 | 6.980 | 6.989 | 6.986 | 7.011 | 7.012 | 6.959 | 6.983 | 6 975 | 7.081 | 7.069 |

* Total Fe as FeO

Table B-2 (continued)



| Sample no. | 1/6291 | 15/6291 | | SD-42 | | | | | | | | | SD-64 | | | |
|---|---|---|---|---|---|---|---|---|---|---|---|---|---|---|---|---|
| Analysis no. | 3 | 1 | 2 | 1 | 2 | 3 | 4 | 5 | 6 | 7 | 8 | 9 | 1 | 2 | 3 | 4 |
| | C5-Ms3 | C13-Ms1 | C13-Ms2 | Ms1/Ab4 | Ms2/Ab4 | Ms3/Ms5 | Ms4/Ab5 | Ms8/Ab | Ms9/Ab | Ms10/Ch | C5-Ms11 | C5-Ms12 | C1-Ms1- | C1-Ms3 | C1-Ms4 | C4-Ms5nChl6 |
| SiO2 | 45.04 | 48.07 | 49.18 | 46.95 | 47.57 | 46.66 | 51.99 | 45.53 | 47.27 | 49.18 | 46.51 | 47.38 | 46.72 | 48 01 | 45.90 | 48.77 |
| TiO2 | 0.21 | 0.24 | 0.07 | 0.14 | 0.16 | 0.13 | 0.11 | 0.14 | 0.29 | 0.16 | 0.99 | 0.20 | 0.22 | 0.18 | 0.17 | 0.15 |
| Al2O3 | 33.75 | 31.31 | 31.78 | 28.25 | 28.35 | 28.09 | 29.11 | 27.50 | 28.41 | 28.65 | 27.99 | 28.43 | 29.98 | 29.95 | 29.72 | 30.69 |
| FeO* | 3.78 | 2.00 | 2.09 | 5.00 | 4.27 | 4.29 | 4.45 | 6.42 | 5.34 | 4.15 | 4.34 | 3.90 | 4.49 | 2.49 | 4.50 | 1.96 |
| MnO | 0.00 | 0.00 | 0.03 | 0.03 | 0.00 | 0.00 | 0.00 | 0.12 | 0.00 | 0.01 | 0.10 | 0.00 | 0.00 | 0.13 | 0.00 | 0.00 |
| MgO | 0.45 | 1.73 | 1.98 | 2.50 | 2.00 | 2.23 | 2.47 | 3.65 | 2.36 | 2.14 | 2.38 | 2.16 | 2.85 | 2.25 | 2.91 | 2.10 |
| CaO | 0 00 | 0.00 | 0.00 | 0.01 | 0.00 | 0.04 | 0.00 | 0.01 | 0.02 | 0.03 | 0.00 | 0.02 | 0.03 | 0.05 | 0.06 | 0.06 |
| Na2O | 0.34 | 0.22 | 0.18 | 0.16 | 0.10 | 0.13 | 0.07 | 0.10 | 0.09 | 0.10 | 0.14 | 0.13 | 0.18 | 0.17 | 0.15 | 0.18 |
| K2O | 10.96 | 9.09 | 9.09 | 10.05 | 10.81 | 10.32 | 9.16 | 9.56 | 9.83 | 10.71 | 10.15 | 10.55 | 9.70 | 10.34 | 9.82 | 10.93 |
| F | 0.01 | 0.00 | 0.00 | 0.00 | 0.19 | 0.00 | 0.16 | 0.08 | 0.44 | 0.21 | 0.00 | 0.00 | 0.00 | 0.00 | 0.00 | 0 00 |
| Cl | 0.02 | 0 00 | 0.00 | 0 01 | 0.00 | 0.02 | 0.03 | 0.00 | 0.00 | 0.02 | 0.01 | 0.00 | 0.00 | 0.02 | 0.00 | 0.00 |
| Total | 94.57 | 92.66 | 94.40 | 93.09 | 93.45 | 91.91 | 97.53 | 93.10 | 94.04 | 95.37 | 92.62 | 92.77 | 94.19 | 93.59 | 93 24 | 94.84 |
| O = F, Cl | -0 01 | 0.00 | 0.00 | 0.00 | -0.08 | 0.00 | -0.07 | -0.03 | -0.19 | -0.09 | 0.00 | 0.00 | 0.00 | 0.00 | 0.00 | 0.00 |
| Total | 94.56 | 92.66 | 94.40 | 93.09 | 93.37 | 91.90 | 97.46 | 93.07 | 93.86 | 95.28 | 92.62 | 92.77 | 94.19 | 93.58 | 93.24 | 94.84 |
| Number of cations on the basis of 11 oxygens: | | | | | | | | | | | | | | | | |
| Si | 3.073 | 3.261 | 3.271 | 3.257 | 3.290 | 3.272 | 3.385 | 3.190 | 3.258 | 3.321 | 3.240 | 3.284 | 3.188 | 3.268 | 3.171 | 3.271 |
| Al iv | 0.927 | 0.739 | 0.729 | 0.743 | 0 710 | 0.728 | 0.615 | 0.810 | 0.742 | 0.679 | 0.760 | 0.716 | 0.812 | 0.732 | 0 829 | 0.729 |
| Sum T | 4.000 | 4.000 | 4.000 | 4.000 | 4.000 | 4.000 | 4.000 | 4.000 | 4.000 | 4.000 | 4.000 | 4.000 | 4.000 | 4.000 | 4.000 | 4.000 |
| Al vi | 1.787 | 1.766 | 1.764 | 1.567 | 1.601 | 1.595 | 1.620 | 1.461 | 1.568 | 1.601 | 1.540 | 1.607 | 1.600 | 1.671 | 1.592 | 1 697 |
| Ti | 0.011 | 0.012 | 0.004 | 0.007 | 0.008 | 0.007 | 0.005 | 0.007 | 0.015 | 0.008 | 0.052 | 0.010 | 0.011 | 0.009 | 0.009 | 0.008 |
| Fe2+ | 0.216 | 0.113 | 0.116 | 0.290 | 0.247 | 0.252 | 0.242 | 0.376 | 0.308 | 0.234 | 0.253 | 0.226 | 0.256 | 0.142 | 0.260 | 0.110 |
| Mn | 0.000 | 0.000 | 0.002 | 0.002 | 0.000 | 0.000 | 0.000 | 0.007 | 0 000 | 0.001 | 0.006 | 0.000 | 0.000 | 0.008 | 0.000 | 0.000 |
| Mg | 0.046 | 0 175 | 0.196 | 0.258 | 0.206 | 0.233 | 0.239 | 0.381 | 0.242 | 0.216 | 0 247 | 0 223 | 0.290 | 0.229 | 0.300 | 0.210 |
| Sum O | 2.060 | 2.066 | 2.081 | 2.125 | 2.063 | 2.086 | 2.107 | 2.233 | 2.133 | 2.060 | 2.097 | 2.067 | 2.158 | 2.058 | 2.162 | 2.024 |
| Ca | 0.000 | 0.000 | 0.000 | 0.001 | 0.000 | 0.003 | 0.000 | 0.001 | 0.001 | 0.003 | 0.000 | 0.002 | 0 002 | 0.003 | 0.005 | 0 004 |
| Na | 0.045 | 0.029 | 0.023 | 0.021 | 0.014 | 0.018 | 0.009 | 0.013 | 0.012 | 0.013 | 0.019 | 0.017 | 0.024 | 0.022 | 0.020 | 0.024 |
| K | 0.954 | 0.787 | 0.772 | 0.890 | 0.954 | 0.923 | 0.761 | 0.854 | 0 864 | 0.923 | 0.902 | 0.933 | 0.845 | 0.898 | 0.866 | 0.936 |
| Sum A | 0.999 | 0.816 | 0.795 | 0.911 | 0.967 | 0.944 | 0.770 | 0.869 | 0.877 | 0.939 | 0.921 | 0.951 | 0.871 | 0.923 | 0.890 | 0.963 |
| Sum Cations | 7.059 | 6.882 | 6.876 | 7.036 | 7.030 | 7 030 | 6.877 | 7.101 | 7.010 | 6.999 | 7.019 | 7.019 | 7.029 | 6.981 | 7 052 | 6.988 |

Table B-2 (continued)

| Sample no. | SD-64 | | SD-104 | | SD-165 | | | | SD-198 | | | | | SD-211 | | |
|---|---|---|---|---|---|---|---|---|---|---|---|---|---|---|---|---|
| Analysis no. | 6 | 7 | 1 | 2 | 1 | 2 | 3 | 4 | 1 | 2 | 3 | 4 | 5 | 1 | 2 | 3 |
| | C3-Ms7n | C5-Ms8n | C5-Wm2 | C5-Wm3 | C2-Ms1 | C2-Ms2 | C2-Ms3 | C2-Ms4 | C1-Wm1 | C1-Wm2 | C1-Wm4 | C1-Wm5 | C1-Wm6 | C1-Ms1E | C1-Ms2E | C1-Ms3D |
| SiO2 | 48.83 | 47.70 | 44.94 | 45.02 | 45.44 | 46.16 | 45.28 | 45.28 | 52.33 | 52.34 | 50.07 | 48.23 | 49.59 | 45.02 | 45.20 | 43.88 |
| TiO2 | 0.16 | 0.24 | 0.05 | 0.13 | 0.39 | 0.47 | 1.05 | 0.39 | 0.00 | 0.04 | 0.02 | 0.10 | 0.08 | 0.32 | 0.39 | 0.46 |
| Al2O3 | 30.68 | 31.29 | 34.76 | 35.07 | 33.33 | 34.03 | 33.45 | 34.42 | 22.05 | 22.07 | 21 48 | 21.17 | 21.85 | 31.75 | 31.68 | 32.01 |
| FeO* | 1.71 | 1.70 | 1.10 | 0.89 | 2.83 | 2.56 | 2.86 | 2.78 | 5.15 | 5.39 | 5.90 | 7.49 | 6.42 | 3.52 | 3 86 | 4.11 |
| MnO | 0.00 | 0.00 | 0.00 | 0.04 | 0.03 | 0.00 | 0.11 | 0.04 | 0.05 | 0.00 | 0.00 | 0.13 | 0.00 | 0.13 | 0.08 | 0.03 |
| MgO | 2.02 | 2.04 | 0.95 | 0.81 | 0.69 | 0.57 | 0.55 | 0.51 | 3.95 | 3.79 | 4.11 | 5.23 | 4.50 | 0.96 | 0.95 | 0.87 |
| CaO | 0.00 | 0.00 | 0.00 | 0.02 | 0.00 | 0.02 | 0.68 | 0.02 | 0.11 | 0.08 | 0.10 | 0.11 | 0.13 | 0.00 | 0.02 | 0.00 |
| Na2O | 0.18 | 0.16 | 0.68 | 0.59 | 0.82 | 0.80 | 0.81 | 0.77 | 0.02 | 0.04 | 0.05 | 0.01 | 0.05 | 0.23 | 0.28 | 0.33 |
| K2O | 11.06 | 10.89 | 10.56 | 10.52 | 10.42 | 10.10 | 10.09 | 10.24 | 10.78 | 10.60 | 10.15 | 9.97 | 10.33 | 10.86 | 10.93 | 10.96 |
| F | 0.00 | 0.00 | 0.00 | 0.00 | 0.00 | 0.00 | 0.00 | 0.00 | 0.00 | 0.00 | 0.00 | 0.00 | 0.00 | 0.08 | 0.00 | 0.21 |
| Cl | 0 00 | 0.00 | 0.02 | 0.00 | 0.01 | 0.02 | 0.01 | 0.00 | 0.02 | 0.00 | 0.17 | 0.00 | 0.02 | 0 01 | 0.00 | 0.00 |
| Total | 94.64 | 94.02 | 93.07 | 93 09 | 93.97 | 94.73 | 94.91 | 94.46 | 94.46 | 94.36 | 92.04 | 92.44 | 92.96 | 92.88 | 93.40 | 92 87 |
| O = F, Cl | 0.00 | 0.00 | -0.01 | 0.00 | 0.00 | -0.01 | 0.00 | 0.00 | -0.01 | 0.00 | 0.00 | 0.00 | 0.00 | -0.04 | 0.00 | -0.09 |
| Total | 94.64 | 94.02 | 93.06 | 93.09 | 93.96 | 94.73 | 94.91 | 94.46 | 94.46 | 94.36 | 92.03 | 92.44 | 92.95 | 92.85 | 93.40 | 92.78 |
| Number of cations on the basis of 11 oxygens: | | | | | | | | | | | | | | | | |
| Si | 3.279 | 3.226 | 3.067 | 3.066 | 3.099 | 3.107 | 3.064 | 3.066 | 3.577 | 3.580 | 3.534 | 3.429 | 3.479 | 3.128 | 3.127 | 3 072 |
| Al iv | 0.721 | 0.774 | 0.933 | 0.934 | 0.901 | 0.893 | 0.936 | 0.934 | 0.423 | 0.420 | 0.466 | 0.571 | 0.521 | 0.872 | 0.873 | 0.928 |
| Sum T | 4.000 | 4.000 | 4 000 | 4.000 | 4.000 | 4.000 | 4.000 | 4.000 | 4.000 | 4.000 | 4.000 | 4.000 | 4.000 | 4 000 | 4 000 | 4.000 |
| Al vi | 1.707 | 1.720 | 1.865 | 1.881 | 1.779 | 1.807 | 1.733 | 1.814 | 1.355 | 1.360 | 1.322 | 1.204 | 1.286 | 1.729 | 1.711 | 1.714 |
| Ti | 0.008 | 0.012 | 0.003 | 0.007 | 0.020 | 0.024 | 0.053 | 0.020 | 0.000 | 0.002 | 0.001 | 0.005 | 0.004 | 0.017 | 0.020 | 0.024 |
| Fe2+ | 0 096 | 0.096 | 0.063 | 0.051 | 0.162 | 0.144 | 0.162 | 0.158 | 0.294 | 0.308 | 0.348 | 0.445 | 0.377 | 0.205 | 0.223 | 0.241 |
| Mn | 0.000 | 0.000 | 0.000 | 0.003 | 0.002 | 0.000 | 0.006 | 0.002 | 0.003 | 0.000 | 0.000 | 0.008 | 0 000 | 0 008 | 0.005 | 0.002 |
| Mg | 0.202 | 0.205 | 0.097 | 0.083 | 0.071 | 0.057 | 0.056 | 0 051 | 0.402 | 0.386 | 0.432 | 0.554 | 0.470 | 0.099 | 0.098 | 0.090 |
| Sum O | 2.014 | 2.034 | 2.027 | 2.023 | 2.033 | 2.032 | 2.010 | 2 045 | 2.054 | 2.057 | 2.103 | 2.217 | 2.137 | 2.057 | 2.058 | 2.071 |
| Ca | 0.000 | 0.000 | 0.000 | 0.001 | 0.000 | 0 002 | 0.049 | 0.002 | 0 008 | 0.006 | 0.007 | 0.008 | 0.010 | 0.000 | 0.002 | 0.000 |
| Na | 0.023 | 0.022 | 0.090 | 0.077 | 0.109 | 0.105 | 0.106 | 0.101 | 0.003 | 0.005 | 0.006 | 0.001 | 0.007 | 0.031 | 0.038 | 0 044 |
| K | 0.947 | 0.940 | 0.919 | 0.914 | 0.907 | 0.867 | 0.871 | 0.885 | 0.940 | 0.925 | 0.914 | 0.905 | 0.925 | 0.963 | 0.965 | 0.979 |
| Sum A | 0.970 | 0.961 | 1.010 | 0.992 | 1.015 | 0.974 | 1.027 | 0.988 | 0.951 | 0.936 | 0.928 | 0.915 | 0.942 | 0.994 | 1.004 | 1.024 |
| Sum Cations | 6 984 | 6.996 | 7.036 | 7.016 | 7.048 | 7.005 | 7.037 | 7 033 | 7.006 | 6.993 | 7.031 | 7.131 | 7.079 | 7.052 | 7 062 | 7.095 |

* Total Fe as FeO

Table B-2 (continued)

| Sample no. | SD-211 | | | SD-213 | | | | | | | | SD-217 | SD-221 | | | |
|---|---|---|---|---|---|---|---|---|---|---|---|---|---|---|---|---|
| Analysis no. | 4 | 5 | 6 | 1 | 2 | 3 | 4 | 5 | 6 | 7 | 8 | 1 | 1 | 2 | 3 | 4 |
| | C1-Ms5 | C3-Ms6 | C3-Ms7 | C5-Ms1 | C5-Ms2 | C5-Ms3 | C5-Ms4 | C5-Ms5 | C5-Ms6 | C1-Ms7 | Ms10/A | C3-Ms2 | C2-Ms2 | C2-Ms3 | C2-Ms4 | C2-Ms5 |
| SiO2 | 47.08 | 45.86 | 46.77 | 44.87 | 45.86 | 45.26 | 48.68 | 45.36 | 45 62 | 45.78 | 46 01 | 44.77 | 48 25 | 48.50 | 48.30 | 49.65 |
| TiO2 | 0.29 | 0.33 | 0.17 | 0.58 | 0.72 | 0 65 | 0.18 | 0.23 | 1.25 | 0.72 | 0 02 | 0 07 | 0.09 | 0.08 | 0.02 | 0.00 |
| Al2O3 | 31.56 | 32.28 | 31.84 | 29.93 | 30.23 | 29.84 | 31.50 | 32.59 | 33.34 | 35.24 | 35.39 | 29.47 | 32.71 | 32.12 | 32.53 | 31.53 |
| FeO* | 1.48 | 1.72 | 1.31 | 4.79 | 4 87 | 5.08 | 1.48 | 2.76 | 1.21 | 0.70 | 1.34 | 5 65 | 1.09 | 1.16 | 1.13 | 1.32 |
| MnO | 0.07 | 0 00 | 0.01 | 0.01 | 0.00 | 0.05 | 0 02 | 0.02 | 0 00 | 0.10 | 0 00 | 0.09 | 0.00 | 0.00 | 0 05 | 0 00 |
| MgO | 1.67 | 1.42 | 1.34 | 1.30 | 1.24 | 1.30 | 0.96 | 0.49 | 0.80 | 0.59 | 0.27 | 3.46 | 1.62 | 1.73 | 1.58 | 1.88 |
| CaO | 0 02 | 0 02 | 0.00 | 0.02 | 0 01 | 0.00 | 0.01 | 0.00 | 0 04 | 0 00 | 0.06 | 0.11 | 0.00 | 0 00 | 0.04 | 0 00 |
| Na2O | 0.24 | 0.59 | 0.29 | 0.27 | 0.29 | 0.29 | 0.37 | 0.39 | 0.36 | 0.68 | 0.35 | 0.12 | 0.35 | 0.31 | 0.23 | 0.23 |
| K2O | 10.51 | 10.13 | 10.13 | 10 63 | 10.92 | 10.80 | 9.90 | 10.70 | 10 03 | 10.36 | 10.73 | 8.16 | 9 24 | 9.46 | 9.54 | 9.29 |
| F | 0.54 | 0.11 | 0.38 | 0.00 | 0.08 | 0 05 | 0.22 | 0.16 | 0.05 | 0 03 | 0 08 | 0 08 | 0.00 | 0.19 | 0.00 | 0.29 |
| Cl | 0.00 | 0.02 | 0.00 | 0.00 | 0.01 | 0 00 | 0.00 | 0.00 | 0.01 | 0.05 | 0.00 | 0.00 | 0.00 | 0 03 | 0.01 | 0.02 |
| Total | 93.47 | 92.49 | 92.24 | 92.39 | 94 24 | 93.32 | 93.32 | 92.69 | 92.71 | 94.26 | 94.25 | 91.97 | 93.35 | 93.57 | 93.43 | 94.22 |
| O = F, Cl | -0.23 | -0.05 | -0.16 | 0.00 | -0 04 | -0.02 | -0.09 | -0.07 | -0.03 | -0.02 | -0 03 | -0.03 | 0.00 | -0.08 | 0 00 | -0.13 |
| Total | 93.24 | 92.44 | 92.08 | 92.39 | 94.21 | 93.30 | 93.23 | 92.62 | 92.69 | 94.23 | 94.22 | 91 93 | 93.35 | 93.48 | 93.42 | 94.09 |
| Number of cations on the basis of 11 oxygens: | | | | | | | | | | | | | | | | |
| Si | 3.214 | 3.155 | 3.216 | 3.153 | 3.164 | 3.158 | 3.291 | 3.139 | 3.115 | 3.074 | 3.097 | 3.134 | 3.235 | 3.257 | 3.243 | 3.308 |
| Al iv | 0.786 | 0.845 | 0.784 | 0 847 | 0.836 | 0.842 | 0.709 | 0.861 | 0.885 | 0.926 | 0.903 | 0.866 | 0.765 | 0.743 | 0.757 | 0.692 |
| Sum T | 4.000 | 4.000 | 4.000 | 4.000 | 4.000 | 4.000 | 4.000 | 4 000 | 4.000 | 4.000 | 4.000 | 4.000 | 4.000 | 4.000 | 4.000 | 4.000 |
| Al vi | 1.753 | 1.772 | 1.798 | 1 632 | 1.622 | 1.612 | 1 802 | 1.798 | 1.800 | 1.865 | 1.906 | 1.566 | 1.822 | 1.800 | 1.817 | 1.784 |
| Ti | 0 015 | 0.017 | 0 009 | 0.031 | 0.037 | 0.034 | 0.009 | 0 012 | 0.064 | 0.037 | 0.001 | 0.004 | 0 004 | 0.004 | 0.001 | 0.000 |
| Fe2+ | 0.084 | 0.099 | 0.075 | 0.281 | 0 281 | 0.296 | 0 084 | 0.160 | 0.069 | 0.039 | 0.075 | 0.331 | 0.061 | 0.065 | 0 063 | 0 074 |
| Mn | 0 004 | 0.000 | 0.001 | 0.001 | 0.000 | 0 003 | 0.001 | 0.001 | 0.000 | 0 006 | 0 000 | 0.005 | 0 000 | 0.000 | 0 003 | 0.000 |
| Mg | 0.170 | 0.145 | 0.137 | 0.136 | 0.128 | 0.135 | 0.097 | 0.051 | 0.081 | 0.059 | 0 027 | 0.361 | 0.162 | 0.173 | 0.158 | 0.186 |
| Sum O | 2.027 | 2.034 | 2 020 | 2.081 | 2.069 | 2.081 | 1.993 | 2.021 | 2.014 | 2.005 | 2.010 | 2.266 | 2.049 | 2.042 | 2.043 | 2.044 |
| Ca | 0.001 | 0.001 | 0.000 | 0.001 | 0.001 | 0.000 | 0 001 | 0 000 | 0.003 | 0.000 | 0.004 | 0.008 | 0.000 | 0.000 | 0 003 | 0.000 |
| Na | 0.032 | 0.078 | 0.038 | 0.037 | 0.039 | 0 039 | 0 049 | 0.052 | 0.047 | 0.089 | 0.046 | 0.016 | 0 045 | 0 040 | 0.030 | 0 029 |
| K | 0.915 | 0.889 | 0 889 | 0 953 | 0.961 | 0.961 | 0.854 | 0.945 | 0 874 | 0 888 | 0 922 | 0.729 | 0.791 | 0.811 | 0.817 | 0.790 |
| Sum A | 0.949 | 0.969 | 0.928 | 0.991 | 1.001 | 1.000 | 0.903 | 0.996 | 0.924 | 0.977 | 0.972 | 0.753 | 0.836 | 0.851 | 0.850 | 0.819 |
| Sum Cations | 6.975 | 7.003 | 6.948 | 7 072 | 7.070 | 7 081 | 6.896 | 7.018 | 6.939 | 6.982 | 6 981 | 7.019 | 6 885 | 6.893 | 6.893 | 6 863 |

Table B-2 (continued)

| Sample no. | SD-221 | | | P-106 | | | | | | P-107 | | | | | | | | | |
|---|---|---|---|---|---|---|---|---|---|---|---|---|---|---|---|---|---|---|---|
| Analysis no. | 5 | 6 | 7 | 1 | 2 | 3 | 4 | 5 | 6 | 1 | 2 | 3 | 4 | 5 | 6 | 7 | 8 | 9 |
| | C2-Ms6 | C2-Ms7 | C2-Ms8 | C6-Ms2 | C6-Ms3 | C6-Ms4 | C6-Ms5 | C6-Ms6 | C6-Ms7 | C9-Ms1 | C9-Ms2 | C9-Ms1/ | C9-Ms3 | C9-Ms4 | C9-Ms5 | C9-Ms6 | C13-Ms7 | C13-Ms8 |
| SiO2 | 48 65 | 48.33 | 48.54 | 46.28 | 48.27 | 48 08 | 47.52 | 47.49 | 46.40 | 49.84 | 49 85 | 49 84 | 49.39 | 49.70 | 49 81 | 49.57 | 48 35 | 49.22 |
| TiO2 | 0 01 | 0.04 | 0.10 | 0.05 | 0.10 | 0.07 | 0.00 | 0.01 | 0.00 | 0.00 | 0.04 | 0.00 | 0.01 | 0.04 | 0.05 | 0 01 | 0.08 | 0.00 |
| Al2O3 | 32.33 | 32.58 | 32.45 | 25.08 | 25.84 | 26.46 | 26.75 | 26.31 | 26.07 | 28.20 | 28.45 | 28.28 | 29.45 | 28.34 | 29.78 | 29.16 | 31.89 | 32.16 |
| FeO* | 1.11 | 1.07 | 1.13 | 5.68 | 4.77 | 4.68 | 3.74 | 3.95 | 4.77 | 3.03 | 2.60 | 3.05 | 3.04 | 2.93 | 2.45 | 3.10 | 2.07 | 2.13 |
| MnO | 0.04 | 0.00 | 0.00 | 0.05 | 0.06 | 0.04 | 0.02 | 0.08 | 0.17 | 0 00 | 0 05 | 0.10 | 0.00 | 0.11 | 0.17 | 0.05 | 0.04 | 0 07 |
| MgO | 1.75 | 1 65 | 1.61 | 4.23 | 2.89 | 3.51 | 3.06 | 3.45 | 3.70 | 2.75 | 3.00 | 2.81 | 1.99 | 2.69 | 2.15 | 2.35 | 1.44 | 1.19 |
| CaO | 0.05 | 0.00 | 0.00 | 0.03 | 0.00 | 0.00 | 0.00 | 0.01 | 0.01 | 0.02 | 0.06 | 0.03 | 0.04 | 0.05 | 0.02 | 0.02 | 0.07 | 0 07 |
| Na2O | 0.26 | 0.27 | 0.27 | 0.10 | 0.08 | 0.08 | 0.09 | 0.05 | 0.07 | 0.13 | 0.17 | 0.12 | 0.21 | 0.09 | 0.10 | 0.07 | 0.15 | 0.10 |
| K2O | 9.58 | 9.49/ | 9.22 | 11.06 | 11.15 | 11.55 | 11 27 | 11.46 | 11.10 | 11.23 | 11.29 | 11.39 | 11.23 | 11.26 | 11.21 | 11.36 | 11 27 | 10.94 |
| F | 0.13 | 0 05 | 0 00 | 0.39 | 0.00 | 0.00 | 0.53 | 0.35 | 0.26 | 0.22 | 0.11 | 0.00 | 0.09 | 0.29 | 0.11 | 0.24 | 0.00 | 0.00 |
| Cl | 0 03 | 0.04 | 0.03 | 0.02 | 0.00 | 0.01 | 0.01 | 0.00 | 0.00 | 0.02 | 0.00 | 0.00 | 0.01 | 0.02 | 0 00 | 0.01 | 0.04 | 0.01 |
| Total | 93.95 | 93.52 | 93.36 | 92.98 | 93.17 | 94.49 | 92.99 | 93.17 | 92.55 | 95.45 | 95.61 | 95.63 | 95.47 | 95.53 | 95.85 | 95.94 | 95.41 | 95.90 |
| O = F, Cl | -0 06 | -0.03 | -0.01 | -0.17 | 0.00 | 0.00 | -0.23 | -0.15 | -0.11 | -0.10 | -0 04 | 0.00 | -0.04 | -0.13 | -0 05 | -0.10 | -0.01 | 0.00 |
| Total | 93 88 | 93 49 | 93.36 | 92.81 | 93.17 | 94.49 | 92.77 | 93.03 | 92.43 | 95.35 | 95.56 | 95.63 | 95.43 | 95.40 | 95.81 | 95.84 | 95.41 | 95.89 |
| Number of cations on the basis of 11 oxygens: | | | | | | | | | | | | | | | | | | |
| Si | 3.254 | 3.242 | 3.254 | 3.278 | 3.362 | 3.312 | 3.323 | 3.318 | 3.278 | 3.353 | 3.340 | 3.344 | 3.317 | 3.344 | 3.320 | 3.321 | 3.232 | 3.260 |
| Al iv | 0.746 | 0.758 | 0.746 | 0.722 | 0.638 | 0.688 | 0.677 | 0 682 | 0.722 | 0.647 | 0.660 | 0.656 | 0.683 | 0.656 | 0.680 | 0 679 | 0.768 | 0 740 |
| Sum T | 4.000 | 4.000 | 4 000 | 4.000 | 4.000 | 4.000 | 4 000 | 4.000 | 4.000 | 4.000 | 4.000 | 4.000 | 4.000 | 4.000 | 4.000 | 4.000 | 4.000 | 4.000 |
| Al vi | 1.803 | 1.818 | 1.818 | 1.373 | 1.484 | 1.461 | 1.528 | 1.486 | 1.450 | 1.590 | 1.587 | 1.581 | 1.648 | 1.593 | 1.660 | 1.624 | 1.745 | 1.771 |
| Ti | 0.001 | 0.002 | 0.005 | 0.003 | 0.005 | 0 003 | 0.000 | 0.001 | 0.000 | 0.000 | 0 002 | 0.000 | 0.001 | 0.002 | 0.003 | 0 001 | 0.004 | 0 000 |
| Fe2+ | 0.062 | 0.060 | 0.064 | 0.336 | 0.278 | 0.270 | 0.219 | 0.231 | 0 282 | 0.171 | 0.146 | 0.171 | 0.171 | 0.165 | 0.137 | 0.174 | 0.116 | 0.118 |
| Mn | 0.002 | 0.000 | 0.000 | 0.003 | 0.004 | 0.002 | 0.001 | 0.005 | 0.010 | 0.000 | 0 003 | 0.006 | 0.000 | 0 007 | 0.010 | 0.003 | 0.002 | 0.004 |
| Mg | 0.175 | 0.165 | 0.161 | 0.447 | 0.300 | 0.360 | 0 318 | 0.360 | 0.389 | 0.276 | 0.299 | 0.281 | 0.199 | 0.270 | 0.214 | 0.235 | 0 144 | 0.117 |
| Sum O | 2.042 | 2.044 | 2.047 | 2.163 | 2 071 | 2.097 | 2.066 | 2.082 | 2.130 | 2.036 | 2.037 | 2.040 | 2.019 | 2 036 | 2.022 | 2.036 | 2.012 | 2 010 |
| Ca | 0 003 | 0.000 | 0.000 | 0.002 | 0.000 | 0.000 | 0.000 | 0.001 | 0 001 | 0 001 | 0 004 | 0.002 | 0.003 | 0 003 | 0 002 | 0 001 | 0.005 | 0.005 |
| Na | 0.034 | 0 035 | 0.035 | 0.014 | 0.010 | 0.011 | 0.012 | 0.007 | 0 010 | 0.017 | 0.022 | 0.015 | 0.028 | 0 012 | 0 014 | 0.009 | 0.020 | 0 013 |
| K | 0.818 | 0.812 | 0.789 | 1.000 | 0.991 | 1.015 | 1.005 | 1.022 | 1.000 | 0.964 | 0.965 | 0.975 | 0.963 | 0.967 | 0 953 | 0 971 | 0.961 | 0.924 |
| Sum A | 0.855 | 0 848 | 0.824 | 1.015 | 1.001 | 1.026 | 1.017 | 1.030 | 1.011 | 0.982 | 0.991 | 0.992 | 0.993 | 0.982 | 0 968 | 0.982 | 0.986 | 0.943 |
| Sum Cations | 6 897 | 6.892 | 6 871 | 7.178 | 7 072 | 7.123 | 7.083 | 7.112 | 7 142 | 7 019 | 7 028 | 7.032 | 7 012 | 7.019 | 6.991 | 7 017 | 6 998 | 6 953 |

* Total Fe as FeO

Table B-3 Electron microprobe analyses of chlorites (metasediments of the Pha Som Metamorphic Complex).

| Sample no. | 2/5291 | 5/8291 | | | | | | 3/9291 | | | | 6/9291 | | | 3/8291 | |
|---|---|---|---|---|---|---|---|---|---|---|---|---|---|---|---|---|
| Analysis no. | 1 | 1 | 2 | 3 | 4 | 5 | 6 | 1 | 2 | 3 | 4 | 1 | 2 | 3 | 1 | 2 |
| SiO2 | 25.31 | 23.82 | 24.24 | 23.97 | 23.98 | 23.88 | 24.55 | 24.05 | 24.28 | 23.62 | 23.27 | 27.80 | 26.35 | 26.22 | 26.54 | 26 30 |
| TiO2 | 0.00 | 0.05 | 0.04 | 0.06 | 0.05 | 0.05 | 0.06 | 0.00 | 0.00 | 0.00 | 0.00 | 0.07 | 0.07 | 0 00 | 0 09 | 0.03 |
| Al2O3 | 23.65 | 22.54 | 22.37 | 23.13 | 22.84 | 23.01 | 23 07 | 23.33 | 24.10 | 23.78 | 23.44 | 23.53 | 23.93 | 23.78 | 19.18 | 19.24 |
| Cr2O3 | 0.14 | 0.00 | 0.00 | 0.01 | 0.00 | 0.02 | 0.05 | 0.00 | 0 00 | 0.00 | 0.04 | 0.01 | 0.00 | 0.00 | 0.00 | 0.05 |
| FeO* | 30.27 | 26.41 | 24.87 | 27.07 | 26.82 | 26.44 | 26.91 | 25.98 | 25.16 | 26.34 | 27.03 | 22.05 | 19.74 | 19.43 | 27.89 | 28.41 |
| MnO | 0.01 | 0.60 | 0.41 | 0.36 | 0.38 | 0.40 | 0.46 | 0.17 | 0.18 | 0.06 | 0 05 | 0.07 | 0.47 | 0.41 | 0.57 | 0.62 |
| MgO | 9.04 | 12.13 | 13.81 | 11.66 | 11.68 | 11.67 | 11.36 | 12.19 | 13 08 | 12.32 | 11.82 | 13.66 | 14.91 | 15.36 | 12.74 | 12.24 |
| Total | 88.42 | 85.55 | 85.74 | 86.26 | 85.75 | 85.47 | 86.46 | 85.72 | 86.80 | 86.12 | 85 65 | 87.19 | 85.47 | 85.20 | 87.01 | 86.89 |
| Number of cations on the basis of 14 oxygens: | | | | | | | | | | | | | | | | |
| Si | 2.696 | 2.600 | 2.614 | 2.595 | 2.611 | 2.604 | 2.646 | 2.601 | 2.576 | 2.537 | 2.534 | 2.858 | 2.748 | 2.740 | 2.858 | 2.847 |
| Al iv | 1.304 | 1.400 | 1.386 | 1.405 | 1.389 | 1.396 | 1.354 | 1.399 | 1.424 | 1.463 | 1.466 | 1.142 | 1.252 | 1.260 | 1.142 | 1.153 |
| Sum T | 4.000 | 4.000 | 4.000 | 4.000 | 4.000 | 4.000 | 4.000 | 4.000 | 4.000 | 4.000 | 4.000 | 4.000 | 4.000 | 4.000 | 4.000 | 4 000 |
| Al vi | 1.667 | 1.501 | 1.457 | 1.547 | 1.543 | 1.562 | 1.578 | 1.576 | 1.590 | 1.549 | 1.544 | 1.710 | 1.690 | 1.669 | 1.293 | 1.303 |
| Ti | 0.000 | 0.004 | 0.003 | 0.005 | 0.004 | 0.004 | 0.005 | 0.000 | 0.000 | 0.000 | 0.000 | 0.005 | 0.005 | 0.000 | 0.007 | 0.002 |
| Cr | 0.012 | 0.000 | 0.000 | 0.001 | 0.000 | 0.002 | 0.004 | 0.000 | 0 000 | 0.000 | 0.003 | 0.001 | 0.000 | 0.000 | 0.000 | 0.004 |
| Fe | 2.697 | 2.411 | 2.243 | 2.451 | 2.442 | 2.411 | 2.426 | 2.350 | 2.232 | 2.366 | 2.462 | 1.896 | 1.722 | 1.698 | 2.512 | 2.572 |
| Mn | 0.001 | 0 055 | 0.037 | 0.033 | 0.035 | 0.037 | 0 042 | 0.016 | 0.016 | 0.005 | 0.005 | 0.006 | 0.042 | 0.036 | 0.052 | 0.057 |
| Mg | 1.435 | 1.973 | 2.219 | 1.881 | 1.895 | 1.896 | 1.825 | 1.965 | 2.068 | 1.972 | 1.919 | 2.093 | 2.317 | 2.392 | 2.045 | 1.975 |
| Sum O | 5.811 | 5.945 | 5.959 | 5.919 | 5.919 | 5.912 | 5.880 | 5.907 | 5.907 | 5 893 | 5.933 | 5.710 | 5.776 | 5.795 | 5.909 | 5.913 |
| Sum Cations | 9.811 | 9.945 | 9.959 | 9.919 | 9.919 | 9.912 | 9.880 | 9.907 | 9.907 | 9.893 | 9.933 | 9.710 | 9.776 | 9.795 | 9.909 | 9.913 |
| Mg/(Mg+Fe2) | 0.347 | 0.450 | 0.497 | 0.434 | 0.437 | 0.440 | 0.429 | 0.455 | 0.481 | 0.455 | 0.438 | 0.525 | 0.574 | 0.585 | 0.449 | 0.434 |

Table B-3 (continued)

| Sample no. | 3/8291 | SD-97 | | | | | | SD-225 | | | | | | | | SD-227 |
|---|---|---|---|---|---|---|---|---|---|---|---|---|---|---|---|---|
| Analysis no. | 3 | 1 | 2 | 3 | 4 | 5 | 6 | 1 | 2 | 3 | 4 | 5 | 6 | 7 | 8 | 1 |
| | | C1-Chl1 | C1-Chl2 | C1-Chl3 | C6-Chl4 | C6-Chl5 | C6-Chl6 | C7-Chl1 | C7-Chl2 | C7-Chl3 | C7-Chl4 | C7-Chl5 | C7-Chl6 | C7-Chl7 | C7-Chl8 | C5-Chl1 |
| SiO2 | 28.26 | 24.91 | 24.80 | 25.06 | 25.35 | 26.06 | 27.27 | 27.13 | 26.49 | 27 00 | 27.27 | 26.45 | 26.77 | 26.48 | 26.86 | 26.63 |
| TiO2 | 0.00 | 0.11 | 0.07 | 0.14 | 0.09 | 0.00 | 0.04 | 0.10 | 0.00 | 0.01 | 0.07 | 0.00 | 0.00 | 0.01 | 0.00 | 0.00 |
| Al2O3 | 20.44 | 22.51 | 22.01 | 22.42 | 18.74 | 18.88 | 19.26 | 17.78 | 18.55 | 17.66 | 17.87 | 18.21 | 18.08 | 17.71 | 18.42 | 20.78 |
| Cr2O3 | 0.09 | 0.00 | 0.03 | 0.00 | 0.05 | 0.07 | 0.25 | 0.04 | 0.00 | 0.00 | 0.02 | 0.03 | 0.06 | 0.00 | 0.02 | 0.01 |
| FeO* | 23.96 | 21.03 | 20.93 | 20.72 | 29.39 | 28.63 | 18.87 | 25.72 | 25.72 | 26.22 | 26.33 | 27.26 | 27.20 | 27.46 | 26.93 | 27.60 |
| MnO | 0.71 | 0.41 | 0.34 | 0.40 | 0.27 | 0.31 | 0.22 | 0.39 | 0.38 | 0.35 | 0.36 | 0.30 | 0.36 | 0.36 | 0.41 | 0.41 |
| MgO | 14.46 | 17.06 | 17.16 | 17.79 | 12.25 | 12.85 | 19.94 | 15.23 | 15.02 | 15.00 | 15.05 | 14.44 | 14.33 | 14.35 | 14.65 | 11.29 |
| Total | 87.92 | 86.03 | 85.33 | 86.53 | 86.15 | 86.79 | 85.86 | 86.39 | 86.16 | 86.23 | 86.98 | 86.68 | 86.79 | 86.37 | 87.29 | 86.74 |
| Number of cations on the basis of 14 oxygens: | | | | | | | | | | | | | | | | |
| Si | 2.929 | 2.619 | 2.629 | 2.613 | 2.791 | 2.827 | 2.834 | 2.909 | 2.852 | 2.911 | 2.912 | 2.853 | 2.882 | 2.873 | 2.868 | 2.860 |
| Al iv | 1.071 | 1.381 | 1.371 | 1.387 | 1.209 | 1.173 | 1.166 | 1.091 | 1.148 | 1.089 | 1.088 | 1.147 | 1.118 | 1.127 | 1.132 | 1.140 |
| Sum T | 4.000 | 4.000 | 4.000 | 4.000 | 4.000 | 4.000 | 4.000 | 4.000 | 4.000 | 4.000 | 4.000 | 4.000 | 4.000 | 4.000 | 4.000 | 4.000 |
| Al vi | 1.427 | 1.409 | 1.379 | 1.370 | 1.224 | 1.241 | 1.194 | 1.158 | 1.207 | 1.155 | 1.161 | 1.170 | 1.176 | 1.139 | 1.187 | 1.492 |
| Ti | 0.000 | 0.008 | 0.005 | 0.011 | 0 007 | 0.000 | 0.003 | 0.008 | 0.000 | 0.001 | 0.005 | 0 000 | 0.000 | 0.001 | 0.000 | 0.000 |
| Cr | 0.007 | 0.000 | 0.002 | 0.000 | 0.005 | 0.006 | 0.021 | 0.004 | 0.000 | 0.000 | 0.002 | 0.002 | 0.005 | 0.000 | 0.002 | 0.001 |
| Fe | 2.077 | 1.849 | 1.855 | 1 807 | 2.707 | 2.597 | 1.640 | 2.307 | 2.316 | 2.364 | 2.351 | 2.459 | 2.448 | 2.491 | 2.405 | 2.479 |
| Mn | 0.062 | 0 036 | 0.030 | 0.036 | 0.025 | 0.029 | 0.020 | 0.035 | 0.035 | 0.032 | 0.033 | 0.027 | 0.032 | 0.033 | 0.037 | 0.038 |
| Mg | 2.234 | 2.673 | 2.710 | 2.766 | 2.011 | 2.077 | 3.089 | 2.435 | 2.410 | 2.410 | 2.395 | 2.321 | 2.299 | 2.319 | 2.332 | 1.808 |
| Sum O | 5.808 | 5.976 | 5.983 | 5.989 | 5.980 | 5.950 | 5.966 | 5.947 | 5.968 | 5.961 | 5.947 | 5.979 | 5.961 | 5.983 | 5.963 | 5.817 |
| Sum Cations | 9.808 | 9.976 | 9.983 | 9.989 | 9.980 | 9.950 | 9.966 | 9.947 | 9.968 | 9.961 | 9.947 | 9.979 | 9.961 | 9.983 | 9.963 | 9.817 |
| Mg/(Mg+Fe2) | 0.518 | 0.591 | 0.594 | 0.605 | 0.426 | 0.444 | 0.653 | 0.513 | 0.510 | 0.505 | 0.505 | 0.486 | 0.484 | 0.482 | 0.492 | 0.422 |

* Total Fe as FeO

Table B-3 (continued)

| Sample no. | SD-227 | | | | | | 1/7291 | | | | | | | SD-60 | | |
|---|---|---|---|---|---|---|---|---|---|---|---|---|---|---|---|---|
| Analysis no. | 2 | 3 | 4 | 5 | 6 | 7 | 1 | 2 | 3 | 4 | 5 | 6 | 7 | 1 | 2 | |
| | C5-Chl3 | C5-Chl4 | C5-Chl5 | C6-Chl6 | C6-Chl7 | C6-Chl8 | C8-Chl1 | C8-Chl2 | C5-Chl3 | C5-Chl4 | C5-Chl5 | C1-Chl6 | C1-Chl7 | C7-Chl1 | C7-Chl2 | |
| SiO2 | 25.75 | 25.33 | 25.86 | 25.54 | 25.74 | 26.25 | 28.06 | 28.50 | 27 20 | 27.19 | 27.37 | 27.16 | 26.83 | 24.79 | 24.39 | |
| TiO2 | 0.07 | 0.00 | 0.03 | 0 00 | 0.02 | 0 00 | 1.34 | 1.25 | 1.19 | 1.22 | 1 03 | 0 02 | 0.04 | 0.03 | 0 00 | |
| Al2O3 | 21.55 | 19.45 | 19.12 | 19.52 | 19.33 | 19.34 | 18.31 | 18.49 | 16 27 | 16.50 | 17.36 | 18.91 | 18.74 | 21.22 | 20.99 | |
| Cr2O3 | 0.04 | 0.00 | 0.05 | 0 00 | 0.01 | 0 04 | 0.04 | 0.00 | 0.17 | 0.12 | 0 00 | 0 01 | 0.00 | 0.02 | 0.06 | |
| FeO* | 27.62 | 28.87 | 28.87 | 28 92 | 29.11 | 28 01 | 24 06 | 23.45 | 25.43 | 25.48 | 24.72 | 23.79 | 25.38 | 25 43 | 26.03 | |
| MnO | 0.38 | 0.38 | 0.46 | 0.53 | 0.53 | 0.51 | 0.16 | 0.06 | 0 19 | 0.15 | 0.08 | 0.49 | 0.42 | 0.30 | 0.20 | |
| MgO | 10.54 | 12.19 | 11.91 | 12.74 | 12.41 | 12.84 | 13 63 | 13.49 | 14.12 | 14 32 | 13.33 | 14 86 | 13.98 | 13.51 | 13.64 | |
| CaO | 0.12 | 0.09 | 0.10 | 0 00 | 0.04 | 0 06 | 0.06 | 0.11 | 0.10 | 0.05 | 0 08 | 0 03 | 0.05 | 0 01 | 0.05 | |
| Total | 86 08 | 86.30 | 86.40 | 87 26 | 87.18 | 87.04 | 85.66 | 85.35 | 84 67 | 85.03 | 83.97 | 85.27 | 85.44 | 85.33 | 85.35 | |
| Number of cations on the basis of 14 oxygens: | | | | | | | | | | | | | | | | |
| Si | 2.794 | 2.776 | 2.827 | 2.766 | 2.793 | 2.831 | 2.994 | 3 035 | 2.981 | 2 965 | 3 001 | 2.918 | 2 904 | 2.693 | 2.662 | |
| Al iv | 1.206 | 1.224 | 1.173 | 1.234 | 1.207 | 1.169 | 1.006 | 0.965 | 1 019 | 1 035 | 0.999 | 1.082 | 1 096 | 1.307 | 1.338 | |
| Sum T | 4.000 | 4.000 | 4.000 | 4.000 | 4.000 | 4.000 | 4.000 | 4.000 | 4 000 | 4.000 | 4.000 | 4.000 | 4.000 | 4.000 | 4.000 | |
| Al vi | 1.551 | 1.288 | 1.293 | 1.260 | 1.265 | 1.290 | 1.298 | 1.356 | 1.083 | 1.087 | 1.245 | 1 314 | 1.296 | 1.411 | 1.362 | |
| Ti | 0.006 | 0.000 | 0.003 | 0 000 | 0.001 | 0.000 | 0.108 | 0.100 | 0 098 | 0.100 | 0 085 | 0.002 | 0 003 | 0.003 | 0 000 | |
| Cr | 0.003 | 0.000 | 0.004 | 0.000 | 0.001 | 0.004 | 0.003 | 0.000 | 0.015 | 0 010 | 0.000 | 0.001 | 0.000 | 0.002 | 0.005 | |
| Fe | 2.506 | 2.646 | 2.640 | 2.620 | 2.641 | 2.527 | 2.147 | 2.089 | 2.331 | 2.324 | 2.267 | 2.138 | 2.298 | 2.311 | 2.376 | |
| Mn | 0 035 | 0.035 | 0.043 | 0 049 | 0.049 | 0.046 | 0.014 | 0 005 | 0.018 | 0.014 | 0 007 | 0.045 | 0 039 | 0.028 | 0 018 | |
| Mg | 1.705 | 1.990 | 1.941 | 2.058 | 2.006 | 2.064 | 2.168 | 2.141 | 2.306 | 2.328 | 2.178 | 2.380 | 2.255 | 2.188 | 2.219 | |
| Sum O | 5.806 | 5.958 | 5.923 | 5 987 | 5.964 | 5.931 | 5.738 | 5 692 | 5.851 | 5.863 | 5.783 | 5.878 | 5.891 | 5 943 | 5.980 | |
| Ca | 0.014 | 0.010 | 0.012 | 0.000 | 0.005 | 0.007 | 0.007 | 0.013 | 0.012 | 0.006 | 0.009 | 0.003 | 0.006 | 0 002 | 0.005 | |
| Sum Cations | 9.820 | 9.968 | 9 935 | 9.987 | 9.969 | 9.937 | 9.745 | 9.704 | 9 862 | 9.869 | 9.792 | 9 882 | 9.897 | 9.944 | 9.985 | |
| Mg/(Mg+Fe) | 0.405 | 0.429 | 0.424 | 0.440 | 0.432 | 0.450 | 0.502 | 0.506 | 0 497 | 0.500 | 0 490 | 0 527 | 0.495 | 0.486 | 0.483 | |

Table B-3 (continued)

| Sample no. | SD-60 | SD-99 | | | | | | | SD-193 | | | | | | | | 15/6291 |
|---|---|---|---|---|---|---|---|---|---|---|---|---|---|---|---|---|---|
| Analysis no. | 3 | 1 | 2 | 3 | 4 | 5 | 6 | | 1 | 2 | 3 | 4 | 5 | 6 | 7 | 8 | 1 |
| | C7-Chl3 | C3-Chl1 | C3-Chl2 | C3-Chl3 | C8-Chl4 | C8-Chl5 | C9-Chl6 | | C1-Chl1 | C1-Chl2 | C1-Chl3 | C2-Chl4 | C2-Chl5 | C3-Chl6 | C3-Chl7 | Chl8/Ms | C4-Chl1 |
| SiO2 | 24.96 | 28.27 | 25.00 | 25.32 | 23.14 | 23.48 | 25.12 | | 26.83 | 26.67 | 26.91 | 27.48 | 27.65 | 28.17 | 28.65 | 27.96 | 26.60 |
| TiO2 | 0.05 | 1.02 | 0.12 | 0.02 | 0.05 | 0.10 | 0.12 | | 3.74 | 2.68 | 2.22 | 2.96 | 3.70 | 1.88 | 1.26 | 3.06 | 0.00 |
| Al2O3 | 20.84 | 16.74 | 22.45 | 22.75 | 21.78 | 21.65 | 20.20 | | 19.74 | 20.29 | 20.53 | 20.83 | 20.72 | 18.99 | 19.69 | 19.86 | 18.39 |
| Cr2O3 | 0.00 | 0.00 | 0.04 | 0.00 | 0.00 | 0.07 | 0.14 | | 0.00 | 0.00 | 0.03 | 0.07 | 0.01 | 0.03 | 0.00 | 0.02 | 0.00 |
| FeO* | 25.91 | 24.24 | 22.34 | 22.70 | 31.60 | 32.17 | 26.79 | | 24.43 | 24.57 | 25.12 | 23.31 | 23.36 | 23.21 | 23 03 | 24.02 | 27.11 |
| MnO | 0.21 | 0.06 | 0.41 | 0.24 | 0.21 | 0.12 | 0.20 | | 0.10 | 0.04 | 0.20 | 0.18 | 0.11 | 0.09 | 0.07 | 0.12 | 0.16 |
| MgO | 13.53 | 15.64 | 16.08 | 15.68 | 9.57 | 9.93 | 13.80 | | 11.22 | 11.17 | 11.49 | 11.75 | 10.85 | 12.94 | 12.37 | 11.23 | 13.99 |
| Total | 85.49 | 85.96 | 86.44 | 86.70 | 86.34 | 87.52 | 86.37 | | 86.06 | 85.42 | 86.50 | 86.60 | 86.41 | 85.30 | 85.06 | 86.27 | 86.25 |
| Number of cations on the basis of 14 oxygens: | | | | | | | | | | | | | | | | | |
| Si | 2.711 | 3.012 | 2.632 | 2.655 | 2.576 | 2.582 | 2.715 | | 2.852 | 2.857 | 2.854 | 2.878 | 2.897 | 2.994 | 3.039 | 2.947 | 2.876 |
| Al iv | 1.289 | 0.988 | 1.368 | 1.345 | 1.424 | 1.418 | 1.285 | | 1.148 | 1.143 | 1.146 | 1.122 | 1.103 | 1.006 | 0.961 | 1.053 | 1.124 |
| Sum T | 4.000 | 4.000 | 4.000 | 4.000 | 4.000 | 4.000 | 4.000 | | 4.000 | 4.000 | 4.000 | 4.000 | 4.000 | 4.000 | 4.000 | 4 000 | 4.000 |
| Al vi | 1.379 | 1.114 | 1.418 | 1.467 | 1.434 | 1.389 | 1.290 | | 1.326 | 1.420 | 1.421 | 1.450 | 1.456 | 1.373 | 1.501 | 1.414 | 1.221 |
| Ti | 0.004 | 0.082 | 0.010 | 0.002 | 0.004 | 0.008 | 0.010 | | 0.299 | 0.216 | 0.177 | 0.233 | 0.292 | 0.150 | 0.101 | 0.243 | 0.000 |
| Cr | 0.000 | 0.000 | 0.003 | 0.000 | 0.000 | 0 006 | 0.012 | | 0.000 | 0.000 | 0.003 | 0.006 | 0.001 | 0.003 | 0.000 | 0.002 | 0.000 |
| Fe | 2.353 | 2.160 | 1.967 | 1.991 | 2.942 | 2.958 | 2.422 | | 2.172 | 2.202 | 2.228 | 2.042 | 2.047 | 2.063 | 2.043 | 2.117 | 2.452 |
| Mn | 0.019 | 0.005 | 0.037 | 0.021 | 0.019 | 0.011 | 0.018 | | 0.009 | 0.003 | 0.018 | 0.016 | 0 010 | 0.008 | 0.006 | 0.011 | 0.015 |
| Mg | 2.191 | 2.483 | 2.523 | 2.450 | 1.587 | 1.627 | 2.223 | | 1.778 | 1.784 | 1.815 | 1.834 | 1.695 | 2.049 | 1.956 | 1.763 | 2.255 |
| Sum O | 5.946 | 5.844 | 5.957 | 5.929 | 5.987 | 6.000 | 5.976 | | 5.583 | 5.625 | 5.663 | 5.582 | 5.501 | 5.645 | 5.607 | 5.549 | 5.942 |
| Sum Cations | 9.946 | 9.844 | 9.957 | 9.929 | 9.987 | 10.000 | 9.976 | | 9.583 | 9 625 | 9.663 | 9.582 | 9.501 | 9.645 | 9.607 | 9.549 | 9.942 |
| Mg/(Mg+Fe2) | 0.482 | 0.535 | 0.562 | 0.552 | 0.350 | 0.355 | 0.479 | | 0.450 | 0.448 | 0.449 | 0.473 | 0.453 | 0.498 | 0 489 | 0.454 | 0.479 |

* Total Fe as FeO

Table B-3 (continued)

| Sample no. | 15/6291 | | | | | | SD-42 | | | | | SD-64 | | | | |
|---|---|---|---|---|---|---|---|---|---|---|---|---|---|---|---|---|
| Analysis no. | 2 | 3 | 4 | 5 | 6 | 7 | 1 | 2 | 3 | 4 | 5 | 1 | 2 | 3 | 4 | 5 |
| | C4-Chl2 | C4-Chl3 | C4-Chl4 | C4-Chl5 | C4-Chl6 | C4-Chl7 | C4-Chl1 | C4-Chl2 | C4-Chl5 | C4-Chl4 | C4-Chl5 | C2-Chl1 | C2-Chl2 | C2-Chl4 | C2-Chl5 | C3-Chl6nMs5 |
| SiO2 | 26.73 | 26.78 | 27.02 | 27.07 | 27.45 | 27.38 | 24.67 | 24.90 | 25.27 | 24.82 | 24.79 | 25.76 | 25.36 | 25.34 | 25.74 | 24.55 |
| TiO2 | 0.03 | 0 01 | 0.01 | 0.00 | 0.01 | 0.00 | 0.09 | 0.01 | 0.05 | 0.05 | 0.01 | 0.07 | 0.07 | 0.08 | 0.10 | 0.07 |
| Al2O3 | 18.03 | 18.57 | 18.47 | 18.42 | 18.45 | 18.87 | 20.47 | 20.43 | 19.94 | 20.67 | 20.36 | 19.61 | 20.02 | 20.96 | 20 28 | 21.05 |
| Cr2O3 | 0.04 | 0.00 | 0.00 | 0.03 | 0.06 | 0.04 | 0.10 | 0.01 | 0.01 | 0.00 | 0.01 | 0.07 | 0.01 | 0.05 | 0.06 | 0.04 |
| FeO* | 26.22 | 25.91 | 26.35 | 25.50 | 24.24 | 26.48 | 28.12 | 28.39 | 26.52 | 27.37 | 26.88 | 27.45 | 28.76 | 27.51 | 27.37 | 28.57 |
| MnO | 0.34 | 0.13 | 0.31 | 0.30 | 0.16 | 0.22 | 0.14 | 0.06 | 0.19 | 0.12 | 0.09 | 0.34 | 0.25 | 0.28 | 0.18 | 0.13 |
| MgO | 13.82 | 14.29 | 14.87 | 14.62 | 14.70 | 14.77 | 13.25 | 13.64 | 14.20 | 13.96 | 13.98 | 13.35 | 13.15 | 12.40 | 13.15 | 12.76 |
| Total | 85.21 | 85.69 | 87.03 | 85.94 | 85.07 | 87.76 | 86.82 | 87.45 | 86.18 | 86.99 | 86.13 | 86.66 | 87.62 | 86.61 | 86.88 | 87.17 |
| Number of cations on the basis of 14 oxygens: | | | | | | | | | | | | | | | | |
| Si | 2.917 | 2.895 | 2.884 | 2.913 | 2.957 | 2.892 | 2.673 | 2.678 | 2.734 | 2.671 | 2.690 | 2.781 | 2.727 | 2.734 | 2.765 | 2.653 |
| Al iv | 1.083 | 1.105 | 1.116 | 1.087 | 1.043 | 1.108 | 1.327 | 1.322 | 1.266 | 1.329 | 1.310 | 1.219 | 1.273 | 1.266 | 1.235 | 1.347 |
| Sum T | 4.000 | 4 000 | 4.000 | 4 000 | 4.000 | 4.000 | 4.000 | 4.000 | 4.000 | 4 000 | 4.000 | 4.000 | 4.000 | 4 000 | 4.000 | 4.000 |
| Al vi | 1.236 | 1 262 | 1.208 | 1.249 | 1.299 | 1.242 | 1.288 | 1.269 | 1.277 | 1.292 | 1.295 | 1.278 | 1.265 | 1.399 | 1.335 | 1.334 |
| Ti | 0.002 | 0.001 | 0.001 | 0.000 | 0 001 | 0.000 | 0.007 | 0.001 | 0.004 | 0.004 | 0.000 | 0.005 | 0.005 | 0.006 | 0.008 | 0.005 |
| Cr | 0.003 | 0.000 | 0.000 | 0.003 | 0.005 | 0.003 | 0.008 | 0.001 | 0.001 | 0.000 | 0.001 | 0 006 | 0.001 | 0.004 | 0.005 | 0.003 |
| Fe | 2.393 | 2.343 | 2.352 | 2.295 | 2.183 | 2.339 | 2.548 | 2.554 | 2.400 | 2.463 | 2.440 | 2.479 | 2.587 | 2.482 | 2.459 | 2.581 |
| Mn | 0 031 | 0.012 | 0.028 | 0.027 | 0.015 | 0.020 | 0.012 | 0.005 | 0.017 | 0.011 | 0.009 | 0.031 | 0.022 | 0.026 | 0.016 | 0.012 |
| Mg | 2.247 | 2.302 | 2.365 | 2.344 | 2.360 | 2.325 | 2.139 | 2.187 | 2.290 | 2.238 | 2.262 | 2.148 | 2.107 | 1.993 | 2.105 | 2.055 |
| Sum O | 5.914 | 5.920 | 5.954 | 5.918 | 5.863 | 5.930 | 6.004 | 6.018 | 5.989 | 6.008 | 6.007 | 5.947 | 5.988 | 5.911 | 5.928 | 5.990 |
| Sum Cations | 9.914 | 9.920 | 9.954 | 9.918 | 9.863 | 9.930 | 10.004 | 10.018 | 9.989 | 10.008 | 10.007 | 9.947 | 9.988 | 9.911 | 9.928 | 9.990 |
| Mg/(Mg+Fe2) | 0.484 | 0.496 | 0.501 | 0.505 | 0.519 | 0.498 | 0.456 | 0.461 | 0.488 | 0.476 | 0.481 | 0.464 | 0 449 | 0.445 | 0.461 | 0.443 |

Table B-3 (continued)

| Sample no. | SD-64 | | | | SD-148 | | | | SD-148.1 | | | | | SD-150 | | |
|---|---|---|---|---|---|---|---|---|---|---|---|---|---|---|---|---|
| Analysis no. | 6 | 7 | 8 | 9 | 1 | 2 | 3 | 4 | 1 | 2 | 3 | 4 | 5 | 1 | 2 | 3 |
| | C3-Chl7r | C3-Chl8r | C5-Chl9r | C5-Chl1( | C1-Chl1 | C1-Chl2 | C1-Chl3 | C1-Chl4 | C2-Chl3 | C2-Chl4 | C4-Chl5 | C4-Chl6 | C4-Chl7 | C3-Chl1 | C3-Chl2 | C3-Chl5 |
| SiO2 | 24.67 | 26.34 | 24.45 | 24.82 | 23.34 | 23.52 | 23.42 | 24.08 | 24.96 | 25.25 | 25.09 | 25.06 | 25.34 | 23.10 | 23.54 | 23.68 |
| TiO2 | 0.06 | 0.06 | 0.00 | 0.03 | 0.02 | 0.06 | 0.04 | 0.03 | 0.01 | 0 00 | 0.00 | 0.09 | 0.00 | 0.05 | 0.04 | 0.03 |
| Al2O3 | 21.14 | 22.54 | 21.22 | 21.49 | 22.05 | 22.28 | 22.39 | 22.11 | 21.28 | 21.17 | 21.98 | 21.90 | 21.72 | 20.73 | 20.37 | 21.09 |
| Cr2O3 | 0.00 | 0.04 | 0.00 | 0.14 | 0.00 | 0.04 | 0.00 | 0.00 | 0.07 | 0.04 | 0.00 | 0.00 | 0.03 | 0.17 | 0.04 | 0.07 |
| FeO* | 28.87 | 27.27 | 27.99 | 28.23 | 27.39 | 28.28 | 28.19 | 26.65 | 24.80 | 24.61 | 24.91 | 24.42 | 25.21 | 31.52 | 31.71 | 32.32 |
| MnO | 0 20 | 0.30 | 0.24 | 0.21 | 0.31 | 0.08 | 0.15 | 0.16 | 0.48 | 0.20 | 0.26 | 0.32 | 0.39 | 0.30 | 0.33 | 0.43 |
| MgO | 12.71 | 11.82 | 12.72 | 12.77 | 12.28 | 11.39 | 11.74 | 12.50 | 14.90 | 15.01 | 14.38 | 14.99 | 14.51 | 9.04 | 9.72 | 9.60 |
| Total | 87.65 | 88.39 | 86.61 | 87.71 | 85.39 | 85.65 | 85.94 | 85.53 | 86.50 | 86.29 | 86.61 | 86.77 | 87.21 | 84.91 | 85.76 | 87.22 |
| Number of cations on the basis of 14 oxygens: | | | | | | | | | | | | | | | | |
| Si | 2.655 | 2.765 | 2.652 | 2.657 | 2.569 | 2.587 | 2.567 | 2.626 | 2.665 | 2.695 | 2.670 | 2.657 | 2.684 | 2.623 | 2.645 | 2.620 |
| Al iv | 1.345 | 1.235 | 1.348 | 1.343 | 1.431 | 1.413 | 1.433 | 1.374 | 1.335 | 1.305 | 1.330 | 1.343 | 1.316 | 1.377 | 1.355 | 1.380 |
| Sum T | 4.000 | 4.000 | 4.000 | 4.000 | 4 000 | 4.000 | 4.000 | 4.000 | 4.000 | 4.000 | 4.000 | 4.000 | 4.000 | 4 000 | 4.000 | 4.000 |
| Al vi | 1.336 | 1.555 | 1.366 | 1.369 | 1.431 | 1.476 | 1.462 | 1.468 | 1.345 | 1.358 | 1.428 | 1.394 | 1.397 | 1.398 | 1.344 | 1.371 |
| Ti | 0.005 | 0.005 | 0.000 | 0.003 | 0.002 | 0.005 | 0.003 | 0.003 | 0.000 | 0.000 | 0.000 | 0.007 | 0.000 | 0.004 | 0.004 | 0.003 |
| Cr | 0.000 | 0.004 | 0.000 | 0.012 | 0.000 | 0.004 | 0.000 | 0.000 | 0.006 | 0 003 | 0.000 | 0.000 | 0.003 | 0.015 | 0.004 | 0.006 |
| Fe | 2.599 | 2.394 | 2.539 | 2.528 | 2.522 | 2.602 | 2.584 | 2.430 | 2.215 | 2.197 | 2.217 | 2.165 | 2.233 | 2.993 | 2.980 | 2.991 |
| Mn | 0.018 | 0.027 | 0.022 | 0.019 | 0.028 | 0.007 | 0.014 | 0.015 | 0.043 | 0.018 | 0.023 | 0.029 | 0.035 | 0.029 | 0.031 | 0.040 |
| Mg | 2.039 | 1.849 | 2.056 | 2.038 | 2.015 | 1.867 | 1.919 | 2.031 | 2.372 | 2.387 | 2.281 | 2.368 | 2.290 | 1.529 | 1.627 | 1.582 |
| Sum O | 5.997 | 5 833 | 5.983 | 5.970 | 5.998 | 5.960 | 5.982 | 5.947 | 5.981 | 5.963 | 5.948 | 5.964 | 5.958 | 5.969 | 5.989 | 5.992 |
| Sum Cations | 9.997 | 9.833 | 9.983 | 9.970 | 9.998 | 9.960 | 9.982 | 9.947 | 9.981 | 9.963 | 9.948 | 9.964 | 9.958 | 9.969 | 9.989 | 9.992 |
| Mg/(Mg+Fe2) | 0.440 | 0.436 | 0.447 | 0.446 | 0.444 | 0.418 | 0.426 | 0.455 | 0.517 | 0.521 | 0.507 | 0.522 | 0.506 | 0.338 | 0.353 | 0.346 |

* Total Fe as FeO

Table B-3 (continued)

| Sample no. | SD-150 | SD-165 | | | SD-198 | | | | | SD-209 | | | | | SD-211 | |
|---|---|---|---|---|---|---|---|---|---|---|---|---|---|---|---|---|
| Analysis no. | 4 | 1 | 2 | 3 | 1 | 2 | 3 | 4 | 5 | 1 | 2 | 3 | 4 | 5 | 1 | 2 |
| | C3-Chl4 | C5-Chl1 | C5-Chl2 | C5-Chl5 | C2-Chl1 | C2-Chl2 | C7-Chl5 | C7-Chl6 | C4-Chl8 | C5-Chl2 | C5-Chl3 | C5-Chl4 | C5-Chl5 | C5-Chl6 | C1-Chl1 | C1-Chl3 |
| SiO2 | 22.70 | 29 26 | 24.76 | 29.80 | 26.84 | 26.63 | 27.11 | 27.19 | 26.85 | 25.88 | 25.61 | 26.12 | 26 26 | 26.00 | 29.49 | 25.05 |
| TiO2 | 0.00 | 0.02 | 0.04 | 0.04 | 0.03 | 0.03 | 0.00 | 0.00 | 0.01 | 0.01 | 0.02 | 0.11 | 0.01 | 0.07 | 0.06 | 0.00 |
| Al2O3 | 21.28 | 23.68 | 21.65 | 23.82 | 16.98 | 16.99 | 16.49 | 16.33 | 16.77 | 18.43 | 18.64 | 18.31 | 18.40 | 18.85 | 23.90 | 21.25 |
| Cr2O3 | 0.00 | 0.04 | 0.00 | 0.03 | 0.00 | 0.00 | 0.03 | 0.00 | 0.02 | 0.05 | 0.00 | 0.02 | 0.02 | 0.07 | 0.05 | 0.10 |
| FeO* | 31.61 | 23.85 | 27.54 | 20.97 | 24.58 | 24.76 | 24.25 | 24.25 | 23.80 | 28.05 | 29.09 | 27.74 | 27.58 | 28 88 | 21.55 | 26.40 |
| MnO | 0.40 | 0.13 | 0.24 | 0.14 | 0.45 | 0.33 | 0.33 | 0.37 | 0.38 | 0.63 | 0.38 | 0.38 | 0.57 | 0.50 | 0.11 | 0.11 |
| MgO | 9.27 | 11.43 | 12.99 | 11.17 | 16.91 | 17.28 | 17.68 | 18.11 | 17.70 | 13.41 | 13.11 | 13.57 | 13.61 | 12.30 | 10.15 | 12.41 |
| Total | 85.26 | 88.41 | 87.22 | 85.96 | 85.78 | 86.01 | 85.89 | 86.26 | 85.51 | 86.46 | 86.86 | 86.25 | 86.45 | 86.68 | 85.31 | 85.33 |
| Number of cations on the basis of 14 oxygens: | | | | | | | | | | | | | | | | |
| Si | 2.563 | 2.976 | 2.655 | 3.064 | 2.891 | 2.865 | 2.911 | 2.908 | 2.892 | 2.819 | 2.789 | 2.840 | 2.848 | 2.828 | 3.065 | 2.728 |
| Al iv | 1.437 | 1.024 | 1.345 | 0.936 | 1.109 | 1.135 | 1.089 | 1.092 | 1.108 | 1.181 | 1.211 | 1.160 | 1.152 | 1.172 | 0.935 | 1.272 |
| Sum T | 4.000 | 4.000 | 4.000 | 4.000 | 4.000 | 4.000 | 4.000 | 4 000 | 4.000 | 4.000 | 4 000 | 4.000 | 4.000 | 4.000 | 4.000 | 4.000 |
| Al vi | 1.397 | 1.816 | 1.393 | 1.951 | 1.047 | 1.019 | 0.998 | 0.966 | 1.021 | 1.184 | 1.182 | 1.187 | 1.200 | 1.244 | 1.994 | 1.457 |
| Ti | 0.000 | 0.002 | 0.003 | 0.003 | 0.002 | 0.003 | 0.000 | 0 000 | 0.000 | 0.001 | 0.002 | 0 009 | 0.001 | 0.006 | 0.005 | 0.000 |
| Cr | 0.000 | 0.003 | 0.000 | 0.002 | 0.000 | 0.000 | 0.002 | 0.000 | 0.002 | 0.005 | 0.000 | 0.001 | 0.002 | 0.006 | 0.004 | 0.008 |
| Fe | 2.985 | 2.029 | 2.470 | 1.804 | 2.214 | 2.227 | 2.178 | 2.169 | 2.144 | 2.555 | 2.649 | 2.522 | 2.501 | 2.627 | 1.873 | 2.404 |
| Mn | 0.038 | 0.011 | 0.022 | 0.012 | 0.041 | 0 030 | 0.030 | 0.034 | 0.035 | 0.058 | 0.035 | 0.035 | 0.052 | 0.046 | 0.010 | 0.011 |
| Mg | 1.561 | 1.733 | 2.077 | 1.712 | 2.714 | 2.771 | 2.829 | 2.886 | 2.840 | 2.176 | 2.128 | 2.198 | 2.200 | 1.994 | 1.572 | 2.015 |
| Sum O | 5.981 | 5.593 | 5.965 | 5.485 | 6.018 | 6.051 | 6.037 | 6.056 | 6.042 | 5.979 | 5.997 | 5.953 | 5.956 | 5.924 | 5.458 | 5.895 |
| Sum Cations | 9.981 | 9.593 | 9.965 | 9.485 | 10.018 | 10.051 | 10.037 | 10.056 | 10.042 | 9.979 | 9.997 | 9.953 | 9.956 | 9.924 | 9.458 | 9.895 |
| Mg/(Mg+Fe2) | 0.343 | 0.461 | 0.457 | 0.487 | 0.551 | 0.554 | 0.565 | 0.571 | 0.570 | 0.460 | 0.445 | 0.466 | 0.468 | 0.432 | 0.456 | 0.456 |

Table B-3 (continued)

| Sample no. | SD-211 | | SD-213 | | | | | SD-217 | SD-221 | | | | | P-102 | | |
|---|---|---|---|---|---|---|---|---|---|---|---|---|---|---|---|---|
| Analysis no. | 3 | 4 | 1 | 2 | 3 | 4 | 5 | 1 | 1 | 2 | 3 | 4 | 5 | 1 | 2 | 3 |
| | C1-Chl4 | C3-Chl5 | C3-Chl1 | C3-Chl2 | C3-Chl3 | C3-Chl4 | C3-Chl5 | C1-Chl3 | C6-Chl1 | C6-Chl2 | C6-Chl3 | C6-Chl4 | C6-Chl5 | C7-Chl2 | C7-Chl3 | C7-Chl4 |
| SiO2 | 24.84 | 24.36 | 25.31 | 25.29 | 26.55 | 25.60 | 24.97 | 25.04 | 24.63 | 29.80 | 24.54 | 24.60 | 24.91 | 26.22 | 26.40 | 25.57 |
| TiO2 | 0.04 | 0.04 | 0.09 | 0.01 | 0.05 | 0.09 | 0.05 | 0.19 | 0.00 | 0.00 | 0.00 | 0.00 | 0.00 | 0.01 | 0.00 | 0.05 |
| Al2O3 | 22.25 | 21.70 | 18.73 | 18.89 | 20.21 | 19.44 | 19.37 | 20.35 | 22.22 | 24.29 | 22.29 | 21.91 | 22.03 | 19.75 | 20.06 | 19.51 |
| Cr2O3 | 0.00 | 0.07 | 0.10 | 0.00 | 0 01 | 0.00 | 0.00 | 0.06 | 0.06 | 0.06 | 0.00 | 0.01 | 0.04 | 0.00 | 0.00 | 0.08 |
| FeO* | 25.55 | 26.92 | 26.73 | 26.48 | 25.63 | 26.57 | 26.36 | 27.56 | 26.07 | 20.35 | 25.34 | 25.55 | 24.99 | 29.59 | 29.62 | 29.58 |
| MnO | 0.15 | 0.12 | 0.30 | 0.18 | 0.16 | 0.22 | 0.30 | 0.38 | 0.23 | 0.26 | 0.38 | 0.31 | 0.25 | 0.23 | 0.26 | 0.23 |
| MgO | 11.96 | 12.53 | 13.37 | 13.15 | 12.33 | 13.31 | 12.95 | 12.01 | 13.45 | 11.11 | 13.28 | 13.41 | 13.59 | 12.77 | 13.07 | 12.64 |
| Total | 84.79 | 85.75 | 84.63 | 84.01 | 84.95 | 85.23 | 84.02 | 85.59 | 86.66 | 85.88 | 85.84 | 85.78 | 85.82 | 88.57 | 89.42 | 87.65 |
| Number of cations on the basis of 14 oxygens: | | | | | | | | | | | | | | | | |
| Si | 2.707 | 2.652 | 2.798 | 2.808 | 2.882 | 2.800 | 2.774 | 2.741 | 2.636 | 3 056 | 2.645 | 2.654 | 2.676 | 2.793 | 2.783 | 2.760 |
| Al iv | 1.293 | 1.348 | 1.202 | 1.192 | 1.118 | 1.200 | 1.226 | 1.259 | 1.364 | 0.944 | 1.355 | 1.346 | 1.324 | 1.207 | 1.217 | 1.240 |
| Sum T | 4.000 | 4.000 | 4.000 | 4.000 | 4.000 | 4.000 | 4.000 | 4.000 | 4.000 | 4.000 | 4.000 | 4.000 | 4.000 | 4.000 | 4.000 | 4.000 |
| Al vi | 1.567 | 1.437 | 1.240 | 1.280 | 1.469 | 1.306 | 1.311 | 1.368 | 1.439 | 1.994 | 1.477 | 1.441 | 1.466 | 1.273 | 1.275 | 1.243 |
| Ti | 0.003 | 0.003 | 0.008 | 0.001 | 0.004 | 0.007 | 0.005 | 0.016 | 0.000 | 0 000 | 0.000 | 0.000 | 0.000 | 0 001 | 0.000 | 0.004 |
| Cr | 0.000 | 0.006 | 0.009 | 0.000 | 0.001 | 0.000 | 0.000 | 0.005 | 0.005 | 0.005 | 0.000 | 0.001 | 0.003 | 0.000 | 0.000 | 0.007 |
| Fe | 2.329 | 2.450 | 2.472 | 2.459 | 2.327 | 2.431 | 2.449 | 2.524 | 2.333 | 1.746 | 2.283 | 2.305 | 2.245 | 2.636 | 2.610 | 2.670 |
| Mn | 0.014 | 0.011 | 0.028 | 0.017 | 0.015 | 0.021 | 0.028 | 0.035 | 0 021 | 0.023 | 0.034 | 0.029 | 0.023 | 0.021 | 0.023 | 0.021 |
| Mg | 1.943 | 2.032 | 2.203 | 2.177 | 1.995 | 2.169 | 2.144 | 1.960 | 2.145 | 1.699 | 2.133 | 2.156 | 2.176 | 2.027 | 2.053 | 2.034 |
| Sum O | 5.856 | 5.940 | 5.959 | 5.935 | 5.811 | 5.933 | 5.937 | 5.907 | 5.942 | 5.466 | 5.928 | 5.931 | 5.913 | 5.958 | 5.962 | 5.979 |
| Sum Cations | 9.856 | 9.940 | 9.959 | 9.935 | 9.811 | 9.933 | 9.937 | 9.907 | 9.942 | 9.466 | 9.928 | 9.931 | 9.913 | 9.958 | 9.962 | 9.979 |
| Mg/(Mg+Fe2) | 0.455 | 0.453 | 0.471 | 0.470 | 0.462 | 0.472 | 0.467 | 0.437 | 0.479 | 0.493 | 0.483 | 0.483 | 0.492 | 0.435 | 0.440 | 0.432 |

* Total Fe as FeO

Table B-3 (continued)

| Sample no. | P-102 | P-104 | | | | | | | | |
|---|---|---|---|---|---|---|---|---|---|---|
| Analysis no. | 4 | 1 | 2 | 3 | 4 | 5 | 6 | 7 | 8 | 9 |
| | C1-Chl5 | C8 Chl1 | C8 Chl2 | C8 Chl3 | C8 Chl4 | C8 Chl5 | C9 Chl6 | C9 Chl7 | C9 Chl8 | C9 Chl9 |
| SiO2 | 26.03 | 26.01 | 26.53 | 26.48 | 25.83 | 26.47 | 25.88 | 25.88 | 26.11 | 26.65 |
| TiO2 | 0.04 | 0.00 | 0.00 | 0.03 | 0.01 | 0.07 | 0.00 | 0.00 | 0.04 | 0.04 |
| Al2O3 | 19.45 | 19.54 | 19.34 | 19.13 | 19.86 | 19.41 | 19.72 | 19.54 | 19.46 | 19.45 |
| Cr2O3 | 0.09 | 0.01 | 0.01 | 0.00 | 0.02 | 0.08 | 0.04 | 0.00 | 0.00 | 0.03 |
| FeO* | 28.13 | 25.84 | 25.15 | 25.53 | 24.88 | 25.45 | 24.93 | 26.20 | 24.97 | 25.15 |
| MnO | 0.20 | 0.28 | 0.27 | 0.25 | 0.10 | 0.29 | 0.27 | 0.23 | 0.23 | 0.28 |
| MgO | 13.35 | 15.63 | 15.66 | 16.14 | 15.83 | 16.29 | 15.84 | 15.03 | 15.93 | 15.95 |
| Total | 87.29 | 87.31 | 86.96 | 87.56 | 86.53 | 88.07 | 86.68 | 86.88 | 86.73 | 87.53 |
| Number of cations on the basis of 14 oxygens: | | | | | | | | | | |
| Si | 2.795 | 2.762 | 2.815 | 2.797 | 2.752 | 2.778 | 2.757 | 2.767 | 2.778 | 2.806 |
| Al iv | 1.205 | 1.238 | 1.185 | 1.203 | 1.248 | 1.222 | 1.243 | 1.233 | 1.222 | 1.194 |
| Sum T | 4.000 | 4.000 | 4.000 | 4.000 | 4.000 | 4.000 | 4.000 | 4.000 | 4.000 | 4.000 |
| Al vi | 1.257 | 1.209 | 1.234 | 1.178 | 1.247 | 1.180 | 1.234 | 1.230 | 1.219 | 1.220 |
| Ti | 0.003 | 0.000 | 0.000 | 0.003 | 0.001 | 0.006 | 0.000 | 0.000 | 0.003 | 0.003 |
| Cr | 0.008 | 0.001 | 0.001 | 0.000 | 0.001 | 0.007 | 0.003 | 0.000 | 0.000 | 0.003 |
| Fe | 2.527 | 2.295 | 2.232 | 2.254 | 2.217 | 2.234 | 2.221 | 2.343 | 2.222 | 2.215 |
| Mn | 0.018 | 0.026 | 0.024 | 0.022 | 0.009 | 0.026 | 0.024 | 0.021 | 0.020 | 0.025 |
| Mg | 2.136 | 2.474 | 2.476 | 2.540 | 2.514 | 2.549 | 2.514 | 2.395 | 2.526 | 2.503 |
| Sum O | 5.949 | 6.004 | 5.967 | 5.998 | 5.989 | 6.000 | 5.996 | 5.988 | 5.991 | 5.968 |
| Sum Cations | 9.949 | 10.004 | 9.967 | 9.998 | 9.989 | 10.000 | 9.996 | 9.988 | 9.991 | 9.968 |
| Mg/(Mg+Fe2) | 0.458 | 0.519 | 0.526 | 0.530 | 0.531 | 0.533 | 0.531 | 0.506 | 0.532 | 0.531 |

* Total Fe as FeO

Table B-4 Electron microprobe analyses of epidotes (metasediments of the Pha Som Metamorphic Complex).

| Sample no. | 5/8291 | | 3/8291 | | | SD-225 | | | | | | SD-227 | | | | |
|---|---|---|---|---|---|---|---|---|---|---|---|---|---|---|---|---|
| Analysis no. | 1 | 2 | 1 | 2 | 3 | 1 | 2 | 3 | 4 | 5 | 6 | 1 | 2 | 3 | 4 | 5 |
| | | | | | | C1-Ep1 | C1-Ep2 | C1-Ep3 | C2-Ep4 | C2-Ep5 | C2-Ep6 | C6-Ep1 | C6-Ep2 | C6-Ep3 | C7-Ep5 | C7-Ep6 |
| SiO2 | 37 71 | 37.79 | 37.64 | 37.85 | 37.62 | 37.78 | 38.02 | 37.91 | 37.15 | 36.90 | 36.56 | 37.15 | 37.49 | 36.47 | 37 13 | 37 07 |
| TiO2 | 0.11 | 0.11 | 0.03 | 0.04 | 0.02 | 0 00 | 0.00 | 0.04 | 0.02 | 0.00 | 0.05 | 0.56 | 0.21 | 1.09 | 0.06 | 0.05 |
| Al2O3 | 21 68 | 21.65 | 24.59 | 24.72 | 24.01 | 25.54 | 26.38 | 25 26 | 23.27 | 22.32 | 21.07 | 23.02 | 22.72 | 22.00 | 23.39 | 23.43 |
| Fe2O3* | 14.16 | 13.90 | 12.19 | 12.02 | .10.69 | 10.40 | 9.25 | 11.11 | 14.42 | 14.22 | 15.82 | 12.84 | 14.09 | 13.85 | 13.83 | 13.52 |
| MnO | 0.12 | 0.40 | 0.01 | 0.17 | 0.27 | 0.31 | 0.20 | 0 10 | 0.08 | 0.00 | 0.06 | 0.36 | 0.19 | 0.21 | 0.20 | 0.17 |
| MgO | 0.01 | 0.00 | 0.05 | 0.05 | 0.00 | 0 02 | 0.02 | 0 00 | 0.02 | 0.00 | 0 03 | 0 07 | 0.23 | 0.18 | 0 01 | 0.01 |
| CaO | 22.74 | 22.94 | 24.04 | 23.75 | 24.01 | 24 05 | 24.35 | 24 52 | 24.45 | 24.07 | 23.35 | 24.01 | 23.88 | 24.01 | 24.44 | 24.41 |
| Total | 96.53 | 96.79 | 98.55 | 98.60 | 96.62 | 98.10 | 98.23 | 98.95 | 99.41 | 97.50 | 96.94 | 98.01 | 98.80 | 97.80 | 99 07 | 98.68 |
| Number of cations on the basis of 12.5 oxygens: | | | | | | | | | | | | | | | | |
| Si | 3.053 | 3.055 | 2.970 | 2.981 | 3.019 | 2.979 | 2.981 | 2.972 | 2.938 | 2.974 | 2.979 | 2.968 | 2.976 | 2.936 | 2.943 | 2.947 |
| Al iv | 0.000 | 0.000 | 0.030 | 0 019 | 0.000 | 0 021 | 0.019 | 0.028 | 0.062 | 0.026 | 0.021 | 0.032 | 0.024 | 0.064 | 0.057 | 0.053 |
| Sum Z | 3 053 | 3.055 | 3.000 | 3.000 | 3.019 | 3.000 | 3 000 | 3 000 | 3.000 | 3.000 | 3.000 | 3.000 | 3.000 | 3.000 | 3 000 | 3.000 |
| Al vi | 2.069 | 2.063 | 2.258 | 2.277 | 2.272 | 2.353 | 2.419 | 2.306 | 2.108 | 2.095 | 2.003 | 2.135 | 2.103 | 2.023 | 2.129 | 2.143 |
| Ti | 0.007 | 0.007 | 0.002 | 0.002 | 0.001 | 0.000 | 0.000 | 0 002 | 0.001 | 0.000 | 0 003 | 0.034 | 0.012 | 0 066 | 0 003 | 0.003 |
| Fe3+ | 0 863 | 0.846 | 0.724 | 0.712 | 0.646 | 0.617 | 0.546 | 0.656 | 0.858 | 0.862 | 0.970 | 0.772 | 0.842 | 0.839 | 0.825 | 0.809 |
| Sum Y | 2.939 | 2.915 | 2.983 | 2.991 | 2.919 | 2.970 | 2.965 | 2.964 | 2.967 | 2.957 | 2.975 | 2.941 | 2.957 | 2.928 | 2.957 | 2.955 |
| Mn | 0 008 | 0.027 | 0.001 | 0.011 | 0.018 | 0.021 | 0.014 | 0.007 | 0.005 | 0.000 | 0.004 | 0.024 | 0.013 | 0.014 | 0.014 | 0.012 |
| Mg | 0.001 | 0.000 | 0.006 | 0.006 | 0.000 | 0 002 | 0.002 | 0.000 | 0.002 | 0.000 | 0.004 | 0.008 | 0.027 | 0.022 | 0.002 | 0.001 |
| Ca | 1.973 | 1.987 | 2.033 | 2.004 | 2.065 | 2.032 | 2.046 | 2.060 | 2 072 | 2.078 | 2.038 | 2.055 | 2.031 | 2.071 | 2.075 | 2.079 |
| Sum W | 1.982 | 2.014 | 2.039 | 2.022 | 2.083 | 2 055 | 2 062 | 2.067 | 2.079 | 2.078 | 2.046 | 2.088 | 2.071 | 2.107 | 2.091 | 2.092 |
| Sum Cations | 7.974 | 7.984 | 8.022 | 8.013 | 8.021 | 8.025 | 8.027 | 8.031 | 8.047 | 8.035 | 8.021 | 8.029 | 8.027 | 8.035 | 8.048 | 8.047 |
| Fe3/(Fe3+Al) | 0.294 | 0 291 | 0.240 | 0.237 | 0.221 | 0.206 | 0.183 | 0.219 | 0 283 | 0.289 | 0.324 | 0.263 | 0.284 | 0.287 | 0.274 | 0 269 |

Table B-4 (continued)

| Sample no. | SD-227 | SD-60 | | 1/6291 | | | 15/6291 | | | | | SD-104 | | | |
|---|---|---|---|---|---|---|---|---|---|---|---|---|---|---|---|
| Analysis no. | 6 | 1 | 2 | 1 | 2 | 3 | 1 | 2 | 3 | 4 | 5 | 1 | 2 | 3 | 4 |
| | C7-Ep7 | C7-Ep1 | C7-Ep2 | | | | C8-Ep1 | C8-Ep2 | C8-Ep3 | C7-Ep4 | C7-Ep5 | C4-Ep1 | C4-Ep2 | C3-Ep3 | C3-Ep4 |
| SiO2 | 37.01 | 36.47 | 36.77 | 37 66 | 36.96 | 37.72 | 37.95 | 37.84 | 37.58 | 37.31 | 36.77 | 36.64 | 37.17 | 36.89 | 36.84 |
| TiO2 | 0.07 | 0.22 | 0.33 | 0.03 | 0 05 | 0.06 | 0.06 | 0.14 | 0.08 | 0.07 | 0.12 | 0 02 | 0.00 | 0.01 | 0.03 |
| Al2O3 | 23.44 | 21.34 | 22.04 | 22.87 | 20.91 | 22.92 | 24.16 | 24.14 | 24.07 | 21.39 | 21.42 | 22.18 | 22.03 | 20.10 | 20.08 |
| Fe2O3* | 13.45 | 14.82 | 13.89 | 13.28 | 16.10 | 13.58 | 12.13 | 11.60 | 11.71 | 15.80 | 15.93 | 13.39 | 14.68 | 16.99 | 16.83 |
| MnO | 0.11 | 0.18 | 0 09 | 0.00 | 0.00 | 0.00 | 0 03 | 0.16 | 0.06 | 0.17 | 0.14 | 0.25 | 0.36 | 0.26 | 0.30 |
| MgO | 0.00 | 0.01 | 0.00 | 0.05 | 0.00 | 0.00 | 0 04 | 0.00 | 0.00 | 0.00 | 0 00 | 0.02 | 0.04 | 0.01 | 0.00 |
| CaO | 24.01 | 23.53 | 23.52 | 22.60 | 23.65 | 23.38 | 23.66 | 23.68 | 23.52 | 23.58 | 23 82 | 22.61 | 23.13 | 23 22 | 23.19 |
| Total | 98.10 | 96.57 | 96.65 | 96.49 | 97.67 | 97 66 | 98.03 | 97.56 | 97.02 | 98.32 | 98 20 | 95.12 | 97.41 | 97.49 | 97.28 |
| Number of cations on the basis of 12.5 oxygens: | | | | | | | | | | | | | | | |
| Si | 2.954 | 2.977 | 2.985 | 3.035 | 2.990 | 3.014 | 3 005 | 3.009 | 3 005 | 2.994 | 2 961 | 3.010 | 2.997 | 3.001 | 3.004 |
| Al iv | 0.046 | 0.023 | 0.015 | 0.000 | 0.010 | 0 000 | 0.000 | 0.000 | 0 000 | 0.006 | 0.039 | 0.000 | 0 003 | 0.000 | 0 000 |
| Sum Z | 3.000 | 3.000 | 3.000 | 3 035 | 3.000 | 3.014 | 3 005 | 3.009 | 3.005 | 3.000 | 3 000 | 3.010 | 3.000 | 3.001 | 3.004 |
| Al vi | 2.160 | 2 032 | 2.095 | 2.173 | 1.985 | 2.159 | 2.256 | 2.263 | 2.269 | 2.017 | 1.994 | 2.149 | 2.092 | 1.928 | 1.929 |
| Ti | 0.004 | 0 013 | 0.020 | 0.002 | 0.003 | 0.004 | 0.004 | 0.008 | 0.005 | 0.004 | 0.007 | 0.001 | 0.000 | 0 000 | 0.002 |
| Fe3+ | 0 808 | 0.910 | 0.848 | 0.805 | 0.981 | 0.817 | 0.723 | 0.694 | 0.705 | 0.954 | 0.966 | 0.828 | 0.891 | 1.040 | 1.032 |
| Sum Y | 2.972 | 2.955 | 2.963 | 2.980 | 2.969 | 2.979 | 2.982 | 2.966 | 2.979 | 2.975 | 2.967 | 2 978 | 2.982 | 2.969 | 2.963 |
| Mn | 0 008 | 0.012 | 0.006 | 0.000 | 0.000 | 0.000 | 0.002 | 0.011 | 0.004 | 0.012 | 0.010 | 0.018 | 0.025 | 0.018 | 0.021 |
| Mg | 0.000 | 0 001 | 0.000 | 0.006 | 0.000 | 0.000 | 0.005 | 0.000 | 0.000 | 0.000 | 0.000 | 0.003 | 0.005 | 0.002 | 0.000 |
| Ca | 2.054 | 2.058 | 2.046 | 1.952 | 2.050 | 2.002 | 2.008 | 2.018 | 2.015 | 2.027 | 2.055 | 1.991 | 1.999 | 2.025 | 2.026 |
| Sum W | 2.062 | 2.072 | 2.052 | 1.958 | 2.050 | 2.002 | 2.014 | 2.029 | 2.019 | 2.039 | 2.065 | 2.011 | 2.028 | 2.044 | 2.047 |
| Sum Cations | 8 035 | 8.027 | 8.016 | 7.974 | 8.019 | 7.995 | 8.002 | 8.004 | 8.003 | 8.014 | 8.032 | 8.000 | 8.010 | 8.014 | 8.014 |
| Fe3/(Fe3+Al) | 0 268 | 0.307 | 0.287 | 0.270 | 0 330 | 0.274 | 0.243 | 0.235 | 0.237 | 0 320 | 0.322 | 0 278 | 0.298 | 0.350 | 0 349 |

* Total Fe as Fe2O3

Table B-4 (continued)

| Sample no. | SD-104 | SD-148.1 | | | | | SD-165 | | | | | SD-198 | | | | SD-209 |
|---|---|---|---|---|---|---|---|---|---|---|---|---|---|---|---|---|
| Analysis no. | 5 | 1 | 2 | 3 | 4 | 5 | 1 | 2 | 3 | 4 | 5 | 1 | 2 | 3 | 4 | 1 |
| | C3-Ep5 | C4-Ep1 | C4-Ep2 | C3-Ep3 | C3-Ep4 | C3-Ep5 | C4-Ep1 | C4-Ep2 | C4-Ep3 | C4-Ep4 | C4-Ep5 | C2-Ep3 | C2-Ep4 | C2-Ep5 | C2-Ep1 | C5-Ep1 |
| SiO2 | 36.84 | 36 64 | 37.17 | 36.89 | 36.84 | 36 84 | 37.76 | 36.87 | 37.46 | 36.61 | 37.32 | 36.78 | 36.48 | 36.25 | 37.11 | 37.39 |
| TiO2 | 0.03 | 0.02 | 0 00 | 0 01 | 0.03 | 0.03 | 0.05 | 0.01 | 0.05 | 0.02 | 0.06 | 0.10 | 0.00 | 0 07 | 0 03 | 0 03 |
| Al2O3 | 20.08 | 22.18 | 22.03 | 20.10 | 20.08 | 20 08 | 21.81 | 21.84 | 23.27 | 23.10 | 22.28 | 20.27 | 20.49 | 20 65 | 21.55 | 22.67 |
| Fe2O3* | 16 83 | 13.39 | 14.68 | 16.99 | 16.83 | 16.83 | 13.56 | 14.87 | 13.65 | 13.71 | 14.33 | 16.25 | 15.55 | 16.43 | 15.35 | 14.07 |
| MnO | 0.30 | 0.25 | 0.36 | 0.26 | 0.30 | 0.30 | 0.05 | 0.00 | 0.01 | 0.20 | 0.14 | 0.11 | 0.30 | 0.26 | 0.33 | 0 00 |
| MgO | 0.00 | 0 02 | 0.04 | 0.01 | 0.00 | 0 00 | 0.00 | 0.00 | 0 00 | 0 00 | 0.00 | 0.00 | 0.00 | 0 00 | 0.00 | 0.12 |
| CaO | 23.19 | 22.61 | 23.13 | 23.22 | 23.19 | 23.19 | 23.35 | 23.33 | 23.76 | 23.47 | 23.71 | 23.41 | 23 01 | 23.13 | 23.17 | 23 88 |
| Total | 97.28 | 95.12 | 97.41 | 97.49 | 97.28 | 97.28 | 96.58 | 96.91 | 98.20 | 97.12 | 97 84 | 96.92 | 95.84 | 96.79 | 97.54 | 98.16 |
| Number of cations on the basis of 12.5 oxygens: | | | | | | | | | | | | | | | | |
| Si | 3.004 | 3.010 | 2.997 | 3.001 | 3.004 | 3.004 | 3.054 | 2.990 | 2.982 | 2.954 | 2.994 | 3.003 | 3.007 | 2.968 | 2.997 | 2.985 |
| Al iv | 0.000 | 0.000 | 0.003 | 0.000 | 0.000 | 0.000 | 0.000 | 0.010 | 0.018 | 0.046 | 0.006 | 0.000 | 0.000 | 0.032 | 0.003 | 0 015 |
| Sum Z | 3 004 | 3.010 | 3.000 | 3.001 | 3.004 | 3.004 | 3.054 | 3.000 | 3 000 | 3.000 | 3.000 | 3 003 | 3 007 | 3.000 | 3.000 | 3 000 |
| Al vi | 1.929 | 2.149 | 2.092 | 1.928 | 1.929 | 1.929 | 2.080 | 2.077 | 2.166 | 2.152 | 2.100 | 1.951 | 1.991 | 1.961 | 2.048 | 2.119 |
| Ti | 0.002 | 0.001 | 0.000 | 0 000 | 0.002 | 0.002 | 0.003 | 0.001 | 0 003 | 0.001 | 0.004 | 0.006 | 0.000 | 0.004 | 0.002 | 0.002 |
| Fe3+ | 1.032 | 0.828 | 0.891 | 1.040 | 1.032 | 1.032 | 0 826 | 0.907 | 0.818 | 0.833 | 0.865 | 0.999 | 0.965 | 1 012 | 0.933 | 0.845 |
| Sum Y | 2.963 | 2.978 | 2.982 | 2.969 | 2.963 | 2.963 | 2.909 | 2.985 | 2.987 | 2.986 | 2.970 | 2.956 | 2.955 | 2.978 | 2.983 | 2.966 |
| Mn | 0.021 | 0 018 | 0.025 | 0.018 | 0.021 | 0.021 | 0.003 | 0 000 | 0.001 | 0.014 | 0.009 | 0.008 | 0.021 | 0 018 | 0.022 | 0.000 |
| Mg | 0.000 | 0 003 | 0.005 | 0.002 | 0.000 | 0.000 | 0.000 | 0.000 | 0 000 | 0.000 | 0.000 | 0 000 | 0.000 | 0.000 | 0.000 | 0.014 |
| Ca | 2.026 | 1.991 | 1.999 | 2.025 | 2.026 | 2.026 | 2.024 | 2.027 | 2.027 | 2.029 | 2.038 | 2.048 | 2.032 | 2.029 | 2.005 | 2 043 |
| Sum W | 2.047 | 2.011 | 2.028 | 2.044 | 2.047 | 2 047 | 2.027 | 2.027 | 2.027 | 2.043 | 2.047 | 2.056 | 2.053 | 2.047 | 2.027 | 2.057 |
| Sum Cations | 8.014 | 8.000 | 8 010 | 8.014 | 8.014 | 8.014 | 7.990 | 8.012 | 8.014 | 8 029 | 8.016 | 8.015 | 8.015 | 8.025 | 8.009 | 8.024 |
| Fe3/(Fe3+Al) | 0.349 | 0.278 | 0.298 | 0.350 | 0.349 | 0.349 | 0 284 | 0.303 | 0 272 | 0.275 | 0.291 | 0.339 | 0.326 | 0.337 | 0.313 | 0 284 |

Table B-4 (continued)

| Sample no. | | | | | | SD-217 | | | | | | SD-221 | | | P-102 | |
|---|---|---|---|---|---|---|---|---|---|---|---|---|---|---|---|---|
| Analysis no. | 2 | 3 | 4 | 5 | 6 | 1 | 2 | 3 | 4 | 5 | 6 | 1 | 2 | 3 | 1 | 2 |
| | C5-Ep2 | C1-Ep4 | C3-Ep6 | C6-Ep7 | C6-Ep8 | C6-Ep1 | C6-Ep2 | C6-Ep3 | C7-Ep4 | C8-Ep5 | C8-Ep6 | C1-Ep6 | C1-Ep7 | C1-Ep8 | C1-Ep1 | C1-Ep2 |
| SiO2 | 37.35 | 37.17 | 36.73 | 37.00 | 38.16 | 37.41 | 37.04 | 37.37 | 37.67 | 37.41 | 37.46 | 36.87 | 37.11 | 37.34 | 36.84 | 37.02 |
| TiO2 | 0.01 | 0.08 | 0.06 | 0.01 | 0.03 | 0 01 | 0.15 | 0.04 | 0.09 | 0.09 | 0.02 | 0.12 | 0.03 | 0.06 | 0.07 | 0.04 |
| Al2O3 | 23.17 | 23.29 | 23.59 | 24.15 | 23.38 | 23.97 | 23.36 | 24.72 | 25.59 | 24.09 | 22.82 | 20.78 | 21.31 | 22.18 | 21.33 | 21.28 |
| Fe2O3* | 13.82 | 12.72 | 11.67 | 10 69 | 10.63 | 11.95 | 13.16 | 11.84 | 9.95 | 11.47 | 13.57 | 16.21 | 15.59 | 14.96 | 15.45 | 15.87 |
| MnO | 0.20 | 0.20 | 0.23 | 0.22 | 0.28 | 0.09 | 0.47 | 0.01 | 0.42 | 0.76 | 0.31 | 0.18 | 0.39 | 0.16 | 0.52 | 0.35 |
| MgO | 0.08 | 0 10 | 0.22 | 0.10 | 0.17 | 0.05 | 0.02 | 0.04 | 0 00 | 0.05 | 0.01 | 0.05 | 0.15 | 0.00 | 0.11 | 0.03 |
| CaO | 23.96 | 23.59 | 23.23 | 22.86 | 22.90 | 24.16 | 23.79 | 24.39 | 23.78 | 23.55 | 23.84 | 24.03 | 23.66 | 23.83 | 22.55 | 22.18 |
| Total | 98.59 | 97.16 | 95.72 | 95.02 | 95.54 | 97.64 | 97.99 | 98.41 | 97.49 | 97.41 | 98 02 | 98.24 | 98.25 | 98.52 | 96.87 | 96.76 |
| Number of cations on the basis of 12.5 oxygens: | | | | | | | | | | | | | | | | |
| Si | 2 969 | 2.986 | 2.984 | 3.011 | 3.083 | 2.983 | 2.961 | 2.955 | 2.984 | 2.989 | 2.993 | 2.975 | 2.984 | 2.982 | 2.996 | 3.010 |
| Al iv | 0.031 | 0.014 | 0.016 | 0.000 | 0.000 | 0.017 | 0 039 | 0.045 | 0.016 | 0.011 | 0.007 | 0.025 | 0 016 | 0.018 | 0.004 | 0.000 |
| Sum Z | 3.000 | 3 000 | 3.000 | 3.011 | 3.083 | 3.000 | 3 000 | 3.000 | 3.000 | 3.000 | 3.000 | 3.000 | 3.000 | 3.000 | 3.000 | 3.010 |
| Al vi | 2.140 | 2.191 | 2.244 | 2.317 | 2 227 | 2.237 | 2.162 | 2.259 | 2.374 | 2.258 | 2.143 | 1.951 | 2.004 | 2.069 | 2.041 | 2.040 |
| Ti | 0 000 | 0.005 | 0.003 | 0.000 | 0.002 | 0.001 | 0.009 | 0.002 | 0.005 | 0.006 | 0.001 | 0.007 | 0.002 | 0 004 | 0.005 | 0.002 |
| Fe3+ | 0.827 | 0.769 | 0.714 | 0 654 | 0.646 | 0.717 | 0.792 | 0.705 | 0.593 | 0.690 | 0.816 | 0.984 | 0.944 | 0.899 | 0.945 | 0.971 |
| Sum Y | 2.967 | 2.965 | 2.961 | 2.972 | 2.875 | 2.955 | 2.963 | 2.966 | 2.972 | 2.953 | 2.960 | 2.942 | 2.949 | 2.972 | 2.991 | 3.013 |
| Mn | 0 013 | 0.014 | 0.016 | 0.015 | 0.019 | 0.006 | 0.032 | 0.001 | 0.028 | 0.051 | 0.021 | 0.012 | 0.026 | 0.011 | 0.036 | 0.024 |
| Mg | 0.010 | 0.012 | 0.026 | 0.013 | 0.021 | 0.006 | 0.002 | 0.005 | 0.000 | 0.005 | 0.001 | 0.006 | 0.018 | 0.000 | 0.013 | 0.004 |
| Ca | 2.041 | 2.031 | 2.022 | 1.993 | 1.982 | 2.064 | 2.037 | 2.066 | 2.019 | 2.016 | 2.041 | 2.077 | 2.038 | 2.039 | 1.964 | 1.932 |
| Sum W | 2.064 | 2.057 | 2.064 | 2.021 | 2.022 | 2.076 | 2.071 | 2.072 | 2.047 | 2.073 | 2.063 | 2.095 | 2.083 | 2.050 | 2.014 | 1.961 |
| Sum Cations | 8 032 | 8.022 | 8.025 | 8.003 | 7.979 | 8.031 | 8.034 | 8.038 | 8.019 | 8.026 | 8.023 | 8.038 | 8.032 | 8.021 | 8.004 | 7.983 |
| Fe3/(Fe3+Al) | 0 276 | 0.259 | 0.240 | 0 220 | 0 225 | 0 241 | 0.264 | 0.234 | 0.199 | 0.233 | 0 275 | 0.332 | 0.318 | 0.301 | 0.316 | 0.322 |

* Total Fe as Fe2O3

Table B-4 (continued)

| Sample no. | P-102 | | | P-104 | | | | | | | | | | | | |
|---|---|---|---|---|---|---|---|---|---|---|---|---|---|---|---|---|
| Analysis no. | 3 | 4 | 5 | 1 | 2 | 3 | 4 | 5 | 6 | | 7 | 8 | 9 | 10 | 11 | 12 |
| | C5-Ep5 | C6-Ep6 | C6-Ep7 | C4-Ep2 | C5-Ep3 | C5-Ep4 | C9-Ep5 | C14-Ep6 | Core | First | | | | | | |
| SiO2 | 37.65 | 37 81 | 37.70 | 37.54 | 37.27 | 37.19 | 37.39 | 37.20 | 37.93 | 37.90 | 37.70 | 37 65 | 37.71 | 37 92 | 37.86 | 37.48 |
| TiO2 | 0.00 | 0.00 | 0.02 | 0.06 | 0.15 | 0.20 | 0.06 | 0.07 | 0.11 | 0.00 | 0.14 | 0.20 | 0.22 | 0 05 | 0.00 | 0.03 |
| Al2O3 | 23.30 | 24.34 | 24.57 | 23.60 | 23.24 | 22.81 | 24 98 | 22.80 | 24.86 | 26.46 | 24.66 | 24 45 | 24 01 | 26 98 | 26 81 | 25 26 |
| Fe2O3* | 12.58 | 11.79 | 11.58 | 11.53 | 12.39 | 13.38 | 10.62 | 13.43 | 11.10 | 9.62 | 10.50 | 11.49 | 12.01 | 8.74 | 8 70 | 10.77 |
| MnO | 0.08 | 0.40 | 0.11 | 0.18 | 0.21 | 0.22 | 0.04 | 0 23 | 0.17 | 0.52 | 0.11 | 0 19 | 0.10 | 0.32 | 0 32 | 0.14 |
| MgO | 0.10 | 0.02 | 0.01 | 0.04 | 0.05 | 0.05 | 0.06 | 0 07 | 0 07 | 0.00 | 0.03 | 0 05 | 0.05 | 0 01 | 0.00 | 0.00 |
| CaO | 23.70 | 23.82 | 23.81 | 23.78 | 23 57 | 24 16 | 24.34 | 23.79 | 24.38 | 24.28 | 24.38 | 24.32 | 24 06 | 24.25 | 24.17 | 24 27 |
| Total | 97.40 | 98.19 | 97.80 | 96.74 | 96.88 | 98.01 | 97.50 | 97 59 | 98 62 | 98.77 | 97.53 | 98.35 | 98 16 | 98.28 | 97.85 | 97.95 |
| Number of cations on the basis of 12.5 oxygens: | | | | | | | | | | | | | | | | |
| Si | 3.011 | 2.994 | 2.991 | 3.015 | 2.999 | 2.975 | 2.972 | 2.985 | 2.984 | 2.963 | 2.995 | 2 977 | 2.989 | 2.967 | 2.974 | 2.966 |
| Al iv | 0.000 | 0.006 | 0.009 | 0.000 | 0.001 | 0 025 | 0 028 | 0 015 | 0 016 | 0 037 | 0.005 | 0.023 | 0.011 | 0.033 | 0 026 | 0.034 |
| Sum Z | 3 011 | 3 000 | 3.000 | 3 015 | 3.000 | 3 000 | 3.000 | 3.000 | 3 000 | 3 000 | 3.000 | 3.000 | 3.000 | 3.000 | 3 000 | 3.000 |
| Al vi | 2.197 | 2.266 | 2.288 | 2.235 | 2.204 | 2.126 | 2.314 | 2.142 | 2.290 | 2.402 | 2.304 | 2.256 | 2.232 | 2.455 | 2.457 | 2.323 |
| Ti | 0 000 | 0.000 | 0.001 | 0.003 | 0 009 | 0 012 | 0 004 | 0.004 | 0 007 | 0.000 | 0 009 | 0.012 | 0.013 | 0.003 | 0.000 | 0.002 |
| Fe3+ | 0.757 | 0.702 | 0.691 | 0 697 | 0.750 | 0 805 | 0.635 | 0.811 | 0 657 | 0.566 | 0 628 | 0.684 | 0.716 | 0.515 | 0.514 | 0.641 |
| Sum Y | 2.953 | 2.968 | 2.981 | 2.936 | 2.963 | 2.943 | 2.953 | 2.957 | 2.953 | 2.967 | 2.941 | 2.952 | 2.962 | 2.973 | 2.972 | 2.966 |
| Mn | 0.005 | 0 027 | 0.008 | 0.012 | 0.014 | 0.015 | 0.003 | 0.015 | 0.011 | 0.034 | 0.008 | 0.013 | 0.007 | 0.021 | 0.021 | 0.009 |
| Mg | 0.012 | 0.003 | 0.002 | 0.005 | 0.006 | 0 005 | 0.007 | 0.009 | 0.008 | 0.000 | 0 004 | 0.005 | 0.006 | 0.002 | 0.000 | 0.000 |
| Ca | 2.031 | 2.021 | 2.024 | 2.047 | 2.032 | 2.071 | 2.073 | 2.046 | 2.055 | 2.033 | 2.076 | 2.060 | 2.043 | 2.033 | 2.034 | 2.058 |
| Sum W | 2.048 | 2.051 | 2.034 | 2.064 | 2.052 | 2.091 | 2.083 | 2.070 | 2.075 | 2.068 | 2 087 | 2.078 | 2.056 | 2.056 | 2.056 | 2 067 |
| Sum Cations | 8.012 | 8.019 | 8.014 | 8.015 | 8.015 | 8.035 | 8.036 | 8.027 | 8.028 | 8 035 | 8.028 | 8.030 | 8.018 | 8.029 | 8.027 | 8.033 |
| Fe3/(Fe3+Al) | 0.256 | 0 236 | 0.231 | 0.238 | 0 254 | 0 272 | 0.213 | 0 273 | 0 222 | 0 188 | 0.214 | 0.231 | 0 242 | 0.171 | 0.172 | 0 214 |

Table B-4 (continued)

| Sample no. | P-104 | | P-106 | | | | | | P-107 | | | | | | | |
|---|---|---|---|---|---|---|---|---|---|---|---|---|---|---|---|---|
| Analysis no. | 13 | 14 | 1 | 2 | 3 | 4 | 5 | 6 | 1 | 2 | 3 | 4 | 5 | 6 | 7 | 8 |
| | | Last | C1-Ep1 | C7-Ep2 | C7-Ep3 | C7-Ep4 | C7-Ep5 | C7-Ep6 | C5-Ep2 | C5-Ep3 | C7-Ep5 | C7-Ep6 | -Ep9nAb | Ep10nAb | Ep11nQtz | Ep12nQtz |
| SiO2 | 38 00 | 37.72 | 35.99 | 36.16 | 35.52 | 35.95 | 36.18 | 36.44 | 36.99 | 37.19 | 37.45 | 37.50 | 37.48 | 37.86 | 37.65 | 37.49 |
| TiO2 | 0.07 | 0.03 | 0.09 | 0.10 | 1.44 | 0.02 | 0 17 | 0.13 | 0.04 | 0.06 | 0.08 | 0.05 | 0.10 | 0.08 | 0.06 | 0.12 |
| Al2O3 | 25.34 | 25 04 | 21.98 | 21.21 | 21 52 | 21.07 | 22.03 | 21.47 | 21.27 | 21.60 | 22.33 | 23.15 | 24.19 | 24.41 | 23.67 | 23.07 |
| Fe2O3* | 11.03 | 11.38 | 15.02 | 15.99 | 14.51 | 16.64 | 14.95 | 15 60 | 16.40 | 15.36 | 14.37 | 13 90 | 12.20 | 12.02 | 12.05 | 13.29 |
| MnO | 0.11 | 0.37 | 0.21 | 0.00 | 0 08 | 0.18 | 0.06 | 0.01 | 0.22 | 0.31 | 0.11 | 0 16 | 0.42 | 0.19 | 0.18 | 0.02 |
| MgO | 0.00 | 0.02 | 0.00 | 0.02 | 0.00 | 0.03 | 0.02 | 0.01 | 0.00 | 0.02 | 0 05 | 0.03 | 0.02 | 0.03 | 0.01 | 0.03 |
| CaO | 24.39 | 24.09 | 24.09 | 24.07 | 23.89 | 23 93 | 24.10 | 24.18 | 23.41 | 23.54 | 24.01 | 23.98 | 23.67 | 23.71 | 23.57 | 23.51 |
| Total | 98.94 | 98.65 | 97.37 | 97.56 | 96.96 | 97.81 | 97.52 | 97.84 | 98.32 | 98.09 | 98.41 | 98.76 | 98.07 | 98.31 | 97.18 | 97.52 |
| Number of cations on the basis of 12.5 oxygens: | | | | | | | | | | | | | | | | |
| Si | 2.976 | 2.970 | 2.923 | 2.938 | 2.896 | 2.921 | 2.930 | 2.947 | 2.975 | 2.989 | 2.989 | 2.975 | 2.977 | 2.992 | 3.012 | 3.000 |
| Al iv | 0.024 | 0.030 | 0.077 | 0.062 | 0.104 | 0.079 | 0.070 | 0 053 | 0.025 | 0.011 | 0 011 | 0.025 | 0.023 | 0.008 | 0 000 | 0 000 |
| Sum Z | 3.000 | 3 000 | 3.000 | 3.000 | 3.000 | 3.000 | 3.000 | 3.000 | 3 000 | 3.000 | 3.000 | 3.000 | 3.000 | 3 000 | 3.012 | 3 000 |
| Al vi | 2.316 | 2.294 | 2.027 | 1.969 | 1.965 | 1.940 | 2.033 | 1.993 | 1.991 | 2 036 | 2.090 | 2.140 | 2.241 | 2.266 | 2.232 | 2.177 |
| Ti | 0.004 | 0.002 | 0.005 | 0.006 | 0.088 | 0.002 | 0.011 | 0.008 | 0.002 | 0.004 | 0.005 | 0.003 | 0.006 | 0.005 | 0.004 | 0.007 |
| Fe3+ | 0.650 | 0.674 | 0.918 | 0.978 | 0.890 | 1.018 | 0.911 | 0.950 | 0.992 | 0.929 | 0.863 | 0.830 | 0.729 | 0.715 | 0.725 | 0 800 |
| Sum Y | 2.970 | 2.970 | 2.950 | 2.953 | 2.943 | 2.959 | 2.955 | 2.951 | 2.986 | 2.969 | 2.958 | 2.973 | 2.976 | 2.985 | 2.961 | 2.984 |
| Mn | 0.008 | 0.025 | 0.014 | 0.000 | 0.006 | 0.012 | 0.004 | 0.001 | 0.015 | 0.021 | 0.007 | 0.011 | 0.028 | 0 013 | 0.012 | 0.002 |
| Mg | 0.000 | 0.002 | 0.000 | 0.003 | 0.000 | 0.003 | 0 002 | 0.001 | 0.000 | 0.002 | 0.006 | 0.003 | 0.002 | 0.003 | 0.001 | 0 003 |
| Ca | 2.047 | 2.033 | 2.096 | 2.096 | 2.087 | 2.084 | 2.091 | 2.095 | 2.017 | 2.027 | 2.053 | 2.038 | 2.014 | 2.008 | 2.020 | 2.016 |
| Sum W | 2.054 | 2.060 | 2.110 | 2.098 | 2.093 | 2.099 | 2.097 | 2.097 | 2.032 | 2.050 | 2.066 | 2.052 | 2.045 | 2.024 | 2.034 | 2.020 |
| Sum Cations | 8.025 | 8.029 | 8.061 | 8 051 | 8.036 | 8.059 | 8.052 | 8.047 | 8.018 | 8.019 | 8 024 | 8.025 | 8.021 | 8.009 | 8.006 | 8.004 |
| Fe3/(Fe3+Al) | 0 217 | 0.225 | 0.304 | 0.325 | 0 301 | 0.335 | 0.302 | 0 317 | 0.330 | 0 312 | 0.291 | 0.277 | 0 244 | 0.239 | 0.245 | 0 269 |

* Total Fe as Fe2O3

Table B-5 Electron microprobe analyses of actinolites (metasediments of the Pha Som Metamorphic Complex).

| Sample no. | SD-198 | | | | | | | | | | P-102 | | | | |
|---|---|---|---|---|---|---|---|---|---|---|---|---|---|---|---|
| Analysis no. | 1 | 2 | 3 | 4 | 5 | 6 | 7 | 8 | 9 | 10 | 1 | 2 | 3 | 4 | 5 |
| | C4-Act1 | C8-Act1 | C8-Act2 | C8-Act3 | C4-Act4 | C4-Act5 | C4-Act6 | C1-Act7 | C1-Act8 | C1-Act9 | C2-Amp1 | C2-Amp2 | C2-Amp3 | C4-Act2 | C4-Act5 |
| SiO2 | 52.26 | 53.26 | 53.48 | 53.53 | 51.60 | 50.68 | 51.85 | 50.93 | 51.77 | 51.41 | 53.00 | 50.90 | 50.06 | 50.94 | 51.55 |
| TiO2 | 0.09 | 0.07 | 0.01 | 0.03 | 0.03 | 0.49 | 0.00 | 0.26 | 0.04 | 0.31 | 0.16 | 0.41 | 0.35 | 0.68 | 0.42 |
| Al2O3 | 1.59 | 1.28 | 1.11 | 1.39 | 2.05 | 2.31 | 1.66 | 1.59 | 1.53 | 1.96 | 1.56 | 3.37 | 3.93 | 4.72 | 3.61 |
| Cr2O3 | 0.02 | 0.00 | 0.06 | 0.10 | 0.00 | 0.00 | 0.05 | 0.04 | 0.02 | 0.00 | 0.02 | 0.04 | 0.03 | 0.00 | 0.02 |
| FeO* | 14.70 | 14.16 | 13.69 | 14.28 | 15.71 | 16.66 | 14.94 | 18.05 | 17.20 | 15.45 | 14.42 | 14.68 | 16.52 | 14.38 | 15.32 |
| MnO | 0.35 | 0.45 | 0.28 | 0.39 | 0.39 | 0.53 | 0.19 | 0.78 | 0.38 | 0.38 | 0.42 | 0.42 | 0.26 | 0.27 | 0.36 |
| MgO | 13.95 | 14.63 | 14.98 | 14.58 | 13.15 | 12.31 | 13.92 | 11.49 | 12.19 | 13.32 | 14.38 | 14.23 | 12.97 | 14.13 | 13.39 |
| CaO | 11.37 | 11.31 | 11.84 | 11.63 | 11.10 | 11.29 | 11.71 | 10.41 | 10.40 | 11.51 | 12.61 | 12.39 | 12.61 | 11.73 | 12.44 |
| Na2O | 0.93 | 0.91 | 0.82 | 0.83 | 1.06 | 1.09 | 0.85 | 1.36 | 1.41 | 0.88 | 0.28 | 0.60 | 0.53 | 0.79 | 0.48 |
| K2O | 0.05 | 0.07 | 0.10 | 0.10 | 0.12 | 0.16 | 0.11 | 0.15 | 0.12 | 0.13 | 0.08 | 0.15 | 0.21 | 0.20 | 0.21 |
| F | 0.02 | 0.10 | 0.03 | 0.02 | 0.00 | 0.20 | 0.00 | 0.00 | 0.00 | 0.00 | 0.05 | 0.00 | 0.10 | 0.17 | 0.20 |
| Cl | 0.01 | 0.00 | 0.00 | 0.01 | 0.02 | 0.01 | 0.00 | 0.00 | 0.00 | 0.00 | 0.02 | 0.06 | 0.03 | 0.03 | 0.03 |
| Total | 95.32 | 96.24 | 96.42 | 96.89 | 95.24 | 95.72 | 95.29 | 95.05 | 95.06 | 95.34 | 96.99 | 97.26 | 97.59 | 98.03 | 98.03 |
| O = F, Cl | -0.01 | -0.04 | -0.01 | -0.01 | 0.00 | 0.00 | 0.00 | 0.00 | 0.00 | 0.00 | -0.02 | -0.01 | -0.05 | -0.08 | -0.09 |
| Total | 95.31 | 96.20 | 96.41 | 96.88 | 95.24 | 95.72 | 95.29 | 95.05 | 95.06 | 95.34 | 96.97 | 97.25 | 97.54 | 97.95 | 97.93 |
| Number of cations on the basis of 23 oxygens:# | | | | | | | | | | | | | | | |
| Si | 7.756 | 7.794 | 7.825 | 7.795 | 7.700 | 7.616 | 7.725 | 7.707 | 7.780 | 7.678 | 7.758 | 7.430 | 7.366 | 7.332 | 7.511 |
| Al iv | 0.244 | 0.206 | 0.175 | 0.205 | 0.300 | 0.384 | 0.275 | 0.293 | 0.220 | 0.322 | 0.242 | 0.570 | 0.634 | 0.668 | 0.489 |
| Sum T | 8.000 | 8.000 | 8.000 | 8.000 | 8.000 | 8.000 | 8.000 | 8.000 | 8.000 | 8.000 | 8.000 | 8.000 | 8.000 | 8.000 | 8.000 |
| Al vi | 0.035 | 0.015 | 0.016 | 0.034 | 0.061 | 0.026 | 0.017 | 0.000 | 0.052 | 0.023 | 0.026 | 0.010 | 0.048 | 0.132 | 0.132 |
| Ti | 0.010 | 0.007 | 0.001 | 0.003 | 0.004 | 0.056 | 0.000 | 0.029 | 0.004 | 0.035 | 0.018 | 0.045 | 0.039 | 0.074 | 0.046 |
| Cr | 0.002 | 0.000 | 0.007 | 0.011 | 0.000 | 0.000 | 0.006 | 0.005 | 0.003 | 0.000 | 0.002 | 0.005 | 0.003 | 0.000 | 0.002 |
| Fe3+ | 0.293 | 0.358 | 0.183 | 0.269 | 0.351 | 0.264 | 0.248 | 0.437 | 0.375 | 0.267 | 0.129 | 0.391 | 0.337 | 0.514 | 0.203 |
| Mg | 3.086 | 3.189 | 3.265 | 3.164 | 2.925 | 2.757 | 3.091 | 2.592 | 2.731 | 2.964 | 3.137 | 3.097 | 2.844 | 3.031 | 2.908 |
| Fe2+ | 1.531 | 1.375 | 1.493 | 1.471 | 1.610 | 1.831 | 1.614 | 1.847 | 1.787 | 1.663 | 1.636 | 1.400 | 1.696 | 1.217 | 1.663 |
| Mn | 0.044 | 0.056 | 0.034 | 0.048 | 0.050 | 0.068 | 0.024 | 0.100 | 0.049 | 0.048 | 0.052 | 0.052 | 0.032 | 0.033 | 0.044 |
| Sum C | 5.000 | 5.000 | 5.000 | 5.000 | 5.000 | 5.000 | 5.000 | 5.000 | 5.000 | 5.000 | 5.000 | 5.000 | 5.000 | 5.000 | 5.000 |
| Fe2+ | 0.000 | 0.000 | 0.000 | 0.000 | 0.000 | 0.000 | 0.000 | 0.000 | 0.000 | 0.000 | 0.000 | 0.000 | 0.000 | 0.000 | 0.000 |
| Mn | 0.000 | 0.000 | 0.000 | 0.000 | 0.000 | 0.000 | 0.000 | 0.000 | 0.000 | 0.000 | 0.000 | 0.000 | 0.000 | 0.000 | 0.000 |
| Ca | 1.809 | 1.773 | 1.857 | 1.815 | 1.775 | 1.817 | 1.869 | 1.687 | 1.675 | 1.841 | 1.978 | 1.938 | 1.988 | 1.809 | 1.943 |
| Na | 0.191 | 0.227 | 0.143 | 0.185 | 0.225 | 0.183 | 0.131 | 0.313 | 0.325 | 0.159 | 0.022 | 0.062 | 0.012 | 0.191 | 0.057 |
| Sum B | 2.000 | 2.000 | 2.000 | 2.000 | 2.000 | 2.000 | 2.000 | 2.000 | 2.000 | 2.000 | 2.000 | 2.000 | 2.000 | 2.000 | 2.000 |
| Ca | 0.000 | 0.000 | 0.000 | 0.000 | 0.000 | 0.000 | 0.000 | 0.000 | 0.000 | 0.000 | 0.000 | 0.000 | 0.000 | 0.000 | 0.000 |
| Na | 0.077 | 0.032 | 0.090 | 0.050 | 0.083 | 0.136 | 0.115 | 0.086 | 0.084 | 0.097 | 0.057 | 0.109 | 0.140 | 0.030 | 0.078 |
| K | 0.009 | 0.013 | 0.019 | 0.018 | 0.023 | 0.030 | 0.021 | 0.029 | 0.023 | 0.024 | 0.015 | 0.028 | 0.039 | 0.036 | 0.038 |
| Sum A | 0.086 | 0.045 | 0.109 | 0.068 | 0.106 | 0.166 | 0.136 | 0.115 | 0.107 | 0.121 | 0.072 | 0.137 | 0.179 | 0.066 | 0.116 |
| Sum Cations | 15.086 | 15.045 | 15.109 | 15.068 | 15.106 | 15.166 | 15.136 | 15.115 | 15.107 | 15.121 | 15.072 | 15.137 | 15.179 | 15.066 | 15.116 |
| Mg/(Mg+Fe2) | 0.668 | 0.699 | 0.686 | 0.683 | 0.645 | 0.601 | 0.657 | 0.584 | 0.604 | 0.641 | 0.657 | 0.689 | 0.626 | 0.713 | 0.636 |

* Total Fe as FeO.

# Calculated by normalising the number of cations other than Ca, Na and K to 13.

Table B-5 (continued)

| Sample no. | P-104 | P-106 | | | | | P-107 | | | | | | |
|---|---|---|---|---|---|---|---|---|---|---|---|---|---|
| Analysis no. | 1 | 1 | 2 | 3 | 4 | 5 | 1 | 2 | 3 | 4 | 5 | 6 | 7 |
| | | C2-Act1 | C2-Act2 | C2-Act2 | C3-Act7 | C3-Act8 | C1 Act | C1 Act1 | C1 Act2 | C1 Act3 | C2 Act4 | C2 Act5 | C3 Act6 |
| SiO2 | 52.00 | 53.05 | 51.29 | 52.84 | 52.14 | 52.70 | 54.59 | 54.30 | 53.81 | 54.79 | 52.60 | 52.85 | 52.97 |
| TiO2 | 0.51 | 0.04 | 0.02 | 0.00 | 0.02 | 0.07 | 0.05 | 0.05 | 0.57 | 0.09 | 0.07 | 0.03 | 0.00 |
| Al2O3 | 3.15 | 1.21 | 2.44 | 1.15 | 2.14 | 2.35 | 1.15 | 1.48 | 1.37 | 1.90 | 1.96 | 1.96 | 1.96 |
| Cr2O3 | 0.00 | 0.00 | 0.00 | 0.29 | 0.06 | 0.12 | 0.05 | 0.00 | 0.00 | 0.00 | 0.04 | 0.00 | 0.11 |
| FeO* | 14.05 | 14.68 | 15.33 | 15.03 | 15.89 | 15.43 | 14.66 | 14.56 | 15.15 | 14.96 | 17.15 | 16.41 | 15.08 |
| MnO | 0.40 | 0.23 | 0.27 | 0.42 | 0.38 | 0.19 | 0.24 | 0.38 | 0.46 | 0.39 | 0.62 | 0.40 | 0.28 |
| MgO | 14.25 | 14.24 | 13.15 | 13.75 | 13.08 | 12.93 | 14.41 | 14.05 | 13.87 | 13.75 | 12.15 | 12.85 | 14.30 |
| CaO | 12.34 | 13.23 | 12.82 | 13.25 | 13.07 | 12.77 | 12.66 | 12.24 | 12.41 | 11.76 | 12.52 | 12.51 | 12.15 |
| Na2O | 0.61 | 0.12 | 0.29 | 0.09 | 0.19 | 0.22 | 0.09 | 0.08 | 0.10 | 0.07 | 0.17 | 0.16 | 0.11 |
| K2O | 0.15 | 0.09 | 0.12 | 0.09 | 0.11 | 0.13 | 0 07 | 0.13 | 0.05 | 0.03 | 0.06 | 0.10 | 0.07 |
| F | 0.00 | 0.15 | 0.18 | 0.38 | 0.23 | 0.13 | 0.03 | 0.13 | 0.00 | 0.08 | 0.00 | 0.18 | 0.00 |
| Cl | 0.04 | 0.00 | 0.00 | 0.00 | 0.00 | 0.01 | 0.00 | 0.00 | 0.02 | 0.00 | 0.00 | 0.00 | 0.01 |
| Total | 97.50 | 97.05 | 95.91 | 97.28 | 97.31 | 97.06 | 98.00 | 97.40 | 97 82 | 97.82 | 97.33 | 97.45 | 97.03 |
| O = F, Cl | -0.01 | -0.06 | -0.08 | -0.16 | -0.10 | -0.06 | -0.01 | -0.06 | -0.01 | -0.03 | 0.00 | -0.07 | 0.00 |
| Total | 97.49 | 96.99 | 95.84 | 97.13 | 97.22 | 97.00 | 97.98 | 97.34 | 97.81 | 97.79 | 97.33 | 97.38 | 97.03 |
| Number of cations on the basis of 23 oxygens:# | | | | | | | | | | | | | |
| Si | 7.559 | 7.818 | 7.680 | 7.819 | 7.717 | 7.789 | 7.889 | 7.885 | 7 809 | 7.876 | 7.774 | 7.773 | 7.693 |
| Al iv | 0.441 | 0.182 | 0.320 | 0.181 | 0.283 | 0.211 | 0.111 | 0.115 | 0.191 | 0.124 | 0.226 | 0.227 | 0.307 |
| Sum T | 8.000 | 8.000 | 8.000 | 8.000 | 8.000 | 8.000 | 8.000 | 8.000 | 8.000 | 8.000 | 8.000 | 8.000 | 8.000 |
| Al vi | 0.099 | 0.028 | 0.110 | 0.020 | 0.090 | 0.198 | 0.085 | 0.139 | 0.044 | 0.198 | 0.116 | 0.113 | 0.028 |
| Ti | 0.055 | 0.005 | 0.002 | 0.000 | 0.002 | 0.008 | 0.005 | 0.006 | 0.062 | 0.010 | 0.008 | 0.004 | 0.000 |
| Cr | 0.000 | 0.000 | 0.000 | 0.034 | 0.007 | 0.014 | 0.005 | 0.000 | 0.000 | 0.000 | 0.004 | 0.000 | 0.012 |
| Fe3+ | 0.187 | 0.000 | 0.000 | 0.000 | 0.000 | 0.000 | 0.054 | 0.107 | 0.126 | 0.258 | 0.065 | 0.099 | 0.442 |
| Mg | 3.088 | 3.128 | 2.934 | 3.033 | 2.886 | 2.848 | 3.103 | 3.041 | 2.999 | 2.945 | 2.675 | 2.816 | 3.094 |
| Fe2+ | 1.521 | 1.839 | 1.934 | 1.913 | 2.008 | 1.932 | 1.717 | 1.661 | 1.712 | 1.541 | 2.055 | 1.919 | 1.389 |
| Mn | 0.050 | 0.000 | 0.020 | 0.000 | 0.007 | 0.000 | 0.030 | 0.046 | 0.056 | 0.048 | 0.077 | 0.049 | 0.034 |
| Sum C | 5.000 | 5.000 | 5.000 | 5.000 | 5.000 | 5.000 | 5.000 | 5.000 | 5.000 | 5.000 | 5.000 | 5.000 | 5.000 |
| Fe2+ | 0.000 | 0.059 | 0.000 | 0.065 | 0.000 | 0.126 | 0.000 | 0.000 | 0.000 | 0.000 | 0.000 | 0.000 | 0.000 |
| Mn | 0.000 | 0.029 | 0.014 | 0.053 | 0.041 | 0.024 | 0.000 | 0.000 | 0.000 | 0.000 | 0.000 | 0.000 | 0.000 |
| Ca | 1.922 | 1.912 | 1.986 | 1.883 | 1.959 | 1.850 | 1.960 | 1.905 | 1.930 | 1.812 | 1.982 | 1.971 | 1.890 |
| Na | 0.078 | 0.000 | 0.000 | 0.000 | 0.000 | 0.000 | 0.024 | 0.023 | 0 029 | 0.020 | 0.018 | 0.029 | 0.031 |
| Sum B | 2.000 | 2.000 | 2.000 | 2.000 | 2.000 | 2.000 | 1.984 | 1.928 | 1.958 | 1.831 | 2.000 | 2.000 | 1.921 |
| Ca | 0.000 | 0.177 | 0.070 | 0.218 | 0.114 | 0.172 | 0.000 | 0.000 | 0.000 | 0.000 | 0.000 | 0.000 | 0.000 |
| Na | 0.094 | 0.034 | 0.084 | 0.025 | 0.056 | 0.062 | 0.000 | 0 000 | 0.000 | 0.000 | 0.031 | 0.017 | 0.000 |
| K | 0.028 | 0.017 | 0.024 | 0.017 | 0.020 | 0.025 | 0.012 | 0.024 | 0.009 | 0.005 | 0.011 | 0.020 | 0.013 |
| Sum A | 0.122 | 0.229 | 0.178 | 0.261 | 0.190 | 0.259 | 0.012 | 0.024 | 0.009 | 0.005 | 0.042 | 0.036 | 0.013 |
| Sum Cations | 15.122 | 15.229 | 15.178 | 15.261 | 15.190 | 15.259 | 14.996 | 14.952 | 14.967 | 14.837 | 15.042 | 15.036 | 14.934 |
| Mg/(Mg+Fe2) | 0.670 | 0.622 | 0.603 | 0.605 | 0.523 | 0.590 | 0.644 | 0.647 | 0.637 | 0.657 | 0.566 | 0.595 | 0.690 |

* Total Fe as FeO.

# Calculated by normalising the number of cations other than Ca, Na and K to 13.

Table B-6 Electron microprobe analyses of pumpellyites (the Pha Som metasediments).

| Sample no. | SD-104 | | SD-198 | | | SD-221 | |
|---|---|---|---|---|---|---|---|
| Analysis no. | 1 | 2 | 1 | 2 | 3 | 1 | 2 |
| | C4-Ep6 | C4-Ep7 | C1-Fe-Pu | C1-Fe-Pu | C1-Fe-Pu | C1-Ep2 | C1-Ep4 |
| SiO2 | 37.21 | 37.22 | 36.82 | 36.64 | 36.92 | 36.65 | 36.25 |
| TiO2 | 0.08 | 0.07 | 0.04 | 0.05 | 0.06 | 1.09 | 0.17 |
| Al2O3 | 21.58 | 21.23 | 20.76 | 20.75 | 20.68 | 20.47 | 20.33 |
| FeO* | 12.09 | 11.96 | 13.67 | 13.86 | 13.14 | 12.49 | 12.18 |
| MnO | 0.06 | 0.21 | 0.11 | 0.16 | 0.08 | 0.19 | 0.21 |
| MgO | 0.42 | 0.34 | 0.01 | 0.00 | 0.00 | 0.37 | 0.52 |
| CaO | 20.82 | 21.80 | 21.59 | 21.84 | 22.53 | 21.85 | 22.40 |
| Total | 92.26 | 92.82 | 92.99 | 93.29 | 93.41 | 93.10 | 92.05 |
| Number of cations = 16# | | | | | | | |
| Si | 6.214 | 6.182 | 6.137 | 6.090 | 6.119 | 6.098 | 6.075 |
| Al iv | 0.000 | 0.000 | 0.000 | 0.000 | 0.000 | 0.000 | 0.000 |
| Sum Z | 6.214 | 6.182 | 6.137 | 6.090 | 6.119 | 6.098 | 6.075 |
| Al vi | 4.249 | 4.157 | 4.080 | 4.065 | 4.040 | 4.014 | 4.016 |
| Ti | 0.011 | 0.009 | 0.004 | 0.006 | 0.008 | 0.136 | 0.021 |
| Fe3+ | 0.740 | 0.834 | 0.916 | 0.929 | 0.952 | 0.849 | 0.963 |
| Sum Y | 5.000 | 5.000 | 5.000 | 5.000 | 5.000 | 5.000 | 5.000 |
| Fe2+ | 0.948 | 0.826 | 0.990 | 0.999 | 0.870 | 0.888 | 0.744 |
| Mn | 0.008 | 0.029 | 0.016 | 0.022 | 0.011 | 0.027 | 0.029 |
| Mg | 0.104 | 0.083 | 0.002 | 0.000 | 0.000 | 0.092 | 0.129 |
| Sum X | 1.060 | 0.938 | 1.007 | 1.021 | 0.880 | 1.007 | 0.903 |
| Ca | 3.726 | 3.879 | 3.856 | 3.889 | 4.001 | 3.895 | 4.022 |
| Sum Cat. | 16.000 | 16.000 | 16.000 | 16.000 | 16.000 | 16.000 | 16.000 |
| Fe3/(Fe3+Al) | 0.148 | 0.167 | 0.183 | 0.186 | 0.191 | 0.175 | 0.193 |

* Total Fe as FeO

# Calculated assuming an ideal formula Ca4(Mg,Fe2)(Al,Fe3)5Si6O21(OH)7

Table B-7 Electron microprobe analyses of calcites (metasediments of the Pha Som Metamorphic Complex).

| Sample no. | 2/5291 | | | | | | | 2/5291 | | 3/9291 | | | | | SD-225 | |
|---|---|---|---|---|---|---|---|---|---|---|---|---|---|---|---|---|
| Analysis no. | 1 | 2 | 3 | 4 | 5 | 6 | 7 | 1 | 2 | 1 | 2 | 3 | 4 | 5 | 1 | 2 |
| | Ankerite | | | | | | | | | | | | | | C1-Cal1 | C1-Cal3 |
| FeO* | 16.47 | 14.49 | 15.28 | 16.38 | 15.82 | 14.11 | 14.78 | 0.85 | 0.97 | 0.89 | 1.12 | 1.14 | 0.95 | 1.09 | 0.62 | 0.00 |
| MnO | 0.62 | 0 84 | 0.99 | 0.77 | 0.98 | 0.83 | 0.87 | 0.49 | 0.59 | 0.67 | 0.87 | 0.88 | 0.89 | 0.99 | 0.14 | 0.23 |
| MgO | 9.88 | 10.77 | 10.76 | 9.97 | 10.65 | 11.92 | 11.26 | 0.00 | 0.05 | 0.37 | 0.28 | 0.58 | 0.38 | 0.28 | 0.24 | 0 00 |
| CaO | 28.67 | 28.34 | 28.05 | 28.17 | 28.70 | 27.95 | 27.52 | 55.16 | 54.51 | 53.93 | 53.55 | 53.75 | 54.12 | 53 60 | 54.20 | 54.58 |
| CO2# | 43.76 | 43.39 | 43.73 | 43.50 | 44.45 | 44.10 | 43.48 | 44.12 | 43.79 | 43.69 | 43.56 | 44 06 | 44.02 | 43 65 | 43.26 | 42.98 |
| Total | 99.40 | 97.83 | 98.81 | 98.79 | 100.60 | 98.91 | 97.91 | 100.62 | 99.90 | 99.55 | 99.38 | 100.41 | 100.36 | 99 61 | 98.46 | 97.79 |
| Number of cations on the basis of 6 oxygens: | | | | | | | | | | | | | | | | |
| Fe | 0.461 | 0.409 | 0.428 | 0.461 | 0.436 | 0.392 | 0.416 | 0.024 | 0 027 | 0.025 | 0.032 | 0.032 | 0.026 | 0.031 | 0.017 | 0.000 |
| Mn | 0.018 | 0.024 | 0 028 | 0.022 | 0.027 | 0.023 | 0.025 | 0.014 | 0.017 | 0.019 | 0 025 | 0 025 | 0 025 | 0.028 | 0.004 | 0.007 |
| Mg | 0.493 | 0.542 | 0.537 | 0.500 | 0.523 | 0.590 | 0.565 | 0.000 | 0.002 | 0.018 | 0.014 | 0.029 | 0 019 | 0.014 | 0.012 | 0.000 |
| Ca | 1 028 | 1.025 | 1 007 | 1.016 | 1.014 | 0.995 | 0.993 | 1.963 | 1.954 | 1.938 | 1.930 | 1.915 | 1.930 | 1.927 | 1.966 | 1.993 |
| Sum Cat. | 2.000 | 2.000 | 2.000 | 2.000 | 2.000 | 2.000 | 2.000 | 2.000 | 2.000 | 2.000 | 2.000 | 2.000 | 2.000 | 2.000 | 2.000 | 2.000 |
| Molecular proportions of end-members: | | | | | | | | | | | | | | | | |
| FeCO3 | 0.231 | 0.205 | 0.214 | 0.231 | 0.218 | 0.196 | 0.208 | 0.012 | 0.014 | 0.012 | 0.016 | 0.016 | 0.013 | 0.015 | 0.009 | 0.000 |
| MnCO3 | 0.009 | 0.012 | 0.014 | 0.011 | 0.014 | 0 012 | 0.012 | 0.007 | 0.008 | 0.010 | 0.012 | 0.012 | 0.013 | 0.014 | 0.002 | 0.003 |
| MgCO3 | 0.246 | 0 271 | 0.269 | 0.250 | 0.262 | 0.295 | 0.283 | 0.000 | 0 001 | 0.009 | 0.007 | 0.014 | 0.009 | 0.007 | 0.006 | 0.000 |
| CaCO3 | 0.514 | 0 513 | 0.503 | 0.508 | 0.507 | 0.497 | 0.497 | 0.981 | 0.977 | 0.969 | 0.965 | 0.957 | 0.965 | 0.964 | 0.983 | 0.997 |

Table B-7 (continued)

| Sample no. | SD-225 | SD-227 | | | 1/7291 | SD-60 | | | 15/6291 | SD-42 | | | | SD-64 | | |
|---|---|---|---|---|---|---|---|---|---|---|---|---|---|---|---|---|
| Analysis no. | 3 | 1 | 2 | 3 | 1 | 1 | 2 | 3 | 1 | 1 | 2 | 3 | 4 | 1 | 2 | 3 |
| | C1-Cal4 | C4-Cal1 | C4-Cal2 | C4-Cal3 | C10-Cal | C8_cal1 | C8-Cal2 | C8-Cal3 | | C4-Cal1 | C4-Cal2 | C4-Cal3 | C2-Cal4 | C2-Cal1 | C6-Cal2 | C6-Cal3 |
| FeO* | 0.09 | 0.09 | 0.04 | 0.06 | 1.88 | 0.33 | 0.37 | 0.33 | 0.29 | 0.48 | 0.59 | 0.67 | 0.59 | 0.12 | 0.41 | 0.55 |
| MnO | 0.24 | 0.20 | 0.00 | 0.04 | 0.71 | 0.59 | 0.65 | 0.43 | 0.49 | 0.74 | 0.67 | 0.65 | 0.80 | 0.47 | 0.56 | 0.55 |
| MgO | 0.00 | 0.00 | 0.00 | 0.00 | 0.74 | 0.09 | 0.11 | 0.07 | 0.08 | 0.16 | 0.19 | 0.17 | 0.21 | 0.00 | 0.03 | 0.13 |
| CaO | 55.14 | 54.64 | 55.16 | 54.63 | 53.27 | 53.48 | 53.49 | 52.96 | 55.15 | 53.10 | 54.15 | 53.94 | 54.64 | 54.97 | 53.87 | 54.09 |
| CO2# | 43.47 | 43.05 | 43.31 | 42.93 | 44.20 | 42.64 | 42.73 | 42.11 | 43.85 | 42.60 | 43.48 | 43.33 | 43.97 | 43.51 | 42.90 | 43.27 |
| Total | 98.93 | 97.97 | 98.51 | 97.66 | 100.80 | 97.14 | 97.35 | 95.90 | 99.86 | 97.08 | 99.09 | 98.76 | 100.21 | 99.07 | 97.77 | 98.60 |
| Number of cations on the basis of 6 oxygens: | | | | | | | | | | | | | | | | |
| Fe | 0.003 | 0.002 | 0.001 | 0.002 | 0.052 | 0.010 | 0.011 | 0.010 | 0.008 | 0.014 | 0.017 | 0.019 | 0.017 | 0.003 | 0.012 | 0.016 |
| Mn | 0.007 | 0.006 | 0.000 | 0.001 | 0.020 | 0.017 | 0.019 | 0.013 | 0.014 | 0.021 | 0 019 | 0.019 | 0.023 | 0.013 | 0.016 | 0 016 |
| Mg | 0.000 | 0.000 | 0.000 | 0.000 | 0.037 | 0.005 | 0.006 | 0.004 | 0.004 | 0.008 | 0.010 | 0.009 | 0.011 | 0.000 | 0.001 | 0.006 |
| Ca | 1.991 | 1.992 | 1.999 | 1.997 | 1.891 | 1 969 | 1.965 | 1.974 | 1.974 | 1.957 | 1.955 | 1.954 | 1.950 | 1.983 | 1.971 | 1.962 |
| Sum Cat. | 2.000 | 2.000 | 2.000 | 2.000 | 2.000 | 2.000 | 2.000 | 2.000 | 2.000 | 2.000 | 2.000 | 2.000 | 2.000 | 2.000 | 2 000 | 2.000 |
| Molecular proportions of end-members: | | | | | | | | | | | | | | | | |
| FeCO3 | 0.001 | 0.001 | 0.000 | 0.001 | 0.026 | 0.005 | 0.005 | 0.005 | 0.004 | 0.007 | 0.008 | 0.009 | 0.008 | 0.002 | 0.006 | 0.008 |
| MnCO3 | 0.003 | 0.003 | 0.000 | 0.001 | 0.010 | 0.009 | 0.009 | 0.006 | 0.007 | 0.011 | 0.010 | 0.009 | 0.011 | 0.007 | 0.008 | 0 008 |
| MgCO3 | 0.000 | 0.000 | 0.000 | 0.000 | 0.018 | 0.002 | 0.003 | 0.002 | 0.002 | 0.004 | 0.005 | 0.004 | 0.005 | 0.000 | 0.001 | 0.003 |
| CaCO3 | 0 995 | 0.996 | 1.000 | 0.999 | 0.946 | 0.984 | 0.982 | 0.987 | 0.987 | 0.978 | 0.977 | 0 977 | 0.975 | 0.992 | 0.985 | 0.981 |

* Total Fe as FeO

# Calculated from stoichiometry

Table B-7 (continued)

| Sample no. | SD-64 | SD-104 | | | | SD-148 | SD-148.1 | | | | | SD-150 | | SD-165 | | |
|---|---|---|---|---|---|---|---|---|---|---|---|---|---|---|---|---|
| Analysis no. | 4 | 1 | 2 | 3 | 4 | 1 | 1 | 2 | 3 | 4 | 5 | 1 | 2 | 1 | 2 | 3 |
| | C6-Cal4 | C9-Cal1 | C9-Cal2 | C9-Cal3 | C9-Cal4 | C1-Cal3 | C3-Cal1 | C3-Cal2 | C4-Cal3 | C4-Cal4 | C4-Cal5 | C3-Cal1 | C3-Cal2 | C2-Cal1 | C2-Cal2 | C2-Cal3 |
| FeO* | 0.30 | 0.30 | 0.39 | 0.48 | 0.19 | 0.86 | 0.32 | 0.49 | 0.47 | 1.66 | 1.68 | 0.46 | 0.24 | 0.36 | 0.50 | 0.13 |
| MnO | 0.63 | 0.90 | 0.80 | 0.94 | 0.94 | 1.36 | 0.64 | 0.87 | 0 81 | 3.05 | 3.10 | 0.72 | 0.71 | 0.47 | 0.62 | 0.60 |
| MgO | 0.00 | 0.09 | 0.11 | 0.10 | 0.11 | 0.30 | 0.09 | 0.22 | 0.21 | 0.51 | 0.59 | 0.04 | 0.00 | 0.04 | 0.00 | 0 00 |
| CaO | 55.13 | 53.78 | 54.01 | 54.02 | 54.72 | 52.36 | 54.44 | 53.34 | 53.05 | 49.92 | 49.71 | 54.56 | 53.67 | 53.65 | 53.64 | 54 67 |
| CO2# | 43.84 | 43.04 | 43.24 | 43.37 | 43.76 | 42.79 | 43.41 | 42.95 | 42.65 | 42.65 | 42.61 | 43.59 | 42.71 | 42.66 | 42.78 | 43.36 |
| Total | 99.89 | 98.10 | 98.56 | 98.90 | 99.73 | 97.67 | 98.90 | 97.88 | 97.19 | 97.80 | 97.69 | 99.36 | 97.33 | 97.17 | 97.54 | 98.76 |
| Number of cations on the basis of 6 oxygens: | | | | | | | | | | | | | | | | |
| Fe | 0.008 | 0 008 | 0.011 | 0.013 | 0.005 | 0.025 | 0 009 | 0.014 | 0.013 | 0.048 | 0 048 | 0.013 | 0.007 | 0.010 | 0.014 | 0.004 |
| Mn | 0.018 | 0.026 | 0.023 | 0.027 | 0.027 | 0.040 | 0.018 | 0.025 | 0.024 | 0.089 | 0 090 | 0.021 | 0 021 | 0 014 | 0.018 | 0.017 |
| Mg | 0.000 | 0.005 | 0.006 | 0.005 | 0.006 | 0.016 | 0.004 | 0.011 | 0.010 | 0.026 | 0.030 | 0.002 | 0 000 | 0.002 | 0.000 | 0.000 |
| Ca | 1.974 | 1.961 | 1.960 | 1.955 | 1.962 | 1.920 | 1.968 | 1.950 | 1.952 | 1.837 | 1.831 | 1.965 | 1.972 | 1.974 | 1.968 | 1.979 |
| Sum Cat. | 2.000 | 2.000 | 2.000 | 2.000 | 2.000 | 2.000 | 2.000 | 2.000 | 2.000 | 2.000 | 2.000 | 2.000 | 2.000 | 2.000 | 2.000 | 2.000 |
| Molecular proportions of end-members: | | | | | | | | | | | | | | | | |
| FeCO3 | 0.004 | 0.004 | 0.006 | 0.007 | 0.003 | 0.012 | 0.005 | 0.007 | 0.007 | 0.024 | 0.024 | 0.006 | 0.003 | 0.005 | 0.007 | 0.002 |
| MnCO3 | 0.009 | 0.013 | 0.012 | 0.013 | 0.013 | 0.020 | 0.009 | 0.013 | 0.012 | 0.044 | 0.045 | 0.010 | 0.010 | 0 007 | 0.009 | 0.009 |
| MgCO3 | 0.000 | 0.002 | 0.003 | 0.002 | 0.003 | 0.008 | 0.002 | 0.006 | 0.005 | 0.013 | 0 015 | 0.001 | 0.000 | 0.001 | 0.000 | 0.000 |
| CaCO3 | 0.987 | 0.981 | 0.980 | 0.977 | 0.981 | 0.960 | 0.984 | 0.975 | 0.976 | 0.919 | 0 916 | 0.982 | 0.986 | 0.987 | 0.984 | 0.990 |

Table B-7 (continued)

| Sample no. | SD-211 | | SD-213 | SD-217 | | | SD-221 | |
|---|---|---|---|---|---|---|---|---|
| Analysis no. | 1 | 2 | 1 | 1 | 2 | 3 | 1 | 2 |
| | C2-Cal1 | C2-Cal4 | C2-Cal2 | C5-Cal1 | C5-Cal2 | C5-Cal3 | C6-Cal1 | C6-Cal4 |
| FeO* | 0.43 | 0.26 | 0.24 | 0.15 | 0.15 | 0.04 | 0.09 | 0.09 |
| MnO | 0.76 | 0.47 | 0.20 | 0.00 | 0.24 | 0.07 | 0.15 | 0.73 |
| MgO | 0.15 | 0.11 | 0.62 | 0.00 | 0.00 | 0.00 | 0.36 | 0.00 |
| CaO | 52.77 | 53.68 | 52.52 | 54.85 | 54.40 | 54.81 | 54.32 | 53.79 |
| CO2# | 42.31 | 42.70 | 42.16 | 43.14 | 42.93 | 43.08 | 43.18 | 42.71 |
| Total | 96.41 | 97.22 | 95.74 | 98.14 | 97.71 | 98.00 | 98.10 | 97.31 |
| Number of cations on the basis of 6 oxygens: | | | | | | | | |
| Fe | 0.012 | 0.008 | 0.007 | 0 004 | 0.004 | 0.001 | 0.002 | 0.002 |
| Mn | 0.022 | 0.014 | 0.006 | 0.000 | 0.007 | 0.002 | 0.004 | 0.021 |
| Mg | 0.008 | 0.006 | 0.032 | 0.000 | 0.000 | 0.000 | 0.018 | 0.000 |
| Ca | 1.958 | 1.973 | 1.955 | 1.996 | 1.989 | 1.997 | 1.975 | 1.976 |
| Sum Cat. | 2.000 | 2.000 | 2.000 | 2.000 | 2.000 | 2.000 | 2.000 | 2.000 |
| Molecular proportions of end-members: | | | | | | | | |
| FeCO3 | 0.006 | 0.004 | 0.003 | 0.002 | 0.002 | 0.001 | 0.001 | 0.001 |
| MnCO3 | 0.011 | 0.007 | 0.003 | 0.000 | 0.003 | 0.001 | 0.002 | 0.011 |
| MgCO3 | 0.004 | 0.003 | 0.016 | 0.000 | 0.000 | 0.000 | 0.009 | 0.000 |
| CaCO3 | 0.979 | 0.987 | 0.977 | 0.998 | 0.994 | 0.998 | 0.987 | 0.988 |

* Total Fe as FeO

# Calculated from stoichiometry

Table B-8 Electron microprobe analyses of sphenes (metasediments of the Pha Som Metamorphic Complex).

| Sample no. | 1/6291 | | SD-104 | | | SD-165 | | | | P-102 | | | | | | |
|---|---|---|---|---|---|---|---|---|---|---|---|---|---|---|---|---|
| Analysis no. | 1 | 2 | 1 | 2 | 3 | 1 | 2 | 3 | | 1 | 2 | 3 | 4 | 5 | 6 | 7 |
| | C3-Spn | Spn | C12-Spn | C12-Spn2 | C912-Spn | C3-Spn1 | C3-Spn2 | C3-Spn3 | C5-Spn4 | C9-Spn1 | C9-Spn2 | C9-Spn3 | C9-Spn4 | C9-Spn5 | C9-Spn6 | C9-Spn7 |
| SiO2 | 29.40 | 29.97 | 29.62 | 29.76 | 33.02 | 30.01 | 30.17 | 29.97 | 30.06 | 31.01 | 30.16 | 30.00 | 29.65 | 30.27 | 30.05 | 30.11 |
| TiO2 | 34.70 | 34.27 | 35.82 | 36.01 | 34.28 | 35.69 | 36.26 | 35.74 | 36.00 | 32.76 | 36.81 | 36.18 | 36.80 | 36.61 | 36.03 | 36.13 |
| Al2O3 | 1.28 | 1.43 | 1.39 | 1.17 | 1.70 | 1.21 | 1.18 | 1.22 | 0.89 | 3.81 | 1.14 | 1.46 | 0.99 | 1.23 | 1.36 | 1.63 |
| Fe2O3* | 1.61 | 1.97 | 1.11 | 1.31 | 1.42 | 1.45 | 1.37 | 1.77 | 1.27 | 2.08 | 0.76 | 0.64 | 1.51 | 0.93 | 0.98 | 0.92 |
| MnO | 0.20 | 0.18 | 0.09 | 0.19 | 0.06 | 0.11 | 0.13 | 0.11 | 0.15 | 0.05 | 0.08 | 0.07 | 0.11 | 0 02 | 0.07 | 0.10 |
| MgO | 0.00 | 0.00 | 0.00 | 0.00 | 0.12 | 0.00 | 0.00 | 0.00 | 0.00 | 0.03 | 0.00 | 0.00 | 0.00 | 0 00 | 0.01 | 0.00 |
| CaO | 27.31 | 27.81 | 27.92 | 27.45 | 26.10 | 29.02 | 28.81 | 28.55 | 28.53 | 27.82 | 28.27 | 27.21 | 28.41 | 27.53 | 27.26 | 27.25 |
| Total | 94.49 | 95.62 | 95.95 | 95.89 | 96.71 | 97.50 | 97.91 | 97.36 | 96.90 | 97.57 | 97.23 | 95.56 | 97.47 | 96.59 | 95.75 | 96.14 |
| Number of cations on the basis of 20 (O,OH,F)#: | | | | | | | | | | | | | | | | |
| Si | 4.000 | 4.000 | 4.000 | 4.000 | 4.000 | 4.000 | 4.000 | 4.000 | 4.000 | 4.000 | 4.000 | 4.000 | 4.000 | 4.000 | 4.000 | 4.000 |
| Ti | 3.574 | 3.481 | 3.631 | 3.661 | 3.438 | 3.557 | 3.603 | 3.572 | 3.616 | 3.228 | 3.686 | 3.685 | 3.683 | 3.694 | 3.665 | 3.656 |
| Al | 0.207 | 0.227 | 0.221 | 0.186 | 0.268 | 0.189 | 0.184 | 0.191 | 0.140 | 0.588 | 0.179 | 0.234 | 0.155 | 0.194 | 0.216 | 0.259 |
| Fe3+ | 0 220 | 0.292 | 0.148 | 0.153 | 0.294 | 0.254 | 0.214 | 0 238 | 0.244 | 0.184 | 0.135 | 0.082 | 0.162 | 0.112 | 0.119 | 0.085 |
| Sum Y | 4.000 | 4.000 | 4.000 | 4.000 | 4.000 | 4.000 | 4.000 | 4.000 | 4.000 | 4.000 | 4.000 | 4.000 | 4.000 | 4.000 | 4.000 | 4.000 |
| Fe2+ | 0.000 | 0.000 | 0.000 | 0.000 | 0.000 | 0.000 | 0 000 | 0.000 | 0.000 | 0.018 | 0.000 | 0.000 | 0.000 | 0 000 | 0.000 | 0.007 |
| Mn | 0 023 | 0.020 | 0.010 | 0.022 | 0.006 | 0.012 | 0.014 | 0.013 | 0.017 | 0.006 | 0.009 | 0.008 | 0.013 | 0 003 | 0.008 | 0.012 |
| Mg | 0.000 | 0.000 | 0.000 | 0.000 | 0.024 | 0.000 | 0.000 | 0.000 | 0.000 | 0.006 | 0.000 | 0.000 | 0.000 | 0.000 | 0.001 | 0.000 |
| Ca | 4.007 | 4.025 | 4.033 | 3.976 | 3.730 | 4.120 | 4.078 | 4.065 | 4.084 | 3.906 | 4.034 | 3.948 | 4 051 | 3.956 | 3.950 | 3.930 |
| Sum W | 4.030 | 4.046 | 4.043 | 3.998 | 3.761 | 4.132 | 4.092 | 4.078 | 4.101 | 3.936 | 4.043 | 3.956 | 4.064 | 3.959 | 3.959 | 3.948 |
| Sum Cations | 12.030 | 12.046 | 12.043 | 11.998 | 11.761 | 12.132 | 12.092 | 12.078 | 12.101 | 11.936 | 12.043 | 11.956 | 12.064 | 11.959 | 11.959 | 11.948 |
| (OH,F) | 0.367 | 0.428 | 0.283 | 0.343 | 1.041 | 0.178 | 0.213 | 0.272 | 0.181 | 0.899 | 0.228 | 0.404 | 0.190 | 0.389 | 0.417 | 0.448 |
| O | 19.633 | 19.572 | 19 717 | 19.657 | 18.959 | 19.822 | 19.787 | 19.728 | 19.819 | 19.101 | 19.772 | 19 596 | 19 810 | 19 611 | 19.583 | 19.552 |

Table B-8 (continued)

| Sample no. | P-104 | | | | P-107 | | | | | | | |
|---|---|---|---|---|---|---|---|---|---|---|---|---|
| Analysis no. | 1 | 2 | 3 | 4 | 1 | 2 | 3 | 4 | 5 | 6 | 7 | 8 |
| | C3-Spn1 | C3-Spn2 | C3-Spn3 | C3-Spn4 | C4Spn? | C4-Spn1 | C4-Spn2 | C4-Spn3 | C15-Spn4 | C15-Spn5 | C15-Spn6 | C15-Spn7 |
| SiO2 | 29.61 | 29.74 | 29.41 | 29.65 | 31.55 | 30.60 | 30.57 | 29.88 | 29.88 | 30.06 | 29.95 | 29.98 |
| TiO2 | 36.66 | 36.52 | 36.83 | 36.80 | 32.34 | 32.65 | 32.72 | 30.00 | 36.36 | 35.53 | 35.67 | 36.10 |
| Al2O3 | 0.99 | 0.95 | 0.90 | 0.99 | 3.44 | 3.05 | 3.17 | 4.40 | 1.05 | 1.16 | .06 | 1.06 |
| Fe2O3* | 1.37 | 1.45 | 1.51 | 1.37 | 2.17 | 2.30 | 2.30 | 4.54 | 1.81 | 1.57 | 1.62 | 1.53 |
| MnO | 0.21 | 0.20 | 0.29 | 0.11 | 0.07 | 0.00 | 0.04 | 0.15 | 0.25 | 0.27 | 0.32 | 0.20 |
| MgO | 0.00 | 0.00 | 0.00 | 0.00 | 0.45 | 0 69 | 0.68 | 1.92 | 0.00 | 0.03 | 0.00 | 0.00 |
| CaO | 28.29 | 28.39 | 28.27 | 28.41 | 27.71 | 28 07 | 27.74 | 25.54 | 28.44 | 28.12 | 28.50 | 28.68 |
| Total | 97.14 | 97.26 | 97.20 | 97.34 | 97.73 | 97.36 | 97.22 | 96.45 | 97.80 | 96.75 | 97.12 | 97.55 |
| Number of cations on the basis of 20 (O,OH,F)#: | | | | | | | | | | | | |
| Si | 4.000 | 4.000 | 4.000 | 4 000 | 4.000 | 4.000 | 4.000 | 4.000 | 4.000 | 4.000 | 4.000 | 4.000 |
| Ti | 3.681 | 3 661 | 3.699 | 3.687 | 3.175 | 3.218 | 3.230 | 2.959 | 3.625 | 3.573 | 3.575 | 3.603 |
| Al | 0.156 | 0.150 | 0.142 | 0.155 | 0.529 | 0.471 | 0.490 | 0.681 | 0.165 | 0.184 | 0.167 | 0.166 |
| Fe3+ | 0.163 | 0.189 | 0.159 | 0.158 | 0.296 | 0.312 | 0.279 | 0.360 | 0.211 | 0.243 | 0.258 | 0.232 |
| Sum Y | 4.000 | 4 000 | 4.000 | 4.000 | 4.000 | 4.000 | 4.000 | 4.000 | 4.000 | 4.000 | 4.000 | 4.000 |
| Fe2+ | 0.000 | 0.000 | 0.000 | 0.000 | 0.000 | 0.000 | 0.000 | 0.098 | 0.000 | 0.000 | 0.000 | 0.000 |
| Mn | 0.024 | 0.022 | 0.033 | 0.013 | 0.008 | 0.000 | 0.005 | 0.017 | 0.028 | 0.030 | 0.036 | 0.022 |
| Mg | 0.000 | 0.000 | 0.000 | 0.000 | 0 088 | 0.134 | 0.132 | 0.376 | 0 000 | 0.006 | 0.000 | 0.000 |
| Ca | 4.046 | 4.055 | 4.045 | 4.055 | 3.876 | 3.941 | 3.903 | 3.590 | 4.040 | 4.030 | 4.069 | 4.077 |
| Sum W | 4.070 | 4.077 | 4.078 | 4.068 | 3.971 | 4.075 | 4.040 | 4.081 | 4.067 | 4.066 | 4.105 | 4.099 |
| Sum Cations | 12.070 | 12.077 | 12.078 | 12.068 | 11.971 | 12.075 | 12.040 | 12.081 | 12.067 | 12.066 | 12.105 | 12.099 |
| (OH,F) | 0.179 | 0.184 | 0.146 | 0.176 | 0.884 | 0.632 | 0 690 | 0.880 | 0.241 | 0.294 | 0.216 | 0.199 |
| O | 19.821 | 19 816 | 19 854 | 19.824 | 19.116 | 19.368 | 19.310 | 19.120 | 19.759 | 19.706 | 19.784 | 19 801 |

* Total Fe as Fe2O3

# Assuming Si = 4.00

# Appendix C

Table C-1 Electron microprobe analyses of amphiboles (ophiolite association of the Pha Som Metamorphic Complex).

| Sample no. | 5/6291 | | | | | | 6/9291 | | | | | | 2/7291 | | | | | 4/7291 | | | | |
|---|---|---|---|---|---|---|---|---|---|---|---|---|---|---|---|---|---|---|---|---|---|---|
| Analysis no. | 1 | 2 | 3 | 4 | 5 | 6 | 1 | 2 | 3 | 4 | 5 | 6 | 1 | 2 | 3 | 4 | 5 | 1 | 2 | 3 | 4 | 5 |
| | | | | | | | | | | | | | Core | Core | Rim | Rim | Rim | core | core | core | core | core |
| SiO2 | 50.02 | 50.88 | 49.41 | 49.51 | 49.63 | 50.31 | 49.45 | 48.81 | 49.05 | 48.64 | 49.64 | 49.48 | 48.12 | 48.20 | 47.86 | 48.88 | 47.85 | 44.67 | 43.61 | 44.57 | 43.15 | 42.96 |
| TiO2 | 0.38 | 0.30 | 0.37 | 0.42 | 0.41 | 0.37 | 0.45 | 0.45 | 0.47 | 0.52 | 0.42 | 0.44 | 0.35 | 0.34 | 0.28 | 0.26 | 0.29 | 0.29 | 0.30 | 0.30 | 0.27 | 0.29 |
| Al2O3 | 5.72 | 4.74 | 6.52 | 6.72 | 6.82 | 5.96 | 7.11 | 7.89 | 8.01 | 7.94 | 7.06 | 7.24 | 9.79 | 9.29 | 9.11 | 7.72 | 8.81 | 13.47 | 14.59 | 13.69 | 14.55 | 14.72 |
| Cr2O3 | 0.09 | 0.09 | 0.10 | 0.15 | 0.05 | 0.02 | 0.12 | 0.12 | 0.12 | 0.23 | 0.12 | 0.17 | 0.03 | 0.12 | 0.05 | 0.22 | 0.12 | 0.07 | 0.07 | 0.14 | 0.07 | 0.08 |
| FeO* | 10.66 | 10.38 | 11.02 | 10.60 | 11.42 | 10.78 | 10.54 | 10.89 | 10.84 | 10.84 | 10.27 | 10.13 | 10.60 | 10.46 | 10.64 | 10.02 | 10.19 | 9.95 | 10.21 | 9.96 | 10.01 | 10.12 |
| MnO | 0.19 | 0.34 | 0.24 | 0.25 | 0.25 | 0.28 | 0.09 | 0.25 | 0.20 | 0.16 | 0.21 | 0.21 | 0.16 | 0.25 | 0.28 | 0.24 | 0.07 | 0.25 | 0.14 | 0.03 | 0.18 | 0.00 |
| MgO | 15.81 | 16.11 | 15.99 | 16.09 | 16.04 | 16.25 | 15.81 | 15.63 | 15.73 | 15.49 | 15.88 | 16.13 | 15.20 | 15.44 | 15.46 | 16.09 | 15.14 | 13.84 | 13.28 | 13.78 | 13.17 | 13.38 |
| CaO | 12.75 | 12.81 | 12.41 | 12.55 | 12.53 | 12.32 | 12.59 | 12.26 | 12.62 | 12.34 | 12.06 | 12.36 | 12.88 | 12.72 | 12.61 | 12.58 | 12.89 | 12.58 | 12.67 | 12.79 | 12.81 | 12.82 |
| Na2O | 0.82 | 0.79 | 0.99 | 0.93 | 0.99 | 0.83 | 0.73 | 0.76 | 0.73 | 0.72 | 0.70 | 0.71 | 1.47 | 1.29 | 1.37 | 1.08 | 1.23 | 1.74 | 1.86 | 1.74 | 1.91 | 1.78 |
| K2O | 0.06 | 0.05 | 0.05 | 0.04 | 0.07 | 0.04 | 0.06 | 0.04 | 0.06 | 0.06 | 0.04 | 0.05 | 0.08 | 0.06 | 0.05 | 0.10 | 0.07 | 0.14 | 0.02 | 0.13 | 0.15 | 0.15 |
| F | 0.00 | 0.00 | 0.00 | 0.00 | 0.00 | 0.00 | 0.00 | 0.00 | 0.00 | 0.00 | 0.00 | 0.00 | 0.00 | 0.00 | 0.00 | 0.00 | 0.00 | 0.00 | 0.00 | 0.00 | 0.00 | 0.00 |
| Cl | 0.00 | 0.00 | 0.00 | 0.00 | 0.00 | 0.02 | 0.00 | 0.00 | 0.00 | 0.00 | 0.00 | 0.00 | 0.00 | 0.00 | 0.02 | 0.00 | 0.00 | 0.02 | 0.02 | 0.00 | 0.04 | 0.02 |
| Total | 96.50 | 96.49 | 97.10 | 97.26 | 98.21 | 97.19 | 96.95 | 97.10 | 97.83 | 96.94 | 96.40 | 96.92 | 98.68 | 98.17 | 97.73 | 97.19 | 96.66 | 97.02 | 96.77 | 97.13 | 96.31 | 96.31 |
| O = F, Cl | 0.00 | 0.00 | 0.00 | 0.00 | 0.00 | 0.00 | 0.00 | 0.00 | 0.00 | 0.00 | 0.00 | 0.00 | 0.00 | 0.00 | 0.00 | 0.00 | 0.00 | 0.00 | 0.00 | 0.00 | -0 01 | 0.00 |
| Total | 96.50 | 96.49 | 97.10 | 97.26 | 98.21 | 97.19 | 96.95 | 97.10 | 97.83 | 96.94 | 96.40 | 96.92 | 98.68 | 98.17 | 97.73 | 97.19 | 96.66 | 97.01 | 96.77 | 97.13 | 96.30 | 96.31 |
| Number of cations on the basis of 23 oxygens:# | | | | | | | | | | | | | | | | | | | | | | |
| Si | 7.245 | 7.370 | 7.082 | 7.079 | 7.037 | 7.180 | 7.086 | 6.961 | 6.960 | 6.959 | 7.106 | 7.055 | 6.829 | 6.850 | 6.835 | 6.990 | 6.935 | 6.454 | 6.332 | 6.442 | 6.324 | 6.276 |
| Al iv | 0.755 | 0.630 | 0.918 | 0.921 | 0.963 | 0.820 | 0.914 | 1.039 | 1.040 | 1.041 | 0.894 | 0.945 | 1.171 | 1.150 | 1.165 | 1.010 | 1.065 | 1.546 | 1.668 | 1.558 | 1.676 | 1.724 |
| Sum T | 8.000 | 8.000 | 8.000 | 8.000 | 8.000 | 8.000 | 8.000 | 8.000 | 8.000 | 8.000 | 8.000 | 8.000 | 8.000 | 8.000 | 8.000 | 8.000 | 8.000 | 8.000 | 8.000 | 8.000 | 8.000 | 8.000 |
| Al vi | 0.221 | 0.180 | 0.183 | 0.212 | 0.177 | 0.182 | 0.287 | 0.287 | 0.300 | 0.299 | 0.298 | 0.273 | 0.467 | 0.407 | 0.369 | 0.291 | 0.441 | 0.748 | 0.829 | 0.775 | 0.837 | 0.811 |
| Ti | 0.041 | 0.033 | 0.040 | 0.045 | 0.044 | 0.039 | 0 048 | 0.048 | 0.050 | 0.056 | 0.045 | 0.047 | 0.037 | 0.036 | 0.031 | 0.028 | 0.032 | 0.032 | 0.033 | 0.033 | 0.030 | 0.032 |
| Cr | 0.010 | 0.010 | 0.011 | 0.017 | 0.006 | 0.003 | 0.014 | 0.014 | 0.013 | 0.026 | 0.014 | 0.019 | 0.003 | 0.013 | 0.005 | 0 025 | 0.014 | 0.008 | 0.008 | 0.016 | 0.008 | 0.009 |
| Fe3+ | 0.242 | 0.166 | 0.548 | 0.492 | 0.601 | 0.550 | 0.436 | 0.678 | 0.578 | 0.610 | 0.590 | 0.576 | 0.290 | 0.417 | 0.482 | 0.466 | 0.185 | 0.320 | 0.297 | 0.228 | 0.178 | 0.294 |
| Mg | 3.413 | 3.478 | 3.415 | 3.429 | 3.389 | 3.455 | 3.376 | 3.322 | 3.326 | 3.303 | 3.388 | 3.428 | 3.215 | 3.270 | 3.290 | 3.429 | 3.270 | 2.980 | 2.873 | 2.968 | 2.875 | 2.912 |
| Fe2+ | 1.049 | 1.091 | 0.773 | 0.776 | 0.753 | 0.736 | 0.827 | 0.621 | 0.709 | 0.687 | 0.640 | 0.632 | 0.969 | 0.826 | 0.788 | 0.732 | 1.050 | 0.883 | 0.943 | 0.976 | 1.049 | 0.942 |
| Mn | 0.023 | 0.042 | 0.029 | 0.030 | 0.030 | 0.034 | 0.011 | 0.030 | 0.024 | 0.019 | 0.025 | 0.025 | 0.019 | 0.030 | 0.034 | 0.029 | 0.009 | 0.031 | 0.017 | 0.004 | 0.023 | 0.000 |
| Sum C | 5.000 | 5.000 | 5.000 | 5.000 | 5.000 | 5.000 | 5.000 | 5.000 | 5.000 | 5.000 | 5.000 | 5.000 | 5.000 | 5.000 | 5.000 | 5.000 | 5.000 | 5.000 | 5.000 | 5.000 | 5.000 | 5.000 |
| Fe2+ | 0.000 | 0.000 | 0.000 | 0.000 | 0.000 | 0.000 | 0.000 | 0.000 | 0.000 | 0.000 | 0.000 | 0.000 | 0.000 | 0.000 | 0.000 | 0.000 | 0.000 | 0.000 | 0.000 | 0.000 | 0.000 | 0.000 |
| Mn | 0.000 | 0.000 | 0.000 | 0.000 | 0.000 | 0.000 | 0.000 | 0.000 | 0.000 | 0.000 | 0.000 | 0.000 | 0 000 | 0.000 | 0.000 | 0.000 | 0.000 | 0.000 | 0.000 | 0.000 | 0.000 | 0.000 |
| Ca | 1.979 | 1.988 | 1.906 | 1.923 | 1.904 | 1.884 | 1.933 | 1.873 | 1.919 | 1.892 | 1.850 | 1.888 | 1.959 | 1.937 | 1.930 | 1.927 | 2.000 | 1.947 | 1.971 | 1.981 | 2.000 | 2.000 |
| Na | 0.021 | 0.012 | 0.094 | 0.077 | 0.096 | 0.116 | 0.067 | 0.127 | 0.081 | 0.108 | 0.150 | 0.112 | 0.041 | 0.063 | 0.070 | 0.073 | 0.000 | 0.053 | 0.029 | 0.019 | 0.000 | 0.000 |
| Sum B | 2.000 | 2.000 | 2.000 | 2.000 | 2.000 | 2.000 | 2.000 | 2.000 | 2.000 | 2.000 | 2.000 | 2.000 | 2 000 | 2.000 | 2.000 | 2.000 | 2.000 | 2.000 | 2.000 | 2.000 | 2.000 | 2.000 |
| Ca | 0.000 | 0.000 | 0.000 | 0.000 | 0.000 | 0.000 | 0.000 | 0.000 | 0.000 | 0.000 | 0.000 | 0.000 | 0.000 | 0.000 | 0.000 | 0.000 | 0.002 | 0.000 | 0 000 | 0.000 | 0.012 | 0.007 |
| Na | 0.209 | 0.210 | 0.181 | 0.181 | 0.176 | 0.115 | 0.136 | 0.084 | 0.120 | 0.092 | 0.044 | 0.085 | 0.363 | 0.292 | 0.308 | 0.227 | 0.346 | 0.435 | 0.495 | 0.469 | 0.542 | 0 505 |
| K | 0.011 | 0.009 | 0.009 | 0 007 | 0.013 | 0.007 | 0.011 | 0.007 | 0.011 | 0.011 | 0.007 | 0.009 | 0.014 | 0.011 | 0.009 | 0.018 | 0.013 | 0.026 | 0.004 | 0.024 | 0.029 | 0.028 |
| Sum A | 0.220 | 0.219 | 0.190 | 0.188 | 0.188 | 0.122 | 0.147 | 0.091 | 0.130 | 0.103 | 0.052 | 0.094 | 0.378 | 0.303 | 0.317 | 0.245 | 0.360 | 0.461 | 0.498 | 0.493 | 0.583 | 0.540 |
| Sum Cations | 15.220 | 15.219 | 15.190 | 15.188 | 15.188 | 15.122 | 15.147 | 15.091 | 15.130 | 15.103 | 15.052 | 15.094 | 15.378 | 15.303 | 15.317 | 15.245 | 15.360 | 15.461 | 15.498 | 15.493 | 15.583 | 15.540 |
| Mg/(Mg+Fe2) | 0.765 | 0.761 | 0.815 | 0.815 | 0.818 | 0.824 | 0.803 | 0.842 | 0.824 | 0.828 | 0.841 | 0.844 | 0.768 | 0.798 | 0.807 | 0.824 | 0.757 | 0.771 | 0.753 | 0.753 | 0.733 | 0.756 |

* Total Fe as FeO.

# Calculated by normalising the number of cations other than Ca, Na and K to 13.

Table C-1 (continued)

| Sample no. | 4/7291 | | 5/7291 | | | | | 7/7291 | | | 8/7291 | | | | | | | | | 9/7291 | | | |
|---|---|---|---|---|---|---|---|---|---|---|---|---|---|---|---|---|---|---|---|---|---|---|---|
| Analysis no. | 6 | 7 | 1 | 2 | 3 | 4 | 5 | 1 | 2 | 3 | 1 | 2 | 3 | 4 | 5 | 6 | 7 | 8 | 9 | 1 | 2 | 3 | 4 |
| | rim | rim | | | | | | | | | | | | | | | | | | core | core | core rim | grt |
| SiO2 | 43.62 | 43.87 | 43.14 | 43.45 | 43.06 | 43.18 | 43.16 | 46.45 | 45.79 | 46.41 | 45.39 | 44.68 | 44.62 | 46.08 | 46.67 | 46.35 | 45.91 | 45.71 | 44.84 | 44.41 | 44.17 | 44.52 | 42.34 |
| TiO2 | 0.25 | 0.62 | 0.66 | 0.56 | 0.60 | 0.67 | 0.51 | 0.31 | 0.38 | 0.35 | 0.36 | 0.42 | 0.35 | 0.29 | 0.27 | 0.25 | 0.27 | 0.35 | 0.29 | 0.58 | 0.52 | 0.56 | 0.68 |
| Al2O3 | 14.49 | 13.41 | 12.96 | 13.08 | 13.25 | 12.94 | 13.05 | 13.08 | 13.57 | 13.36 | 12.49 | 12.93 | 12.99 | 11.20 | 10.68 | 11.69 | 11.87 | 12.16 | 12.67 | 13.67 | 13.65 | 12.92 | 15.64 |
| Cr2O3 | 0.11 | 0.06 | 0.13 | 0.07 | 0.04 | 0.00 | 0.04 | 0.00 | 0.03 | 0.00 | 0.00 | 0.00 | 0.20 | 0.00 | 0.00 | 0.18 | 0.00 | 0.00 | 0.00 | 0.08 | 0.02 | 0.05 | 0.00 |
| FeO* | 9.90 | 11.68 | 14.06 | 13.65 | 13.79 | 14.29 | 14.26 | 10.23 | 10.10 | 9.70 | 10.52 | 10.47 | 10.63 | 10.00 | 9.74 | 9.97 | 10.16 | 10.14 | 10.11 | 12.03 | 12.06 | 12.25 | 12.54 |
| MnO | 0.08 | 0.06 | 0.14 | 0.15 | 0.17 | 0.21 | 0.17 | 0.18 | 0.08 | 0.05 | 0.22 | 0.15 | 0.14 | 0.11 | 0.19 | 0.20 | 0.16 | 0.14 | 0.15 | 0.00 | 0.00 | 0.01 | 0.06 |
| MgO | 13.36 | 12.29 | 11.45 | 11.56 | 11.31 | 11.21 | 11.42 | 13.90 | 13.24 | 13.53 | 13.76 | 13.73 | 13.82 | 14.57 | 14.95 | 14.52 | 14.37 | 14.24 | 14.06 | 12.65 | 12.65 | 12.54 | 11.42 |
| CaO | 12.81 | 12.88 | 12.36 | 12.19 | 12.29 | 12.32 | 12.20 | 12.39 | 12.64 | 12.36 | 12.32 | 12.68 | 12.37 | 12.34 | 12.43 | 12.65 | 12.26 | 12.40 | 12.31 | 12.84 | 12.62 | 12.77 | 12.68 |
| Na2O | 1.78 | 1.23 | 1.63 | 1.56 | 1.56 | 1.63 | 1.60 | 2.10 | 2.19 | 1.94 | 1.89 | 1.92 | 1.92 | 1.71 | 1.64 | 1.75 | 1.74 | 1.85 | 1.98 | 1.33 | 1.37 | 1.19 | 1.52 |
| K2O | 0.15 | 0.03 | 0.11 | 0.11 | 0.12 | 0.09 | 0.09 | 0.19 | 0.23 | 0.21 | 0.15 | 0.15 | 0.16 | 0.12 | 0.09 | 0.11 | 0.14 | 0.12 | 0.15 | 0.04 | 0.02 | 0.03 | 0.01 |
| F | 0.00 | 0.00 | 0.00 | 0.06 | 0.06 | 0.00 | 0.00 | 0.00 | 0.00 | 0.00 | 0.00 | 0.00 | 0.25 | 0.00 | 0.00 | 0.00 | 0.00 | 0.00 | 0.12 | 0.00 | 0.00 | 0.00 | 0.00 |
| Cl | 0.00 | 0.04 | 0.03 | 0.03 | 0.00 | 0.00 | 0.00 | 0.00 | 0.00 | 0.00 | 0.00 | 0.00 | 0.03 | 0.00 | 0.00 | 0.06 | 0.00 | 0.00 | 0.00 | 0.01 | 0.02 | 0.04 | 0.02 |
| Total | 96.56 | 96.17 | 96.65 | 96.45 | 96.27 | 96.53 | 96.50 | 98.83 | 98.25 | 97.91 | 97.10 | 97.11 | 97.47 | 96.42 | 96.67 | 97.71 | 96.87 | 97.11 | 96.69 | 97.64 | 97.10 | 96.89 | 96.91 |
| O = F, Cl | 0.00 | -0.01 | -0.01 | -0.03 | -0.03 | 0.00 | 0.00 | 0.00 | 0.00 | 0.00 | 0.00 | 0.00 | -0.11 | 0.00 | 0.00 | -0.01 | 0.00 | 0.00 | -0.05 | 0.00 | 0.00 | -0.01 | 0.00 |
| Total | 96.56 | 96.16 | 96.64 | 96.42 | 96.25 | 96.53 | 96.50 | 98.83 | 98.25 | 97.91 | 97.10 | 97.11 | 97.36 | 96.42 | 96.67 | 97.70 | 96 87 | 97.11 | 96.64 | 97.64 | 97.09 | 96.88 | 96.90 |
| Number of cations on the basis of 23 oxygens:# | | | | | | | | | | | | | | | | | | | | | | | |
| Si | 6.355 | 6.457 | 6.201 | 6.256 | 6.217 | 6.220 | 6.211 | 6.597 | 6.589 | 6.649 | 6.565 | 6.484 | 6.449 | 6.681 | 6.736 | 6.650 | 6.621 | 6.593 | 6.511 | 6.419 | 6.408 | 6.492 | 6.195 |
| Al iv | 1.645 | 1.543 | 1.799 | 1.744 | 1.783 | 1.780 | 1.789 | 1.403 | 1.411 | 1.351 | 1.435 | 1.516 | 1.551 | 1.319 | 1.264 | 1.350 | 1.379 | 1.407 | 1.489 | 1.581 | 1.592 | 1.508 | 1.805 |
| Sum T | 8.000 | 8.000 | 8.000 | 8.000 | 8.000 | 8.000 | 8.000 | 8.000 | 8.000 | 8.000 | 8.000 | 8.000 | 8.000 | 8.000 | 8.000 | 8.000 | 8.000 | 8.000 | 8.000 | 8.000 | 8.000 | 8.000 | 8.000 |
| Al vi | 0.843 | 0.784 | 0.397 | 0.475 | 0.471 | 0.417 | 0.425 | 0.788 | 0.891 | 0.905 | 0.695 | 0.696 | 0.661 | 0.595 | 0.554 | 0 628 | 0.639 | 0.661 | 0.679 | 0.749 | 0.743 | 0.712 | 0.893 |
| Ti | 0.028 | 0.068 | 0.071 | 0.060 | 0.065 | 0.072 | 0.055 | 0.033 | 0.041 | 0.038 | 0.039 | 0.046 | 0.038 | 0.032 | 0.029 | 0.027 | 0.029 | 0.038 | 0.032 | 0.063 | 0.057 | 0.061 | 0.075 |
| Cr | 0.013 | 0.007 | 0.015 | 0.008 | 0.005 | 0.000 | 0.005 | 0.000 | 0.003 | 0.000 | 0.000 | 0.000 | 0.023 | 0.000 | 0.000 | 0.020 | 0.000 | 0.000 | 0.000 | 0.009 | 0.002 | 0.006 | 0.000 |
| Fe3+ | 0.204 | 0.196 | 1.679 | 1.556 | 1.592 | 1.658 | 1.679 | 0.165 | 0.000 | 0.000 | 0.285 | 0.219 | 0.391 | 0.323 | 0.332 | 0.254 | 0.383 | 0.300 | 0.331 | 0.340 | 0.421 | 0.334 | 0.353 |
| Mg | 2.901 | 2.695 | 2.452 | 2.481 | 2.433 | 2.406 | 2.450 | 2.942 | 2.839 | 2.889 | 2.967 | 2.970 | 2.977 | 3.147 | 3.217 | 3.105 | 3.088 | 3.060 | 3.043 | 2.725 | 2.735 | 2.726 | 2.490 |
| Fe2+ | 1.002 | 1.242 | 0.011 | 0.087 | 0.073 | 0.064 | 0.037 | 1.051 | 1.332 | 1.164 | 0.987 | 1.052 | 0.893 | 0.890 | 0.844 | 0.942 | 0.842 | 0.924 | 0.897 | 1.115 | 1.042 | 1.160 | 1.181 |
| Mn | 0.010 | 0.008 | 0.017 | 0.018 | 0.021 | 0.026 | 0.021 | 0.022 | 0.010 | 0.006 | 0.026 | 0.018 | 0.017 | 0.013 | 0.024 | 0.025 | 0.019 | 0.018 | 0.018 | 0.000 | 0.000 | 0.002 | 0.007 |
| Sum C | 5.000 | 5.000 | 5.000 | 5.000 | 5.000 | 5.000 | 5.000 | 5.000 | 5.000 | 5.000 | 5.000 | 5.000 | 5.000 | 5.000 | 5.000 | 5.000 | 5.000 | 5.000 | 5.000 | 5.000 | 5.000 | 5.000 | 5.000 |
| Fe2+ | 0.000 | 0.000 | 0.000 | 0.000 | 0.000 | 0.000 | 0.000 | 0.000 | 0.000 | 0.000 | 0.000 | 0.000 | 0.000 | 0.000 | 0.000 | 0.000 | 0.000 | 0.000 | 0.000 | 0.000 | 0.000 | 0.000 | 0.000 |
| Mn | 0.000 | 0.000 | 0.000 | 0.000 | 0.000 | 0.000 | 0.000 | 0.000 | 0.000 | 0.000 | 0.000 | 0.000 | 0.000 | 0.000 | 0.000 | 0.000 | 0.000 | 0.000 | 0.000 | 0.000 | 0.000 | 0.000 | 0.000 |
| Ca | 2.000 | 2.000 | 1.546 | 1.565 | 1.562 | 1.545 | 1.554 | 1.886 | 1.949 | 1.897 | 1.909 | 1.971 | 1.916 | 1.917 | 1.922 | 1.944 | 1.894 | 1.916 | 1.914 | 1.989 | 1.962 | 1.996 | 1.988 |
| Na | 0.000 | 0.000 | 0.454 | 0.435 | 0.438 | 0.455 | 0.446 | 0.114 | 0.051 | 0.103 | 0.091 | 0.029 | 0.084 | 0.083 | 0.078 | 0.056 | 0.106 | 0.084 | 0.086 | 0.011 | 0.038 | 0.004 | 0.012 |
| Sum B | 2.000 | 2.000 | 2.000 | 2.000 | 2.000 | 2.000 | 2.000 | 2.000 | 2.000 | 2.000 | 2.000 | 2.000 | 2.000 | 2.000 | 2.000 | 2 000 | 2.000 | 2.000 | 2.000 | 2 000 | 2.000 | 2.000 | 2.000 |
| Ca | 0.000 | 0.031 | 0.000 | 0.000 | 0.000 | 0.000 | 0.000 | 0.000 | 0.000 | 0.000 | 0.000 | 0.000 | 0.000 | 0.000 | 0.000 | 0.000 | 0.000 | 0.000 | 0.000 | 0.000 | 0.000 | 0.000 | 0.000 |
| Na | 0.502 | 0.350 | 0.000 | 0.000 | 0.000 | 0.000 | 0.000 | 0.464 | 0.560 | 0.436 | 0.439 | 0.510 | 0.454 | 0.399 | 0.381 | 0.430 | 0.379 | 0.432 | 0.473 | 0.361 | 0.347 | 0.333 | 0.419 |
| K | 0.029 | 0.007 | 0.020 | 0.021 | 0.023 | 0.016 | 0.017 | 0.034 | 0.042 | 0.038 | 0.027 | 0.028 | 0.030 | 0.021 | 0.016 | 0.020 | 0.027 | 0.022 | 0.028 | 0.007 | 0.004 | 0.006 | 0.002 |
| Sum A | 0.531 | 0.388 | 0.020 | 0.021 | 0.023 | 0.016 | 0.017 | 0.498 | 0.602 | 0.475 | 0.467 | 0.538 | 0.484 | 0.420 | 0.397 | 0.450 | 0.406 | 0.455 | 0.501 | 0.369 | 0.351 | 0.339 | 0.421 |
| Sum Cations | 15.531 | 15.388 | 15.020 | 15.021 | 15.023 | 15.016 | 15.017 | 15.498 | 15.602 | 15.475 | 15.467 | 15.538 | 15.484 | 15.420 | 15.397 | 15.450 | 15.406 | 15.455 | 15.501 | 15.369 | 15.351 | 15.339 | 15.421 |
| Mg/(Mg+Fe2) | 0.743 | 0.685 | 0.995 | 0.966 | 0.971 | 0.974 | 0.985 | 0.737 | 0.681 | 0.713 | 0.750 | 0.738 | 0.769 | 0.780 | 0.792 | 0.767 | 0.786 | 0.768 | 0.772 | 0.710 | 0.724 | 0.702 | 0.678 |

* Total Fe as FeO.

# Calculated by normalising the number of cations other than Ca, Na and K to 13.

Table C-1 (continued)

| Sample no. | 9/7291 | | | | | | | | | | | 12/7291 | | | | | | | | | | | |
|---|---|---|---|---|---|---|---|---|---|---|---|---|---|---|---|---|---|---|---|---|---|---|---|
| Analysis no. | 5 | 6 | 7 | 8 | 9 | 10 | 11 | 12 | 13 | 14 | 15 | 1 | 2 | 3 | 4 | 5 | 6 | 7 | 8 | 9 | 10 | 11 | 12 |
| | rim grt | rim grt | rim grt | rim grt | rim cpx | | | | | | | C1-Hbl1 | C1-Hbl2 | C1-Hbl3 | C1-Hbl4 | C2-Hbl5 | C4-Hbl6 | C4-Hbl7 | C5-Hbl8 | C6-Hbl9 | C5-Hbl1 | C1-Hbl1 | C1-Hbl2b |
| SiO2 | 44.00 | 44.18 | 42.68 | 43.42 | 44.24 | 44.03 | 43.85 | 43.86 | 44.14 | 43.62 | 43.69 | 44.79 | 44.21 | 44.24 | 44.10 | 43.94 | 44.81 | 44.49 | 44.82 | 44.03 | 44.56 | 44.48 | 44.60 |
| TiO2 | 0.59 | 0.64 | 0.68 | 0.57 | 0.58 | 0.54 | 0.76 | 0.71 | 0.63 | 0.73 | 0.63 | 0.41 | 0.51 | 0.47 | 0.50 | 0.48 | 0.48 | 0.41 | 0.53 | 0.40 | 0.42 | 0.41 | 0.47 |
| Al2O3 | 13.96 | 14.16 | 14.95 | 14.88 | 12.60 | 13.56 | 13.90 | 13.56 | 13.40 | 13.39 | 13.58 | 12.48 | 12.85 | 12.40 | 12.62 | 12.65 | 12.15 | 12.25 | 12.93 | 12.16 | 11.97 | 12.76 | 12.42 |
| Cr2O3 | 0.00 | 0.10 | 0.06 | 0.00 | 0.00 | 0.03 | 0.00 | 0.03 | 0.04 | 0.00 | 0.01 | 0.05 | 0.02 | 0.07 | 0.03 | 0.07 | 0.11 | 0.00 | 0.09 | 0.00 | 0.00 | 0.08 | 0.00 |
| FeO* | 11.97 | 12.32 | 12.17 | 11.83 | 11.84 | 12.55 | 12.65 | 12.58 | 12.70 | 12.73 | 12.69 | 12.14 | 12.04 | 12.88 | 12.91 | 12.67 | 13.18 | 13.03 | 11.58 | 13.00 | 12.86 | 12.47 | 12.47 |
| MnO | 0.02 | 0.01 | 0.11 | 0.00 | 0.00 | 0.04 | 0.08 | 0.00 | 0.02 | 0.06 | 0.04 | 0.17 | 0.19 | 0.18 | 0.27 | 0.17 | 0.09 | 0.21 | 0.19 | 0.20 | 0.16 | 0.29 | 0.18 |
| MgO | 12.37 | 12.34 | 11.96 | 12.17 | 12.79 | 12.25 | 11.99 | 12.00 | 12.36 | 12.30 | 12.34 | 12.99 | 12.86 | 12.64 | 12.40 | 12.50 | 12.42 | 12.51 | 12.99 | 12.72 | 12.82 | 12.84 | 12.81 |
| CaO | 12.62 | 13.00 | 12.04 | 12.38 | 12.84 | 12.81 | 12.68 | 12.64 | 12.69 | 12.44 | 12.74 | 12.58 | 12.81 | 12.70 | 12.59 | 12.41 | 12.94 | 12.61 | 12.71 | 12.87 | 12.24 | 12.30 | 12.24 |
| Na2O | 1.30 | 1.28 | 1.49 | 1.42 | 1.23 | 1.23 | 1.24 | 1.31 | 1.22 | 1.25 | 1.21 | 1.91 | 1.91 | 1.85 | 1.83 | 1.79 | 1.84 | 1.84 | 1.77 | 1.89 | 1.76 | 1.77 | 1.67 |
| K2O | 0.02 | 0.03 | 0.01 | 0.08 | 0.05 | 0.05 | 0.05 | 0.07 | 0.02 | 0.09 | 0.05 | 0.13 | 0.13 | 0.13 | 0.14 | 0.14 | 0.13 | 0.13 | 0.13 | 0.13 | 0.09 | 0.14 | 0.12 |
| F | 0.00 | 0.00 | 0.00 | 0.00 | 0.00 | 0.00 | 0.00 | 0.00 | 0.09 | 0.07 | 0.00 | 0.00 | 0 00 | 0 00 | 0.00 | 0.00 | 0.00 | 0.00 | 0.00 | 0.00 | 0.12 | 0.00 | 0.00 |
| Cl | 0.01 | 0.05 | 0.00 | 0.05 | 0.04 | 0.03 | 0.05 | 0.02 | 0.04 | 0.05 | 0.03 | 0.00 | 0.05 | 0.01 | 0.07 | 0.08 | 0.00 | 0.01 | 0.02 | 0.02 | 0 00 | 0.03 | 0.00 |
| Total | 96.86 | 98.11 | 96.15 | 96.79 | 96.21 | 97.11 | 97.24 | 96.78 | 97.33 | 96.72 | 97.02 | 97.65 | 97.58 | 97.57 | 97.46 | 96.90 | 98.15 | 97.49 | 97.76 | 97.42 | 96.99 | 97.56 | 96.98 |
| O = F, Cl | 0.00 | -0.01 | 0.00 | -0.01 | -0.01 | 0.00 | -0.01 | 0.00 | -0.04 | -0.04 | -0.01 | 0.00 | -0.01 | 0.00 | -0.02 | -0.02 | 0.00 | 0.00 | 0.00 | 0.00 | -0.05 | -0.01 | 0.00 |
| Total | 96.86 | 98.10 | 96.15 | 96.78 | 96.20 | 97.11 | 97.23 | 96.78 | 97.29 | 96.68 | 97.01 | 97.65 | 97.57 | 97.57 | 97.44 | 96.88 | 98.15 | 97.49 | 97.75 | 97.41 | 96.94 | 97.55 | 96.98 |
| Number of cations on the basis of 23 oxygens:# | | | | | | | | | | | | | | | | | | | | | | | |
| Si | 6.401 | 6.372 | 6.238 | 6.312 | 6.499 | 6.416 | 6.382 | 6.420 | 6.411 | 6.373 | 6.367 | 6.505 | 6.446 | 6.460 | 6.450 | 6.444 | 6 531 | 6.502 | 6.493 | 6.456 | 6.510 | 6.446 | 6.495 |
| Al iv | 1.599 | 1.628 | 1.762 | 1.688 | 1.501 | 1.584 | 1.618 | 1.580 | 1.589 | 1.627 | 1.633 | 1.495 | 1.554 | 1.540 | 1.550 | 1.556 | 1.469 | 1.498 | 1.507 | 1.544 | 1.490 | 1.554 | 1.505 |
| Sum T | 8.000 | 8.000 | 8.000 | 8.000 | 8.000 | 8.000 | 8.000 | 8.000 | 8.000 | 8.000 | 8.000 | 8.000 | 8.000 | 8.000 | 8.000 | 8.000 | 8.000 | 8.000 | 8.000 | 8.000 | 8.000 | 8.000 | 8.000 |
| Al vi | 0.795 | 0.780 | 0.813 | 0.862 | 0.682 | 0.745 | 0.767 | 0.760 | 0.705 | 0 679 | 0.700 | 0.642 | 0.655 | 0 594 | 0.626 | 0.632 | 0.619 | 0.612 | 0.701 | 0.558 | 0.572 | 0.626 | 0.627 |
| Ti | 0.065 | 0.069 | 0.075 | 0.062 | 0.064 | 0.059 | 0.083 | 0.079 | 0.068 | 0.080 | 0.069 | 0.045 | 0.056 | 0.052 | 0.055 | 0 053 | 0.053 | 0.045 | 0.058 | 0.044 | 0.046 | 0.045 | 0.052 |
| Cr | 0.000 | 0.011 | 0.007 | 0.000 | 0.000 | 0.004 | 0.000 | 0.004 | 0.004 | 0.000 | 0.001 | 0.006 | 0.002 | 0.008 | 0.003 | 0.008 | 0.013 | 0.000 | 0.010 | 0.000 | 0.000 | 0.009 | 0.000 |
| Fe3+ | 0.371 | 0.317 | 0.595 | 0.429 | 0.289 | 0.361 | 0.369 | 0.312 | 0.448 | 0.524 | 0.464 | 0.280 | 0.217 | 0.312 | 0.319 | 0.374 | 0.146 | 0.302 | 0 213 | 0.293 | 0.479 | 0.486 | 0.461 |
| Mg | 2.682 | 2.652 | 2.605 | 2.637 | 2.799 | 2.659 | 2.600 | 2.618 | 2.676 | 2.678 | 2.680 | 2.812 | 2.795 | 2.751 | 2.703 | 2.732 | 2.698 | 2.725 | 2.805 | 2.779 | 2.792 | 2.773 | 2.781 |
| Fe2+ | 1.086 | 1.169 | 0.892 | 1.009 | 1.166 | 1.168 | 1.171 | 1.229 | 1.096 | 1.031 | 1.081 | 1.195 | 1.251 | 1.261 | 1.260 | 1.180 | 1.461 | 1.291 | 1.190 | 1.301 | 1.092 | 1.025 | 1.058 |
| Mn | 0.002 | 0.001 | 0.014 | 0.000 | 0.000 | 0.005 | 0.009 | 0.000 | 0.003 | 0.007 | 0.005 | 0.021 | 0 023 | 0.022 | 0.033 | 0.021 | 0.011 | 0.026 | 0.023 | 0.025 | 0.019 | 0.036 | 0.022 |
| Sum C | 5.000 | 5.000 | 5.000 | 5.000 | 5.000 | 5.000 | 5.000 | 5.000 | 5.000 | 5.000 | 5.000 | 5.000 | 5.000 | 5.000 | 5.000 | 5.000 | 5.000 | 5.000 | 5.000 | 5.000 | 5.000 | 5.000 | 5.000 |
| Fe2+ | 0.000 | 0.000 | 0.000 | 0.000 | 0.000 | 0.000 | 0.000 | 0.000 | 0.000 | 0.000 | 0.000 | 0.000 | 0.000 | 0.000 | 0.000 | 0.000 | 0.000 | 0.000 | 0.000 | 0.000 | 0.000 | 0.000 | 0.000 |
| Mn | 0.000 | 0.000 | 0 000 | 0.000 | 0.000 | 0.000 | 0.000 | 0.000 | 0.000 | 0.000 | 0.000 | 0.000 | 0.000 | 0.000 | 0.000 | 0.000 | 0.000 | 0.000 | 0.000 | 0.000 | 0.000 | 0.000 | 0.000 |
| Ca | 1.967 | 2.000 | 1.886 | 1.928 | 2.000 | 2.000 | 1.978 | 1.982 | 1.974 | 1.947 | 1.989 | 1.958 | 2.000 | 1.987 | 1.973 | 1.950 | 2.000 | 1.975 | 1.973 | 2.000 | 1.916 | 1.910 | 1.910 |
| Na | 0.033 | 0.000 | 0.114 | 0.072 | 0.000 | 0.000 | 0.022 | 0.018 | 0.026 | 0.053 | 0.011 | 0.042 | 0.000 | 0.013 | 0.027 | 0.050 | 0 000 | 0.025 | 0.027 | 0.000 | 0.084 | 0.090 | 0.090 |
| Sum B | 2.000 | 2.000 | 2.000 | 2.000 | 2.000 | 2.000 | 2.000 | 2.000 | 2.000 | 2.000 | 2.000 | 2.000 | 2.000 | 2.000 | 2.000 | 2.000 | 2.000 | 2.000 | 2.000 | 2.000 | 2.000 | 2.000 | 2.000 |
| Ca | 0.000 | 0.009 | 0.000 | 0.000 | 0 021 | 0.000 | 0.000 | 0.000 | 0.000 | 0.000 | 0.000 | 0.000 | 0.001 | 0.000 | 0.000 | 0.000 | 0.021 | 0.000 | 0.000 | 0.022 | 0.000 | 0.000 | 0.000 |
| Na | 0.334 | 0.358 | 0.310 | 0.329 | 0.351 | 0.348 | 0.328 | 0.354 | 0.317 | 0.301 | 0.331 | 0.496 | 0.540 | 0.511 | 0.492 | 0.459 | 0.520 | 0.496 | 0.470 | 0.537 | 0.413 | 0.407 | 0.381 |
| K | 0.004 | 0.006 | 0.002 | 0.014 | 0.010 | 0.009 | 0.009 | 0.013 | 0.004 | 0.016 | 0.010 | 0.024 | 0.024 | 0.024 | 0.026 | 0.026 | 0 024 | 0.024 | 0.024 | 0.024 | 0.017 | 0 026 | 0.023 |
| Sum A | 0.338 | 0.372 | 0.311 | 0.344 | 0.381 | 0.357 | 0.338 | 0.366 | 0.321 | 0.317 | 0.341 | 0.520 | 0.566 | 0 535 | 0.518 | 0.485 | 0 565 | 0.520 | 0.494 | 0.584 | 0.430 | 0.433 | 0 404 |
| Sum Cations | 15.338 | 15.372 | 15.311 | 15.344 | 15.381 | 15.357 | 15.338 | 15.366 | 15.321 | 15.317 | 15.341 | 15.520 | 15.566 | 15.535 | 15.518 | 15.485 | 15.565 | 15.520 | 15.494 | 15.584 | 15.430 | 15.433 | 15.404 |
| Mg/(Mg+Fe2) | 0.712 | 0.694 | 0.745 | 0 723 | 0.706 | 0.695 | 0.689 | 0.681 | 0.710 | 0.722 | 0.712 | 0.702 | 0.691 | 0.686 | 0 682 | 0.698 | 0.649 | 0 679 | 0 702 | 0.681 | 0.719 | 0.730 | 0.724 |

* Total Fe as FeO.

# Calculated by normalising the number of cations other than Ca, Na and K to 13.

Table C-2 Electron microprobe analyses of clinopyroxenes

| Sample no. | 5/6291 | | | | | | | 4/7291 | | | 8/7291 | | | | | | | | | 9/7291 | | |
|---|---|---|---|---|---|---|---|---|---|---|---|---|---|---|---|---|---|---|---|---|---|---|
| Analysis no. | 1 | 2 | 3 | 4 | 5 | 6 | 7 | 1 core | 2 core | 3 core | 1 | 2 | 3 | 4 | 5 | 6 | 7 | 8 | 9 | 1 Core | 2 Core | 3 Core |
| SiO2 | 52.06 | 52.13 | 52.22 | 52.38 | 52.28 | 51.49 | 51.84 | 52.15 | 52.89 | 53.19 | 52.93 | 53.10 | 53.09 | 53.43 | 53.51 | 52.84 | 53.54 | 53.73 | 53.01 | 49.68 | 51.25 | 49.81 |
| TiO2 | 0.09 | 0.07 | 0.07 | 0.02 | 0.07 | 0.13 | 0.05 | 0.07 | 0.08 | 0.06 | 0 05 | 0.04 | 0.05 | 0.06 | 0.06 | 0.05 | 0.04 | 0.04 | 0.04 | 0.44 | 0.45 | 0.40 |
| Al2O3 | 1.11 | 1.03 | 1.14 | 0.73 | 0.91 | 1.22 | 1.15 | 6.57 | 1.46 | 1.10 | 1.83 | 1.70 | 1.51 | 1.66 | 1.64 | 2.22 | 1.72 | 1.54 | 1.63 | 5.87 | 3.30 | 4.76 |
| Cr2O3 | 0.07 | 0.06 | 0.07 | 0.07 | 0.08 | 0.07 | 0.11 | 0.05 | 0.10 | 0.02 | 0.00 | 0.03 | 0.00 | 0.04 | 0.05 | 0.04 | 0.02 | 0.00 | 0.00 | 0.00 | 0.00 | 0.05 |
| Fe2O3* | 3.11 | 3.40 | 2.44 | 2.67 | 2.56 | 4.61 | 3.73 | 0.00 | 0.94 | 1.37 | 1.15 | 1.20 | 0.80 | 1.36 | 1.18 | 1.13 | 1.05 | 1.22 | 1.75 | 2.26 | 1.90 | 3.08 |
| FeO* | 4.02 | 3.73 | 4.54 | 3.64 | 4.13 | 2.80 | 3.50 | 4.16 | 4.16 | 3.64 | 4.86 | 4.55 | 4.85 | 4.14 | 4.57 | 4.47 | 4.70 | 4.01 | 4.07 | 6.63 | 5.00 | 4.38 |
| MnO | 0.39 | 0.41 | 0.39 | 0.38 | 0.32 | 0.38 | 0.35 | 0.20 | 0.12 | 0.13 | 0.28 | 0.21 | 0.20 | 0.26 | 0.19 | 0.26 | 0.20 | 0.27 | 0.27 | 0.04 | 0.00 | 0.06 |
| MgO | 14.30 | 14.12 | 14.15 | 14.49 | 14.31 | 14.04 | 14.02 | 13.12 | 14.79 | 15.06 | 14.06 | 14.37 | 14.21 | 14.33 | 14.41 | 14.18 | 14.32 | 14.46 | 14.30 | 13.18 | 13.64 | 13.64 |
| CaO | 24.05 | 24.27 | 23.77 | 24.63 | 24.13 | 24.72 | 24.57 | 23.07 | 25.00 | 25.32 | 24.25 | 24.12 | 24.27 | 24.55 | 24.65 | 24.40 | 24.46 | 24.42 | 24.56 | 21.51 | 24.51 | 23.24 |
| Na2O | 0.35 | 0.43 | 0.41 | 0.27 | 0.36 | 0.39 | 0.37 | 0.33 | 0.14 | 0.13 | 0.45 | 0.49 | 0.44 | 0.55 | 0.46 | 0.43 | 0.50 | 0.63 | 0.46 | 0.45 | 0.21 | 0.30 |
| Total | 99.54 | 99.65 | 99.19 | 99.28 | 99.16 | 99.85 | 99.68 | 99.72 | 99.67 | 100.02 | 99.86 | 99.80 | 99.43 | 100.38 | 100.71 | 100.01 | 100.55 | 100.34 | 100.09 | 100.06 | 100.26 | 99.73 |
| Number of cations on the basis of 6 oxygens : | | | | | | | | | | | | | | | | | | | | | | |
| Si | 1.941 | 1.942 | 1.952 | 1.955 | 1.954 | 1.918 | 1.933 | 1.922 | 1.956 | 1.960 | 1.959 | 1.962 | 1.970 | 1.963 | 1.962 | 1.949 | 1.964 | 1.971 | 1.955 | 1.844 | 1.897 | 1.851 |
| Al iv | 0.049 | 0.045 | 0.048 | 0 032 | 0.040 | 0.054 | 0.051 | 0.078 | 0.044 | 0.040 | 0.041 | 0.038 | 0.030 | 0.037 | 0.038 | 0 051 | 0.036 | 0.029 | 0.045 | 0.156 | 0.103 | 0.149 |
| Fe3+ | 0.010 | 0.012 | 0.000 | 0.013 | 0.006 | 0.028 | 0.017 | 0.000 | 0.000 | 0.000 | 0.000 | 0.000 | 0.000 | 0.000 | 0.000 | 0.000 | 0.000 | 0.000 | 0.000 | 0.000 | 0.000 | 0.000 |
| Sum T | 2.000 | 2.000 | 2.000 | 2.000 | 2.000 | 2.000 | 2.000 | 2.000 | 2.000 | 2.000 | 2.000 | 2.000 | 2.000 | 2.000 | 2 000 | 2.000 | 2.000 | 2 000 | 2 000 | 2.000 | 2.000 | 2.000 |
| Al vi | 0.000 | 0.000 | 0.003 | 0.000 | 0.000 | 0.000 | 0.000 | 0.207 | 0.020 | 0.008 | 0.038 | 0.036 | 0.036 | 0.035 | 0.033 | 0.046 | 0.039 | 0.038 | 0.027 | 0.101 | 0.041 | 0.060 |
| Ti | 0.003 | 0.002 | 0.002 | 0.001 | 0.002 | 0.004 | 0.001 | 0.002 | 0.002 | 0.002 | 0 002 | 0.001 | 0.001 | 0.002 | 0.002 | 0.002 | 0.001 | 0.001 | 0.001 | 0.012 | 0.013 | 0 011 |
| Cr | 0.002 | 0.002 | 0.002 | 0.002 | 0.002 | 0.002 | 0.003 | 0.001 | 0.003 | 0.001 | 0.000 | 0.001 | 0.000 | 0.001 | 0.001 | 0.001 | 0.001 | 0.000 | 0.000 | 0.000 | 0.000 | 0.001 |
| Fe3+ | 0.077 | 0.083 | 0.069 | 0.062 | 0.066 | 0.101 | 0.088 | 0.000 | 0.026 | 0.038 | 0.032 | 0.033 | 0.022 | 0 038 | 0.033 | 0.031 | 0.029 | 0 034 | 0.048 | 0.063 | 0.053 | 0.086 |
| Fe2+ | 0.125 | 0.116 | 0.142 | 0.113 | 0.130 | 0.087 | 0.109 | 0.128 | 0.129 | 0.112 | 0.151 | 0.140 | 0.151 | 0.127 | 0.137 | 0.138 | 0.144 | 0.123 | 0.126 | 0.206 | 0.155 | 0.136 |
| Mn | 0.012 | 0.013 | 0.012 | 0.012 | 0.010 | 0.012 | 0.011 | 0.006 | 0.004 | 0.004 | 0.009 | 0.007 | 0.006 | 0.008 | 0.006 | 0.008 | 0.006 | 0.008 | 0.008 | 0.001 | 0.000 | 0.002 |
| Mg | 0.795 | 0.784 | 0.788 | 0.806 | 0.797 | 0.779 | 0.779 | 0.721 | 0.815 | 0.827 | 0.775 | 0.791 | 0.786 | 0.784 | 0.787 | 0.779 | 0.783 | 0.791 | 0.786 | 0.729 | 0.752 | 0.756 |
| Sum O | 1.014 | 1.000 | 1.018 | 0.996 | 1.008 | 0.985 | 0.992 | 1.065 | 0.999 | 0.991 | 1.006 | 1.010 | 1.003 | 0.995 | 0.999 | 1.005 | 1 003 | 0.995 | 0.996 | 1.112 | 1.013 | 1.053 |
| Ca | 0.961 | 0.969 | 0.952 | 0.985 | 0.966 | 0.987 | 0.982 | 0.911 | 0.991 | 1.000 | 0.961 | 0.955 | 0.965 | 0.966 | 0.969 | 0.964 | 0.961 | 0.960 | 0.971 | 0.855 | 0.972 | 0.926 |
| Na | 0.025 | 0.031 | 0.030 | 0.020 | 0.026 | 0.028 | 0.027 | 0.024 | 0.010 | 0.009 | 0 032 | 0.035 | 0.032 | 0 039 | 0.033 | 0.031 | 0.035 | 0.045 | 0.033 | 0.032 | 0.015 | 0.022 |
| Sum Cations | 4.000 | 4.000 | 4.000 | 4.000 | 4.000 | 4.000 | 4.000 | 4.000 | 4.000 | 4.000 | 4.000 | 4.000 | 4.000 | 4.000 | 4.000 | 4.000 | 4.000 | 4.000 | 4.000 | 4.000 | 4.000 | 4.000 |
| Mg/(Mg+Fe2) | 0.864 | 0.871 | 0.848 | 0.877 | 0.860 | 0.899 | 0.877 | 0.849 | 0.864 | 0.881 | 0.837 | 0.849 | 0.839 | 0.860 | 0.852 | 0.850 | 0.845 | 0.865 | 0.862 | 0.780 | 0.829 | 0.847 |
| Molecular proportions of end-members# : | | | | | | | | | | | | | | | | | | | | | | |
| Wo | 0.488 | 0.493 | 0.485 | 0.498 | 0.491 | 0.502 | 0.499 | 0.516 | 0.504 | 0.505 | 0.499 | 0.496 | 0.500 | 0.502 | 0.502 | 0 502 | 0 500 | 0.501 | 0.501 | 0.461 | 0.503 | 0 486 |
| En | 0.403 | 0.399 | 0.402 | 0.407 | 0.405 | 0.396 | 0.396 | 0.408 | 0.415 | 0.417 | 0.402 | 0.411 | 0.407 | 0.408 | 0.408 | 0.406 | 0.407 | 0 413 | 0.405 | 0.393 | 0.389 | 0.397 |
| Fs | 0 109 | 0.108 | 0.113 | 0.095 | 0.105 | 0.102 | 0.106 | 0.076 | 0.081 | 0 078 | 0.099 | 0.094 | 0 093 | 0.090 | 0 091 | 0.092 | 0.093 | 0.086 | 0.094 | 0.146 | 0.107 | 0.118 |

* Calculated assuming stoichiometry on the basis of 4 cations and 6 oxygens.

# Calculated after the Subcommittee on Pyroxenes, IMA (1988)

Table C-2 (continued)

| Sample no. | 9/7291 | | | | | | | | | | | | | | 12/7291 | | | | | | |
|---|---|---|---|---|---|---|---|---|---|---|---|---|---|---|---|---|---|---|---|---|---|
| Analysis no. | 4 | 5 | 6 | 7 | 8 | 9 | 10 | 11 | 12 | 13 | 14 | 15 | 16 | 17 | 1 | 2 | 3 | 4 | 5 | 6 | 7 |
| | Core | Core | Core | Rim hbl | Rim hbl | Rim hbl | Rim hbl | Rim grt | Rim grt | | | | | | | | | | | | |
| SiO2 | 50.56 | 50.04 | 51.19 | 51.01 | 50.39 | 50.87 | 50.18 | 50.80 | 50.52 | 50.40 | 50.14 | 49.84 | 49.82 | 49.86 | 51.86 | 51.73 | 51.84 | 51.46 | 51.95 | 52.01 | 52.09 |
| TiO2 | 0.41 | 0.60 | 0.39 | 0.59 | 0.32 | 0.35 | 0.46 | 0.49 | 0.74 | 0.65 | 0.67 | 0.50 | 0.63 | 0.70 | 0.10 | 0.08 | 0.08 | 0.12 | 0.12 | 0.12 | 0.11 |
| Al2O3 | 4.16 | 4.28 | 2.80 | 3.90 | 3.44 | 3.45 | 4.71 | 4.00 | 4.13 | 3.97 | 5.03 | 6.60 | 5.27 | 4.76 | 2.79 | 2.81 | 2.11 | 2.74 | 3.07 | 3.02 | 2.60 |
| Cr2O3 | 0.02 | 0.00 | 0.02 | 0.00 | 0.04 | 0.02 | 0.00 | 0.00 | 0.00 | 0.03 | 0.07 | 0.00 | 0.04 | 0.00 | 0.00 | 0.02 | 0.00 | 0.00 | 0.00 | 0.00 | 0.03 |
| Fe2O3* | 2.61 | 2.66 | 2.33 | 1.79 | 2.51 | 2.60 | 2.23 | 1.76 | 2.15 | 1.45 | 1.56 | 1.00 | 1.01 | 1.65 | 3.21 | 3.75 | 3.74 | 4.31 | 2.93 | 2.47 | 3.25 |
| FeO* | 5.12 | 4.48 | 4.54 | 5.25 | 5.06 | 4.96 | 5.49 | 5.46 | 5.12 | 5.45 | 5.65 | 6.38 | 6.16 | 5.35 | 4.41 | 3.95 | 3.88 | 3.66 | 4.81 | 5.45 | 4.48 |
| MnO | 0.00 | 0.00 | 0.02 | 0.00 | 0.07 | 0.00 | 0.03 | 0.00 | 0.00 | 0.00 | 0.05 | 0.00 | 0.07 | 0.00 | 0.17 | 0.28 | 0.18 | 0.24 | 0.23 | 0.18 | 0.27 |
| MgO | 13.21 | 13.40 | 13.64 | 13.35 | 13.57 | 13.65 | 13.24 | 13.24 | 12.91 | 13.21 | 13.10 | 13.23 | 12.98 | 13.02 | 13.29 | 13.19 | 13.50 | 13.20 | 13.00 | 12.95 | 13.27 |
| CaO | 24.45 | 24.36 | 25.19 | 24.92 | 23.72 | 24.21 | 23.42 | 24.50 | 25.17 | 24.36 | 23.75 | 21.82 | 23.09 | 23.76 | 24.53 | 24.69 | 24.64 | 24.64 | 24.44 | 24.19 | 24.46 |
| Na2O | 0.18 | 0.17 | 0.09 | 0.12 | 0.18 | 0.18 | 0.28 | 0.16 | 0.15 | 0.14 | 0.24 | 0.46 | 0.26 | 0.20 | 0.52 | 0.55 | 0.51 | 0.57 | 0.55 | 0.56 | 0.57 |
| Total | 100.72 | 100.00 | 100.21 | 100.93 | 99.30 | 100.29 | 100.03 | 100.41 | 100.90 | 99.65 | 100.26 | 99.83 | 99.33 | 99.30 | 100.87 | 101.06 | 100.48 | 100.94 | 101.10 | 100.95 | 101.14 |
| Number of cations on the basis of 6 oxygens : | | | | | | | | | | | | | | | | | | | | | |
| Si | 1.868 | 1.858 | 1.898 | 1.878 | 1.886 | 1.885 | 1.863 | 1.880 | 1.865 | 1.879 | 1.857 | 1.845 | 1.861 | 1.860 | 1.911 | 1.904 | 1.918 | 1.898 | 1.909 | 1.917 | 1.915 |
| Al iv | 0.132 | 0.142 | 0.102 | 0.122 | 0.114 | 0.115 | 0.137 | 0.120 | 0.135 | 0.121 | 0.143 | 0.155 | 0.139 | 0.140 | 0.089 | 0.096 | 0.082 | 0.102 | 0.091 | 0.083 | 0.085 |
| Fe3+ | 0.000 | 0.000 | 0.000 | 0.000 | 0.000 | 0.000 | 0.000 | 0.000 | 0.000 | 0.000 | 0.000 | 0.000 | 0.000 | 0.000 | 0.000 | 0.000 | 0.000 | 0.000 | 0.000 | 0 000 | 0.000 |
| Sum T | 2.000 | 2.000 | 2.000 | 2.000 | 2.000 | 2.000 | 2.000 | 2.000 | 2.000 | 2.000 | 2.000 | 2.000 | 2.000 | 2.000 | 2.000 | 2.000 | 2.000 | 2.000 | 2.000 | 2.000 | 2.000 |
| Al vi | 0.049 | 0.046 | 0.021 | 0.048 | 0.037 | 0.036 | 0.069 | 0.055 | 0.045 | 0.053 | 0.077 | 0.133 | 0.093 | 0.069 | 0.032 | 0.026 | 0.010 | 0.017 | 0.042 | 0.048 | 0.028 |
| Ti | 0.011 | 0.017 | 0.011 | 0.016 | 0.009 | 0.010 | 0.013 | 0.014 | 0.021 | 0.018 | 0.019 | 0.014 | 0.018 | 0.020 | 0.003 | 0.002 | 0.002 | 0.003 | 0.003 | 0.003 | 0.003 |
| Cr | 0.001 | 0.000 | 0.001 | 0.000 | 0.001 | 0.001 | 0.000 | 0.000 | 0.000 | 0.001 | 0.002 | 0.000 | 0.001 | 0.000 | 0.000 | 0.001 | 0.000 | 0.000 | 0.000 | 0.000 | 0.001 |
| Fe3+ | 0.073 | 0.074 | 0.065 | 0.050 | 0.071 | 0.072 | 0.062 | 0.049 | 0.060 | 0.041 | 0.043 | 0.028 | 0.028 | 0.046 | 0.089 | 0.104 | 0.104 | 0.120 | 0.081 | 0.068 | 0.090 |
| Fe2+ | 0.158 | 0.140 | 0.141 | 0.162 | 0.158 | 0.154 | 0.170 | 0.169 | 0.158 | 0.170 | 0.175 | 0.198 | 0.192 | 0.177 | 0.136 | 0.122 | 0.120 | 0.113 | 0.153 | 0.168 | 0.138 |
| Mn | 0.000 | 0.000 | 0.001 | 0.000 | 0.002 | 0.000 | 0.001 | 0.000 | 0.000 | 0.000 | 0.001 | 0.000 | 0.002 | 0.000 | 0 005 | 0.009 | 0.006 | 0.007 | 0.007 | 0.006 | 0.008 |
| Mg | 0.727 | 0.742 | 0.754 | 0.733 | 0.757 | 0.754 | 0.733 | 0.730 | 0.710 | 0.734 | 0.723 | 0.730 | 0.722 | 0.724 | 0.730 | 0.724 | 0.744 | 0.725 | 0.712 | 0.711 | 0.727 |
| Sum O | 1.019 | 1.018 | 0.993 | 1.008 | 1.036 | 1.026 | 1.048 | 1.017 | 0.994 | 1.017 | 1.041 | 1.102 | 1.057 | 1.036 | 0.994 | 0.987 | 0.987 | 0.986 | 0.998 | 1.005 | 0.996 |
| Ca | 0.968 | 0.969 | 1.001 | 0.983 | 0.951 | 0.961 | 0.932 | 0.972 | 0.996 | 0.973 | 0.942 | 0.865 | 0.924 | 0.950 | 0.968 | 0 974 | 0.977 | 0.974 | 0.962 | 0.955 | 0.964 |
| Na | 0.013 | 0.012 | 0.006 | 0.009 | 0.013 | 0.013 | 0.020 | 0.011 | 0.011 | 0.010 | 0.017 | 0.033 | 0.019 | 0.014 | 0.037 | 0.039 | 0.037 | 0.041 | 0.039 | 0.040 | 0.041 |
| Sum Cations | 4.000 | 4.000 | 4.000 | 4.000 | 4.000 | 4.000 | 4.000 | 4.000 | 4.000 | 4.000 | 4.000 | 4.000 | 4.000 | 4.000 | 4.000 | 4.000 | 4.000 | 4.000 | 4.000 | 4.000 | 4.000 |
| Mg/(Mg+Fe2) | 0.821 | 0.842 | 0.843 | 0.819 | 0.827 | 0.831 | 0.811 | 0.812 | 0.818 | 0.812 | 0.805 | 0.787 | 0.790 | 0.804 | 0.843 | 0.856 | 0.861 | 0.865 | 0.824 | 0.809 | 0.841 |
| Molecular proportions of end-members# : | | | | | | | | | | | | | | | | | | | | | |
| Wo | 0.503 | 0.504 | 0.510 | 0.510 | 0.490 | 0.495 | 0.491 | 0.506 | 0.518 | 0.507 | 0.500 | 0.475 | 0.494 | 0.501 | 0.502 | 0.504 | 0.501 | 0 502 | 0.503 | 0.501 | 0.500 |
| En | 0.378 | 0.385 | 0.384 | 0.380 | 0.390 | 0.388 | 0.386 | 0.380 | 0.369 | 0.383 | 0.383 | 0.401 | 0.386 | 0.382 | 0.378 | 0.375 | 0.382 | 0.374 | 0.372 | 0.373 | 0.377 |
| Fs | 0.120 | 0.111 | 0.105 | 0.110 | 0.119 | 0.117 | 0.123 | 0.114 | 0.113 | 0.110 | 0.117 | 0.124 | 0 119 | 0.118 | 0.119 | 0.121 | 0.118 | 0.124 | 0.126 | 0.127 | 0.123 |

* Calculated assuming stoichiometry on the basis of 4 cations and 6 oxygens.
# Calculated after the Subcommittee on Pyroxenes, IMA (1988)

Table C-3 Electron microprobe analyses of garnets (ophiolite association of the Pna Som Metamorphic Complex).

| Sample no. | 9/7291 | | | | | | | | | | | | | | | | | | | | |
|---|---|---|---|---|---|---|---|---|---|---|---|---|---|---|---|---|---|---|---|---|---|
| Analysis no. | 1 | 2 | 3 | 4 | 5 | 6 | 7 | 8 | 9 | 10 | 11 | 12 | 13 | 14.00 | 154 | 16 | 17 | 18 | 19 | 20 | 21 |
| | rim hbl | rim hbl | rim hbl | rim hbl | core | core | core | core | rim cpx | rim cpx | rim cpx | | | | | | | | | | |
| SiO2 | 38.74 | 38.56 | 38.52 | 38.19 | 38.92 | 38.07 | 38.87 | 38.68 | 37.80 | 38.41 | 38.11 | 38.61 | 38.63 | 38.61 | 38.11 | 38.31 | 39.00 | 38.58 | 38.20 | 38.42 | 38.71 |
| TiO2 | 0.05 | 0.00 | 0.06 | 0.05 | 0.00 | 0.10 | 0.11 | 0.10 | 0.11 | 0.12 | 0.04 | 0.13 | 0.12 | 0.10 | 0.15 | 0.06 | 0.06 | 0.10 | 0.04 | 0.08 | 0.11 |
| Al2O3 | 21.21 | 21.37 | 21.66 | 21.48 | 21.87 | 20.98 | 21.44 | 21.35 | 21.10 | 21.12 | 21.20 | 21.18 | 21.21 | 21.13 | 20.97 | 20.91 | 21.37 | 21.26 | 21.22 | 21.14 | 21.27 |
| Cr2O3 | 0.14 | 0.00 | 0.00 | 0.03 | 0.03 | 0.00 | 0.04 | 0.00 | 0.07 | 0.05 | 0.00 | 0.06 | 0 00 | 0 00 | 0.01 | 0 05 | 0.00 | 0.02 | 0.08 | 0.00 | 0.05 |
| Fe2O3* | 0.69 | 0.16 | 0.76 | 1.63 | 0.87 | 3.27 | 2.00 | 1.80 | 1.72 | 2.20 | 1.79 | 1.35 | 0.41 | 0.33 | 1.28 | 1.61 | 1.02 | 0.38 | 1.08 | 0.77 | 0.98 |
| FeO* | 22.40 | 20.82 | 20.16 | 19.76 | 20.24 | 21.77 | 22.17 | 21.65 | 21.80 | 22.62 | 19.84 | 22.80 | 22.95 | 23.48 | 21.99 | 21.30 | 20.75 | 21.44 | 21.23 | 20.49 | 21.20 |
| MnO | 0.61 | 0.49 | 0.41 | 0 62 | 0.42 | 0.60 | 0.44 | 0.46 | 0.34 | 0.51 | 0.41 | 0.68 | 0.65 | 0.51 | 0.50 | 0 66 | 0.50 | 0.52 | 0.43 | 0.42 | 0.53 |
| MgO | 4.77 | 2.64 | 4.17 | 2.14 | 4.72 | 6.46 | 7.07 | 7.13 | 4.63 | 4.71 | 3.78 | 5.14 | 4.94 | 5.56 | 4.54 | 4.00 | 5.84 | 5.38 | 5.06 | 5.84 | 5.75 |
| CaO | 11.59 | 15.68 | 14.13 | 16.79 | 13.63 | 9.15 | 8.87 | 8.99 | 11.63 | 11.32 | 14.53 | 10.65 | 10.83 | 9.64 | 11.79 | 13.04 | 11.72 | 11.46 | 11.73 | 11.46 | 11.24 |
| Total | 100.20 | 99.72 | 99.88 | 100.69 | 100.70 | 100.40 | 101.01 | 100.16 | 99.20 | 101.06 | 99.70 | 100.61 | 99.75 | 99.35 | 99.34 | 99.94 | 100.27 | 99.14 | 99.07 | 98.62 | 99.84 |
| Number of cations on the basis of 12 oxygens : | | | | | | | | | | | | | | | | | | | | | |
| Si | 3.003 | 3.012 | 2.985 | 2.965 | 2.985 | 2.943 | 2.969 | 2.974 | 2.965 | 2.966 | 2.971 | 2.986 | 3.008 | 3.013 | 2 985 | 2.987 | 2.998 | 3.006 | 2 986 | 3.000 | 2.994 |
| Al iv | 0.000 | 0.000 | 0.015 | 0.035 | 0.015 | 0.057 | 0.031 | 0.026 | 0.035 | 0.034 | 0.029 | 0.014 | 0.000 | 0.000 | 0.015 | 0.013 | 0.002 | 0.000 | 0.014 | 0.000 | 0.006 |
| Al vi | 1.942 | 1.979 | 1.964 | 1.932 | 1.963 | 1.855 | 1.900 | 1.910 | 1.916 | 1.889 | 1.919 | 1.917 | 1.955 | 1.957 | 1.922 | 1.909 | 1.935 | 1.958 | 1.941 | 1.946 | 1.933 |
| Ti | 0.003 | 0.000 | 0.003 | 0.003 | 0.000 | 0.006 | 0.006 | 0.006 | 0.006 | 0.007 | 0 002 | 0.007 | 0.007 | 0.006 | 0.009 | 0.004 | 0.004 | 0.006 | 0.003 | 0 005 | 0.006 |
| Cr | 0.009 | 0.000 | 0.000 | 0.002 | 0.002 | 0.000 | 0 002 | 0.000 | 0.004 | 0.003 | 0.000 | 0.004 | 0.000 | 0 000 | 0.001 | 0 003 | 0.000 | 0.001 | 0.005 | 0.000 | 0.003 |
| Fe3+ | 0.040 | 0.009 | 0.045 | 0.095 | 0.050 | 0.190 | 0.115 | 0.104 | 0.102 | 0.128 | 0.105 | 0.079 | 0.024 | 0.019 | 0 075 | 0 094 | 0.059 | 0 022 | 0.063 | 0.045 | 0.057 |
| Fe2+ | 1.452 | 1.360 | 1.307 | 1.283 | 1.298 | 1.407 | 1.416 | 1.392 | 1.430 | 1.461 | 1.293 | 1.474 | 1.494 | 1.533 | 1.440 | 1.392 | 1.334 | 1.397 | 1.388 | 1.338 | 1.371 |
| Mn | 0 040 | 0.032 | 0.027 | 0.041 | 0.027 | 0.039 | 0.028 | 0 030 | 0.023 | 0 033 | 0 027 | 0.045 | 0.043 | 0 033 | 0.033 | 0.044 | 0.033 | 0.034 | 0.029 | 0 028 | 0.034 |
| Mg | 0.551 | 0.307 | 0.482 | 0.248 | 0.540 | 0.744 | 0.805 | 0.817 | 0.541 | 0.542 | 0.439 | 0.592 | 0.573 | 0.646 | 0.530 | 0.465 | 0.669 | 0.625 | 0.589 | 0.680 | 0.663 |
| Ca | 0.963 | 1.312 | 1.173 | 1.397 | 1.120 | 0.758 | 0.726 | 0.741 | 0.977 | 0.937 | 1.214 | 0.882 | 0.904 | 0.806 | 0.989 | 1.089 | 0.965 | 0.956 | 0.982 | 0.959 | 0.931 |
| Sum Cations | 8.000 | 8.000 | 8.000 | 8.000 | 8.000 | 8.000 | 8.000 | 8.000 | 8.000 | 8.000 | 8.000 | 8.000 | 8.000 | 8.000 | 8.000 | 8.000 | 8.000 | 8.000 | 8.000 | 8.000 | 8.000 |
| Mg/Mg+Fe2 | 0 275 | 0.184 | 0.269 | 0.162 | 0.294 | 0.346 | 0.362 | 0.370 | 0.275 | 0.271 | 0.253 | 0.287 | 0.277 | 0.297 | 0.269 | 0.250 | 0.334 | 0.309 | 0.298 | 0.337 | 0.326 |
| Molecular proportions of end-members : | | | | | | | | | | | | | | | | | | | | | |
| Alm | 0.483 | 0.451 | 0.437 | 0.432 | 0.435 | 0.477 | 0.476 | 0.467 | 0.481 | 0.491 | 0.435 | 0.493 | 0.496 | 0.508 | 0.481 | 0.466 | 0.445 | 0.464 | 0 465 | 0.445 | 0.457 |
| Py | 0.183 | 0.102 | 0.161 | 0.083 | 0.181 | 0 252 | 0.270 | 0.274 | 0.182 | 0.182 | 0.148 | 0.198 | 0.190 | 0.214 | 0.177 | 0.155 | 0.223 | 0.207 | 0.197 | 0 226 | 0.221 |
| Sp | 0 013 | 0.011 | 0.009 | 0.014 | 0.009 | 0.013 | 0.010 | 0 010 | 0.008 | 0.011 | 0.009 | 0.015 | 0 014 | 0.011 | 0 011 | 0 015 | 0.011 | 0.011 | 0 010 | 0.009 | 0.011 |
| Gr | 0.300 | 0.431 | 0.370 | 0.423 | 0.350 | 0.160 | 0.186 | 0.196 | 0.278 | 0.251 | 0.355 | 0 255 | 0.288 | 0.258 | 0.293 | 0.317 | 0 292 | 0.306 | 0.297 | 0 296 | 0.282 |
| Adr | 0 020 | 0 005 | 0 022 | 0.048 | 0.025 | 0.097 | 0 058 | 0.052 | 0 051 | 0 064 | 0 053 | 0 040 | 0 012 | 0 010 | 0 038 | 0 047 | 0.029 | 0.011 | 0 032 | 0.023 | 0.029 |

* Calculated assuming stoichiometry on the basis of 8 cations and 12 oxygens.

Table C-4 Electron microprobe analyses of zoisites

| Sample no. | 4/7291 | | 5/7291 | | | | | | 7/7291 | | | | 8/7291 | | | |
|---|---|---|---|---|---|---|---|---|---|---|---|---|---|---|---|---|
| Analysis no. | 1 | 2 | 1 | 2 | 3 | 4 | 5 | 6 | 1 | 2 | 3 | 4 | 1 | 2 | 3 | 4 |
| SiO2 | 38.82 | 38.88 | 38.20 | 37.83 | 38.05 | 37.98 | 37.98 | 37.96 | 39.58 | 38.95 | 39.40 | 39.22 | 38.59 | 38.62 | 38.52 | 38.69 |
| TiO2 | 0.08 | 0.02 | 0.33 | 0.26 | 0.10 | 0.13 | 0.27 | 0.23 | 0.00 | 0.10 | 0.03 | 0.06 | 0.06 | 0 07 | 0.05 | 0.10 |
| Al2O3 | 31.45 | 31.44 | 27.75 | 27.24 | 27.72 | 27.52 | 27.45 | 26.87 | 32.06 | 31.85 | 31.90 | 32.07 | 31.49 | 31.24 | 31.32 | 30 61 |
| Fe2O3* | 3.00 | 3.13 | 7.33 | 7.73 | 7.77 | 7.47 | 7.52 | 8.17 | 2.39 | 2.70 | 2.39 | 2.47 | 2.72 | 2.72 | 2.95 | 3.52 |
| MnO | 0.00 | 0.06 | 0.04 | 0.08 | 0.12 | 0.08 | 0.04 | 0.06 | 0.00 | 0.00 | 0.07 | 0.06 | 0.05 | 0.00 | 0.02 | 0.05 |
| MgO | 0.03 | 0.05 | 0.05 | 0.05 | 0.06 | 0.05 | 0.09 | 0.05 | 0.00 | 0 00 | 0.02 | 0.01 | 0.02 | 0.01 | 0.02 | 0 03 |
| CaO | 24.76 | 24.62 | 24.28 | 24.12 | 24.46 | 24.18 | 24.10 | 24.22 | 25.08 | 24.99 | 24.69 | 25.01 | 24.75 | 24.86 | 25.19 | 24 85 |
| Total | 98.14 | 98.20 | 97.98 | 97.31 | 98.28 | 97.41 | 97.44 | 97.55 | 99.11 | 98.59 | 98.50 | 98.90 | 97.69 | 97.52 | 98.07 | 97.85 |
| Number of cations on the basis of 12.5 oxygens: | | | | | | | | | | | | | | | | |
| Si | 2.971 | 2.974 | 2.977 | 2.975 | 2.964 | 2.980 | 2.979 | 2.983 | 2.991 | 2.965 | 2.994 | 2.973 | 2.966 | 2.974 | 2.956 | 2.979 |
| Al iv | 0.029 | 0.026 | 0.023 | 0.025 | 0.036 | 0.020 | 0.021 | 0.017 | 0.009 | 0.035 | 0.006 | 0.027 | 0.034 | 0.026 | 0.044 | 0 021 |
| Sum Z | 3.000 | 3.000 | 3.000 | 3.000 | 3.000 | 3.000 | 3.000 | 3.000 | 3.000 | 3.000 | 3.000 | 3.000 | 3.000 | 3.000 | 3.000 | 3.000 |
| Al vi | 2.808 | 2.809 | 2.528 | 2.501 | 2.511 | 2.526 | 2.517 | 2 473 | 2.847 | 2 823 | 2.852 | 2.839 | 2.820 | 2.811 | 2.790 | 2.757 |
| Ti | 0.005 | 0.001 | 0.019 | 0.015 | 0.006 | 0.007 | 0 016 | 0.013 | 0.000 | 0.006 | 0.002 | 0 003 | 0.003 | 0 004 | 0.003 | 0.006 |
| Fe3+ | 0.173 | 0.180 | 0.430 | 0.458 | 0.455 | 0.441 | 0 444 | 0.483 | 0.136 | 0.155 | 0.137 | 0.141 | 0.158 | 0.157 | 0 171 | 0.204 |
| Sum Y | 2.986 | 2.990 | 2.977 | 2.974 | 2.972 | 2.975 | 2.977 | 2.969 | 2.983 | 2.984 | 2.990 | 2.984 | 2.981 | 2.972 | 2.964 | 2 967 |
| Fe2+ | 0.000 | 0.000 | 0.000 | 0.000 | 0.000 | 0.000 | 0.000 | 0.000 | 0.000 | 0.000 | 0.000 | 0.000 | 0 000 | 0 000 | 0.000 | 0 000 |
| Mn | 0.000 | 0.004 | 0.002 | 0.006 | 0.008 | 0 005 | 0.002 | 0.004 | 0.000 | 0.000 | 0.005 | 0 004 | 0 003 | 0 000 | 0.001 | 0 004 |
| Mg | 0.003 | 0.006 | 0.006 | 0.006 | 0.007 | 0.006 | 0.010 | 0.006 | 0 000 | 0 000 | 0.002 | 0.001 | 0 003 | 0.001 | 0.002 | 0.004 |
| Ca | 2.030 | 2.018 | 2.028 | 2.033 | 2.042 | 2.033 | 2.025 | 2.039 | 2.031 | 2.038 | 2.010 | 2.031 | 2.038 | 2.051 | 2.072 | 2.050 |
| Sum W | 2.034 | 2.027 | 2.037 | 2.044 | 2.057 | 2.044 | 2.038 | 2 048 | 2 031 | 2 038 | 2.017 | 2.036 | 2 044 | 2.052 | 2.074 | 2.057 |
| Sum Cations | 8.019 | 8.017 | 8.013 | 8.018 | 8.029 | 8.019 | 8.014 | 8.017 | 8 013 | 8.023 | 8 007 | 8 020 | 8 025 | 8.025 | 8.038 | 8.024 |
| Fe3/(Fe3+Al) | 0 057 | 0.060 | 0.144 | 0.153 | 0.152 | 0.148 | 0.149 | 0.162 | 0.045 | 0.051 | 0.046 | 0.047 | 0 052 | 0 053 | 0 057 | 0 068 |

* Total Fe as Fe2O3

Table C-5 Electron microprobe analyses of piemontites (Piemontite-bearing quartz schist).

| Sample no. | 2/6291 | | | | | | | | | | |
|---|---|---|---|---|---|---|---|---|---|---|---|
| Analysis no. | 1 | 2 | 3 | 4 | 5 | 6 | 7 | 8 | 9 | Mean | SD |
| SiO2 | 36.50 | 37.15 | 36.90 | 37.09 | 37.06 | 37.20 | 36.49 | 36.51 | 36.55 | 36.83 | 0.31 |
| TiO2 | 0.00 | 0.00 | 0.04 | 0.00 | 0.00 | 0.07 | 0.03 | 0.00 | 0.02 | 0.02 | 0.02 |
| Al2O3 | 20.53 | 20.73 | 20.50 | 20.68 | 21.89 | 20.96 | 20.31 | 20.91 | 21.19 | 20.86 | 0.47 |
| Fe2O3 | 6.78 | 7.01 | 5.20 | 8.04 | 7.50 | 7.86 | 5.44 | 6.81 | 6.80 | 6.83 | 0.97 |
| Mn2O3 | 8.58 | 8.22 | 10.08 | 7.34 | 6.54 | 7.36 | 10.08 | 8.02 | 7.70 | 8.21 | 1.21 |
| MnO | 1.93 | 0.82 | 0.00 | 0.80 | 1.02 | 0.90 | 1.37 | 1.78 | 1.31 | 1.10 | 0.58 |
| MgO | 0.10 | 0.14 | 0.00 | 0.10 | 0.08 | 0.08 | 0.02 | 0.14 | 0.15 | 0.09 | 0.05 |
| CaO | 21.03 | 20.89 | 22.50 | 21.04 | 21.82 | 21.41 | 21.59 | 21.08 | 21.50 | 21.43 | 0.51 |
| Total | 95.45 | 94.96 | 94.68 | 95.09 | 95.91 | 95.84 | 95.32 | 95.25 | 95.22 | 95.30 | 0.39 |
| Number of cations on the basis of 12.5 oxygens | | | | | | | | | | | |
| Si | 3.001 | 3.045 | 3.029 | 3.042 | 3.011 | 3.029 | 2.999 | 3.001 | 2.999 | 3.017 | 0.019 |
| Al iv | 0.000 | 0.000 | 0.000 | 0.000 | 0.000 | 0.000 | 0.001 | 0.000 | 0.001 | 0.000 | 0.000 |
| Sum Z | 3.001 | 3.045 | 3.029 | 3.042 | 3.011 | 3.029 | 3.000 | 3.001 | 3.000 | 3.017 | 0.019 |
| Al vi | 1.990 | 2.003 | 1.984 | 1.999 | 2.096 | 2.012 | 1.967 | 2.026 | 2.049 | 2.014 | 0.039 |
| Ti | 0.000 | 0.000 | 0.002 | 0.000 | 0.000 | 0.004 | 0.002 | 0.000 | 0.001 | 0.001 | 0.002 |
| Fe3+ | 0.419 | 0.432 | 0.321 | 0.496 | 0.458 | 0.482 | 0.337 | 0.421 | 0.420 | 0.421 | 0.059 |
| Mn3+ | 0.591 | 0.564 | 0.693 | 0.504 | 0.445 | 0.502 | 0.695 | 0.552 | 0.530 | 0.564 | 0.085 |
| Sum Y | 3.000 | 3.000 | 3.000 | 3.000 | 3.000 | 3.000 | 3.000 | 3.000 | 3.000 | 3.000 | 0.000 |
| Fe2+ | 0.000 | 0.000 | 0.000 | 0.000 | 0.000 | 0.000 | 0.000 | 0.000 | 0.000 | 0.000 | 0.000 |
| Mn | 0.134 | 0.057 | 0.000 | 0.055 | 0.070 | 0.062 | 0.095 | 0.124 | 0.091 | 0.077 | 0.040 |
| Mg | 0.012 | 0.017 | 0.000 | 0.012 | 0.010 | 0.010 | 0.002 | 0.017 | 0.018 | 0.011 | 0.006 |
| Ca | 1.852 | 1.835 | 1.979 | 1.849 | 1.899 | 1.868 | 1.902 | 1.857 | 1.890 | 1.881 | 0.044 |
| Sum X | 1.999 | 1.909 | 1.942 | 1.917 | 1.979 | 1.940 | 1.999 | 1.998 | 2.000 | 1.965 | 0.038 |
| Total cat. | 7.999 | 7.955 | 7.970 | 7.958 | 7.989 | 7.969 | 7.999 | 7.999 | 8.000 | 7.982 | 0.019 |
| Molecular proportions of end-members : | | | | | | | | | | | |
| Cz | 0.663 | 0.668 | 0.662 | 0.666 | 0.699 | 0.672 | 0.656 | 0.675 | 0.683 | 0.672 | 0.013 |
| Ps | 0.140 | 0.144 | 0.107 | 0.165 | 0.153 | 0.161 | 0.112 | 0.140 | 0.140 | 0.140 | 0.020 |
| Pm | 0.197 | 0.188 | 0.231 | 0.168 | 0.148 | 0.168 | 0.232 | 0.184 | 0.177 | 0.188 | 0.028 |

* Total Fe as Fe2O3

# MnO and Mn2O3 are calculated assuming Al vi+Fe3+Mn3 = 3.

Table C-6 Electron microprobe analyses of muscovites (Piemontite-bearing quartz schist).

| Sample no. | 2/6291 | | | | | | | | | | | | | | | | | | | | | |
|---|---|---|---|---|---|---|---|---|---|---|---|---|---|---|---|---|---|---|---|---|---|---|
| Analysis no. | 1 | 2 | 3 | 4 | 5 | 6 | 7 | 8 | 9 | 10 | 11 | 12 | 13 | 14 | 15 | 16 | 17 | 18 | 19 | 20 | Mean | SD |
| SiO2 | 48.57 | 48.01 | 47.57 | 47.55 | 47.82 | 48.11 | 48.37 | 47.47 | 49.02 | 49.88 | 49.46 | 50.55 | 51.22 | 51.68 | 49.69 | 49.55 | 50.96 | 47.12 | 51.18 | 50.34 | 49.21 | 1.44 |
| TiO2 | 0.32 | 0.26 | 0.30 | 0.20 | 0.33 | 0.22 | 0.12 | 0.33 | 0.27 | 0.22 | 0.31 | 0.32 | 0.02 | 0.24 | 0.21 | 0.30 | 0.24 | 0.27 | 0 09 | 0.09 | 0.23 | 0.09 |
| Al2O3 | 30.13 | 29.05 | 30.05 | 28.81 | 29.48 | 29.24 | 29.77 | 30.01 | 27.72 | 27.94 | 30.40 | 29.61 | 30.34 | 29.24 | 30.56 | 30.33 | 29.00 | 30.18 | 27.62 | 27.47 | 29.35 | 0.99 |
| FeO* | 3.59 | 3.46 | 3.69 | 3.55 | 3.44 | 3.63 | 3.20 | 3.46 | 3.35 | 3.37 | 3.58 | 3.44 | 2.42 | 3.56 | 3.44 | 3.66 | 3.51 | 3.28 | 2.40 | 2.28 | 3.32 | 0.43 |
| MnO | 0.27 | 0.12 | 0.24 | 0.36 | 0 33 | 0.45 | 0.18 | 0.22 | 0.38 | 0.38 | 0.33 | 0.36 | 0.12 | 0.43 | 0 24 | 0.22 | 0.29 | 0.26 | 0.04 | 0.11 | 0.27 | 0.11 |
| MgO | 2.49 | 2.61 | 2.26 | 2.54 | 2.58 | 2.82 | 2.58 | 2.38 | 2.93 | 3.03 | 2.46 | 2.81 | 2.74 | 3.14 | 2.50 | 2.40 | 3.16 | 2.27 | 2.28 | 3.20 | 2.66 | 0.31 |
| CaO | 0.00 | 0.03 | 0.00 | 0.00 | 0.00 | 0.01 | 0.00 | 0.05 | 0.02 | 0.03 | 0.01 | 0.04 | 0.03 | 0.04 | 0.05 | 0.04 | 0.00 | 0.02 | 0.00 | 0.00 | 0.02 | 0.02 |
| Na2O | 1.35 | 1.23 | 1.43 | 1.27 | 1.31 | 1.31 | 0.77 | 1.39 | 0.98 | 0.88 | 1.21 | 0.98 | 0.28 | 1.08 | 0.94 | 1.33 | 1.25 | 1.19 | 0.15 | 0.17 | 1.02 | 0.40 |
| K2O | 8.97 | 9.04 | 9.28 | 9.32 | 9.45 | 9.50 | 9.70 | 8.98 | 9.41 | 9.24 | 8.55 | 8.61 | 9.50 | 8.94 | 7.59 | 8.75 | 9.54 | 8.62 | 9.59 | 10.03 | 9.13 | 0.54 |
| F | 0.00 | 0.00 | 0.00 | 0.00 | 0.00 | 0.00 | 0.00 | 0.00 | 0.00 | 0.00 | 0.00 | 0.00 | 0.00 | 0.00 | 0.00 | 0.00 | 0.00 | 0.00 | 0.00 | 0.00 | 0.00 | 0.00 |
| Cl | 0.00 | 0.00 | 0.00 | 0.02 | 0.03 | 0.02 | 0.03 | 0.02 | 0.04 | 0.00 | 0.05 | 0.02 | 0.05 | 0.05 | 0.02 | 0.00 | 0.05 | 0.09 | 0.04 | 0.06 | 0.03 | 0.02 |
| Total | 95.69 | 93.81 | 94.82 | 93.62 | 94.77 | 95.31 | 94.72 | 94.31 | 94.12 | 94.97 | 96.37 | 96.74 | 96.73 | 98.41 | 95.24 | 96.59 | 98.01 | 93.29 | 93.39 | 93.73 | 95.23 | 1.50 |
| O = F, Cl | 0.00 | 0.00 | 0.00 | -0.01 | -0.01 | -0.01 | -0.01 | -0.01 | -0.01 | 0.00 | 0.00 | 0.00 | 0.00 | -0.01 | -0.01 | -0.01 | -0.01 | -0.01 | -0 01 | 0.00 | 0.00 | 0.00 |
| Total | 95.69 | 93.81 | 94.82 | 93.62 | 94.76 | 95.31 | 94.71 | 94.30 | 94.11 | 94.97 | 96 37 | 96.74 | 96.73 | 98.40 | 95.24 | 96.58 | 98.00 | 93 28 | 93.38 | 93.73 | 95 23 | 1.50 |
| Number of cations on the basis of 11 oxygens : | | | | | | | | | | | | | | | | | | | | | | |
| Si | 3.273 | 3.299 | 3.250 | 3.291 | 3.267 | 3.276 | 3.290 | 3.250 | 3.362 | 3.379 | 3.296 | 3.345 | 3.362 | 3.372 | 3.317 | 3.299 | 3 354 | 3.249 | 3.477 | 3.425 | 3.322 | 0.061 |
| Al iv | 0.727 | 0.701 | 0.750 | 0.709 | 0.733 | 0.724 | 0.710 | 0.750 | 0.638 | 0.621 | 0.704 | 0.655 | 0.638 | 0.628 | 0.683 | 0.701 | 0.646 | 0.751 | 0.523 | 0.575 | 0.678 | 0.061 |
| Sum T | 4.000 | 4.000 | 4.000 | 4.000 | 4.000 | 4.000 | 4.000 | 4.000 | 4.000 | 4.000 | 4.000 | 4.000 | 4 000 | 4.000 | 4.000 | 4.000 | 4.000 | 4.000 | 4.000 | 4.000 | 4.000 | 0.000 |
| Al vi | 1.667 | 1.653 | 1.671 | 1.641 | 1.642 | 1.623 | 1.678 | 1.672 | 1.603 | 1.610 | 1.684 | 1.655 | 1.710 | 1.621 | 1.722 | 1.679 | 1.604 | 1.703 | 1.688 | 1.629 | 1.658 | 0.036 |
| Ti | 0.016 | 0.013 | 0.015 | 0.010 | 0.017 | 0.011 | 0.006 | 0.017 | 0.014 | 0.011 | 0.016 | 0.016 | 0.001 | 0.012 | 0.011 | 0 015 | 0.012 | 0.014 | 0.005 | 0.004 | 0.012 | 0.005 |
| Fe2+ | 0.091 | 0.089 | 0.095 | 0.092 | 0.088 | 0.093 | 0.082 | 0.089 | 0.086 | 0.086 | 0.090 | 0.086 | 0.060 | 0.088 | 0.086 | 0.092 | 0.087 | 0.085 | 0.061 | 0.058 | 0.084 | 0.011 |
| Mn | 0.015 | 0 007 | 0.014 | 0.021 | 0.019 | 0.026 | 0.010 | 0.013 | 0.022 | 0.022 | 0 019 | 0.020 | 0.007 | 0.024 | 0.014 | 0.012 | 0.016 | 0.015 | 0.002 | 0.006 | 0.015 | 0.006 |
| Mg | 0.250 | 0.267 | 0.230 | 0.262 | 0.263 | 0.286 | 0.262 | 0.243 | 0.299 | 0.306 | 0.244 | 0.277 | 0.268 | 0.306 | 0.249 | 0.238 | 0.310 | 0.233 | 0.230 | 0.324 | 0.267 | 0.029 |
| Sum O | 2.040 | 2.030 | 2.025 | 2.027 | 2.029 | 2.039 | 2.038 | 2.034 | 2.025 | 2.035 | 2.052 | 2.054 | 2.045 | 2.049 | 2.082 | 2.036 | 2.029 | 2.050 | 1.987 | 2.022 | 2.036 | 0.018 |
| Ca | 0.000 | 0.002 | 0 000 | 0.000 | 0.000 | 0.001 | 0.000 | 0.004 | 0.001 | 0.002 | 0.001 | 0.003 | 0 002 | 0.003 | 0.003 | 0.003 | 0.000 | 0.001 | 0.000 | 0.000 | 0.001 | 0.001 |
| Na | 0.176 | 0.164 | 0.189 | 0.170 | 0.174 | 0.173 | 0.102 | 0.185 | 0.130 | 0.116 | 0.157 | 0.125 | 0.036 | 0.136 | 0.122 | 0.171 | 0.159 | 0.159 | 0.020 | 0.022 | 0.134 | 0.053 |
| K | 0.771 | 0.793 | 0.809 | 0.823 | 0.824 | 0.825 | 0.842 | 0.784 | 0.823 | 0.799 | 0.727 | 0.727 | 0.796 | 0.744 | 0.646 | 0.743 | 0.801 | 0.759 | 0.831 | 0.871 | 0.787 | 0.051 |
| Sum A | 0.948 | 0.959 | 0.998 | 0.993 | 0.997 | 0.999 | 0.943 | 0.973 | 0.955 | 0.916 | 0.884 | 0.855 | 0.834 | 0.883 | 0.772 | 0.917 | 0.961 | 0.919 | 0.852 | 0.893 | 0.923 | 0.062 |
| Sum Cations | 6 987 | 6.989 | 7.023 | 7.020 | 7.027 | 7.038 | 6.981 | 7.006 | 6.980 | 6 951 | 6.936 | 6.910 | 6.879 | 6.932 | 6 854 | 6.953 | 6 990 | 6.969 | 6.839 | 6.915 | 6 959 | 0.057 |

* Total Fe as FeO

Table C-7 Electron microprobe analyses of chlorites (Piemontite-bearing quartz schist).

| Sample no. | 2/6291 | | | | | | | | | | | | | |
|---|---|---|---|---|---|---|---|---|---|---|---|---|---|---|
| Analysis no. | 1 | 2 | 3 | 4 | 5 | 6 | 7 | 8 | 9 | 10 | 11 | 12 | Mean | SD |
| SiO2 | 30.09 | 29.86 | 30.22 | 30.23 | 30.79 | 30.37 | 31.37 | 31.01 | 31.22 | 30.58 | 31.82 | 31.36 | 30.74 | 0.61 |
| TiO2 | 0.04 | 0.05 | 0.00 | 0.00 | 0.05 | 0.00 | 0.04 | 0.07 | 0.00 | 0.03 | 0.04 | 0.00 | 0.03 | 0.03 |
| Al2O3 | 21.64 | 21.13 | 21.28 | 21.20 | 21.58 | 21.27 | 22.32 | 20.89 | 21.49 | 21.88 | 21.34 | 20.72 | 21.40 | 0.43 |
| Cr2O3 | 0.00 | 0.00 | 0.00 | 0.00 | 0.06 | 0.00 | 0.10 | 0.00 | 0.02 | 0.14 | 0.00 | 0.00 | 0.03 | 0.05 |
| FeO* | 0.83 | 0.82 | 0.84 | 0.83 | 0.81 | 0.85 | 0.66 | 0.71 | 0.65 | 0.66 | 0.83 | 0.69 | 0.77 | 0.08 |
| MnO | 0.69 | 0.53 | 0.70 | 0.57 | 0.72 | 0.61 | 0.55 | 0.84 | 1.10 | 0.97 | 0.67 | 0.84 | 0.73 | 0.18 |
| MgO | 33.26 | 33.39 | 33.51 | 33.05 | 32.00 | 32.53 | 31.06 | 32.03 | 30.84 | 30.71 | 32.01 | 31.34 | 32.14 | 1.01 |
| Total | 86.55 | 85.78 | 86.55 | 85.88 | 86.01 | 85.63 | 86.10 | 85.55 | 85.32 | 84.97 | 86.71 | 84.95 | 85.83 | 2.39 |
| Number of cations on the basis of 14 oxygens : | | | | | | | | | | | | | | |
| Si | 2.821 | 2.823 | 2.833 | 2.852 | 2.895 | 2.871 | 2.933 | 2.931 | 2.955 | 2.908 | 2.961 | 2.979 | 2.897 | 0.056 |
| Al iv | 1.179 | 1.177 | 1.167 | 1.148 | 1.105 | 1.129 | 1.067 | 1.069 | 1.045 | 1.092 | 1.039 | 1.021 | 1.103 | 0.056 |
| Sum T | 4.000 | 4.000 | 4.000 | 4.000 | 4.000 | 4.000 | 4.000 | 4.000 | 4.000 | 4.000 | 4.000 | 4.000 | 4.000 | 0.000 |
| Al vi | 1.212 | 1.177 | 1.184 | 1.210 | 1.287 | 1.242 | 1.393 | 1.258 | 1.353 | 1.360 | 1.302 | 1.299 | 1.273 | 0.071 |
| Ti | 0.003 | 0.004 | 0.000 | 0.000 | 0.004 | 0.000 | 0.003 | 0.005 | 0.000 | 0.002 | 0.003 | 0.000 | 0.002 | 0.002 |
| Cr | 0.000 | 0.000 | 0.000 | 0.000 | 0.004 | 0.000 | 0.007 | 0.000 | 0.001 | 0.011 | 0.000 | 0.000 | 0.002 | 0.004 |
| Fe | 0.065 | 0.065 | 0.066 | 0.065 | 0.064 | 0.067 | 0.052 | 0.056 | 0.051 | 0.052 | 0.065 | 0.055 | 0.060 | 0.006 |
| Mn | 0.055 | 0.042 | 0.056 | 0.046 | 0.057 | 0.049 | 0.044 | 0.067 | 0.088 | 0.078 | 0.053 | 0.068 | 0.059 | 0.014 |
| Mg | 4.646 | 4.704 | 4.681 | 4.647 | 4.484 | 4.584 | 4.328 | 4.511 | 4.350 | 4.352 | 4.439 | 4.437 | 4.514 | 0.136 |
| Sum O | 5.981 | 5.996 | 5.991 | 5.969 | 5.903 | 5.943 | 5.831 | 5.901 | 5.846 | 5.859 | 5.866 | 5.861 | 5.912 | 0.061 |
| Sum Cations | 9.981 | 9.996 | 9.991 | 9.969 | 9.903 | 9.943 | 9.831 | 9.901 | 9.846 | 9.859 | 9.866 | 9.861 | 9.912 | 0.061 |
| Mg/(Mg+Fe2) | 0.986 | 0.986 | 0.986 | 0.986 | 0.986 | 0.986 | 0.988 | 0.988 | 0.988 | 0.988 | 0.986 | 0.988 | 0.987 | 0.001 |

* Total Fe as FeO

Table C-8 Electron microprobe analyses of serpentines

| Sample no. | 13/7291 | | | | | | | | | SD-136 | | | | | | | SD-176 | | | |
|---|---|---|---|---|---|---|---|---|---|---|---|---|---|---|---|---|---|---|---|---|
| Analysis no. | 1 | 2 | 3 | 4 | 5 | 6 | 7 | 8 | 9 | 1 | 2 | 3 | 4 | 5 | 6 | 7 | 1 | 2 | 3 | 4 |
| SiO2 | 44.32 | 45.79 | 45.05 | 45.43 | 45.40 | 45.92 | 45.20 | 45.71 | 45.94 | 43.23 | 44.03 | 44.54 | 43.97 | 43.89 | 44 20 | 44.99 | 43.84 | 43.96 | 44.18 | 43.72 |
| TiO2 | 0.02 | 0.00 | 0.00 | 0.01 | 0.03 | 0.00 | 0.00 | 0.00 | 0.00 | 0.02 | 0 01 | 0.00 | 0.00 | 0 00 | 0 00 | 0.00 | 0.04 | 0.01 | 0.01 | 0.04 |
| Al2O3 | 0.14 | 0.08 | 0.19 | 0.16 | 0.35 | 0.22 | 0.18 | 0.15 | 0.12 | 0.36 | 0.36 | 0.31 | 0.33 | 0.69 | 0.27 | 0.20 | 0.07 | 0.10 | 0.25 | 0.16 |
| Cr2O3 | 0.06 | 0.00 | 0.00 | 0.04 | 0.07 | 0.00 | 0.00 | 0.06 | 0.00 | 0.03 | 0.01 | 0.00 | 0 01 | 0 31 | 0.00 | 0.00 | 0.00 | 0.08 | 0.00 | 0.00 |
| FeO* | 3.42 | 3.54 | 4.79 | 2.96 | 3.01 | 3.19 | 2.97 | 2.63 | 2.53 | 2.40 | 2.31 | 2.17 | 2.23 | 3 27 | 3.03 | 2.87 | 1.35 | 1.12 | 1.08 | 1.26 |
| MnO | 0.12 | 0.03 | 0.00 | 0.00 | 0.00 | 0.00 | 0.01 | 0.00 | 0.05 | 0.03 | 0.04 | 0.02 | 0.04 | 0.05 | 0.05 | 0 00 | 0.05 | 0.02 | 0 10 | 0 08 |
| MgO | 39.71 | 40.36 | 37.59 | 40.34 | 40.08 | 39.88 | 39.67 | 40.36 | 40.12 | 39.05 | 40.12 | 40.43 | 40.14 | 40.13 | 40.35 | 40.55 | 41.87 | 41.92 | 41.21 | 41.33 |
| Total | 87.84 | 89.85 | 87.67 | 89.00 | 89.00 | 89.29 | 88.08 | 88.95 | 88.81 | 85.15 | 86.91 | 87.51 | 86.76 | 88.33 | 87.93 | 88.61 | 87.22 | 87.23 | 86.85 | 86.60 |
| Number of cations on the basis of 7 oxygens : | | | | | | | | | | | | | | | | | | | | |
| Si | 2 052 | 2.069 | 2.095 | 2.067 | 2.066 | 2 082 | 2.076 | 2 076 | 2.087 | 2.053 | 2.048 | 2.054 | 2.048 | 2.022 | 2.041 | 2.056 | 2.026 | 2.029 | 2.045 | 2.034 |
| Al iv | 0.000 | 0.000 | 0 000 | 0.000 | 0.000 | 0.000 | 0.000 | 0.000 | 0.000 | 0.000 | 0.000 | 0.000 | 0.000 | 0.000 | 0.000 | 0 000 | 0.000 | 0.000 | 0.000 | 0.000 |
| Sum T | 2.052 | 2.069 | 2.095 | 2 067 | 2.066 | 2.082 | 2.076 | 2.076 | 2.087 | 2.053 | 2.048 | 2.054 | 2.048 | 2.022 | 2.041 | 2.056 | 2.026 | 2.029 | 2.045 | 2.034 |
| Al | 0.008 | 0.004 | 0.010 | 0.009 | 0.019 | 0.012 | 0.010 | 0.008 | 0.006 | 0.020 | 0.020 | 0.017 | 0.018 | 0.037 | 0.015 | 0.011 | 0.004 | 0.006 | 0 014 | 0.009 |
| Ti | 0 001 | 0.000 | 0.000 | 0.000 | 0.001 | 0.000 | 0.000 | 0.000 | 0.000 | 0 001 | 0.000 | 0.000 | 0.000 | 0 000 | 0.000 | 0.000 | 0.001 | 0.000 | 0.000 | 0.001 |
| Cr | 0.002 | 0.000 | 0.000 | 0 001 | 0.003 | 0.000 | 0.000 | 0.002 | 0.000 | 0.001 | 0.000 | 0.000 | 0.000 | 0.011 | 0 000 | 0.000 | 0.000 | 0.003 | 0.000 | 0.000 |
| Fe | 0.132 | 0.134 | 0.186 | 0.113 | 0.115 | 0.121 | 0.114 | 0.100 | 0.096 | 0.095 | 0.090 | 0.084 | 0.087 | 0.126 | 0.117 | 0.110 | 0.052 | 0.043 | 0.042 | 0.049 |
| Mn | 0.005 | 0.001 | 0.000 | 0.000 | 0.000 | 0.000 | 0 000 | 0.000 | 0.002 | 0.001 | 0.002 | 0.001 | 0.002 | 0.002 | 0.002 | 0.000 | 0.002 | 0.001 | 0.004 | 0.003 |
| Mg | 2.740 | 2.718 | 2 605 | 2.735 | 2.718 | 2.694 | 2.716 | 2.731 | 2.716 | 2.763 | 2.781 | 2.779 | 2.786 | 2.755 | 2 776 | 2 762 | 2.884 | 2.884 | 2.842 | 2.865 |
| Sum O | 2.890 | 2.860 | 2 805 | 2.861 | 2.857 | 2.831 | 2.843 | 2.843 | 2.823 | 2.883 | 2.894 | 2.883 | 2.895 | 2.932 | 2.911 | 2.882 | 2.944 | 2.937 | 2 903 | 2.927 |
| Sum Cations | 4.942 | 4.929 | 4.900 | 4.928 | 4.923 | 4.912 | 4.919 | 4.919 | 4.910 | 4.936 | 4.942 | 4.937 | 4.943 | 4.954 | 4.952 | 4.939 | 4.970 | 4 966 | 4.948 | 4.961 |
| Mg/(Mg+Fe2) | 0.954 | 0.953 | 0.933 | 0.960 | 0 960 | 0.957 | 0 960 | 0.965 | 0.966 | 0 967 | 0 969 | 0.971 | 0.970 | 0.956 | 0 960 | 0.962 | 0 982 | 0.985 | 0.985 | 0.983 |

* Total Fe as FeO

Table C-8 (continued)

| Sample no. | SD-176 | | | SD-178 | | | | | | | SD-179.2 | | | | | | | | |
|---|---|---|---|---|---|---|---|---|---|---|---|---|---|---|---|---|---|---|---|
| Analysis no. | 5 | 6 | 7 | 1 | 2 | 3 | 4 | 5 | 6 | 7 | 1 | 2 | 3 | 4 | 5 | 6 | 7 | 8 | 9 |
| | | | | C1-Spt2 | C1-Spt3 | C1-Spt4 | C1-Spt5 | C1-Spt6 | C1-Spt7 | C1-Spt1 | C1-Spt1 | C1-Spt2 | C1-Spt3 | C1-Spt4 | C2-Spt5 | C2Spt6 | C2-Spt7 | C2-Spt8 | C2-Spt9 |
| SiO2 | 44.01 | 43.71 | 43.83 | 42.43 | 42.29 | 42.40 | 42.51 | 42.43 | 42.35 | 42.56 | 43.51 | 43.12 | 43.59 | 43.68 | 42 22 | 43.02 | 43.94 | 43.65 | 43.35 |
| TiO2 | 0.00 | 0.01 | 0.00 | 0.00 | 0.00 | 0.01 | 0.01 | 0.03 | 0.00 | 0.00 | 0 00 | 0.03 | 0.00 | 0.03 | 0.02 | 0.00 | 0.02 | 0 00 | 0 01 |
| Al2O3 | 0.21 | 0.14 | 0 10 | 0.04 | 0.03 | 0.08 | 0.02 | 0.04 | 0.05 | 0.05 | 0.23 | 0.20 | 0.23 | 0.24 | 0.61 | 0.12 | 0 21 | 0.05 | 0.22 |
| Cr2O3 | 0.00 | 0.00 | 0.00 | 0.03 | 0.00 | 0.00 | 0.02 | 0.01 | 0 00 | 0.00 | 0.13 | 0.07 | 0.04 | 0.07 | 0.16 | 0.00 | 0.00 | 0.01 | 0.01 |
| FeO* | 1.20 | 1.12 | 1.00 | 6.30 | 6.50 | 6.91 | 6.89 | 6.66 | 8.06 | 6.40 | 3.68 | 3.58 | 2.99 | 3.25 | 3.50 | 3.21 | 2.89 | 3.17 | 3.18 |
| MnO | 0.04 | 0.10 | 0.00 | 0.01 | 0.13 | 0.00 | 0.05 | 0.08 | 0.10 | 0.03 | 0.03 | 0.11 | 0.05 | 0.04 | 0.03 | 0.04 | 0.04 | 0.09 | 0.15 |
| MgO | 41.51 | 41.71 | 41.25 | 37.35 | 37.35 | 37.16 | 37.59 | 37.34 | 35.92 | 37.20 | 39.89 | 39.24 | 40.21 | 40.36 | 39.50 | 39.86 | 40 23 | 39.72 | 40.14 |
| Total | 86.97 | 86.78 | 86.20 | 86.16 | 86.30 | 86.55 | 87.08 | 86.60 | 86.48 | 86 25 | 87.47 | 86.36 | 87.11 | 87.68 | 86.03 | 86.25 | 87.33 | 86 69 | 87.05 |
| Number of cations on the basis of 7 oxygens : | | | | | | | | | | | | | | | | | | | |
| Si | 2.036 | 2.028 | 2.043 | 2.035 | 2.029 | 2.031 | 2.026 | 2.030 | 2.042 | 2 040 | 2.028 | 2.035 | 2.033 | 2.027 | 2.001 | 2.030 | 2.041 | 2.045 | 2.026 |
| Al iv | 0.000 | 0.000 | 0.000 | 0.000 | 0.000 | 0.000 | 0.000 | 0.000 | 0.000 | 0.000 | 0 000 | 0.000 | 0.000 | 0.000 | 0.000 | 0.000 | 0.000 | 0 000 | 0.000 |
| Sum T | 2.036 | 2.028 | 2.043 | 2.035 | 2.029 | 2.031 | 2.026 | 2.030 | 2.042 | 2.040 | 2.028 | 2.035 | 2.033 | 2.027 | 2.001 | 2.030 | 2.041 | 2 045 | 2.026 |
| Al | 0.011 | 0.008 | 0.006 | 0.002 | 0.001 | 0.004 | 0.001 | 0.002 | 0.003 | 0.003 | 0.013 | 0.011 | 0 013 | 0.013 | 0 034 | 0.007 | 0.012 | 0.003 | 0.012 |
| Ti | 0.000 | 0.000 | 0.000 | 0.000 | 0.000 | 0.000 | 0 000 | 0.001 | 0 000 | 0.000 | 0 000 | 0.001 | 0.000 | 0 001 | 0.001 | 0 000 | 0.001 | 0 000 | 0.000 |
| Cr | 0.000 | 0.000 | 0.000 | 0.001 | 0.000 | 0.000 | 0.001 | 0.000 | 0.000 | 0.000 | 0.005 | 0.003 | 0.002 | 0.003 | 0 006 | 0.000 | 0.000 | 0.000 | 0 000 |
| Fe | 0.046 | 0.043 | 0.039 | 0.253 | 0.261 | 0.277 | 0.275 | 0.266 | 0.325 | 0.257 | 0.143 | 0.141 | 0.117 | 0.126 | 0.139 | 0.127 | 0.112 | 0.124 | 0.124 |
| Mn | 0.002 | 0.004 | 0.000 | 0.000 | 0.005 | 0.000 | 0.002 | 0.003 | 0.004 | 0.001 | 0.001 | 0.004 | 0 002 | 0.002 | 0.001 | 0.001 | 0.002 | 0 004 | 0.006 |
| Mg | 2.862 | 2.885 | 2.866 | 2.670 | 2.671 | 2.653 | 2.670 | 2.663 | 2.581 | 2.657 | 2.771 | 2.760 | 2.794 | 2.791 | 2.791 | 2.803 | 2.784 | 2 773 | 2.796 |
| Sum O | 2.922 | 2.940 | 2.911 | 2.928 | 2.941 | 2.937 | 2.948 | 2.937 | 2.914 | 2.918 | 2.934 | 2.921 | 2.927 | 2.937 | 2.977 | 2.938 | 2.912 | 2.909 | 2.941 |
| Sum Cations | 4.958 | 4.968 | 4.954 | 4.963 | 4.970 | 4.967 | 4.974 | 4.967 | 4.956 | 4.958 | 4.963 | 4.957 | 4.960 | 4.964 | 4.978 | 4.967 | 4.953 | 4.954 | 4.967 |
| Mg/(Mg+Fe2) | 0 984 | 0.985 | 0 987 | 0.914 | 0.911 | 0 906 | 0 907 | 0.909 | 0 888 | 0 912 | 0 951 | 0 951 | 0.960 | 0.957 | 0 953 | 0 957 | 0 961 | 0 957 | 0.957 |

* Total Fe as FeO

Table C-9 Electron microprobe analyses of chlorites (ophiolite association of the Pha Som Metamorphic Complex).

| Sample no. | 13/7291 | | | | | | | | SD-136 | SD-178 | | | | | | SD-179.2 | | | | | | |
|---|---|---|---|---|---|---|---|---|---|---|---|---|---|---|---|---|---|---|---|---|---|---|
| Analysis no. | 1 | 2 | 3 | 4 | 5 | 6 | 7 | 8 | 1 | 1 | 2 | 3 | 4 | 5 | 6 | 1 | 2 | 3 | 4 | 5 | 6 | 7 |
| | | | | | | | | | | C4-Chl1 | C4-Chl2 | C4-Chl3 | C4-Chl4 | C4-Chl5 | C4-Chl1 | C4-Chl1 | C1-Chl2 | C1-Chl3 | C1-Chl4 | C1-Chl5 | C1-Chl6 | C4-Chl7 |
| SiO2 | 33.26 | 32.00 | 33.34 | 32.67 | 31.81 | 32.38 | 31.62 | 33 00 | 33.85 | 31.63 | 33.64 | 32.40 | 36.30 | 31.75 | 31.46 | 31.61 | 32.44 | 35.36 | 31.42 | 31.95 | 34.05 | 33.91 |
| TiO2 | 0.02 | 0.06 | 0.06 | 0.04 | 0.08 | 0.07 | 0.06 | 0.06 | 0 03 | 0.03 | 0.00 | 0.03 | 0.01 | 0.02 | 0.01 | 0.05 | 0.03 | 0.00 | 0.01 | 0.09 | 0.04 | 0.00 |
| Al2O3 | 14.30 | 14.98 | 13.98 | 13.86 | 15.72 | 14.89 | 16.08 | 14.60 | 10.80 | 13 62 | 12.75 | 12.42 | 7.44 | 13.14 | 13.74 | 13.29 | 12.25 | 9.83 | 13.02 | 13.05 | 10.26 | 10.33 |
| Cr2O3 | 2.60 | 2.43 | 2.53 | 2.88 | 2.42 | 2.54 | 2.49 | 2.80 | 4.29 | 3.45 | 3.14 | 3.24 | 2.17 | 3.57 | 3.29 | 3.21 | 2.65 | 2.57 | 3.44 | 3.23 | 2.94 | 2.96 |
| FeO* | 3.01 | 3.81 | 3.18 | 3.10 | 3.63 | 3.50 | 3.46 | 3.15 | 2.97 | 2.42 | 2.76 | 3.04 | 3.77 | 2.30 | 2.43 | 2.73 | 3.05 | 3.28 | 2.73 | 2.97 | 3.49 | 2.88 |
| MnO | 0.07 | 0.00 | 0.00 | 0.00 | 0.00 | 0.00 | 0.00 | 0.02 | 0.01 | 0.00 | 0.00 | 0.00 | 0.05 | 0.00 | 0.00 | 0.00 | 0.00 | 0.00 | 0.00 | 0.00 | 0.05 | 0.00 |
| MgO | 34.26 | 33.71 | 33.97 | 33.40 | 33.02 | 33.04 | 32.24 | 33.63 | 35.23 | 34.37 | 34.20 | 34.36 | 36.01 | 34.40 | 34.17 | 34.15 | 34.22 | 35.73 | 33.84 | 33.98 | 35.07 | 35.30 |
| Total | 87.52 | 86.99 | 87.06 | 85.95 | 86.68 | 86.42 | 85.95 | 87.26 | 87.18 | 85.52 | 86.50 | 85.48 | 85.74 | 85.18 | 85.10 | 85.05 | 84.64 | 86 76 | 84.47 | 85.27 | 85.92 | 85.38 |
| Number of cations on the basis of 14 oxygens : | | | | | | | | | | | | | | | | | | | | | | |
| Si | 3.134 | 3.049 | 3.159 | 3.139 | 3.036 | 3.097 | 3.039 | 3.121 | 3.225 | 3.060 | 3.207 | 3.141 | 3.499 | 3.083 | 3.056 | 3.077 | 3.170 | 3.364 | 3.083 | 3.104 | 3.286 | 3.282 |
| Al iv | 0.866 | 0.951 | 0.841 | 0.861 | 0.964 | 0.903 | 0.961 | 0.879 | 0.775 | 0.940 | 0.793 | 0.859 | 0.501 | 0.917 | 0 944 | 0.923 | 0.830 | 0.636 | 0.917 | 0.896 | 0.714 | 0.718 |
| Sum T | 4.000 | 4.000 | 4.000 | 4.000 | 4.000 | 4.000 | 4.000 | 4.000 | 4.000 | 4.000 | 4.000 | 4.000 | 4.000 | 4.000 | 4.000 | 4.000 | 4.000 | 4.000 | 4.000 | 4 000 | 4.000 | 4.000 |
| Al | 0.723 | 0.732 | 0.720 | 0.709 | 0.805 | 0.776 | 0.860 | 0.749 | 0.439 | 0.612 | 0.640 | 0.560 | 0.345 | 0.587 | 0.630 | 0.602 | 0.580 | 0.466 | 0.588 | 0.599 | 0.453 | 0.461 |
| Ti | 0.001 | 0.004 | 0.004 | 0.003 | 0.006 | 0.005 | 0.004 | 0.004 | 0.002 | 0.002 | 0.000 | 0.002 | 0.001 | 0 001 | 0.001 | 0.004 | 0.002 | 0.000 | 0.001 | 0.007 | 0.003 | 0.000 |
| Cr | 0.194 | 0.183 | 0.189 | 0.219 | 0.183 | 0.192 | 0.189 | 0.209 | 0.323 | 0.264 | 0.237 | 0.249 | 0.165 | 0.274 | 0.253 | 0.247 | 0.205 | 0.193 | 0.267 | 0.249 | 0.225 | 0.227 |
| Fe | 0.237 | 0.304 | 0.252 | 0.249 | 0.290 | 0.280 | 0.278 | 0.249 | 0.237 | 0.196 | 0.220 | 0.246 | 0.304 | 0.187 | 0.197 | 0.222 | 0 249 | 0.261 | 0.224 | 0.241 | 0.282 | 0.233 |
| Mn | 0.006 | 0.000 | 0.000 | 0.000 | 0.000 | 0.000 | 0.000 | 0.002 | 0.001 | 0.000 | 0.000 | 0.000 | 0.004 | 0 000 | 0.000 | 0.000 | 0.000 | 0.000 | 0.000 | 0.000 | 0.004 | 0.000 |
| Mg | 4.811 | 4.787 | 4.796 | 4.783 | 4.697 | 4.710 | 4.617 | 4.740 | 5.003 | 4.955 | 4.860 | 4.965 | 5.173 | 4.977 | 4.947 | 4.954 | 4.982 | 5.067 | 4.949 | 4.921 | 5.044 | 5.093 |
| Sum O | 5.972 | 6.010 | 5.962 | 5.963 | 5.981 | 5.963 | 5.949 | 5.954 | 6.004 | 6.030 | 5.957 | 6.021 | 5.992 | 6.025 | 6.027 | 6.030 | 6.019 | 5.987 | 6.030 | 6.017 | 6.011 | 6.015 |
| Sum Cations | 9.972 | 10.010 | 9.962 | 9.963 | 9.981 | 9.963 | 9.949 | 9.954 | 10.004 | 10.030 | 9.957 | 10.021 | 9.992 | 10.025 | 10.027 | 10.030 | 10.019 | 9.987 | 10.030 | 10.017 | 10.011 | 10.015 |
| Mg/(Mg+Fe2) | 0.953 | 0 940 | 0.950 | 0.950 | 0.942 | 0.944 | 0.943 | 0 950 | 0.955 | 0.962 | 0 957 | 0.953 | 0.945 | 0.964 | 0.962 | 0.957 | 0.952 | 0.951 | 0 957 | 0.953 | 0.947 | 0.956 |

* Total Fe as FeO

# Appendix D

Table D-1 Electron microprobe analyses of chlorites (the Pak Pat Volcanics).

| Sample no. | NZ-1.1 | | | | | | | | NZ-1.2 | | | | | | | |
|---|---|---|---|---|---|---|---|---|---|---|---|---|---|---|---|---|
| Analysis no. | 1 | 2 | 3 | 4 | 5 | 6 | 7 | 8 | 1 | 2 | 3 | 4 | 5 | 6 | 7 | 8 |
| | C1-Chl1. | C1-Chl1. | C1-Chl1. | C1-Chl1. | C3-Chl3. | C3-Chl3. | C3-Chl3. | C3-Chl3 | C1-Chl1. | C1-Chl1. | C1-Chl1. | C1-Chl1 | C2-Chl2. | C2-Chl2. | C3-Chl3. | C3-Chl3.2 |
| SiO2 | 24.58 | 24.82 | 24.65 | 24.52 | 25.92 | 25 61 | 24.76 | 25.88 | 27.71 | 27.01 | 27.19 | 26 98 | 25.79 | 26.22 | 27.01 | 26.85 |
| TiO2 | 0.00 | 0 01 | 0.05 | 0.00 | 0.05 | 0.01 | 0.06 | 0.08 | 0.01 | 0.00 | 0.01 | 0.04 | 0.00 | 0.00 | 0.00 | 0 04 |
| Al2O3 | 21.76 | 21 42 | 22.18 | 21.89 | 21.77 | 21.72 | 21.35 | 22.23 | 20.69 | 20.94 | 21.16 | 21.88 | 22.17 | 21.69 | 21.04 | 20.39 |
| Cr2O3 | 0.00 | 0.05 | 0.02 | 0.02 | 0.12 | 0.10 | 0.06 | 0.04 | 0.08 | 0.03 | 0.04 | 0.02 | 0.00 | 0.03 | 0.00 | 0.01 |
| FeO* | 26.84 | 27.13 | 26.23 | 27.30 | 25.67 | 26 21 | 27.38 | 24.55 | 19 23 | 19.93 | 19.05 | 19.73 | 20.79 | 20 63 | 19.93 | 20.25 |
| MnO | 0.52 | 0.58 | 0.53 | 0.61 | 0.29 | 0.54 | 0.54 | 0.42 | 0 24 | 0.28 | 0.25 | 0.35 | 0.34 | 0.37 | 0.42 | 0.29 |
| MgO | 12.86 | 12.65 | 13.50 | 12.68 | 12.54 | 12.39 | 12 84 | 12.53 | 18.23 | 18.00 | 18.17 | 17 70 | 17.34 | 17.76 | 18.56 | 18.32 |
| Total | 86.56 | 86.66 | 87.15 | 87.01 | 86.34 | 86.57 | 86.99 | 85.74 | 86 18 | 86.19 | 85.86 | 86.68 | 86.44 | 86.71 | 86.97 | 86.15 |
| Number of cations on the basis of 14 oxygens: | | | | | | | | | | | | | | | | |
| Si | 2.652 | 2.678 | 2.631 | 2.635 | 2.770 | 2.745 | 2.668 | 2.769 | 2.859 | 2.802 | 2.815 | 2.777 | 2.688 | 2.721 | 2.780 | 2.797 |
| Al iv | 1.348 | 1.322 | 1.369 | 1.365 | 1.230 | 1.255 | 1.332 | 1.231 | 1.141 | 1.198 | 1.185 | 1.223 | 1.312 | 1.279 | 1 220 | 1.203 |
| Sum T | 4.000 | 4.000 | 4.000 | 4.000 | 4.000 | 4.000 | 4.000 | 4.000 | 4 000 | 4.000 | 4.000 | 4.000 | 4.000 | 4.000 | 4.000 | 4.000 |
| Al vi | 1.420 | 1.402 | 1.422 | 1.407 | 1.513 | 1.489 | 1.379 | 1.573 | 1.376 | 1.364 | 1.399 | 1.432 | 1.411 | 1.374 | 1.334 | 1.302 |
| Ti | 0.000 | 0.001 | 0.004 | 0.000 | 0 004 | 0.001 | 0.005 | 0 006 | 0.000 | 0.000 | 0.000 | 0.003 | 0 000 | 0 000 | 0.000 | 0.003 |
| Cr | 0.000 | 0.005 | 0.002 | 0.001 | 0.010 | 0.008 | 0.005 | 0.004 | 0.006 | 0.002 | 0.003 | 0.001 | 0.000 | 0 002 | 0.000 | 0.001 |
| Fe2+ | 2.422 | 2.448 | 2.341 | 2.453 | 2.295 | 2.349 | 2.467 | 2.197 | 1.660 | 1.729 | 1.650 | 1 698 | 1.812 | 1.790 | 1.716 | 1.765 |
| Mn | 0.048 | 0.053 | 0.048 | 0.056 | 0.026 | 0.049 | 0.049 | 0.038 | 0.021 | 0.025 | 0.022 | 0 030 | 0.030 | 0 033 | 0.036 | 0.026 |
| Mg | 2.068 | 2.034 | 2.147 | 2.030 | 1.997 | 1.979 | 2.062 | 1.997 | 2.803 | 2.784 | 2.805 | 2.715 | 2.694 | 2.747 | 2 848 | 2.845 |
| Sum O | 5.957 | 5.942 | 5.964 | 5.947 | 5.845 | 5 875 | 5.967 | 5.815 | 5.866 | 5.903 | 5.878 | 5.879 | 5.947 | 5.946 | 5.934 | 5.942 |
| Sum Cations | 9.957 | 9.942 | 9.964 | 9.947 | 9.845 | 9.875 | 9 967 | 9.815 | 9.866 | 9.903 | 9.878 | 9 879 | 9.947 | 9.946 | 9.934 | 9.942 |
| Mg/(Mg+Fe2) | 0.461 | 0.454 | 0.478 | 0 453 | 0.465 | 0.457 | 0.455 | 0.476 | 0.628 | 0.617 | 0.630 | 0 615 | 0.598 | 0.605 | 0 624 | 0.617 |

Table D-1 (continued)

| Sample no. | NZ-1.3 | | | | | | | NZ-8.1 | | | | | | |
|---|---|---|---|---|---|---|---|---|---|---|---|---|---|---|
| Analysis no. | 1 | 2 | 3 | 4 | 5 | 6 | 7 | 1 | 2 | 3 | 4 | 5 | 6 | 7 |
| | C1-Chl1. | C1-Chl1. | C1-Chl1. | C2-Chl2. | C2-Chl2. | C2-Chl2. | C2-Chl2 | C2-Chl2. | C2-Chl2. | C2-Chl2. | C2-Chl2. | C3-Chl3. | C3-Chl3. | C3-Chl3.3 |
| SiO2 | 26.65 | 26.76 | 26.99 | 26.86 | 26.70 | 27.24 | 27.01 | 25.69 | 25.93 | 26.39 | 26.14 | 25.73 | 27.72 | 26.67 |
| TiO2 | 0.00 | 0 00 | 0.08 | 0.00 | 0.00 | 0.04 | 0.00 | 0.05 | 0.05 | 0.01 | 0.00 | 0.03 | 0.01 | 0 07 |
| Al2O3 | 21.85 | 21.47 | 21.16 | 21.32 | 21.29 | 20.92 | 21.25 | 21.10 | 21.01 | 20.95 | 20.60 | 21.42 | 21.52 | 21.61 |
| Cr2O3 | 0.07 | 0.08 | 0.00 | 0.01 | 0.00 | 0.01 | 0 03 | 0.00 | 0.00 | 0.00 | 0.04 | 0.04 | 0.03 | 0 02 |
| FeO* | 20.82 | 19.17 | 19.81 | 19.62 | 20.08 | 19.31 | 19.67 | 23.51 | 24.03 | 22.89 | 22.70 | 23.75 | 19.59 | 20.79 |
| MnO | 0.40 | 0.23 | 0.39 | 0.40 | 0.33 | 0.33 | 0.36 | 0 67 | 0.99 | 0.75 | 0.79 | 0.80 | 0.33 | 0 69 |
| MgO | 18.01 | 18.25 | 18.42 | 18.23 | 18.29 | 17.92 | 18.30 | 16.04 | 15.70 | 16 01 | 15.77 | 14.43 | 16.59 | 16.23 |
| Total | 87.80 | 85.96 | 86.84 | 86.43 | 86.69 | 85.77 | 86.62 | 87.06 | 87.70 | 87.00 | 86.05 | 86.20 | 85.79 | 86.09 |
| Number of cations on the basis of 14 oxygens: | | | | | | | | | | | | | | |
| Si | 2.729 | 2.774 | 2.779 | 2.777 | 2.758 | 2.829 | 2.785 | 2.705 | 2.720 | 2.767 | 2.774 | 2.739 | 2.874 | 2.787 |
| Al iv | 1.271 | 1.226 | 1.221 | 1.223 | 1.242 | 1.171 | 1.215 | 1.295 | 1.280 | 1.233 | 1.226 | 1.261 | 1.126 | 1.213 |
| Sum T | 4.000 | 4.000 | 4.000 | 4.000 | 4.000 | 4.000 | 4.000 | 4.000 | 4.000 | 4 000 | 4.000 | 4.000 | 4 000 | 4.000 |
| Al vi | 1.366 | 1.398 | 1.348 | 1.376 | 1.351 | 1.391 | 1.368 | 1.326 | 1.318 | 1.358 | 1.351 | 1.426 | 1.503 | 1.450 |
| Ti | 0.000 | 0.000 | 0.006 | 0.000 | 0.000 | 0.003 | 0.000 | 0 004 | 0.004 | 0.001 | 0.000 | 0 002 | 0.001 | 0.005 |
| Cr | 0.006 | 0.007 | 0.000 | 0.000 | 0.000 | 0.000 | 0.003 | 0.000 | 0.000 | 0.000 | 0.004 | 0 003 | 0.002 | 0.002 |
| Fe2+ | 1.783 | 1.662 | 1.705 | 1.697 | 1.735 | 1.677 | 1.696 | 2.071 | 2.108 | 2.008 | 2.015 | 2.114 | 1 698 | 1.817 |
| Mn | 0.035 | 0.020 | 0.034 | 0 035 | 0.028 | 0.029 | 0.032 | 0.060 | 0.088 | 0.066 | 0.071 | 0.072 | 0 029 | 0.061 |
| Mg | 2.748 | 2.819 | 2.826 | 2.809 | 2.817 | 2.774 | 2.812 | 2.517 | 2.454 | 2.502 | 2.494 | 2.288 | 2.563 | 2.527 |
| Sum O | 5.938 | 5.906 | 5.919 | 5.917 | 5.932 | 5.875 | 5.911 | 5.977 | 5.972 | 5.935 | 5.934 | 5.906 | 5.796 | 5.863 |
| Sum Cations | 9.938 | 9.906 | 9.919 | 9.917 | 9.932 | 9.875 | 9.911 | 9.977 | 9.972 | 9.935 | 9.934 | 9.906 | 9.796 | 9 863 |
| Mg/(Mg+Fe2) | 0 606 | 0.629 | 0 624 | 0 623 | 0 619 | 0 623 | 0 624 | 0.549 | 0.538 | 0.555 | 0 553 | 0.520 | 0 601 | 0.582 |

* Total Fe as FeO

Table D-2 Electron microprobe analyses of epidotes (the Pak Pat Volcanics).

| Sample no. | NZ-8.1 | | | |
|---|---|---|---|---|
| Analysis no. | 1 | 2 | 3 | 4 |
| | C3-Ep1 | C3-Ep2 | C3-Ep3 | C3-Ep5 |
| SiO2 | 37.06 | 37.37 | 37.49 | 37.60 |
| TiO2 | 0.03 | 0.08 | 0.09 | 0.13 |
| Al2O3 | 24.22 | 24.51 | 24.87 | 24.43 |
| Fe2O3* | 11.71 | 11.43 | 11.86 | 11.92 |
| MnO | 0.32 | 0.28 | 0.44 | 0.27 |
| MgO | 0.00 | 0.00 | 0.00 | 0.00 |
| CaO | 23.55 | 23.99 | 23.96 | 24.17 |
| Total | 96.89 | 97.67 | 98.71 | 98.52 |
| Number of cations on the basis of 12.5 oxygens: | | | | |
| Si | 2.975 | 2.974 | 2.956 | 2.972 |
| Al iv | 0.025 | 0.026 | 0.044 | 0.028 |
| Sum Z | 3.000 | 3.000 | 3.000 | 3.000 |
| Al vi | 2.266 | 2.274 | 2.268 | 2.247 |
| Ti | 0.002 | 0.005 | 0.005 | 0.007 |
| Fe3+ | 0.708 | 0.685 | 0.704 | 0.709 |
| Sum Y | 2.976 | 2.963 | 2.977 | 2.964 |
| Fe2+ | 0.000 | 0.000 | 0.000 | 0.000 |
| Mn | 0.022 | 0.019 | 0.030 | 0.018 |
| Mg | 0.000 | 0.000 | 0.000 | 0.000 |
| Ca | 2.026 | 2.046 | 2.024 | 2.047 |
| Sum W | 2.047 | 2.065 | 2.054 | 2.065 |
| Sum Cations | 8.024 | 8.029 | 8.031 | 8.029 |
| Fe3/(Fe3+Al) | 0.236 | 0.229 | 0.233 | 0.237 |

* Total Fe as Fe2O3

# Appendix E

Table E-1 Electron microprobe analyses of amphiboles (Hornfelses).

| Sample no. | 4/111290 | | | | | | | | | | | 7/111290 | | | | | | | | | | | |
|---|---|---|---|---|---|---|---|---|---|---|---|---|---|---|---|---|---|---|---|---|---|---|---|
| Analysis no. | 1 | 2 | 3 | 4 | 5 | 6 | 7 | 8 | 9 | 10 | 11 | 1 | 2 | 3 | 4 | 5 | 6 | 7 | 8 | 9 | 10 | 11 | 12 |
| SiO2 | 37.53 | 38.38 | 36.65 | 37.50 | 37.16 | 37.00 | 38.99 | 38.45 | 38.30 | 38.97 | 36.41 | 37.05 | 36.69 | 36.50 | 36.44 | 37.96 | 38.01 | 35.68 | 35.91 | 35.27 | 38.96 | 37.42 | 37.80 |
| TiO2 | 0.70 | 0.51 | 0.47 | 0.49 | 0.33 | 0.43 | 0.19 | 0.36 | 0.23 | 0.32 | 0.55 | 0.32 | 0.31 | 0.31 | 0.44 | 0.23 | 0.55 | 0.53 | 0.10 | 0.12 | 0.18 | 0.29 | 0 34 |
| Al2O3 | 11.66 | 10.89 | 11.61 | 11.42 | 11.65 | 11.44 | 10.92 | 12.03 | 12.01 | 11.09 | 11.87 | 10.84 | 11.79 | 10.67 | 11.57 | 9.37 | 9.48 | 11.11 | 10.36 | 10 28 | 9.07 | 9.91 | 11.05 |
| Cr2O3 | 0.03 | 0.00 | 0.06 | 0.00 | 0.02 | 0.00 | 0.03 | 0.00 | 0.00 | 0.00 | 0.00 | 0.00 | 0.00 | 0.18 | 0.02 | 0.00 | 0.12 | 0.00 | 0.02 | 0.00 | 0.00 | 0 00 | 0 00 |
| FeO* | 29.33 | 29.51 | 28.66 | 29.76 | 29.77 | 29.61 | 28.39 | 27.12 | 26.90 | 29.14 | 29.28 | 30.47 | 28.53 | 30.77 | 29 09 | 31.10 | 30.08 | 31.22 | 32.39 | 32.92 | 32.21 | 29.23 | 29.55 |
| MnO | 0.51 | 0.50 | 0.50 | 0.42 | 0.48 | 0.51 | 0.44 | 0.42 | 0.39 | 0.42 | 0.51 | 0.45 | 0.44 | 0.46 | 0 46 | 0.43 | 0.49 | 0.52 | 0.45 | 0.42 | 0.50 | 0.55 | 0.44 |
| MgO | 2.29 | 2.69 | 2.64 | 2.22 | 2.19 | 2.15 | 3.55 | 3.54 | 3.61 | 2.81 | 2.27 | 2.29 | 2.85 | 2.04 | 2.96 | 1.97 | 2.23 | 1.76 | 1.26 | 0.99 | 1.76 | 2.74 | 2.80 |
| CaO | 11.61 | 11.51 | 11.33 | 11.70 | 11.74 | 11.76 | 11.46 | 12.01 | 11.64 | 11.83 | 11.70 | 11.71 | 11.68 | 11.80 | 11.91 | 11.58 | 11.74 | 11.69 | 11.48 | 11.29 | 11.60 | 11.07 | 11.47 |
| Na2O | 1.45 | 1.49 | 1.44 | 1.65 | 1.69 | 1.61 | 1.49 | 1.56 | 1.78 | 1.82 | 1.61 | 1.67 | 1.75 | 0.46 | 1.61 | 1.57 | 1.41 | 1.57 | 1.51 | 1.59 | 1.72 | 1.48 | 1.73 |
| K2O | 2.00 | 1.73 | 1.72 | 1.74 | 1.78 | 1.74 | 1.44 | 1.72 | 1.49 | 1.36 | 1.89 | 1.62 | 1.69 | 2.04 | 1.87 | 1.68 | 1.64 | 2.02 | 2.04 | 1.99 | 1.43 | 1.59 | 1.76 |
| F | 0.00 | 0.00 | 0.00 | 0 00 | 0.00 | 0.00 | 0.00 | 0.00 | 0.00 | 0.00 | 0.00 | 0.00 | 0.00 | 0.00 | 0.00 | 0 00 | 0.00 | 0.00 | 0.00 | 0 00 | 0.00 | 0.00 | 0 00 |
| Cl | 1.77 | 1.29 | 1.01 | 1.28 | 1.26 | 1.37 | 0 60 | 0.89 | 0.84 | 0.73 | 1.42 | 0.98 | 1.06 | 1.40 | 1.47 | 1.14 | 1.40 | 1.63 | 1.99 | 2.06 | 0.93 | 1.34 | 1.18 |
| Total | 98.87 | 98.50 | 96 08 | 98.18 | 98.07 | 97.63 | 97.51 | 98.10 | 97.17 | 98.49 | 97.52 | 97.40 | 96.79 | 96.63 | 97.84 | 97.03 | 97.15 | 97.73 | 97.51 | 96.93 | 98.37 | 95.62 | 98.11 |
| O = F, Cl | -0.40 | -0.29 | -0 22 | -0.29 | -0.28 | -0.31 | -0.14 | -0.20 | -0.19 | -0.16 | -0.32 | -0.22 | -0.24 | -0.32 | -0.33 | -0.26 | -0.32 | -0.37 | -0.45 | -0.46 | -0.21 | -0.30 | -0.27 |
| Total | 98.47 | 98.21 | 95 86 | 97.89 | 97.78 | 97.32 | 97.37 | 97.90 | 96.98 | 98.32 | 97.20 | 97.18 | 96.55 | 96 32 | 97.51 | 96.77 | 96 84 | 97.36 | 97.06 | 96.46 | 98.16 | 95 32 | 97.84 |
| Number of cations on the basis of 23 oxygens:# | | | | | | | | | | | | | | | | | | | | | | | |
| Si | 6.084 | 6.182 | 6.026 | 6.102 | 6 059 | 6.071 | 6.225 | 6.155 | 6.161 | 6.240 | 5.982 | 6 070 | 6.015 | 6.035 | 5.954 | 6 287 | 6.287 | 5 920 | 6.019 | 5.967 | 6.349 | 6 212 | 6.117 |
| Al iv | 1.916 | 1.818 | 1.974 | 1.898 | 1.941 | 1.929 | 1.775 | 1.845 | 1.839 | 1.760 | 2.018 | 1.930 | 1.985 | 1 965 | 2.046 | 1.713 | 1.713 | 2.080 | 1.981 | 2.033 | 1.651 | 1.788 | 1.883 |
| Sum T | 8 000 | 8.000 | 8.000 | 8.000 | 8.000 | 8.000 | 8.000 | 8.000 | 8.000 | 8.000 | 8.000 | 8 000 | 8.000 | 8.000 | 8.000 | 8 000 | 8.000 | 8 000 | 8.000 | 8 000 | 8.000 | 8.000 | 8 000 |
| Al vi | 0.312 | 0 249 | 0.277 | 0.293 | 0.299 | 0.285 | 0.279 | 0.426 | 0.437 | 0.334 | 0.281 | 0.164 | 0.293 | 0.116 | 0 183 | 0 117 | 0.136 | 0 093 | 0.066 | 0 017 | 0.091 | 0.151 | 0.225 |
| Ti | 0 085 | 0.062 | 0 058 | 0.060 | 0.040 | 0.053 | 0.023 | 0.043 | 0.027 | 0.038 | 0.068 | 0 039 | 0.038 | 0 039 | 0 054 | 0.029 | 0 068 | 0 066 | 0.013 | 0 015 | 0.022 | 0 037 | 0.041 |
| Cr | 0 004 | 0.000 | 0.008 | 0.001 | 0.002 | 0.001 | 0.003 | 0.000 | 0.001 | 0 000 | 0.000 | 0.000 | 0.000 | 0.024 | 0.003 | 0 000 | 0.016 | 0.000 | 0 003 | 0.000 | 0.000 | 0 000 | 0.000 |
| Fe3+ | 0.529 | 0.650 | 0.761 | 0.524 | 0.555 | 0.528 | 0.770 | 0.377 | 0.477 | 0.448 | 0.570 | 0.706 | 0.603 | 0.989 | 0.681 | 0.569 | 0 464 | 0.765 | 0.837 | 0.941 | 0.623 | 0.813 | 0.695 |
| Mg | 0.552 | 0.646 | 0.646 | 0.538 | 0.533 | 0.526 | 0.844 | 0.844 | 0.865 | 0 669 | 0.556 | 0.559 | 0.696 | 0.503 | 0 721 | 0.486 | 0.550 | 0 435 | 0.315 | 0.250 | 0.427 | 0 677 | 0.675 |
| Fe2+ | 3.447 | 3.325 | 3.180 | 3.527 | 3 505 | 3.536 | 3.021 | 3.253 | 3.141 | 3.454 | 3.453 | 3.469 | 3.308 | 3.266 | 3.295 | 3.739 | 3.697 | 3.567 | 3.703 | 3.717 | 3.767 | 3.244 | 3.304 |
| Mn | 0.070 | 0 068 | 0.069 | 0.058 | 0.066 | 0.072 | 0.059 | 0.057 | 0.053 | 0.057 | 0.071 | 0.062 | 0.061 | 0.064 | 0 064 | 0.060 | 0.069 | 0.073 | 0 064 | 0.060 | 0 069 | 0.078 | 0.060 |
| Sum C | 5.000 | 5.000 | 5.000 | 5.000 | 5.000 | 5.000 | 5.000 | 5.000 | 5.000 | 5.000 | 5.000 | 5.000 | 5.000 | 5.000 | 5.000 | 5.000 | 5.000 | 5.000 | 5.000 | 5 000 | 5.000 | 5.000 | 5.000 |
| Fe2+ | 0.000 | 0.000 | 0.000 | 0 000 | 0.000 | 0.000 | 0.000 | 0.000 | 0.000 | 0.000 | 0.000 | 0.000 | 0.000 | 0.000 | 0.000 | 0.000 | 0.000 | 0.000 | 0.000 | 0.000 | 0.000 | 0.000 | 0.000 |
| Mn | 0 000 | 0.000 | 0.000 | 0.000 | 0.000 | 0.000 | 0.000 | 0.000 | 0.000 | 0.000 | 0.000 | 0.000 | 0.000 | 0.000 | 0 000 | 0.000 | 0.000 | 0.000 | 0 000 | 0 000 | 0 000 | 0.000 | 0.000 |
| Ca | 2 000 | 1.987 | 1.996 | 2.000 | 2.000 | 2.000 | 1.961 | 2.000 | 2.000 | 2.000 | 2.000 | 2.000 | 2 000 | 2 000 | 2.000 | 2.000 | 2.000 | 2.000 | 2.000 | 2.000 | 2.000 | 1.969 | 1.988 |
| Na | 0 000 | 0.013 | 0.004 | 0.000 | 0.000 | 0.000 | 0.039 | 0.000 | 0.000 | 0 000 | 0.000 | 0.000 | 0.000 | 0 000 | 0 000 | 0.000 | 0 000 | 0.000 | 0 000 | 0.000 | 0.000 | 0.031 | 0.012 |
| Sum B | 2.000 | 2.000 | 2.000 | 2.000 | 2.000 | 2.000 | 2.000 | 2.000 | 2.000 | 2.000 | 2.000 | 2.000 | 2 000 | 2.000 | 2.000 | 2 000 | 2.000 | 2.000 | 2 000 | 2.000 | 2 000 | 2 000 | 2.000 |
| Ca | 0.016 | 0.000 | 0.000 | 0.039 | 0.050 | 0 067 | 0.000 | 0.060 | 0.006 | 0.029 | 0.060 | 0.056 | 0 052 | 0.091 | 0 085 | 0 055 | 0.081 | 0 078 | 0.062 | 0 047 | 0.026 | 0.000 | 0.000 |
| Na | 0.454 | 0.453 | 0.456 | 0.520 | 0.535 | 0.512 | 0.422 | 0.485 | 0.554 | 0.566 | 0.514 | 0.531 | 0.556 | 0.147 | 0 510 | 0.504 | 0 452 | 0.505 | 0.491 | 0 522 | 0.544 | 0.446 | 0.529 |
| K | 0.414 | 0.355 | 0 360 | 0.361 | 0.369 | 0 364 | 0 293 | 0.351 | 0.305 | 0.277 | 0.396 | 0.339 | 0.353 | 0.430 | 0 390 | 0.355 | 0 346 | 0.428 | 0.436 | 0.430 | 0.297 | 0.336 | 0.364 |
| Sum A | 0.884 | 0.808 | 0.816 | 0.921 | 0.954 | 0.943 | 0.715 | 0.896 | 0.865 | 0.872 | 0.970 | 0.925 | 0.961 | 0.669 | 0 985 | 0.914 | 0.879 | 1.011 | 0.989 | 0.998 | 0.866 | 0.782 | 0.893 |
| Sum Cations | 15.884 | 15.808 | 15.816 | 15.921 | 15.954 | 15.943 | 15.715 | 15.896 | 15.865 | 15.872 | 15.970 | 15.925 | 15.961 | 15.669 | 15.985 | 15.914 | 15.879 | 16.011 | 15.989 | 15.998 | 15.866 | 15.782 | 15.893 |
| Mg/(Mg+Fe2) | 0.138 | 0.163 | 0.169 | 0 132 | 0.132 | 0.130 | 0.218 | 0.206 | 0 216 | 0 162 | 0 139 | 0.139 | 0.174 | 0.133 | 0.180 | 0.115 | 0.129 | 0.109 | 0.078 | 0 063 | 0.102 | 0 173 | 0.170 |

* Total Fe as FeO.

# Calculated by normalising the number of cations other than Ca, Na and K to 13.

Table E-2 Electron microprobe analyses of clinopyroxenes (Hornfelses).

| Sample no. | 4/121190 | | | | | | | | | 7/111290 | | | | | | |
|---|---|---|---|---|---|---|---|---|---|---|---|---|---|---|---|---|
| Analysis no. | 1 | 2 | 3 | 4 | 5 | 6 | 7 | 8 | 9 | 1 | 2 | 3 | 4 | 5 | 6 | 7 |
| | in Amp | rim Cc | in Amp | rim Grt | core | | | in Amp | in Amp | | | | | | | |
| SiO2 | 53.68 | 53.22 | 53.38 | 50.82 | 51.60 | 49.34 | 49.50 | 49.33 | 50.82 | 50.15 | 49.69 | 49.38 | 49.61 | 50.40 | 50.46 | 49.55 |
| TiO2 | 0.04 | 0.00 | 0 02 | 0.00 | 0.00 | 0.11 | 0.05 | 0.16 | 0.01 | 0.05 | 0.04 | 0.05 | 0.06 | 0.04 | 0.00 | 0.00 |
| Al2O3 | 0.32 | 0.24 | 0.35 | 0.29 | 0.25 | 1.23 | 1.13 | 1.40 | 0.17 | 0.35 | 0.70 | 0.59 | 0.41 | 0.45 | 0.92 | 0.39 |
| Cr2O3 | 0.00 | 0.00 | 0.02 | 0.00 | 0.00 | 0.07 | 0.00 | 0.00 | 0.03 | 0.04 | 0 04 | 0.09 | 0.00 | 0.00 | 0.03 | 0.00 |
| Fe2O3* | 1.01 | 1.53 | 1.64 | 1.91 | 1.05 | 2.63 | 2.61 | 1.55 | 1.42 | 2 85 | 4.13 | 2.61 | 2.43 | 1.61 | 2.82 | 2.18 |
| FeO* | 1.85 | 3.34 | 1.48 | 12.19 | 10.60 | 15.13 | 15.17 | 17.37 | 10.57 | 14.90 | 12.99 | 16 51 | 15.07 | 17.81 | 15.72 | 21.50 |
| MnO | 0.71 | 1.52 | 1.08 | 1.44 | 1.63 | 0.93 | 0.93 | 0.87 | 3.84 | 0.91 | 0.71 | 0 73 | 0 85 | 0.97 | 0.72 | 0.90 |
| MgO | 16.13 | 14.50 | 15.72 | 8.65 | 9.90 | 6.38 | 6 37 | 5.57 | 8.40 | 6 96 | 7.60 | 5.89 | 6 66 | 5.84 | 6.58 | 2.98 |
| CaO | 25.68 | 25.16 | 25.93 | 24.30 | 24.42 | 23.74 | 23.91 | 23.36 | 24.13 | 24.25 | 24.36 | 23.92 | 23.94 | 23.84 | 24.36 | 23.71 |
| Na2O | 0.00 | 0 15 | 0.01 | 0.12 | 0.13 | 0.27 | 0.25 | 0 22 | 0.09 | 0.15 | 0.22 | 0.15 | 0.19 | 0.12 | 0.21 | 0.25 |
| Total | 99.43 | 99.66 | 99.62 | 99.73 | 99.59 | 99.82 | 99.92 | 99.82 | 99.48 | 100.63 | 100.46 | 99.92 | 99.21 | 101.07 | 101.80 | 101.45 |
| Number of cations on the basis of 6 oxygens: | | | | | | | | | | | | | | | | |
| Si | 1.978 | 1.978 | 1.969 | 1.970 | 1.984 | 1.939 | 1.943 | 1.948 | 1.978 | 1.954 | 1.930 | 1.950 | 1 960 | 1.970 | 1.945 | 1.968 |
| Al iv | 0.014 | 0.011 | 0.015 | 0.013 | 0.011 | 0.057 | 0.052 | 0.052 | 0.008 | 0.016 | 0 032 | 0.028 | 0.019 | 0 021 | 0.042 | 0.018 |
| Fe3+ | 0.008 | 0 011 | 0.016 | 0.017 | 0.005 | 0.004 | 0.005 | 0.000 | 0.014 | 0.030 | 0.038 | 0.022 | 0.021 | 0.010 | 0.013 | 0.014 |
| Sum T | 2.000 | 2 000 | 2.000 | 2.000 | 2.000 | 2.000 | 2.000 | 2.000 | 2.000 | 2.000 | 2.000 | 2 000 | 2 000 | 2.000 | 2.000 | 2.000 |
| Al vi | 0 000 | 0.000 | 0.000 | 0.000 | 0.000 | 0.000 | 0.000 | 0 013 | 0.000 | 0.000 | 0.000 | 0 000 | 0 000 | 0.000 | 0 000 | 0 000 |
| Ti | 0.001 | 0.000 | 0.001 | 0.000 | 0.000 | 0.003 | 0.002 | 0.005 | 0 000 | 0 001 | 0.001 | 0.001 | 0 002 | 0.001 | 0.000 | 0.000 |
| Cr | 0.000 | 0.000 | 0.001 | 0.000 | 0.000 | 0 002 | 0.000 | 0.000 | 0.001 | 0.001 | 0 001 | 0.003 | 0.000 | 0.000 | 0 001 | 0.000 |
| Fe3+ | 0.020 | 0.032 | 0.030 | 0 039 | 0.026 | 0 073 | 0.072 | 0.046 | 0.027 | 0.053 | 0 083 | 0.056 | 0 051 | 0.038 | 0.069 | 0.051 |
| Fe2+ | 0.057 | 0.104 | 0.046 | 0.395 | 0.338 | 0.497 | 0.498 | 0.574 | 0.344 | 0.485 | 0 422 | 0 545 | 0 498 | 0.582 | 0.507 | 0.714 |
| Mn | 0.022 | 0.048 | 0.034 | 0.047 | 0.053 | 0.031 | 0.031 | 0.029 | 0.127 | 0.030 | 0.023 | 0.024 | 0.028 | 0.032 | 0.023 | 0.030 |
| Mg | 0 886 | 0.803 | 0.864 | 0.500 | 0.567 | 0.373 | 0.372 | 0.328 | 0.487 | 0.404 | 0.440 | 0.347 | 0.392 | 0 340 | 0 378 | 0.176 |
| Sum O | 0.986 | 0.987 | 0.974 | 0.981 | 0.984 | 0.980 | 0.976 | 0.994 | 0.987 | 0.976 | 0.970 | 0 976 | 0.971 | 0.993 | 0 978 | 0.972 |
| Ca | 1.014 | 1.002 | 1.025 | 1.009 | 1.006 | 0.999 | 1.006 | 0.988 | 1.007 | 1.012 | 1.014 | 1.012 | 1.014 | 0.998 | 1.006 | 1.009 |
| Na | 0.000 | 0.011 | 0.001 | 0.009 | 0.010 | 0.020 | 0.019 | 0.017 | 0 007 | 0.012 | 0.016 | 0 011 | 0 015 | 0 009 | 0.015 | 0.019 |
| Sum Cations | 4.000 | 4.000 | 4.000 | 4.000 | 4.000 | 4.000 | 4.000 | 4.000 | 4.000 | 4 000 | 4.000 | 4.000 | 4.000 | 4.000 | 4.000 | 4.000 |
| Mg/((Mg+Fe2 | 0.940 | 0.886 | 0 950 | 0.558 | 0.627 | 0.429 | 0.428 | 0.364 | 0 586 | 0.454 | 0.510 | 0.389 | 0.440 | 0.369 | 0.427 | 0.198 |
| Molecular proportions of end-members# : | | | | | | | | | | | | | | | | |
| Wo | 0.507 | 0 504 | 0.513 | 0.507 | 0.505 | 0 506 | 0.508 | 0.503 | 0.505 | 0.510 | 0.512 | 0.510 | 0.511 | 0.502 | 0 507 | 0 509 |
| En | 0.443 | 0.404 | 0 432 | 0.251 | 0.285 | 0.189 | 0.188 | 0.167 | 0.245 | 0 204 | 0 222 | 0.175 | 0.198 | 0.171 | 0.191 | 0 089 |
| Fs | 0.050 | 0.092 | 0.055 | 0.242 | 0.209 | 0.305 | 0.304 | 0.330 | 0.250 | 0 287 | 0.266 | 0.315 | 0 291 | 0.327 | 0.302 | 0 401 |

* Calculated assuming stoichiometry on the basis of 4 cations and 6 oxygens.

# Calculated after the Subcommittee on Pyroxenes, IMA (9188).

Table E-3 Electron microprobe analyses of garnets (Hornfelses).

| Sample no. | 4/111290 | | | | | | | | | |
|---|---|---|---|---|---|---|---|---|---|---|
| Analysis no. | 1 | 2 | 3 | 4 | 5 | 6 | 7 | 8 | 9 | 10 |
| | | | | | | | RimCpx | RimCpx | RimCpx | RimCpx |
| SiO2 | 36.74 | 37.02 | 36.65 | 36.78 | 37.00 | 36.77 | 37.03 | 36.70 | 37.11 | 36.90 |
| TiO2 | 0.23 | 0.00 | 0.00 | 0.02 | 0.18 | 0.00 | 0.87 | 0.63 | 1.02 | 0.73 |
| Al2O3 | 5.48 | 6.11 | 4.99 | 5.66 | 6.61 | 6.54 | 7.68 | 6.39 | 7.89 | 9.02 |
| Cr2O3 | 0.02 | 0.01 | 0.00 | 0.04 | 0.00 | 0.01 | 0.00 | 0.00 | 0.08 | 0.03 |
| Fe2O3* | 23.35 | 22.63 | 24.03 | 23.78 | 22.29 | 22.06 | 20.02 | 21.76 | 20.33 | 18.59 |
| FeO* | 0.00 | 0.00 | 0.00 | 0.00 | 0.00 | 0.00 | 0.00 | 0.00 | 0.03 | 0.00 |
| MnO | 0.79 | 0.77 | 0.81 | 0.77 | 0.74 | 1.14 | 0.77 | 0.46 | 0.45 | 0.91 |
| MgO | 0.05 | 0.03 | 0.03 | 0.01 | 0.01 | 0.06 | 0.01 | 0.02 | 0.04 | 0.04 |
| CaO | 34.59 | 34.31 | 34.60 | 34.60 | 34.52 | 34.32 | 34.76 | 35.29 | 34.84 | 35.04 |
| Total | 101.25 | 100.88 | 101.11 | 101.66 | 101.35 | 100.90 | 101.14 | 101.25 | 101.89 | 101.26 |
| Number of cations on the basis of 12 oxygens: | | | | | | | | | | |
| Si | 2.976 | 3.000 | 2.979 | 2.968 | 2.980 | 2.974 | 2.971 | 2.956 | 2.956 | 2.938 |
| Al iv | 0.024 | 0.000 | 0.021 | 0.032 | 0.020 | 0.026 | 0.029 | 0.044 | 0.044 | 0.062 |
| Al vi | 0.499 | 0.584 | 0.457 | 0.507 | 0.608 | 0.597 | 0.697 | 0.563 | 0.697 | 0.785 |
| Ti | 0.014 | 0.000 | 0.000 | 0.001 | 0.011 | 0.000 | 0.052 | 0.038 | 0.061 | 0.044 |
| Cr | 0.001 | 0.001 | 0.000 | 0.003 | 0.000 | 0.001 | 0.000 | 0.000 | 0.005 | 0.002 |
| Fe3+ | 1.424 | 1.380 | 1.470 | 1.444 | 1.351 | 1.343 | 1.209 | 1.319 | 1.219 | 1.114 |
| Fe2+ | 0.000 | 0.000 | 0.000 | 0.000 | 0.000 | 0.000 | 0.000 | 0.000 | 0.000 | 0.000 |
| Mn | 0.054 | 0.053 | 0.056 | 0.053 | 0.050 | 0.078 | 0.052 | 0.031 | 0.030 | 0.061 |
| Mg | 0.006 | 0.004 | 0.004 | 0.001 | 0.001 | 0.007 | 0.001 | 0.002 | 0.005 | 0.005 |
| Ca | 3.002 | 2.979 | 3.013 | 2.992 | 2.979 | 2.974 | 2.988 | 3.046 | 2.974 | 2.989 |
| Sum Cations | 8.000 | 8.000 | 8.000 | 8.000 | 8.000 | 8.000 | 8.000 | 8.000 | 8.000 | 8.000 |
| Mg/Mg+Fe2 | 1.000 | 1.000 | 1.000 | 1.000 | 1.000 | 1.000 | 1.000 | 1.000 | 1.000 | 1.000 |
| Molecular proportions of end-members : | | | | | | | | | | |
| Alm | 0.000 | 0.000 | 0.000 | 0.000 | 0.000 | 0.000 | 0.000 | 0.000 | 0.000 | 0.000 |
| Py | 0.002 | 0.001 | 0.001 | 0.000 | 0.000 | 0.002 | 0.000 | 0.001 | 0.002 | 0.002 |
| Sp | 0.018 | 0.017 | 0.018 | 0.017 | 0.017 | 0.026 | 0.017 | 0.010 | 0.010 | 0.020 |
| Gr | 0.283 | 0.299 | 0.263 | 0.271 | 0.314 | 0.314 | 0.386 | 0.347 | 0.380 | 0.431 |
| Adr | 0.697 | 0.682 | 0.718 | 0.711 | 0.669 | 0.658 | 0.596 | 0.642 | 0.608 | 0.547 |

* Calculated assuming stoichiometry on the basis of 8 cations and 12 oxygens.

Table E-4 Electron microprobe analyses of epidotes (Hornfelses).

| Sample no. | 4/111290 | | | | 7/111290 | | |
|---|---|---|---|---|---|---|---|
| Analysis no. | 1 | 2 | 3 | 4 | 1 | 2 | 3 |
| SiO2 | 37.36 | 37.15 | 37.62 | 37.86 | 37.64 | 37 85 | 37.62 |
| TiO2 | 0.03 | 0.01 | 0.02 | 0.03 | 0.03 | 0.04 | 0.02 |
| Al2O3 | 20.86 | 20.79 | 23.07 | 22.38 | 24.59 | 24.72 | 24.01 |
| Fe2O3* | 15.95 | 16.69 | 14.03 | 13.94 | 12.19 | 12.02 | 10.69 |
| MnO | 0.06 | 0.00 | 1.07 | 0.32 | 0.01 | 0.17 | 0.27 |
| MgO | 0.00 | 0.00 | 0.00 | 0.01 | 0.05 | 0.05 | 0.00 |
| CaO | 23.95 | 23.79 | 22.88 | 23.46 | 24.04 | 23.75 | 24.01 |
| Total | 98.21 | 98.43 | 98.67 | 97.99 | 98.55 | 98.60 | 96.62 |
| Number of cations on the basis of 12.5 oxygens: | | | | | | | |
| Si | 3.006 | 2.988 | 2.989 | 3.024 | 2.970 | 2.981 | 3.019 |
| Al iv | 0.000 | 0.012 | 0.011 | 0.000 | 0.030 | 0.019 | 0.000 |
| Sum Z | 3.006 | 3.000 | 3.000 | 3.024 | 3.000 | 3.000 | 3.019 |
| Al vi | 1.978 | 1.960 | 2.150 | 2.107 | 2.258 | 2.277 | 2.272 |
| Ti | 0.002 | 0.000 | 0.001 | 0.002 | 0.002 | 0.002 | 0.001 |
| Fe3+ | 0.966 | 1.010 | 0.839 | 0.838 | 0.724 | 0.712 | 0.646 |
| Sum Y | 2.946 | 2.970 | 2.990 | 2.947 | 2.983 | 2.991 | 2.919 |
| Mn | 0.004 | 0 000 | 0.072 | 0.021 | 0.001 | 0.011 | 0.018 |
| Mg | 0.000 | 0.000 | 0.000 | 0.001 | 0.006 | 0.006 | 0.000 |
| Ca | 2.065 | 2.050 | 1.948 | 2.007 | 2.033 | 2.004 | 2.065 |
| Sum W | 2.069 | 2.050 | 2.020 | 2.030 | 2.039 | 2.022 | 2.083 |
| Sum Cations | 8.020 | 8.021 | 8.010 | 8.002 | 8.022 | 8.013 | 8.021 |
| Fe3/(Fe3+Al) | 0.328 | 0.339 | 0.280 | 0.285 | 0.240 | 0.237 | 0.221 |

* Total Fe as Fe2O3

Table E-5 Electron microprobe analyses of calcite.

| Sample no. | 4/111290 | | | 7/111290 | | | |
|---|---|---|---|---|---|---|---|
| Analysis no. | 1 | 2 | 3 | 1 | 2 | 3 | 4 |
| FeO* | 0.17 | 0.03 | 0.08 | 1.04 | 0.32 | 0.29 | 0.41 |
| MnO | 0.19 | 0.21 | 0.14 | 1.11 | 0.00 | 0.12 | 0.82 |
| MgO | 0.01 | 0.00 | 0.00 | 0.02 | 0.00 | 0.00 | 0.01 |
| CaO | 55.41 | 55.35 | 55.54 | 54.32 | 55.21 | 55.87 | 54.93 |
| CO2# | 43.72 | 43.59 | 43.72 | 43.98 | 43.52 | 44.10 | 43.88 |
| Total | 99.50 | 99.18 | 99.47 | 100.47 | 99.05 | 100.39 | 100.04 |
| Number of cations on the basis of 6 oxygens: | | | | | | | |
| Fe | 0.005 | 0.001 | 0.002 | 0.029 | 0.009 | 0.008 | 0.011 |
| Mn | 0.006 | 0.006 | 0.004 | 0.031 | 0.000 | 0.003 | 0.023 |
| Mg | 0.000 | 0.000 | 0.000 | 0.001 | 0.000 | 0.000 | 0.000 |
| Ca | 1.989 | 1.993 | 1.994 | 1.939 | 1.991 | 1.988 | 1.965 |
| Sum Cat. | 2.000 | 2.000 | 2.000 | 2.000 | 2.000 | 2.000 | 2.000 |
| Molecular proportions of end-members: | | | | | | | |
| FeCO3 | 0.002 | 0.000 | 0.001 | 0.014 | 0.005 | 0.004 | 0.006 |
| MnCO3 | 0.003 | 0.003 | 0.002 | 0.016 | 0.000 | 0.002 | 0.012 |
| MgCO3 | 0.000 | 0.000 | 0.000 | 0.000 | 0.000 | 0 000 | 0.000 |
| CaCO3 | 0.995 | 0.997 | 0.997 | 0.969 | 0.995 | 0.994 | 0.982 |

* Total Fe as FeO

# Calculated from stoichiometry

# Appendix F

Table F-1 Electron microprobe analyses of K-feldspars (Gneisses).

| Sample no. | IN-5 | | | | | IN-10 | | | | | | IN-14 | | | | | | IN-18.1 | | | | | |
|---|---|---|---|---|---|---|---|---|---|---|---|---|---|---|---|---|---|---|---|---|---|---|---|
| Analysis no. | 1 | 2 | 3 | 4 | 5 | 1 | 2 | 3 | 4 | 5 | 6 | 1 | 2 | 3 | 4 | 5 | 6 | 1 | 2 | 3 | 4 | 5 | 6 |
| | C3-Kfs3. | C3-Kfs3. | C3-Kfs3. | C3-Kfs3. | C3-Kfs3. | C1-Kfs1. | C1-Kfs1. | C1-Kfs1. | C1-Kfs1. | C1-Kfs1. | C2-Kfs2. | C6-Kfs1 | C6-Kfs2 | C6-Kfs3 | C2-Kfs4 | C2-Kfs5 | C2-Kfs6 | C3-Kfs1 | C6-Kfs3 | C6-Kfs4 | C6-Kfs5 | C6-Kfs6 | C6-Kfs7 |
| SiO2 | 64.25 | 63.70 | 64.17 | 64.17 | 64.46 | 64.33 | 63.64 | 64.41 | 64.54 | 64.58 | 64.32 | 64.43 | 64.66 | 64.47 | 64.32 | 64.54 | 64.42 | 64.60 | 64.42 | 64.52 | 64.68 | 64.38 | 64.40 |
| Al2O3 | 18.46 | 18.34 | 18.70 | 18.61 | 18.87 | 18.83 | 18.84 | 18.85 | 18.61 | 18.60 | 18.64 | 18.16 | 18.15 | 18.20 | 18.13 | 18.16 | 18.20 | 18.16 | 18.55 | 18.39 | 18.56 | 18.29 | 18.29 |
| FeO* | 0.02 | 0.00 | 0.00 | 0.06 | 0.00 | 0.06 | 0.05 | 0.03 | 0.04 | 0.01 | 0.00 | 0.05 | 0.02 | 0.03 | 0.00 | 0.03 | 0.03 | 0.07 | 0.02 | 0.00 | 0.02 | 0.00 | 0.01 |
| MgO | 0.00 | 0.00 | 0.01 | 0.00 | 0.02 | 0.00 | 0.01 | 0.10 | 0.01 | 0 00 | 0.00 | 0.00 | 0.04 | 0.00 | 0.00 | 0.01 | 0 02 | 0.00 | 0.00 | 0.02 | 0.00 | 0.00 | 0.01 |
| CaO | 0.00 | 0 05 | 0.01 | 0.00 | 0.05 | 0.03 | 0.06 | 0.00 | 0.00 | 0.00 | 0.00 | 0.00 | 0 00 | 0.00 | 0.05 | 0.04 | 0.00 | 0.00 | 0.00 | 0.00 | 0.00 | 0.00 | 0.00 |
| Na2O | 1.53 | 1.47 | 1.45 | 1.54 | 1.44 | 1.50 | 1.40 | 1.65 | 1.63 | 0.57 | 0.86 | 1.21 | 1.25 | 1.31 | 1.54 | 1.45 | 1.24 | 0.75 | 0.71 | 0.91 | 0.89 | 0.68 | 1.09 |
| K2O | 14.46 | 14.44 | 14.29 | 14.13 | 14.40 | 14.38 | 14.65 | 14.13 | 14.24 | 15.82 | 15.48 | 15.22 | 15.50 | 15.39 | 14.69 | 14.76 | 15.37 | 15.70 | 15.38 | 15.75 | 15.36 | 15.76 | 15.23 |
| Total | 98.72 | 98.00 | 98.63 | 98.51 | 99.24 | 99.14 | 98.66 | 99.17 | 99.08 | 99.58 | 99.30 | 99.08 | 99.63 | 99.41 | 98.72 | 98.98 | 99.28 | 99.29 | 99.08 | 99.59 | 99.50 | 99.12 | 99.03 |
| Number of cations on the basis of 8 oxygens: | | | | | | | | | | | | | | | | | | | | | | | |
| Si | 2.990 | 2.988 | 2.986 | 2.986 | 2.982 | 2.978 | 2.969 | 2.980 | 2.989 | 2 991 | 2.986 | 2.997 | 2.997 | 2.993 | 2.998 | 2.999 | 2.994 | 3.001 | 2.993 | 2.992 | 2.993 | 2.997 | 2.996 |
| Al | 1.013 | 1.014 | 1.026 | 1.021 | 1.029 | 1.028 | 1.036 | 1.028 | 1.016 | 1.015 | 1 020 | 0 996 | 0.992 | 0.996 | 0.996 | 0.995 | 0 997 | 0.995 | 1.016 | 1.005 | 1.013 | 1.004 | 1.003 |
| Fe2+ | 0.002 | 0.000 | 0.000 | 0 005 | 0 000 | 0.005 | 0.004 | 0.003 | 0.003 | 0.001 | 0.000 | 0.004 | 0.002 | 0.002 | 0.000 | 0.002 | 0.002 | 0.005 | 0.002 | 0.000 | 0 001 | 0 000 | 0.001 |
| Mg | 0 000 | 0.000 | 0.000 | 0.000 | 0.000 | 0.000 | 0.000 | 0.000 | 0.000 | 0.000 | 0 000 | 0.000 | 0.000 | 0.000 | 0.000 | 0.000 | 0.000 | 0.000 | 0 000 | 0.000 | 0.000 | 0.000 | 0.000 |
| Ca | 0.000 | 0.003 | 0.001 | 0.000 | 0.002 | 0.002 | 0.003 | 0.000 | 0.000 | 0.000 | 0.000 | 0.000 | 0.000 | 0.000 | 0.003 | 0.002 | 0.000 | 0.000 | 0.000 | 0.000 | 0.000 | 0 000 | 0.000 |
| Na | 0.138 | 0.134 | 0.131 | 0.139 | 0.129 | 0.135 | 0.126 | 0.148 | 0.147 | 0.051 | 0.077 | 0.110 | 0.112 | 0.118 | 0.139 | 0.131 | 0.112 | 0.068 | 0.064 | 0 082 | 0.080 | 0.062 | 0.099 |
| K | 0.858 | 0.864 | 0.848 | 0.839 | 0.850 | 0.849 | 0.872 | 0.834 | 0.841 | 0.935 | 0.917 | 0.903 | 0.916 | 0.911 | 0.873 | 0.875 | 0.911 | 0.931 | 0.911 | 0.932 | 0.907 | 0.936 | 0.904 |
| Sum Cations | 5.001 | 5.004 | 4.991 | 4.990 | 4.993 | 4.997 | 5.010 | 4.992 | 4.995 | 4.994 | 5.001 | 5.010 | 5.019 | 5.022 | 5.010 | 5.004 | 5.017 | 4.999 | 4.986 | 5.011 | 4 993 | 4.999 | 5.003 |
| Molecular proportions of end-members: | | | | | | | | | | | | | | | | | | | | | | | |
| An | 0.000 | 0.003 | 0.001 | 0.000 | 0.002 | 0.002 | 0.003 | 0.000 | 0.000 | 0.000 | 0.000 | 0.000 | 0 000 | 0.000 | 0.003 | 0 002 | 0.000 | 0.000 | 0.000 | 0 000 | 0.000 | 0.000 | 0.000 |
| Ab | 0.139 | 0.134 | 0.134 | 0.142 | 0.132 | 0.137 | 0.126 | 0.151 | 0.148 | 0.052 | 0.078 | 0.108 | 0.109 | 0.115 | 0.137 | 0.130 | 0.109 | 0.068 | 0.065 | 0.081 | 0 081 | 0.062 | 0.098 |
| Or | 0 861 | 0.864 | 0.866 | 0.858 | 0.866 | 0.861 | 0 871 | 0.849 | 0.852 | 0.948 | 0.922 | 0.892 | 0 891 | 0.885 | 0.860 | 0 869 | 0.891 | 0.932 | 0.935 | 0.919 | 0 919 | 0 938 | 0.902 |

* Total Fe as FeO

Table F-1 (continued)

| Sample no. | IN-19 | | | | | | | | IN-3 | | | | IN-13.1 | | | | | | IN-13.2 | | | | |
|---|---|---|---|---|---|---|---|---|---|---|---|---|---|---|---|---|---|---|---|---|---|---|---|
| Analysis no. | 1 | 2 | 3 | 4 | 5 | 6 | 7 | 8 | 1 | 2 | 3 | 4 | 1 | 2 | 3 | 4 | 5 | 6 | 1 | 2 | 3 | 4 | 5 |
| | C5-Kfs1 | C5-Kfs1a | C5-Kfs2a | C5-Kfs3a | C5-Kfs4a | C5-Kfs5a | Kfs6a | Kfs74 | C8-Kfs1 | C8-Kfs2 | C8-Kfs3 | C9-Kfs4 | C4-Kfs1 | C4-Kfs2 | C4-Kfs3 | C4-Kfs4 | C4-Kfs5 | C6-Kfs6 | C7-Kfs7. | C7-Kfs7. | C7-Kfs7. | C7-Kfs7. | C7-Kfs7.5 |
| SiO2 | 65.15 | 64.97 | 64.48 | 64.54 | 64.59 | 64.64 | 64.89 | 64.88 | 64.29 | 64.70 | 64.29 | 64.43 | 64.47 | 64.39 | 64.17 | 64.21 | 64.15 | 64.20 | 63.90 | 64.87 | 64.50 | 64.23 | 64.79 |
| Al2O3 | 18.67 | 18.65 | 18.52 | 18.37 | 18.80 | 18.32 | 18.68 | 18.64 | 18.40 | 18.49 | 18.38 | 18.12 | 18.34 | 18.23 | 18.26 | 18.15 | 18.19 | 17.95 | 18.65 | 18.81 | 18.80 | 18.83 | 19.00 |
| FeO* | 0.13 | 0.00 | 0.03 | 0.00 | 0.00 | 0.00 | 0.00 | 0.00 | 0.00 | 0.03 | 0.01 | 0.02 | 0.06 | 0 03 | 0.08 | 0.02 | 0.01 | 0.00 | 0 03 | 0.00 | 0.01 | 0.13 | 0.03 |
| MgO | 0.00 | 0.00 | 0.00 | 0.00 | 0.00 | 0.01 | 0.00 | 0.00 | 0.01 | 0.00 | 0.00 | 0.00 | 0.00 | 0.00 | 0.00 | 0.00 | 0.00 | 0.01 | 0.00 | 0.00 | 0.00 | 0.00 | 0.00 |
| CaO | 0.05 | 0.00 | 0.00 | 0.00 | 0.01 | 0.02 | 0 04 | 0.01 | 0.02 | 0.04 | 0.01 | 0.00 | 0.03 | 0.00 | 0.00 | 0.00 | 0.02 | 0.01 | 0.00 | 0.02 | 0.08 | 0.01 | 0.00 |
| Na2O | 1.06 | 1.15 | 0.81 | 1.22 | 1.31 | 1.21 | 1.24 | 1.24 | 1.03 | 1.00 | 1.00 | 0.92 | 0.79 | 0.80 | 0.76 | 0.71 | 0.86 | 0.82 | 1.07 | 1.87 | 1.63 | 1.51 | 1.67 |
| K2O | 15.59 | 15.46 | 15.92 | 15.30 | 15.08 | 15.00 | 15.14 | 15.15 | 15.36 | 15.17 | 15.31 | 15.37 | 16.06 | 16.00 | 16.19 | 16.02 | 16.15 | 16.05 | 14.99 | 13.88 | 14.26 | 14.36 | 14.34 |
| Total | 100.65 | 100.24 | 99.75 | 99.44 | 99.80 | 99.21 | 99.99 | 99.92 | 99.10 | 99.43 | 99.01 | 98.85 | 99.76 | 99.46 | 99.46 | 99.10 | 99.39 | 99.04 | 98.65 | 99.46 | 99.29 | 99.06 | 99.84 |
| Number of cations on the basis of 8 oxygens: | | | | | | | | | | | | | | | | | | | | | | | |
| Si | 2.984 | 2.989 | 2.987 | 2.993 | 2.981 | 2.999 | 2.988 | 2.990 | 2.991 | 2.994 | 2.992 | 3.003 | 2.988 | 2.994 | 2.986 | 2.996 | 2.990 | 3.000 | 2.981 | 2 988 | 2.982 | 2.975 | 2.978 |
| Al | 1.008 | 1.011 | 1.011 | 1.004 | 1.023 | 1.002 | 1.014 | 1.012 | 1.009 | 1.009 | 1.009 | 0.996 | 1.002 | 0.999 | 1.002 | 0.998 | 0.999 | 0.989 | 1.026 | 1.021 | 1.025 | 1.028 | 1.030 |
| Fe2+ | 0.010 | 0.000 | 0.002 | 0.000 | 0.000 | 0.000 | 0.000 | 0.000 | 0.000 | 0.002 | 0.001 | 0.001 | 0.005 | 0.002 | 0.006 | 0.001 | 0 001 | 0.000 | 0.003 | 0.000 | 0.001 | 0.010 | 0.003 |
| Mg | 0.000 | 0.000 | 0.000 | 0.000 | 0.000 | 0.000 | 0.000 | 0.000 | 0.000 | 0.000 | 0.000 | 0.000 | 0.000 | 0 000 | 0.000 | 0.000 | 0.000 | 0.000 | 0.000 | 0.000 | 0.000 | 0.000 | 0.000 |
| Ca | 0.002 | 0.000 | 0.000 | 0.000 | 0.001 | 0.001 | 0.002 | 0.000 | 0.001 | 0 002 | 0 000 | 0.000 | 0.002 | 0.000 | 0.000 | 0 000 | 0 001 | 0.001 | 0.000 | 0.001 | 0.004 | 0.000 | 0 000 |
| Na | 0.095 | 0.103 | 0.073 | 0.109 | 0.117 | 0.109 | 0.111 | 0.111 | 0.093 | 0 090 | 0.091 | 0.083 | 0 071 | 0.072 | 0.069 | 0.064 | 0.078 | 0.075 | 0.097 | 0.167 | 0.146 | 0.135 | 0.149 |
| K | 0.911 | 0.908 | 0.941 | 0.905 | 0.888 | 0.888 | 0.889 | 0.891 | 0.912 | 0.896 | 0.909 | 0.914 | 0.950 | 0.949 | 0.961 | 0.954 | 0.960 | 0.957 | 0.892 | 0.816 | 0.841 | 0.849 | 0.841 |
| Sum Cations | 5.010 | 5.011 | 5.013 | 5.012 | 5.010 | 4.999 | 5.005 | 5.005 | 5.006 | 4.993 | 5.003 | 4.997 | 5.018 | 5.017 | 5.025 | 5.013 | 5.029 | 5.021 | 4.999 | 4.993 | 4.999 | 4.998 | 5.001 |
| Molecular proportions of end-members: | | | | | | | | | | | | | | | | | | | | | | | |
| An | 0 002 | 0.000 | 0.000 | 0.000 | 0.001 | 0.001 | 0.002 | 0.000 | 0.001 | 0.002 | 0.000 | 0.000 | 0.002 | 0.000 | 0.000 | 0.000 | 0 001 | 0 001 | 0.000 | 0.001 | 0.004 | 0.000 | 0.000 |
| Ab | 0.094 | 0.102 | 0.072 | 0.108 | 0.116 | 0.109 | 0.111 | 0.111 | 0.092 | 0.091 | 0.091 | 0.083 | 0.070 | 0.071 | 0.067 | 0.063 | 0.075 | 0.072 | 0.098 | 0.170 | 0.148 | 0.137 | 0.150 |
| Or | 0.904 | 0 898 | 0.928 | 0 892 | 0.883 | 0.890 | 0.888 | 0.889 | 0.907 | 0.907 | 0.909 | 0.917 | 0.929 | 0.929 | 0.933 | 0 937 | 0 924 | 0 927 | 0.902 | 0 829 | 0 848 | 0 862 | 0.850 |

* Total Fe as FeO

Table F-2 Electron microprobe analyses of plagioclases (Gneisses).

| Sample no. | IN-1 | | | | | | | IN-10 | | | | IN-14 | | | | | | IN-18.1 | |
|---|---|---|---|---|---|---|---|---|---|---|---|---|---|---|---|---|---|---|---|
| Analysis no. | 1 | 2 | 3 | 4 | 5 | 6 | 7 | 1 | 2 | 3 | 4 | 1 | 2 | 3 | 4 | 5 | 6 | 1 | 2 |
| | C1-Pl1 | C1Pl2 | C1-Pl3 | C1-Pl4 | C1-Pl5 | C1-Pl6 | C1-Pl7 | C2-Pl2.1 | C3-Pl3.1 | C3-Pl3.2 | C3-Pl3.3 | C5-Pl1 | C5-Pl2 | C5-Pl3 | C5-Pl4 | C5-Pl5 | C3-Pl6 | C6-Pl1 | C6-Pl2 |
| SiO2 | 58.85 | 59.89 | 59.92 | 59.26 | 59.66 | 59.85 | 59.71 | 63.00 | 62.68 | 63.20 | 62.20 | 63.11 | 63.24 | 63.22 | 63.32 | 63.53 | 63.44 | 67.77 | 67.34 |
| Al2O3 | 25.56 | 25.43 | 25.87 | 25.81 | 25.73 | 25.64 | 25.46 | 22.98 | 23.41 | 22.97 | 24.06 | 22.56 | 23.33 | 23.29 | 22.95 | 23.10 | 23.45 | 20.07 | 20.25 |
| FeO* | 0.10 | 0.01 | 0.02 | 0.11 | 0.08 | 0.03 | 0.00 | 0.00 | 0.00 | 0.00 | 0.07 | 0.00 | 0.04 | 0.12 | 0.03 | 0.09 | 0.07 | 0.01 | 0.00 |
| MgO | 0.03 | 0.00 | 0.00 | 0.01 | 0.00 | 0.00 | 0.00 | 0.01 | 0.00 | 0.01 | 0.00 | 0.01 | 0.00 | 0.02 | 0.00 | 0.00 | 0.02 | 0.00 | 0.00 |
| CaO | 7.37 | 7.07 | 7.27 | 7.07 | 7.36 | 6.97 | 7.29 | 4.02 | 4.29 | 4.15 | 5.04 | 4.41 | 4.68 | 4.81 | 4.72 | 4.53 | 4.67 | 0.72 | 0.68 |
| Na2O | 7.03 | 6.98 | 6.94 | 6.98 | 6.98 | 7.17 | 6.94 | 8.73 | 8.80 | 8.69 | 8.31 | 8.63 | 8.43 | 8.44 | 8.39 | 8.76 | 8.37 | 11.10 | 10.74 |
| K2O | 0.28 | 0.32 | 0.42 | 0.35 | 0.51 | 0.31 | 0.37 | 0.37 | 0.30 | 0.23 | 0.35 | 0.35 | 0.31 | 0.30 | 0.37 | 0.45 | 0.34 | 0.08 | 0.08 |
| Total | 99.22 | 99.72 | 100.44 | 99.59 | 100.30 | 99.97 | 99.76 | 99.10 | 99.48 | 99.25 | 100.04 | 99.07 | 100.02 | 100.19 | 99.78 | 100.45 | 100.35 | 99.75 | 99.10 |
| Number of cations on the basis of 8 oxygens: | | | | | | | | | | | | | | | | | | | |
| Si | 2.644 | 2.672 | 2.657 | 2.648 | 2.652 | 2.664 | 2.665 | 2.805 | 2.785 | 2.808 | 2.752 | 2.813 | 2.792 | 2.787 | 2.803 | 2.796 | 2.791 | 2.969 | 2.965 |
| Al | 1.354 | 1.337 | 1.352 | 1.360 | 1.348 | 1.345 | 1.340 | 1.206 | 1.226 | 1.203 | 1.255 | 1.186 | 1.214 | 1.210 | 1.198 | 1.199 | 1.216 | 1.037 | 1.051 |
| Fe2+ | 0.007 | 0.001 | 0.002 | 0.008 | 0.006 | 0.002 | 0.000 | 0.000 | 0.000 | 0.000 | 0.005 | 0.000 | 0.003 | 0.009 | 0.002 | 0.006 | 0.005 | 0.001 | 0.000 |
| Mg | 0.000 | 0.000 | 0.000 | 0.000 | 0.000 | 0.000 | 0.000 | 0.000 | 0.000 | 0.000 | 0.000 | 0.000 | 0.000 | 0.000 | 0.000 | 0.000 | 0.000 | 0.000 | 0.000 |
| Ca | 0.355 | 0.338 | 0.346 | 0.338 | 0.350 | 0.332 | 0.349 | 0.192 | 0.204 | 0.198 | 0.239 | 0 211 | 0.221 | 0.227 | 0.224 | 0.213 | 0.220 | 0.034 | 0.032 |
| Na | 0.613 | 0.604 | 0.597 | 0.605 | 0.601 | 0.619 | 0.601 | 0.754 | 0.758 | 0.749 | 0.713 | 0.746 | 0.721 | 0.721 | 0.720 | 0.748 | 0.714 | 0.943 | 0.916 |
| K | 0.016 | 0.018 | 0.024 | 0.020 | 0.029 | 0.018 | 0.021 | 0.021 | 0.017 | 0.013 | 0.020 | 0.020 | 0.017 | 0.017 | 0.021 | 0.025 | 0.019 | 0.005 | 0.005 |
| Sum Cations | 4.989 | 4.970 | 4.976 | 4.980 | 4.986 | 4.981 | 4.976 | 4.978 | 4.990 | 4.971 | 4.984 | 4.976 | 4.969 | 4.971 | 4.968 | 4.988 | 4.965 | 4.987 | 4.970 |
| Molecular proportions of end-members: | | | | | | | | | | | | | | | | | | | |
| An | 0.361 | 0.352 | 0.358 | 0.351 | 0.357 | 0.343 | 0.359 | 0.199 | 0.208 | 0.206 | 0.246 | 0.216 | 0.231 | 0.235 | 0.232 | 0.216 | 0.231 | 0.035 | 0.033 |
| Ab | 0.623 | 0.629 | 0.618 | 0.628 | 0.613 | 0.639 | 0.619 | 0.780 | 0.774 | 0.780 | 0.734 | 0.764 | 0.751 | 0.747 | 0.747 | 0.758 | 0.749 | 0.961 | 0.962 |
| Or | 0.017 | 0.019 | 0.024 | 0.021 | 0.029 | 0.018 | 0.022 | 0.022 | 0.018 | 0.014 | 0.020 | 0.020 | 0.018 | 0.017 | 0.022 | 0.025 | 0 020 | 0 005 | 0.005 |

* Total Fe as FeO

Table F-2 (continued)

| Sample no. | IN-18.1 | | | | | | | | IN-19 | | | | | | | IN-2 | | | |
|---|---|---|---|---|---|---|---|---|---|---|---|---|---|---|---|---|---|---|---|
| Analysis no. | 3 | 4 | 5 | 6 | 7 | 8 | 9 | 10 | 1 | 2 | 3 | 4 | 5 | 6 | 7 | 1 | 2 | 3 | 4 |
| | C6-Pl3 | C6-Pl4 | C6-Pl5 | C6-Pl6 | C6-PL7 | C6-Pl8 | C6-Pl9 | C6-Pl10 | C4-Pl1 | C4-Pl2 | C1-Pl3 | C4-Pl1a | C4-PL2a | C4-Pl3a | C4-Pl4a | C1-Pl1.1 | C1-Pl1.2 | C2-Pl2.1 | C2-Pl2.2 |
| SiO2 | 67.38 | 67.31 | 67.31 | 67.39 | 66.59 | 67.26 | 67.05 | 66.51 | 65.54 | 65.56 | 65.06 | 66.03 | 65.58 | 65.72 | 65.44 | 58.89 | 59.04 | 59.22 | 59.94 |
| Al2O3 | 19.77 | 20.05 | 19.87 | 19.89 | 20.53 | 19.83 | 20.35 | 20.47 | 21.49 | 21.33 | 21.62 | 21.20 | 21.17 | 21.23 | 21.00 | 25.39 | 25.58 | 25.33 | 24.92 |
| FeO* | 0.04 | 0.02 | 0.00 | 0.02 | 0.01 | 0.00 | 0.00 | 0.00 | 0.06 | 0.00 | 0.03 | 0.02 | 0.03 | 0.01 | 0.02 | 0.06 | 0.11 | 0.04 | 0.10 |
| MgO | 0.01 | 0.00 | 0.01 | 0.00 | 0.00 | 0.00 | 0.01 | 1.51 | 0.02 | 0.00 | 0.00 | 0 01 | 0.00 | 0.00 | 0.00 | 0.00 | 0.00 | 0.00 | 0.00 |
| CaO | 0.56 | 0.84 | 0.64 | 0.84 | 1.66 | 0.76 | 1.13 | 1.57 | 2.50 | 2.54 | 2.77 | 2.34 | 2.43 | 2.33 | 2.44 | 7.11 | 6.90 | 6.91 | 6.42 |
| Na2O | 11.09 | 10.89 | 10.97 | 10.56 | 10.56 | 10.97 | 10.63 | 10.59 | 9.64 | 9.60 | 9.51 | 9.80 | 9.80 | 9.82 | 9.99 | 6.74 | 7.04 | 7.07 | 7.37 |
| K2O | 0.12 | 0.08 | 0.11 | 0.11 | 0.12 | 0.12 | 0.07 | 0.06 | 0.24 | 0.20 | 0.25 | 0.25 | 0.26 | 0.25 | 0.25 | 0.37 | 0.41 | 0.33 | 0.35 |
| Total | 98.98 | 99.20 | 98.91 | 98.80 | 99.47 | 98.95 | 99.24 | 100.71 | 99.49 | 99.23 | 99.23 | 99.64 | 99.27 | 99.37 | 99.15 | 98.57 | 99.07 | 98.89 | 99.11 |
| Number of cations on the basis of 8 oxygens: | | | | | | | | | | | | | | | | | | | |
| Si | 2.974 | 2.964 | 2.973 | 2.975 | 2.933 | 2.971 | 2.953 | 2.916 | 2.890 | 2.898 | 2.879 | 2.906 | 2.899 | 2.902 | 2.900 | 2.658 | 2.653 | 2.665 | 2.687 |
| Al | 1.029 | 1.041 | 1.034 | 1.035 | 1.066 | 1.033 | 1.057 | 1.058 | 1.117 | 1.112 | 1.128 | 1.100 | 1.103 | 1.105 | 1.097 | 1.351 | 1.355 | 1.344 | 1.317 |
| Fe2+ | 0.003 | 0.002 | 0.000 | 0.001 | 0 001 | 0.000 | 0.000 | 0.000 | 0.004 | 0.000 | 0.002 | 0.001 | 0.003 | 0.001 | 0.002 | 0.005 | 0.008 | 0.003 | 0.008 |
| Mg | 0.000 | 0.000 | 0.000 | 0.000 | 0.000 | 0.000 | 0.000 | 0.000 | 0.000 | 0.000 | 0.000 | 0.000 | 0.000 | 0.000 | 0.000 | 0.000 | 0 000 | 0.000 | 0.000 |
| Ca | 0.027 | 0.040 | 0.030 | 0.040 | 0.078 | 0.036 | 0.053 | 0.074 | 0.118 | 0.120 | 0.132 | 0.110 | 0.115 | 0.110 | 0.116 | 0.344 | 0.332 | 0.333 | 0.309 |
| Na | 0.949 | 0.930 | 0.939 | 0.904 | 0.902 | 0.940 | 0.908 | 0.900 | 0.824 | 0.823 | 0.816 | 0.836 | 0.840 | 0.841 | 0.859 | 0.590 | 0 613 | 0.617 | 0.640 |
| K | 0.007 | 0.005 | 0.006 | 0.006 | 0.007 | 0 007 | 0.004 | 0.003 | 0.014 | 0.011 | 0.014 | 0.014 | 0 015 | 0.014 | 0.014 | 0.021 | 0.023 | 0.019 | 0.020 |
| Sum Cations | 4.988 | 4.981 | 4.982 | 4.962 | 4.987 | 4.986 | 4.975 | 4.951 | 4.967 | 4.963 | 4.970 | 4.968 | 4.975 | 4.973 | 4.987 | 4.969 | 4.984 | 4.980 | 4.981 |
| Molecular proportions of end-members: | | | | | | | | | | | | | | | | | | | |
| An | 0.027 | 0.041 | 0.031 | 0.042 | 0.079 | 0.037 | 0.055 | 0.076 | 0.124 | 0.126 | 0.137 | 0.115 | 0.119 | 0.114 | 0.117 | 0.360 | 0.343 | 0.344 | 0.318 |
| Ab | 0.966 | 0.955 | 0.962 | 0.952 | 0.914 | 0.956 | 0.941 | 0.921 | 0.862 | 0 862 | 0.849 | 0 871 | 0.866 | 0 871 | 0.869 | 0.618 | 0.633 | 0.637 | 0.661 |
| Or | 0.007 | 0.005 | 0.006 | 0.006 | 0.007 | 0.007 | 0.004 | 0 004 | 0 014 | 0.012 | 0.014 | 0 014 | 0.015 | 0 015 | 0.014 | 0.022 | 0.024 | 0.020 | 0.021 |

* Total Fe as FeO

Table F-2 (continued)

| Sample no. | IN-2 | IN-3 | | | | | IN-13.1 | | | | | IN-13.2 | | | | | |
|---|---|---|---|---|---|---|---|---|---|---|---|---|---|---|---|---|---|
| Analysis no. | 5 | 1 | 2 | 3 | 4 | 5 | 1 | 2 | 3 | 4 | 5 | 1 | 2 | 3 | 4 | 5 | 6 |
| | C2-Pl2.3 | C1-Pl1 | C1-Pl2 | C1-Pl3 | C1-Pl4 | C1-Pl5 | C6-Pl1 | C6-Pl2 | C6-Pl3 | C6-Pl4 | C6-Pl6 | C9-Pl9.1 | C9-Pl9.2 | C29Pl9.3 | C9-Pl9.4 | C9-Pl9.5 | C9-Pl9.6 |
| SiO2 | 58.76 | 47.04 | 46.88 | 47.81 | 47.70 | 47.62 | 44.46 | 44.69 | 45.04 | 45.15 | 45.51 | 61.49 | 61.80 | 62.20 | 61.51 | 62.66 | 63.49 |
| Al2O3 | 25.14 | 33.61 | 33.07 | 33.24 | 33.33 | 33.08 | 34.60 | 34.41 | 34.33 | 34.18 | 33.87 | 23.98 | 23.94 | 23.60 | 24.00 | 23.28 | 23.18 |
| FeO* | 0.06 | 0 00 | 0.04 | 0.10 | 0.02 | 0.08 | 0.16 | 0.06 | 0.18 | 0.11 | 0.06 | 0.05 | 0.00 | 0.01 | 0.02 | 0.09 | 0.00 |
| MgO | 0.00 | 0.00 | 0.00 | 0.00 | 0.00 | 0.00 | 0.00 | 0.00 | 0.00 | 0.00 | 0.00 | 0.00 | 0 00 | 0 00 | 0.02 | 0.00 | 0.00 |
| CaO | 7.19 | 17.30 | 16.92 | 16.87 | 16.72 | 16.68 | 19.27 | 19.04 | 18.44 | 18.53 | 18.83 | 4.87 | 5.23 | 4.82 | 5.55 | 4.50 | 4.33 |
| Na2O | 7.18 | 1.79 | 1.80 | 1.85 | 1.86 | 1.96 | 0.80 | 0.80 | 1.09 | 1.07 | 1.09 | 7.90 | 7.88 | 7.94 | 7.67 | 8 40 | 8.39 |
| K2O | 0.32 | 0.02 | 0.03 | 0.05 | 0.04 | 0.03 | 0.02 | 0.02 | 0.01 | 0.05 | 0 03 | 0.51 | 0.38 | 0.36 | 0.25 | 0.21 | 0.27 |
| Total | 98.64 | 99.75 | 98.74 | 99.92 | 99.66 | 99.46 | 99.31 | 99.02 | 99.10 | 99.09 | 99.39 | 98.80 | 99.24 | 98.94 | 99.02 | 99.13 | 99.66 |
| Number of cations on the basis of 8 oxygens: | | | | | | | | | | | | | | | | | |
| Si | 2.656 | 2.165 | 2.178 | 2.191 | 2.191 | 2.193 | 2.069 | 2.084 | 2 094 | 2.101 | 2.113 | 2.753 | 2.755 | 2.776 | 2.748 | 2.788 | 2.808 |
| Al | 1.340 | 1.824 | 1.811 | 1.796 | 1.805 | 1.796 | 1.898 | 1.891 | 1.882 | 1.875 | 1.854 | 1.265 | 1.258 | 1.242 | 1.264 | 1.221 | 1.208 |
| Fe2+ | 0.004 | 0.000 | 0.003 | 0.008 | 0.002 | 0.006 | 0 012 | 0.005 | 0.014 | 0 008 | 0.005 | 0 004 | 0.000 | 0.001 | 0.002 | 0.007 | 0.000 |
| Mg | 0.000 | 0.000 | 0.000 | 0.000 | 0.000 | 0.000 | 0.000 | 0.000 | 0.000 | 0.000 | 0.000 | 0.000 | 0.000 | 0.000 | 0.000 | 0.000 | 0.000 |
| Ca | 0.348 | 0.853 | 0.842 | 0.828 | 0.823 | 0.823 | 0.961 | 0.951 | 0.919 | 0.924 | 0.937 | 0 234 | 0.250 | 0.230 | 0.266 | 0.214 | 0.205 |
| Na | 0.629 | 0.159 | 0.162 | 0.164 | 0.166 | 0.175 | 0.072 | 0.072 | 0.098 | 0.096 | 0.098 | 0.685 | 0.682 | 0 687 | 0.665 | 0.725 | 0.719 |
| K | 0.018 | 0.001 | 0.002 | 0.003 | 0.002 | 0.002 | 0.001 | 0.001 | 0.001 | 0.003 | 0.002 | 0.029 | 0.022 | 0.021 | 0.014 | 0.012 | 0.015 |
| Sum Cations | 4.995 | 5.003 | 4.997 | 4.990 | 4.989 | 4.994 | 5.013 | 5.005 | 5.008 | 5.007 | 5.008 | 4.970 | 4.967 | 4.957 | 4.958 | 4.966 | 4.956 |
| Molecular proportions of end-members: | | | | | | | | | | | | | | | | | |
| An | 0.350 | 0.842 | 0.837 | 0.833 | 0.831 | 0.823 | 0.929 | 0.928 | 0.903 | 0.903 | 0.903 | 0 246 | 0.262 | 0.246 | 0.281 | 0.225 | 0.218 |
| Ab | 0.632 | 0.157 | 0.161 | 0.165 | 0.167 | 0.175 | 0.070 | 0.071 | 0.097 | 0.094 | 0.095 | 0.723 | 0.715 | 0.732 | 0.704 | 0.762 | 0 766 |
| Or | 0.018 | 0.001 | 0 002 | 0.003 | 0.002 | 0.002 | 0.001 | 0.001 | 0.001 | 0.003 | 0.002 | 0.031 | 0.023 | 0.022 | 0.015 | 0.012 | 0 016 |

* Total Fe as FeO

Table F-3 Electron microprobe analyses of biotites (Gneisses).

| Sample no. | IN-1 | | | | | | | IN-5 | | | | | | | IN-10 | | | |
|---|---|---|---|---|---|---|---|---|---|---|---|---|---|---|---|---|---|---|
| Analysis no. | 1 | 2 | 3 | 4 | 5 | 6 | 7 | 1 | 2 | 3 | 4 | 5 | 6 | 7 | 1 | 2 | 3 | 4 |
| | C1-Bt1.1 | C1-Bt1.2 | C1-Bt1.3 | C3-Bt3.1 | C3-Bt3.2 | C3-Bt3.3 | C3-Bt3.4 | C3-Bt3.1 | C3-Bt3 2 | C3-Bt3.3 | C3-Bt3 4 | C7-Bt7.1 | C7-Bt7.2 | C7-Bt7.3 | C4-Bt4.1 | C4-Bt4.2 | C4-Bt4.3 | C9-Bt9 1 |
| SiO2 | 36.22 | 36.09 | 36.21 | 36.73 | 36.55 | 36.33 | 36.62 | 34.73 | 34.67 | 35.17 | 34.37 | 34.90 | 35.09 | 34.90 | 33.86 | 33.87 | 33.88 | 33.86 |
| TiO2 | 3.32 | 3.38 | 3.26 | 2.91 | 2.90 | 3.15 | 3.45 | 3.78 | 3.81 | 3.19 | 3.71 | 3.96 | 3.89 | 4.04 | 2.57 | 2.28 | 2.84 | 2.58 |
| Al2O3 | 14.94 | 15.13 | 15.11 | 14.77 | 14.66 | 14.76 | 15.32 | 15.71 | 15.64 | 15.50 | 15.56 | 15.39 | 15.49 | 15.28 | 18.78 | 18.92 | 19.03 | 18.97 |
| FeO* | 18.42 | 19.41 | 19.35 | 18.50 | 18.85 | 18.65 | 18.37 | 21.65 | 21.13 | 21.76 | 21.84 | 21.75 | 21.65 | 21.47 | 22.60 | 22.19 | 22.37 | 23.36 |
| MnO | 0.26 | 0.37 | 0.52 | 0.34 | 0.38 | 0.48 | 0.20 | 0.56 | 0.42 | 0.45 | 0.22 | 0.17 | 0.27 | 0.35 | 0.54 | 0.58 | 0.64 | 0.44 |
| MgO | 11.33 | 11.09 | 11.14 | 11.42 | 11.50 | 11.13 | 11.17 | 8.59 | 8.61 | 8.93 | 8.30 | 8.70 | 8.55 | 8.55 | 6.12 | 5.76 | 5.49 | 5.96 |
| CaO | 0.05 | 0.00 | 0.05 | 0.01 | 0.00 | 0.04 | 0.00 | 0.00 | 0.01 | 0.00 | 0.01 | 0.00 | 0.01 | 0.00 | 0.03 | 0.05 | 0.05 | 0.05 |
| Na2O | 0.12 | 0.07 | 0.07 | 0.11 | 0.10 | 0.05 | 0.01 | 0.10 | 0.11 | 0.08 | 0.09 | 0.10 | 0.09 | 0.05 | 0.10 | 0.10 | 0.16 | 0.10 |
| K2O | 9.60 | 9.73 | 9.66 | 9.67 | 9.74 | 9.68 | 9.89 | 9.44 | 9.50 | 9.49 | 9.61 | 9.65 | 9.56 | 9.68 | 9.10 | 9.24 | 9.35 | 9.47 |
| F | 0.87 | 0.19 | 0.30 | 0.54 | 0.33 | 1.08 | 0.42 | 0.40 | 0.31 | 0.81 | 0.67 | 1.01 | 0.30 | 0 56 | 0.51 | 0.56 | 0.58 | 0.71 |
| Cl | 0.02 | 0.01 | 0.00 | 0.03 | 0.00 | 0.06 | 0.00 | 0.03 | 0.08 | 0.02 | 0.01 | 0.00 | 0.05 | 0 00 | 0 03 | 0 04 | 0.08 | 0.04 |
| Total | 95.16 | 95.46 | 95.68 | 95.04 | 95.01 | 95.41 | 95.44 | 94.98 | 94.29 | 95.39 | 94.40 | 95.62 | 94.97 | 94.89 | 94.23 | 93.58 | 94.46 | 95.54 |
| O = F, Cl | -0.37 | -0.08 | -0.14 | -0.24 | -0.14 | -0.47 | -0.18 | -0.17 | -0.15 | -0.35 | -0.28 | -0.43 | -0.14 | -0.24 | -0.22 | -0.24 | -0.26 | -0.31 |
| Total | 94.79 | 95.38 | 95.54 | 94.80 | 94.87 | 94.94 | 95.26 | 94.81 | 94.14 | 95.04 | 94.11 | 95.19 | 94.83 | 94.66 | 94.01 | 93.34 | 94.20 | 95.23 |
| Number of cations on the basis of 11 oxygens: | | | | | | | | | | | | | | | | | | |
| Si | 2.793 | 2.769 | 2.775 | 2.825 | 2.813 | 2.807 | 2.797 | 2.720 | 2.729 | 2.752 | 2.722 | 2.732 | 2.743 | 2.740 | 2 675 | 2.694 | 2.676 | 2.658 |
| Al iv | 1.207 | 1.231 | 1.225 | 1.175 | 1.187 | 1.193 | 1.203 | 1.280 | 1.271 | 1.248 | 1.278 | 1.268 | 1.257 | 1.260 | 1.325 | 1.306 | 1.324 | 1.342 |
| Sum T | 4.000 | 4.000 | 4.000 | 4.000 | 4.000 | 4.000 | 4.000 | 4.000 | 4.000 | 4.000 | 4.000 | 4.000 | 4.000 | 4.000 | 4.000 | 4.000 | 4.000 | 4.000 |
| Al vi | 0.150 | 0.138 | 0.140 | 0.164 | 0.143 | 0.152 | 0.177 | 0.171 | 0.180 | 0.182 | 0.174 | 0.152 | 0.171 | 0.154 | 0.425 | 0.468 | 0.448 | 0.414 |
| Ti | 0.193 | 0.195 | 0.188 | 0.168 | 0.168 | 0.183 | 0.198 | 0.223 | 0.226 | 0.188 | 0.221 | 0.233 | 0.229 | 0.239 | 0.152 | 0.136 | 0.168 | 0.152 |
| Fe2+ | 1.188 | 1.245 | 1.240 | 1.190 | 1.213 | 1.205 | 1.173 | 1.419 | 1.391 | 1.424 | 1.447 | 1.424 | 1.415 | 1.410 | 1.494 | 1.476 | 1.477 | 1.534 |
| Mn | 0.017 | 0.024 | 0.034 | 0.022 | 0.025 | 0.032 | 0.013 | 0.037 | 0.028 | 0 030 | 0.015 | 0.011 | 0.018 | 0.024 | 0.036 | 0.039 | 0.043 | 0.029 |
| Mg | 1.302 | 1.269 | 1.272 | 1.309 | 1.319 | 1.281 | 1.271 | 1.003 | 1.010 | 1.041 | 0.980 | 1.015 | 0.996 | 1.000 | 0.721 | 0.683 | 0.646 | 0.698 |
| Sum O | 2.850 | 2.870 | 2.873 | 2.853 | 2.868 | 2.853 | 2.832 | 2.852 | 2.834 | 2.865 | 2.837 | 2.836 | 2.830 | 2.826 | 2.828 | 2.802 | 2.783 | 2.826 |
| Ca | 0.005 | 0.000 | 0.004 | 0.001 | 0.000 | 0.003 | 0.000 | 0.000 | 0.001 | 0.000 | 0.001 | 0 000 | 0.001 | 0.000 | 0.002 | 0.004 | 0.004 | 0.004 |
| Na | 0.018 | 0.010 | 0.011 | 0.017 | 0.015 | 0.008 | 0.002 | 0.016 | 0.017 | 0.013 | 0.014 | 0.015 | 0.014 | 0.008 | 0.016 | 0.015 | 0.024 | 0.015 |
| K | 0.945 | 0.952 | 0.945 | 0.949 | 0.957 | 0.954 | 0.964 | 0.944 | 0.954 | 0.947 | 0.971 | 0.964 | 0 954 | 0.969 | 0.917 | 0.937 | 0.942 | 0.949 |
| Sum A | 0.967 | 0.963 | 0.959 | 0.966 | 0.971 | 0.965 | 0.965 | 0.959 | 0.971 | 0 960 | 0.987 | 0.978 | 0.968 | 0.977 | 0.936 | 0.957 | 0.970 | 0.968 |
| Sum Cations | 7.817 | 7.833 | 7.833 | 7.820 | 7.840 | 7.819 | 7.798 | 7.811 | 7.805 | 7.825 | 7.823 | 7.814 | 7.798 | 7.803 | 7.764 | 7.759 | 7.753 | 7.794 |
| Mg/(Mg+Fe2) | 0.523 | 0 505 | 0.506 | 0.524 | 0.521 | 0.515 | 0.520 | 0.414 | 0.421 | 0.422 | 0.404 | 0.416 | 0.413 | 0.415 | 0.326 | 0.316 | 0 304 | 0.313 |

* Total Fe as FeO

Table F-3 (continued)

| Sample no. | IN-10 | | IN-14 | | | | | | | | | | IN-18.1 | | | | | |
|---|---|---|---|---|---|---|---|---|---|---|---|---|---|---|---|---|---|---|
| Analysis no. | 5 | 6 | 1 | 2 | 3 | 4 | 5 | 6 | 7 | 8 | 9 | 10 | 1 | 2 | 3 | 4 | 5 | 6 |
| | C9-Bt9.2 | C9-Bt9.3 | C1-Bt1 | C1-Bt2 | C1-Bt3 | C1-Bt4 | C1-Bt5 | C4-Bt6 | C4-Bt7 | C4-Bt8 | C6-Bt9 | C6-Bt10 | C1-Bt1 | C1-Bt2 | C1-Bt3 | C1-Bt4 | C1-Bt5 | C1-Bt6 |
| SiO2 | 33.97 | 33.87 | 35.78 | 35.81 | 35.93 | 35.68 | 36.08 | 35.87 | 35.86 | 36.03 | 35.90 | 36.15 | 36.61 | 36.18 | 35.87 | 36.94 | 36.66 | 36.41 |
| TiO2 | 3.09 | 3.06 | 3.11 | 3.23 | 3.46 | 3.34 | 3.39 | 3.33 | 3.58 | 3.71 | 3.40 | 3.47 | 2.21 | 2.34 | 2.37 | 2.23 | 2.18 | 2.38 |
| Al2O3 | 19.18 | 19.47 | 17.55 | 17.75 | 17.77 | 17.07 | 18.08 | 17.55 | 17.56 | 17.62 | 17.88 | 17.79 | 17.28 | 17.01 | 16.68 | 16.27 | 17.34 | 17.08 |
| FeO* | 22.29 | 21.37 | 20.29 | 20.31 | 20.23 | 20.36 | 19.46 | 19.47 | 20.30 | 19.73 | 20.38 | 20.20 | 21.75 | 21.47 | 21.70 | 21.31 | 21.40 | 21.87 |
| MnO | 0.83 | 0.74 | 0.43 | 0.46 | 0.30 | 0.40 | 0.38 | 0.27 | 0.46 | 0.42 | 0.32 | 0.39 | 0.30 | 0.47 | 0.43 | 0.34 | 0.40 | 0.49 |
| MgO | 5.69 | 5.39 | 8.85 | 8.72 | 8.69 | 9.01 | 8.57 | 8.67 | 8.43 | 8.27 | 8.78 | 8.60 | 8.56 | 8.29 | 8.39 | 9.08 | 8.48 | 8.51 |
| CaO | 0.01 | 0.06 | 0.00 | 0.00 | 0.00 | 0.00 | 0.00 | 0.00 | 0.00 | 0.00 | 0.00 | 0.01 | 0.00 | 0.01 | 0.04 | 0.00 | 0.02 | 0.00 |
| Na2O | 0.13 | 0.11 | 0.08 | 0.10 | 0.09 | 0.10 | 0.09 | 0.07 | 0.09 | 0.07 | 0.05 | 0.10 | 0.06 | 0.06 | 0.06 | 0.11 | 0.07 | 0.07 |
| K2O | 9.25 | 9.46 | 9.74 | 9.71 | 9.73 | 9.86 | 9.87 | 9.88 | 9.76 | 9.66 | 9.87 | 9.94 | 9.64 | 9.81 | 9.70 | 9.98 | 9.67 | 9.75 |
| F | 0.37 | 0.33 | 0.57 | 0.57 | 0.69 | 0.74 | 0.65 | 0.58 | 0.80 | 0.57 | 0.63 | 0.69 | 1.89 | 1.81 | 1.75 | 1.93 | 2.16 | 1.90 |
| Cl | 0.04 | 0.07 | 0.05 | 0.03 | 0.03 | 0.02 | 0.02 | 0.00 | 0.05 | 0.05 | 0.01 | 0.03 | 0.06 | 0.04 | 0.05 | 0.06 | 0.01 | 0.04 |
| Total | 94.84 | 93.93 | 96.43 | 96.67 | 96.91 | 96.57 | 96.58 | 95.70 | 96.89 | 96.13 | 97.23 | 97.36 | 98.35 | 97.49 | 97.04 | 98.25 | 98.39 | 98.50 |
| O = F, Cl | -0.17 | -0.15 | -0.25 | -0.25 | -0.30 | -0.31 | -0.28 | -0.25 | -0.35 | -0.25 | -0.27 | -0.30 | -0.81 | -0.77 | -0.75 | -0.82 | -0.91 | -0.81 |
| Total | 94.68 | 93.77 | 96.18 | 96.43 | 96.62 | 96.26 | 96.30 | 95.46 | 96.55 | 95.88 | 96.96 | 97.06 | 97.55 | 96.72 | 96.29 | 97.43 | 97.48 | 97.69 |
| Number of cations on the basis of 11 oxygens: | | | | | | | | | | | | | | | | | | |
| Si | 2.662 | 2.671 | 2.732 | 2.726 | 2.727 | 2.730 | 2.737 | 2.748 | 2.732 | 2.748 | 2.718 | 2.734 | 2.787 | 2.783 | 2.776 | 2.819 | 2.793 | 2.776 |
| Al iv | 1.338 | 1.329 | 1.268 | 1.274 | 1.273 | 1.270 | 1.263 | 1.252 | 1.268 | 1.252 | 1.282 | 1.266 | 1.213 | 1.217 | 1.224 | 1.181 | 1.207 | 1.224 |
| Sum T | 4.000 | 4.000 | 4.000 | 4.000 | 4.000 | 4.000 | 4.000 | 4.000 | 4.000 | 4.000 | 4.000 | 4.000 | 4.000 | 4.000 | 4.000 | 4.000 | 4.000 | 4.000 |
| Al vi | 0.434 | 0.480 | 0.311 | 0.319 | 0.318 | 0.270 | 0.355 | 0.333 | 0.309 | 0.333 | 0.315 | 0.320 | 0.337 | 0.326 | 0.298 | 0.283 | 0.350 | 0.311 |
| Ti | 0.182 | 0.181 | 0.178 | 0.185 | 0.198 | 0.192 | 0.193 | 0.192 | 0.205 | 0.213 | 0.193 | 0.197 | 0.126 | 0.135 | 0.138 | 0.128 | 0.125 | 0.136 |
| Fe2+ | 1.461 | 1.409 | 1.295 | 1.293 | 1.284 | 1.303 | 1.235 | 1.247 | 1.293 | 1.259 | 1.290 | 1.277 | 1.384 | 1.381 | 1.405 | 1.360 | 1.364 | 1.395 |
| Mn | 0.055 | 0.049 | 0.028 | 0.030 | 0.019 | 0.026 | 0.024 | 0.018 | 0.029 | 0.027 | 0.020 | 0.025 | 0.019 | 0.031 | 0.028 | 0.022 | 0.026 | 0.032 |
| Mg | 0.664 | 0.634 | 1.007 | 0.989 | 0.983 | 1.027 | 0.970 | 0.990 | 0.957 | 0.940 | 0.991 | 0.970 | 0.971 | 0.950 | 0.968 | 1.033 | 0.963 | 0.968 |
| Sum O | 2.797 | 2.754 | 2.820 | 2.815 | 2.802 | 2.819 | 2.777 | 2.780 | 2.793 | 2.771 | 2.809 | 2.789 | 2.839 | 2.823 | 2.838 | 2.827 | 2.827 | 2.841 |
| Ca | 0.001 | 0.005 | 0.000 | 0.000 | 0.000 | 0.000 | 0.000 | 0.000 | 0.000 | 0.000 | 0.000 | 0.000 | 0.000 | 0.001 | 0.003 | 0.000 | 0.002 | 0.000 |
| Na | 0.020 | 0.016 | 0.011 | 0.014 | 0.014 | 0.015 | 0.013 | 0.010 | 0.014 | 0.010 | 0.008 | 0.014 | 0.009 | 0.009 | 0.009 | 0.016 | 0.010 | 0.011 |
| K | 0.925 | 0.952 | 0.949 | 0.942 | 0.942 | 0.962 | 0.955 | 0.966 | 0.949 | 0.940 | 0.953 | 0.959 | 0.936 | 0.963 | 0.958 | 0.972 | 0.940 | 0.948 |
| Sum A | 0.945 | 0.973 | 0.960 | 0.957 | 0.956 | 0.977 | 0.968 | 0.976 | 0.962 | 0.950 | 0.961 | 0.974 | 0.945 | 0.972 | 0.970 | 0.989 | 0.952 | 0.959 |
| Sum Cations | 7.742 | 7.727 | 7.780 | 7.772 | 7.757 | 7.796 | 7.744 | 7.756 | 7.756 | 7.721 | 7.771 | 7.763 | 7.784 | 7.796 | 7.808 | 7.815 | 7.779 | 7.800 |
| Mg/(Mg+Fe2) | 0.313 | 0.310 | 0.437 | 0.433 | 0.434 | 0.441 | 0.440 | 0.442 | 0.425 | 0.428 | 0.434 | 0.432 | 0.412 | 0.407 | 0.408 | 0.432 | 0.414 | 0.410 |

* Total Fe as FeO

Table F-3 (continued)

| Sample no. | IN-10 | | | | IN-19 | | | | | | | | IN-13.2 | | | | | | |
|---|---|---|---|---|---|---|---|---|---|---|---|---|---|---|---|---|---|---|---|
| Analysis no. | 7 | 8 | 9 | 10 | 1 | 2 | 3 | 4 | 5 | 6 | 7 | 8 | 1 | 2 | 3 | 4 | 5 | 6 | 7 |
| | C4-Bt7 | C4-Bt8 | C4-Bt9 | C4-Bt10 | C3-Bt1 | C3-Bt2 | C2-Bt1a | C2-Bt2a | C2-Bt3a | C2-Bt4a | C2-Bt5a | C2-Bt6a | C1-Bt1.7 | C1-Bt1 2 | C1-Bt1.3 | C1-Bt1.4 | C1-Bt1.5 | C1-Bt1.6 | C1-Bt1.7 |
| SiO2 | 36.42 | 36.43 | 36.52 | 36.81 | 35.71 | 35.68 | 36.10 | 36.45 | 36.21 | 35.75 | 36.57 | 36.21 | 36.62 | 36.72 | 36.69 | 36.64 | 36.68 | 37.14 | 36.89 |
| TiO2 | 2.37 | 2.37 | 2.30 | 2.49 | 2.28 | 2.15 | 2.29 | 2.12 | 2.25 | 2.29 | 2.13 | 2.24 | 3.17 | 3.22 | 2.89 | 3.31 | 3.19 | 2.37 | 2.89 |
| Al2O3 | 17.71 | 17.18 | 17.23 | 17.57 | 16.85 | 16.85 | 17.05 | 16.87 | 16.96 | 16.66 | 17.29 | 17.29 | 13.00 | 13.13 | 13.19 | 13.01 | 13.08 | 13.13 | 13.09 |
| FeO* | 20.99 | 20.84 | 21.11 | 21.13 | 22.24 | 22.07 | 21.54 | 21.69 | 21.83 | 22.18 | 22.47 | 22.16 | 20.84 | 21.81 | 22.13 | 21.41 | 20.66 | 20.14 | 21.74 |
| MnO | 0.31 | 0.28 | 0.43 | 0.43 | 0.44 | 0.38 | 0.54 | 0.56 | 0.43 | 0.58 | 0.55 | 0.51 | 0.17 | 0.32 | 0.27 | 0.36 | 0.29 | 0.41 | 0.39 |
| MgO | 8.50 | 8.48 | 8.50 | 8.30 | 8.19 | 8.11 | 8.13 | 8.25 | 8.15 | 8.09 | 8.20 | 8.12 | 10.92 | 10.84 | 10.96 | 10.65 | 10.55 | 11.21 | 10.77 |
| CaO | 0.01 | 0.00 | 0.00 | 0.00 | 0.00 | 0.00 | 0.03 | 0.02 | 0.00 | 0.00 | 0.02 | 0.03 | 0.00 | 0.00 | 0.00 | 0.02 | 0.00 | 0 00 | 0.02 |
| Na2O | 0.10 | 0.08 | 0.09 | 0.08 | 0.06 | 0.07 | 0.10 | 0.12 | 0.09 | 0.08 | 0.10 | 0.10 | 0.00 | 0.05 | 0.08 | 0.00 | 0.06 | 0.01 | 0.02 |
| K2O | 9.94 | 9.90 | 9.93 | 9.67 | 9.81 | 9.91 | 9.71 | 9.78 | 9.74 | 9 68 | 9.47 | 9.69 | 9.66 | 9.68 | 10 05 | 9.78 | 9.72 | 10.04 | 9.80 |
| F | 2.08 | 2.13 | 2.12 | 1.69 | 1.76 | 2.06 | 2.09 | 2.13 | 2.36 | 2.33 | 2.19 | 2.24 | 1.15 | 0.80 | 0.89 | 0.85 | 1.07 | 1.09 | 1.16 |
| Cl | 0.06 | 0.04 | 0.05 | 0.04 | 0.04 | 0.03 | 0.05 | 0.05 | 0.06 | 0.04 | 0 03 | 0.07 | 0.02 | 0.05 | 0.02 | 0.02 | 0 03 | 0.03 | 0.01 |
| Total | 98.48 | 97.72 | 98.29 | 98.21 | 97.39 | 97.31 | 97.62 | 98.04 | 98.07 | 97.68 | 99.02 | 98.66 | 95.56 | 96 62 | 97.14 | 96.05 | 95.30 | 95.57 | 96.80 |
| O = F, Cl | -0.89 | -0.90 | -0.90 | -0.72 | -0.75 | -0.87 | -0 89 | -0.91 | -1.01 | -0.99 | -0.93 | -0.96 | -0.49 | -0.35 | -0.38 | -0.36 | -0.44 | -0.46 | -0.49 |
| Total | 97.59 | 96.82 | 97.38 | 97.48 | 96.64 | 96.44 | 96.73 | 97.13 | 97.07 | 96.69 | 98.09 | 97.70 | 95.07 | 96 27 | 96.77 | 95.69 | 94.86 | 95.10 | 96.30 |
| Number of cations on the basis of 11 oxygens: | | | | | | | | | | | | | | | | | | | |
| Si | 2.770 | 2.793 | 2.788 | 2.791 | 2.763 | 2.770 | 2.783 | 2.800 | 2.788 | 2.774 | 2.783 | 2.771 | 2.857 | 2 837 | 2.831 | 2.846 | 2.866 | 2.890 | 2.855 |
| Al iv | 1.230 | 1.207 | 1.212 | 1.209 | 1.237 | 1.230 | 1.217 | 1.200 | 1.212 | 1.226 | 1.217 | 1.229 | 1.143 | 1.163 | 1.169 | 1.154 | 1.134 | 1.110 | 1.145 |
| Sum T | 4.000 | 4.000 | 4.000 | 4.000 | 4.000 | 4.000 | 4.000 | 4.000 | 4.000 | 4.000 | 4.000 | 4.000 | 4.000 | 4.000 | 4.000 | 4.000 | 4.000 | 4.000 | 4.000 |
| Al vi | 0.357 | 0.345 | 0.339 | 0.361 | 0.301 | 0.313 | 0.332 | 0.327 | 0.328 | 0.298 | 0 334 | 0.331 | 0.052 | 0.033 | 0.030 | 0.038 | 0.071 | 0.094 | 0.049 |
| Ti | 0.135 | 0.136 | 0.132 | 0.142 | 0.133 | 0.126 | 0.133 | 0.122 | 0.130 | 0.134 | 0.122 | 0.129 | 0.186 | 0.187 | 0.167 | 0.193 | 0.187 | 0.139 | 0.168 |
| Fe2+ | 1.335 | 1.336 | 1.348 | 1.340 | 1.440 | 1.433 | 1.388 | 1.393 | 1.406 | 1.439 | 1.430 | 1.419 | 1.360 | 1.409 | 1.428 | 1.391 | 1.350 | 1.310 | 1.407 |
| Mn | 0.020 | 0.018 | 0.028 | 0 028 | 0.029 | 0.025 | 0.035 | 0.037 | 0.028 | 0.038 | 0.035 | 0 033 | 0.011 | 0.021 | 0.017 | 0.023 | 0.019 | 0.027 | 0.025 |
| Mg | 0.963 | 0.968 | 0.967 | 0.937 | 0.944 | 0.939 | 0.934 | 0.945 | 0.935 | 0.935 | 0.929 | 0.926 | 1.270 | 1.248 | 1.260 | 1.233 | 1.229 | 1.300 | 1.242 |
| Sum O | 2.810 | 2.804 | 2.814 | 2.808 | 2.846 | 2.836 | 2.823 | 2.824 | 2.826 | 2.845 | 2.851 | 2.837 | 2.879 | 2.897 | 2.902 | 2.878 | 2.855 | 2.870 | 2.893 |
| Ca | 0.001 | 0.000 | 0.000 | 0.000 | 0.000 | 0.000 | 0.002 | 0 001 | 0.000 | 0.000 | 0.002 | 0.002 | 0.000 | 0.000 | 0.000 | 0.001 | 0 000 | 0 000 | 0.001 |
| Na | 0.014 | 0.012 | 0.013 | 0.012 | 0.009 | 0.011 | 0.014 | 0 018 | 0.013 | 0.012 | 0 014 | 0.014 | 0 000 | 0.007 | 0.012 | 0.000 | 0.009 | 0 002 | 0.003 |
| K | 0.965 | 0.968 | 0.967 | 0.935 | 0.969 | 0.982 | 0.955 | 0.959 | 0.957 | 0.958 | 0.919 | 0.946 | 0.962 | 0.954 | 0.989 | 0.969 | 0.969 | 0.997 | 0.968 |
| Sum A | 0.980 | 0.980 | 0.981 | 0.947 | 0.978 | 0.993 | 0.971 | 0.978 | 0.970 | 0.971 | 0.935 | 0.963 | 0.962 | 0.961 | 1.001 | 0.971 | 0.977 | 0.999 | 0.972 |
| Sum Cations | 7.791 | 7.785 | 7.794 | 7.755 | 7.825 | 7.829 | 7.794 | 7.802 | 7.797 | 7.815 | 7.786 | 7.800 | 7.840 | 7.858 | 7.903 | 7.850 | 7.833 | 7.869 | 7.865 |
| Mg/(Mg+Fe2) | 0.419 | 0.420 | 0.418 | 0.412 | 0.396 | 0.396 | 0.402 | 0.404 | 0.399 | 0.394 | 0.394 | 0 419 | 0.483 | 0.470 | 0.469 | 0.470 | 0.476 | 0 498 | 0.469 |

* Total Fe as FeO

Table F-4 Electron microprobe analyses of muscovites (Gneisses).

| Sample no. | IN-10 | | | | | | IN-14 | | | | | | | | | IN-18.1 | | |
|---|---|---|---|---|---|---|---|---|---|---|---|---|---|---|---|---|---|---|
| Analysis no. | 1 | 2 | 3 | 4 | 5 | 6 | 1 | 2 | 3 | 4 | 5 | 6 | 7 | 8 | 9 | 1 | 2 | 3 |
| | C4-Ms4. | C4-Ms4. | C4-Ms-4. | C6-Ms6. | C6-Ms6. | C6-Ms6.3 | | | | | | | | | | C1-Ms1 | C1-Ms1 | C1-Ms1 |
| SiO2 | 45.39 | 45.38 | 45.81 | 44.94 | 45.26 | 45.66 | 45.52 | 45.85 | 45.75 | 47.08 | 46.72 | 46.98 | 46.97 | 46.59 | 46.17 | 46.66 | 46.61 | 46.41 |
| TiO2 | 0.68 | 0.68 | 0.54 | 0.58 | 0.62 | 0.62 | 1.39 | 1.15 | 0.69 | 1.13 | 0.90 | 1.00 | 1.19 | 1.27 | 1.20 | 1.28 | 0.99 | 1.35 |
| Al2O3 | 35.48 | 35.30 | 35.04 | 35.14 | 34.91 | 35.03 | 32.87 | 32.77 | 33.72 | 32.52 | 32.99 | 32.55 | 32.42 | 33.22 | 33.20 | 33.50 | 33.18 | 33.32 |
| FeO* | 1.32 | 1.37 | 1.27 | 1.11 | 1.22 | 1.17 | 1.50 | 1.80 | 1.80 | 1.99 | 1.95 | 2.26 | 2.04 | 1.91 | 1.67 | 1.72 | 1.74 | 1.55 |
| MnO | 0.05 | 0.09 | 0.00 | 0.00 | 0.04 | 0.00 | 0.02 | 0.07 | 0.00 | 0.00 | 0.00 | 0.10 | 0.00 | 0.02 | 0.08 | 0.01 | 0.00 | 0.00 |
| MgO | 0.49 | 0.64 | 0.61 | 0.60 | 0.54 | 0.52 | 1.21 | 1.21 | 1.13 | 1.42 | 1.38 | 1.39 | 1.35 | 1.29 | 1.19 | 1.19 | 1.21 | 1.14 |
| CaO | 0.03 | 0.00 | 0.00 | 0.00 | 0.01 | 0.00 | 0.00 | 0.00 | 0.00 | 0.00 | 0.00 | 0.00 | 0.00 | 0.00 | 0.00 | 0.00 | 0.00 | 0.00 |
| Na2O | 0.51 | 0.57 | 0.55 | 0.56 | 0.50 | 0.55 | 0.39 | 0.37 | 0.35 | 0.34 | 0.26 | 0.29 | 0.27 | 0.33 | 0.46 | 0.47 | 0.36 | 0.38 |
| K2O | 10.22 | 10.65 | 10.51 | 10.67 | 10.60 | 10.54 | 11.19 | 11.35 | 11.16 | 11.08 | 11.07 | 11.15 | 11.26 | 11.03 | 10.97 | 11.00 | 11.11 | 10.97 |
| F | 0.11 | 0.22 | 0.19 | 0.30 | 0.62 | 0.22 | 0.64 | 0.67 | 0.73 | 1.00 | 1.02 | 1.04 | 0.97 | 0.76 | 0.92 | 0.73 | 0.78 | 0.59 |
| Cl | 0.00 | 0.03 | 0.00 | 0.00 | 0.00 | 0.00 | 0.00 | 0.00 | 0.00 | 0.01 | 0.00 | 0.00 | 0.00 | 0.01 | 0.00 | 0.00 | 0.01 | 0.00 |
| Total | 94.26 | 94.92 | 94.52 | 93.90 | 94.32 | 94.30 | 94.73 | 95.26 | 95.34 | 96.58 | 96.29 | 96.74 | 96.46 | 96.43 | 95.85 | 96.55 | 95.99 | 95.72 |
| O = F, Cl | -0.05 | -0.10 | -0.08 | -0.13 | -0.26 | -0.09 | -0.27 | -0.28 | -0.31 | -0.42 | -0.43 | -0.44 | -0.41 | -0.32 | -0.39 | -0.31 | -0.33 | -0.25 |
| Total | 94.22 | 94.82 | 94.44 | 93.78 | 94.05 | 94.21 | 94.46 | 94.98 | 95.03 | 96.15 | 95.86 | 96.31 | 96.06 | 96.11 | 95.47 | 96.25 | 95.66 | 95.47 |
| Number of cations on the basis of 11 oxygens: | | | | | | | | | | | | | | | | | | |
| Si | 3.055 | 3.049 | 3.080 | 3.050 | 3.068 | 3.077 | 3.094 | 3.107 | 3.091 | 3.147 | 3.131 | 3.142 | 3.146 | 3.111 | 3.106 | 3.107 | 3.125 | 3.110 |
| Al iv | 0.945 | 0.951 | 0.920 | 0.950 | 0.932 | 0.923 | 0.906 | 0.893 | 0.909 | 0.853 | 0.869 | 0.858 | 0.854 | 0.889 | 0.894 | 0.893 | 0.875 | 0.890 |
| Sum T | 4.000 | 4.000 | 4.000 | 4.000 | 4.000 | 4.000 | 4.000 | 4.000 | 4.000 | 4.000 | 4.000 | 4.000 | 4.000 | 4.000 | 4.000 | 4.000 | 4.000 | 4.000 |
| Al vi | 1.869 | 1.845 | 1.857 | 1.862 | 1.857 | 1.861 | 1.728 | 1.724 | 1.777 | 1.710 | 1.738 | 1.709 | 1.706 | 1.726 | 1.738 | 1.737 | 1.747 | 1.742 |
| Ti | 0.034 | 0.034 | 0.027 | 0.030 | 0.032 | 0.032 | 0.071 | 0.059 | 0.035 | 0.057 | 0.045 | 0.050 | 0.060 | 0.064 | 0.060 | 0.064 | 0.050 | 0.068 |
| Fe2+ | 0.074 | 0.077 | 0.071 | 0.063 | 0.069 | 0.066 | 0.085 | 0.102 | 0.102 | 0.111 | 0.110 | 0.126 | 0.114 | 0.107 | 0.094 | 0.096 | 0.098 | 0.087 |
| Mn | 0.003 | 0.005 | 0.000 | 0.000 | 0.002 | 0.000 | 0.001 | 0.004 | 0.000 | 0.000 | 0.000 | 0.006 | 0.000 | 0.001 | 0.005 | 0.001 | 0.000 | 0.000 |
| Mg | 0.049 | 0.064 | 0.061 | 0.060 | 0.054 | 0.052 | 0.123 | 0.122 | 0.114 | 0.142 | 0.138 | 0.138 | 0.135 | 0.128 | 0.120 | 0.118 | 0.121 | 0.114 |
| Sum O | 2.030 | 2.025 | 2.018 | 2.015 | 2.014 | 2.010 | 2.007 | 2.011 | 2.027 | 2.020 | 2.030 | 2.030 | 2.015 | 2.027 | 2.017 | 2.016 | 2.016 | 2.012 |
| Ca | 0.002 | 0.000 | 0.000 | 0.000 | 0.001 | 0.000 | 0.000 | 0.000 | 0.000 | 0.000 | 0.000 | 0.000 | 0.000 | 0.000 | 0.000 | 0.000 | 0.000 | 0.000 |
| Na | 0.066 | 0.074 | 0.071 | 0.073 | 0.066 | 0.071 | 0.052 | 0.049 | 0.046 | 0.044 | 0.034 | 0.037 | 0.036 | 0.042 | 0.060 | 0.061 | 0.047 | 0.050 |
| K | 0.877 | 0.913 | 0.901 | 0.924 | 0.917 | 0.907 | 0.970 | 0.981 | 0.962 | 0.945 | 0.946 | 0.952 | 0.963 | 0.940 | 0.941 | 0.935 | 0.950 | 0.938 |
| Sum A | 0.945 | 0.987 | 0.973 | 0.998 | 0.984 | 0.978 | 1.022 | 1.030 | 1.008 | 0.990 | 0.980 | 0.989 | 0.998 | 0.982 | 1.001 | 0.996 | 0.997 | 0.988 |
| Sum Cations | 6.975 | 7.012 | 6.990 | 7.013 | 6.998 | 6.988 | 7.029 | 7.041 | 7.035 | 7.009 | 7.010 | 7.018 | 7.013 | 7.009 | 7.018 | 7.011 | 7.013 | 6.999 |

* Total Fe as FeO

Table F-4 (continued)

| Sample no. | IN-18.1 | | | | | | | | | IN-19 | | | | | | | | |
|---|---|---|---|---|---|---|---|---|---|---|---|---|---|---|---|---|---|---|
| Analysis no. | 4 | 5 | 6 | 7 | 8 | 9 | 10 | 11 | 12 | 1 | 2 | 3 | 4 | 5 | 6 | 7 | 8 | 9 |
| | C1-Ms1 | C1-Ms1 | C2-Ms6 | C2-Ms7 | C2-Ms8 | C7-Ms9 | C7-Ms10 | C7-Ms11 | C7-Ms12 | C3-Ms1 | C3-Ms2 | C1-Ms1a | C2-Ms2a | C2-Ms3a | C2-Ms4a | C2-Ms5a | C2-Ms6a | C2-Ms7a |
| SiO2 | 46.95 | 46.73 | 47.24 | 46.95 | 46.86 | 47.10 | 46.36 | 46.16 | 46.44 | 45.52 | 45.85 | 45.75 | 47.08 | 46.72 | 46.98 | 46.97 | 46.59 | 46.17 |
| TiO2 | 1.34 | 1.19 | 0.85 | 0.80 | 1.10 | 0.27 | 0.20 | 0.21 | 0.34 | 1.39 | 1.15 | 0.69 | 1.13 | 0.90 | 1.00 | 1.19 | 1.27 | 1.20 |
| Al2O3 | 33.46 | 33.16 | 33.71 | 33.92 | 34.28 | 35.47 | 35.54 | 35.77 | 34.78 | 32.87 | 32.77 | 33.72 | 32.52 | 32.99 | 32.55 | 32.42 | 33.22 | 33.20 |
| FeO* | 1.74 | 1.75 | 1.87 | 1.67 | 1.64 | 1.27 | 1.51 | 1.53 | 1.77 | 1.50 | 1.80 | 1.80 | 1.99 | 1.95 | 2.26 | 2.04 | 1.91 | 1.67 |
| MnO | 0.04 | 0.06 | 0.00 | 0.07 | 0.02 | 0.06 | 0.08 | 0.08 | 0.03 | 0.02 | 0.07 | 0.00 | 0.00 | 0.00 | 0.10 | 0.00 | 0.02 | 0.08 |
| MgO | 1.14 | 1.14 | 1.11 | 1.19 | 1.19 | 0.78 | 0.75 | 0.67 | 0.96 | 1.21 | 1.21 | 1.13 | 1.42 | 1.38 | 1.39 | 1.35 | 1.29 | 1.19 |
| CaO | 0.00 | 0.00 | 0.01 | 0.00 | 0.02 | 0.01 | 0.00 | 0.00 | 0.02 | 0.00 | 0.00 | 0.00 | 0.00 | 0.00 | 0.00 | 0.00 | 0.00 | 0.00 |
| Na2O | 0.43 | 0.34 | 0.39 | 0.46 | 0.40 | 0.36 | 0.36 | 0.35 | 0.29 | 0.39 | 0.37 | 0.35 | 0.34 | 0.26 | 0.29 | 0.27 | 0.33 | 0.46 |
| K2O | 10.84 | 10.86 | 11.11 | 11.03 | 11.10 | 11.07 | 11.22 | 11.36 | 11.26 | 11.19 | 11.35 | 11.16 | 11.08 | 11.07 | 11.15 | 11.26 | 11.03 | 10.97 |
| F | 0.73 | 0.79 | 0.79 | 0.65 | 0.75 | 0.48 | 0.75 | 0.57 | 0.76 | 0.64 | 0.67 | 0.73 | 1.00 | 1.02 | 1.04 | 0.97 | 0.76 | 0.92 |
| Cl | 0.00 | 0.00 | 0.00 | 0.00 | 0.01 | 0.00 | 0.00 | 0.01 | 0.00 | 0.00 | 0.00 | 0.00 | 0.01 | 0.00 | 0.00 | 0.00 | 0.01 | 0.00 |
| Total | 96.67 | 96.03 | 97.08 | 96.75 | 97.38 | 96.86 | 96.77 | 96.71 | 96.65 | 94.73 | 95.26 | 95.34 | 96.58 | 96.29 | 96.74 | 96.46 | 96.43 | 95.85 |
| O = F, Cl | -0.31 | -0.33 | -0.33 | -0.27 | -0.32 | -0.20 | -0.32 | -0.24 | -0.32 | -0.27 | -0.28 | -0.31 | -0.42 | -0.43 | -0.44 | -0.41 | -0.32 | -0.39 |
| Total | 96.37 | 95.69 | 96.75 | 96.48 | 97.07 | 96.66 | 96.45 | 96.47 | 96.33 | 94.46 | 94.98 | 95.03 | 96.15 | 95.86 | 96.31 | 96.06 | 96.11 | 95.47 |
| Number of cations on the basis of 11 oxygens: | | | | | | | | | | | | | | | | | | |
| Si | 3.119 | 3.128 | 3.129 | 3.115 | 3.093 | 3.102 | 3.075 | 3.062 | 3.090 | 3.094 | 3.107 | 3.091 | 3.147 | 3.131 | 3.142 | 3.146 | 3.111 | 3.106 |
| Al iv | 0.881 | 0.872 | 0.871 | 0.885 | 0.907 | 0.898 | 0.925 | 0.938 | 0.910 | 0.906 | 0.893 | 0.909 | 0.853 | 0.869 | 0.858 | 0.854 | 0.889 | 0.894 |
| Sum T | 4.000 | 4.000 | 4.000 | 4.000 | 4.000 | 4.000 | 4.000 | 4.000 | 4.000 | 4.000 | 4.000 | 4.000 | 4.000 | 4.000 | 4.000 | 4.000 | 4.000 | 4.000 |
| Al vi | 1.739 | 1.744 | 1.762 | 1.768 | 1.761 | 1.856 | 1.855 | 1.860 | 1.818 | 1.728 | 1.724 | 1.777 | 1.710 | 1.738 | 1.709 | 1.706 | 1.726 | 1.738 |
| Ti | 0.067 | 0.060 | 0.042 | 0.040 | 0.054 | 0.013 | 0.010 | 0.010 | 0.017 | 0.071 | 0.059 | 0.035 | 0.057 | 0.045 | 0.050 | 0.060 | 0.064 | 0.060 |
| Fe2+ | 0.097 | 0.098 | 0.104 | 0.093 | 0.091 | 0.070 | 0.084 | 0.085 | 0.099 | 0.085 | 0.102 | 0.102 | 0.111 | 0.110 | 0.126 | 0.114 | 0.107 | 0.094 |
| Mn | 0.002 | 0.003 | 0.000 | 0.004 | 0.001 | 0.003 | 0.004 | 0.005 | 0.002 | 0.001 | 0.004 | 0.000 | 0.000 | 0.000 | 0.006 | 0.000 | 0.001 | 0.005 |
| Mg | 0.113 | 0.113 | 0.110 | 0.118 | 0.117 | 0 076 | 0.074 | 0.067 | 0.096 | 0.123 | 0.122 | 0.114 | 0.142 | 0.138 | 0.138 | 0.135 | 0.128 | 0.120 |
| Sum O | 2.017 | 2.018 | 2.017 | 2.022 | 2.024 | 2.019 | 2.027 | 2.026 | 2.031 | 2.007 | 2 011 | 2.027 | 2.020 | 2.030 | 2.030 | 2.015 | 2.027 | 2.017 |
| Ca | 0.000 | 0.000 | 0.001 | 0.000 | 0.002 | 0.001 | 0.000 | 0.000 | 0.001 | 0.000 | 0.000 | 0.000 | 0.000 | 0.000 | 0.000 | 0.000 | 0.000 | 0.000 |
| Na | 0.055 | 0.045 | 0.050 | 0.059 | 0.052 | 0.046 | 0.046 | 0.045 | 0.037 | 0.052 | 0.049 | 0.046 | 0.044 | 0.034 | 0.037 | 0.036 | 0.042 | 0.060 |
| K | 0.918 | 0.928 | 0.939 | 0.934 | 0.935 | 0.930 | 0.950 | 0.961 | 0.956 | 0.970 | 0.981 | 0.962 | 0.945 | 0.946 | 0.952 | 0.963 | 0.940 | 0.941 |
| Sum A | 0.974 | 0.972 | 0.989 | 0.992 | 0.988 | 0.977 | 0 996 | 1.006 | 0.994 | 1.022 | 1.030 | 1.008 | 0.990 | 0.980 | 0.989 | 0.998 | 0.982 | 1.001 |
| Sum Cations | 6.991 | 6.991 | 7.007 | 7.015 | 7.012 | 6.996 | 7.023 | 7.032 | 7.025 | 7.029 | 7.041 | 7.035 | 7.009 | 7.010 | 7.018 | 7.013 | 7.009 | 7.018 |

* Total Fe as FeO

Table F-5 Electron microprobe analyses of clinopyroxenes (Gneisses).

| Sample no. | IN-2 | | | | | | | IN-3 | | | | | | |
|---|---|---|---|---|---|---|---|---|---|---|---|---|---|---|
| Analysis no. | 1 | 2 | 3 | 4 | 5 | 6 | 7 | 1 | 2 | 3 | 4 | 5 | 6 | 7 |
| | C6-Cpx6 | C6-Cpx6 | C6-Cpx6 | C11-Cpx | C11-Cpx | C12-Cpx | C12-Cpx | C1-Cpx1 | C1-Cpx2 | C1-Cpx3 | C1-Cpx4 | C1-Cpx5 | C1-Cpx1 | C1-Cpx2a |
| SiO2 | 51.37 | 50.75 | 51.45 | 51.76 | 51.54 | 50.76 | 51.32 | 52.13 | 52.34 | 52.08 | 52.36 | 52.26 | 51.40 | 51.34 |
| TiO2 | 0.04 | 0.07 | 0.02 | 0.02 | 0.02 | 0.00 | 0.01 | 0.02 | 0.04 | 0.01 | 0.02 | 0.00 | 0.00 | 0.00 |
| Al2O3 | 0.46 | 0.38 | 0.36 | 0.32 | 0.30 | 0.33 | 0.39 | 0.35 | 0.31 | 0.33 | 0.50 | 0.40 | 0.37 | 0.40 |
| Cr2O3 | 0.05 | 0.06 | 0.05 | 0.03 | 0.00 | 0.01 | 0.01 | 0.00 | 0.01 | 0.04 | 0.07 | 0.07 | 0.04 | 0.04 |
| Fe2O3* | 2.48 | 2.54 | 1.46 | 2.33 | 1.41 | 2.17 | 1.78 | 1.48 | 1.12 | 1.59 | 2.25 | 2.24 | 1.36 | 2.66 |
| FeO* | 9.27 | 9.39 | 11.37 | 8.54 | 8.88 | 10.93 | 11.74 | 12.10 | 11.35 | 11.05 | 8.53 | 9.38 | 12.06 | 10.56 |
| MnO | 0.83 | 0.82 | 0.49 | 0.61 | 0.58 | 0.83 | 1.01 | 0.52 | 0.48 | 0.54 | 1.04 | 0.97 | 0.61 | 0.46 |
| MgO | 10.84 | 10.40 | 9.93 | 11.29 | 11.25 | 9.33 | 9.25 | 9.87 | 10.41 | 10.32 | 11.33 | 10.86 | 9.57 | 9.79 |
| CaO | 24.10 | 24.00 | 24.49 | 25.19 | 24.77 | 24.74 | 24.62 | 24.62 | 24.90 | 24.84 | 25.16 | 25.06 | 24.48 | 25.15 |
| Na2O | 0.25 | 0.27 | 0.13 | 0.08 | 0.09 | 0.13 | 0.13 | 0.13 | 0.07 | 0.10 | 0.13 | 0.14 | 0.08 | 0.15 |
| Total | 99.69 | 98.67 | 99.75 | 100.17 | 98.84 | 99.22 | 100.26 | 101.22 | 101.02 | 100.90 | 101.40 | 101.38 | 99.97 | 100.54 |
| Number of cations on the basis of 6 oxygens: | | | | | | | | | | | | | | |
| Si | 1.961 | 1.962 | 1.974 | 1.961 | 1.976 | 1.966 | 1.970 | 1.975 | 1.979 | 1.973 | 1.960 | 1.963 | 1.974 | 1.958 |
| Al iv | 0.021 | 0.017 | 0.016 | 0.014 | 0.014 | 0.015 | 0.017 | 0.016 | 0.014 | 0.015 | 0.022 | 0.018 | 0.017 | 0.018 |
| Fe3+ | 0.018 | 0.021 | 0.009 | 0.024 | 0.011 | 0.019 | 0.013 | 0.009 | 0.008 | 0.012 | 0.017 | 0.019 | 0.009 | 0.024 |
| Sum T | 2.000 | 2.000 | 2.000 | 2.000 | 2.000 | 2.000 | 2.000 | 2.000 | 2.000 | 2.000 | 2.000 | 2.000 | 2.000 | 2.000 |
| Al vi | 0.000 | 0.000 | 0.000 | 0.000 | 0.000 | 0.000 | 0.000 | 0.000 | 0.000 | 0.000 | 0.000 | 0.000 | 0.000 | 0.000 |
| Ti | 0.001 | 0.002 | 0.000 | 0.001 | 0.001 | 0.000 | 0.000 | 0.001 | 0.001 | 0.000 | 0.001 | 0.000 | 0.000 | 0.000 |
| Cr | 0.002 | 0.002 | 0.002 | 0.001 | 0.000 | 0.000 | 0.000 | 0.000 | 0.000 | 0.001 | 0.002 | 0.002 | 0.001 | 0.001 |
| Fe3+ | 0.053 | 0.053 | 0.033 | 0.042 | 0.030 | 0.044 | 0.039 | 0.033 | 0.024 | 0.033 | 0.046 | 0.045 | 0.030 | 0.052 |
| Fe2+ | 0.296 | 0.304 | 0.365 | 0.271 | 0.284 | 0.354 | 0.377 | 0.383 | 0.359 | 0.350 | 0.267 | 0.296 | 0.387 | 0.337 |
| Mn | 0.027 | 0.027 | 0.016 | 0.020 | 0.019 | 0.027 | 0.033 | 0.017 | 0.015 | 0.017 | 0.033 | 0.031 | 0.020 | 0.015 |
| Mg | 0.617 | 0.599 | 0.568 | 0.638 | 0.643 | 0.539 | 0.529 | 0.557 | 0.587 | 0.582 | 0.632 | 0.608 | 0.548 | 0.556 |
| Sum O | 0.995 | 0.986 | 0.983 | 0.972 | 0.976 | 0.964 | 0.978 | 0.991 | 0.986 | 0.984 | 0.981 | 0.981 | 0.987 | 0.961 |
| Ca | 0.986 | 0.994 | 1.007 | 1.023 | 1.018 | 1.027 | 1.013 | 1.000 | 1.009 | 1.008 | 1.010 | 1.009 | 1.007 | 1.028 |
| Na | 0.019 | 0.020 | 0.009 | 0.006 | 0.007 | 0.010 | 0.009 | 0.009 | 0.005 | 0.008 | 0.010 | 0.010 | 0.006 | 0.011 |
| Sum Cations | 4.000 | 4.000 | 4.000 | 4.000 | 4.000 | 4.000 | 4.000 | 4.000 | 4.000 | 4.000 | 4.000 | 4.000 | 4.000 | 4.000 |
| Mg/((Mg+Fe2 | 0.676 | 0.664 | 0.609 | 0.702 | 0.694 | 0.604 | 0.584 | 0.592 | 0.621 | 0.625 | 0.703 | 0.673 | 0.586 | 0.623 |
| Molecular proportions of end-members# : | | | | | | | | | | | | | | |
| Wo | 0.498 | 0.503 | 0.506 | 0.513 | 0.511 | 0.516 | 0.509 | 0.502 | 0.506 | 0.506 | 0.508 | 0.507 | 0.506 | 0.517 |
| En | 0.312 | 0.303 | 0.286 | 0.320 | 0.323 | 0.271 | 0.266 | 0.280 | 0.294 | 0.293 | 0.318 | 0.306 | 0.275 | 0.280 |
| Fs | 0.190 | 0.194 | 0.208 | 0.167 | 0.167 | 0.213 | 0.225 | 0.218 | 0.200 | 0.201 | 0.174 | 0.187 | 0.220 | 0.203 |

* Calculated assuming stoichiometry on the basis of 4 cations and 6 oxygens.
# Calculated after the Subcommittee on Pyroxenes, IMA (1988).

Table F-5 (continued)

| Sample no. | IN-13.1 | | | | | | | | | IN-13.2 | | | | | |
|---|---|---|---|---|---|---|---|---|---|---|---|---|---|---|---|
| Analysis no. | 1 | 2 | 3 | 4 | 5 | 6 | 7 | 8 | 9 | 1 | 2 | 3 | 4 | 5 | 6 |
| | C1-Cpx1 | C1-Cpx2 | C1-Cpx3 | C1-Cpx4 | C2-Cpx5 | C2-Cpx6 | C2-Cpx7 | C3-Cpx8 | C3-Cpx9 | C5-Cpx5 | C5-Cpx5 | C5-Cpx5 | C5-Cpx5 | C6-Cpx6 | C6-Cpx6.2 |
| SiO2 | 52.52 | 52.10 | 50.92 | 51.46 | 51.79 | 52.03 | 51.21 | 52.13 | 51.90 | 51.39 | 51.58 | 51.27 | 51.38 | 51.72 | 50.97 |
| TiO2 | 0.00 | 0.01 | 0.05 | 0.04 | 0.04 | 0.00 | 0.01 | 0.03 | 0.02 | 0.07 | 0.07 | 0.00 | 0.07 | 0.06 | 0.01 |
| Al2O3 | 0.40 | 0.43 | 0.44 | 0.41 | 1.60 | 0.33 | 0.39 | 0.48 | 0.40 | 0.37 | 0.38 | 1.01 | 0.37 | 0.38 | 0.25 |
| Cr2O3 | 0.01 | 0.04 | 0.00 | 0.00 | 0.01 | 0.04 | 0.00 | 0.02 | 0.00 | 0.05 | 0.05 | 0.07 | 0.02 | 0.00 | 0.00 |
| Fe2O3* | 2.59 | 1.94 | 2.41 | 2.03 | 2.07 | 2.43 | 2.20 | 2.31 | 2.08 | 2.38 | 1.81 | 1.26 | 1.88 | 2.77 | 2.28 |
| FeO* | 6.14 | 7.81 | 11.89 | 11.04 | 7.42 | 9.66 | 11.73 | 9.39 | 9.61 | 12.16 | 12.63 | 13.00 | 13.18 | 12.25 | 13.92 |
| MnO | 0.19 | 0.21 | 0.28 | 0.30 | 0.22 | 0.39 | 0.29 | 0.37 | 0.40 | 0.66 | 0.70 | 0.67 | 0.53 | 0.56 | 0.51 |
| MgO | 12.96 | 11.95 | 9.28 | 9.90 | 12.09 | 10.81 | 9.45 | 11.05 | 11.22 | 9.44 | 9.29 | 9.16 | 9.06 | 9.17 | 8.33 |
| CaO | 25.68 | 25.21 | 24.73 | 24.96 | 25.08 | 25.31 | 24.88 | 25.20 | 24.36 | 24.07 | 23.93 | 23.69 | 23.90 | 24.26 | 24.05 |
| Na2O | 0.10 | 0.15 | 0.12 | 0.13 | 0.12 | 0.10 | 0.11 | 0.13 | 0.18 | 0.22 | 0.26 | 0.20 | 0 22 | 0.35 | 0.19 |
| Total | 100.60 | 99.84 | 100.11 | 100.28 | 100.44 | 101.10 | 100.26 | 101.13 | 100.17 | 100.82 | 100.69 | 100.34 | 100.60 | 101.51 | 100.48 |
| Number of cations on the basis of 6 oxygens: | | | | | | | | | | | | | | | |
| Si | 1.958 | 1.968 | 1.958 | 1.965 | 1.938 | 1.961 | 1.963 | 1.960 | 1.968 | 1.963 | 1.972 | 1.966 | 1.970 | 1.963 | 1.968 |
| Al iv | 0.018 | 0.019 | 0.020 | 0.018 | 0.062 | 0.015 | 0.017 | 0.021 | 0 018 | 0.016 | 0.017 | 0 034 | 0.017 | 0.017 | 0.011 |
| Fe3+ | 0.024 | 0.013 | 0.022 | 0.016 | 0.000 | 0.024 | 0.019 | 0.018 | 0 014 | 0.021 | 0.011 | 0 000 | 0.013 | 0.020 | 0.021 |
| Sum T | 2.000 | 2.000 | 2.000 | 2.000 | 2.000 | 2.000 | 2.000 | 2.000 | 2 000 | 2 000 | 2.000 | 2.000 | 2.000 | 2.000 | 2 000 |
| Al vi | 0.000 | 0.000 | 0.000 | 0.000 | 0.009 | 0.000 | 0.000 | 0.000 | 0.000 | 0.000 | 0.000 | 0.011 | 0.000 | 0.000 | 0.000 |
| Ti | 0.000 | 0.000 | 0.001 | 0.001 | 0.001 | 0.000 | 0.000 | 0.001 | 0.000 | 0.002 | 0.002 | 0.000 | 0.002 | 0.002 | 0.000 |
| Cr | 0.000 | 0.001 | 0.000 | 0.000 | 0.000 | 0.001 | 0.000 | 0.001 | 0.000 | 0.002 | 0.002 | 0.002 | 0.001 | 0.000 | 0.000 |
| Fe3+ | 0.049 | 0.042 | 0.048 | 0.042 | 0.058 | 0.045 | 0.044 | 0.047 | 0.045 | 0.048 | 0.041 | 0.036 | 0.041 | 0.059 | 0.045 |
| Fe2+ | 0.191 | 0.247 | 0.382 | 0.353 | 0.236 | 0.304 | 0.376 | 0.295 | 0.305 | 0.388 | 0.404 | 0 417 | 0.423 | 0.390 | 0.449 |
| Mn | 0.006 | 0.007 | 0.009 | 0.010 | 0.007 | 0.013 | 0.009 | 0.012 | 0.013 | 0.021 | 0.023 | 0.022 | 0.017 | 0.018 | 0.017 |
| Mg | 0.720 | 0.672 | 0.532 | 0.564 | 0.674 | 0.607 | 0.540 | 0.619 | 0.634 | 0.537 | 0.529 | 0.523 | 0.518 | 0.519 | 0.479 |
| Sum O | 0.967 | 0.969 | 0.972 | 0.969 | 0.986 | 0.970 | 0.970 | 0.975 | 0.997 | 0.999 | 1.001 | 1.012 | 1.001 | 0.988 | 0.991 |
| Ca | 1.026 | 1.020 | 1.019 | 1.021 | 1.006 | 1.022 | 1.022 | 1.015 | 0.990 | 0.985 | 0.980 | 0.973 | 0.982 | 0.987 | 0.995 |
| Na | 0.007 | 0.011 | 0.009 | 0.010 | 0.008 | 0.007 | 0.008 | 0.010 | 0.014 | 0.016 | 0.019 | 0.015 | 0.016 | 0.026 | 0.014 |
| Sum Cations | 4.000 | 4.000 | 4.000 | 4.000 | 4.000 | 4.000 | 4.000 | 4.000 | 4.000 | 4.000 | 4.000 | 4.000 | 4.000 | 4.000 | 4.000 |
| Mg/((Mg+Fe2 | 0.790 | 0.732 | 0.582 | 0.615 | 0.741 | 0.666 | 0.589 | 0.677 | 0.675 | 0.580 | 0.567 | 0.557 | 0.551 | 0.571 | 0.516 |
| Molecular proportions of end-members# : | | | | | | | | | | | | | | | |
| Wo | 0.515 | 0.513 | 0.512 | 0.513 | 0.508 | 0.513 | 0.513 | 0.511 | 0.498 | 0.497 | 0.496 | 0.494 | 0.496 | 0 500 | 0.501 |
| En | 0.361 | 0.338 | 0.267 | 0.283 | 0.340 | 0.305 | 0.271 | 0.311 | 0.319 | 0.271 | 0.268 | 0.265 | 0.261 | 0.263 | 0.241 |
| Fs | 0 124 | 0.148 | 0.221 | 0.203 | 0.152 | 0.182 | 0.216 | 0.178 | 0.182 | 0 231 | 0.237 | 0 241 | 0 243 | 0 237 | 0.258 |

* Calculated assuming stoichiometry on the basis of 4 cations and 6 oxygens.
# Calculated after the Subcommittee on Pyroxenes, IMA (1988).

Table F-6 Electron microprobe analyses of garnets (Gneisses).

| Sample no. | IN-2 | | | | | | | | IN-3 | | | | | | | | |
|---|---|---|---|---|---|---|---|---|---|---|---|---|---|---|---|---|---|
| Analysis no. | 1 | 2 | 3 | 4 | 5 | 6 | 7 | 8 | 1 | 2 | 3 | 4 | 5 | 6 | 7 | 8 | 9 |
| | C12-Grt1 | C12-Grt1 | C12-Grt1 | C12-Grt1 | C13-Grt1 | C13-Grt1 | C13-Grt1 | C13-Grt13.4 | | | | | | | | | |
| SiO2 | 38.47 | 37.99 | 38.56 | 38.12 | 38.57 | 38.45 | 38.07 | 38.36 | 38.35 | 38.48 | 38.47 | 38.63 | 38.99 | 38.49 | 39.20 | 37.58 | 38.83 |
| TiO2 | 0.38 | 0.29 | 0.40 | 0.33 | 0.30 | 0.18 | 0.22 | 0.30 | 0.20 | 0.27 | 0.21 | 0.18 | 0.30 | 0.27 | 0.21 | 0.20 | 0.23 |
| Al2O3 | 20.16 | 19.81 | 20.43 | 20.27 | 20.34 | 20.71 | 20.31 | 20.61 | 19.79 | 19.46 | 20.01 | 20.86 | 20.63 | 20.60 | 20.89 | 22.75 | 20.29 |
| Cr2O3 | 0.07 | 0.35 | 0.02 | 0.20 | 0.00 | 0.00 | 0.08 | 0.05 | 0.00 | 0.04 | 0.00 | 0.01 | 0.00 | 0.00 | 0.00 | 0.02 | 0.00 |
| Fe2O3* | 4.02 | 4.88 | 3.77 | 4.69 | 4.66 | 4.08 | 4.54 | 3.95 | 4.60 | 5.30 | 4.86 | 4.00 | 3.65 | 4.03 | 4.29 | 4.42 | 4.21 |
| FeO* | 0.00 | 0.00 | 0.00 | 0.00 | 0.00 | 0.00 | 0.25 | 0.00 | 1.11 | 0.58 | 0.84 | 0.58 | 1.12 | 0.53 | 0.93 | 0.17 | 0.60 |
| MnO | 0.84 | 1.92 | 0.64 | 1.08 | 0.74 | 0.61 | 0.91 | 0.50 | 1.00 | 1.11 | 0.84 | 0.69 | 0.73 | 0.60 | 0.70 | 0.56 | 0.58 |
| MgO | 0.07 | 0.08 | 0.09 | 0.07 | 0.09 | 0.07 | 0.05 | 0.06 | 0.03 | 0.04 | 0.06 | 0.10 | 0.08 | 0.08 | 0.09 | 0.11 | 0.08 |
| CaO | 35.72 | 34.67 | 36.57 | 35.53 | 35.59 | 36.00 | 34.70 | 35.71 | 34.22 | 34.72 | 34.65 | 35.04 | 35.05 | 35.12 | 35.33 | 34.49 | 35.36 |
| Total | 99.74 | 99.99 | 100.48 | 100.27 | 100.29 | 100.10 | 99.14 | 99.53 | 99.31 | 100.00 | 99.94 | 100.10 | 100.55 | 99.72 | 101.63 | 100.30 | 100.18 |
| Number of cations on the basis of 12 oxygens: | | | | | | | | | | | | | | | | | |
| Si | 2.940 | 2.911 | 2.920 | 2.903 | 2.933 | 2.922 | 2.931 | 2.932 | 2.956 | 2.951 | 2.945 | 2.939 | 2.956 | 2.941 | 2.943 | 2.847 | 2.956 |
| Al iv | 0.060 | 0.089 | 0 080 | 0.097 | 0.067 | 0.078 | 0.069 | 0.068 | 0.044 | 0.049 | 0.055 | 0.061 | 0.044 | 0.059 | 0.057 | 0.153 | 0.044 |
| Al vi | 1.756 | 1.700 | 1.743 | 1.723 | 1.757 | 1.777 | 1.775 | 1.789 | 1.754 | 1.710 | 1.751 | 1.810 | 1.801 | 1.796 | 1.791 | 1.878 | 1.776 |
| Ti | 0.022 | 0.017 | 0.023 | 0.019 | 0.017 | 0.010 | 0.013 | 0.017 | 0.011 | 0.016 | 0.012 | 0.010 | 0.017 | 0.016 | 0.012 | 0.011 | 0.013 |
| Cr | 0.004 | 0.021 | 0.001 | 0.012 | 0.000 | 0.000 | 0.005 | 0.003 | 0.000 | 0.002 | 0.000 | 0.001 | 0.000 | 0.000 | 0.000 | 0.001 | 0.000 |
| Fe3+ | 0.231 | 0.282 | 0.215 | 0.269 | 0.267 | 0.233 | 0.263 | 0.227 | 0.267 | 0.306 | 0.280 | 0.229 | 0.208 | 0.232 | 0.242 | 0.252 | 0.241 |
| Fe2+ | 0.000 | 0.000 | 0.000 | 0.000 | 0.000 | 0.000 | 0.016 | 0.000 | 0.072 | 0.037 | 0.054 | 0.037 | 0.070 | 0.034 | 0.058 | 0.011 | 0.038 |
| Mn | 0.055 | 0.125 | 0.041 | 0.069 | 0.048 | 0.039 | 0.060 | 0.032 | 0.065 | 0.072 | 0.054 | 0.044 | 0.047 | 0.039 | 0.044 | 0.036 | 0.038 |
| Mg | 0.008 | 0.009 | 0.010 | 0.008 | 0.011 | 0.008 | 0.006 | 0.007 | 0.004 | 0.005 | 0.007 | 0.011 | 0.009 | 0.009 | 0.010 | 0.012 | 0.009 |
| Ca | 2.924 | 2.847 | 2.967 | 2.900 | 2.901 | 2.931 | 2.863 | 2.925 | 2.826 | 2.853 | 2.842 | 2.857 | 2.848 | 2.875 | 2.842 | 2.799 | 2.884 |
| Sum Cations | 8.000 | 8.000 | 8.000 | 8.000 | 8.000 | 8.000 | 8.000 | 8.000 | 8.000 | 8.000 | 8.000 | 8.000 | 8.000 | 8.000 | 8.000 | 8.000 | 8.000 |
| Mg/Mg+Fe2 | 1.000 | 1.000 | 1.000 | 1.000 | 1.000 | 1.000 | 0.266 | 1.000 | 0.050 | 0.109 | 0.109 | 0.236 | 0.110 | 0.215 | 0.146 | 0.539 | 0.191 |
| Molecular proportions of end-members : | | | | | | | | | | | | | | | | | |
| Alm | 0.000 | 0.000 | 0.000 | 0.000 | 0.000 | 0.000 | 0.006 | 0.000 | 0.024 | 0.012 | 0.018 | 0.013 | 0.024 | 0.011 | 0.020 | 0.004 | 0.013 |
| Py | 0.003 | 0.003 | 0.003 | 0.003 | 0.004 | 0.003 | 0.002 | 0.002 | 0.001 | 0.002 | 0.002 | 0.004 | 0.003 | 0.003 | 0.003 | 0.004 | 0.003 |
| Sp | 0.018 | 0.042 | 0.014 | 0.023 | 0.016 | 0.013 | 0.020 | 0.011 | 0.022 | 0.024 | 0.018 | 0.015 | 0.016 | 0.013 | 0.015 | 0.013 | 0.013 |
| Gr | 0.863 | 0.813 | 0.876 | 0.839 | 0.845 | 0.867 | 0.838 | 0.872 | 0.818 | 0.807 | 0.819 | 0.852 | 0.853 | 0.855 | 0.839 | 0.847 | 0.849 |
| Adr | 0.116 | 0.142 | 0.107 | 0.135 | 0.135 | 0.117 | 0.134 | 0.115 | 0.135 | 0.155 | 0.142 | 0.117 | 0.105 | 0.118 | 0.123 | 0.132 | 0.122 |

* Calculated assuming stoichiometry on the basis of 8 cations and 12 oxygens.

Table F-6 (continued)

| Sample no. | IN-3 | | | | | | | | | | | | | | | | |
|---|---|---|---|---|---|---|---|---|---|---|---|---|---|---|---|---|---|
| Analysis no. | 10 | 11 | 12 | 13 | 14 | 15 | 16 | 17 | 18 | 19 | 20 | 21 | 22 | 23 | 24 | 25 | 26 |
| | | | | | | | | | | | | | | | | | C3-Grt1 |
| SiO2 | 38.36 | 38.37 | 38.38 | 38.63 | 38.53 | 38.44 | 38.26 | 38.50 | 38.65 | 38.35 | 38.43 | 38.51 | 38.24 | 38.52 | 38.33 | 38.25 | 39.05 |
| TiO2 | 0.27 | 0.19 | 0.23 | 0.23 | 0.12 | 0.19 | 0.16 | 0.25 | 0.22 | 0.21 | 0.23 | 0.26 | 0.26 | 0.15 | 0.17 | 0.17 | 0.20 |
| Al2O3 | 20.53 | 20.86 | 20.59 | 20.61 | 20.02 | 20.42 | 20.73 | 20.46 | 20.55 | 20.73 | 20.73 | 20.58 | 20.01 | 19.79 | 19.73 | 19.95 | 20.85 |
| Cr2O3 | 0.00 | 0.04 | 0.01 | 0.00 | 0.07 | 0.00 | 0.02 | 0.00 | 0.00 | 0.00 | 0.00 | 0.02 | 0.04 | 0.06 | 0.01 | 0.00 | 0.00 |
| Fe2O3* | 4.89 | 4.11 | 4.63 | 4.72 | 5.23 | 4.72 | 4.81 | 4.19 | 3.77 | 4.41 | 4.75 | 5.32 | 5.82 | 5.71 | 5.77 | 5.46 | 4.52 |
| FeO* | 0.07 | 0.78 | 0.46 | 0.14 | 0.48 | 0.26 | 0.17 | 0.78 | 0.84 | 0.40 | 0.08 | -0.14 | 0.30 | 0.80 | 0.55 | 0.43 | 1.04 |
| MnO | 0.54 | 0.61 | 0.66 | 0.65 | 1.21 | 0.70 | 0.51 | 0.56 | 0.63 | 0.53 | 0.64 | 0.75 | 1.09 | 1.22 | 1.32 | 1.14 | 0.86 |
| MgO | 0.07 | 0.08 | 0.06 | 0.08 | 0.05 | 0.06 | 0.07 | 0.08 | 0.07 | 0.08 | 0.06 | 0.08 | 0.07 | 0.08 | 0.05 | 0.09 | 0.07 |
| CaO | 35.42 | 34.74 | 35.01 | 35.47 | 34.64 | 35.16 | 35.19 | 34.95 | 34.98 | 35.10 | 35.37 | 35.52 | 34.67 | 34.36 | 34.36 | 34.46 | 34.99 |
| Total | 100.14 | 99.78 | 100.04 | 100.54 | 100.34 | 99.95 | 99.92 | 99.76 | 99.71 | 99.81 | 100.29 | 100.90 | 100.50 | 100.69 | 100.28 | 99.94 | 101.58 |
| Number of cations on the basis of 12 oxygens: | | | | | | | | | | | | | | | | | |
| Si | 2.922 | 2.930 | 2.928 | 2.931 | 2.940 | 2.935 | 2.920 | 2.943 | 2.953 | 2.928 | 2.922 | 2.915 | 2.917 | 2.937 | 2.934 | 2.932 | 2.936 |
| Al iv | 0.078 | 0.070 | 0.072 | 0.069 | 0.060 | 0.065 | 0.080 | 0.057 | 0.047 | 0.072 | 0.078 | 0.085 | 0.083 | 0.063 | 0.066 | 0.068 | 0.064 |
| Al vi | 1.767 | 1.809 | 1.780 | 1.774 | 1.741 | 1.773 | 1.784 | 1.787 | 1.805 | 1.794 | 1.780 | 1.751 | 1.717 | 1.715 | 1.714 | 1.734 | 1.785 |
| Ti | 0.015 | 0.011 | 0.013 | 0.013 | 0.007 | 0.011 | 0.009 | 0.014 | 0.013 | 0.012 | 0.013 | 0.015 | 0.015 | 0.008 | 0.010 | 0.010 | 0.011 |
| Cr | 0.000 | 0.002 | 0.001 | 0.000 | 0.004 | 0.000 | 0.001 | 0.000 | 0.000 | 0.000 | 0.000 | 0.001 | 0.002 | 0.004 | 0.001 | 0.000 | 0.000 |
| Fe3+ | 0.281 | 0.236 | 0.266 | 0.269 | 0.300 | 0.271 | 0.276 | 0.241 | 0.217 | 0.254 | 0.272 | 0.303 | 0.334 | 0.328 | 0.332 | 0.315 | 0.256 |
| Fe2+ | 0.005 | 0.050 | 0.029 | 0.009 | 0.031 | 0.017 | 0.011 | 0.050 | 0.053 | 0.026 | 0.005 | -0.009 | 0.019 | 0.051 | 0.035 | 0.027 | 0.065 |
| Mn | 0.035 | 0.039 | 0.043 | 0.042 | 0.078 | 0.045 | 0.033 | 0.036 | 0.041 | 0.034 | 0.041 | 0.048 | 0.071 | 0.078 | 0.085 | 0.074 | 0.055 |
| Mg | 0.008 | 0.009 | 0.007 | 0.009 | 0.006 | 0.007 | 0.008 | 0.009 | 0.008 | 0.009 | 0.007 | 0.009 | 0.008 | 0.009 | 0.005 | 0.010 | 0.008 |
| Ca | 2.891 | 2.843 | 2.862 | 2.883 | 2.832 | 2.876 | 2.877 | 2.863 | 2.864 | 2.871 | 2.882 | 2.881 | 2.834 | 2.807 | 2.817 | 2.830 | 2.820 |
| Sum Cations | 8.000 | 8.000 | 8.000 | 8.000 | 8.000 | 8.000 | 8.000 | 8.000 | 8.000 | 8.000 | 8.000 | 8.000 | 8.000 | 8.000 | 8.000 | 8.000 | 8.000 |
| Mg/Mg+Fe2 | 0.625 | 0.148 | 0.196 | 0.508 | 0.167 | 0.294 | 0.435 | 0.148 | 0.124 | 0.261 | 0.584 | 69.209 | 0.308 | 0.145 | 0.133 | 0.269 | 0.108 |
| Molecular proportions of end-members : | | | | | | | | | | | | | | | | | |
| Alm | 0.002 | 0.017 | 0.010 | 0.003 | 0.010 | 0.006 | 0.004 | 0.017 | 0.018 | 0.009 | 0.002 | -0.003 | 0.006 | 0.017 | 0.012 | 0.009 | 0.022 |
| Py | 0.003 | 0.003 | 0.002 | 0.003 | 0.002 | 0.002 | 0.003 | 0.003 | 0.003 | 0.003 | 0.002 | 0.003 | 0.003 | 0.003 | 0.002 | 0.003 | 0.003 |
| Sp | 0.012 | 0.013 | 0.015 | 0.014 | 0.027 | 0.015 | 0.011 | 0.012 | 0.014 | 0.012 | 0.014 | 0.016 | 0.024 | 0.027 | 0.029 | 0.025 | 0.019 |
| Gr | 0.841 | 0.846 | 0.838 | 0.842 | 0.808 | 0.838 | 0.841 | 0.846 | 0.856 | 0.847 | 0.843 | 0.828 | 0.796 | 0.786 | 0.788 | 0.802 | 0.826 |
| Adr | 0.143 | 0.120 | 0.135 | 0.137 | 0.153 | 0.138 | 0.141 | 0.122 | 0.110 | 0.129 | 0.139 | 0.155 | 0.171 | 0.167 | 0.169 | 0.160 | 0.130 |

* Calculated assuming stoichiometry on the basis of 8 cations and 12 oxygens.

Table F-6 (continued)

| Sample no. | IN-3 | | | | | | | | | IN-13.1 | | | | | | |
|---|---|---|---|---|---|---|---|---|---|---|---|---|---|---|---|---|
| Analysis no. | 27 | 28 | 29 | 30 | 31 | 32 | 33 | 34 | 35 | 1 | 2 | 3 | 4 | 5 | 6 | 7 |
| | C3-Grt2 | C3-Grt3 | C3-Grt4 | C3-Grt5 | C5-Grt6 | C5-Grt7 | C5-Grt8 | C5-Grt9 | C5-Grt10 | C1-Grt1 | C1-Grt2 | C1-Grt3 | C1-Grt4 | C1-Grt5 | C2-Grt6 | C2-Grt7 |
| SiO2 | 39.14 | 39.02 | 39.02 | 39.07 | 38.63 | 38.88 | 39.08 | 38.89 | 38.92 | 37.90 | 37.64 | 37.94 | 37.88 | 37.78 | 38.00 | 37.61 |
| TiO2 | 0.22 | 0.36 | 0.26 | 0.18 | 0.28 | 0.22 | 0.27 | 0.24 | 0.21 | 0.53 | 0.72 | 0.52 | 0.80 | 0.76 | 0.41 | 0.49 |
| Al2O3 | 20.91 | 20.90 | 20.80 | 20.52 | 19.44 | 20.36 | 20.79 | 20.70 | 20.71 | 18.23 | 18.47 | 17.96 | 17.97 | 18.07 | 19.49 | 18.74 |
| Cr2O3 | 0.01 | 0.00 | 0.05 | 0.01 | 0.03 | 0.00 | 0.03 | 0.06 | 0.01 | 0.00 | 0.00 | 0.02 | 0.01 | 0.10 | 0.02 | 0.04 |
| Fe2O3* | 4.11 | 3.52 | 3.90 | 4.39 | 5.85 | 4.23 | 4.30 | 4.52 | 4.05 | 6.87 | 6.04 | 6.92 | 6.69 | 6.84 | 7.06 | 7.60 |
| FeO* | 1.31 | 0.61 | 0.35 | 1.15 | 0.56 | 1.89 | 1.05 | 0.89 | 1.43 | 0.00 | 0.00 | 0.00 | 0.00 | 0.00 | 0.25 | 0.00 |
| MnO | 0.85 | 0.48 | 0.50 | 1.01 | 1.20 | 1.19 | 0.87 | 0.80 | 0.85 | 0.28 | 0.26 | 0.19 | 0.18 | 0.36 | 0.34 | 0.24 |
| MgO | 0.10 | 0.06 | 0.07 | 0.08 | 0.05 | 0.05 | 0.09 | 0.06 | 0.10 | 0.06 | 0.07 | 0.06 | 0.10 | 0.06 | 0.07 | 0.06 |
| CaO | 34.85 | 35.73 | 35.84 | 34.79 | 34.79 | 33.95 | 35.03 | 35.04 | 34.55 | 37.05 | 37.07 | 36.08 | 36.66 | 36.55 | 35.20 | 35.47 |
| Total | 101.49 | 100.69 | 100.79 | 101.19 | 100.83 | 100.77 | 101.52 | 101.21 | 100.84 | 100.91 | 100.27 | 99.69 | 100.30 | 100.54 | 100.84 | 100.25 |
| Number of cations on the basis of 12 oxygens: | | | | | | | | | | | | | | | | |
| Si | 2.944 | 2.949 | 2.947 | 2.951 | 2.942 | 2.954 | 2.940 | 2.935 | 2.948 | 2.888 | 2.881 | 2.929 | 2.905 | 2.894 | 2.898 | 2.890 |
| Al iv | 0.056 | 0.051 | 0.053 | 0.049 | 0.058 | 0.046 | 0.060 | 0.065 | 0.052 | 0.112 | 0.119 | 0.071 | 0.095 | 0.106 | 0.102 | 0.110 |
| Al vi | 1.798 | 1.810 | 1.798 | 1.778 | 1.688 | 1.779 | 1.784 | 1.778 | 1.797 | 1.526 | 1.547 | 1.563 | 1.530 | 1.525 | 1.650 | 1.587 |
| Ti | 0.012 | 0.021 | 0.015 | 0.010 | 0.016 | 0.012 | 0.016 | 0.013 | 0.012 | 0.030 | 0.041 | 0.030 | 0.046 | 0.044 | 0.023 | 0.029 |
| Cr | 0.001 | 0.000 | 0.003 | 0.001 | 0.002 | 0.000 | 0.002 | 0.004 | 0.001 | 0.000 | 0.000 | 0.001 | 0.001 | 0.006 | 0.001 | 0.002 |
| Fe3+ | 0.233 | 0.200 | 0.222 | 0.249 | 0.335 | 0.242 | 0.243 | 0.257 | 0.231 | 0.394 | 0.348 | 0.402 | 0.386 | 0.394 | 0.405 | 0.439 |
| Fe2+ | 0.082 | 0.038 | 0.022 | 0.073 | 0.035 | 0.120 | 0.066 | 0.056 | 0.090 | 0.000 | 0.000 | 0.000 | 0.000 | 0.000 | 0.016 | 0.000 |
| Mn | 0.054 | 0.031 | 0.032 | 0.065 | 0.077 | 0.077 | 0.055 | 0.051 | 0.054 | 0.018 | 0.017 | 0.012 | 0.012 | 0.024 | 0.022 | 0.016 |
| Mg | 0.011 | 0.007 | 0.008 | 0.009 | 0.006 | 0.006 | 0.010 | 0.007 | 0.011 | 0.007 | 0.008 | 0.007 | 0.012 | 0.007 | 0.008 | 0.007 |
| Ca | 2.809 | 2.893 | 2.900 | 2.815 | 2.840 | 2.764 | 2.824 | 2.834 | 2.804 | 3.025 | 3.039 | 2.984 | 3.013 | 2.999 | 2.876 | 2.920 |
| Sum Cations | 8.000 | 8.000 | 8.000 | 8.000 | 8.000 | 8.000 | 8.000 | 8.000 | 8.000 | 8.000 | 8.000 | 8.000 | 8.000 | 8.000 | 8.000 | 8.000 |
| Mg/Mg+Fe2 | 0.119 | 0.155 | 0.264 | 0.109 | 0.146 | 0.049 | 0.134 | 0.112 | 0.112 | 1.000 | 1.000 | 1.000 | 1.000 | 1.000 | 0.323 | 1.000 |
| Molecular proportions of end-members : | | | | | | | | | | | | | | | | |
| Alm | 0.028 | 0.013 | 0.007 | 0.025 | 0.012 | 0.040 | 0.022 | 0.019 | 0.030 | 0.000 | 0.000 | 0.000 | 0.000 | 0.000 | 0.005 | 0.000 |
| Py | 0.004 | 0.002 | 0.003 | 0.003 | 0.002 | 0.002 | 0.003 | 0.002 | 0.004 | 0.002 | 0.003 | 0.002 | 0.004 | 0.002 | 0.003 | 0.002 |
| Sp | 0.018 | 0.010 | 0.011 | 0.022 | 0.026 | 0.026 | 0.019 | 0.017 | 0.018 | 0.006 | 0.005 | 0.004 | 0.004 | 0.008 | 0.008 | 0.005 |
| Gr | 0.832 | 0.873 | 0.867 | 0.824 | 0.790 | 0.809 | 0.832 | 0.831 | 0.830 | 0.798 | 0.822 | 0.793 | 0.801 | 0.795 | 0.776 | 0.768 |
| Adr | 0.118 | 0.101 | 0.112 | 0.126 | 0.170 | 0.122 | 0.124 | 0.131 | 0.117 | 0.194 | 0.170 | 0.201 | 0.191 | 0.195 | 0 208 | 0.224 |

* Calculated assuming stoichiometry on the basis of 8 cations and 12 oxygens.

Table F-7 Electron microprobe analyses of amphiboles (Gneisses).

| Sample no. | IN-2 | | | | | | |
|---|---|---|---|---|---|---|---|
| Analysis no. | 1 | 2 | 3 | 4 | 5 | 6 | 7 |
| | C3-Ampl | C3-Ampl | C3-Ampl | C5-Ampl | C5-Ampl | C5-Ampl | C5-Amph5.4 |
| SiO2 | 44.79 | 44.21 | 44.24 | 44.10 | 43.94 | 44.81 | 44.49 |
| TiO2 | 0.41 | 0.51 | 0.47 | 0.50 | 0.48 | 0.48 | 0.41 |
| Al2O3 | 12.48 | 12.85 | 12.40 | 12.62 | 12.65 | 12.15 | 12.25 |
| Cr2O3 | 0.05 | 0.02 | 0.07 | 0.03 | 0.07 | 0.11 | 0.00 |
| FeO* | 12.14 | 12.04 | 12.88 | 12.91 | 12.67 | 13.18 | 13.03 |
| MnO | 0.17 | 0.19 | 0.18 | 0.27 | 0.17 | 0.09 | 0.21 |
| MgO | 12.99 | 12.86 | 12.64 | 12.40 | 12.50 | 12.42 | 12.51 |
| CaO | 12.58 | 12.81 | 12.70 | 12.59 | 12.41 | 12.94 | 12.61 |
| Na2O | 1.91 | 1.91 | 1.85 | 1.83 | 1.79 | 1.84 | 1.84 |
| K2O | 0.13 | 0.13 | 0.13 | 0.14 | 0.14 | 0.13 | 0.13 |
| F | 0.00 | 0.00 | 0.00 | 0.00 | 0.00 | 0.00 | 0.00 |
| Cl | 0.00 | 0.05 | 0.01 | 0.07 | 0.08 | 0.00 | 0.01 |
| Total | 97.65 | 97.58 | 97.57 | 97.46 | 96.90 | 98.15 | 97.49 |
| O = F, Cl | 0.00 | -0.01 | 0.00 | -0.02 | -0.02 | 0.00 | 0.00 |
| Total | 97.65 | 97.57 | 97.57 | 97.44 | 96.88 | 98.15 | 97.49 |
| Number of cations on the basis of 23 oxygens:# | | | | | | | |
| Si | 6.505 | 6.446 | 6.460 | 6.450 | 6.444 | 6.531 | 6.502 |
| Al iv | 1.495 | 1.554 | 1.540 | 1.550 | 1.556 | 1.469 | 1.498 |
| Sum T | 8.000 | 8.000 | 8.000 | 8.000 | 8.000 | 8.000 | 8.000 |
| Al vi | 0.642 | 0.655 | 0.594 | 0.626 | 0.632 | 0.619 | 0.612 |
| Ti | 0.045 | 0.056 | 0.052 | 0.055 | 0.053 | 0.053 | 0.045 |
| Cr | 0.006 | 0.002 | 0.008 | 0.003 | 0.008 | 0.013 | 0.000 |
| Fe3+ | 0.280 | 0.217 | 0.312 | 0.319 | 0.374 | 0.146 | 0.302 |
| Mg | 2.812 | 2.795 | 2.751 | 2.703 | 2.732 | 2.698 | 2.725 |
| Fe2+ | 1.195 | 1.251 | 1.261 | 1.260 | 1.180 | 1.461 | 1.291 |
| Mn | 0.021 | 0.023 | 0.022 | 0.033 | 0.021 | 0.011 | 0.026 |
| Sum C | 5.000 | 5.000 | 5.000 | 5.000 | 5.000 | 5.000 | 5.000 |
| Fe2+ | 0.000 | 0.000 | 0.000 | 0.000 | 0.000 | 0.000 | 0.000 |
| Mn | 0.000 | 0.000 | 0.000 | 0.000 | 0.000 | 0.000 | 0.000 |
| Ca | 1.958 | 2.000 | 1.987 | 1.973 | 1.950 | 2.000 | 1.975 |
| Na | 0.042 | 0.000 | 0.013 | 0.027 | 0.050 | 0.000 | 0.025 |
| Sum B | 2.000 | 2.000 | 2.000 | 2.000 | 2.000 | 2.000 | 2.000 |
| Ca | 0.000 | 0.001 | 0.000 | 0.000 | 0.000 | 0.021 | 0.000 |
| Na | 0.496 | 0.540 | 0.511 | 0.492 | 0.459 | 0.520 | 0.496 |
| K | 0.024 | 0.024 | 0.024 | 0.026 | 0.026 | 0.024 | 0.024 |
| Sum A | 0.520 | 0.566 | 0.535 | 0.518 | 0.485 | 0.565 | 0.520 |
| Sum Cations | 15.520 | 15.566 | 15.535 | 15.518 | 15.485 | 15.565 | 15.520 |
| Mg/(Mg+Fe2) | 0.702 | 0.691 | 0.686 | 0.682 | 0.698 | 0.649 | 0.679 |

* Total Fe as FeO.

# Calculated by normalising the number of cations other than Ca, Na and K to 13.

Table F-8 Electron microprobe analyses of sillimanites (Gneisses)

| Sample no. | IN-18.1 | IN-19 | |
|---|---|---|---|
| Analysis no. | 1 | 1 | 2 |
| | | C6-Sill1 | C6-Sill2 |
| SiO2 | 36.77 | 36.45 | 36.84 |
| TiO2 | 0.02 | 0.02 | 0.04 |
| Al2O3 | 62.27 | 63.01 | 63.14 |
| Cr2O3 | 0.00 | 0.00 | 0.00 |
| Fe2O3* | 0.24 | 0.25 | 0.16 |
| MnO | 0.00 | 0.00 | 0.00 |
| MgO | 0.00 | 0.01 | 0.00 |
| CaO | 0.02 | 0.01 | 0.00 |
| Total | 99.32 | 99.75 | 100.18 |
| Number of cations on the basis of 5 oxygens : | | | |
| Si | 0.999 | 0.987 | 0.993 |
| Ti | 0.000 | 0.000 | 0.001 |
| Al | 1.995 | 2.011 | 2.006 |
| Cr | 0.000 | 0.000 | 0.000 |
| Fe3+ | 0.005 | 0.005 | 0.003 |
| Mn | 0.000 | 0.000 | 0.000 |
| Mg | 0.000 | 0.000 | 0.000 |
| Ca | 0.000 | 0.000 | 0.000 |
| Sum Cations | 3.000 | 3.004 | 3.002 |

* Total Fe as Fe2O3.

Table F-9 Electron microprobe analyses of calcites (Gneisses).

| Sample no. | IN-2 | |
|---|---|---|
| Analysis no. | 1 | 2 |
| | C13-Cal1 | C13-Cal13.2 |
| FeO* | 0.10 | 0.00 |
| MnO | 0.12 | 0.00 |
| MgO | 0.00 | 0.00 |
| CaO | 54.76 | 54.99 |
| CO2# | 43.11 | 43.16 |
| Total | 98.10 | 98.15 |
| Number of cations on the basis of 6 oxygens: | | |
| Fe | 0.003 | 0.000 |
| Mn | 0.003 | 0.000 |
| Mg | 0.000 | 0.000 |
| Ca | 1.994 | 2.000 |
| Sum Cat. | 2.000 | 2.000 |
| Molecular proportions of end-members: | | |
| FeCO3 | 0.001 | 0.000 |
| MnCO3 | 0.002 | 0.000 |
| MgCO3 | 0.000 | 0.000 |
| CaCO3 | 0.997 | 1.000 |

* Total Fe as FeO
# Calculated from stoichiometry

Table F-10 Electron microprobe analyses of zoisites (Gneisses).

| Sample no. | IN-3 | | | | |
|---|---|---|---|---|---|
| Analysis no. | 1 | 2 | 3 | 4 | 5 |
| SiO2 | 38.68 | 38.65 | 38.42 | 38.33 | 38.41 |
| TiO2 | 0.03 | 0.02 | 0.08 | 0.06 | 0.05 |
| Al2O3 | 28.99 | 28.27 | 29.03 | 28.77 | 29.08 |
| Fe2O3* | 6.32 | 6.86 | 6.12 | 6.79 | 6.18 |
| MnO | 0.60 | 0.59 | 0.69 | 0.48 | 0.26 |
| MgO | 0.00 | 0.03 | 0.02 | 0.00 | 0.01 |
| CaO | 24.08 | 24.21 | 23.95 | 24.14 | 24.33 |
| Total | 98.72 | 98.63 | 98.31 | 98.57 | 98.31 |
| Number of cations on the basis of 12.5 oxygens: | | | | | |
| Si | 2.982 | 2.991 | 2.974 | 2.966 | 2.971 |
| Al iv | 0.018 | 0.009 | 0.026 | 0.034 | 0.029 |
| Sum Z | 3.000 | 3.000 | 3.000 | 3.000 | 3.000 |
| Al vi | 2.617 | 2.569 | 2.623 | 2.590 | 2.623 |
| Ti | 0.002 | 0.001 | 0.005 | 0.003 | 0.003 |
| Fe3+ | 0.367 | 0.399 | 0.356 | 0.395 | 0.360 |
| Sum Y | 2.986 | 2.969 | 2.984 | 2.989 | 2.986 |
| Mn | 0.040 | 0.039 | 0.046 | 0.032 | 0.017 |
| Mg | 0.000 | 0.004 | 0.002 | 0.000 | 0.001 |
| Ca | 1.989 | 2.007 | 1.986 | 2.001 | 2.017 |
| Sum W | 2.029 | 2.050 | 2.034 | 2.033 | 2.034 |
| Sum Cations | 8.015 | 8.019 | 8.019 | 8.021 | 8.020 |
| Fe3/(Fe3+Al) | 0.122 | 0.134 | 0.119 | 0.131 | 0.119 |

* Total Fe as Fe2O3